



HAL
open science

Catalytic activation of CO towards carboxylic acids and esters mediated by ruthenium precursors

Kana Kunihiro

► **To cite this version:**

Kana Kunihiro. Catalytic activation of CO towards carboxylic acids and esters mediated by ruthenium precursors. Organic chemistry. Université de Rennes, 2022. English. NNT : 2022REN1S025 . tel-03859459

HAL Id: tel-03859459

<https://theses.hal.science/tel-03859459>

Submitted on 18 Nov 2022

HAL is a multi-disciplinary open access archive for the deposit and dissemination of scientific research documents, whether they are published or not. The documents may come from teaching and research institutions in France or abroad, or from public or private research centers.

L'archive ouverte pluridisciplinaire **HAL**, est destinée au dépôt et à la diffusion de documents scientifiques de niveau recherche, publiés ou non, émanant des établissements d'enseignement et de recherche français ou étrangers, des laboratoires publics ou privés.

THESE DE DOCTORAT DE

L'UNIVERSITE DE RENNES 1

ECOLE DOCTORALE N° 596

Matière, Molécules, Matériaux

Spécialité : Chimie Moléculaire et Macromoléculaire

Par

Kana Yasmine KUNIHIO

Catalytic activation of CO₂ towards carboxylic acids and esters mediated by ruthenium precursors

Thèse présentée et soutenue à Rennes, le 20/01/2022

Unité de recherche : UMR 6226 CNRS Institut des Sciences Chimiques de Rennes

Thèse N° :

Rapporteurs avant soutenance :

Walter Leitner Professeur, Max Planck Institute for Chemical Energy Conversion, Mülheim an der Ruhr,
Allemagne
Kazushi Mashima Professeur, Univ. d'Osaka, Japon

Composition du Jury :

Président : Pierre Dixneuf Prof. émérite des Universités, Univ. Rennes 1
Examinatrice : Hélène Olivier-Bourbigou Directrice scientifique, IFP Energies nouvelles
Dir. de thèse : Evgueni Kirillov Maître de conférences, Univ. Rennes 1
Co-dir. de thèse : Jean-François Carpentier Prof. des Universités, Univ. Rennes 1

Invité(s)

Pierre Dixneuf Prof. émérite des Universités, Univ. Rennes 1

Activation du CO₂ pour la formation d'acides et d'esters
carboxyliques catalysée par des précurseurs au ruthénium

Kana Yasmine KUNIHIO

A thesis submitted for the degree of Doctor of Philosophy

Université de Rennes 1

UMR 6226, ISCR, Rennes, France

20th of January 2022

*“We do not inherit the earth from our ancestors; we borrow it
from our children” – Native American proverb*

Table of Contents

Acknowledgements	11
Foreword	15
Declaration of authorship	17
Abstract	19
Résumé	21
List of abbreviations, chemical products, molecules and units	23
General introduction	27
1. Context	27
2. History of carbon dioxide: from its discovery to its first uses	28
3. Sources of CO ₂	29
3.1. Occurrence of CO ₂ in nature	29
3.2. Anthropogenic CO ₂ emissions	30
4. Technologies for CO ₂ reduction.....	33
4.1. CO ₂ capture	33
4.2. CO ₂ , an industrial by-product.....	35
4.3. Carbon capture and storage (CCS).....	37
4.4. Price and availability of CO ₂	37
4.5. Carbon Capture and Utilisation (CCU).....	38
5. Chemical valorization of CO ₂	40
5.1. Urea production.....	42
5.2. Dry-reforming	42
5.3. Methanol production	43
5.4. Salicylic acid production.....	43
5.5. Cyclic carbonates	44
5.6. Polymers from CO ₂	44

5.7. Organic acids from CO ₂	45
6. Goal of the thesis	48
7. References	50

Part I

Introduction	57
Chapter 1 – CO₂ as a C1 source to access carboxylic acids: State-of-the-art	59
1.1. Carboxylic acid syntheses from CO ₂ : General aspects	59
1.2. Transition metal-catalyzed carboxylation reactions	61
1.2.1. Carbon dioxide activation with mononuclear transition metal complexes	61
1.2.2. Metal-catalyzed carboxylation reaction of organometallic reagents	63
a. Catalytic carboxylation of organotin derivatives	63
b. Catalytic carboxylation of organoboron and other organometallic reagents	64
1.2.3. Catalytic reductive carboxylation of non-activated substrates	67
a. Catalytic carboxylation of organic halides	67
b. Catalytic reductive carboxylation of C–O and C–N electrophiles	70
1.2.4. Catalytic carboxylation of unsaturated hydrocarbons	73
a. C(<i>sp</i>)–H bonds (alkynes)	73
b. C(<i>sp</i> ²)–H bonds (alkenes)	76
• Early discovery: metallalactone formation	76
• Towards acrylic acid synthesis	79
• Acrylate recovery via M–O metallactone bond cleavage	81
• Hydrocarboxylation reaction of alkenes	84
• Carbonylation and hydroformylation reactions	89
c. Catalytic carboxylation of dienes and other polyunsaturated systems	92
1.2.5. Catalytic carboxylation techniques via C–H functionalization	94
a. <i>sp</i> C–H carboxylation	95

b. sp^2 C–H carboxylation	97
• Friedel-Crafts carboxylation of aromatics.....	97
• Base-mediated carboxylation	98
• Transition-metal-catalyzed carboxylation of Csp^2 –H bonds	100
c. sp^3 C–H carboxylation.....	102
1.3. Conclusion and outlook.....	104
1.4. References	105
Chapter 2 – Efficient catalytic systems toward carboxylation reaction of C_2H_4 with CO_2: from discovery to optimization by means of High Throughput Experimentation.....	111
2.1. High-Throughput Experimentation	111
2.1.1. Introduction	111
2.1.2. Objectives and background	112
a. Ethylene carboxylation reaction using triethylsilane.....	112
b. Preliminary results	113
c. HTS methodology.....	117
2.2. Results and discussion.....	118
2.2.1. HTS catalytic results of the reductive coupling of CO_2 with C_2H_4 and Et_3SiH ... 118	
2.2.2. Batch-scale metal-catalyzed synthesis of silylesters from CO_2 and C_2H_4	122
a. Upscaling to batch scale reactors	122
b. Optimization of the reaction conditions.....	125
2.2.3. Toward metal-catalyzed synthesis of carboxylic acids from CO_2 , C_2H_4 and H_2 ? 127	
2.3. Conclusion.....	129
2.4. References	130

Part II

Introduction.....	137
Chapter 3 – Catalytic CO_2-C_2H_4 coupling mediated by ruthenium(II) complexes bearing bidentate chelating phosphines	139

3.1. Evaluation of the ligand effect on the catalytic activity	139
3.1.1. Background	139
3.1.2. Evaluating the catalytic performances of Ru(H)(Cl)(CO)(PPh ₃) ₃ in combination with bidentate phosphine ligands	141
3.2. Towards identifying reaction intermediates: syntheses and characterization of new Ru ^{II} phosphine chelated Ru(H)(Cl)(CO)(DCPB)(PPh ₃) and Ru(H)(Cl)(CO)(DCPF)(PPh ₃) complexes.....	145
3.2.1. X-Ray characterization of Ru(H)(Cl)(CO)(DCPB)(PPh ₃) and Ru(H)(Cl)(CO)(DCPF)(PPh ₃) complexes originating from the reaction of Ru-1 with DCPB and DCPF, respectively	145
3.2.2. NMR studies of the reaction of Ru-1 with DCPF: formation of Ru(H)(Cl)(CO)(PPh ₃)(DCPF) complex (Ru-2).....	148
3.2.3. NMR studies of the reaction of Ru-1 with DCPB: formation of Ru(H)(Cl)(CO)(DCPB)(PPh ₃) (Ru-3)	150
3.3. Influence of the metal/ligand ratio in ligand exchange reaction and catalysis.....	161
3.3.1. Influence of the Ru(H)(Cl)(CO)(PPh ₃) ₃ /DCPB ratios in complexation reaction.	161
3.3.2. Application to catalysis	165
3.4. Reactivity of Et ₃ SiH toward ruthenium complexes	166
3.4.1. Stoichiometric reaction of Ru-1 , DCPB and Et ₃ SiH	166
3.4.2. Synthesis, characterization and catalytic activity of the dihydrido Ru(H) ₂ (CO)(DCPB)(PPh ₃) complex (Ru-5).....	167
3.5. Conclusion.....	170
3.6. References	172
Chapter 4 – Mechanistic Investigations on the Ruthenium-Catalyzed Synthesis of Silyl Esters from C₂H₄ and CO₂	175
4.1. Background	175
4.2. Mechanistic insights on the formation of the targeted triethylsilyl acrylate (A1) and propionate (P1) products.....	177

4.2.1. Ru(H)(Cl)(CO)(PPh ₃)(DCPB) mediated coupling of CO ₂ and C ₂ H ₄ : formation of the [Ru(Cl)(CO)(DCPB)(κ ² O, O-CO ₂ CH=CH ₂)] (Ru-6)	177
4.2.2. Possible mechanism for the formation of Ru-6	190
4.2.3. Computational studies	192
4.2.4. Release of triethylsilyl acrylate from acrylate-ruthenium Ru(Cl)(CO)(DCPB)(κ ² O, O-CO ₂ CH=CH ₂) and regeneration of Ru(H)(Cl)(CO)(DCPB)(PPh ₃)	192
4.2.5. Possible mechanism for the formation of Ru-6 and Ru-7 leading to triethylsilyl acrylate and triethylsilyl propionate	203
4.3. Mechanistic insights on the formation of the triethylsilyl formate (F1) by-product ..	205
4.3.1. State-of-the-art	205
4.3.2. Catalytic hydrosilylation of CO ₂ using Ru-3 complex; DFT calculations and mechanism.....	208
4.4. Mechanistic insights on the formation of the triethylvinylsilane (TEVS) and tetraethylsilane (TES) by-products	209
4.4.1. State-of-the-art	209
4.4.2. Catalytic hydrosilylation and dehydrogenative silylation of C ₂ H ₄ using the Ru-3 system; DFT calculations and mechanism proposal	212
4.5. Optimization of the catalytic formation of triethylsilylacrylate and propionate from CO ₂ , C ₂ H ₄ , Et ₃ SiH and additives	214
4.6. Conclusion.....	218
4.7. References	220
General conclusion and perspectives	225
Experimental section	229
Annexes	253
Compte-rendu en langue française	263
Organic products and complex structures reminder	291

Acknowledgements

I would like to firstly express my gratitude to the member of the jury, Dr. H el ene Olivier-Bourbigou, Prof. Pierre Dixneuf, Prof. Walter Leitner and Prof. Kazushi Mashima, for accepting to evaluate my work and for the rich scientific discussion we had during the defense.

My journey at the University of Rennes was a marathon, and it would not have been possible for me to reach the finish line without the support of many people. The following pages can only begin to express my full gratitude toward all the people that have helped me along the way.

I would like to thank my supervisors, Dr. Evgueni Kirillov and Prof. Jean-Fran ois Carpentier, for allowing me to join the OCP group and for giving me the opportunity to work on the CO22CHEM project. Thank you for your guidance, for the scientific discussions and feedbacks and for being supportive throughout my research work.

Our collaborators outside Rennes University have been of great importance in the start and throughout my project. I have had the pleasure to work at the Realcat Platform in Lille, for several months, to perform the HTS primary studies. Prof. P. S ebastien and Prof. F. Dumeignil welcomed us kindly, sharing their time, expertise and guiding us through the futuristic world of HTS. Special thanks goes to Dr. S. Heyte, the most impressive, patient, efficient, resourceful woman I have ever met! Thank you for training me on the different HTS facilities and for making my stay comfortable in Lille. I also had the pleasure to meet the bright Eagon, the kind and determined Roxane and the funny Antoine. Thank you for your cheerfulness and for spending hours with me at glove box writing down my weight values! Wish you all the best for your careers.

Prof. L. Maron and Dr. R. Thayalan have brought their computational knowledge to the project. Thank you for helping us getting a better understanding of the CO₂ reactional mechanism in our system.

As a great part of this manuscript is based on NMR experiments, such studies would not have been possible without the help of Dr. E. Caytan and C. Orione. I thank you both for your time, for sharing your expertise with me and for your valuable advices regarding my chemistry. Thank you Elsa for ordering, every winter, delicious oranges and lemons all the way down from Corsica. Cl ement, I enjoyed very much our manga and anime discussions! I hope you will have the opportunity to visit Japan one day, and who knows, we may be able to play "G o" on the land of the rising sun!

I also had the pleasure to work with Dr. P. J ehan – thank you for your hard work and dedication to analysing my complexes by mass spectrometry, even those who were difficult to observe.

During these three years and half, I also had the privilege to interact with amazing permanent members. I had the great pleasure to meet Prof. Dixneuf, whom was always eager to help, give enriching

scientific advices and who taught me a lot about french culture and gastronomy. Thank you for taking me under your wing. You are a mentor to me.

To my floor neighbours, Dr. O. Galangau, Dr. L. Norel, Dr. J. Boixel and Dr. S. Guillaume, thank you for your advices. I am also deeply grateful for the rich scientific discussions I had with Dr. G. Alcaraz. Thank you for your time and for having given me such great ideas, both experimentally and theoretically inspiring.

I am thankful to many other OMC group members: Dr. C. Fischmeister, Dr. C. Darcel, Dr. J.-F. Soulé have been very helpful especially at the beginning of my PhD.

A huge THANK YOU also goes to the amazing staff members that have guide me throughout my PhD. These people are behind the scene superheroes: Mrs. B. Mahi, Mrs. C. Jolivet, Mrs. K. Robin, Mrs. C. Perier and Mr. D. Paris.

Thankful thoughts goes also to all my teachers, from my early middle school (Lycée Cheikh Bouamama, Algiers, Algeria) and high school years (LIAD, Algiers), back when science was still taught on a chalkboard, and not through computer screens (#Covid19)! Mrs. Ounas, Mrs. Terba, Mr. Menasria, Mrs. Bouisri, Mrs. Barnet, Mr. Guidez, Mr. Tahar, Mr. Joucdar, thank you for teaching me the basics of science with passion and altruism. To my university education professors, Dr. Pipon, Dr. Dechy-Cabaret, Dr. Volkman, Dr. Urrutigoity, Dr. Vaca-Garcia, and my internship supervisors Dr. Thomas and Dr. Harris, thank you for your encouragements, your advices and your trust. Each of you contributed to build the scientist I am today.

My time in Rennes would not have been the same without my lab mates. During these 3 years, I had the chance to meet people from different backgrounds. With them, I was able to travel from China to New Zealand, through the Mauritius Islands, Greece, Lebanon, Italy, India, Romania, Iran until reaching my final destination; Brittany.

When I first joined the lab, “the elders”, Dr. O. Santoro, Dr. T. Chavagnan, Dr. E. Le Coz, Dr. H. Roueindeji, were great sources of help and wisdom and I am deeply grateful for their kindness.

I had the pleasure to share an office for over two years with the funniest of all, Dr. X. Desert, who obviously should consider a comedian career, not to mention his crazy dancing skills! The future Dr. D. Theodosopoulou, the youngest of the EK team, have been refreshing to work with; stay as you are, optimistic and sweet. And thank you for introducing me to the delicious Greek olive oil :D. To Dr. J. Hammoud, the most enthusiastic, caring, joyful lebanese girl I have ever met. Thank you for always feeding me hummos whenever I craved some. To Dr. P. Chapple, the coolest and the most relaxed labmate I know, thank you for the discussions we had. Weither it was about food, drinks, sports or trips, I have always learned new stuff while talking to you. Can’t wait to visit New Zealand !

Dr. R. Shakaroun, *a.k.a* Ramaちゃん, my labmate and friend who had an incredibly positive influence on my time in the lab. You have been to me an inspiration through your hard work and perseverance. There are no words to properly describe the many lessons I learned from you. Wherever

will be, let us be strong and dreamy, shy and determined, let us be the best versions of ourselves... IN_P power!!

There have been many other postdocs, visiting students and undergrads that have influenced my time in the JFC lab: Dr. V. Hardouin-Duparc, Dr. S. Abouderhamine, Dr. R. Raghavendra, H. Li, L. Qu, Y. Nafeh and the future doctors W. Huang and V. Chugh (my fellow CO₂ partners!), V. Manayath, J. Savarithai, A. Dhaini – thank you all!

I also had the pleasure to interact with many other students from other teams. Dr. H. AlSabea, Shayma El Shahimi, Nour El Beyrouti, Marie Barale, Marie Peng, Nour, Zhuan, Amal Benzai, Arpan, Meriem, Fadwa, Delphine, Jennifer, Adrien, Idriss. I'm grateful for your comradery. A super special acknowledgement goes to Mr. J. Ollivier for the deep, long, philosophical and metaphysical discussions we shared, helping me escaping the lab for few moments.

I can only hope to have future coworkers as pleasant and easy to work with as you guys!

During my stay in Rennes, I have had the pleasure also to meet Dr. D. Müller and his lovely wife Agnès and kids. I am so happy to seeing you fulfilled in your chemist career that you deserve so much. Thank you for sharing with me your life and scientific experiences, which allowed me to become aware of many things. But most importantly, thanks for the homemade pizzas and the warm dinners after babysitting the kids :p !

I wouldn't forget to acknowledge Dr. M. Devillard, for whom I have the deepest respect and admiration. Not just one of the brightest chemists I've ever met, you're one of the most interesting person I've known, and probably will soon be the coolest Dad in the world ☺ Wish you and Dr. N. Del Rio the best for the future!

Dr. A. Zeineddine, my partner in crime for three years, thank you for being by my side. Your encouragements have always been a source of incredible energy and motivation. I am truly grateful for your support and kindness. In addition, sharing with you the same burning passion for food has been, and will always be, a real source of happiness (hahah, ouuuh poulet rôti à la broche au four avec des potatoes garliki, parmeggiani... la liste est longue :p)!

Far from the eyes but close to the heart, my bffs have always had my back! To my dear Zoé Koeller, stucked with me since 2011 (#galèredelaprèpa), thank you for the free psychological phone call sessions and for always caring about me! Meuf, I am so proud of both of us and for what we have accomplished! Love you habibti

Amandine Trottet, the beautiful, kind, sweet, smart chemist engineer and soon, Master of flowers, I am so happy to see our friendship grow in a very meaningful way, even far from each other.

To the future Dr. Gabriela del Carmen Espadas Aldana Adam (this is long haha), my irreplaceable, smart, irresistible Mexican sister, and her amazing parents (Jorge and Marta), thank you for always keeping an eye on me and for being part of my family. Os quiero mucho.

Sanouna (Dr. Rebbah), khti, el dem, you simply have always been there for me. I love you bb, and words cannot describe how much I do! Cannot wait to see what the future holds for us (zwedj? a3ardini balaki haha)!

Dr. Marion Duval, *a.k.a* kabukiii, my PhD, sushis, ice cream, travel, DALs partner... and so much more! Thank you for your authenticity and loyalty. The deep, meaningful connection our friendship has is a cherished treasure. Stay as amazing as you are bibu!

Thanks to this PhD, I also had the opportunity to discover the beauty of Brittany, through its beaches, its gastronomy (long live to the Kouign amann and les galettes sarazin!), its landscapes but also through its schizophrenic changes of weather (#crachinbreton)!

Without the support of my family, I would probably not have been able to get this far. To all the Soukeur-Mabrouki-Kunihiro, with a special mention to Mohieddine, Choab, Yacine, Mimi, Yemma, Nana, Mami and Jeddo, thank you for your affection and support, I hope I made you proud. Papa, Mama, Lyes, I am truly grateful for all the sacrifices you have done for me and for your encouragement throughout my studies (even though they were understanding nothing of what I was doing: “tu finis quand ton stage? Mama je suis en thèse...”). Thank you for your endless and unconditional love. Nhabkoum.

Foreword

The present manuscript includes two parts, each being divided into two chapters. The first Part describes the investigations conducted towards the search of new catalytic systems for the ethylene carboxylation reaction, starting from an exhaustive bibliographical study (Chapter 1), then followed by a high throughput experimental approach using hydrosilanes as reductant (Chapter 2). The second Part aims at optimizing the ruthenium-catalyzed coupling reaction of carbon dioxide, ethylene and triethylsilane toward silylesters, by improving the reactivity and selectivity of the system (Chapter 3) and elucidating the mechanisms at work through identification and isolation of the intermediates and active species (Chapter 4). These two parts are preceded by a General Introduction and followed by a General Conclusion, a summary of thesis in French, and an experimental part. The references numbered in Roman figures include the publications cited in this manuscript, relating to bibliographic references, located at the end of each chapter. Footnotes are given in alphabetical order, intended to clarify or supplement any comments written in the body text.

A folding A3 page, including the structures of the synthesized complexes as well as those of the organic products obtained in catalysis, can be found at the end of the manuscript (page 255) in order to facilitate and guide the reader throughout his reading.

Declaration of authorship

I, Kana Yasmine Kunihiro, hereby declare being the author of this thesis, and the work described therein was carried out by myself, with the following exceptions:

All X-ray measurements contained in this thesis, together with single-crystal structures solving and refinement, were carried out by one of the following: Dr. T. Roisnel or Dr. V. Dorcet of the Centre de DIFractométrie – UMR 6226, ISCR, Université de Rennes 1, France. Initial High Throughput Screening experiments were conducted at the Argonne National Laboratory and were carried out by Dr. E. Bunel, Chemical Sciences and Engineering Division, USA, group of Dr. T. Krause. Variable Temperature NMR experiments of **Ru-3** complex described in Chapter 3 were carried out by Dr. E. Caytan, CNRS – UMR 6226, ISCR, Université de Rennes 1, France. All Density Functional Theory (DFT) calculations contained within Chapter 4 were carried out by Dr. R. Thayalan under the direction of Prof. L. Maron, Laboratoire de Physique et Chimie des Nano-objets (LPCNO), INSA Toulouse, France.

Abstract

In recent decades, the use of CO₂ as a carbon source has gained considerable interest due to its non-toxicity and abundance. CO₂ represents an attractive renewable resource to decrease the massive consumption of fossil fuels as well as the environmental difficulties associated with their exploitation. More recently, the development of new strategies for carboxylic acids synthesis has emerged as these compounds are versatile starting materials for the fine chemical industry. However, due to the inherent stability of CO₂, the use of highly reactive and waste-generating substrates is often needed.

The present project finds interest in developing new systems for reductive carboxylation reactions, catalyzed by transition metals, allowing to avoid the use of polluting co-reactants. This work first focuses on the study of different catalytic systems activities, previously selected through a literature study. Using a high throughput screening approach, some promising systems for the reductive carboxylation reaction of C₂H₄, in the presence of the reducing agent Et₃SiH, have been identified and then optimized in terms of conversion and selectivity.

The second part of the manuscript aims at understanding the corresponding reaction mechanisms giving access to the targeted alkyl and alkenyl silyl esters. In particular, it describes the structural investigations carried out on the catalytic intermediate species generated in situ from ruthenium precursors and bidentate phosphine ligands. The knowledge acquired through experimental NMR studies, supplemented by DFT calculations, allowed to propose several reaction mechanisms potentially involved.

Keywords: CO₂ – C₂H₄ – carboxylation – ruthenium – phosphine – mechanism – silyl esters

Résumé

Au cours des dernières décennies, l'utilisation du CO₂ comme matière première carbonée a suscité un intérêt considérable de par sa non toxicité et son abondance. Le CO₂ représente une ressource renouvelable attrayante pour pallier à la consommation massive de ressources fossiles et aux difficultés environnementales liées à leur exploitation. Plus récemment, le développement de nouvelles stratégies de synthèse d'acides carboxyliques, molécules polyvalentes pour la chimie fine, ont vu le jour. Néanmoins, en raison de la stabilité inhérente du CO₂, l'utilisation de substrats hautement réactifs et générateurs de déchets est souvent nécessaire.

Le présent travail doctoral s'est intéressé au développement de nouveaux systèmes pour les réactions de carboxylation réductrice, catalysées par des métaux de transition, permettant de s'affranchir de co-réactifs polluants. Ces travaux de thèse s'intéressent d'abord à l'étude de l'activité de différents systèmes catalytiques, préalablement sélectionnés au travers d'une étude de la littérature existante. En utilisant une approche de criblage à haut débit, certains systèmes prometteurs pour la réaction de carboxylation réductrice du C₂H₄, en présence du réducteur Et₃SiH, ont été identifiés puis optimisés en termes de conversion et de sélectivité.

La seconde partie du manuscrit vise à la compréhension des mécanismes réactionnels donnant accès aux esters d'alkyle et d'alcényle silylés désirés. Elle décrit en particulier l'élucidation structurale des espèces catalytiques intermédiaires générées in situ à partir de précurseurs au ruthénium et de ligands phosphine bidentés. Les connaissances acquises à travers des études RMN expérimentales, complétées par des calculs DFT, ont permis de proposer plusieurs mécanismes réactionnels potentiellement mis en jeu.

Mots clés : CO₂ – C₂H₄ – carboxylation – ruthénium – phosphine – mécanisme – esters silyliques

List of abbreviations, chemical products, molecules and units

Acronymes		Chemical Products	
APPI	Atmospheric Pressure Photoionization Analysis	4CzIPN	1,2,3,5-tetrakis(carbazol-9-yl)-4,6-dicyanobenzene
BDE	Bond Dissociation Energy	9-BBN	9-Borabicyclo[3.3.1]nonane
C1	One-Carbon	$[(\text{CH}_3)_3\text{Si}]_4\text{Si}$	Tetrakis(trimethylsilyl)silane
CCS	Carbon Capture And Storage	$[\text{Rh}(\text{COD})\text{Cl}]_2$	Chloro(1,5-cyclooctadiene)rhodium(I) dimer
CCU	Carbon Capture And Utilisation	$[\text{Rh}(\text{coe})_2\text{Cl}]_2$	Chlorobis(cyclooctene)rhodium(I), dimer
COP 21	Climate Change Conference	(IPr)CuCl	Chloro[1,3-bis(2,6-diisopropylphenyl)imidazol-2-ylidene]copper(I)
DFT	Density Functional Theory	acac ⁻	acetylacetonate anion
DG	Directing Group	Ar	Argon
DRM	Dry Reforming Of Methane	BAr^{F_3}	tris[3,5-bis(trifluoromethyl)phenyl]borane
EOR	Enhanced Oil Recovery	BiPheEPhos	6,6'-[(3,3'-Di-tert-butyl-5,5'-dimethoxy-1,1'-biphenyl-2,2'-diyl)bis(oxy)]bis(dibenzo[d,f][1,3,2]dioxaphosphepin)
ESI	Electrospray Ionization	BiPheP	2,2'-Bis(diphenylphosphino)-1,1'-biphenyl
EXSY	Exchange Spectroscopy)	Cy	Cyclohexyl group
F-gases	Fluorinated Gases	DBU	1,8-Diazabicyclo[5.4.0]undec-7-ene
FID	Flame Ionization Detector	DCPB	1,4-Bis(dicyclohexylphosphino)butane
GC	Gas Chromatography	DCPE	1,2-Bis(dicyclohexylphosphino)ethane
GHG	Greenhouse Gases	DCPF	1,1'-Ferrocenediyl-bis(dicyclohexylphosphine)
HMBC	Heteronuclear Multiple Bond Correlation	DCPM	bis(dicyclohexylphosphino)methane
HMQC	Heteronuclear Multiple Quantum Coherence	DCPP	1,3-bis(dicyclohexylphosphino)propane
HOMO	Highest Occupied Molecular Orbital	DMF	N,N-Diméthylformamide
HSQC	Heteronuclear Single Quantum Correlation	DPPB	1,4-Bis(diphenylphosphino)butane
HTS	High Throughput Screening	DPPBz	1,2-Bis(diphenylphosphino)benzene
IEA	International Energy Agency	DPPF	1,1'-Ferrocenediyl-bis(diphenylphosphine)
IPCC	Intergovernmental Panel on Climate Change	Karstedt catalyst, 3wt% Pt in xylene	Platinum(0)-1,3-divinyl-1,1,3,3-tetramethyldisiloxane complex solution
LA	Lewis Acid		
LUMO	Lowest Unoccupied Molecular Orbital		
MO	Molecular Orbital		

MS	Mass Spectrometry	NiBr ₂ .glyme	(1,2-Dimethoxyethane)nickel dibromide
NEOSY	Nuclear Overhauser Effect Spectroscopy	Ni(cdt)	1 <i>E</i> ,5 <i>E</i> ,9 <i>E</i> -cyclododeca-1,5,9-triene;nickel
NHC	<i>N</i> -heterocyclic carbenes	NMP	1-Methyl-2-pyrrolidinone
NMR	Nuclear Magnetic Resonance	PCy ₃	Tricyclohexylphosphine
OA	Oxidative Addition	Pd/C	Palladium on carbon
PFCs	Perfluorocarbons	PMHS	Polymethylhydrosiloxane
R&D	Research & Development	PP ₃	Tris[2-(diphenylphosphino)ethyl]phosphine
r.t.	Room Temperature	PPh ₃	Triphenylphosphine
TON	Turn Over Number	<i>p</i> TSA·H ₂ O	<i>p</i> -Toluenesulfonic acid monohydrate
USD	US Dollar	TES	Tetraethylsilane
VT	Variable Temperature	TEVS	triethylvinylsilane
WGS	Water-Gas Shift	THF	Tetrahydrofurane
XRD	X-Ray Diffraction	TMEDA	Tetramethylethylenediamine
		TMSCHN ₂	Trimethylsilyldiazomethane
		Xantphos	4,5-Bis(diphenylphosphino)-9,9-dimethylxanthene
Units			
ΔG^\ddagger	Gibbs Enthalpy Of Activation		
ΔS	Entropy		
ΔH	Enthalpy		
°C	Celsius		
Å	Ångström		
bar	Metric Unit Of Pressure (= 100 000 Pa)		
CO ₂ -eq	Carbon Dioxide Equivalents		
D	Debye		
Gt	Billion Tonnes		
<i>J</i>	Coupling Constant (Hz)		
K	Kelvin		
Mt	Megaton		
δ	Chemical Shift (Ppm, NMR)		
ΔG_f°	Free Energy Formation		

General introduction

1. Context

After the industrial revolution, the increase in the world population and the intensive consumption of non-renewable fossil resources have led to a noticeable increase in the concentrations of heat-trapping pollutants in the atmosphere, specifically carbon dioxide (CO₂), methane (CH₄), nitrous oxide (N₂O) and, late on, synthetic fluorinated gases (F-gases).^[a] These excessive anthropogenic emissions of greenhouse gases (GHGs) (27 billion tonnes of CO₂-eq/year in 1970 vs. 49 billion tonnes of CO₂-eq/year in 2016)^{[1],[b]} have been responsible of a global annual increase of temperature by a little more than 1 degree Celsius.^[2] CO₂, which represents 74% of total mankind emissions,^[c] is considered as the largest contributor to global warming, which levels are higher now than at any time in the last 800,000 years.^[1] As a consequence, glaciers are melting, sea levels are rising, forests are burning, and wildlife is scrambling to keep pace (extinction of many plant and animal species). Decreasing CO₂ emissions is therefore a key issue and has become an area of active scientific study and political concern. In December 2015, at the United Nations Climate Change Conference (COP 21) held in Paris, policy makers agreed on the ambition to keep the temperature increase below 2 °C aiming for 1.5 °C. While searching for solutions to quantitatively reduce CO₂ emissions of the fossil-based energy system, a perspective of circular economy appears to be economically and ecologically attractive, by capturing and reusing waste stream CO₂. Such alternative feedstock comes into view to open new doors for a new carbon source.

This introduction provides a brief history on the discovery and uses of CO₂, its different emission sources and consumption sinks, as well as a description of its accumulation impacts in the atmosphere. With the aim of decreasing its unbalanced emissions, different technologies and utilisations of CO₂ have therefore emerged, among which, chemical valorisation have found some industrial applications.

^[a] The targets for the first commitment period of the Kyoto Protocol cover emissions of the six main greenhouse gases, namely: CO₂; CH₄; N₂O; Hydrofluorocarbons (HFCs); Perfluorocarbons (PFCs) and Sulphur hexafluoride (SF₆).

^[b] A carbon dioxide equivalent or CO₂ equivalent, abbreviated as CO₂-eq is a metric measure used to compare the emissions from various greenhouse gases on the basis of their global-warming potential (GWP), by converting amounts of other gases to the equivalent amount of CO₂ with the same global warming potential.

^[c] CH₄, 17.3%; N₂O, 6.2%; and other emissions (HFCs, CFCs, SF₆), 2.1%

Yet, none of these chemical utilizations of CO₂ is able to replace CO₂ storage as an efficient tool for reducing anthropogenic emissions and limiting climate change.

Since CO₂ activation represents a thermodynamic and kinetic challenge, utilisation of appropriate energy sources and catalysts is mandatory, while maintaining the lowest possible carbon footprint.

The purpose of the present thesis is to understand and rationalize, based on the current knowledge in the field and original works I carried out, the metal-catalysed transformation of CO₂ into the simplest value added acrylic and propionic acids, using ethylene as a coupling partner.

2. History of carbon dioxide: from its discovery to its first uses

The existence of CO₂ has been known since ancient times, back when myths were created around certain places due to the bubbling of “living” water coming from the ground.^[3] These bubbles of CO₂ in water create carbonic acid, which dissolves some mineral salts from bedrock, creating mineral water with its typical salty and sour taste. Long considered having “healing powers”, mineral water’s composition was not investigated until the 16th century. Van Helmont firstly recognized that CO₂ is a distinct gas, by preparing it by various other routes (burning charcoal or slaking lime with an acid) and demonstrating that it was the same gas issued from mineral water. Investigations around CO₂ started in 1757 when Black discovered the lethal effect of such gas on animal life. In 1782, the French chemist Lavoisier was then the first at proving the composition of CO₂: a combination of oxygen and carbon named “*gaz acide carbonique*”. The first exploitation of CO₂ began with attempts to produce artificial mineral water (CO₂ in H₂O) as a medicine.

The industrial utilization of CO₂ really started at the beginning of the 19th century, with Faraday's successful experiments on its liquefaction. Based on his finding, Thilorier and co-workers carried out extensive experiments on the expansion, vapor pressure, density, and enthalpy changes of liquid CO₂ during evaporation, costing them a spectacular explosion and the life of one of their colleagues. As larger quantities of liquid CO₂ were possible to produce, thanks to the development of new compressors, the first factory dedicated to liquid CO₂ was established by Raydt in Germany in 1884. Exported then to the United States, the giant Praxair was born, becoming one of the world market leader distributor of industrial liquid and

compressed CO₂. In 1924, the first solid CO₂ production plant opened in Canada, mainly used for the distribution and preservation of food items.

More industrial applications were then found, in particular in ice-making, carbonation of beverages, refrigeration, fire extinguisher or, more recently, incorporated into processes, such as Enhanced Oil Recovery (EOR, see section 5.5.1.).

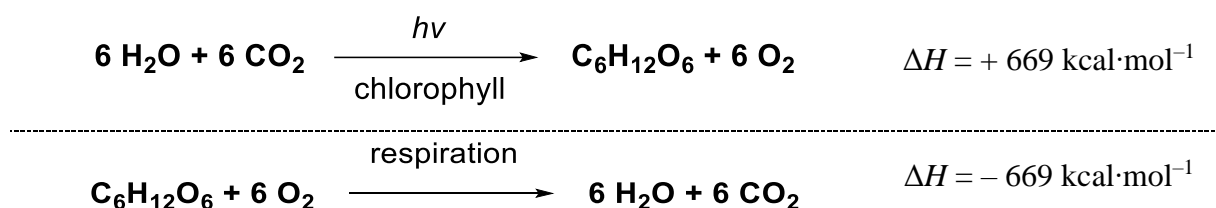
3. Sources of CO₂

3.1. Occurrence of CO₂ in nature

CO₂ is naturally present in earth's lithosphere, hydrosphere and atmosphere. Its amount is maintained through a balance between natural processes by which it is produced and used up.

The part of the earth not covered by the oceans is called lithosphere, where an estimated 5.5×10^{16} tons of CO₂ are present in the form of calcium carbonate (chalk), dolomite (CaMg(CO₃)₂), and other metal carbonates. Rocks containing carbonates easily emit, when heated strongly under vacuum, a mixture of gases mainly constituted of CO₂, H₂O, and H₂. Therefore, at volcanoes and eruptive vents, gases are constantly escaping as a result of the action of heat on earth's crust rocks. In addition, CO₂ also escapes from earth natural sparkling water sources.^[4] On the other hand, the hydrosphere, including the oceans, seas, lakes, streams, and other water sources, can hold an average of five volumes of CO₂ per ten thousand volumes of water (about 1.4×10^{14} tons of CO₂). In seawater, CO₂ exists as carbonates, hydrogenocarbonates, carbonic acid, and as the dissolved gas itself.^[4] Depending on the temperature of water, a dynamic equilibrium exists whereby the colder parts of the ocean absorb CO₂ and the warmer parts expel it into the atmosphere.

CO₂ is therefore naturally released from volcanoes, wells, gaseous water sources, combustion of carbonate materials and decomposition of organic materials. CO₂ is also exchanged between the atmosphere and the land-based biosphere. The plant world absorbs CO₂ from the atmosphere by the leaves to generate energy through photosynthesis, which is the reaction that converts CO₂, H₂O and energy from sunlight into glucose.



Plants subsequently convert glucose into sugar and starch. Organisms depending on vegetation for food transform these carbohydrates through respiration process. A series of biochemical reactions decomposes the stored energy into H₂O and CO₂.

During Earth's glacial–interglacial cycles over the past 2 million years, the climates have never been identical, according to the scientific and historical evidences^[d] furnished by the IPCC and the NASA (Figure 1).^[1,2,5,6] Atmospheric concentration of CO₂ have faced large variations, oscillating between 180 and 300 ppm, but remained stable at around 280 ppm. From the beginning of the 19th century, atmospheric CO₂ has slowly increased, betraying an imbalance in the carbon cycle.

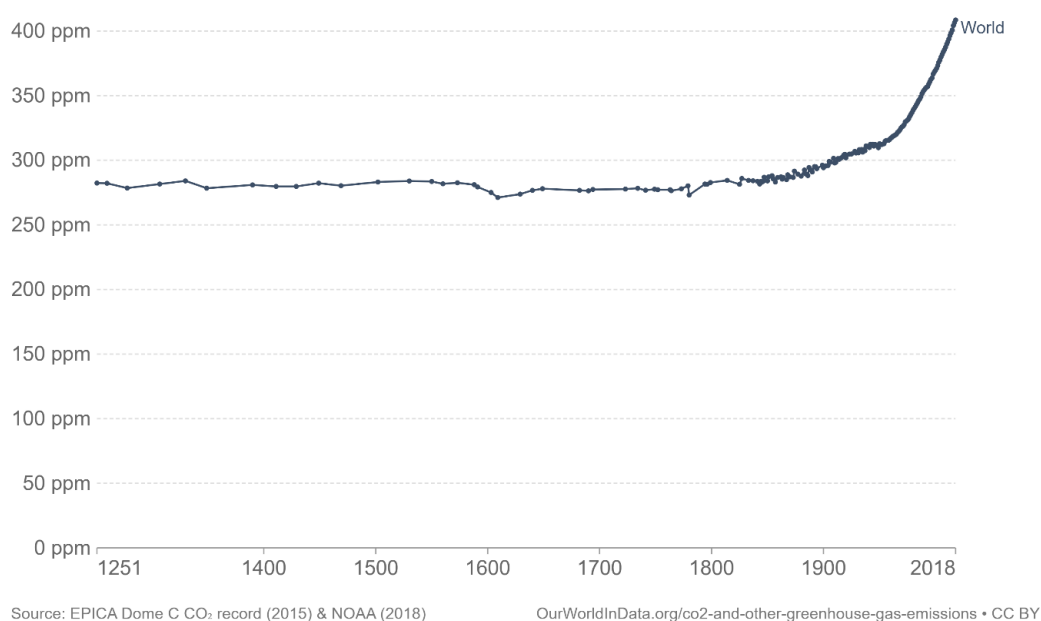


Figure 1. Global average long-term atmospheric concentrations of CO₂, measured in parts per million (ppm). Long-term trends in CO₂ concentrations can be measured at high-resolution using preserved air samples from ice cores.^[1]

3.2. Anthropogenic CO₂ emissions

Today, CO₂ concentrations in the atmosphere raised up to 0.041%,^[e] making it the fourth most abundant gas after N₂ (78.08%), O₂ (20.95 %) and Ar (0.93%).^[7] Obviously, to the natural CO₂ variations, those related to human activity must be added. In fact, from the pre-industrial times to the present day, the carbon cycle was abruptly disrupted due to the massive

^[d] Intergovernmental Panel on Climate Change (IPCC) and the National Aeronautics and Space Administration (NASA).

^[e] One ppm of CO₂ represents one molecule of CO₂ in a million molecules of air, i.e. 0.0001%. 278 ppm therefore represents 0.0278% or approximately 0.03%.

increase of all GHGs, especially CO₂, reaching 419 ppm in 2021.^[8] Anthropogenic activities emit around 50 billion tonnes (Gt)^[f] of GHGs each year (measured in carbon dioxide equivalents (CO₂-eq)). From the diagram shown in Figure 2, almost three-quarters of emissions come from energy use; 18% from agriculture and land-use; and the remaining 8% from industry and waste.^[5]

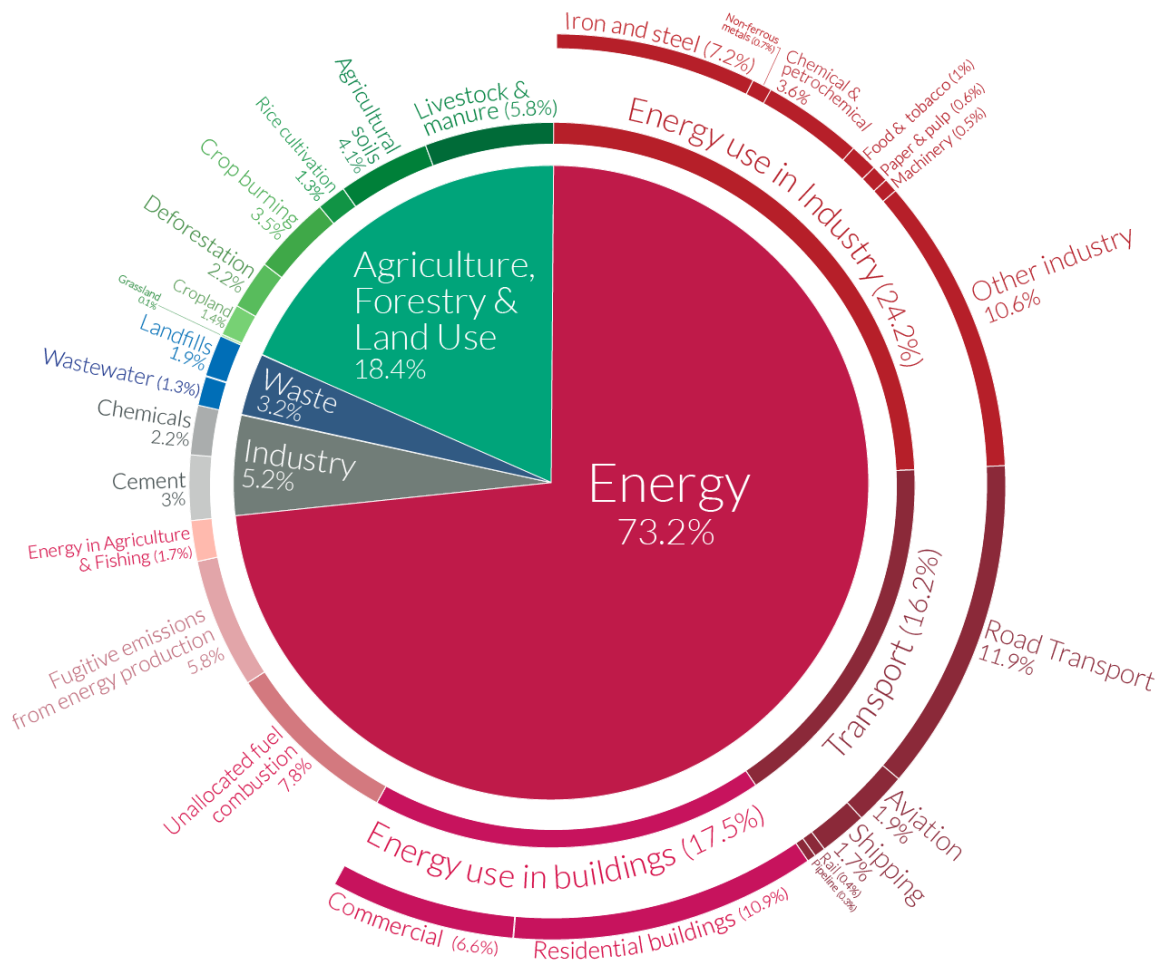


Figure 2. Global greenhouse gas emissions by sector shown for the year 2016. Global GHGs emissions were 49.4 GtCO₂-eq.^[1]

What is the fate of these CO₂ emissions once emitted into the atmosphere? A schematic representation of the overall perturbation of the global CO₂ cycle caused by anthropogenic activities, averaged globally for the decade 2010–2019, is given in Figure 3. Over this period, emissions from the combustion of coal, oil and gas were estimated to 34 GtCO₂ a year, to which must be added 6 GtCO₂ due to deforestation and land uses. The oceans and the terrestrial biosphere can absorb only half of the CO₂ emitted currently in the atmosphere each year (9 and 13 GtCO₂ respectively), leaving an abnormal positive carbon balance of 19 GtCO₂ on Earth.^[9]

^[f] One megaton (1 Mt) is worth one million (10⁶) tons, or 10⁹ kg. One gigaton (1 Gt) is worth one billion (10⁹) tons, or 10¹² kg.

General introduction

This accumulation, which remains for many thousands of years in the atmosphere, is sufficient to create an imbalance, thus causing global warming. In fact, since 1906, these changes in the carbon cycle have led to an increase in the global average surface temperature by a little more than 1 degree Celsius.^[2] As a matter of fact, CO₂ is considered to be the most important gas for controlling Earth's temperature, mainly through its infrared active molecular vibrations.

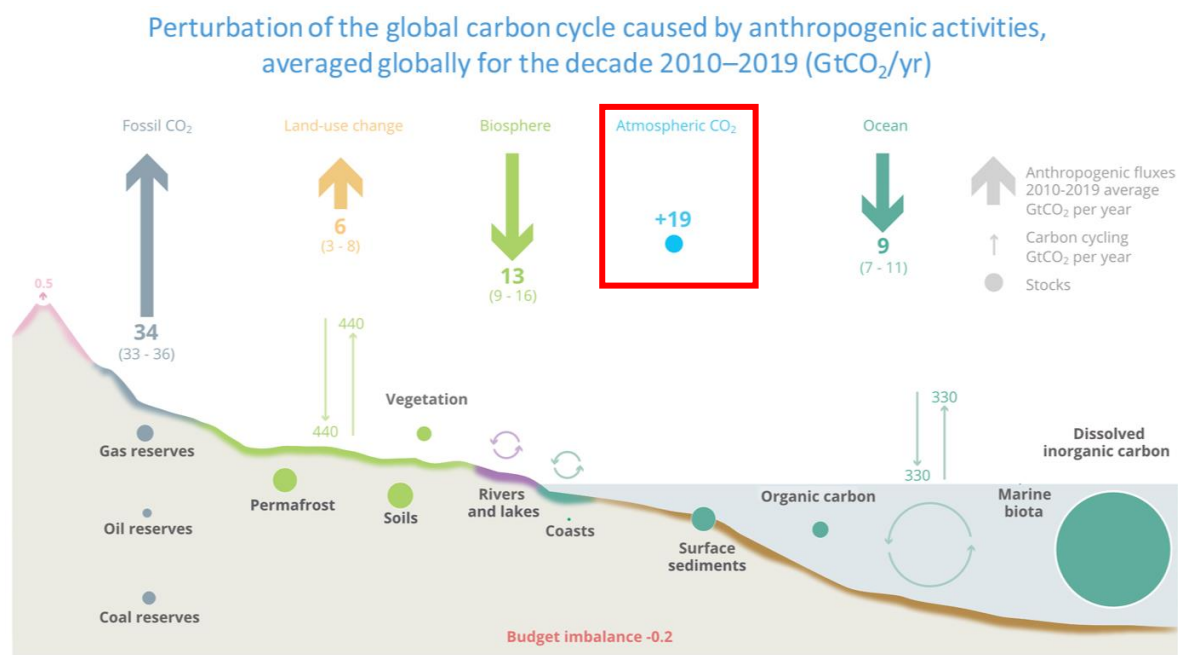


Figure 3. Schematic representation of the overall perturbation of the global CO₂ cycle caused by anthropogenic activities, averaged globally for the decade 2010–2019. See legends for the corresponding arrows and units.^[9,10]

Considering the severe effects of global warming, various energy sources have been proposed to replace traditional fossil fuels and reduce CO₂ emissions into the atmosphere. For example, to achieve close-to-zero greenhouse gas emissions power stations, there is a long-term need to make more active use of solar energy, hydroelectricity, biomass, biofuel, wind power, geothermal, wave power, tidal power etc. Adopting renewable energy resources and designing better conversion systems without negative impacts on the environment are very complex tasks, but at the same time very exciting. However, global energy demands are so high that it is impossible to substitute fossil fuels in the short term. In order to minimizing CO₂ anthropogenic emissions different strategies have been proposed (Figure 4). Considering these premises, the most mature strategies are focused on the design of more efficient processes to minimize CO₂ emissions and on its sequestration. **CO₂ subsequent valorisation and transformation into value added chemicals can provide climate benefits only if the application is scalable, uses low-carbon energy, and displaces a product that ultimately releases CO₂ into the**

atmosphere, such as fuels and chemicals, with products that involve permanent carbon retention and offer larger emissions reductions.^[11]

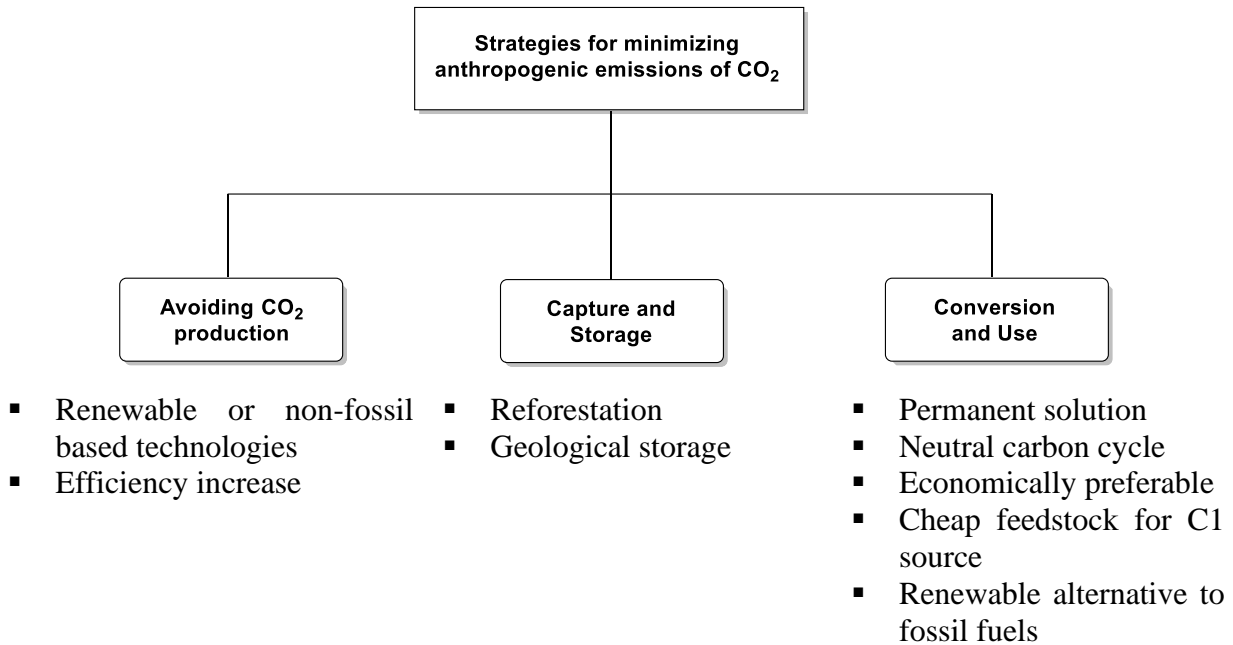


Figure 4. Strategies for minimizing CO₂ emissions.^[11]

4. Technologies for CO₂ reduction

One way to achieve climate neutrality in the energy sector is to separate the CO₂ of the power plant before its emission into the atmosphere. However, because there was no incentive or requirement to store it, CO₂ has been captured from industrial process streams and released into the atmosphere for almost 80 years.

4.1. CO₂ capture

Nowadays, there are three main technologically feasible approaches to capture CO₂ from the combustion of fossil fuels: post-combustion, pre-combustion and oxy-fuel combustion captures (Figure 5).

Post-combustion CO₂ capture is well known from the 70s as a potential economic source of CO₂ (for enhanced oil recovery (EOR) operations, see section 5.5.1).^[12] In this approach, instead of being discharged directly to the atmosphere, the CO₂ produced from flue gases by combustion of fossil fuels and biomass is captured. The flue gas is next passed through equipment which separates most of the CO₂. However, the key drawbacks hindering the large-scale implementation of this technology remains in separating the relatively low concentration

of CO₂ from the large amounts of N₂ in the flue gas (~ 4% CO₂ by volume from natural gas plants and 12-15% from coal plants). In addition, high energy inputs related to CO₂ desorption process and separation from zero heavy metal pollutants are needed.^[13] There are several technologies available for post-combustion capture, which can be achieved by several physical and chemical separation methods, such as absorption, membranes, adsorption and cryogenic processes.^[12] Nowadays, the most efficient and closest to market technology is based mainly on CO₂ absorption using amines. Amine solvents are well-suited for capturing CO₂ from dilute, low pressure streams, reacting reversibly with CO₂ and forming water-soluble salts.^[14]

In pre-combustion capture, CO₂ separation occurs prior to fuel combustion and power generation (Figure 5). Fuel reacts with O₂ or air and steam at high temperatures and pressures to give mainly a gas stream mixture primarily composed of CO and H₂, also known as syngas. CO is then converted through water-gas shift (WGS) reaction, to give high pressure CO₂ and higher amounts of H₂. By using a physical or chemical absorption process, CO₂ is separated, resulting in a H₂-rich fuel, which can be used in many applications (boilers, furnaces, gas turbines). The advantages of this route are the elevated pressures (15–40 bar) and the medium CO₂ fraction of 15–40% v/v, which offer ideal conditions for an energy efficient CO₂ separation.^[13] While the capital cost of capture equipment is not insignificant, the major goal in R&D for CO₂ capture prior to combustion designs is to reduce the energy penalties.

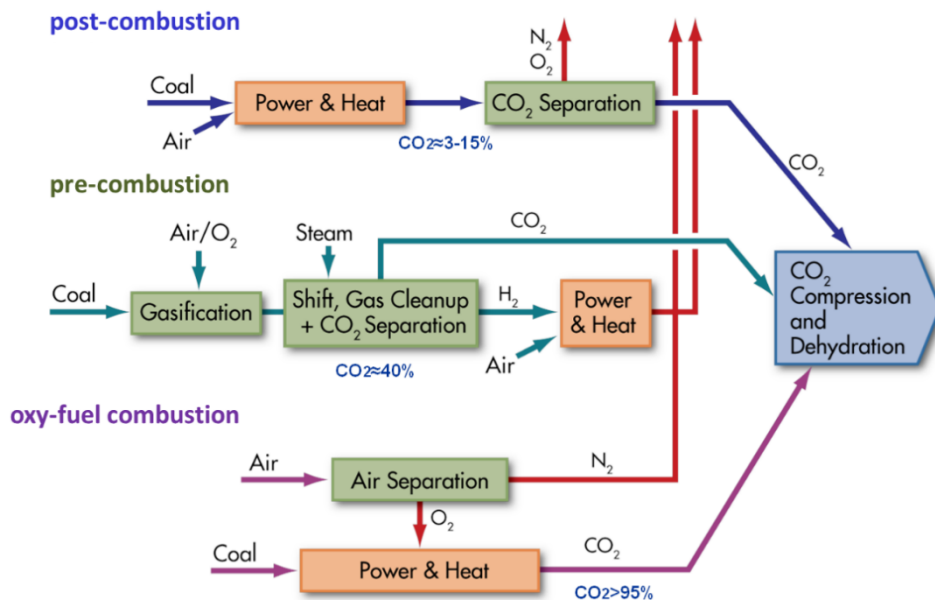


Figure 5. Summary of CO₂ capture technologies.^[13]

Oxy-combustion process (or oxy-fuel capture) is considered as one of the most attractive and simple CO₂ capture technologies that would be economically viable in fossil-fuel power

plants and industrial facilities.^[13] The fuel is burned using high purity O₂ as oxidiser, separated from air, producing a flue gas which is predominantly nearly pure CO₂ and H₂O.^[15] Water can be easily removed by condensation, producing a highly CO₂ concentrated flue gas (70 to 95% v/v) compared to air-fired combustion. However, the capital cost, energy consumption, and operational challenges of O₂ separation from air are the primary challenge of cost-competitive oxy-combustion systems.^[15]

4.2. CO₂, an industrial by-product

The CO₂ used today is predominantly sourced from industrial processes that produce high purity CO₂ as a by-product, such as ammonia production and biomass fermentation, or extracted from natural underground CO₂ deposits.

4.2.1. From ammonia plants

The Haber-Bosch process, which converts hydrogen and nitrogen to ammonia, is one of the most important industrial chemical reactions ever developed.^[16] The process made ammonia-based fertilizers widely available, with a production of 157.3 Mt in 2010, according to the Institute for Industrial Productivity's Industrial Efficiency Technology database.^[17] About 50% of the world's food production relies on ammonia fertilizers. Therefore, with ammonia being the second most produced chemical worldwide, its production accounts for approximately 2% of worldwide fossil energy use and generates over 420 Mt of CO₂ annually.^[18] The process for the production of ammonia is shown in Figure 6.^[4] The first step consists in the desulfurization of the hydrocarbon feedstock (e.g., natural gas). Next, by adding water vapour, followed by air, the catalytic steam reforming of the hydrocarbons transforms CH₄ into a gaseous mixture of H₂, CO₂, and CO. Catalysed WGS reaction converts then CO into H₂ and CO₂, which the latter is removed by absorption into a solution containing alkali metal carbonates and ethanolamine, under pressure. Then, the absorbed CO₂ is liberated in a separate vessel by raising/lowering the temperature/pressure. While most of the CO₂ generated during ammonia production is used in onsite-urea manufacturing, some of the CO₂ is released into the atmosphere or sold for the CO₂ market, especially when more ammonia (and thus CO₂) is produced than is needed for urea manufacturing.

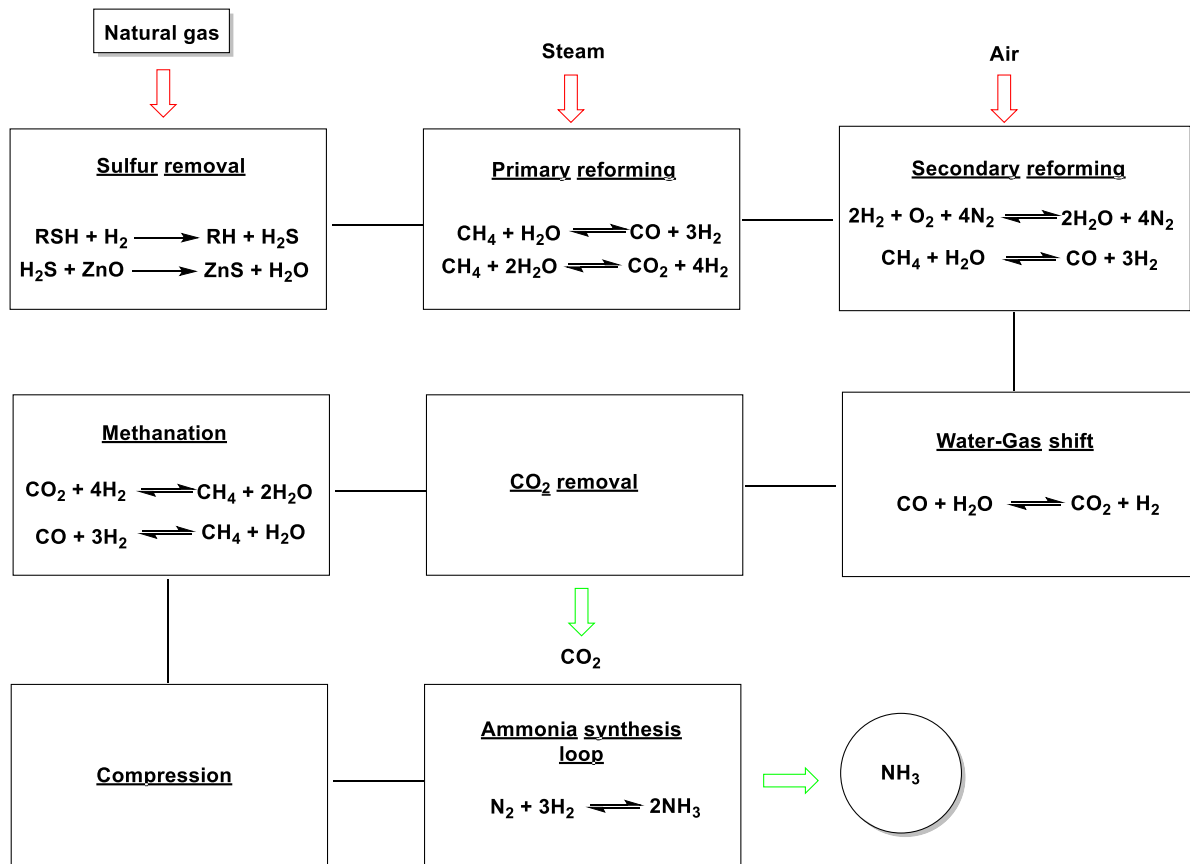


Figure 6. Schematic representation of an ammonia plant.^[4]

4.2.2. From flue gases

Since the industrial revolution, annual CO₂ emissions from fuel combustion have dramatically increased from near zero to over 33 GtCO₂ in 2015.^[19] In conventional fossil fuel power plants, CO₂ is produced by the complete combustion of carbon based fuels, such as coal or natural gas, to generate heat energy, which is converted to electricity. CO₂ concentration in the flue gas from a combustion process varies from 4 to 14% in natural gas and coal-power plants, while other industries such as cement, iron and steel and petrochemical industries produce flue gas ranging between 14 and 33%.^[13] Unlike CO₂ from ammonia plant, the product obtained from flue gases is generally contaminated by large amounts of dust, O₂, SO_x, NO_x and trace pollutants such as Hg.^[13,20]

High-concentration/high-partial-pressure sources (e.g., from ammonia/hydrogen production and gas processing operations) could represent early prospects for the implementation of CO₂ capture and storage. If these sources can then be linked to enhanced production schemes in the vicinity, they could be low-cost options for CO₂ capture and storage.

4.3. Carbon capture and storage (CCS)

Carbon capture and storage (CCS) has become a topic of debate among scientific community and questions are raised on its feasibility and its long-term consequences.^[11] It consists on tackling climate change by capturing the CO₂ generated by large point sources before its release into the atmosphere, transporting it usually by pipeline and injecting it into suitable deep rock formations or releasing it in the ocean or on the sea floor.^[21] CO₂ can be primarily available in thermal power generation, including fossil fuels, biomass, municipal waste and other waste to energy plants, and captured after the combustion process (Post-Combustion Capture, see above). The technology that demonstrated the best results to absorb CO₂ is the one using amines. However, drawbacks were observed related to the high corrosivity and the costs required for the regeneration of the amines.^[12] Moreover, additional requirement such as transport, injection and storage of CO₂ have to be taken into account.^[22] Ideally, to make a significant contribution to the mitigation of climate change, CO₂ storage will need to be done in quantities of GtCO₂/year. In addition, significant uncertainties are remaining, which will need to be addressed to provide sufficient confidence and safety over the long-term geological and ocean storage.

4.4. Price and availability of CO₂

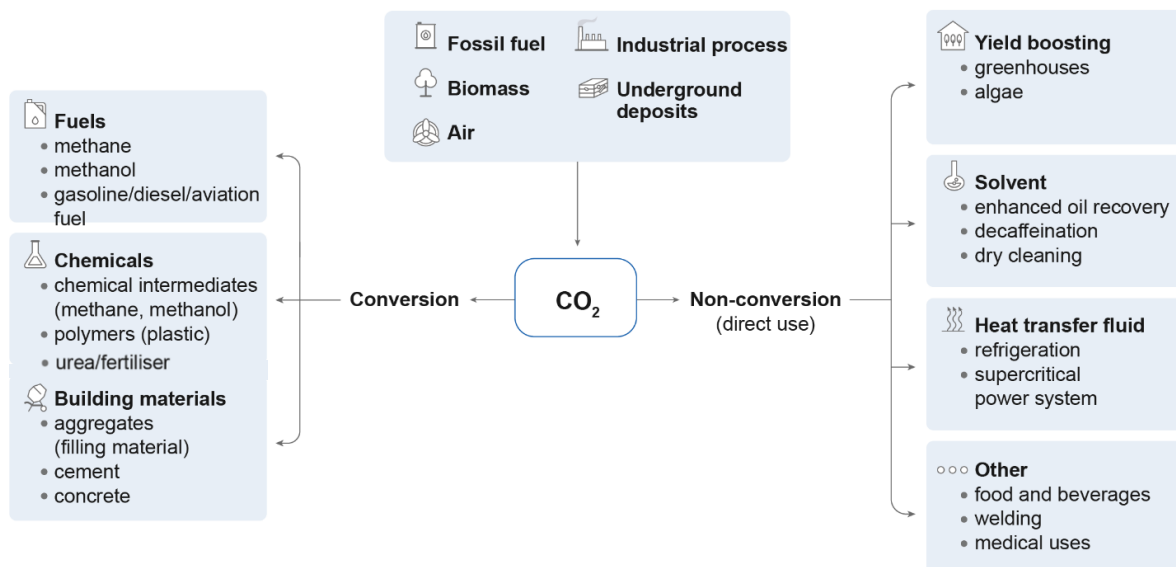
As noted above, the costs of CO₂ capture and purification vary greatly by point source. Natural wells are an important and cheap source of pure CO₂ (> 99%, 15–20 €/tCO₂ in 2010).^[23] Prices of CO₂ issued from industrial processes vary in a range of 15–20 €/tCO₂ for producing “pure” or highly concentrated CO₂ streams (such as ethanol production or natural gas processing) to 35–100 €/tCO₂ for processes with “dilute” gas streams (such as cement production and power generation).^[24] Capturing CO₂ directly from the air remain the most expensive method, with costs reported in academic literature ranging from roughly 94 to 232 USD/tCO₂, as it implies a much greater energy input than CO₂ capture from concentrated point sources.^[25]

The price of CO₂ is not only affected by the cost of its capture and transport, but also by local market conditions and climate policies. In Europe, the price of carbon has been rising sharply from 8€/tCO₂ in 2018 to around 52€/tCO₂ in 2021. It is mainly due to the CO₂ emissions trading system set up by the European Union in 2005. This decision follows on the Kyoto Protocol commitments aimed at reducing GHGs emissions.^[26,27] The authorities set a market mechanism known as carbon pricing, which covers a part of a country’s total emissions by charging CO₂ emitters for each ton released through a tax or a fee. In a cap-and-trade system of

carbon pricing, the government sets a cap on the total amount of emissions allowed, and CO₂ emitters are either given permits (or allowances) or must buy the right to emit CO₂. Companies whose total emissions fall under the cap may choose to sell their unused emissions credits to those who surpass its carbon allotment. Until 2012, almost all allowances were allocated free of charge. However, in recent years, more than half of the allowances were sold to companies, consequently rising CO₂ prices.

4.5. Carbon Capture and Utilisation (CCU)

A potential complementary alternative to CCS would be Carbon Capture and Utilisation (CCU), which explores the use of CO₂ in applications other than storage. This process can be classified into two ways; direct use processes (non-conversion) and conversion processes (Figure 7).



IEA 2019. All rights reserved.

Figure 7. Simple classification of CO₂ use pathways.^[25]

Once captured, CO₂ can be valorised through a physical or chemical utilization to form valuable products. It finds applications in food and beverage production, metal fabrication, cooling, fire extinguishers as well as other uses. Globally, some 230 Mt of CO₂ are used every year, with the largest consumer being the fertiliser industry, where 130 Mt CO₂ is used in urea manufacturing, followed by oil and gas, with a consumption of 70 to 80 Mt CO₂ for enhanced oil recovery (EOR).^[25]

4.5.1. Enhanced oil recovery (EOR)

The oil industry is the largest consumer of externally sourced CO₂, by injecting it into the subsurface to boost oil recovery.^[28] Oil field development is generally carried out in two or three recovery stages. During the primary stage, oil is produced by natural drive mechanisms (dissolved gas expansion, gas cap expansion, saline water influx).^[29] As the fluids are being extracted, the reservoir pressure decreases, and so do oil production rates. In order to maximize the duration of the primary production, pressure maintenance and fluid lifting techniques are employed. Hence, the secondary recovery injects most commonly water (waterflooding), not only to maintain reservoir pressure, but also to displace oil toward producing wells. At this stage, an average of only 30–50% of oil is recovered, the rest remaining in the reservoir. Enhanced oil recovery (EOR), often considered as a tertiary recovery phase, is a process recovering the oil by the injection of a material that is not originally present in the reservoir (Figure 8).^[29] In the case of CO₂-EOR, CO₂ is the injected material, which can help increasing the overall pressure within the reservoir, forcing the oil towards production wells. In addition, CO₂ can dissolve in the oil to lower its viscosity and improves its flow rate. First tried in 1972 in Scurry County, CO₂ injection has been used successfully throughout the Permian Basin of West Texas and eastern New Mexico.^[30] The International Energy Agency's (IEA) database shows that, globally, around 500,000 barrels of oil are produced daily using CO₂-EOR processes, representing around 20% of total oil production from EOR.^[31] Ironically, most of the CO₂ used for EOR comes from naturally-occurring reservoirs. For example, in the United States, less than 30% of the near 70 Mt CO₂ injected each year for CO₂-EOR is captured from anthropogenic sources. In order to be considered for its climate mitigation value, new transport infrastructures are needed, together with low-cost and reliable CO₂ sources in close proximity to oil fields.

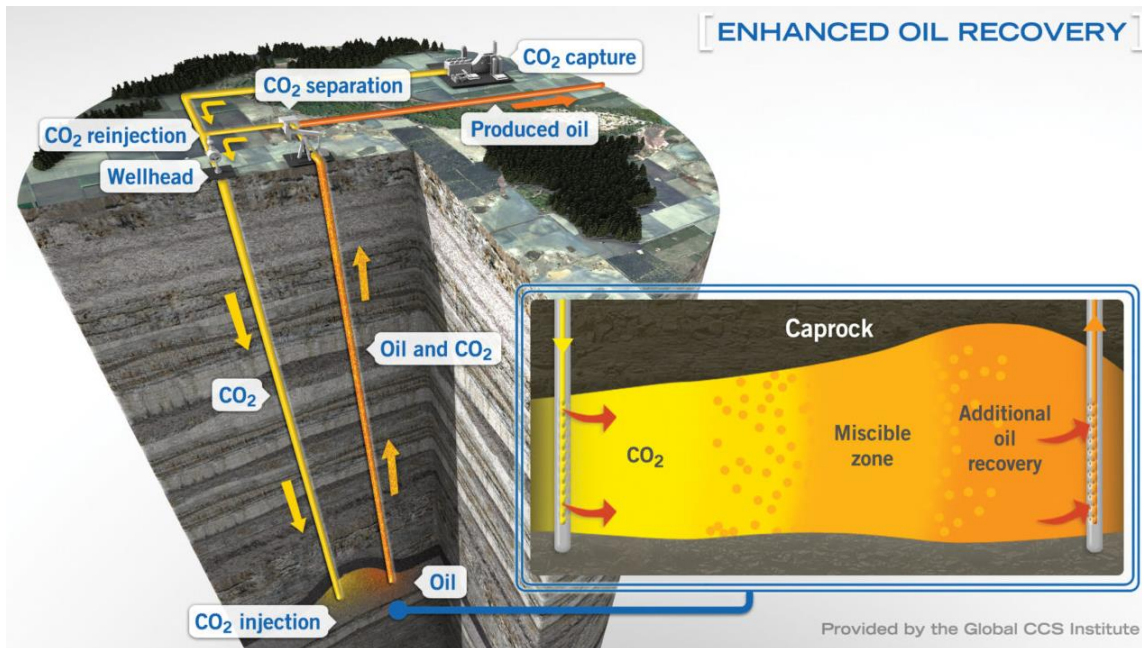


Figure 8. Schematic CO₂-EOR operation.^[32]

Because of the many sectors and processes contributing to global emissions, a single or simple solution to tackle climate change does not exist. For example, focusing only on the energy sector would imply a fully decarbonized electricity supply, suggesting electrifying all of the heating and road transport. More challenging, emissions from shipping and aviation will still have to be tackled, for which low-carbon technologies do not exist yet. Hence dealing independently with energy or transport or deforestation alone is insufficient. To reach net-zero emissions, innovations across many sectors are needed.

5. Chemical valorization of CO₂

CO₂ is a nontoxic, economic and vastly abundant C1 resource that can be used to produce value-added chemicals/fuels and materials. The biggest challenge in chemical utilization of CO₂ is, however, its high thermodynamic barrier as it is almost inert (free energy formation of CO₂ $\Delta G_f^\circ = -393.52$ kJ/mol).^[33] Therefore, most reactions of conversions of CO₂ are endothermic and require substantial amounts of energy whereas others have a high kinetic barrier and need efficient catalysts to promote the reaction.^[4] In addition to heterogeneous and homogeneous catalysis, thermal, photochemical, and electrochemical conversions of CO₂ have been explored.

Two main approaches to convert CO₂ into fine chemicals can be considered. The first one is the reductive conversion of CO₂ to produce, for example, chemicals such as methanol or

formic acid (referred to as “vertical reduction” by Cantat and co-workers, Figure 9).^[34] This methodology requires a large amount of energy and quite powerful reducing agents (e.g. H₂). The other one is non-reductive (the +IV oxidation state of the carbon is maintained) and widely used to produce urea, carbonates, polycarbonates, polyurethanes, carboxylates, lactones or carbamates (“horizontal utilization”, Figure 9). Despite playing an important role in the present and future fuels economy, these chemicals do not cover the whole feedstock necessary for fine chemicals synthesis.^[23] To enlarge the range of compounds directly available from CO₂, novel methods aiming at combining both reduction of CO₂ and formation of C–C, C–N and C–O bonds need to be developed (diagonal transformations, Figure 9). Traditionally, to access these chemicals, petrochemicals (hydrocarbons) are extensively used as fuels and basic reagents as they can be easily derivatized. To compete with petrochemistry, the ideal diagonal transformations, in which the oxidation state of the CO₂ carbon atom varies from +III (for carboxylic acids) to –II (for ethers), should ensure energy economy and a positive carbon balance. Yet, viable examples remain scarce and to date, only a handful processes utilizing CO₂ have been industrialized.^[35]

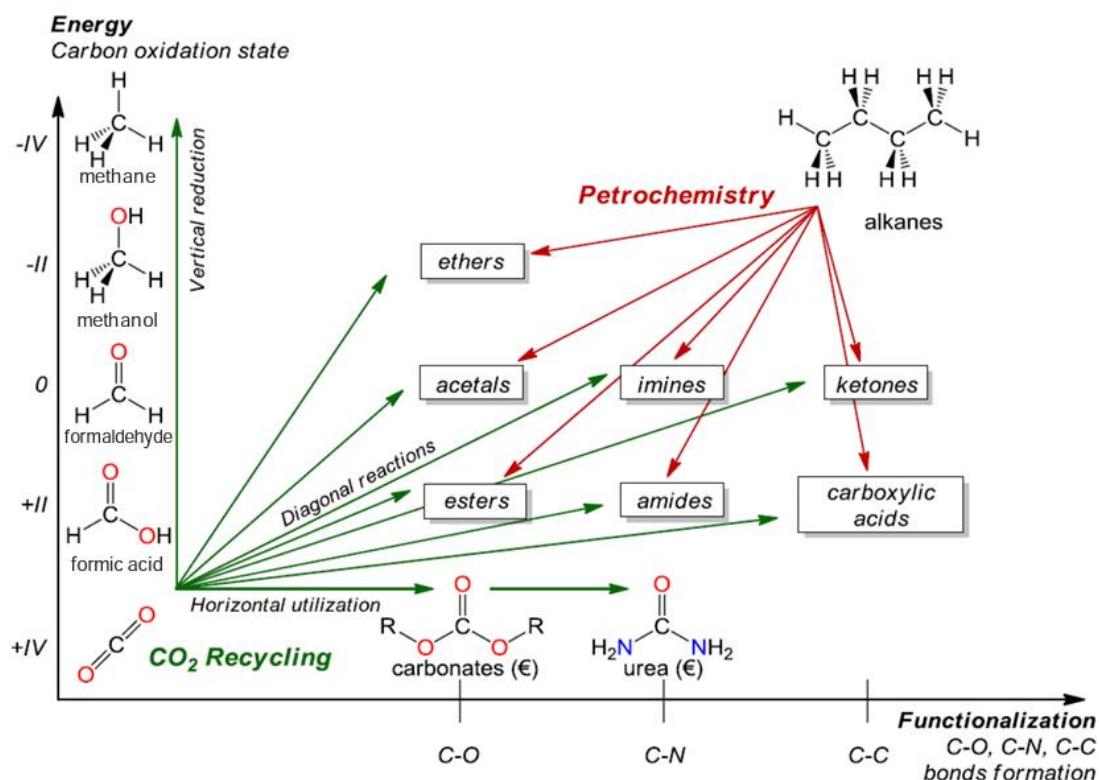
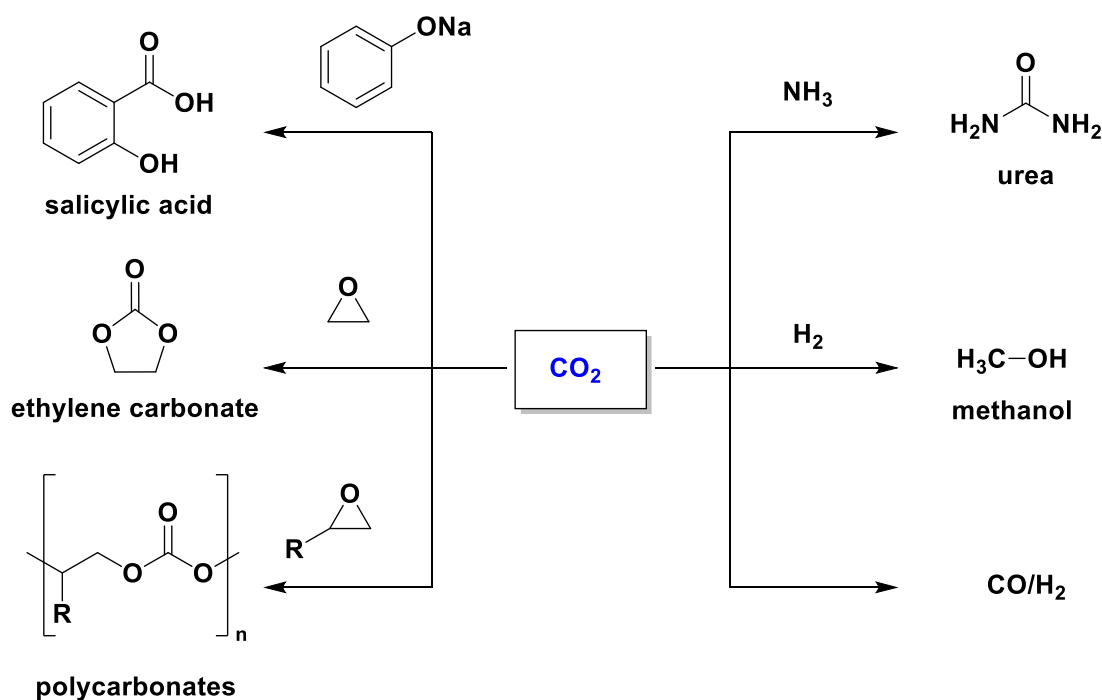


Figure 9. Approaches to recycling transformations of CO₂ as alternatives to petrochemical methods, as depicted by Cantat *et al.*^[36]

Today, the main chemical products obtained at the industrial scale using CO₂ as a raw material are urea, methanol, methane, salicylic acid, organic and inorganic carbonates,

polymers (Scheme 1). Among them, the synthesis of urea (130 Mt/year) and methanol (2.7 Mt/year) are the predominant consumers of CO₂ (pure or derived from CO by the Water Gas Shift reaction (WGS)).



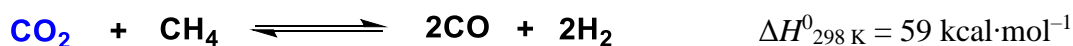
Scheme 1. Industrialized chemical transformations of CO₂ into commodity chemicals.

5.1. Urea production

By far, the largest application using CO₂ is urea production, mostly used as an agricultural fertiliser. The industrial synthesis of urea (NH₂)₂CO is based on the reaction of NH₃ (which is generated by the Haber–Bosch process; $3\text{H}_2 + \text{N}_2 \rightarrow 2\text{NH}_3$) with CO₂ by dehydration of intermediate ammonium carbamate. Urea plants are connected to ammonia synthesizing plants, where relatively pure CO₂ is available from the steam reforming process.

5.2. Dry-reforming

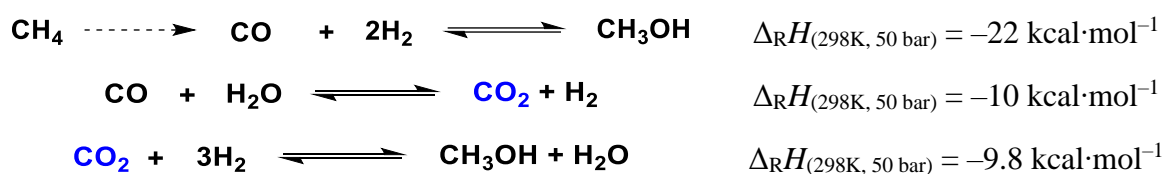
Syngas can be produced by reacting CO₂ through dry-reforming (DRM) of CH₄, which is the major constituent of natural gas (Scheme 2). DRM is a strongly endothermic reaction, requiring temperatures of 750 °C and the use of heterogeneous catalysts. Since CH₄ is derived from landfills or fossil resources, high amounts of impurities, such as sulfur gases, cause catalyst poisoning and deactivation.



Scheme 2. Dry reforming of Methane (DRM) with CO₂ to form synthesis gas.

5.3. Methanol production

With a current global demand of around 98 Mt in 2021, methanol is one of the most important bulk chemicals for the industry.^[25,37] Today's most important applications of methanol are the production of formaldehyde, methyl *tert*-butyl ether, Methanol-to-olefins (MTO) reaction, *tert*-amyl methyl ether, and acetic acid.^[38,39] Its application in the mobility sector can also be envisaged through its direct use or its conversion to hydrocarbon fuels via methanol-to-gasoline processes. Currently, almost all industrial methanol is synthesized from syngas (Scheme 3), in the presence of heterogeneous catalysts (Cu/Zn/Al oxides) at elevated pressures and temperatures (50–250 bar, 200–350 °C).^[38] Natural gas is currently the feedstock to define the lowest carbon footprint for world-scale industrial methanol production, whereby steam reforming or partial oxidation can be used for syngas generation.^[38] To date, several processes have been developed to integrate CO₂ into the synthesis of methanol, based either on CO₂ conversion to CO (reverse WGS) and its subsequent hydrogenation or direct hydrogenation of CO₂ (Scheme 3).

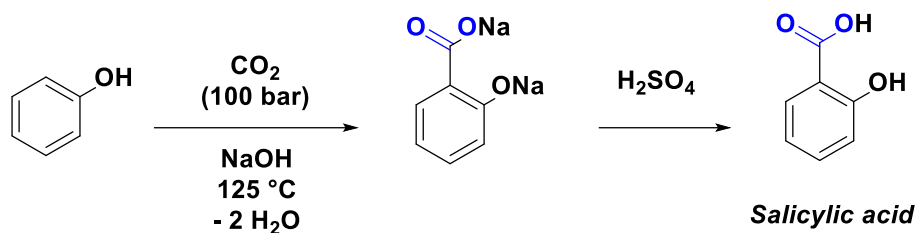


Scheme 3. Production of MeOH from synthesis gas.^[38]

Worldwide first demonstration of the direct conversion process of CO₂ to methanol was reported by Lurgi in 1994. Another laboratory pilot plant built by the NIRE and RITE institutes in Japan, demonstrated the hydrogenation of CO₂ on a 50 kg/day scale. In 2011, the first commercial CO₂-to-methanol has been in operation in Iceland, with a production capacity of ca. 5600 t/year.^[25,38] Although extremely attractive, life cycle analysis studies show that the carbon footprint for direct hydrogenation of CO₂ to methanol is depending on the H₂ supply.

5.4. Salicylic acid production

The synthesis of salicylic acid from CO₂ and phenolates is an old industrial process, dating back to the 19th century. This reaction is used for the synthesis of salicylic acid, as it is the first step in the industrial synthesis of Aspirin, directly consuming 29 kt of CO₂/year.^[40]



Scheme 4. Synthesis of salicylic acid.

5.5. Cyclic carbonates

The market for cyclic carbonates is experiencing rapid growth, owing to their use as aprotic solvent and electrolytes in lithium ion batteries for powering electronic devices. They are produced commercially from CO_2 and epoxides (Scheme 1).^[4] Ethylene and propylene oxides are employed as high-energy substrates to catalytically produce ethylene ($\Delta H_{\text{R}} = -33 \text{ kcal/mol}$) and propylene carbonates, in a highly exothermic reaction. The process has been industrialized in the 1950s, directly utilizing 40 kt CO_2 /year for a production scale of around 80 kt/year. The process is energy-intensive and the reaction requires the use of Lewis acid or base catalysts, which operate at high temperatures and pressures.^[40] Because of the energy required from fossil fuels, the synthesis of cyclic carbonates is considered as a net emitter rather than CO_2 consumer (0.9 ton of CO_2 emitted/1 ton of cyclic carbonate produced). The significant environmental benefits resulting from this strategy is therefore being questioned and further documented. Thus, development and commercial adoption of new catalytic systems would allow the synthesis of cyclic carbonates to occur at room temperature and atmospheric pressure and thus resulting in a significant reduction in total CO_2 emissions.

5.6. Polymers from CO_2

CO_2 can be utilized in various polymerization reactions, either directly by copolymerization, or indirectly by using CO_2 -derived compounds. For example, the possibility of synthesizing aliphatic polycarbonates from copolymerization of CO_2 and epoxides has been known for many decades.^[4,38,40] In 2016, Bayer (now Covestro) launched a production plant for polyether-polycarbonate-polyols in Germany, with a capacity of 5000 t/year.^[38] In this process, Bayer showed that a roughly 20wt% of the propylene oxide within the polyol could be replaced by CO_2 , without affecting physical properties of the polymer. CO_2 is reacted with propylene oxide in the presence of a zinc-based catalyst to produce polyols, which are then used for the production of flexible foam polyurethanes for foam mattresses. The current polyol market is

about 7.5 Mt/year, and with a 20wt% average CO₂ content, up to 1.6 Mt/year of CO₂ could be used directly, which no longer needs to be manufactured from crude oil.^[38]

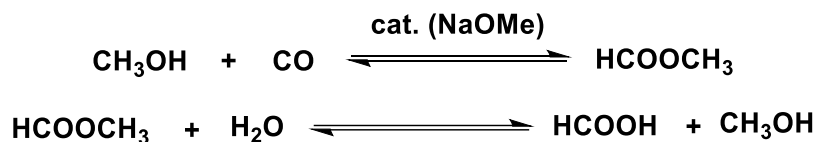
5.7. Organic acids from CO₂

A number of organic acid compounds can, in principle, be produced using CO₂. However, research in this field is still at laboratory scale and efficiency of the investigated catalytic systems is too low to be industrially implemented.

5.7.1. Formic acid

A process of great interest is the synthesis of formic acid via the direct reaction of H₂, generated from renewable resources, and CO₂. The interest toward such a process is mainly due to the potential of formic acid as hydrogen-carrier, as it can be easily decomposed back to H₂ and CO₂ through a quasi- CO₂-neutral cycle.^[41]

Currently, worldwide production of formic acid is obtained from the combination of methanol and CO generated from fossil fuel, with a strong base in a two-step process via methyl formate formation (Scheme 5). Around 1 Mt are used each year in the leather, rubber and textile industries, as well as for the synthesis of organic chemicals.^[38]



Scheme 5. Dry reforming of Methane (DRM) with CO₂ to form synthesis gas.

Unfortunately, the direct hydrogenation of CO₂ is thermodynamically disfavoured. Therefore, to shift the thermodynamic equilibrium, bases are commonly added to reaction mixture. Yet, the reaction has not found industrial application, owing to two main drawbacks: a) the economic costs for the separation of formic acid, from the salts formed in the presence of the added base (typically NEt₃), are not trivial b) recovering the expensive metal-catalysts in an efficient manner.^[41]

5.7.2. Acrylic acid and esters

Acrylic acid is the simplest unsaturated carboxylic acid and an important building block for thousands of consumer products. In 2016, the world production of acrylic acid was estimated to be approximately 5.5 Mt/year.^[42] Such important worldwide market is driven by two main requests. First, due to the increasing lifespan and improving lifestyle, a significant growing

General introduction

demand was observed for the production of diapers and other hygiene products, as acrylic acid is the monomer used for superabsorbent polymers synthesis.

This versatile intermediate is also used for the production of acrylate esters, which are employed in the manufacture of detergents, coatings, adhesives and resin formulations, accounting for more than 50% of acrylic acid worldwide demand.^[43]

i. Chemical properties

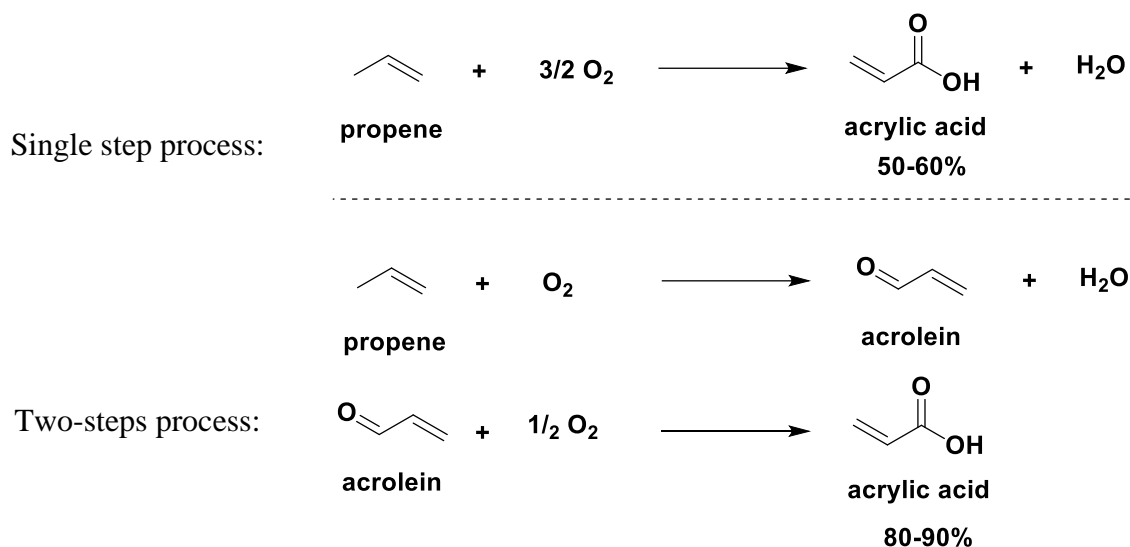
Acrylic acid and its esters are particularly interesting as they can undergo reactions characteristic of both unsaturated compounds and aliphatic carboxylic acids/esters. Due to their pair of conjugated bonds, these compounds possess high reactivity.^[42] The β -carbon atom, polarized by the carbonyl group, behaves as an electrophile, favouring addition of a variety of nucleophiles to the vinyl group. On the other hand, the C=C bond is able to undergo radical-initiated addition reactions, Diels–Alder reactions with dienes and polymerization reactions, while the carboxyl group allows for esterification and transesterification reactions.

ii. Industrial production of acrylic acid

In the past, acrylic acid has been commercially produced through many different processes, including the ethylene cyanohydrine process, the Reppe carbonylation of acetylene process, the ketene process and acrylonitrile hydrolysis.^[42] By the late 1990s, all of these processes were progressively discontinued either for safety and ecological reasons, or due to the increasing cost and limited availability of starting materials (e.g. acetylene).

Currently, commercial acrylic acid is manufactured on by selective oxidation of propene, a process that quickly gained prominence due to the high availability and relatively low cost of the alkene substrate from steam reforming.

The process can be carried out either in single-step direct oxidation or two-step oxidation in the gas-phase, with the latter being the most favoured route to achieve maximum conversion and selectivity, employing heterogeneous catalysts (Scheme 6). The steps employ separate catalysts and are operated at different temperatures to permit high overall efficiency.



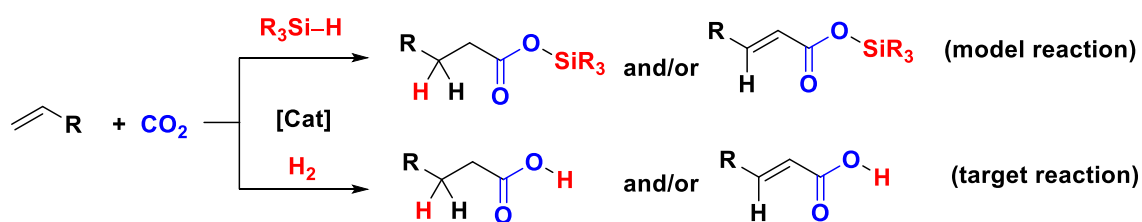
Scheme 6. Acrylic acid industrial production.

In the first step, propene is converted to acrolein in the presence of air at 330 – 380 °C (1-2 bar), using a multicomponent catalytic system incorporating Mo and Bi mixed oxides containing one or more of other elements as promoter (such as Fe, Co, Ni, Tl, W, Al, Zr, Ti, Te, K, P, Sb, Sn, or Si).^[42] In the second step, acrolein is further oxidized to acrylic acid at ~300 °C using catalysts based on Mo-V mixed oxides containing other elements and carriers (W, Cu, Co, Ni, Fe, Pb, Bi, Sn, Sb, or Si). Almost full conversion of acrolein and after several recovery and purification steps (absorbing column, liquid-liquid extraction, distillation carried out in the presence of polymerization inhibitor, re-crystallization), yields greater than 90% of acrylic acid are obtained. It is very likely that the propene oxidation route will continue as the most economical process. However, since the latter is petroleum dependent, continual increases in propene price are unavoidable and affect the market economy of acrylic acid. Thus, it is of great economic interest to ensure acrylic acid production and its price stability with more economic and eco-friendly alternative route.

The synthesis of acrylic acid based on the direct combination of ethylene (C₂H₄) with CO₂ is, in principle, a very attractive alternative as would not only utilize the cheap and abundantly available CO₂ as C1 building block but would also avoid waste formation thanks to its intrinsic atom efficiency. Furthermore, further utilization of renewable ethylene would highlight its positive environmental impact, as it could be derived from dehydration of bio-ethanol.^[44] Recent advances have opened new perspectives in C₂H₄ carboxylation research area (see Part I Chapter 1).

6. Goal of the thesis

In the framework of this project, we will explore and substantiate new homogeneous catalytic processes enabling the reductive carboxylation of ethylene into industrially attractive but also more challenging way, carboxylic acids. In order to better identify valid catalytic systems and unveil the nature of the corresponding catalytic intermediates, catalytic coupling reaction of CO₂ with C₂H₄ will be followed by reduction with hydrosilanes, which would afford valuable carboxylic acid silyl esters (model reaction, Scheme 7).



Scheme 7. Catalytic reductive carboxylation of alkenes into carboxylic acids or their silyl esters.

Readily available, easy-to-handle, harmless and relatively inexpensive (although admittedly still industrially unviable), hydrosilanes are widely used as reducing agents for many functional groups. Given their highly tunable activity by the substituents at the silicon atom, hydrosilanes are eminently competitive reducing agents to organometallic hydrides, and they appear well-suited for preliminary academic investigations.

In its very first phase, the project dealt with identification of promising catalysts systems for the model target reaction by using High Throughput Screening (HTS) techniques. The second and major phase of the project was devoted to the implementation of the results of the first phase into an effective homogeneous catalytic process, to access carboxylic acids and then optimize the selectivity and productivity at the lab scale. Ideally, this could be achieved by using H₂ as reducing agent, which will allow making this process benign, fully atom-efficient and industrially/economically attractive (target reaction, Scheme 7).

Parallel to these catalytic studies, the understanding of reactivity pattern in model organometallic compounds towards CO₂, alkenes and hydrosilanes, and detailed structural information about key intermediates and side-products have been carried out to allow the determination of the actual operative catalytic mechanism. In a longer-term perspective, the collected and analyzed fundamental data shall be of high interest for extrapolation to other related chemical processes associated with metal complexes-mediated protocols of chemical conversion and/or sequestration/recycling of CO₂. Also, unraveling essential problems of

catalytic activation of CO₂ (poor selectivity, low conversion, high energy costs) shall constitute another landmark for future works in this hot area of sustainable development.

7. References

- [1] H. Ritchie, M. Roser, *Our World Data* **2020**.
- [2] N. G. C. Change, “Global Surface Temperature | NASA Global Climate Change,” can be found under <https://climate.nasa.gov/vital-signs/global-temperature>
- [3] E. Almqvist, in *Hist. Ind. Gases* (Ed.: E. Almqvist), Springer US, Boston, MA, **2003**, pp. 47–135.
- [4] S. Topham, A. Bazzanella, S. Schiebahn, S. Luhr, L. Zhao, A. Otto, D. Stolten, in *Ullmanns Encycl. Ind. Chem.*, American Cancer Society, **2014**, pp. 1–43.
- [5] Intergovernmental Panel on Climate Change, O. Edenhofer, Eds. , *Climate Change 2014: Mitigation of Climate Change: Working Group III Contribution to the Fifth Assessment Report of the Intergovernmental Panel on Climate Change*, Cambridge University Press, New York, NY, **2014**.
- [6] “Climate Change: Past, Present, and Future | Wiley,” can be found under <http://www.wiley.com/en-gb/Climate+Change%3A+Past%2C+Present%2C+and+Future-p-9781118708521>
- [7] “Earth Fact Sheet,” can be found under <https://nssdc.gsfc.nasa.gov/planetary/factsheet/earthfact.html>
- [8] “Earth’s CO2 Home Page,” can be found under <https://www.co2.earth/>
- [9] P. Friedlingstein, M. W. Jones, M. O’Sullivan, R. M. Andrew, J. Hauck, G. P. Peters, W. Peters, J. Pongratz, S. Sitch, C. Le Quéré, D. C. E. Bakker, J. G. Canadell, P. Ciais, R. B. Jackson, P. Anthoni, L. Barbero, A. Bastos, V. Bastrikov, M. Becker, L. Bopp, E. Buitenhuis, N. Chandra, F. Chevallier, L. P. Chini, K. I. Currie, R. A. Feely, M. Gehlen, D. Gilfillan, T. Gkritzalis, D. S. Goll, N. Gruber, S. Gutekunst, I. Harris, V. Haverd, R. A. Houghton, G. Hurtt, T. Ilyina, A. K. Jain, E. Joetzjer, J. O. Kaplan, E. Kato, K. Klein Goldewijk, J. I. Korsbakken, P. Landschützer, S. K. Lauvset, N. Lefèvre, A. Lenton, S. Lienert, D. Lombardozzi, G. Marland, P. C. McGuire, J. R. Melton, N. Metzl, D. R. Munro, J. E. M. S. Nabel, S.-I. Nakaoka, C. Neill, A. M. Omar, T. Ono, A. Peregón, D. Pierrot, B. Poulter, G. Rehder, L. Resplandy, E. Robertson, C. Rödenbeck, R. Séférian, J. Schwinger, N. Smith, P. P. Tans, H. Tian, B. Tilbrook, F. N. Tubiello, G. R. van der Werf, A. J. Wiltshire, S. Zaehle, *Earth Syst. Sci. Data* **2019**, *11*, 1783–1838.
- [10] “Global Carbon Project (GCP),” can be found under <https://www.globalcarbonproject.org/carbonbudget/index.htm>
- [11] A. Gulzar, A. Gulzar, M. B. Ansari, F. He, S. Gai, P. Yang, *Chem. Eng. J. Adv.* **2020**, *3*, 100013.
- [12] J. A. Cecilia, D. Ballesteros Plata, E. Vilarrasa García, *Molecules* **2021**, *26*, 500.
- [13] B. Llamas, B. Navarrete, F. Vega, E. Rodriguez, L. F. Mazadiego, Á. Cámara, P. Otero, *Greenhouse Gas Emissions – Carbon Capture, Storage and Utilisation*, IntechOpen, **2016**.
- [14] N. MacDowell, N. Florin, A. Buchard, J. Hallett, A. Galindo, G. Jackson, C. S. Adjiman, C. K. Williams, N. Shah, P. Fennell, *Energy Environ. Sci.* **2010**, *3*, 1645–1669.
- [15] “Oxy-Combustion,” can be found under <https://netl.doe.gov/node/7477>
- [16] “Industrial ammonia production emits more CO2 than any other chemical-making reaction. Chemists want to change that,” can be found under <https://cen.acs.org/environment/green-chemistry/Industrial-ammonia-production-emits-CO2/97/i24>
- [17] “Ammonia,” can be found under <http://www.iipinetwork.org/wp-content/letd/content/ammonia.html>, **2013**.
- [18] X. Liu, A. Elgowainy, M. Wang, *Green Chem.* **2020**, *22*, 5751–5761.
- [19] “Greenhouse Gas Emissions from Energy: Overview – Analysis,” can be found under <https://www.iea.org/reports/greenhouse-gas-emissions-from-energy-overview>

- [20] M. Marczak, S. Budzyń, J. Szczurowski, K. Kogut, P. Burmistrz, *Environ. Sci. Pollut. Res.* **2019**, 26, 8383–8392.
- [21] "Carbon Dioxide Capture and Storage" can be found under <https://www.ipcc.ch/report/carbon-dioxide-capture-and-storage/>
- [22] "Carbon Capture and Storage in Europe," can be found under <https://easac.eu/publications/details/carbon-capture-and-storage-in-europe/>
- [23] M. Aresta, in *Carbon Dioxide Chem. Feedstock*, John Wiley & Sons, Ltd, **2010**, pp. 1–13.
- [24] "Is carbon capture too expensive? – Analysis," can be found under <https://www.iea.org/commentaries/is-carbon-capture-too-expensive>
- [25] "Putting CO₂ to Use – Analysis," can be found under <https://www.iea.org/reports/putting-co2-to-use>
- [26] "L'évolution des différents prix du carbone," can be found under <https://energiesdev.fr/prix-carbone-co2/>, **2020**.
- [27] "What is Carbon Pricing?," can be found under <https://www.spglobal.com/en/research-insights/articles/what-is-carbon-pricing>
- [28] "Enhanced Oil Recovery," can be found under <https://www.energy.gov/fe/science-innovation/oil-gas-research/enhanced-oil-recovery>
- [29] V. Núñez-López, E. Moskal, *Front. Clim.* **2019**, 1, 5.
- [30] "Can CO₂-EOR really provide carbon-negative oil? – Analysis," can be found under <https://www.iea.org/commentaries/can-co2-eor-really-provide-carbon-negative-oil>
- [31] "Whatever happened to enhanced oil recovery? – Analysis," can be found under <https://www.iea.org/commentaries/whatever-happened-to-enhanced-oil-recovery>
- [32] "Storage," can be found under <https://www.globalccsinstitute.com/about/what-is-ccs/storage/>
- [33] T. Allison, **1996**, DOI 10.18434/T42S31.
- [34] C. Das Neves Gomes, O. Jacquet, C. Villiers, P. Thuéry, M. Ephritikhine, T. Cantat, *Angew. Chem. Int. Ed.* **2012**, 51, 187–190.
- [35] E. J. C. Lopes, A. P. C. Ribeiro, L. M. D. R. S. Martins, *Catalysts* **2020**, 10, 479.
- [36] "Valorisation chimique du CO₂ : état des lieux. Quantification des bénéfices é...," can be found under <https://www.ademe.fr/valorisation-chimique-co2-etat-lieux-quantification-benefices-energetiques-environnementaux-evaluation-economique-trois-voies-chimiques>
- [37] "Innovation Outlook: Renewable Methanol," can be found under <https://www.irena.org/publications/2021/Jan/Innovation-Outlook-Renewable-Methanol>
- [38] J. Artz, T. E. Müller, K. Thenert, J. Kleinekorte, R. Meys, A. Sternberg, A. Bardow, W. Leitner, "Sustainable Conversion of Carbon Dioxide: An Integrated Review of Catalysis and Life Cycle Assessment," DOI 10.1021/acs.chemrev.7b00435 can be found under <https://pubs.acs.org/doi/abs/10.1021/acs.chemrev.7b00435>, **2017**.
- [39] M. Bertau, H. Offermanns, L. Plass, F. Schmidt, H.-J. Wernicke, Eds., *Methanol: The Basic Chemical and Energy Feedstock of the Future: Asinger's Vision Today*, Springer-Verlag, Berlin Heidelberg, **2014**.
- [40] A. W. Kleij, M. North, A. Urakawa, *ChemSusChem* **2017**, 10, 1036–1038.
- [41] T. Schaub, R. A. Paciello, *Angew. Chem. Int. Ed.* **2011**, 50, 7278–7282.
- [42] T. Ohara, T. Sato, N. Shimizu, G. Prescher, H. Schwind, O. Weiberg, K. Marten, H. Greim, T. D. Shaffer, P. Nandi, in *Ullmanns Encycl. Ind. Chem.*, American Cancer Society, **2020**, pp. 1–21.
- [43] *Chem. Eng.* **2016**.
- [44] "Surfactants from Renewable Resources | Wiley," can be found under <http://www.wiley.com/en-us/Surfactants+from+Renewable+Resources-p-9780470760413>

Part I

CO₂ as a C1 source toward the direct synthesis of carboxylic acids and their derivatives

Part I

Introduction	57
Chapter 1 – CO₂ as a C1 source to access carboxylic acids: State-of-the-art	59
1.1. Carboxylic acid syntheses from CO ₂ : General aspects	59
1.2. Transition metal-catalyzed carboxylation reactions.....	61
1.2.1. Carbon dioxide activation with mononuclear transition metal complexes	61
1.2.2. Metal-catalyzed carboxylation reaction of organometallic reagents.....	63
1.2.3. Catalytic reductive carboxylation of non-activated substrates.....	67
1.2.4. Catalytic carboxylation of unsaturated hydrocarbons	72
1.2.5. Catalytic carboxylation techniques via C–H functionalization.....	94
1.3. Conclusion and outlook.....	104
1.4. References	105
Chapter 2 – Efficient catalytic systems toward carboxylation reaction of C₂H₄ with CO₂: from discovery to optimization by means of High Throughput Experimentation.....	111
2.1. High–Throughput Experimentation	111
2.1.1. Introduction	111
2.1.2. Objectives and background	112
2.2. Results and discussion.....	118
2.2.1. HTS catalytic results of the reductive coupling of CO ₂ with C ₂ H ₄ and Et ₃ SiH...	118
2.2.2. Batch-scale metal-catalyzed synthesis of silylesters from CO ₂ and C ₂ H ₄	122
2.2.3. Toward metal-catalyzed synthesis of carboxylic acids from CO ₂ , C ₂ H ₄ and H ₂ ?	127
2.3. Conclusion.....	129
2.4. References	130

Part I

Introduction

Given the actual environmental context, conversion of CO₂ as a non-toxic, abundant and inexpensive C1 synthon into platform molecules has gained tremendous interest.^[1,2] More recently, substantial efforts have been made to develop new straightforward carboxylation methodologies toward carboxylic acids and carbonates, which are highly versatile starting materials for fine chemicals and biologically active compounds.^[3]

Due to the inherent stability of CO₂, the utilization of highly reactive starting materials such as organometallic reagents is often needed.^[4] During the last decades, prodigious advances have been reported in the fields of electrochemistry, heterogeneous and homogeneous catalysis towards the chemical activation of CO₂.^[5-7] In particular, transition metal-catalyzed carboxylation reactions with CO₂ have experienced exponential growth, as they are becoming powerful alternative strategies to circumvent early waste-producing synthetic routes.

Focusing on the most important breakthroughs, the first chapter of this manuscript provides a state-of-the-art of the current transition metal methods employed to access carboxylic acids from CO₂. The catalyzed carboxylation portfolio includes a variety of coupling partners depending on the catalytic strategy employed. Herein, a particular emphasis is given to the utilization of simple unsaturated hydrocarbons as coupling partners. Highly appealing yet extremely challenging, the transition-metal catalyzed carboxylation reactions of the simplest alkene, *i.e.* the reductive coupling of CO₂ with ethylene (C₂H₄) to produce acrylic acid, still remain at their infancy. In this context, a new transition metal catalyzed reductive methodology to access carboxylic acids and esters derivatives was investigated. Chapter 2 describes the combinations conducted at identifying new successful catalyst precursor/ligand systems for the reductive carboxylation of ethylene, by means of high-throughput screening (HTS) technologies.

Chapter 1 – CO₂ as a C1 source to access carboxylic acids: State-of-the-art

Easy to store and simple to handle, carboxylic acids are accessible by means of a large number of well-established routes, including the conventional hydrolysis of nitriles and related derivatives or oxidation of alcohols or aldehydes.^[3] However, regardless of the efficiency of these well-known procedures, the most straightforward strategy to access carboxylic acids is the direct carboxylation of carbon nucleophiles using CO₂ as the electrophilic partner. Indeed, this approach has the advantages of generally avoiding harsh conditions and using abundant, inexpensive and non-toxic carbon dioxide as highly attractive source.^[8] Typically, nucleophilic partners used in carboxylation reactions are highly reactive so they can easily overcome the CO₂ kinetic and thermodynamic inertness. For example, the use of organolithium or Grignard reagents allows these carboxylation reactions to proceed smoothly in absence of any transition metal catalyst, reducing therefore synthesis costs. However, these reactions presents the drawback of being incompatible with sensitive functional groups such as ketones, nitriles or aldehydes, and require the use of stoichiometric amounts of metallic reagent. Therefore, alternative organometallic procedures operating under milder conditions, and high chemoselectivity, have emerged.

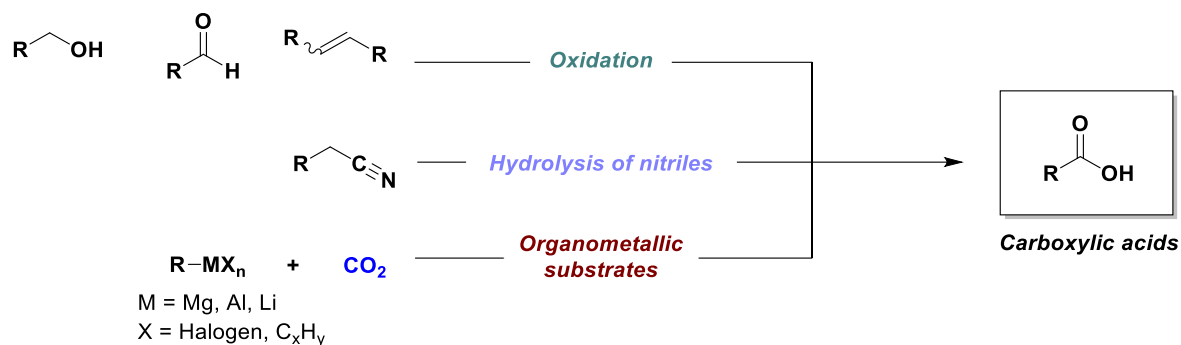
The following Chapter discusses the major breakthroughs reported recently in the field of carboxylation, illustrating the importance of using CO₂ as a carbon source toward more sustainable chemical processes.

1.1. Carboxylic acid syntheses from CO₂: General aspects

Carboxylic acids can be obtained using a wide variety of reactions. For instance, carboxylic derivatives such as esters, amides, and anhydrides can undergo hydrolysis to form the corresponding carboxylic acids. On the other hand, a direct introduction of a carboxylic moiety requests more elaborated and harsher procedures. The most common used syntheses are categorised into three major reaction types (Scheme I.1.1):^[9]

- Oxidation of primary alcohols, aldehydes and alkenes using strong oxidizing reagents (KMnO₄, Jones reagent, Dess–Martin periodinane)
- Hydrolysis of nitriles to carboxylic acids
- Consecutive reactions of highly energetic organometallic substrates, bearing a nucleophilic carbon, with carbon dioxide (electrophilic carbon atom) to yield the

corresponding carboxylate salts, followed by strong aqueous acid treatment to afford carboxylic acid



Scheme I.1.1. Pathways to access carboxylic acids.

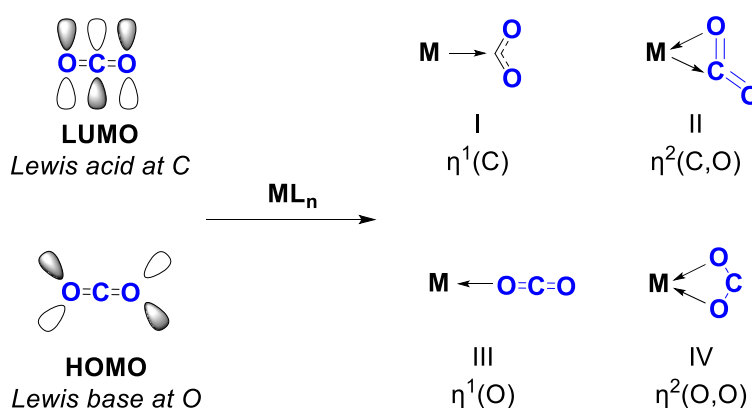
The later strategy relies on the direct CO₂ insertion in a polarized C–metal bond and is therefore promoted using stoichiometric amounts of highly nucleophilic organometallic entities such as Grignard reagents, organolithium or organoaluminum species, furnishing the corresponding carboxylic acids upon hydrolytic workup. However, the poor chemoselectivity of such reagents encouraged the design of catalytic cross-coupling reactions.^[10] Understanding the different CO₂ binding modes to a metal center led to the development of metal-catalyzed carboxylation techniques using less basic/nucleophilic organometallic reagents.

1.2. Transition metal-catalyzed carboxylation reactions

Since catalytic transformations of CO₂ requires primarily its coordination to a metal center, stereo-electronic features of carbon dioxide molecule and its binding modes to transition metals will be firstly described.

1.2.1. Carbon dioxide activation with mononuclear transition metal complexes

In its ground state, CO₂ is a 16 electron linear triatomic molecule having a $D_{\infty h}$ symmetry.^[1] The *sp* hybridized central carbon atom possesses two C=O bonds with a C–O bond distance of 1.16 Å, shorter than a normal C=O bond (*cf.* 1.23 Å).^[11] The linearity and inherent electronegativity difference between carbon and oxygen atoms result in two dipole moments symmetrically opposite to each other, making CO₂ a non-polar molecule kinetically and thermodynamically stable. The reactivity of CO₂ primarily relies on the $1\pi_g$ -occupied molecular orbital (HOMO), centred on the oxygen atoms, and the $2\pi_u$ -unoccupied molecular orbital (LUMO) lying on the carbon atom (Scheme I.1.2).^[11] These features confer an ambiphilic character to the CO₂ molecule, exhibiting both Lewis acidic character at the central carbon and Lewis basic character on the two oxygen atoms. In addition, CO₂ contains two adjacent orthogonal π -orbitals amenable for bonding interactions with the *d* electrons of a metal center. Consequently, because of carbon dioxide's multiple reactive sites, its binding mode to transition metal complexes have been intensively investigated. As judged by the wealth of literature data, four basic chelating modes are possible (Scheme I.1.2).^[12,13]



Scheme I.1.2. Coordination modes of CO₂ to transition metals.^[14]

Metallacarboxylate complexes (I) are typically formed with electron-rich metals via electron density transfer from a d_z^2 metal orbital to the anti-bonding π^* of CO₂.^[15] The $\eta^2(\text{C}, \text{O})$ side-on coordination mode affords a three-membered metallacycle complex II, whereas

electron-deficient metal complexes bind to CO₂ in either a $\eta^1(\text{O})$ end-on coordination mode (III) or with two oxygen atoms (IV, CO₂ acting as a chelating ligand).^[15]

The first transition metal complex with CO₂ as ligand was described by Aresta and co-workers in 1975 (Figure I.1.1).^[16] The product was structurally characterized as the planar complex Ni($\eta^2\text{-CO}_2$)(PCy₃)₂, with “side-on” coordination of CO₂.^[17] Herskovitz *et al.* reported then the first examples of rhodium and iridium $\eta^1(\text{C})$ type complexes.^[18] More interestingly perhaps, end-on type adducts were found to form stable species using oxophilic actinide complexes such as [((^{Ad}ArO)₃tacn)U], ((^{Ad}ArO)₃tacn = 1,4,7-tris(3-adamantyl-5-*tert*-butyl-2-hydroxybenzyl)1,4,7-triazacyclo-nonane)), in which CO₂ adopts a linear geometry.^[19]

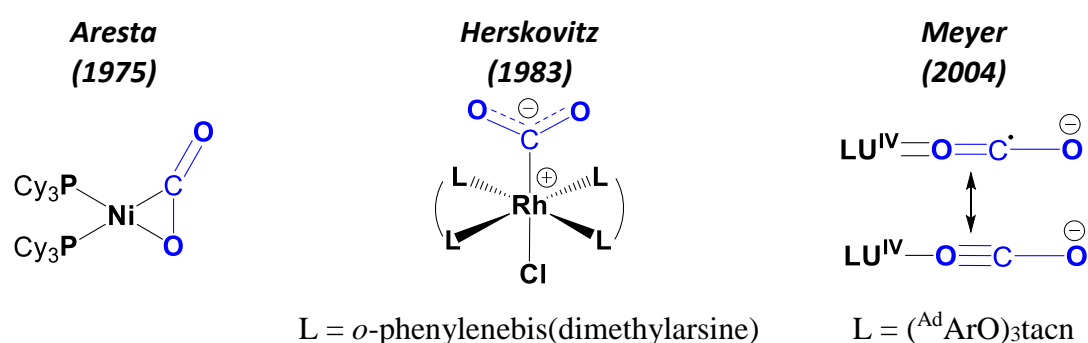


Figure I.1.1. Literature examples of the coordination of CO₂ to metal complexes.

Overall, the $\eta^2(\text{C,O})$ coordination mode appear to be the most common followed by the $\eta^1(\text{C})$ binding mode,^[20] both causing significant distortion of the O–C–O angle from linearity and, therefore, lowering CO₂ activation energy.^[14] Thus, promoting the targeted C–C bond coupling of CO₂ toward carboxylic acids became conceivable. Three different strategies of transition metal-mediated reactions of CO₂ were hence envisaged: (a) prior $\eta^2(\text{C,O})$ or $\eta^1(\text{C})$ coordination of CO₂ followed by a nucleophilic attack of an oxygen atom on electron-deficient substrates (b) oxidative coupling of electron-rich substrates with CO₂, (c) concurrent coordination of CO₂ and substrate to the metal center.^[14]

Taking into account these approaches, a vast panel of metal-catalyzed carboxylation reactions including such substrates as organometallic reagents, organic halides or (un)saturated hydrocarbons has been developed (Figure I.1.2). In this field, Martin and co-workers published a detailed full review giving a 50 years overview on the main strategies and breakthroughs of metal-catalyzed carboxylation reactions using CO₂.^[14]

Herein, a brief summary of these progresses is given to highlight the different methodologies exploited for the successful conversion of kinetically and thermodynamically stable CO₂.

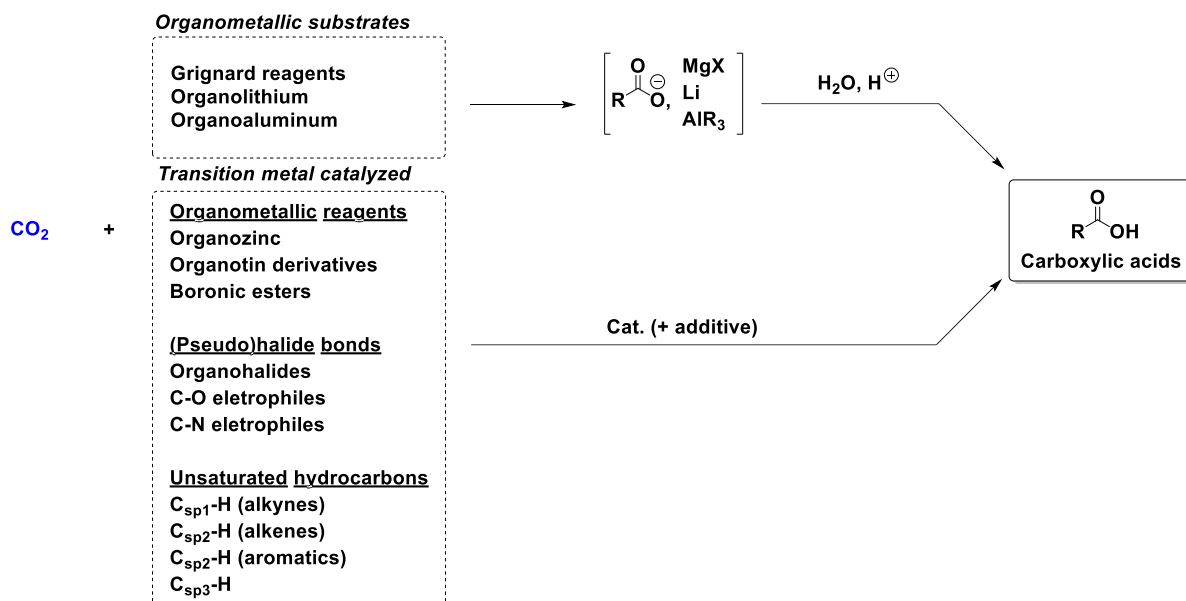


Figure I.1.2. Overview of the catalyzed and non-catalyzed approaches to access carboxylic acids from CO₂.

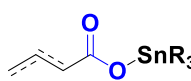
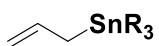
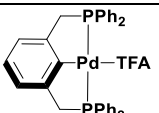
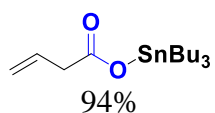
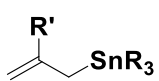
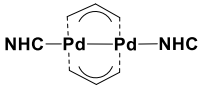
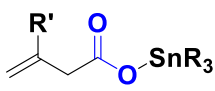
1.2.2. Metal-catalyzed carboxylation reaction of organometallic reagents

a. Catalytic carboxylation of organotin derivatives

Organotin(IV) reagents are particularly interesting coupling partners since they are stable to air, moisture and can be readily purified by chromatography prior to use. Moreover, organotin compounds present the advantage of being less reactive and hence more tolerant with respect to many functional groups.

Firstly reported in 1997 by Shi and Nicholas, metal-catalyzed carboxylation of organometallic substrates with CO₂ was performed using allyl stannanes.^[21] Easily converted to the corresponding allyl tin esters upon using catalytic amounts of Pd(PPh₃)₄, the protocol required however high pressures of CO₂ and could not be extended to bulkier substrates (Table I.1.1, entry 1). Ten years later, the use of palladium catalysts bearing pincer ligands allowed the formation of identical products under milder reaction conditions (Table I.1.1, entry 2).^[22] In 2011, it was found by Hazari's group that utilization of η³-allyl Pd(II) complexes supported by *N*-heterocyclic carbenes (NHC) allowed the reaction to be performed under even milder conditions and led to excellent yields (Table I.1.1, entry 3a.).^[23] Later on, more stable and easy-to-synthesize Pd(I)-bridging allyl dimer was employed for similar transformations (Table I.1.1, entry 3b.).^[24]

Table I.1.1. Examples of metal-catalyzed carboxylation of organotin derivatives.

Entry	Substrate	Catalyst	Reaction conditions	Product Yield [%]
1 ^[21]			Pd(PPh ₃) ₄ (8 mol%) CO ₂ (33 atm) THF, 70 °C	 R ^[a] = Bu, 90% (α,β)/10% (β,γ) R ^[a] = Ph, 70%(α,β)/30% (β,γ)
2 ^[22]			(3.5 mol%) CO ₂ (4 atm) THF, 70 °C	 94%
3 ^[23,24]			a. (2-methylallyl)Pd(O C(O)C ₄ H ₇)(NHC) (5 mol%) CO ₂ (1 atm) PhH, r.t. b.  (5 mol%) CO ₂ (1 atm) PhH, r.t.	 a. 80-95% b. 79-82%

b. Catalytic carboxylation of organoboron and other organometallic reagents

Unlike organotin substrates, the readily available and stable to heat, moisture and oxygen boronic acids and esters has made organoboron reagents particularly attractive.^[14]

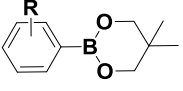
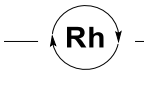
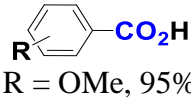
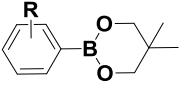
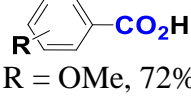
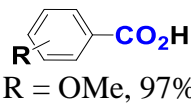
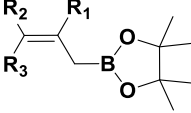
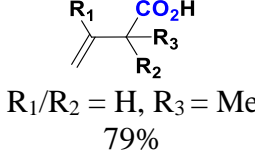
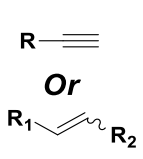
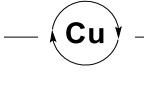
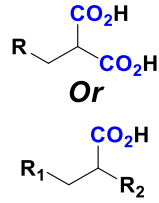
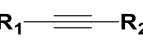
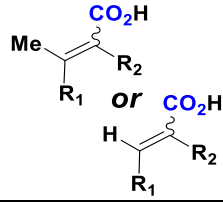
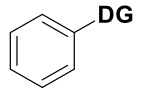
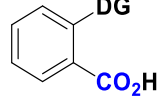
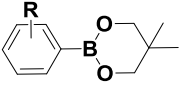
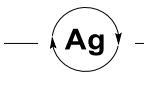
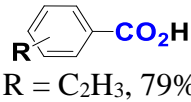
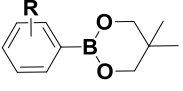
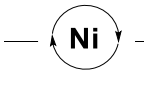
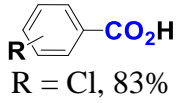
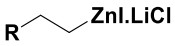
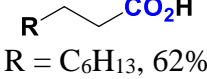
In 2006, the group of Iwasawa reported the first metal-catalyzed carboxylation of neopentyl glycol boronic esters under atmospheric pressure of CO₂, using Rh catalysts supported by bidentate phosphine ligands (Table I.1.2, entry 1).^[25] Later on, the same group described the catalytic activity of cheaper copper catalysts, in combination with bisoxazoline ligands, highlighting their functional group efficiency and compatibility compared to the previous Rh catalysts (Table I.1.2, entry 2).^[26] Hou *et al.* described then the use of NHC ligands, allowing to reduce the [(IPr)CuCl] catalyst loading and to avoid the use of excess amounts of CsF (Table I.1.2, entry 3).^[27] These metal-catalyzed carboxylation reactions of organoboranes were not limited to only aryl boronic esters, or to the presence of a neopentyl glycol unit on the organoborane. In fact, the use of allyl pinacol boronic esters was soon after reported by Duong,


applying similar conditions, and delivering the corresponding branched β,γ -unsaturated carboxylic acids with high regioselectivity (Table I.1.2, entry 4).^[28] Few years later, Skrydstrup *et al.* reported the carboxylation of a range of olefins *via* alkyl borane intermediates formed upon initial exposure to 9-BBN (Table I.1.2, entry 5).^[29] Of particular interest was the ability to access synthetically useful malonic acids from terminal alkynes through double hydroboration, followed by carboxylation. The authors successfully extended their methodology to the carboxylation of natural compounds containing di- and trisubstituted C=C bonds.

Prompted by the successful hydroboration/carboxylation sequence, other organometallic reagents were evaluated and employed toward CO₂ incorporation. For instance, Hou and coworkers reported a new stereoselective carbon(hydro)alumination of alkynes followed by carboxylation to access α,β -unsaturated carboxylic acids, in presence of Cu-based catalysts (Table I.1.2, entry 6).^[30] The authors also developed Cu-catalyzed carboxylation of aromatic and allylic aluminates. The presence of a directing group (DG) appeared to be mandatory with aromatic aluminates whereas a 2-aryloxy motif was required for allylic carboxylic acids preparation (Table I.1.2, entry 7).^[31,32] The above examples demonstrating the ability of Cu and Rh complexes to efficiently develop carboxylation reactions of boronic esters were not only limited to these metals since Lu and co-workers showed similar effectiveness and high functional group tolerance by using Ag catalysts (Table I.1.2, entry 8).^[33] Few years later, the group of Nolan developed an efficient carboxylation protocol of aryl and vinyl neopentyl glycol boronic esters using allyl-nickel(II) catalysts supported by NHC-ligands (Table I.1.2, entry 9).^[34]

While the popularity of organoboron reagents was expanding, carboxylation reaction employing organozinc species also started emerging. Pd and Ni-catalyzed reaction for aromatic organozinc reagents carboxylation were described by Dong and Oshima in 2008.^[35,36] In combination with electron rich and sterically hindered PCy₃ ligand, reactivity of the corresponding Ni catalyst was found to be superior to Pd analogue for aliphatic organozinc reagents coupling with CO₂ (Table I.1.2, entries 10,11 and 12).

Table I.1.2. Examples of metal-catalyzed carboxylation of organoboron and other organometallic substrates.

Entry	Substrate	Catalyst	Reaction conditions	Product Yield [%]
1 ^[25]			[Rh(OH) ₂ (cod)] ₂ (3 mol%) dppp (7 mol%) CO ₂ (1 atm) CsF (3.0 equiv) dioxane, 60 °C	 R = OMe, 95%
2 ^[26]			CuI (5 mol%) Bisoxazoline ligand (6 mol%) CO ₂ (1 atm) CsF (3.0 equiv) DMF, 90 °C	 R = OMe, 72%
3 ^[27]			[(IPr)CuCl] (1 mol%) CO ₂ (1 atm) <i>t</i> BuOK (1.05 equiv) THF, 80 °C	 R = OMe, 97%
4 ^[28]			[(IPr)CuCl] (5 mol%) CO ₂ (1 atm) <i>t</i> BuOK (1.1 equiv) THF, 70 °C	 R ₁ /R ₂ = H, R ₃ = Me 79%
5 ^[29]			CuOAc (10 mol%) 9-BBN IPr (12 mol%) CO ₂ (4 equiv) CsF (3 equiv) dioxane, 120 °C	
6 ^[30]			AlMe ₃ or DIBAL Then [(IPr)CuCl] (5 mol%) CO ₂ (1 atm) Toluene or THF	
7 ^[31,32]			<i>i</i> Bu ₃ Al(TMP)Li (2 equiv) then (NHC)CuCl (5 mol%) <i>t</i> BuOK (5 mol%) CO ₂ (1 atm) THF, -78 °C then r.t.	
8 ^[33]			[Ag] (1 mol%) PPh ₃ (1.5 mol%) CO ₂ (20 atm) <i>t</i> BuOK (2 equiv) dioxane, 100 °C	 R = C ₂ H ₅ , 79%
9 ^[34]			[Ni(NHC)(allyl)Cl] (5 mol%) CO ₂ (1 atm) <i>t</i> BuOK (1.2 equiv) toluene, 100 °C	 R = Cl, 83%
10 ^[36]			[Ni(acac)] (5 mol%) PCy ₃ (10 mol%) CO ₂ (1 atm)	 R = C ₆ H ₁₃ , 62%

DME, r.t.		
11 ^[35]	R–ZnBr <i>or</i> R–ZnI.LiCl	[Ni(PCy ₃) ₂] ₂ (N ₂) (5 mol%) CO ₂ (1 atm) toluene, 0 °C R–CO ₂ H R = -(CH ₂) ₃ Cl, 92%
12 ^[35]		Pd(OAc) (10 mol%) PCy ₃ (20 mol%) CO ₂ (1 atm) THF, 0 °C R–CO ₂ H R = -Ph, 90%

1.2.3. Catalytic reductive carboxylation of non-activated substrates

a. Catalytic carboxylation of organic halides

All the catalytic carboxylation reactions described above, although efficient, required the use stoichiometric amounts of organometallic species, hampering therefore any potential industrial upscaling. In this context, direct carboxylation of organic (pseudo)halides have been developed, since organometallic reagents are often obtained through metalation techniques from their corresponding organic halides.^[37] Such processes have the advantage of avoiding highly reactive organometallic reagents. They are, however, at first sight, counterintuitive as both CO₂ and C–(pseudo)halide bonds have an electrophilic carbon atom.^[38,39] To achieve these type of cross-electrophile coupling reaction, the presence of an appropriate reducing agent is mandatory to balance redox properties.^[40] The major drawback of this strategy is the possible reaction of the reducing agent with the putative oxidative addition species prior to CO₂ insertion, such as dimerization of electrophiles or competitive transmetalation followed by either β-hydride elimination or reductive elimination. The following section compiles results describing catalytic attempts towards reductive carboxylation reactions of organic (pseudo)halides.

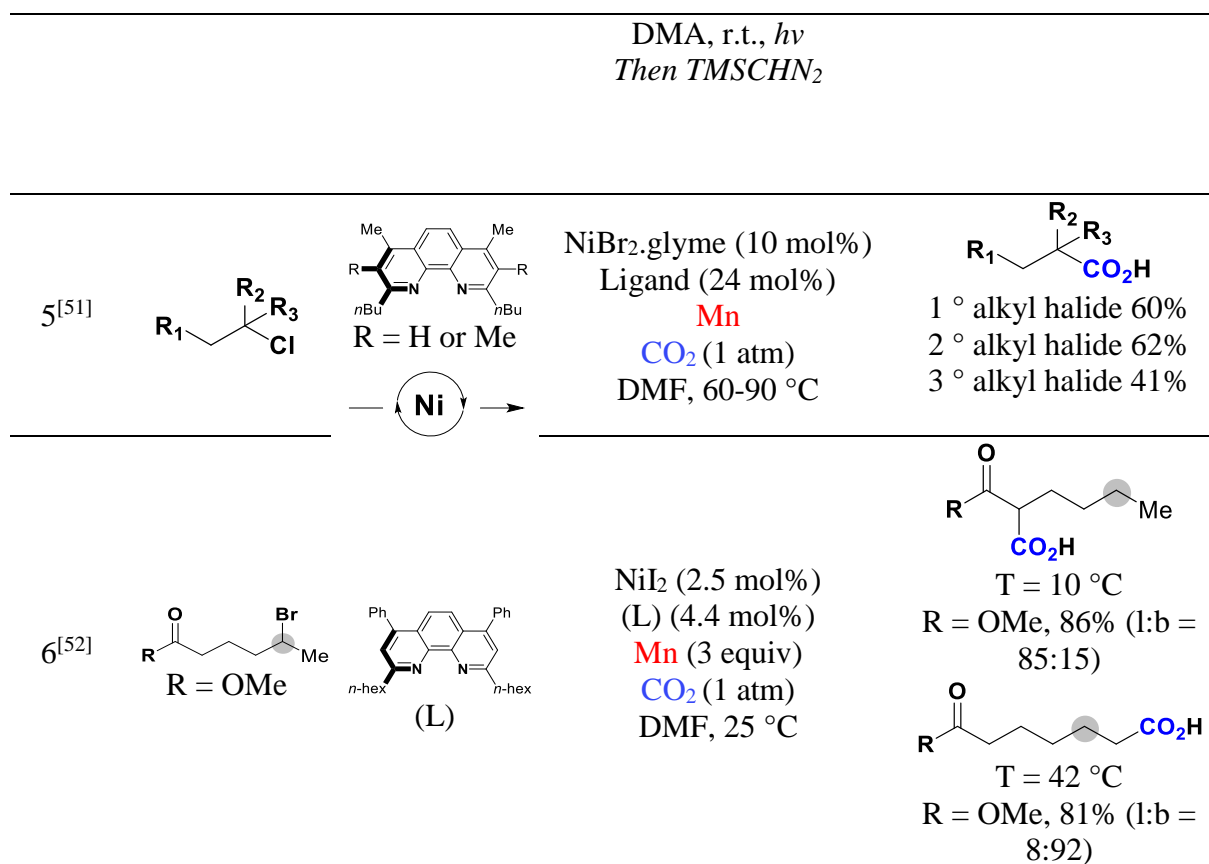
Historically, the first catalytic carboxylation of aryl halides with CO₂ was an electrochemical process employing Ni and Pd catalysts.^[41–43] However, the methodology lacked efficiency and was applied to a limited scope of substrates. Later on, non-electrochemical processes, published by Osakada and Yamamoto in 1994, afforded benzoic acid in moderate yield upon prior exposure of stoichiometric amounts of PhBr to Ni(cod)₂ and bipyridine.^[44] These pioneering results revealed the ability of nickel catalysts to mediate CO₂ insertion into PhNiBr(bpy) complex, and therefore, prepare carboxylic acids starting from simple organic halides. It took almost 15 years until Martin and co-workers reported the first catalytic carboxylation of aryl bromides with CO₂ and Et₂Zn as reductant (Table I.1.3, entries

1).^[45] The use of electron-rich and bulky phosphines helped minimizing Negishi-type cross-coupling side reactions. The reaction exhibited good functional group (e.g. epoxides) tolerance despite operating under high pressures. In 2012, the scope was further extended by Tsuji and Fujihara to aryl and vinylchlorides at atmospheric pressure of CO₂ and using Ni(II) catalysts (Table I.1.3, entry 2).^[46] In fact, incorporating mild and air-stable metallic Mn as reducing agent in combination with ammonium salts was mandatory to achieve reactivity. Theoretical calculations supported a Mn-mediated one-electron reduction of the Ni(II) complex to Ar-Ni(I)(PPh₃)₂ species, followed by CO₂ insertion.^[47]

Next, the group of Martin described a Ni-catalyzed protocol for carboxylation of primary, secondary and tertiary benzyl halides,^[48] while He and co-workers reported the use of primary benzyl chlorides (Table I.1.3, entry 3).^[49] The utilization of a Pd precatalyst with electron-rich and bulky phosphines in the presence of MgCl₂ was found to be critical. In this case, DFT calculations suggested a pathway where MgCl₂ is presumably involved in the process of CO₂ insertion into the (SPhos)₂Pd^{II}-CH₂Ph bond by stabilizing the Pd^{II}-CO₂ adduct and thus accelerating CO₂ insertion.

Table I.1.3. Examples of metal-catalyzed carboxylation of (pseudo)halides substrates.

Entry	Substrate	Catalyst /Ligand	Reaction conditions	Product Yield [%]
1 ^[45]			Pd(OAc) ₂ (8 mol%) <i>t</i> BuXPhos (10mol%) Et ₂ Zn (2.0 equiv) CO ₂ (1-10 atm) DMA, 40 °C	 R = NMe, 40% R = CHCH ₂ , 64%
2 ^[46]			[NiCl ₂ (PPh ₃) ₂] (5 mol%) PPh ₃ (10 mol%) Mn, Et ₄ NI (3.0 equiv, 10 mol%) CO ₂ (1 atm) DMI, r.t.	 R = Bpin, 58% R = CO ₂ Me, 76%
3 ^[49]			Pd(OAc) ₂ (3.3 mol%) SPhos (6.6 mol%) MgCl ₂ (1.4 equiv, CO ₂ (1 atm) DMF, 0 °C	 R = Br, 59% R = COPh, 53%
4 ^[50]			Pd(OAc) ₂ (2.5 mol%) <i>t</i> BuXPhos or PhXPhos (5 mol%) Photocatalyst (1 mol%) CO ₂ (1 atm) Cs ₂ CO ₃ (3.0 equiv) (<i>i</i> Pr) ₂ NEt (3.0 equiv)	 X = Cl, R = CF ₃ , 96% X = Br, <i>o,p</i> R = <i>i</i> Pr, 76%



Over the years, visible light photoredox catalysis strategies avoiding the use of stoichiometric amounts of metallic reductants have emerged as a powerful tool.^[14] For example, Iwasawa and Martin reported a Pd/Ir polypyridyl sensitizer dual catalytic system for the direct photocatalyzed carboxylation of aryl bromides and chlorides (Table I.1.3, entry 4).^[50] The multi-component systems, in the presence of an amine as electron donor, allowed to avoid the need for stoichiometric amounts of metallic single-electron reductants.^[53] Operating under mild conditions, addition of an excess of base was however necessary for neutralizing acids (HX and ArCOOH) generated from the oxidized amine. The corresponding methyl ester derivatives were obtained in good yields after *in situ* methyl esterification with trimethylsilyldiazomethane (TMSCHN₂).

Until 2016, metal-catalyzed reductive carboxylations remained focused on the utilization of substrates capable to readily undergo oxidative addition (aryl, benzyl or allyl (pseudo)halides). In fact, the main reasons hampering the use of simple inactivated alkyl halides was the low concentration of CO₂ in solution rendering difficult to generate alkyl metal species without undergoing parasitic β-hydride elimination or homocoupling reactions.^[14,54] To overcome this challenge, the group of Martin used 1,10-phenanthroline type ligands carrying substituents adjacent to the nitrogen atoms, thus preventing β-H elimination reaction prior to

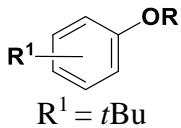

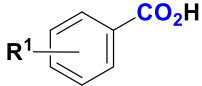
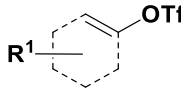
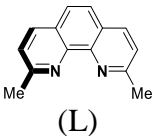
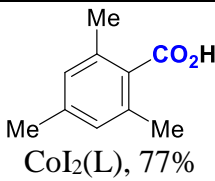
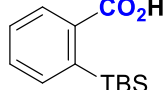
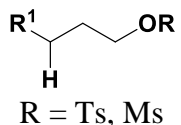
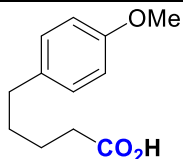
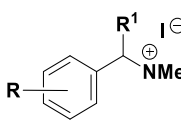
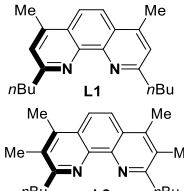
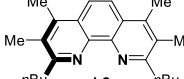
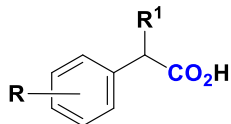
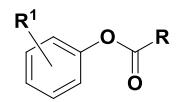
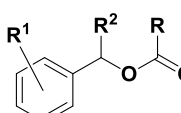
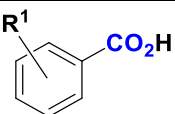
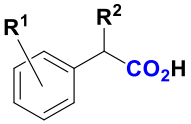
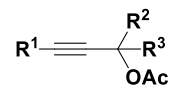
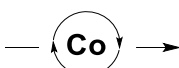
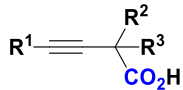
CO₂ insertion (Table I.1.3, entry 5).^[51] Coupling of primary, secondary and tertiary alkyl halides was therefore possible, encouraging the authors to extend the scope to cyclopropyl motifs.^[55,56] Using the same family of ligands, the group of Martin also developed remote carboxylation reaction of halogenated aliphatic hydrocarbons (Table I.1.3, entry 6). The strategy is based on the accelerated iterative β -hydride elimination/migratory insertion sequence setting therefore CO₂ insertion at remote sites.^[52]

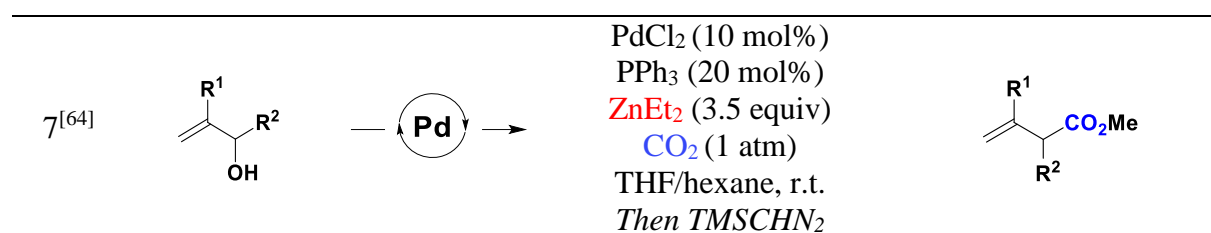
b. Catalytic reductive carboxylation of C–O and C–N electrophiles

An alternative strategy to the use of waste-generating organo-halides substrates is the utilization of C–O electrophiles as organic halides surrogates. Their natural abundance offer the advantage of being readily accessible, practical and less toxic substrates.^[57] However, unlike aryl halides, the cleavage of the stronger C–O bond requires higher energy. Nickel catalysts have proven to be particularly effective for the carboxylation of such esters and aryl sulfonates. Using similar conditions to those previously reported for aryl chlorides (Table I.1.3, entry 2), Tsuji and Fujihara reported the catalytic carboxylation of activated aryl sulfonates with nickel catalyst and PPh₃ ligand (Table I.1.4, entry 1).^[46]

The group of Tsuji extended the scope to more sterically hindered vinyl triflates upon using Ni and Co catalysts in combination with *ortho*-substituted 1,10-phenanthroline ligands (Table I.1.4, entry 2).^[58] Later on, the group of Durandetti assessed the feasibility of the carboxylation of aryl tosylates in the absence of ammonium salts or phosphine ligands, affording the corresponding carboxylic acids in moderate yields.^[59] This process was further extended by the group of Martin to unactivated alkyl mesylates and tosylates (Table I.1.4, entry 3).^[60] Yields comparable to those obtained starting from halide substrates were achieved from the sulfonate surrogates. Utilization of *ortho*-substituted 1,10-phenanthroline ligands, in combination with the Ni catalytic precursors, provided a procedure to access carboxylic acids via *sp*³ C–N cleavage of benzyl ammonium salts (Table I.1.4, entry 4).^[61]

Table I.1.4. Examples of metal-catalyzed carboxylation of C–O and C–N electrophiles.

Entry	Substrate	Catalyst /Ligand	Reaction conditions	Product Yield [%] / TON
1 ^[46]			[NiCl ₂ (PPh ₃) ₂] ₂ (10 mol%) PPh ₃ (20 mol%) Mn, Et ₄ NI (3.0 equiv, 20%) CO ₂ (1 atm) DMI, 60 °C	 R = Ts, 73% R = Tf, 72%
2 ^[58]		 (L)	[NiI ₂ (PPh ₃) ₂] ₂ or CoI ₂ (5 mol%) Mn (1.5 equiv) CO ₂ (1 atm) DMF, 60 °C	 CoI ₂ (L), 77%  NiI ₂ (L), 93%
3 ^[60]			[NiBr ₂ .glyme] (10 mol%) (L) (26 mol%) Mn (2.4 equiv) CO ₂ (1 atm) DMF, 50 °C	 R = Ts, 74% R = Ms, 61%
4 ^[61]		 L1  L2	[NiBr ₂ .glyme] (10 mol%) L1 or L2 (26 mol%) Mn (2.0 equiv) CO ₂ (1 atm) DMF, 70-90 °C	
5 ^[62]	 Or 	NiCl ₂ (dppf) or NiCl ₂ (PMe ₃) ₂	[Ni]-catalyst Mn (1.0-2.0 equiv) CO ₂ (1 atm) DMF or DMA, r.t.-100 °C	 R = tBu, 72% NiCl ₂ dppf Or  R = Me 80%, CH ₂ OMe 61% NiCl ₂ (PMe ₃) ₂
6 ^[63]			CoI ₂ (Phen) ₂ (5 mol%) Mn (3.0 equiv) CO ₂ (1 atm) DMA, r.t.	



In 2014, the Ni-catalyzed carboxylation of C(sp²)– and C(sp³)–bonds was also explored, and the nature of the ligand was found to have a crucial influence on the reactivity of aryl pivalates and benzyl esters (Table I.1.4, entry 5).^[62] The scope was further extended to propargyl acetates, using a cobalt catalyst in presence of 1,10-phenanthroline ligands (Table I.1.4, entry 6).^[63]

The group of Sato studied then the direct carboxylation of alcohols, given that C–O electrophiles are ultimately obtained from their C–OH counterparts.^[64] The high activation energy of the *sp*³ C–OH bond cleavage together with the high polarizability of the O–H bond were overcome in a Pd-catalyzed carboxylation of allylic alcohols using Et₂Zn as transmetalation agent (Table I.1.4, entry 7).^[64,65] In 2017, Martin and co-workers reported an alternative Ni(cod)₂/phenanthroline catalytic system for allylic alcohols in absence of the difficult-to-handle Et₂Zn.^[66]

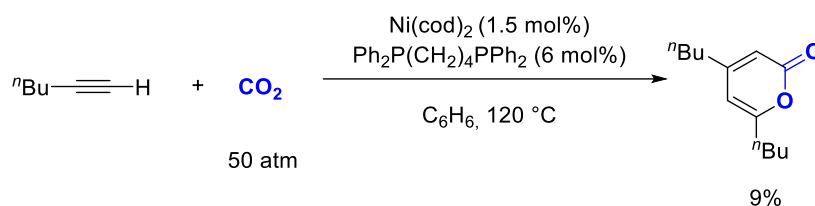
Despite the considerable number of methodologies developed, utilization of naturally abundant phenols, anisoles or aliphatic alcohols as substrates for direct carboxylation remains a challenge. In general, the catalytic cross-coupling reactions of organometallic reagents and organic (pseudo)halides with CO₂ to access value-added carboxylic acid derivatives have been still lacking usability. Although efficient and robust protocols have been developed, pre-functionalization of organic (pseudo)halides and the use of stoichiometric amounts of organometallic reagents are needed. An attractive alternative strategy emerged to perform direct carboxylation of non-activated substrates such as unsaturated hydrocarbons. The progress made during the last 30 years in this field is described in the following section.

1.2.4. Catalytic carboxylation of unsaturated hydrocarbons

a. C(*sp*)–H bonds (alkynes)

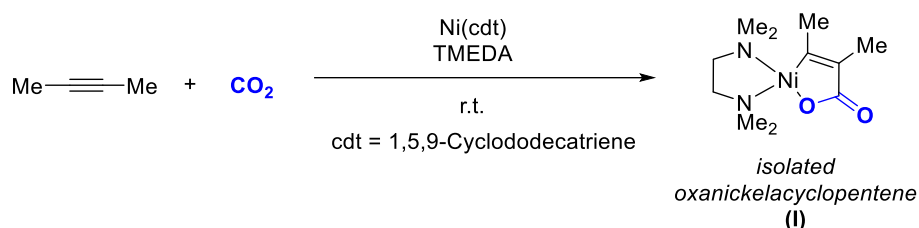
Catalytic CO₂ carboxylation of regular unsaturated substrates is a powerful synthetic approach towards industrially relevant carboxylic acids, such as linear and branched fatty acids. In 1977, the first incorporation of CO₂ into alkynes substrates was reported by Inoue and co-

workers.^[67,68] Ni catalyst supported by phosphine ligands were found efficient in the cycloaddition of carbon dioxide with terminal or internal alkynes, producing 2-pyrone derivatives in low yields (Scheme I.1.3).^[67]



Scheme I.1.3. Inoue's catalytic formation of 2-pyrone derivatives.


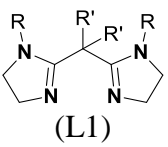
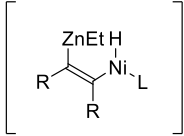
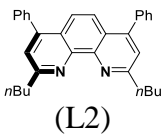
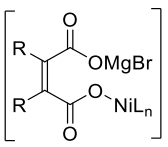
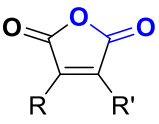
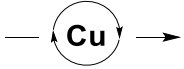
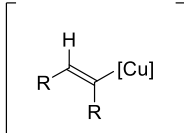
Mechanistic investigations conducted by Walther revealed the formation of an oxanickelacyclopentene species (**I**) via oxidative cyclization of alkynes and CO₂ with Ni(0) complexes.^[69,70] Shortly after, Höberg and co-workers first isolated derivative **I** obtained from the coupling of 2-butyne and CO₂ with Ni(0) and TMEDA ligand (Scheme I.1.4).^[71–73]

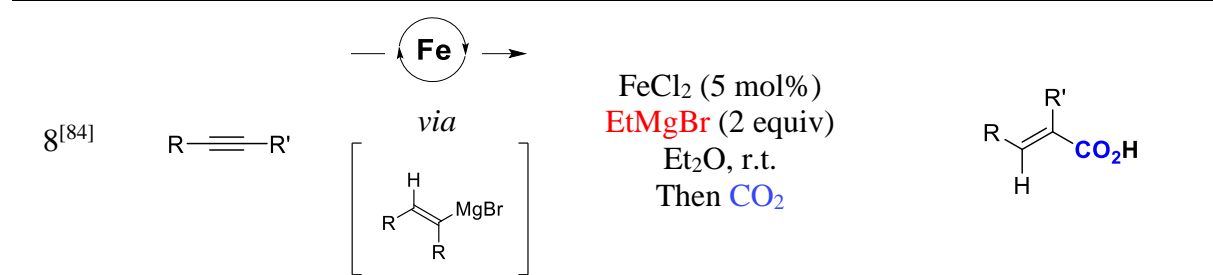


Scheme I.1.4. Isolation of oxanickelacyclopentene.

This stable species exhibited a wide range of reactivity, and a particular interest was given to the transformation of alkynes with CO₂ into acrylic acids.^[71–73] Saito and Yamamoto reported in 1999 the preparation of β -substituted acrylic acids through direct protonolysis of **I** (Table I.1.5, entry 1).^[74] The regioselectivity of Ni-catalyzed carboxylation of terminal alkynes was rationalized by DFT calculations, suggesting that the formation of the kinetically preferred **I** results from CO₂ insertion at the less substituted carbon position.^[75–77]

Table I.1.5. Examples of metal-catalyzed carboxylation of alkynes.

Entry	Substrate	Catalyst /Ligand	Reaction conditions	Product Yield [%]
1 ^[74]	$R-C\equiv C-H$		Ni(cod) ₂ (1 equiv) DBU (2 equiv) CO ₂ (1 atm) THF, 0 °C then H ₃ O ⁺	$R-CH=CH-CO_2H$ R = <i>t</i> Bu, 72% R = TMS, 58%
2 ^[78]	$Ph-C\equiv C-H$	 (L1)	Ni(cod) ₂ (1 equiv) (L1) (2 equiv) CO ₂ (1 atm) THF, 0 °C then H ₃ O ⁺	+ $Ph-C(=CH_2)-CO_2H$ R = H, R' = Me, 60% (98:2) R = Et, R' = H, 20% (7:93)
3 ^[79]	$R-C\equiv C-R'$	<i>via</i> 	Ni(cod) ₂ (1-3 mol%) ZnEt ₂ (3 equiv) CsF (1 equiv) CO ₂ (1 atm) MeCN, 60 °C	$R-CH=C(R')-CO_2H$ R = R' = Ph, 81% R = <i>t</i> Bu, R' = Ph, 91%
4 ^[80]	$Ar-C\equiv C-R$	 (L2)	[NiBr ₂ .glyme] (5 mol%) (L2) (6 mol%) <i>t</i> BuOH (1.5 equiv) Mn (1.5 equiv) CO ₂ (1 atm) DMF, 60 °C	$Ar-CH=C(R)-CO_2H$ Ar = Ph, R = Me, 85%
5 ^[81]	$R-C\equiv C-H$		[NiI ₂] (10 mol%) (L2) (25 mol%) H ₂ O (1.0 equiv) Mn (3.6 equiv) CO ₂ (1 atm) DMF, 25 °C Then H ₂ over Pd/C	$R-CH_2-CH_2-CO_2H$
6 ^[82]	$R-C\equiv C-R'$	<i>via</i> 	[Ni(acac) ₂ (bpy)] (10 mol%) MgBr ₂ (3.0 equiv) Zn (3.0 equiv) CO ₂ (1 atm) DMF, r.t.	 R = R' = Et, 60% R = Me, R' = Cy, 67%
7 ^[83]	$R-C\equiv C-R'$	 <i>via</i> 	Cu(IMes)F (1 mol%) (EtO) ₃ SiH (2 equiv) CO ₂ (1 atm) 1,4-dioxane, 100 °C	$R-CH=C(R')-CO_2H$ R = R' = Ph, 72% R = <i>t</i> Bu, R' = Ph, 71% R = Cy, R' = Ph, 88%



Iwasawa and co-workers demonstrated that the use of sterically hindered methylene substituted bis(amidine)ligands resulted in β -substituted acrylic acids from the cross-coupling of terminal alkynes with CO_2 , whereas reducing steric hinderance of the ligand reversed the regioselectivity toward α -substituted acrylic acids (Table I.1.5, entry 2).^[78] Another strategy proposed by Ma was to generate *in situ* stereo-defined 1-alkenyl zinc species from hydrozincation of alkynes with Et_2Zn ; the latter reacted with CO_2 to afford the corresponding carboxylic acid (Table I.1.5, entry 3).^[79]

While nickel catalysts proved to be particularly suited for CO_2 insertion into $\text{C}(sp)\text{--H}$ bonds, other examples of hydrocarboxylation reaction of alkynes were reported by Tsuji and Fujihara, using Cu catalysts bearing NHC ligands, achieving similar yields and regioselectivities (Table I.1.5, entry 7).^[83] In this case, the Cu^{I} -hydride metal species was generated *in situ* with an hydrosilane. The latter was added to an alkyne substrate to afford the copper alkenyl intermediate, followed by CO_2 insertion and σ -bond metathesis with the hydrosilane, thus, delivering the corresponding silyl ester. A similar strategy was also described by Chen and co-workers using FeCl_2 as catalyst (Table I.1.5, entry 8).^[84] Alkylation of the Fe-(pre)catalyst with EtMgBr , followed by β -H elimination, hydrometalation of the alkyne substrate and transmetalation with the Grignard reagent, afforded the vinylmagnesium bromide intermediate and regenerated the active Fe-alkyl species. The final step inserting CO_2 delivered the carboxylic acid product.

The group of Martin later developed an alternative protocol with organometallic reagents and high-molecular silanes, using simple, available and benign alcohols as hydride source.^[80] The milder Ni-catalyzed regioselective hydrocarboxylation of alkynes allowed to broaden functional group tolerance (Table I.1.5, entry 4). Later on, aliphatic terminal alkynes could be employed, using water as the hydride source, ultimately recovering α -branched aliphatic carboxylic acids after reduction with H_2 over Pd/C (Table I.1.5, entry 5).^[81] Tsuji and Fujihara assessed the feasibility of multiple CO_2 insertions across the alkyne platform toward the corresponding maleic anhydride (Table I.1.5, entry 6). For the second carboxylation to

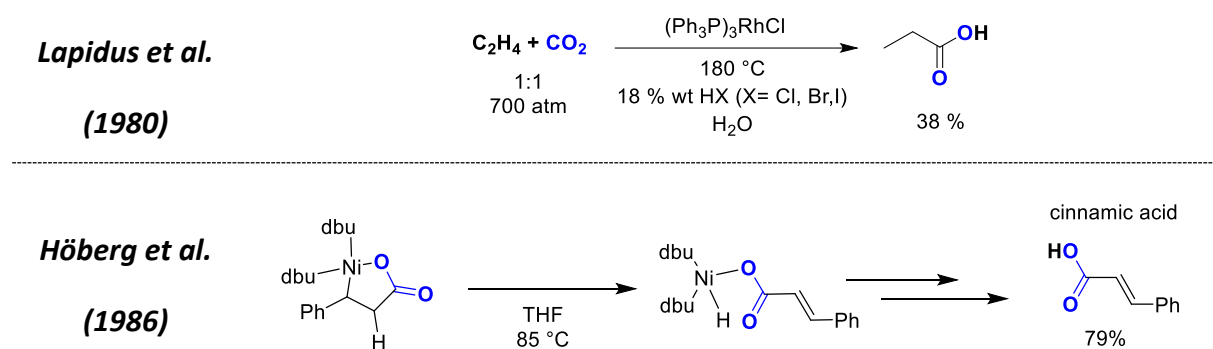
occur, the Lewis acidic MgBr_2 played an important role in facilitating the CO_2 insertion into the Ni–C bond of the oxanickelacyclopentene intermediate (Table I.1.5, entry 6).^[82]

b. $\text{C}(sp^2)$ –H bonds (alkenes)

Carboxylation reactions of olefins have the advantage of using abundant, inexpensive, non-toxic and available feedstocks – CO_2 and unsaturated hydrocarbons. Yet, compared to other activated π -systems (alkynes, allenes, dienes, diynes and so on), olefins display significantly lower reactivity. The following section describes the most relevant results on transition metal-catalyzed carboxylation reactions of alkenes with CO_2 .

Pioneering studies reported by Lapidus *et al.* in 1980 attested the feasibility of transforming ethylene and CO_2 into propionic acid using Rh and Pd catalysts in the presence of HBr under very harsh conditions (700 bar, 180 °C, Scheme I.1.5, top).^[85] This discovery encouraged chemists toward new developments in this area.

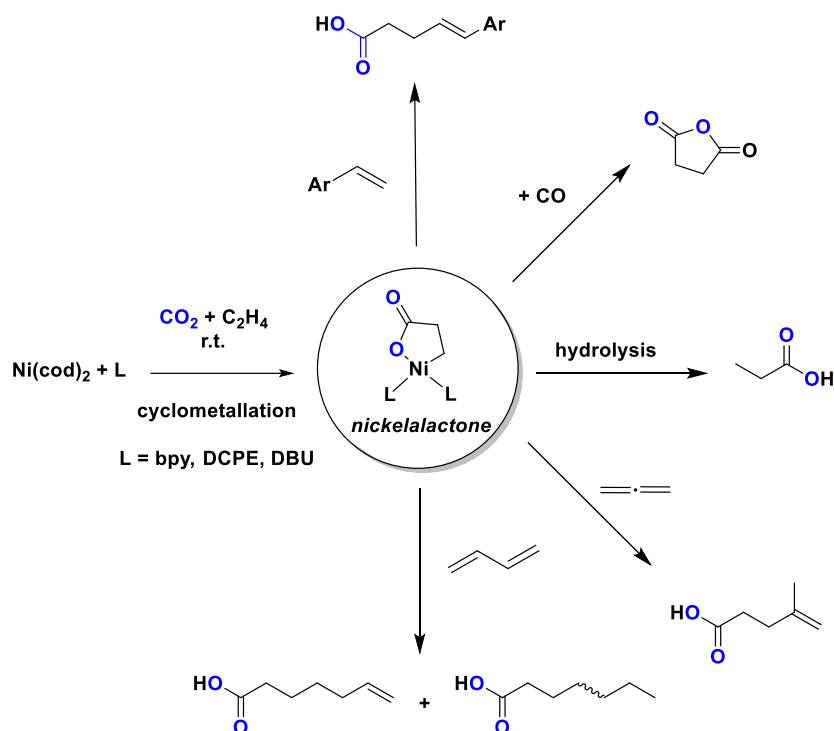
- *Early discovery: metalallactone formation*



Scheme I.1.5. (Top) Carboxylation reaction of carbon dioxide with ethylene using Rh^{I} precursor^[85] (bottom) Höberg's pioneering studies on β -hydride elimination from nickelalactone^[86].

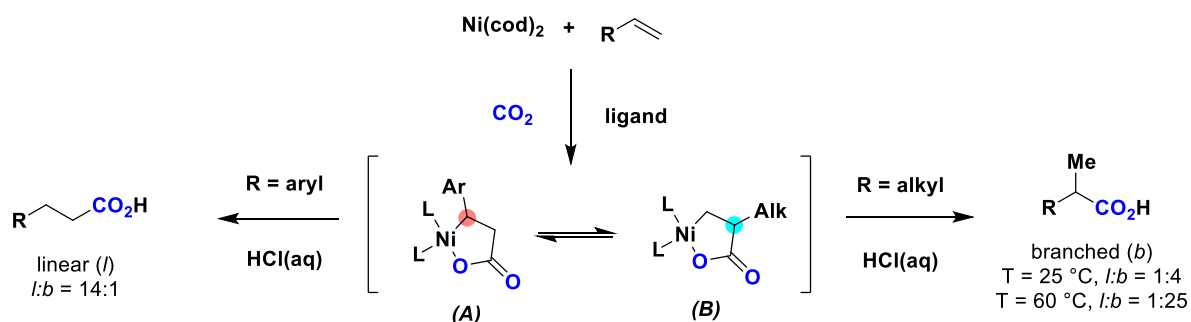
A few years later, Höberg and coworkers carried-out Ni(0)-induced coupling of CO_2 with styrene to afford the corresponding cinnamic acid in 79% yield (Scheme I.1.5, bottom).^[87] In 1987, upon mixing ethylene and CO_2 in presence of DBU, the same authors isolated the intermediate involved, a stable nickelalactone (Scheme I.1.6, 70% yield).^[87] The square planar 16-electron complex, whose structure was confirmed by X-ray crystallographic analysis, turned out to be a versatile reaction intermediate. For example, protonolysis of that nickelalactone afforded propionic acid in good yield (85%). The 5-membered metalallactone also allowed to access various carboxylic acids by coupling with 1,3-dienes, allenes, carbon monoxide and other alkenes.^[86–89] Unfortunately, all reductive eliminations to give carboxylic

acids were not followed by Ni(0) complex regeneration, which is mandatory for the catalytic reaction.



Scheme I.1.6. Formation and reactivity of nickelalactone complex.

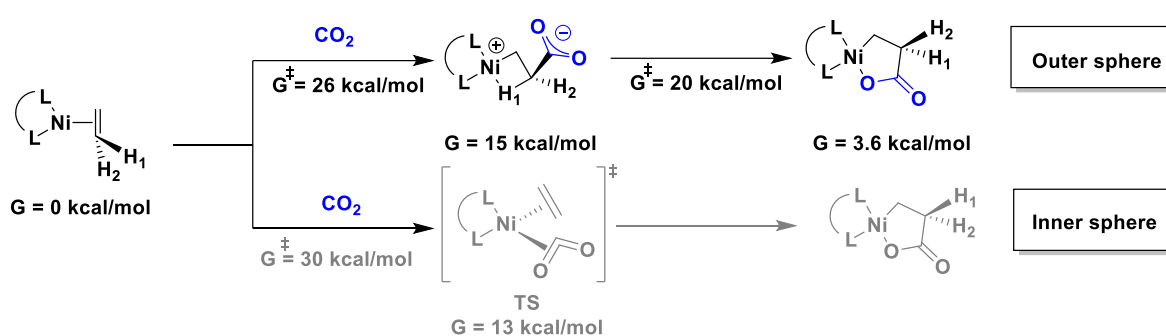
Attempts to tackle regioselectivity issues in the reactions with monosubstituted alkenes were undertaken upon varying the temperature and/or the electronic features of the alkene. For instance, the use of styrenes led to preferably nickelalactones (A) with the metal center bonded at the benzylic position, whereas regular α -olefins gave a mixtures of nickelalactones at room temperature (Scheme I.1.7, (A) and (B)).^[90] Formation of less-sterically-congested nickelalactone was however favored when rising temperature.



Scheme I.1.7. Regioselectivity in the formation of nickelalactone.

In addition, the ligand was found to play an important role on site-selectivity. For example, the use of bidentate phosphines or electron-rich imines allowed achieving good yields whereas disproportionation of CO₂ to CO was observed when using bipyridine ligands.^[90]

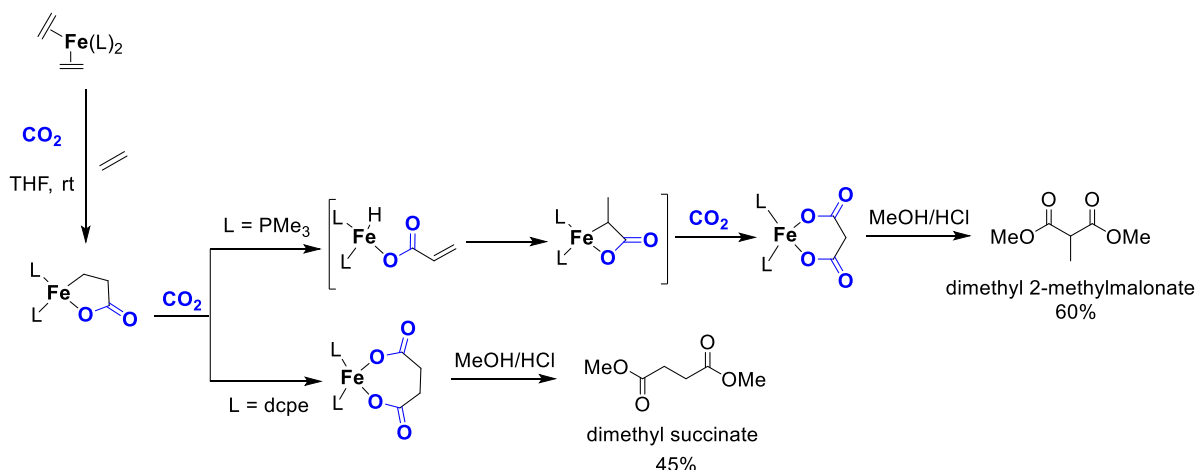
In order to establish the mechanism of nickelalactone formation, DFT calculations were conducted on Ni(0) complexes and bidentate ligands systems.^[17,91–93] These studies suggested that the five-membered metallacycle is formed *via* oxidative cyclization according to an “outer sphere” pathway, starting from a Ni(0) π -complex with ethylene, followed by CO₂ attack at the olefin ligand (Scheme I.1.8).^[94]



Scheme I.1.8. Competing outer- and inner-sphere mechanisms of lactone formation.^[95]

Another possible pathway involves an “inner-sphere” mechanism, which was found to be highly affected by ligand steric hindrance.^[95] Within the homologous series of bidentate phosphines d’bpm, d’bpe and d’bpp, the broadening of the bite angles enhances steric bulk and leads to an increase of the “inner-sphere” barrier mechanism while the analogous barrier for the “outer-sphere” mechanism is less affected.^[95] Moreover, attack of the CO₂ on the ethylene-ligand for the “outer-sphere” mechanism occurs without preliminary coordination of CO₂ to the metal center.

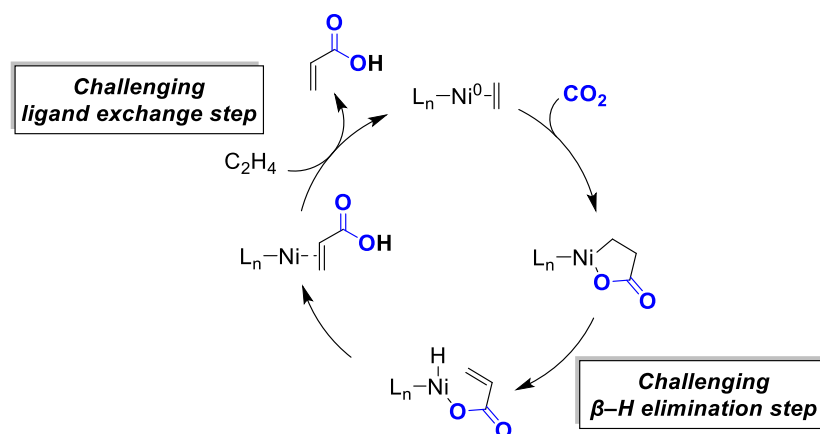
The oxidative cyclization of unsaturated hydrocarbons with CO₂ was however not only limited to Ni(0) species. Similar studies have been conducted upon using Ti(II)^[96], Zr(II)^[97] and Fe(0)^[89] precursors. For example, the use of [(PEt₃)₂Fe(C₂H₄)₂] enabled the formation of oxaferracyclopentanones upon reaction with CO₂ (Scheme I.1.9). Once again, the nature of phosphine ligands demonstrated a significant influence on the regioselectivity. Whereas a monodentate phosphine ligand (PMe₃) gave rise to methylmalonate product, a bidentate ligand (bis(dicyclohexylphosphino)ethane, DCPE) afforded the regioisomeric dimethyl succinate. Herein, multiple CO₂ insertion reactions turned out to be interesting, as nickelalactones do not typically trigger this characteristic.



Scheme I.1.9. Oxidative cyclization of C_2H_4 , CO_2 and $Fe(0)$ species and influence of the ligands on the dicarboxylic acids formation.^[89]

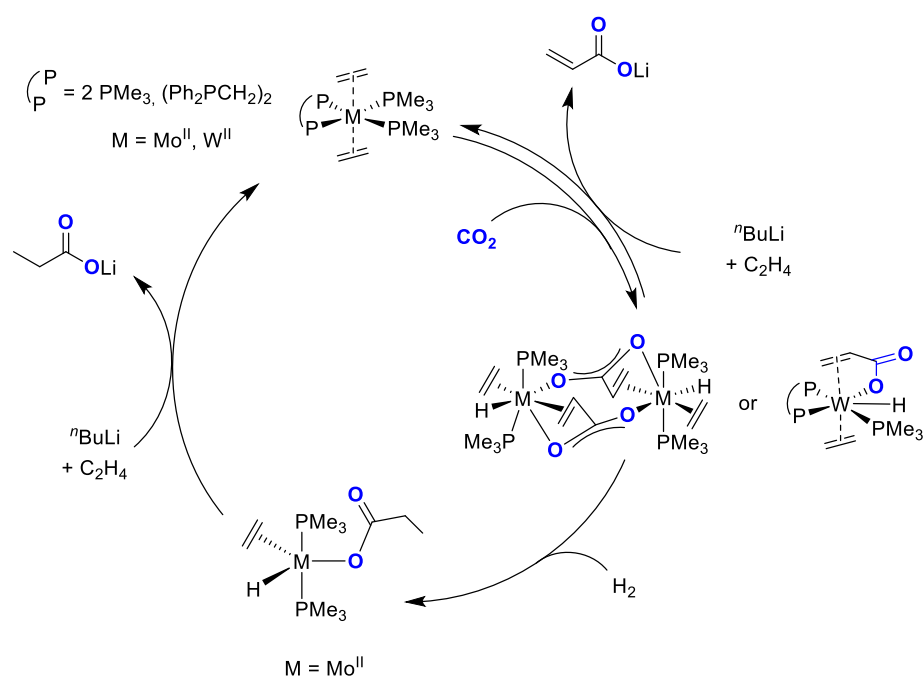
- *Towards acrylic acid synthesis*

Although important achievements have been accomplished in order to facilitate carboxylic acids formation, one “dream reaction” kept intriguing both academic and industrial fields: the direct synthesis of acrylic acid. From an atom economy points of view, the acrylate building block could be directly obtained from the cross-coupling reaction of ethylene and CO_2 . Although extremely attractive, this reaction exhibits many obstacles (Scheme I.1.10). First of all, the overall process is highly endothermic, therefore unfavourable, ($\Delta G_R^0 = 10.2 \text{ kcal}\cdot\text{mol}^{-1}$).^[98] The nickelalactone intermediate appeared to be a relatively stable species.^[99] Furthermore, theoretical calculations showed that the kinetic barrier of the β -H elimination step is particularly high ($\Delta G^\ddagger = +42.5 \text{ kcal}\cdot\text{mol}^{-1}$) due to the substantial five-membered ring strain, which prevents $Ni\cdots H$ agostic interactions.^[92,100,101]



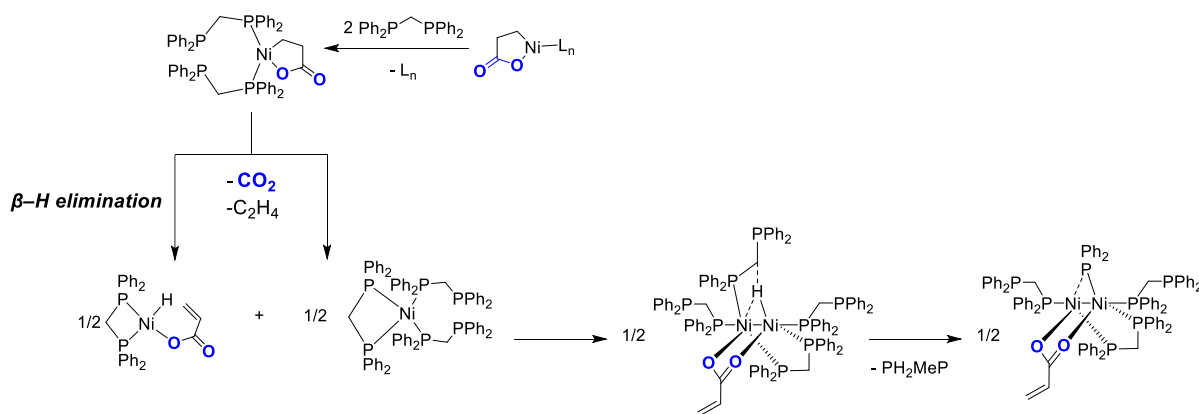
Scheme I.1.10. Direct acrylic acid formation from ethylene carboxylation reaction.

Early works, conducted in 1985 by Carmona and co-workers, dealt with the recovery of the low valent metal active species. Thus, using Mo(0) and W(0) precursors, exposed to ethylene and carbon dioxide readily underwent oxidative coupling reaction, from which stable hydrido-M(II)-acrylate products were isolated (Scheme I.1.11).^[102–105] This work represented the first attempt towards the direct synthesis of acrylic acid from CO₂ and C₂H₄. Unlike Hoberg's stable nickelalactone intermediate, the analogous Mo(II) and W(II) metallacycles were not observable and, thus, it was suggested that a rapid β-H elimination led to the more stable hydrido-M(II)-acrylate complexes. Upon treatment of the Mo hydride-M(II)-acrylate species with ⁿBuLi under ethylene atmosphere, lithium acrylate was identified. On the other hand, hydrogenation of the acrylate complex under H₂ atmosphere (1 bar, 20 °C) provided a hydrido-M(II)-propionate species which further released the propionic acid salt of Li upon treatment with ⁿBuLi (Scheme I.1.11). The use of such a strong nucleophile illustrated the difficulty of achieving reductive elimination to regenerate the ethylene-coordinated complex.



Scheme I.1.11. C₂H₄ carboxylation catalyzed by Mo- and W-ethylene complexes.^[102–105]

In 2006, Walther and co-workers revealed the formation of acrylate from a nickelacycle upon complexation with bidentate ligands.^[106] *In situ* ligand exchange with bis(diphenylphosphino)methane (dppm) allowed the first β-H elimination from a well-defined metalalactone affording a stable Ni(I)-Ni(I) dimer (Scheme I.1.12). However, the release of the acrylic acid product was not achievable in this study.

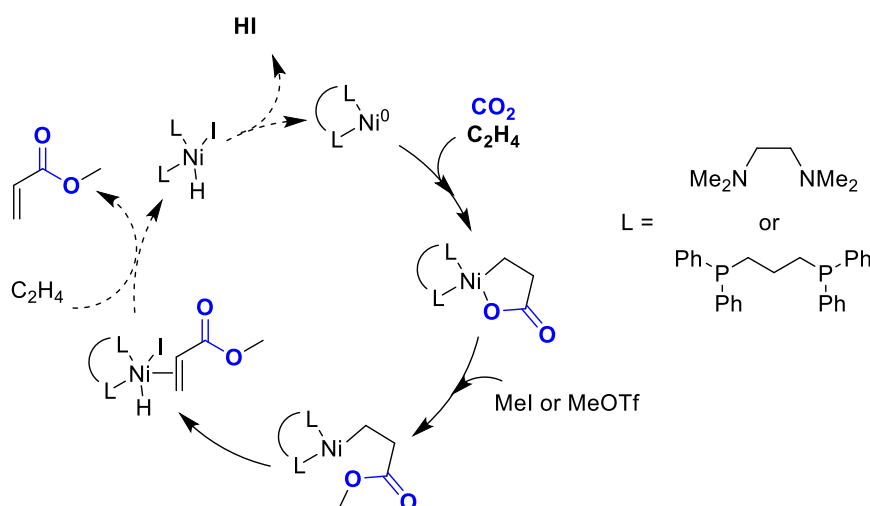


Scheme I.1.12. Walther's possible pathway for the formation of metallacycle nickel carboxylate.^[106]

In view of the unfruitful attempts to enable the prompt release of acrylic acid from the parent metallactones, development of new strategies have emerged, aiming first at releasing ring strain and facilitating β -H elimination.

- *Acrylate recovery via M–O metallactone bond cleavage*

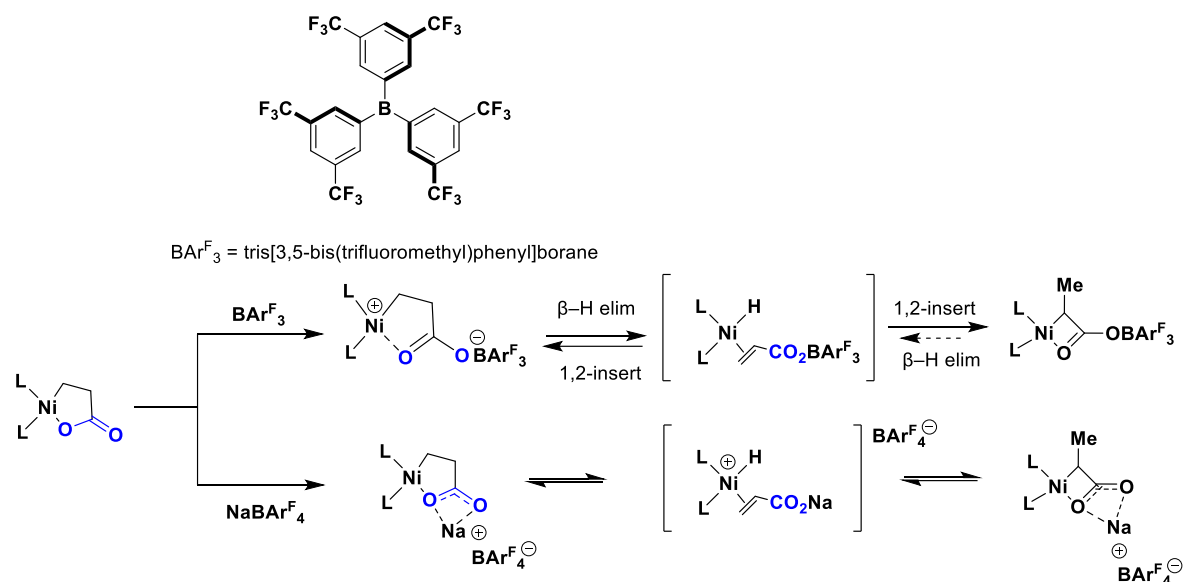
On the basis of the previous results, Riecker and Kühn conducted nickelacycle ring-opening alkylation with methylating agents (Scheme I.1.13).^[107,108] Using diamine or diphosphine bidentate ligands, the nickelacycle underwent β -H elimination in neat MeI. *In situ* methylation released the corresponding methyl acrylate with a maximum yield of 33%. However, the regeneration of the active Ni(0) species was still not accessible, making the reaction so far not catalytic.



Scheme I.1.13. Hypothetical catalytic cycle of nickelactone-ring-opening esterification toward acrylate synthesis.^[107,108]

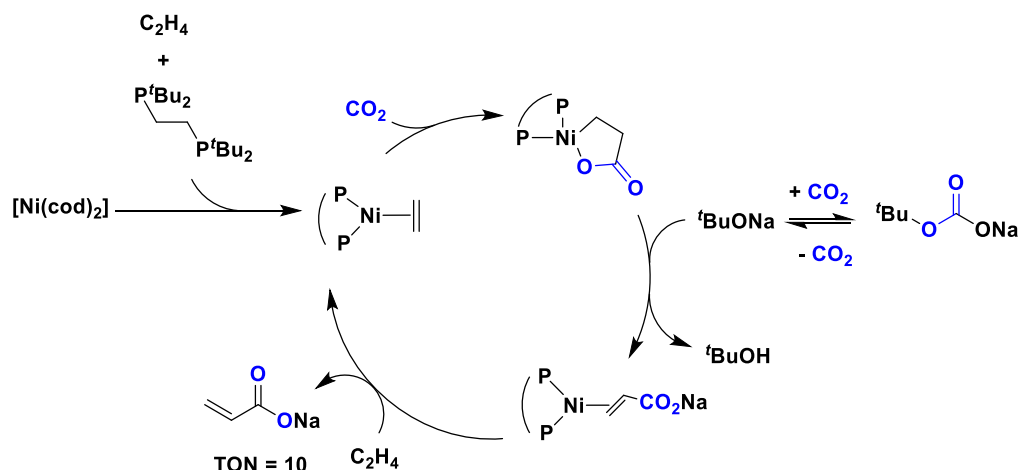
Inspired by the earlier studies based on the hydrolysis of metallactones using Brønsted acids,^[86,87,89,100] Bernskoetter and co-workers were able to ring-open the nickelalactone

intermediate by using Lewis acids (LA).^[109,110] Coordination of the LA (e.g. tris[3,5-bis(trifluoromethyl)phenyl]borane, BAr^{F_3}) to the carboxylate moiety induced β -H elimination followed by subsequent 1,2-insertion of the acryl borate ligand into the Ni–H bond, generating a four-membered nickelacycle. Herein, stoichiometric amounts of metal precursor were used and further decomposed, failing therefore in the catalytic carboxylation reaction of ethylene.



Scheme I.1.14. Pathways for formation of 2,1-acryl borate reinsertion product and reversible β -hydride elimination.

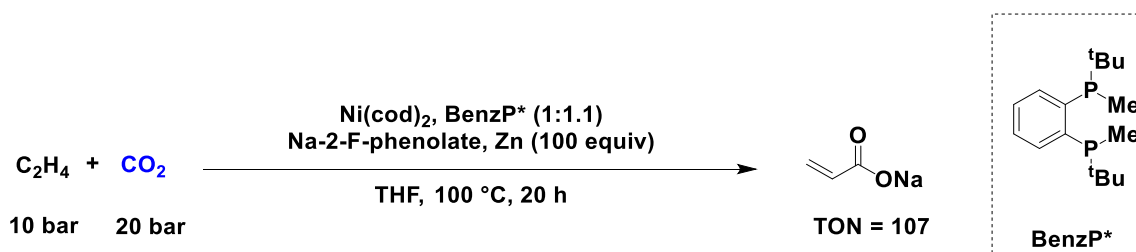
Additional theoretical studies showed the importance of adding a base to capture the Ni–H intermediate and release the targeted acrylate salt.^[111,112] Using the computational results, Limbach and co-workers described in 2012 the first catalytic carboxylation of ethylene and carbon dioxide using $\text{Ni}(\text{cod})_2$, the bidentate phosphine ligand *d*^tbpe and ^tBuONa as a base.^[113] The elementary steps of the catalytic cycle were established; nickelalactone formation was achieved under high pressures of CO_2 , whereas metallacycle cleavage and acrylate/ethylene exchange steps were carried out at lower pressures (Scheme I.1.15). The role of the base was effectively attributed to its capacity to abstract one of the lactone's acidic α -proton to the carbonyl group, which further undergoes ligand exchange with ethylene. On the other hand, the authors pointed out that strong bases, in presence of high pressures of CO_2 , form stable carbonates, becoming therefore useless in the direct deprotonation of the metallalactone under these reaction conditions. To tackle this issue, a two-stage carboxylation methodology was developed, in which pressurization and depressurization cycles were repeated, and thus giving access to a maximum TON of 10 of sodium acrylate.



Scheme I.1.15. Catalytic cycle for the formation of sodium acrylate salts from CO₂, ethylene, and ^tBuONa as a base.

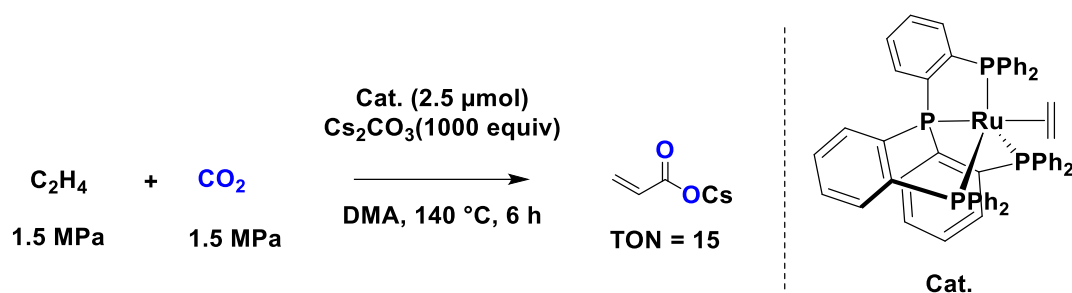
Hence, the following studies aimed at identifying a base compatible with all the individual steps of the catalytic cycle, and featuring (a) sufficient basicity to deprotonate the α -H of the carbonyl group of the metallalactone b) poor nucleophilicity to avoid irreversible reaction with CO₂.

In 2014, Limbach and Schaub efficiently modified the prototype system by using less nucleophilic substituted metal phenoxides to promote the formation of Ni(0)-acrylate complex (Scheme I.1.16).^[114,115] Thus, the targeted sodium acrylate was obtained with TONs up to 107. Apart from ethylene, a broad range of activated alkenes delivered the corresponding α,β -unsaturated carboxylic acid salts.



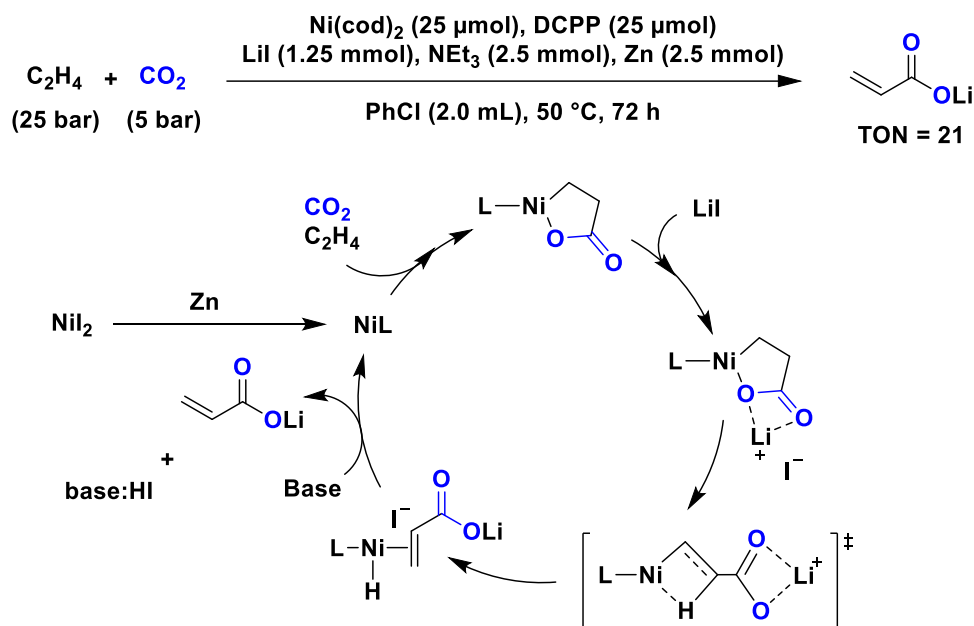
Scheme I.1.16. Formation of sodium acrylate salts from CO₂, ethylene, and metal phenoxide as a base.

On the other hand, Iwasawa and co-workers achieved a TON of 15 using 1000 equiv of Cs₂CO₃ as a base (C₂H₄:CO₂, 1:1, 180°C, 6h). The study reported the first utilization of RuH(OAc)(PPh₃)₃ as precursor, in combination with the tetradentate phosphine ligand tris[2-(diphenylphosphino)phenyl]phosphine, for oxidative cyclization of C₂H₄ and CO₂ (Scheme I.1.17).^[116] The authors published the first example of formation and isolation of ruthenolactone species, which has been confirmed by XRD-analysis.^[117]



Scheme I.1.17. Catalytic synthesis of acrylate salt using Ru(C₂H₄) complex bearing a tetradentate phosphine ligand.

Following a different strategy, Vogt and co-workers elaborated a strong Lewis acid-induced β-H elimination.^[118] In the presence of stoichiometric amounts of LiI, stoichiometric amounts of Et₃N and Zn-dust, regeneration of the active catalyst species was achieved, and lithium acrylate was obtained with a TON of 21 (Scheme I.1.18).



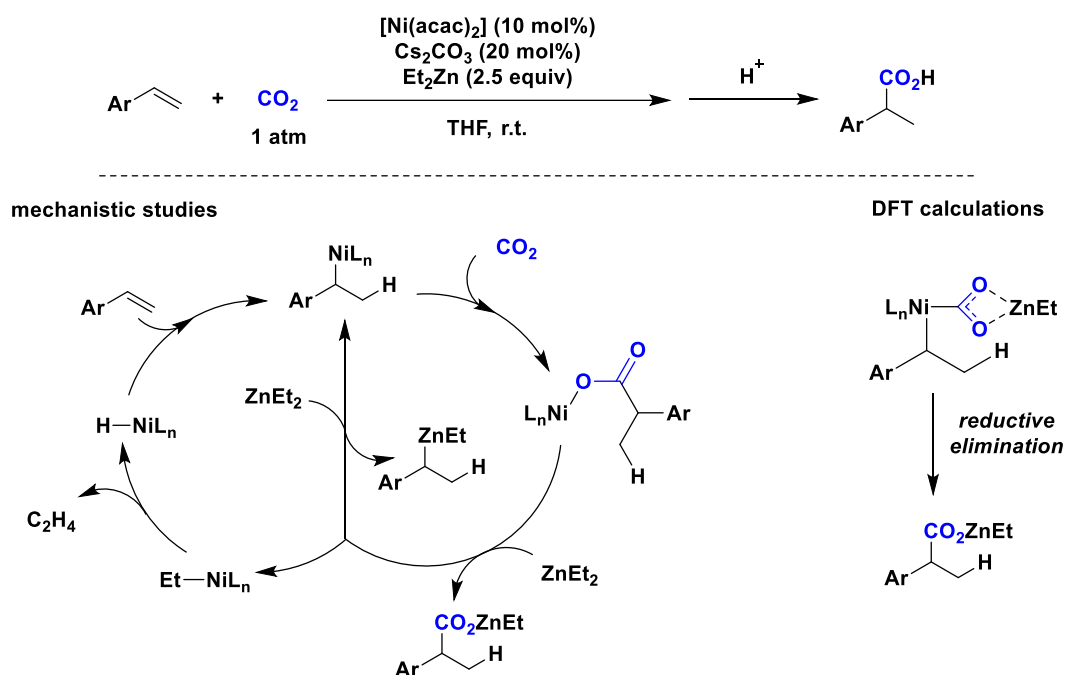
Scheme I.1.18. Vogt and co-workers' strong Lewis-induced β-H elimination.^[118]

Although promising results were obtained, the above suggested protocols still suffered from a lack of efficiency (poor TONs) towards a scalable production of acrylic acid or its derivatives from CO₂ and ethylene.

- *Hydrocarboxylation reaction of alkenes*

In parallel to the above mentioned studies, tremendous efforts were made to incorporate not only ethylene but other alkenes in an effective catalytic process. Inspired by Hoberg's work on nickelalactones, Rovis and co-workers developed in 2008 a nickel-catalyzed

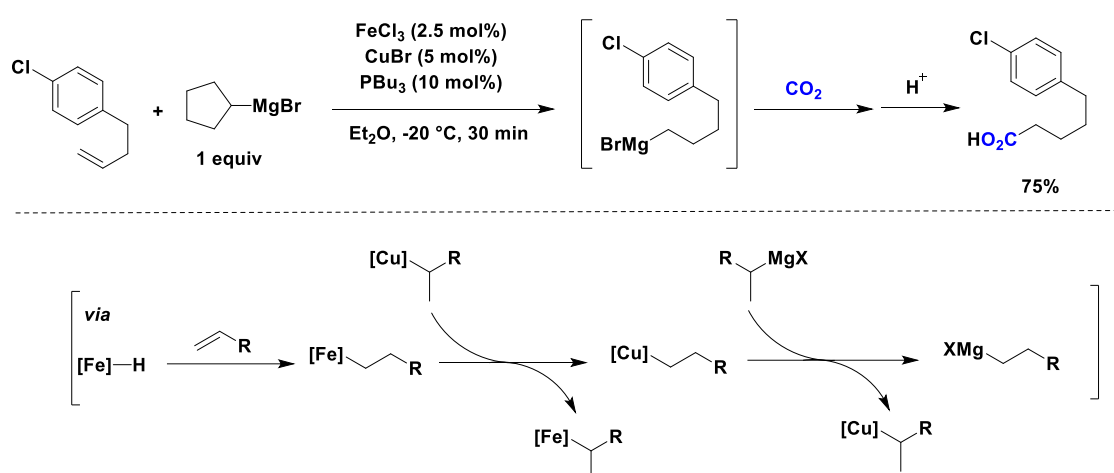
hydrocarboxylation of styrenes with CO₂.^[4,119] Under mild conditions (CO₂ 1 bar, 25 °C), a nickel precursor ([Ni(cod)₂ or [Ni(acac)₂] 10 mol%), a base additive (Cs₂CO₃, 20 mol%) and Et₂Zn as reductant (2.5 equiv) led to the corresponding phenyl acetic acids after hydrolytic workup (Scheme I.1.19). The reaction was tolerant to various functional groups such as nitriles, ketones, esters and aryl chlorides and was extended to other styrene analogues bearing electron-deficient and neutral substituents.



Scheme I.1.19. Rovi's hydrocarboxylation of styrenes.

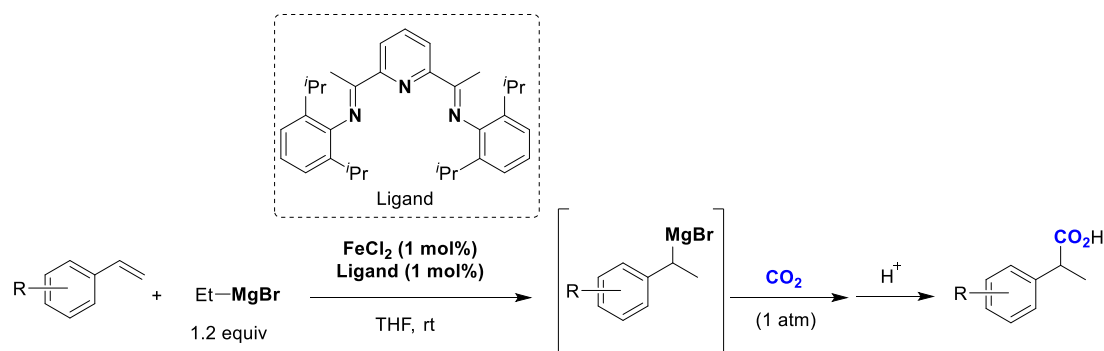
The authors suggested that the active catalyst involved in the mechanism is a Ni-hydride species generated upon transmetalation with Et₂Zn, then β-H elimination steps. Posterior theoretical calculations, conducted by Lin and Yuan for this process, revealed that, while the generation of nickelalactone intermediate was thermodynamically favoured, the mechanism remains kinetically driven by the formation of nickel-hydride species.^[120] The 2,1-insertion of the styrene substrate into the Ni–H bond affords a benzyl nickel species, which undergoes sequential insertion of CO₂ followed by subsequent transmetalation and regeneration of the precatalyst through β-H elimination. Hence, the dual role for Et₂Zn was confirmed, acting both as a hydride source and transmetalating agent for the reaction of benzyl nickel intermediate with CO₂. The system enabled to obtain α-carboxylated product in moderate to high yields. This result constitutes an important advance in the field of catalytic carboxylation reactions. However, the main drawback remained the generation of stoichiometric amounts of waste due to the use of excess of organometallic reductant (Et₂Zn).

Following a different strategy, Hayashi and co-workers developed in 2012 a Fe/Cu cooperative catalytic system for the hydromagnesiation/carboxylation of terminal alkenes.^[121] Interestingly, the first Fe-catalyzed hydrocarboxylation of unactivated alkene substrates and CO₂ was achieved using an alkyl Grignard reagent as the hydride source. In this process, insertion of the alkene into the Fe–H of active species afforded a Fe–alkyl product, which was then converted into the respective alkylcuprate. Subsequent transmetalation with alkyl Grignard reagent resulted in the corresponding primary alkyl Grignard reagent that ultimately lead to the targeted linear carboxylic acids by reaction with CO₂ with high levels of regioselectivity (Scheme I.1.20).



Scheme I.1.20. First Fe-catalyzed hydroxycarboxylation of alkene and CO₂.

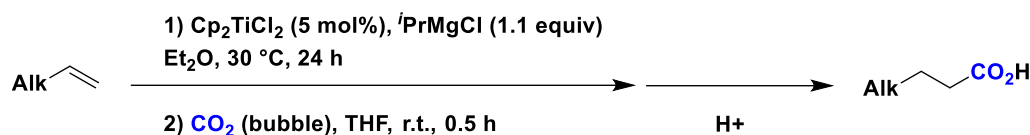
Shortly after, a similar approach was reported by Thomas towards phenyl-substituted acetic acids from electron-rich styrenes using FeCl₂/bis(imino)pyridine combination and EtMgBr reagent as hydride source (Scheme I.1.21).^[122]



Scheme I.1.21. Fe-catalyzed hydromagnesiation and subsequent carboxylation of styrenes.

The use of EtMgBr, rather than Hayashi's previous cyclopentenyl magnesium bromide, resulted in branched carboxylic acids, highlighting the importance of the nature of the hydride source on the regioselectivity. Moreover, mechanistic investigation showed a highly regioselective and reversible Fe-catalyzed hydrometalation, giving an α -aryl Grignard reagent, and occurring without the need for any additional Cu-catalyst.^[14]

In addition to Ni and Fe systems, Xi and co-workers successfully catalyzed hydrocarboxylation of alkenes with CO₂ using Cp₂TiCl₂ as precursor (Scheme I.1.22).^[123] The highly active "titanium hydride" species was generated in the presence of Grignard reagent (ⁱPrMgCl). Similarly to Hayashi's and Shirakawa's catalytic experiments, reactions of aliphatic alkenes provided the corresponding linear carboxylic acids whereas electron-rich styrene derivatives afforded α -aryl-carboxylic acids.

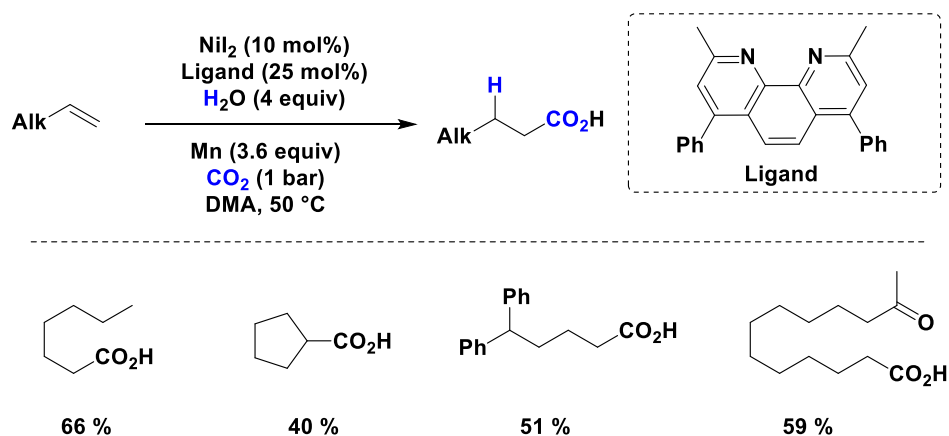


Scheme I.1.22. Ti-catalyzed hydromagnesiation/carboxylation of olefins.

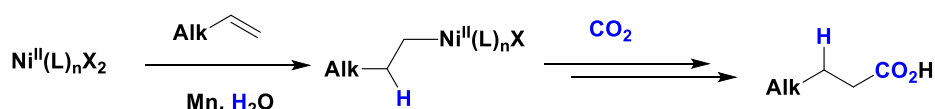
These established methodologies for hydrocarboxylation of activated unsaturated hydrocarbons required stoichiometric amounts of highly reactive organozinc or Grignard reagents. Generation of excess organometallic wastes and harsh reaction conditions remained the main drawbacks of these strategies. Exploring more readily available hydride sources or reductants toward catalytic hydrocarboxylation appeared to be as promising and challenging goal, which are being tackled by several research groups.

For instance, the group of Martin recently discovered the use of water as a mild, inexpensive and safe hydride source in catalytic hydrocarboxylation of unactivated olefins under atmospheric pressure of CO₂.^[124] In contrast to previous procedures, mild conditions were found compatible with a broad range of functional groups, achieving high chemoselectivities (Scheme I.1.23, top). Trying to provide a rationale behind the site selectivity in the case of olefins, the authors hypothesized that the reaction proceeds first via hydrometalation of the alkene substrate, as confirmed by deuteration experiments. Because of the bulkiness of the metal center provided by the adjacent aliphatic side-chain, the formation of a linear alkyl nickel product is more favoured (Scheme I.1.23, bottom). Interestingly, the

protocol could be extended to internal acyclic olefins as well as to ethylene (NiI_2 (0.41 mol%), Ligand (0.98 mol%)), affording in the latter case propionic acid with a TON of 20.

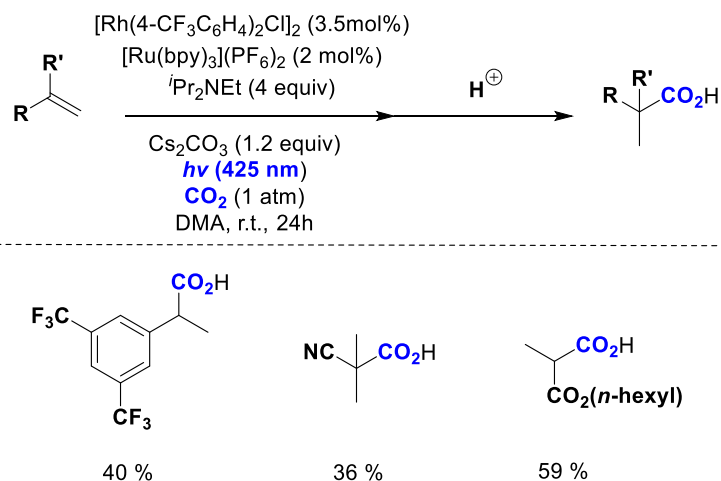


Origin of site-selectivity in the carboxylation of aliphatic alkenes



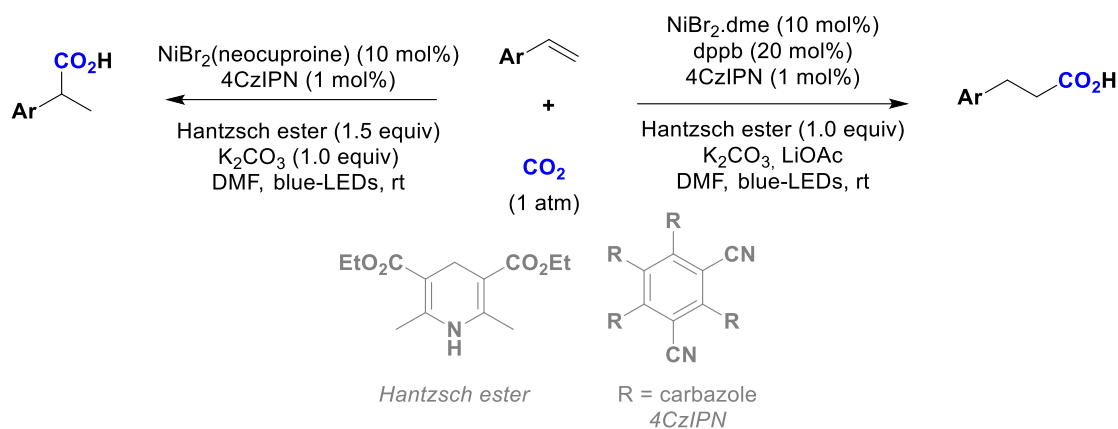
Scheme I.1.23. Carboxylation of unactivated terminal α -olefins.

Inspired by nature to mimic photosynthesis by plants, innovative strategies merging transition-metal catalysis and photocatalysis emerged for the photocarboxylation of styrenes and electrodeficient alkenes. In 2017, the group of Iwasawa reported the utilization of Rh(I) hydride complex, triggering a regioselective hydromatellation of the alkene substrate followed by subsequent carboxylation (Scheme I.1.24).^[125] Regeneration of the Rh(I) hydride species is expected to occur by electrons and proton transfer of the carboxylated Rh alkyl complex, generating a Rh(III) species, and followed by the release of the carboxylic acid in presence of a base.



Scheme I.1.24. Rh-catalyzed photocarboxylation of electrodeficient alkenes.

On the other hand, the group of König described a dual visible-light-Ni catalysis and based on the *in situ* generation of a Ni(0) active species under mild photocatalytic conditions, implying the use of Hantzsch ester as reductant and 1,2,3,5-tetrakis(carbazol-9-yl)-4,6-dicyanobenzene (4CzIPN) as photosensitizer. Interestingly, according to the ligand employed, phenyl acetic acids or linear carboxylic acids are obtained in moderate to good yields (Scheme I.1.25).^[126]



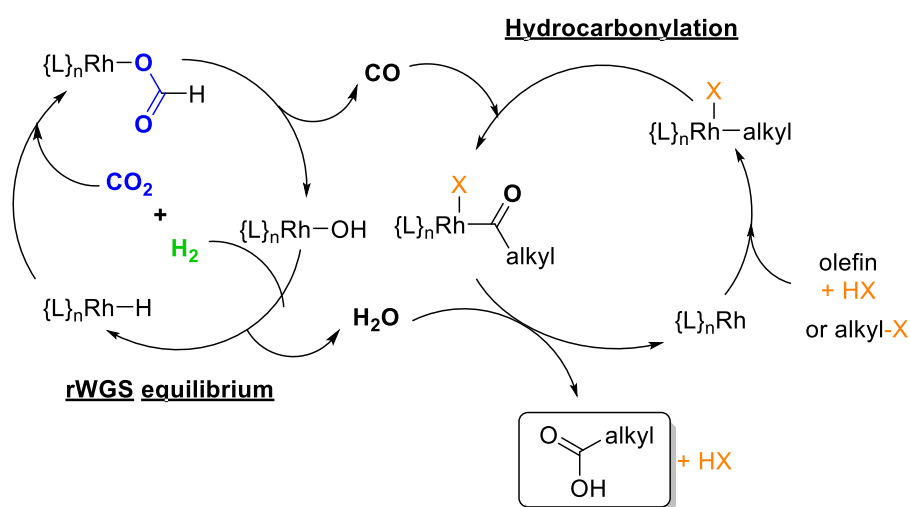
Scheme I.1.25. Ni-catalyzed photocarboxylation of styrene and electrodeficient alkenes.

- **Carbonylation and hydroformylation reactions**

Aside from the direct carboxylation methodologies, carbonylation techniques of unactivated alkenes with CO_2 including a hydroformylation/reduction sequence have emerged. These strategies are based on the reaction of the active C1 synthon (CO), released *via* reverse water-gas-shift reaction (rWGSR) in the presence of reducing agents such as H_2 or alcohols.

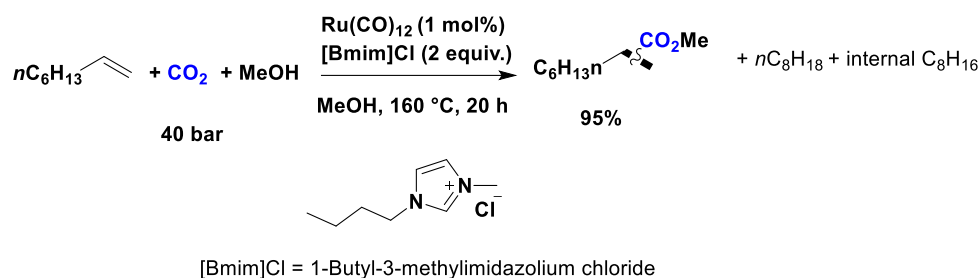
For example, Leitner and coworkers reported the multi-component system involving $[\text{RhCl}(\text{CO})_2]_2/\text{PPh}_3/p\text{TSA}\cdot\text{H}_2\text{O}$ as precatalyst, CH_3I as promoter and H_2 as reductant.^[127] In

that case, the proposed global catalytic cycle incorporates two interlinked loops (Scheme I.1.26): the first one sets up an equilibrium between CO_2/H_2 and $\text{CO}/\text{H}_2\text{O}$ through rWGSR intermediated by a putative Rh-hydrido species, while the second equilibrium leads to formation of a Rh-alkyl intermediate, followed by carbonylation. The intrinsic feature of this mechanism is the absence of a carboxylate intermediate in the hypothesized principal hydroxycarbonylation cycle. The overall reaction occurs in acetic acid under rather harsh conditions (60 bar of CO_2 and 10 bar of H_2 pressure, 180 °C, 2.5 mol% $[\text{RhCl}(\text{CO})_2]_2$, 25 mol% PPh_3).



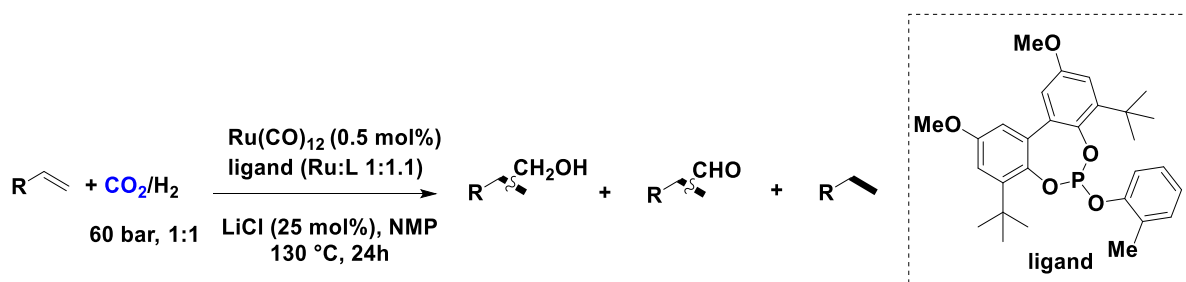
Scheme I.1.26. Proposed mechanism for Rh-catalyzed hydroxycarbonylation–“hydrocarboxylation” of olefins.^[127]

More recently, the group of Beller demonstrated the utility of reacting CO_2 (40 bar, 160 °C, 20 h) and alcohols (MeOH and EtOH) for alkoxy carbonylation of olefins (Scheme I.1.27).^[128] Although the reaction mechanism remained unclear, the first step of the major reaction pathway is believed to be reduction of CO_2 with MeOH to CO. In the next step, alkenes undergo carbonylation and react with alcohol to afford the corresponding esters. A number of aliphatic olefins as well as styrenes were also induced in the reaction with carbon dioxide using $\text{Ru}_3(\text{CO})_{12}$ (1.0 mol%), 1-butyl-3-methylimidazolium chloride (2.0 equiv. vs. alkenes) and the corresponding alcohol, giving high yields of industrially relevant esters without any addition of strong reductant.



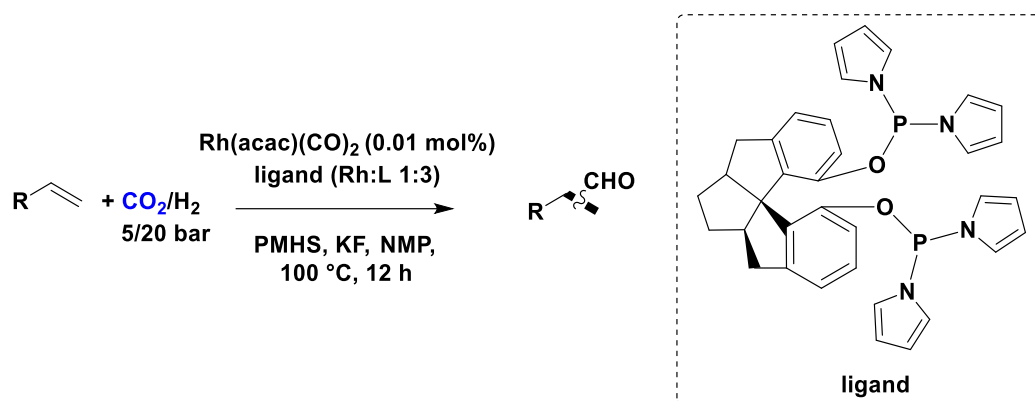
Scheme I.1.27. Methoxycarbonylation of 1-octene with carbon dioxide and methanol.^[128]

Beller and co-workers also showed that the same Ru precursor in combination with phosphite ligands can catalyse carbonylation of both terminal and internal alkenes to linear alcohols through a domino reverse water gas shift (rWGS)/hydroformylation/reduction reaction sequence under CO₂/H₂ atmosphere (30:30 bar, 130 °C, 24 h, Scheme I.1.28).^[129]



Scheme I.1.28. Ru-catalyzed hydroformylation/reduction of alkenes with carbon dioxide.^[129]

In 2017, Xia and coworkers reported a reductive coupling of CO₂ with linear and cyclic alkenes in the simultaneous presence of both H₂ and PMHS (polymethylhydrosiloxane) as reductants, using Rh(acac)(CO)₂/phosphine as precatalyst (0.01 mol%, 0.1 equiv of KF, NMP, 5 bar CO₂ and 20 bar H₂, 100 °C, Scheme I.1.29).^[130] High yields (up to 60%) of linear and branched aldehydes were obtained after 12 h. In the absence of one of the two co-reductants, higher amounts of alkene isomerization products (*i.e.* internal olefins) were formed. The mechanism of this process, apparently intermediated by formation of formic acid, still remains unclear.



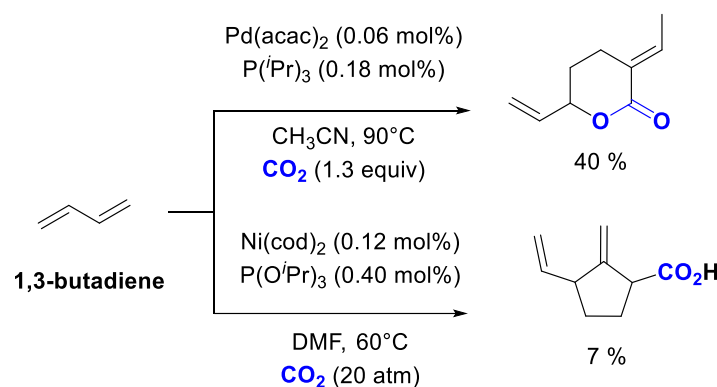
Scheme I.1.29. Transition-metal-catalyzed carbonylation of olefins with CO₂ and H₂.^[130]

Although considered as remarkable developments, the lack of controlled CO₂ regiochemical incorporation into the unsaturated hydrocarbons backbone, as well as the need for elevated temperatures and high pressures, still hamper easy access to carboxylic acids.

c. Catalytic carboxylation of dienes and other polyunsaturated systems

With the advantage of having an additional unsaturated bond for further functionalization, reactions between 1,3-dienes and CO₂ have been extensively studied since the 80's, when Behr and Höberg reported the telomerisation of butadiene in the presence of CO₂.^[131,132]

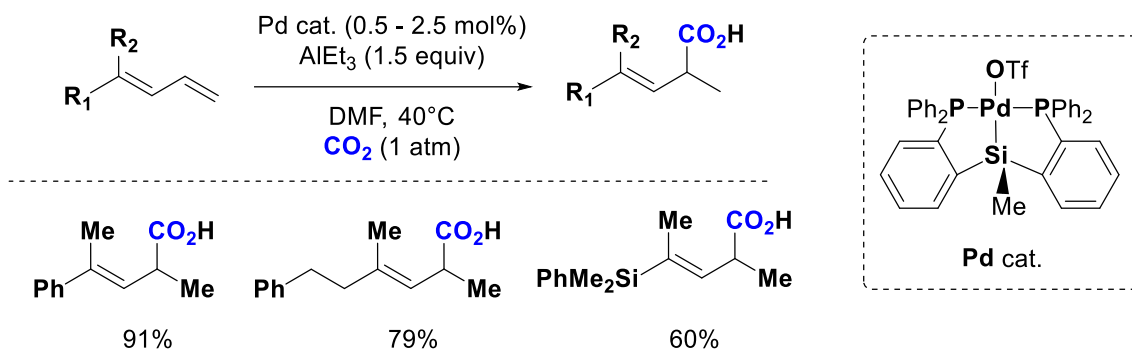
Depending on the nature of the precatalyst, different reactivities and selectivities were observed, as shown in Scheme I.1.30. The Pd-catalyzed reaction of CO₂ and butadiene led to the formation of lactone products, whereas the Ni-catalyzed reaction afforded carboxylic acid, both pathways involving an allylic metal complex as intermediate.



Scheme I.1.30. Carboxylation of 1,3-diene reported by Behr and Höberg.

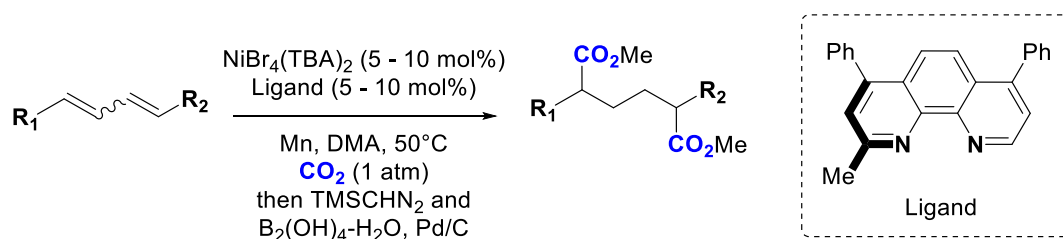
In 2011, the group of Iwasawa described a pincer-type Pd(II)-catalyzed hydrocarboxylation of 1,3-dienes (Scheme I.1.31).^[133] The use of AlEt₃ as the terminal reducing

agent was necessary to form the β,γ -unsaturated carboxylic acids, without traces of neither competitive telomerisation nor 1,2-dicarboxylation side-products.



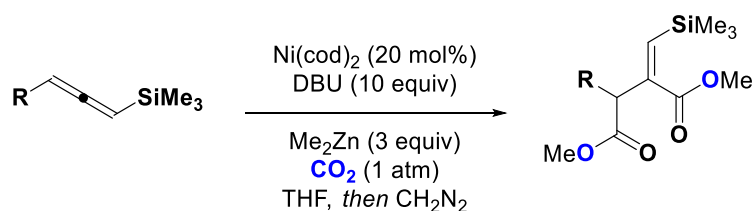
Scheme I.1.31. Hydrocarboxylation of 1,3-dienes.

Few years later, Martin and co-workers published a site selective protocol for the synthesis of adipic acids from 1,3-dienes and CO_2 . It was found that the use of 1,10-phenantroline type ligand enabled site-selective 1,4-incorporation of CO_2 , with high chemoselectivity. Esterification of the carboxylic acid moiety and reduction of the pending double bonds facilitated the purification of the adipic acid derivatives.^[134]



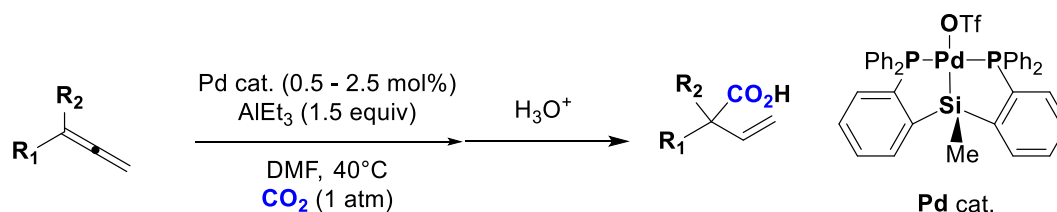
Scheme I.1.32. 1,4-dicarboxylation reaction of 1,3-dienes.

Studies on the telomerisation of 1,2-dienes (allenes) with CO_2 have been firstly described in the 80's, in the presence of Pd(II) complexes. In 2003, Mori and co-workers described the stoichiometric Ni(0)-mediated addition of CO_2 and aryl aldehydes into terminal allenes.^[135] Few years later, the same group published the first catalytic double carboxylation of trimethylsilyl-substituted allenes using $\text{Ni}(\text{cod})_2$, an excess amounts of DBU and Me_2Zn as reducing agent, to afford the corresponding diesters (Scheme I.1.33).^[136]



Scheme I.1.33. Ni-catalyzed decarboxylation of allenes with CO_2 .

In 2008, using similar reaction conditions to those previously shown for 1,3-dienes, the group of Iwasawa reported the hydrocarboxylation of allenes (Scheme I.1.34).^[137] The mechanism of the reaction was further investigated,^[138] and the catalytic cycle is believed to start with generation of a Pd(II) hydride species via transmetalation with AlEt₃, followed by hydrometalation of the allene which undergoes nucleophilic addition of CO₂. A final transmetalation/ β -H elimination step releases the carboxylated aluminium salt product and regenerates the catalytic Pd active species.



Scheme I.1.34. Hydrocarboxylation of allenes.

Since the pioneering stoichiometric studies conducted by Höberg in the early 1980's and his discovery of the nickelalactones from oxidative cyclization of olefins and CO₂, transition-metal catalyzed carboxylation techniques have witnessed considerable advances for promoting CO₂ insertion into unsaturated substrates. Despite the knowledge acquired, the majority of the developed methodologies still require the utilization of well-defined, air-sensitive stoichiometric metal complexes or metal reductants and working under harsh reaction conditions. Moreover, catalytic carboxylation of alkenes is still limited to specific activated substrates. For example, the carboxylation reaction of the simplest olefin, ethylene, to access the industrially relevant acrylic acid, still requires more efficient and milder reaction procedures.

1.2.5. Catalytic carboxylation techniques via C–H functionalization

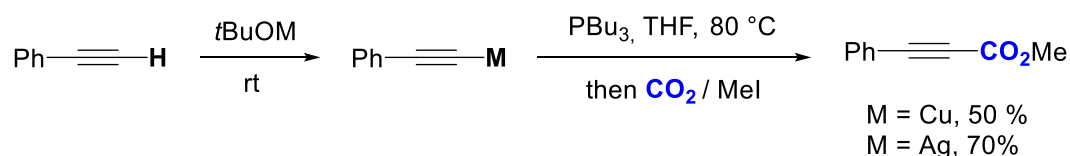
During the last decades, functionalization of C–H bonds have become an interesting cross-coupling methodology to access carbon–carbon and carbon–heteroatom bonds, as it follows the concept of high atom and step economy.^[14] In particular, reacting C–H bonds with CO₂ as a coupling partner possesses a high research value, as it combines two ubiquitous feedstocks. From a synthetic point of view, C–H functionalization has the advantage of avoiding substrate pre-functionalization, since the nucleophilic or electrophilic partner reacting with CO₂ is replaced by an *in situ* generated organometallic reagent. While C–H carboxylation techniques seems to increase the efficiency of the process, the main challenge to overcome remains the differentiation among the multiple C–H bonds of the coupling partner, especially in saturated

hydrocarbons. The following section describes the efforts conducted towards metal-catalyzed C–H carboxylation reactions with CO₂, aiming at reaching satisfactory outcomes in terms of productivity chemo- and regioselectivity.

a. *sp* C–H carboxylation

C–H functions in terminal alkynes possess the particularity of being much more acidic than those of most of the other hydrocarbons, and thus being able to be deprotonated ($pK_a \approx 26$) using an appropriate base. This particularity prompted several groups to study the potential of these substrates to undergo catalytic carboxylation in the presence of CO₂.

In 1974, Saegusa reported the first example of metal-mediated carboxylation of alkynes.^[139] A copper or silver acetylide species was formed *in situ* upon exposing the terminal alkyne to stoichiometric amounts of either CuO^{*t*}Bu or AgO^{*t*}Bu, followed by CO₂ insertion into the metal–carbon bond, in the presence of electron-rich tri-*n*-butyl phosphine ligand (Scheme I.1.35).


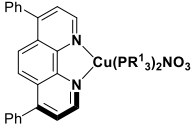
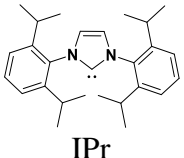
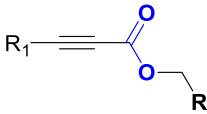
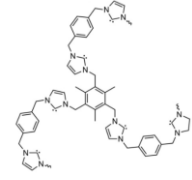



Scheme I.1.35. Metal-mediated carboxylation of terminal alkynes by Saegusa.^[139]

Twenty years later, Inoue reported the first catalytic carboxylative coupling reaction of terminal alkynes with alkyl bromide and CO₂, in the presence of Ag(I) or Cu(I) salts (AgI/AgNO₃ or CuI/CuBr) and overstoichiometric amounts of inorganic salts as the base (Table I.1.6., entry 1).^[140] Further esterification step with bromoalkane allowed to regenerate the copper salt catalyst.

Based on these works, the use of copper catalysts for the direct carboxylation reaction of terminal alkynes was further explored by different research groups. In 2010, simultaneous works published independently, by Gooßen, Lu and Zhang, highlighted the use of Cu(I) complexes under basic conditions. Gooßen and co-workers reported different Cu(I) catalytic systems, containing 1,10-phenantroline and triarylphosphine ligands, for aromatic and aliphatic alkynes carboxylation (entry 2).^[141]

Table I.1.6. Examples of metal-catalyzed carboxylation of *sp* C–H bonds

Entry	Substrate	Catalyst /Ligand	Reaction conditions	Product Yield [%]
1 ^[140]	$R_1\text{—}\equiv\text{—H}$		CuI (4 mol%) R ₂ Br (2.0 equiv) K ₂ CO ₃ (6 equiv) CO ₂ (1 atm) DMA, 100 °C	$R_1\text{—}\equiv\text{—CO}_2R_2$ R ₁ = Ph, R ₂ = C ₆ H ₁₃ , 89% R ₁ = Ph, R ₂ = –CH ₂ – Ph, 55%
2 ^[141]	$R_1\text{—}\equiv\text{—H}$	 [Cu]-1: R ¹ = C ₆ H ₅ [Cu]-2: R ¹ = 4-F-C ₆ H ₄	[Cu]-1/2 (1 – 2 mol%) Cs ₂ CO ₃ (2 equiv) CO ₂ (1 atm) DMF, 35-50 °C	$R_1\text{—}\equiv\text{—CO}_2H$ R ₁ = –Ph, 98%
3 ^[142]	$R_1\text{—}\equiv\text{—H}$	 IPr	[(IPr)CuCl] (10 mol%) R ₂ CH ₂ Cl (1 equiv) K ₂ CO ₃ CO ₂ (10 bar) DMF, 60 °C, 24h	 R ₁ = –Ph–CF ₃ , R ₂ = cinnamyl, 82%
4 ^[143]	$R\text{—}\equiv\text{—H}$	 Poly-NHC ligand	CuCl (2 – 5 mol%) TMEDA or poly-NHC Cs ₂ CO ₃ (1.2 equiv) CO ₂ (1 atm) DMF, 25 °C	$R\text{—}\equiv\text{—CO}_2H$ R = Ph TMEDA : 90% Poly-NHC : 95% R = <i>p</i> (N ₂ O)Ph- TMEDA : <5% Poly-NHC : 70%
5 ^[144]	$R\text{—}\equiv\text{—H}$		AgI (1 mol%) Cs ₂ CO ₃ (1.5 equiv) CO ₂ (2 atm) DMF, 50 °C Then HCl	$R_1\text{—}\equiv\text{—CO}_2H$ R ₁ = Ph, 98%

Lu and co-workers reported the use of N-heterocyclic carbene (NHC) Cu(I) complexes for the carboxylative coupling of terminal alkynes and allylic chlorides to synthesize functionalized allylic 2-alkynoates (entry 3).^[142] The utilization of NHC ligands was found to increase significantly the catalytic activity and selectivity. In addition, a broad range of allylic, propargylic and benzyl chlorides were used, compared to the previous works. Subsequently, Zhang published a CuCl/TMEDA (tetramethylethylenediamine) system avoiding the use of additional base (entry 4).^[143] The same group also developed a protocol based on poly-N-heterocyclic carbenes (PNHCs) ligands, allowing to achieve high yields with electron-withdrawing alkynes (entry 4). The group of Lu reported a ligand-free AgI-catalyzed carboxylation of terminal alkynes (entry 5).^[144] Compared to the previously reported

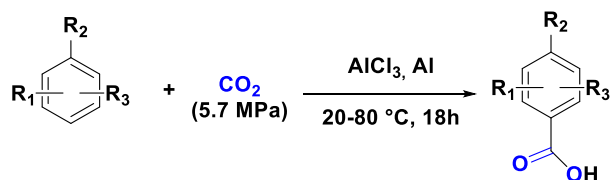
[(IPr)CuCl]/K₂CO₃ system (entry 3), the AgI/Cs₂CO₃ combination showed a superior catalytic activity, even for the ligand-free Ag(I)-catalyzed carboxylative coupling of terminal alkynes, chloride compounds, and CO₂ at very low catalyst loadings (1 mol%).^[145] Encouraged by developing greener processes, additional protocols using supercritical CO₂ as solvent^[146] or reusable Ag-supported nanoparticles^[147,148] have been reported for the carboxylation of terminal alkynes.

b. *sp*² C–H carboxylation

With typical *p*K_a values ranging from ~ 25 to 50 for ethylene, C*sp*²–Hydrogens are less acidic than the C*sp*–H ones. This suggests that depending on the acidity of the targeted C*sp*²–H bond, a wide range of strategies could be applied.^[14]

- *Friedel-Crafts carboxylation of aromatics*

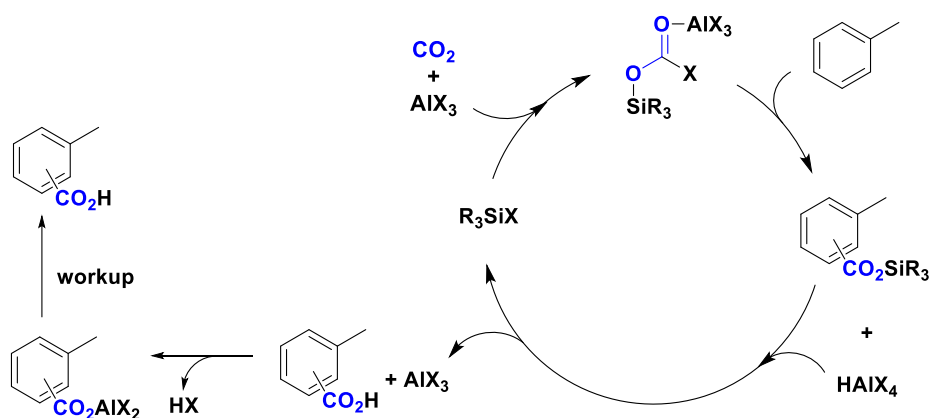
The direct use of CO₂ for the carboxylation of arenes is one of the most desirable pathways to access arylcarboxylic acids. Friedel and Crafts firstly described such practical process, by observing the formation of minor amounts of benzoic acid along with HCl, when CO₂ was bubbled through a mixture of AlCl₃ and benzene, heated at the boiling point of the latter.^[149] The low electrophilicity of CO₂ and the high Lewis acidity of the aluminium-based compounds, prevented from achieving good yields and afforded high amounts of side-products (benzophenones, diphenylmethanes). In 2002, Olah *et al.* improved the yields for the production of aromatic carboxylic acids by using AlCl₃ and aluminium metal powder as an additive (ratios depending on the substrates used), which helped neutralizing the liberated HCl to regenerate the active AlCl₃ species (Scheme I.1.36).^[150] The DFT studies suggested an initial complexation between CO₂ and AlCl₃ forming an electrophilic complex. The latter reacts with the arene and subsequent deprotonation by a chloride anion affords an aluminium carboxylate.



Scheme I.1.36. AlCl₃/Al promoted carboxylation of aromatic compounds

Later on, Munshi and co-workers reported an efficient *p*-toluic acid synthesis by holding AlCl₃ (5.4 mmol) under high pressure of CO₂ prior to adding toluene (70 atm, 1 h incubation time, 80

% yield).^[151] The induction step forces the $\text{AlCl}_3\text{-CO}_2$ adduct formation and prevents the deactivation of AlCl_3 , thus resulting in a more effective carboxylation. On the other hand, the group of Hattori found that large amounts of alkyl or arylsilyl chlorides efficiently promote Lewis acid (AlBr_3)-mediated direct carboxylation of alkylbenzenes and polycyclic arenes, under mild reaction conditions (30 atm of CO_2 , r.t.).^[152,153] The authors suggested that a haloformate-like active species is generated from silyl chlorides, CO_2 and AlX_3 directly reacting with the arene via an $\text{S}_{\text{E}}\text{Ar}$ mechanism (Scheme I.1.37).



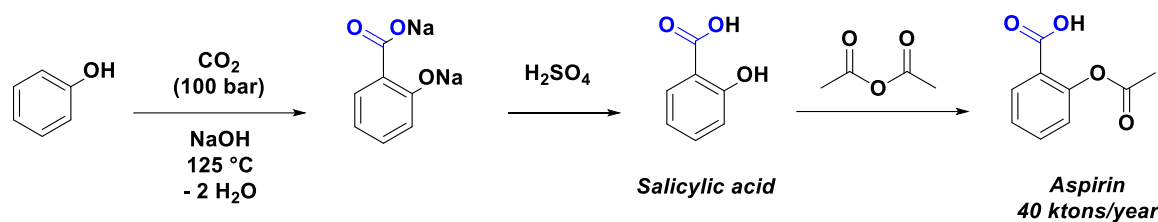
Scheme I.1.37. Proposed mechanism for R_3SiX -promoted carboxylation.

Friedel–Crafts carboxylation with CO_2 was also efficiently applied to 1-substituted indoles and pyrroles using dialkylaluminum chlorides instead of aluminum trihalides as CO_2 -activator.^[154] Thus, indole-3-carboxylic acids and pyrrole-2-carboxylic acids were obtained regioselectively in good yields (61–85 %).

Salicylic acid derivatives have been synthesized mostly upon using the base-mediated Kolbe-Schmitt two-step manufacturing process (see section below). Therefore, to achieve direct carboxylation of phenol with CO_2 , Ijima and Yamaguchi developed a procedure operating under supercritical conditions (scCO_2 , 80 atm, 80 °C, 1h), using AlBr_3 as Lewis-acid, and leading to salicylic acids in approximately 70% yields.^[155]

- **Base-mediated carboxylation**

The first practical example of C–H carboxylation of aromatic compounds was developed by Kolbe and Schmitt in 1860, for the preparation of 2-hydroxy-benzoic acid from CO_2 .^[156,157] This synthesis, called after its inventors, is one of the oldest organic reaction using CO_2 and is widely used in the industry today, notably for the synthesis of Aspirin with a worldwide production of 40 000 tons/year (Scheme I.1.38).^[158]



Scheme I.1.38. Kolbe-Schmitt reaction for the production of salicylic acid.

The reaction provides direct access to salicylic acids through *ortho*-C–H carboxylation of alkali metal phenoxide generated under high pressures of CO₂ (20–100 atm) and high temperatures (125–280 °C) in the presence of NaOH.^[149] Several experimental studies have shown that the nature of the final product depends on the nature of the alkali cation used. For example, sodium phenolates always led to *ortho*-benzoic acid (salicylic acid) whereas potassium phenolate resulted in *para*-benzoic acid formation.^[159,160] Among the numerous DFT studies published,^[159,160] it is generally accepted that CO₂ is first activated by the alkali metal phenoxide, followed by C–alkylation reaction of the CO₂ electrophilic carbon atom with the aryl ring at *ortho* or *para* position, leading to the production of the final alkali metal benzoate. The main drawback of this protocol is the access to completely dry phenoxide from the corresponding phenol, since the generated water molecules could strongly chelate with the alkali metal phenoxides and prevent therefore CO₂ addition.^[161] To avoid undesired formation of H₂O, the group of Larrosa used NaH as a base and allowed the reaction to proceed in a one pot process, under atmospheric of CO₂ in the presence of 2,4,6-trimethylphenol (TMP) as a recyclable additive.^[162] Substrates containing electron-donating groups and halogen substituents were reactive under these conditions whereas substrates with strong electro-withdrawing groups did not undergo carboxylation. Besides phenol substrates, heteroarenes were efficiently carboxylated upon using Cs₂CO₃, KO^tBu or LiO^tBu for the deprotonation of poorly acidic C–H bonds.^[163,164,164,165]

The strategies described above for the carboxylation of aromatic compounds with CO₂ require the use of Lewis-acid or base mediators. Overall, the Lewis-acid-mediated C–H carboxylation reaction targets CO₂ activation through coordination with the Lewis acid, allowing the aromatic compound to react with the activated CO₂. Despite the fact that low reaction temperatures are needed for these processes, high gas pressures are required and poor regioselectivities are observed. On the other hand, the base-mediated C–H approach involves deprotonation of the most acidic proton to form species with a strong nucleophilic carbon, which attacks the weakly electrophilic CO₂. However, high reaction temperatures are often

needed in order to achieve good yields. Therefore, methodologies operating under milder conditions remain a challenge, encouraging, in the last decades, the development of metal-catalyzed C_{sp^2} -H bonds transformations with CO_2 .

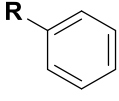

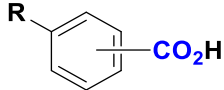
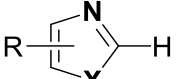
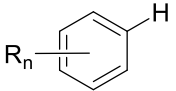

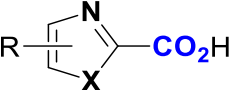
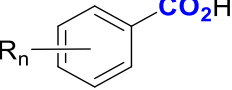
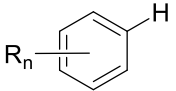

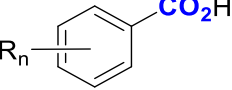
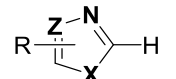
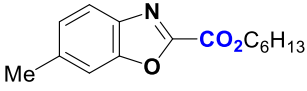
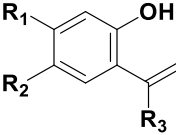
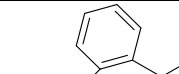
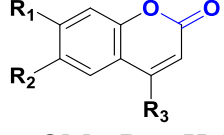
- ***Transition-metal-catalyzed carboxylation of C_{sp^2} -H bonds***

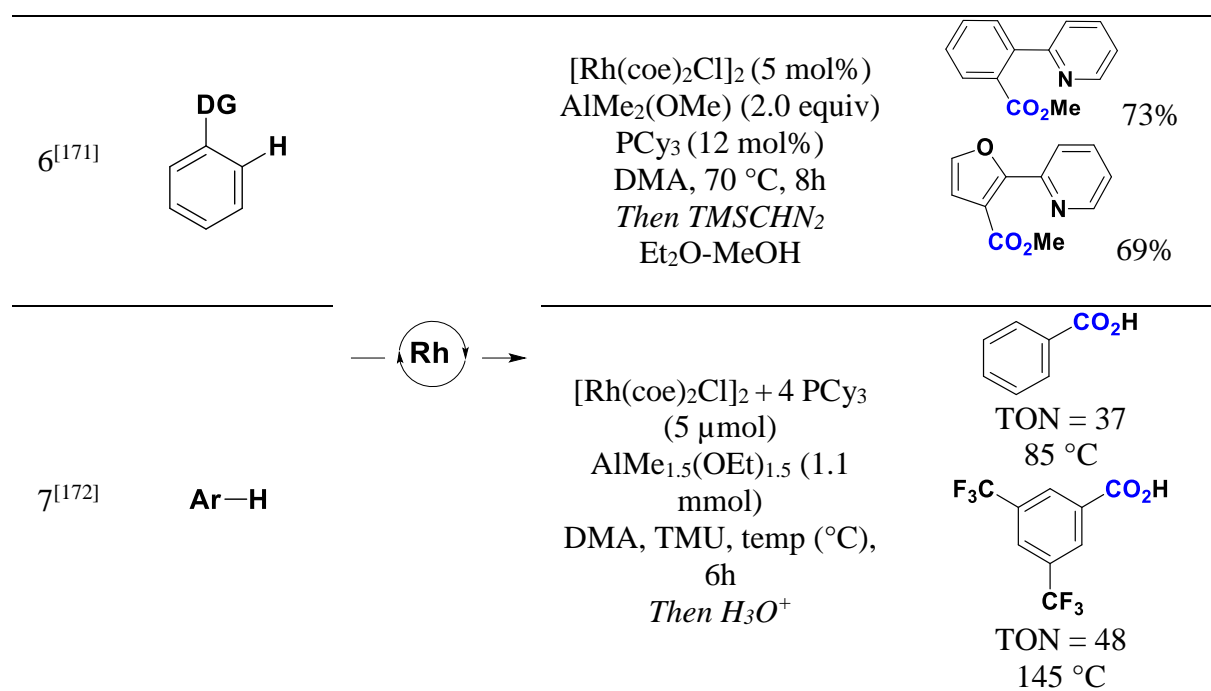
In 1984, Fujiwara and co-workers described the first example of direct transition-metal-catalyzed carboxylation of arenes (benzene, furan, anisole) using Pd(II) salts and t BuOOH as a reoxidizing agent (Table I.1.7, entry 1).^[166] The reaction yielded 127% of benzoic acid and 125% of methoxybenzoic acid with respect to the amount of catalyst, *i.e.* TONs of 1.27 and 1.25 respectively. Although the efficiency of the reaction was very poor, this seminal work showed the feasibility to promote carboxylation of benzene with CO_2 , a reaction that is thermodynamically uphill.

This research field remained dormant for almost three decades until 2010, when Nolan and co-workers demonstrated the C_{sp^2} -H carboxylation reaction of a variety of electron-deficient arenes, based on the use of [(IPr)AuOH] as catalyst and stoichiometric amounts of KOH as base (Table I.1.7, entry 2 (A)).^[167] The system was found efficient for C_{sp^2} -H acidic protons carboxylation of a series of polyhalogenated benzene derivatives, oxazoles and thiazoles compounds ($pK_a < 30.3$). Soon after, Nolan reported an improved catalytic system based on the use of cheaper carbene-Cu(I) hydroxide complexes, yet under harsher reaction conditions and higher catalyst loadings (entry 3).^[168] The same year, Hou and co-workers independently published a protocol using the (IPr)CuCl complex as catalyst and stoichiometric amounts of KO t Bu with a variety of electron-poor heteroaromatics (entry 4).^[169] The corresponding esters derivatives were obtained in moderate to good yields after esterification with an alkyl iodide.

The group of Iwasawa succeeded in the development of a Pd(II)-catalyzed carboxylation of alkenyl C-H bonds with CO_2 , by treatment of 2-hydroxystyrenes under basic conditions, furnishing coumarins derivatives in good yields (entry 5).^[170] From this reaction, a six-membered alkenylpalladium(II) key intermediate was isolated (entry 5), which was obtained by the 2-hydroxystyrene C_{sp^2} -H bond chelation-assisted cleavage in the presence of a base, and followed by CO_2 insertion.

Table I.1.7. Examples of metal-catalyzed carboxylation of sp^2 C–H bonds

Entry	Substrate	Catalyst /Ligand	Reaction conditions	Product Yield [%]
1 ^[166]	 R = H R = OMe (Solvent)		Pd(OAc) ₂ (1 equiv) ^t BuOOH (40 equiv) CO ₂ (1 atm) 70 °C, 3 days	 R = H, 127% R = OMe, 125%
2 ^[167]	 Or 		(A) [(IPr)AuOH] (1.5 mol%) KOH (1.05 equiv) CO ₂ (1.5 atm) THF, 20 °C, 12h <i>Then HCl</i>	 (A) X = O, R = H, 89% (B) X = O, R = H, 77% Or  (A) R _n = 2,6-ortho-Cl, 96%
3 ^[168]			(B) (IPr)CuOH (1.5 mol%) CsOH (1.05 equiv) CO ₂ (1.5 atm) THF, 65 °C, 12h <i>Then HCl</i>	 (A) R _n = 2,6-ortho-Cl, 96%
4 ^[169]			[(IPr)CuOH] (5.0 mol%) KO ^t Bu (1.1 equiv) CO ₂ (1 atm) THF, 80 °C, 14 h Then C ₆ H ₁₃ I (2 equiv), DMF, 80 °C, 5 h	 87%
5 ^[170]			Pd(OAc) ₂ (5 mol%) Cs ₂ CO ₃ (3 equiv) CO ₂ (1 atm) Diglyme, 100 °C <i>Then H₃O⁺</i>	 R ₁ = OMe, R ₂ = H, R ₃ = Ph, 84% R ₁ = R ₂ = H, R ₃ = Me, 83%



As described in the early reports of carboxylation of (hetero)arenes, C–H deprotonation was limited to relatively acidic Csp^2 –H bonds, through a deprotonation step promoted by the use of Au(I) and Cu(I) hydroxyl complexes. Aiming at promoting carboxylation reaction of less acidic Csp^2 –H bonds, Iwasawa developed a Rh(I)-catalyzed C–H activation of aromatic compounds in combination with an appropriate methyl-metallic reagent, AlMe₂(OMe) (entry 6).^[171] The proposed catalytic cycle is initiated by premixing AlMe₂(OMe) and [Rh(coe)₂Cl]₂ to generate the key catalytic L_nRh(I)–Me species by transmetalation. Subsequent oxidative addition into the Csp^2 –H bond, followed by CO₂ insertion, effectively resulted in directed *ortho*-carboxylation of a wide range of phenylpyridines. Few years later, the same authors described an effective Rh(I) catalyst, stabilized by bidentate phosphine ligand (1,2-bis(dicyclophosphino)ethane, dcpe), for the direct carboxylation of toluene or xylene (entry 7).^[172] Moderate to good site-selectivities were obtained, and high TON were observed at high temperatures and in the presence of methyl aluminium complexes. The use of AlMe_{1.5}(OEt)_{1.5} allows to generate, as previously studied by the authors for directing group procedures, the 14-electron L_nRh(I)–Me complex participating in the oxidative addition of the arene.

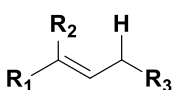
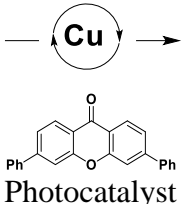
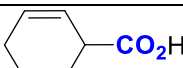
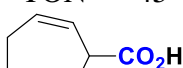
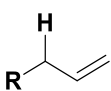
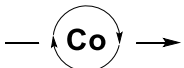
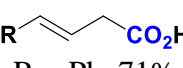
c. sp^3 C–H carboxylation

Among the challenging transformations, the direct carboxylation of Csp^3 –H bonds is considered as the most difficult one reaction to achieve. Although conceivable, the metal-catalyzed functionalization of less active Csp^3 –H bonds is hampered by the lack in substrates

of proximal empty low-energy or filled high-energy orbitals, which could readily interact with the *d* orbitals of the metal center.^[173]

In 2015, the group of Murakami developed a carboxylation of *o*-alkylphenyl ketones with CO₂ simply upon irradiation with UV light or even solar light.^[174] Taking advantage of the knowledge acquired, the same group succeeded in the carboxylation of allylic Csp³-H bonds by combining organic photocatalysts with (IPr)CuCl under UV-light irradiation (Table I.1.8, entry 1).^[175] Although modest TONs were obtained, the methodology developed provided a step forward in the Csp³-H carboxylation field.

Table I.1.8. Examples of metal-catalyzed carboxylation of sp³ C-H bonds

Entry	Substrate	Catalyst /Ligand	Reaction conditions	Product Yield [%]/TON
1 ^[175]		 Photocatalyst	(IPr)CuCl (0.01 mmol) Photocatalyst (0.05 mmol) ^t BuOK (1.0 mmol) CO ₂ (2 atm) UV light (365 nm) benzene, 110 °C, 12 h <i>Then HCl</i>	 TON* = 45  TON* = 17 * based on copper complex
2 ^[176]			Co(acac) ₂ (10 mol%) Xantphos (20 mol%) AlMe ₃ (1.5 equiv) CsF (1 equiv) CO ₂ (1 atm) DMA, 60 °C, 12 h <i>Then HCl</i>	 R = Ph, 71%

Later on, Sato developed Co-catalyzed allylic Csp³-H carboxylation with CO₂ in the presence of AlMe₃ as methylating agent. Similarly to the Rh-catalyzed carboxylation of arenes, a low-valent methyl-cobalt(I) intermediate is generated upon reacting with AlMe₃, followed by oxidative addition of the allyl-arene or simple alkenes and loss of methane (Table I.1.8, entry 2). Then, carbon dioxide is inserted into the resulting allyl-Co(I) species generating the γ -carboxylate-Co(I) species. The latter reacts with AlMe₃ and releases the α,β -unsaturated carboxylic acids.^[176]

Hence, in the recent decades, numerous efforts have been conducted towards transition-metal-catalyzed direct C-H activation reactions. Among the methodologies developed, the substrate scope is often limited to those incorporating activated C-H bonds, such as alkynes, polyhalogenated arenes or heterocyclic compounds. A major advance in the field is

carboxylation of less activated Csp^2 -H bonds using catalysts such as Rh(II) and Pd(II) with the assistance of -N or -O directing groups. Until now, only one example of direct C-H carboxylation of simple arenes such as benzene has been reported, demonstrating the lack of real breakthroughs in this field. On the other hand, Csp^3 -H transformations are still limited to reactive allylic and benzylic C-H bonds.

1.3. Conclusion and outlook

The use of CO_2 as a C1 source represents a key methodology towards the development of greener chemical processes. During the last decades, substantial efforts have been made in the field of carboxylation reactions, using CO_2 as starting material to produce carboxylic acids and derivatives, which are attractive targets for fine chemicals synthesis. Their preparation includes several well-established methods and despite their efficiency, transition metal-catalysed carboxylation reactions have experienced an exponential growth, as they allow the use of a variety of less reactive coupling partners and enhance functional group compatibility.

Although encouraging outcomes are emerging, substantial shortcomings need to be overcome. Indeed, these techniques still often require the use of stoichiometric amounts of organometallic or pre-functionalized reagents, as well as stoichiometric amounts of organometallic or metallic additives, leading to the production of high amounts of wastes, and hampering therefore their potential application. Moreover, the most promising catalytic systems exhibit low TON, reflecting a lack of efficiency. Therefore, the design a simple and functional-group compatible catalytic technology for the carboxylation of poorly polarized substrates with CO_2 is still not reached.

Additionally, depending on both the substrate and the catalyst employed, diversified reaction pathways might be at play, and the exact nature of the putative active species remains speculative.

1.4. References

- [1] T. Sakakura, J.-C. Choi, H. Yasuda, *Chem. Rev.* **2007**, *107*, 2365–2387.
- [2] M. Aresta, A. Dibenedetto, *Dalton Trans.* **2007**, *0*, 2975–2992.
- [3] L. J. Gooßen, N. Rodríguez, K. Gooßen, *Angew. Chem. Int. Ed.* **2008**, *47*, 3100–3120.
- [4] Y. Zhang, S. N. Riduan, *Angew. Chem. Int. Ed.* **2011**, *50*, 6210–6212.
- [5] J. L. White, M. F. Baruch, J. E. Pander, Y. Hu, I. C. Fortmeyer, J. E. Park, T. Zhang, K. Liao, J. Gu, Y. Yan, T. W. Shaw, E. Abelev, A. B. Bocarsly, *Chem. Rev.* **2015**, *115*, 12888–12935.
- [6] M. Yan, Y. Kawamata, P. S. Baran, *Chem. Rev.* **2017**, *117*, 13230–13319.
- [7] A. Dibenedetto, A. Angelini, P. Stufano, *J. Chem. Technol. Biotechnol.* **2014**, *89*, 334–353.
- [8] A. Correa, R. Martín, *Angew. Chem. Int. Ed.* **2009**, *48*, 6201–6204.
- [9] Jonathan Clayden, Nick Greeves, Stuart Warren, *Organic Chemistry Second Edition*, **2012**.
- [10] A. M. Echavarren, A. Homs, in *Met.-Catalyzed Cross-Coupling React. More*, John Wiley & Sons, Ltd, **2014**, pp. 1–64.
- [11] M. Aresta, A. Dibenedetto, E. Quaranta, in *React. Mech. Carbon Dioxide Convers.* (Eds.: M. Aresta, A. Dibenedetto, E. Quaranta), Springer, Berlin, Heidelberg, **2016**, pp. 1–34.
- [12] K. Huang, C.-L. Sun, Z.-J. Shi, *Chem. Soc. Rev.* **2011**, *40*, 2435–2452.
- [13] A. Behr, *Angew. Chem. Int. Ed. Engl.* **1988**, *27*, 661–678.
- [14] A. Tortajada, F. Juliá-Hernández, M. Börjesson, T. Moragas, R. Martin, *Angew. Chem. Int. Ed.* **2018**, *57*, 15948–15982.
- [15] Q. Liu, L. Wu, R. Jackstell, M. Beller, *Nat. Commun.* **2015**, *6*, 5933.
- [16] M. Aresta, C. F. Nobile, V. G. Albano, E. Forni, M. Manassero, *J. Chem. Soc. Chem. Commun.* **1975**, 636–637.
- [17] M. Aresta, R. Gobetto, E. Quaranta, I. Tommasi, *Inorg. Chem.* **1992**, *31*, 4286–4290.
- [18] J. C. Calabrese, T. Herskovitz, J. B. Kinney, *J. Am. Chem. Soc.* **1983**, *105*, 5914–5915.
- [19] I. Castro-Rodríguez, H. Nakai, L. N. Zakharov, A. L. Rheingold, K. Meyer, *Science* **2004**, *305*, 1757–1759.
- [20] K. Tanaka, in *Adv. Inorg. Chem.* (Ed.: A.G. Sykes), Academic Press, **1995**, pp. 409–435.
- [21] M. Shi, K. M. Nicholas, *J. Am. Chem. Soc.* **1997**, *119*, 5057–5058.
- [22] R. Johansson, O. F. Wendt, *Dalton Trans.* **2007**, 488–492.
- [23] J. Wu, N. Hazari, *Chem. Commun.* **2010**, *47*, 1069–1071.
- [24] D. P. Hruszkewycz, J. Wu, N. Hazari, C. D. Incarvito, *J. Am. Chem. Soc.* **2011**, *133*, 3280–3283.
- [25] K. Ukai, M. Aoki, J. Takaya, N. Iwasawa, *J. Am. Chem. Soc.* **2006**, *128*, 8706–8707.
- [26] J. Takaya, S. Tadami, K. Ukai, N. Iwasawa, *Org. Lett.* **2008**, *10*, 2697–2700.
- [27] T. Ohishi, M. Nishiura, Z. Hou, *Angew. Chem. Int. Ed.* **2008**, *47*, 5792–5795.
- [28] H. A. Duong, P. B. Huleatt, Q.-W. Tan, E. L. Shuying, *Org. Lett.* **2013**, *15*, 4034–4037.
- [29] M. Juhl, S. L. R. Laursen, Y. Huang, D. U. Nielsen, K. Daasbjerg, T. Skrydstrup, *ACS Catal.* **2017**, *7*, 1392–1396.
- [30] M. Takimoto, Z. Hou, *Chem. – Eur. J.* **2013**, *19*, 11439–11445.
- [31] A. Ueno, M. Takimoto, W. W. N. O, M. Nishiura, T. Ikariya, Z. Hou, *Chem. – Asian J.* **2015**, *10*, 1010–1016.
- [32] A. Ueno, M. Takimoto, Z. Hou, *Org. Biomol. Chem.* **2017**, *15*, 2370–2375.
- [33] X. Zhang, W.-Z. Zhang, L.-L. Shi, C.-X. Guo, L.-L. Zhang, X.-B. Lu, *Chem. Commun.* **2012**, *48*, 6292–6294.
- [34] Y. Makida, E. Marelli, A. M. Z. Slawin, S. P. Nolan, *Chem. Commun.* **2014**, *50*, 8010–8013.
- [35] C. S. Yeung, V. M. Dong, *J. Am. Chem. Soc.* **2008**, *130*, 7826–7827.
- [36] H. Ochiai, M. Jang, K. Hirano, H. Yorimitsu, K. Oshima, *Org. Lett.* **2008**, *10*, 2681–2683.
- [37] P. Knochel, W. Dohle, N. Gommermann, F. F. Kneisel, F. Kopp, T. Korn, I. Sapountzis, V. A. Vu, *Angew. Chem. Int. Ed.* **2003**, *42*, 4302–4320.
- [38] T. Moragas, A. Correa, R. Martin, *Chem. – Eur. J.* **2014**, *20*, 8242–8258.
- [39] J. Gu, X. Wang, W. Xue, H. Gong, *Org. Chem. Front.* **2015**, *2*, 1411–1421.
- [40] E. Richmond, J. Moran, *Synthesis* **2018**, *50*, 499–513.
- [41] S. Torii, H. Tanaka, T. Hamatani, K. Morisaki, A. Jutand, F. Peluger, J.-F. Fauvarque, *Chem. Lett.* **1986**, *15*, 169–172.

- [42] C. Amatore, A. Jutand, *J. Am. Chem. Soc.* **1991**, *113*, 2819–2825.
- [43] C. Amatore, A. Jutand, F. Khalil, M. F. Nielsen, *J. Am. Chem. Soc.* **1992**, *114*, 7076–7085.
- [44] K. Osakada, R. Sato, T. Yamamoto, *Organometallics* **1994**, *13*, 4645–4647.
- [45] A. Correa, R. Martín, *J. Am. Chem. Soc.* **2009**, *131*, 15974–15975.
- [46] T. Fujihara, K. Nogi, T. Xu, J. Terao, Y. Tsuji, *J. Am. Chem. Soc.* **2012**, *134*, 9106–9109.
- [47] F. B. Sayyed, Y. Tsuji, S. Sakaki, *Chem. Commun.* **2013**, *49*, 10715–10717.
- [48] T. León, A. Correa, R. Martín, *J. Am. Chem. Soc.* **2013**, *135*, 1221–1224.
- [49] S. Zhang, W.-Q. Chen, A. Yu, L.-N. He, *ChemCatChem* **2015**, *7*, 3972–3977.
- [50] K. Shimomaki, K. Murata, R. Martín, N. Iwasawa, *J. Am. Chem. Soc.* **2017**, *139*, 9467–9470.
- [51] M. Börjesson, T. Moragas, R. Martín, *J. Am. Chem. Soc.* **2016**, *138*, 7504–7507.
- [52] F. Juliá-Hernández, T. Moragas, J. Cornella, R. Martín, *Nature* **2017**, *545*, 84–88.
- [53] A. Paul, M. D. Smith, A. K. Vannucci, *J. Org. Chem.* **2017**, *82*, 1996–2003.
- [54] A. Rudolph, M. Lautens, *Angew. Chem.* **2009**, *121*, 2694–2708.
- [55] T. Moragas, R. Martín, *Synthesis* **2016**, *48*, 2816–2822.
- [56] X. Wang, Y. Liu, R. Martín, *J. Am. Chem. Soc.* **2015**, *137*, 6476–6479.
- [57] M. Börjesson, T. Moragas, D. Gallego, R. Martín, *ACS Catal.* **2016**, *6*, 6739–6749.
- [58] K. Nogi, T. Fujihara, J. Terao, Y. Tsuji, *J. Org. Chem.* **2015**, *80*, 11618–11623.
- [59] F. Rebih, M. Andreini, A. Moncomble, A. Harrison-Marchand, J. Maddaluno, M. Durandetti, *Chem. – Eur. J.* **2016**, *22*, 3758–3763.
- [60] Y. Liu, J. Cornella, R. Martín, *J. Am. Chem. Soc.* **2014**, *136*, 11212–11215.
- [61] T. Moragas, M. Gaydou, R. Martín, *Angew. Chem. Int. Ed.* **2016**, *55*, 5053–5057.
- [62] A. Correa, T. León, R. Martín, *J. Am. Chem. Soc.* **2014**, *136*, 1062–1069.
- [63] K. Nogi, T. Fujihara, J. Terao, Y. Tsuji, *Chem. Commun.* **2014**, *50*, 13052–13055.
- [64] T. Mita, Y. Higuchi, Y. Sato, *Chem. – Eur. J.* **2015**, *21*, 16391–16394.
- [65] S. J. Blanksby, G. B. Ellison, *Acc. Chem. Res.* **2003**, *36*, 255–263.
- [66] M. van Gemmeren, M. Börjesson, A. Tortajada, S.-Z. Sun, K. Okura, R. Martín, *Angew. Chem. Int. Ed.* **2017**, *56*, 6558–6562.
- [67] Y. Inoue, Y. Itoh, H. Hashimoto, *Chem. Lett.* **1977**, *6*, 855–856.
- [68] Y. Inoue, Y. Itoh, H. Hashimoto, *Chem. Lett.* **1978**, *7*, 633–634.
- [69] *J. Organomet. Chem.* **1992**, *436*, 109–119.
- [70] *J. Organomet. Chem.* **1987**, *334*, 377–388.
- [71] *J. Organomet. Chem.* **1982**, *238*, 383–387.
- [72] G. Burkhart, H. Hoberg, *Angew. Chem. Int. Ed. Engl.* **1982**, *21*, 76–76.
- [73] *J. Organomet. Chem.* **1982**, *228*, C21–C24.
- [74] S. Saito, S. Nakagawa, T. Koizumi, K. Hirayama, Y. Yamamoto, *J. Org. Chem.* **1999**, *64*, 3975–3978.
- [75] S. Sakaki, K. Mine, D. Taguchi, T. Arai, *Bull. Chem. Soc. Jpn.* **1993**, *66*, 3289–3299.
- [76] S. Sakaki, K. Mine, T. Hamada, T. Arai, *Bull. Chem. Soc. Jpn.* **1995**, *68*, 1873–1882.
- [77] D. C. Graham, M. I. Bruce, G. F. Metha, J. H. Bowie, M. A. Buntine, *J. Organomet. Chem.* **2008**, *693*, 2703–2710.
- [78] M. Aoki, M. Kaneko, S. Izumi, K. Ukai, N. Iwasawa, *Chem. Commun.* **2004**, 2568–2569.
- [79] S. Li, W. Yuan, S. Ma, *Angew. Chem. Int. Ed.* **2011**, *50*, 2578–2582.
- [80] X. Wang, M. Nakajima, R. Martín, *J. Am. Chem. Soc.* **2015**, *137*, 8924–8927.
- [81] M. Gaydou, T. Moragas, F. Juliá-Hernández, R. Martín, *J. Am. Chem. Soc.* **2017**, *139*, 12161–12164.
- [82] T. Fujihara, Y. Horimoto, T. Mizoe, F. B. Sayyed, Y. Tani, J. Terao, S. Sakaki, Y. Tsuji, *Org. Lett.* **2014**, *16*, 4960–4963.
- [83] T. Fujihara, T. Xu, K. Semba, J. Terao, Y. Tsuji, *Angew. Chem. Int. Ed.* **2011**, *50*, 523–527.
- [84] R. Santhoshkumar, Y.-C. Hong, C.-Z. Luo, Y.-C. Wu, C.-H. Hung, K.-Y. Hwang, A.-P. Tu, C.-H. Cheng, *ChemCatChem* **2016**, *8*, 2210–2213.
- [85] A. L. Lapidus, Y. Y. Ping, *Russ. Chem. Rev.* **1981**, *50*, 63.
- [86] H. Hoberg, Y. Peres, A. Milchereit, *J. Organomet. Chem.* **1986**, *307*, C38–C40.
- [87] H. Hoberg, Y. Peres, C. Krüger, Y.-H. Tsay, *Angew. Chem. Int. Ed. Engl.* **1987**, *26*, 771–773.
- [88] H. Hoberg, D. Schaefer, *J. Organomet. Chem.* **1983**, *251*, c51–c53.
- [89] H. Hoberg, K. Jenni, K. Angermund, C. Krüger, *Angew. Chem. Int. Ed. Engl.* **1987**, *26*, 153–155.

- [90] H. Hoberg, D. Schaefer, G. Burkhart, C. Krüger, M. J. Romão, *J. Organomet. Chem.* **1984**, 266, 203–224.
- [91] M. Aresta, E. Quaranta, I. Tommasi, *J. Chem. Soc. Chem. Commun.* **1988**, 450–452.
- [92] I. Pápai, G. Schubert, I. Mayer, G. Besenyi, M. Aresta, *Organometallics* **2004**, 23, 5252–5259.
- [93] G. Yang, B. Schäffner, M. Blug, E. J. M. Hensen, E. A. Pidko, *ChemCatChem* **2014**, 6, 800–807.
- [94] P. N. Plessow, A. Schäfer, M. Limbach, P. Hofmann, *Organometallics* **2014**, 33, 3657–3668.
- [95] M. Limbach, in *Adv. Organomet. Chem.* (Ed.: P.J. Pérez), Academic Press, **2015**, pp. 175–202.
- [96] S. A. Cohen, J. E. Bercaw, *Organometallics* **1985**, 4, 1006–1014.
- [97] H. G. Alt, C. E. Denner, *J. Organomet. Chem.* **1990**, 390, 53–60.
- [98] D. C. Graham, C. Mitchell, M. I. Bruce, G. F. Metha, J. H. Bowie, M. A. Buntine, *Organometallics* **2007**, 26, 6784–6792.
- [99] E. Kirillov, J.-F. Carpentier, E. Bunel, *Dalton Trans.* **2015**, 44, 16212–16223.
- [100] H. Hoberg, A. Ballesteros, A. Sigan, C. Jegat, A. Milchereit, *Synthesis* **1991**, 1991, 395–398.
- [101] G. Schubert, I. Pápai, *J. Am. Chem. Soc.* **2003**, 125, 14847–14858.
- [102] R. Alvarez, E. Carmona, D. J. Cole-Hamilton, A. Galindo, E. Gutierrez-Puebla, A. Monge, M. L. Poveda, C. Ruiz, *J. Am. Chem. Soc.* **1985**, 107, 5529–5531.
- [103] W. H. Bernskoetter, B. T. Tyler, *Organometallics* **2011**, 30, 520–527.
- [104] Rafael. Alvarez, Ernesto. Carmona, Agustin. Galindo, Enrique. Gutierrez, J. M. Marin, Angeles. Monge, M. L. Poveda, Caridad. Ruiz, J. M. Savariault, *Organometallics* **1989**, 8, 2430–2439.
- [105] A. Galindo, A. Pastor, P. J. Perez, E. Carmona, *Organometallics* **1993**, 12, 4443–4451.
- [106] R. Fischer, J. Langer, A. Malassa, D. Walther, H. Görls, G. Vaughan, *Chem. Commun.* **2006**, 2510–2512.
- [107] C. Bruckmeier, M. W. Lehenmeier, R. Reichardt, S. Vagin, B. Rieger, *Organometallics* **2010**, 29, 2199–2202.
- [108] S. Y. T. Lee, M. Cokoja, M. Drees, Y. Li, J. Mink, W. A. Herrmann, F. E. Kühn, *ChemSusChem* **2011**, 4, 1275–1279.
- [109] D. Jin, T. J. Schmeier, P. G. Williard, N. Hazari, W. H. Bernskoetter, *Organometallics* **2013**, 32, 2152–2159.
- [110] D. Jin, P. G. Williard, N. Hazari, W. H. Bernskoetter, *Chem. – Eur. J.* **2014**, 20, 3205–3211.
- [111] P. N. Plessow, L. Weigel, R. Lindner, A. Schäfer, F. Rominger, M. Limbach, P. Hofmann, *Organometallics* **2013**, 32, 3327–3338.
- [112] W. Guo, C. Michel, R. Schwiedernoch, R. Wischert, X. Xu, P. Sautet, *Organometallics* **2014**, 33, 6369–6380.
- [113] M. L. Lejkowski, R. Lindner, T. Kageyama, G. É. Bódizs, P. N. Plessow, I. B. Müller, A. Schäfer, F. Rominger, P. Hofmann, C. Futter, S. A. Schunk, M. Limbach, *Chem. – Eur. J.* **2012**, 18, 14017–14025.
- [114] N. Huguet, I. Jevtovikj, A. Gordillo, M. L. Lejkowski, R. Lindner, M. Bru, A. Y. Khalimon, F. Rominger, S. A. Schunk, P. Hofmann, M. Limbach, *Chem. – Eur. J.* **2014**, 20, 16858–16862.
- [115] I. Jevtovikj, S. Manzini, M. Hanauer, F. Rominger, T. Schaub, *Dalton Trans.* **2015**, 44, 11083–11094.
- [116] K. Takahashi, Y. Hirataka, T. Ito, N. Iwasawa, *Organometallics* **2020**, 39, 1561–1572.
- [117] R. W. Mitchell, A. Spencer, G. Wilkinson, *J. Chem. Soc. Dalton Trans.* **1973**, 846–854.
- [118] C. Hendriksen, E. A. Pidko, G. Yang, B. Schäffner, D. Vogt, *Chem. – Eur. J.* **2014**, 20, 12037–12040.
- [119] C. M. Williams, J. B. Johnson, T. Rovis, *J. Am. Chem. Soc.* **2008**, 130, 14936–14937.
- [120] R. Yuan, Z. Lin, *Organometallics* **2014**, 33, 7147–7156.
- [121] E. Shirakawa, D. Ikeda, S. Masui, M. Yoshida, T. Hayashi, *J. Am. Chem. Soc.* **2012**, 134, 272–279.
- [122] M. D. Greenhalgh, S. P. Thomas, *J. Am. Chem. Soc.* **2012**, 134, 11900–11903.
- [123] P. Shao, S. Wang, C. Chen, C. Xi, *Org. Lett.* **2016**, 18, 2050–2053.
- [124] M. Gaydou, T. Moragas, F. Juliá-Hernández, R. Martin, *J. Am. Chem. Soc.* **2017**, 139, 12161–12164.
- [125] K. Murata, N. Numasawa, K. Shimomaki, J. Takaya, N. Iwasawa, *Chem. Commun.* **2017**, 53, 3098–3101.
- [126] Q.-Y. Meng, S. Wang, G. S. Huff, B. König, *J. Am. Chem. Soc.* **2018**, 140, 3198–3201.

- [127] T. G. Ostapowicz, M. Schmitz, M. Krystof, J. Klankermayer, W. Leitner, *Angew. Chem. Int. Ed.* **2013**, *52*, 12119–12123.
- [128] L. Wu, Q. Liu, I. Fleischer, R. Jackstell, M. Beller, *Nat. Commun.* **2014**, *5*, 3091.
- [129] Q. Liu, L. Wu, I. Fleischer, D. Selent, R. Franke, R. Jackstell, M. Beller, *Chem. – Eur. J.* **2014**, *20*, 6888–6894.
- [130] X. Ren, Z. Zheng, L. Zhang, Z. Wang, C. Xia, K. Ding, *Angew. Chem. Int. Ed.* **2017**, *56*, 310–313.
- [131] *J. Organomet. Chem.* **1983**, *255*, 263–268.
- [132] H. Hoberg, S. Gross, A. Milchereit, *Angew. Chem. Int. Ed. Engl.* **1987**, *26*, 571–572.
- [133] J. Takaya, K. Sasano, N. Iwasawa, *Org. Lett.* **2011**, *13*, 1698–1701.
- [134] A. Tortajada, R. Ninokata, R. Martin, *J. Am. Chem. Soc.* **2018**, *140*, 2050–2053.
- [135] M. Takimoto, M. Kawamura, M. Mori, *Org. Lett.* **2003**, *5*, 2599–2601.
- [136] M. Takimoto, M. Kawamura, M. Mori, Y. Sato, *Synlett* **2005**, *2005*, 2019–2022.
- [137] J. Takaya, N. Iwasawa, *J. Am. Chem. Soc.* **2008**, *130*, 15254–15255.
- [138] H.-W. Suh, L. M. Guard, N. Hazari, *Chem. Sci.* **2014**, *5*, 3859–3872.
- [139] T. Tsuda, K. Ueda, T. Saegusa, *J. Chem. Soc. Chem. Commun.* **1974**, 380–381.
- [140] Y. Fukue, S. Oi, Y. Inoue, *J. Chem. Soc. Chem. Commun.* **1994**, 2091–2091.
- [141] L. J. Gooßen, N. Rodríguez, F. Manjolinho, P. P. Lange, *Adv. Synth. Catal.* **2010**, *352*, 2913–2917.
- [142] W.-Z. Zhang, W.-J. Li, X. Zhang, H. Zhou, X.-B. Lu, *Org. Lett.* **2010**, *12*, 4748–4751.
- [143] D. Yu, Y. Zhang, *Proc. Natl. Acad. Sci.* **2010**, *107*, 20184–20189.
- [144] X. Zhang, W.-Z. Zhang, X. Ren, L.-L. Zhang, X.-B. Lu, *Org. Lett.* **2011**, *13*, 2402–2405.
- [145] X. Zhang, W.-Z. Zhang, L.-L. Shi, C. Zhu, J.-L. Jiang, X.-B. Lu, *Tetrahedron* **2012**, *68*, 9085–9089.
- [146] F.-W. Li, Q.-L. Suo, H.-L. Hong, N. Zhu, Y.-Q. Wang, L.-M. Han, *Tetrahedron Lett.* **2014**, *55*, 3878–3880.
- [147] D. Yu, M. X. Tan, Y. Zhang, *Adv. Synth. Catal.* **2012**, *354*, 969–974.
- [148] X.-H. Liu, J.-G. Ma, Z. Niu, G.-M. Yang, P. Cheng, *Angew. Chem. Int. Ed.* **2015**, *54*, 988–991.
- [149] J. Luo, I. Larrosa, *ChemSusChem* **2017**, *10*, 3317–3332.
- [150] G. A. Olah, B. Török, J. P. Joschek, I. Bucsi, P. M. Esteves, G. Rasul, G. K. Surya Prakash, *J. Am. Chem. Soc.* **2002**, *124*, 11379–11391.
- [151] P. Munshi, E. J. Beckman, *Ind. Eng. Chem. Res.* **2009**, *48*, 1059–1062.
- [152] K. Nemoto, H. Yoshida, Y. Suzuki, N. Morohashi, T. Hattori, *Chem. Lett.* **2006**, *35*, 820–821.
- [153] K. Nemoto, H. Yoshida, N. Egusa, N. Morohashi, T. Hattori, *J. Org. Chem.* **2010**, *75*, 7855–7862.
- [154] K. Nemoto, S. Onozawa, N. Egusa, N. Morohashi, T. Hattori, *Tetrahedron Lett.* **2009**, *50*, 4512–4514.
- [155] T. Iijima, T. Yamaguchi, *J. Mol. Catal. Chem.* **2008**, *295*, 52–56.
- [156] H. Kolbe, *Justus Liebigs Ann. Chem.* **1860**, *113*, 125–127.
- [157] R. Schmitt, *J. Für Prakt. Chem.* **1885**, *31*, 397–411.
- [158] “The History of Aspirin | The International Aspirin Foundation,” can be found under <https://www.aspirin-foundation.com/history/>
- [159] Z. Marković, S. Marković, N. Begović, *J. Chem. Inf. Model.* **2006**, *46*, 1957–1964.
- [160] Z. Marković, S. Marković, N. Manojlović, J. Predojević-Simović, *J. Chem. Inf. Model.* **2007**, *47*, 1520–1525.
- [161] A. S. Lindsey, H. Jeskey, *Chem. Rev.* **1957**, *57*, 583–620.
- [162] J. Luo, S. Preciado, P. Xie, I. Larrosa, *Chem. – Eur. J.* **2016**, *22*, 6798–6802.
- [163] O. Vechorkin, N. Hirt, X. Hu, *Org. Lett.* **2010**, *12*, 3567–3569.
- [164] S. Kobayashi, W.-J. Yoo, T. V. Q. Nguyen, M. Guiteras Capdevila, *HETEROCYCLES* **2015**, *90*, 1196.
- [165] S. Fenner, L. Ackermann, *Green Chem.* **2016**, *18*, 3804–3807.
- [166] *J. Organomet. Chem.* **1984**, *266*, c44–c46.
- [167] I. I. F. Boogaerts, S. P. Nolan, *J. Am. Chem. Soc.* **2010**, *132*, 8858–8859.
- [168] I. I. F. Boogaerts, G. C. Fortman, M. R. L. Furst, C. S. J. Cazin, S. P. Nolan, *Angew. Chem. Int. Ed.* **2010**, *49*, 8674–8677.

- [169] L. Zhang, J. Cheng, T. Ohishi, Z. Hou, *Angew. Chem. Int. Ed.* **2010**, *49*, 8670–8673.
- [170] K. Sasano, J. Takaya, N. Iwasawa, *J. Am. Chem. Soc.* **2013**, *135*, 10954–10957.
- [171] H. Mizuno, J. Takaya, N. Iwasawa, *J. Am. Chem. Soc.* **2011**, *133*, 1251–1253.
- [172] T. Suga, H. Mizuno, J. Takaya, N. Iwasawa, *Chem. Commun.* **2014**, *50*, 14360–14363.
- [173] O. Baudoin, *Chem. Soc. Rev.* **2011**, *40*, 4902–4911.
- [174] Y. Masuda, N. Ishida, M. Murakami, *J. Am. Chem. Soc.* **2015**, *137*, 14063–14066.
- [175] N. Ishida, Y. Masuda, S. Uemoto, M. Murakami, *Chem. – Eur. J.* **2016**, *22*, 6524–6527.
- [176] K. Michigami, T. Mita, Y. Sato, *J. Am. Chem. Soc.* **2017**, *139*, 6094–6097.

Chapter 2 – Efficient catalytic systems toward carboxylation reaction of C₂H₄ with CO₂: from discovery to optimization by means of High Throughput Experimentation

This chapter describes the main works obtained using high throughput techniques. Except the early tests carried out by the “Argonne National Laboratory” (Chemical Sciences and Engineering Division, USA, group of Dr Theodore Krause), the high throughput experiments described in this Chapter were performed in collaboration with Prof. Dr. Sébastien Paul and Dr. Svetlana Heyte at the REALCAT screening platform, Villeneuve d’Ascq France. Part of this chapter has been published, see: Chem. Eur. J. 2021, 27, 3997–4003.

2.1. High-Throughput Experimentation

2.1.1. Introduction

Nowadays, over 80% of commercial chemical processes involve the use of catalysts, becoming by far the most important mean of producing various chemicals such as fertilizers, plastics, drugs and pharmaceuticals.^[1,2] Facing this continual increasing production demand, catalytic chemical processes are required to be more environmentally friendly and energetically efficient by prompt identification of highly active and selective catalysts. However, most current investigations are still commonly based on single experiments, whose results are used to plan the next experimental steps (“trial-and-error” procedures). These exhaustive studies are therefore time- and cost-consuming, requiring new methodologies to enhance research process efficiency. Therefore, acceleration through parallel experimentation has been established and, today, the principles of combinatorial chemistry are well implemented in pharmaceutical drug research (finding hit and lead compounds) and in many companies (AstraZeneca, DOW, BP, Bayer...)^[3-5] Well-known to be more than running large numbers of experiments in parallel, combinatorial chemistry refers to thoroughly planned combinations of parameters (e.g., chemical elements, solvents, additives, pre-and post-treatments, etc.). Hence, in heterogeneous and homogeneous catalysis, High Throughput Screening (HTS) experimentations have been employed to study the effect of various reaction parameters (e.g. temperature, pressure, stirring speed, time, concentration, etc.) and, at the same time, for parallel or rapid sequential testing of desired properties or functions, becoming very popular for catalyst discovery and early phase optimization. Historically, high throughput approach was firstly performed in 1909 by Mittash *et al.* at BASF, for the discovery of the first ammonia-catalyst synthesis using Haber-Bosh process.^[1,2,6] Since then, combinatorial syntheses and screening were widely applied and implemented in the health field for drug discovery, as well as for the synthesis of 25,000 new

luminescent materials.^[7] Consequently, to accelerate the discovery of new or improved homogeneous catalysts, HTS experimentations gained interest in both industry and academia. Moreover, homogeneous metal catalysts are very well suited for HTS, since in many cases, they can be prepared by simply mixing a metal precursor and ligand. Moreover, today's HTS technology promises greater efficiency, through reactor miniaturization, automation and integration.

Herein, we describe the use of HTS strategy for the reductive coupling of CO₂ with C₂H₄ and in the presence of triethylsilane (Et₃SiH), for which potential catalysts precursors and ligands were selected through an extensive literature survey (Chapter 1). The present study reported in the following chapter aims, in first intention, at identifying effective homogeneous catalytic systems toward the formation of silylesters. Once those catalytic systems identified, upscaling and optimization of the reaction conditions, using high-pressure autoclave reactors, were initiated.

2.1.2. Objectives and background

a. Ethylene carboxylation reaction using triethylsilane

Our HTS approach for carboxylation of ethylene with CO₂ relied on the evaluation of combinations of various ligands, with group 8, 9 and 10 metal precursors, in the presence of alternative, readily available reductant, namely hydrosilanes.^[8] In fact, the favoured formation of the Si–O bond (bond dissociation energy: BDE = 110 kcal·mol⁻¹)^[9] due to the oxophilicity of the silicon atom promotes formation of silylesters and therefore CO₂ reductive transformation. In addition, the relatively more facile activation of the Si–H bond (BDE = 91 kcal·mol⁻¹ in SiH₄ compared to the strong non-polar H–H bond BDE = 104 kcal·mol⁻¹ in H₂) makes hydrosilanes good reductants under relatively mild conditions. Therefore, triethylsilane (Et₃SiH) was selected as reductant as it features both high hydride donor ability and nucleophilicity among other commercially available analogues.^[9–11] We thus envisioned that such reactants may enable release of the free acrylate product from a putative metallacycle intermediate, formed by the activation of CO₂ via oxidative coupling with ethylene (details of its formation are given in Chapter I).^[12] Moreover, the highly tunable reactivity of hydrosilanes and their easiness to handle (stable liquids) make them interesting, competitive reducing agents as compared to metals and organometallic reductants. Thus, the above process involving

hydrosilanes as reductants can constitute a reliable model for related carboxylation processes operating with H₂.

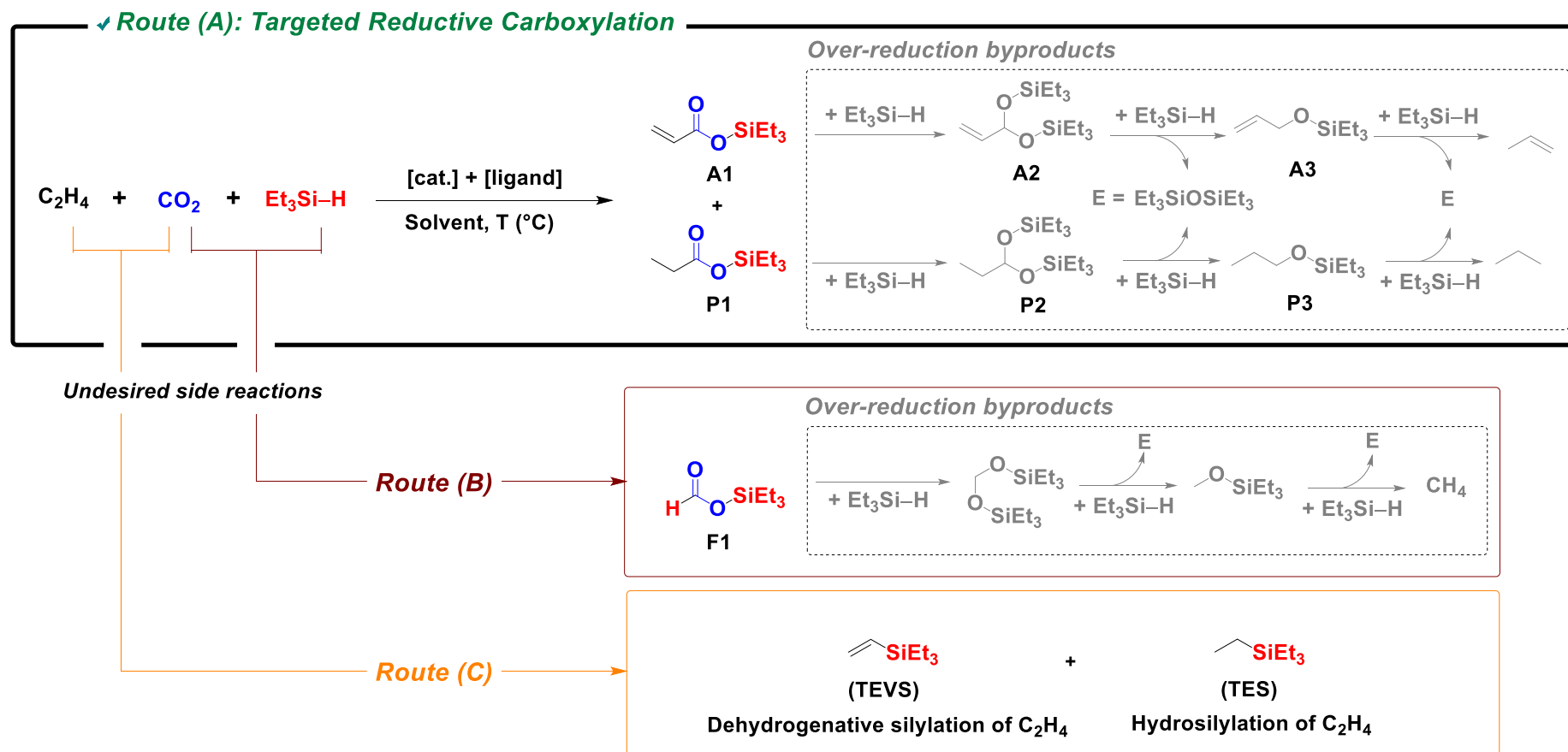
b. Preliminary results

Early studies using HTS techniques have been carried out in collaboration with the Chemical Sciences and Engineering Division of the Argonne National Laboratory, USA. Around 140 combinations of different transition metal precursors across the Periodic Table (essentially first and second row elements), in combination with various ligands, have been tested for ethylene carboxylation with CO₂ in the presence of Et₃SiH. After reaction for a given time (16 h), GC analyses of the crude mixtures revealed the presence of various compounds in the liquid phase (gaseous products such as CO, CH₄, H₂ were not sought).

Scheme I.2.1 summarizes the three possible different series of products that can be formed through the corresponding competing reaction pathways, namely routes A, B and C. The targeted triethylsilyl propionate (**P1**) and acrylate (**A1**) (Scheme I.2.1, Route A), products of the reductive carboxylation reaction of ethylene were successfully obtained with few catalyst/ligand combinations (Figure I.2.1). In some cases, traces of the products of the subsequent over-reduction reaction of triethylsilane with **A1** and **P1** to namely **A2**, **A3**, propene and, **P2**, **P3**, propane, respectively, were detected (Scheme I.2.1, Route A and Figure I.2.1). Note that for each over-reduction step, one molecule of hexaethylidisiloxane (**E**) is generated as a by-product. On the other hand, triethylsilyl formate (**F1**) issued from the hydrosilylation reaction of CO₂ was identified. The later is also subjected to a subsequent series of over-reduction reactions leading to methane (Route B).^[13] Yet, the highest competitive pathway that we observed comprises the two separate reactions between ethylene and hydrosilane (route C), namely hydrosilylation and dehydrogenative coupling, yielding the corresponding tetraethylsilane (**TES**) and triethylvinylsilane (**TEVS**).^[14] Throughout this study, by stating that the selectivity for the catalytic carboxylation reaction of C₂H₄ in the presence of Et₃SiH is enhanced, it implies that the TON towards the desired route A products are increased, while those of the unwanted route B and C are lowered.

Among the combinations tested in HTS, catalytic systems based on Ru have revealed their capability to afford mixtures of the three relevant compounds **A1**, **P1** and **P2**, with (unoptimized) TONs ranging from 5 to 12 (Figure I.2.1). Also, some systems based on Rh yielded mostly produced **P1** and **F1** (TONs of 17 and 7, respectively). Other catalytic

combinations based on Ni have shown propensity to afford selectively (depending on the nature of ligand) only insignificant amounts of one of the four products **A1**, **P1**, **P2** and **F1**.



Scheme I.2.1. Possible products of the coupling reaction of CO₂ with C₂H₄ in the presence of Et₃SiH.

Part I – Chapter 2

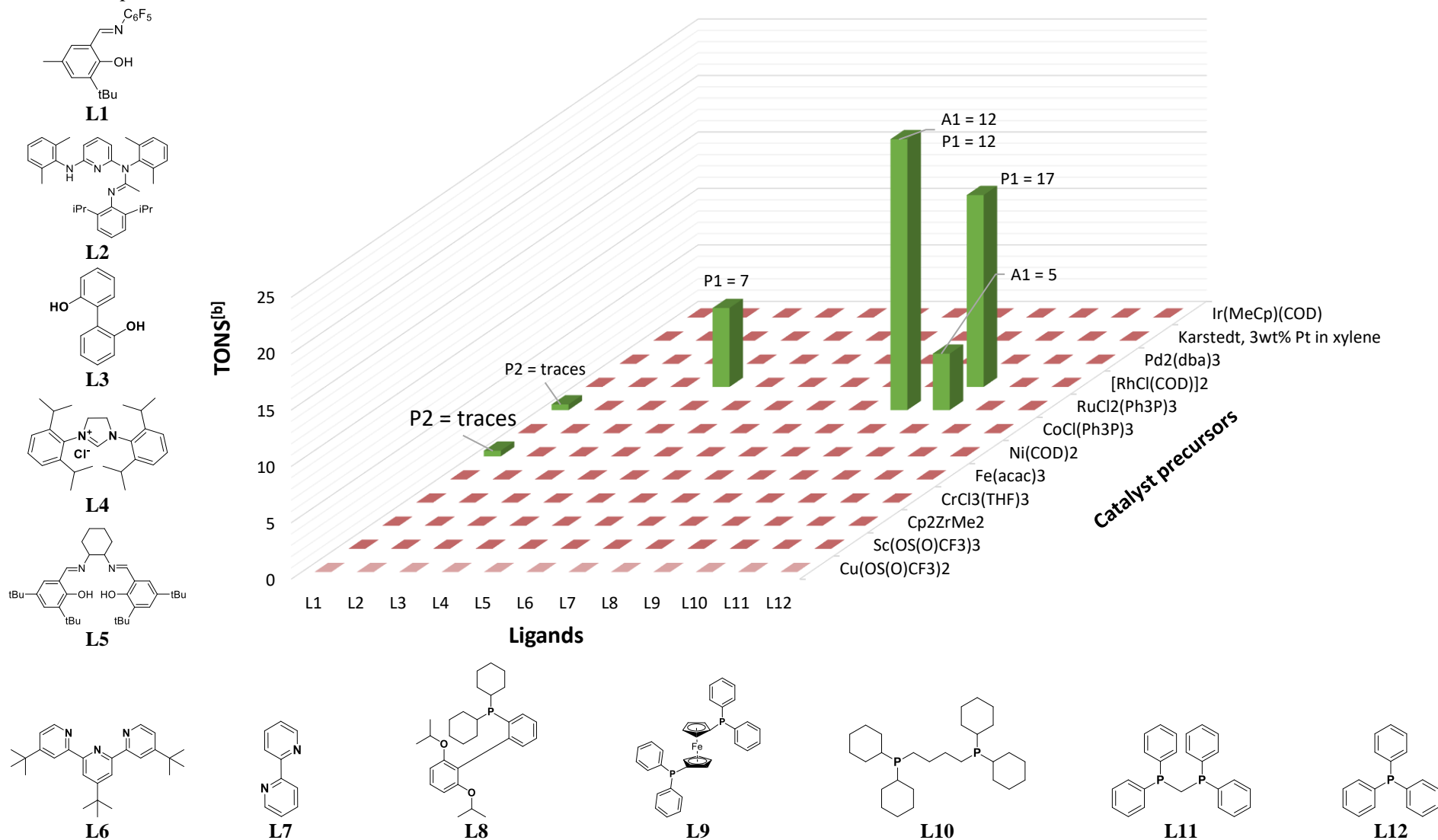


Figure I.2.1. Early catalytic results of the coupling reaction of CO₂ with C₂H₄ in the presence of Et₃SiH.^[a]

^[a] Solvent (1.0 mL), [Si-H]₀ = 0.43 mol·L⁻¹, [Precursor]₀ = [ligand]₀ = 0.002 mol·L⁻¹, CO₂/C₂H₄ 1:1 mol/mol, P(CO₂) + P(C₂H₄) = 2 and 17 bar, 80°C, 20h. ^[b] Turnover number determined by GC-FID using *n*-dodecane as internal standard (0.22 mol·L⁻¹).

c. HTS methodology

Since Ru and Rh catalyst precursors were found active towards the targeted carboxylation reaction of ethylene with CO₂, a series of more detailed HTS investigations was undertaken in collaboration with the REALCAT platform (University of Lille, France). Runs of 24 parallel tests were performed involving commercially available Ru and Rh precatalysts namely [Ru(*p*-cymene)Cl₂]₂, Ru(H)(Cl)(CO)(PPh₃)₃, Rhodium(II) bis(*n*-octanoate), Rh(Cl)(PPh₃)₃ and [RhCl(COD)]₂ in combination with a set of diphosphine ligands featuring variable stereo-electronic properties (Figure I.2.2).

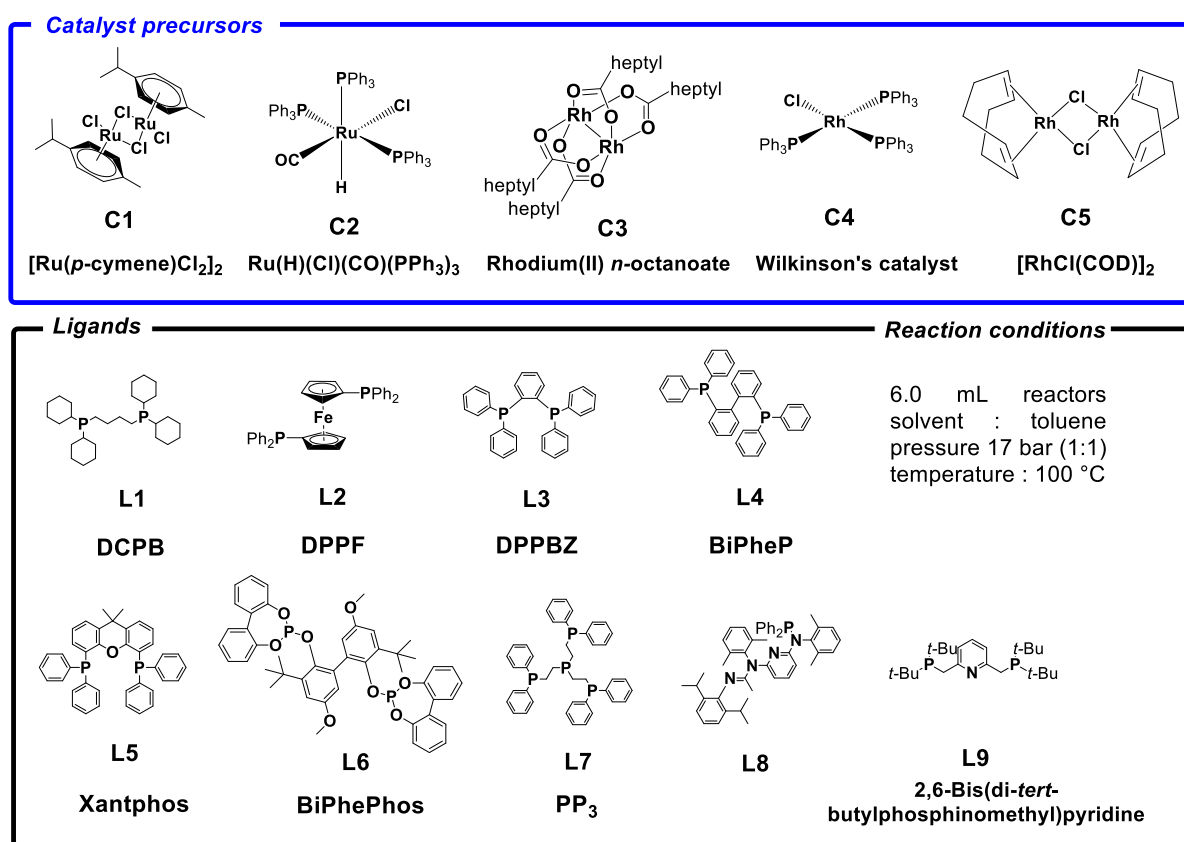


Figure I.2.2. HTS precursor/ligand combinations used at the REALCAT platform (Ecole Centrale de Lille, France).

The following experimental conditions were applied (Figure 1.2.3): 6.0 mL inox reactors were filled with Et₃SiH (0.86 mmol), [precursor]₀ = [ligand]₀ = 0.5 mol% vs. hydrosilane, solvent (toluene, 2 mL), and were pressurized with an equimolar C₂H₄-CO₂ gas mixture (P_{total} = 17 bar) at a reaction temperature of 100 °C for 16 h. The crude reactions mixtures were analyzed by GC-FID and GC-MS. The analytical techniques developed in this study enabled unequivocal separation, authentication and quantification of the most relevant

(**A1**, **P1**) of the above possible products (except the gaseous ones CH₄, H₂, C₃H₆, C₃H₈, CO) and overall Et₃SiH molar balance of 72-98% were obtained in most cases.^[a]

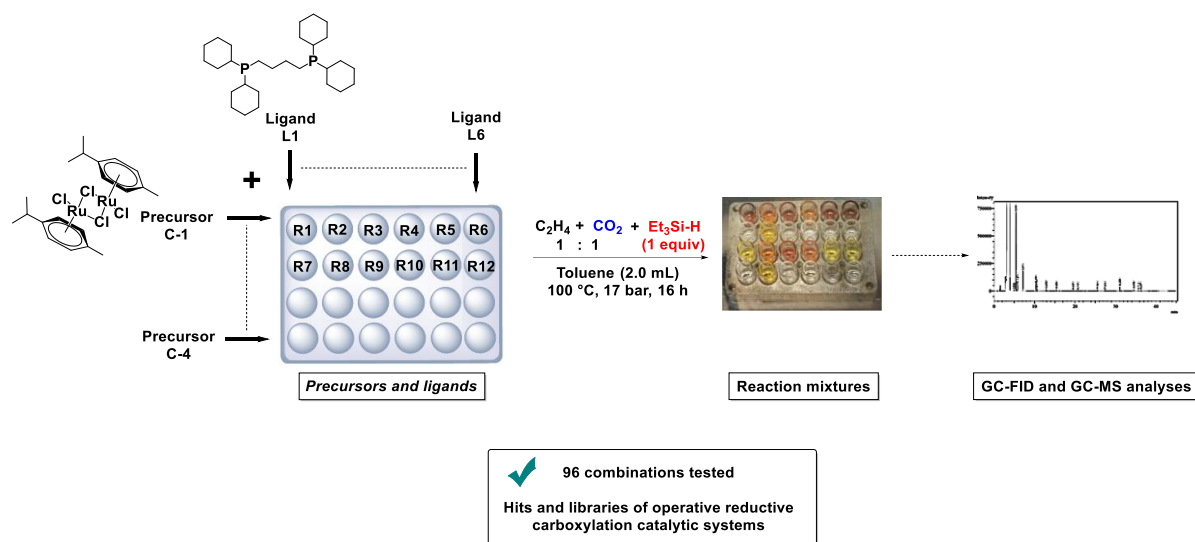


Figure I.2.3. General representation of HTS process for reductive coupling of CO₂ with C₂H₄ in presence of Et₃SiH. Reaction conditions : solvent (toluene, 2 mL), C₂H₄:CO₂ gas mixture (1:1, P_{total} = 17 bar), 100 °C, 16h.

2.2. Results and discussion

2.2.1. HTS catalytic results of the reductive coupling of CO₂ with C₂H₄ and Et₃SiH

The catalytic results obtained through HTS experiments are given in Tables I.2.1 and I.2.2. The first run (#1, Table I.2.1) refers to the utilization of C1, C2, C3, C4 precursors in combination with L1, L2, L3, L4 ligands. As demonstrated by the high conversions of Et₃SiH (> 44%), all of the combination tested were found enabling Et₃SiH transformation. However, as judged by the TONs values, the targeted **A1** and **P1** silyl esters were not selectively formed, as route C products formation was prevalent (TONs > 100 for **TES** and **TEVS**, Table I.2.1). The presence of these co-products is not surprising since hydrosilylation of CO₂ and alkenes in addition to dehydrogenative silylation reaction have been well documented in the scientific communities.^[15,16]

For example, rhodium complexes are known for nearly 40 years as highly effective (pre)catalysts for hydrosilylation.^[17] Many Rh(I) and Rh(III) complexes catalyze this reaction, e.g. [RhX(R₃P)₃] (where X = Cl, R = Ph, Wilkinson's catalyst), [RhX(CO)(R₃P)₂], or RhH(PPh₃)₄.^[17-19] Systems such as [(COD)RhCl]₂/L where L = PPh₃ or ^tBu₂PCH₂P^tBu₂ are also

^[a] Calculated as follows: $100 - [(n_{\text{Et}_3\text{SiH introduced}} - \sum n_{\text{silylated products}}) / n_{\text{Et}_3\text{SiH introduced}}] \times 100$

highly selective towards hydrosilylation of alkenes.^[20,21] Indeed, as shown in Tables I.2.1 and I.2.2, (entries 13 to 18), $[\text{Rh}(\text{COD})\text{Cl}]_2/\text{L}_{1-9}$ and $\text{Rh}(\text{Cl})(\text{PPh}_3)_3/\text{L}_{1-9}$ delivered exclusively **TES** and **TEVS** products, confirming their efficiency toward ethylene hydrosilylation.

On the other hand, the Ru-based precursors C1 and C2 in combination with L1 and L2 ligands delivered, although not selectively, **A1** and **P1** silylesters in quantifiable TONs (Table I.2.1, entries 1, 2, 7, 8, 19 and 20). These combinations were re-evaluated and the TONs values confirmed their ability to access route A products (run #2, Tables I.2.3, entries 1, 2, 7 and 8). Interestingly, experiments conducted with the L7 ligand successfully provided **A1** product with the highest TON of 18 (Table I.2.2, entries 4 and 10).

Initially judged as promising, duplicated experiments using C1 and C2 precursors with ligand L4 failed in delivering **A1** and **P1** products (Table I.2.1, entries 4, 10 vs Table I.2.2, entries 3 and 9). The observed variation of activity is probably due to the possible presence of traces of impurities/poisons in the HTS reactors. Indeed, blank tests carried out without any metal precursor showed a slight production of **F1**, **TEVS** and **TES** (Table I.2.2, entries 19 to 24). Surprisingly, performing the HTS tests in single use glass reactors increased drastically unwanted route B and C products, attesting the probable involvement of the reactors material in promoting some side-reactions.^[b]

In summary, only few combinations of the 48 tested allowed to observe the formation of silyl esters **A1** and **P1** products. In particular, the following Ru-based systems were pinpointed: $\text{Ru}(\text{H})(\text{Cl})(\text{CO})(\text{PPh}_3)_3/1,4\text{-bis}(\text{dicyclohexylphosphino})\text{butane}$ (DCPB), $\text{Ru}(\text{H})(\text{Cl})(\text{CO})(\text{PPh}_3)_3/\text{tris}[2\text{-(diphenylphosphino)ethyl}]\text{phosphine}$ (PP₃), $\text{Ru}(\text{H})(\text{Cl})(\text{CO})(\text{PPh}_3)_3/1,1'\text{-Ferrocenediyl-bis}(\text{diphenylphosphine})$ (DPPF), $[\text{Ru}(p\text{-cymene})\text{Cl}_2]_2/\text{DCPB}$ and $[\text{Ru}(p\text{-cymene})\text{Cl}_2]_2/\text{DPPF}$. Described for the first time, these group 8 metal-based systems appeared to give a direct access to silyl esters from ethylene, CO₂ and hydrosilane, with moderate to high triethylsilane conversions.

^[b] Single-use glass reactors experimental results are not included in the present manuscript.

Table I.2.1. Results from HTS experiments from run #1.^[a]

Entry	Run #1 Precursor/Ligand	Conv. Et ₃ SiH [mol%] ^[b]	TON ^[c]				
			Route A		Route B and C		
			A1	P1	F1	TES + TEVS	E
1	C1/L1	>98	0.4	traces	141	55	2
2	C1/L2	>98	0.2	traces	79	103	4
3	C1/L3	>98	0	traces	38	159	3
4	C1/L4	61	0.4	traces	120	traces	3
5	C1/L5	53	0	0	187	traces	2
6	C1/L6	70	0	0	60	78	2
7	C2/L1	84	0.3	traces	58	102	3
8	C2/L2	92	0.3	traces	72	102	0
9	C2/L3	>98	0	traces	0	200	0
10	C2/L4	44	2	traces	81	5	0
11	C2/L5	>98	0	traces	0	200	0
12	C2/L6	>98	0	0	0	199	0
13	C3/L1	>98	0	0	0	196	0
14	C3/L2	>98	0	0	0	196	0
15	C3/L3	>98	0	0	72	124	3
16	C3/L4	>98	0	0	0	195	5
17	C3/L5	>98	0	0	39	161	0
18	C3/L6	>98	0	0	0	200	0
19	C4/L1	75	0.7	traces	63	86	0
20	C4/L2	>98	0.1	traces	53	147	0
21	C4/L3	56	0	0	69	42	0
22	C4/L4	84	0.2	traces	70	89	5
23	C4/L5	>98	0	0	46	154	0
24	C4/L6	98	0	0	32	162	0

^[a] Solvent (2.0 mL), [Si–H]₀ = 0.043 mol·L⁻¹, [Precursor]₀ = [ligand]₀ = 0.0002 mol·L⁻¹, CO₂/C₂H₄ 1:1 mol/mol, P(CO₂) + P(C₂H₄) = 17 bar. ^[b] Determined by integration of the ¹H NMR peaks vs. those of the standard ((Me₃Si)₄Si. ^[c] Turnover number as determined by GC-FID using *n*-dodecane as internal standard.

Table I.2.2. Results from HTS experiments with run #2.^[a]

Entry	Run #2 Precursor/Ligand	Conv. Et ₃ SiH [mol%] ^[b]	TON ^[c]					
			Route A		Route B and C			
			A1	P1	F1	TES	TEVS	E
1	C1/L1	>98	3	Traces	49	25	123	0.3
2	C1/L2	59	12	Traces	101	29	20	0.2
3	C1/L4	52	0	Traces	7	15	43	0
4	C1/L7	>98	4	Traces	44	51	105	0
5	C1/L8	72	0	0	2	40	67	0
6	C1/L9	97	0	0	3	56	87	0.4
7	C2/L1	55	4	Traces	87	2	23	0
8	C2/L2	95	3	Traces	28	20	124	0
9	C2/L4	90	0	Traces	3	17	118	0.2
10	C2/L7	8	18	Traces	34	0	0	0
11	C2/L8	>98	0	Traces	2	33	132	0
12	C2/L9	>98	0	0	1	37	132	0
13	C5/L1	>98	0	0	14	61	94	0.9
14	C5/L2	>98	0	0	13	60	97	0.8
15	C5/L4	>98	0	0	2	49	111	0
16	C5/L7	88	0	0	2	49	62	1.4
17	C5/L8	>98	0	0	1	42	124	0
18	C5/L9	>98	0	0	2	54	140	0
19	L1	10	0	Traces	20	1	1	0
20	L2	6	0	Traces	24	0	1	0.5
21	L4	3	0	0	1	0	0	0
22	L7	6	0	Traces	33	0	1	0
23	L8	6	0	0	3	0	1	0
24	L9	0	0	0	17	14	32	0

^[a] Solvent (2.0 mL), [Si–H]₀ = 0.043 mol·L⁻¹, [Precursor]₀ = [ligand]₀ = 0.0002 mol·L⁻¹, CO₂/C₂H₄ 1:1 mol/mol, P(CO₂) + P(C₂H₄) = 17 bar. ^[b] Determined by integration of the ¹H NMR peaks vs. those of the standard ((Me₃Si)₄Si). ^[c] Turnover number as determined by GC-FID using *n*-dodecane as internal standard.

2.2.2. Batch-scale metal-catalyzed synthesis of silylesters from CO₂ and C₂H₄

a. Upscaling to batch scale reactors

The previously pinpointed “hit” catalyst combinations were next employed in batch experiments using 50 mL-autoclaves (Figure I.2.4). Table 1.2.3 summarizes HTS results (numbered from 1 to 4) and scaled up batch system (highlighted in grey and numbered from 1’ to 4’). The concentrations of reductant, catalyst and ligand were increased by one order of magnitude compared to HTS protocols and the 50 mL-reactors were pressurized with a CO₂/C₂H₄ gas mixture molar ratio of 1:1 (CO₂/C₂H₄/Et₃SiH = 2:2:1 ratio). After 16 h at 100°C, the crude mixtures were analysed by GC-FID and GC-MS.

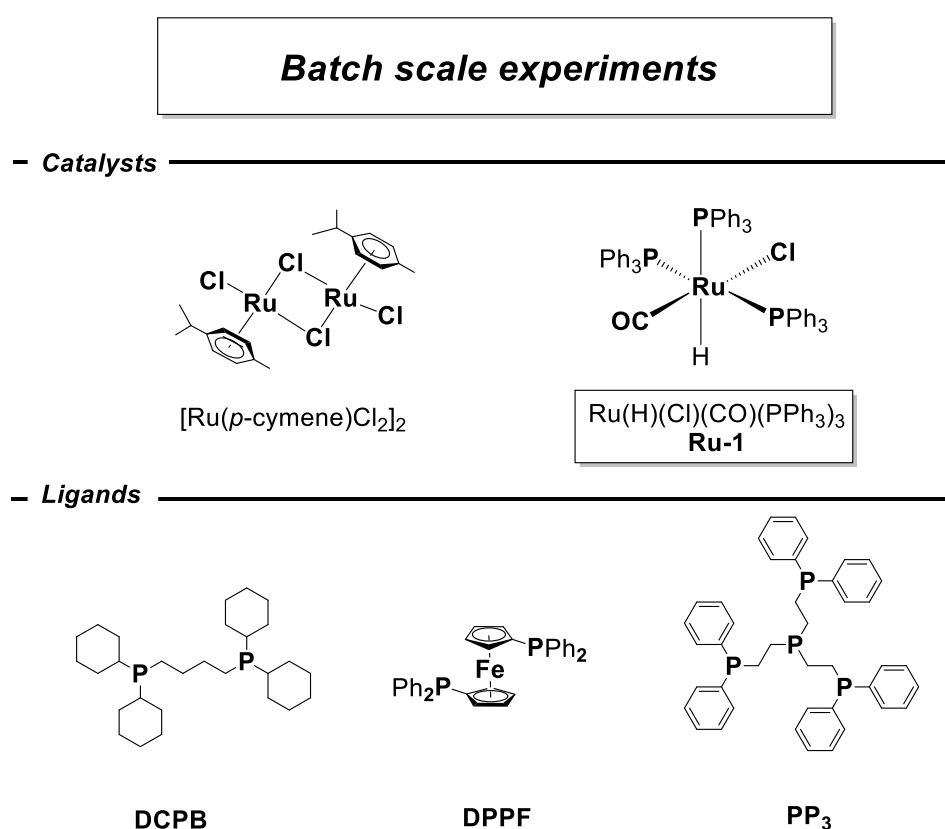


Figure I.2.4. Main Ru(II) precursors and diphosphine ligands used in batch-scale studies.

Table I.2.3. HTS (1 to 4) and autoclave scale (1' to 4') catalytic carboxylation of ethylene with CO₂ and HSiEt₃.

Entry	Precursor / ligand (1:1, 0.5 mol%) (vs. HSiEt ₃)	Conv. HSiEt ₃ [mol%] ^[b]	TON (mol(product)·mol(Ru) ⁻¹) ^[c]									
			Route A products					Route B and C products				
			A1	PI	F1	TES	TEVS	E				
1	[Ru(<i>p</i> -cymene)Cl ₂] ₂ / DCPB	>98	0.4	traces	141	55	2					
1'		>98	0	0	0	180	traces	traces				
2	Ru(H)(Cl)(CO)(PPh ₃) ₃ / PP ₃	8	18	traces	34	0	0					
2'		29	0	0	0	traces	2	0				
3	Ru(H)(Cl)(CO)(PPh ₃) ₃ / DCPB	92	0.3	traces	72	102	0					
3'		54	13	1.3	16	4	53	1.6				
4	[Ru(<i>p</i> -cymene)Cl ₂] ₂ / DPPF	>98	0.2	traces	79	103	4					
4'		67	0	3	0	74	16	2				
5	Ru(H)(Cl)(CO)(PPh ₃) ₃ / DPPF	92	0.3	traces	72	102	0					
5'		16	0.2	0.4	0	10	4	0.4				

In Grey, bench scale reaction conditions: toluene (20 mL), [Si-H]₀ = 0.43 mol·L⁻¹, [Ru]₀ = [ligand]₀ = 0.002 mol·L⁻¹, CO₂/C₂H₄ 1:1 mol/mol, P(CO₂) + P(C₂H₄) = 20 bar; 16 h; results of at least duplicated experiments and averaged TON values. ^[b] Determined by integration of the ¹H NMR signals vs. those of the standard ((Me₃Si)₄Si). ^[c] Turnover number as determined by GC-FID using *n*-dodecane as internal standard.

The precursor $[\text{Ru}(p\text{-cymene})\text{Cl}_2]_2$ in combination with DCPB ligand gave promising results since detectable amounts of **A1** and **P1** were observed, along with high TONs of route B and C products (Table 1.2.3, entry 1). Although high conversions of Et_3SiH were achieved both under HTS and batch reactors conditions (entries 1 and 1'), only route C products were unfortunately detected after performing the reaction in autoclave. The same trend was observed for the $\text{Ru}(\text{H})(\text{Cl})(\text{CO})(\text{PPh}_3)_3 / \text{PP}_3$ combination, for which the HTS TONs were irreproducible under batch conditions.

On the other hand, when combining $\text{Ru}(\text{H})(\text{Cl})(\text{CO})(\text{PPh}_3)_3$ with DCPB, moderate to good conversions were achieved in both HTS and bench scale experiments. An overall TON of 14 was obtained for the formation of **A1** and **P1** silylesters (molar ratio **A1/P1** of 10:1, entries 3 and 3'). Significant amounts of **F1** (silyl formate) were, however, observed concomitantly (entries 3 and 3', TONs of 72–16, respectively), in addition to **TES** and **TEVS** formation in large amounts with TONs exceeding 55.

Combinations of $[\text{Ru}(p\text{-cymene})\text{Cl}_2]_2$ and $\text{Ru}(\text{H})(\text{Cl})(\text{CO})(\text{PPh}_3)_3$ precursors with DPPF were then studied (entries 4 and 5). Although both HTS and bench-scale experiments gave similar results toward route A esters formation, the main products formed remained those of routes B and C, resulting therefore in very low selectivity.

Overall, enhanced selectivity and catalytic activity toward the route A products were observed when the electron-rich DCPB ligand was combined to $\text{Ru}(\text{H})(\text{Cl})(\text{CO})(\text{PPh}_3)_3$ (**Ru-1**) complex. We found that the bench-scale turnover numbers of **Ru-1**/DCPB combination were higher than those obtained through HTS studies. Since reproducibility issues were already observed, the difference of activity witnessed while upscaling the concentrations might probably come from traces of impurities/poisons within the HTS reactors.

In spite of the different promising tests obtained by HTS, only one catalytic combination gave encouraging outcome upon scaling-up to the bench reactors levels. Therefore, in order to optimize further the reaction conditions, we chose to focus on the **Ru-1**/DCPB system. We began our studies by evaluating the effects of other reaction conditions such as the nature of solvent, gas pressures and the temperature.

b. Optimization of the reaction conditions

Choosing a suitable solvent for an effective reaction or process is a key parameter to take into account. Indeed, as an example, the solubility of ethylene is an important criterion required to describe the kinetics but also the selectivity of metallocene-catalyzed olefin polymerization.^[22] Moreover, previous studies have reported solubility data of ethylene in toluene, as it has been often used as a reaction medium for its homopolymerization and copolymerization.^[22,23] Therefore, our first investigations started using toluene as solvent for the coupling reaction of CO₂ with C₂H₄ and Et₃SiH (Table 1.2.4, entry 1). We observed that aprotic solvents such as polar THF and non-polar toluene are quite effective for the transformation, producing **A1** with TON of 3 and 13, respectively (entries 1 and 2). On the other hand, running the reaction in polar DMF (37/3.87 D) and NMP (32/4.09 D) solvents did not yield **A1**, but **P1** with relatively low TONs (entries 3 and 4, TONs of 4 and 7, respectively). However, the competing route C products were obtained in higher TONs, compared to those achieved in experiments in non-polar solvents (entries 2 and 4 vs. 1 and 2). Hence, the targeted **A1** product was obtained in toluene and THF, whereas unwanted route B and C products were mainly favoured in DMF and NMP. In short, we decided to perform further experiments using toluene.

Table I.2.4. Catalytic results from batch experiments carried out in different solvents.^[a]

Entry ^[a]	Solvent (20 mL)	Conv. Et ₃ SiH [mol%] ^[b]	TON ^[c]					
			Route A		Route B and C			
			A1	P1	F1	TES	TEVS	E
1	Toluene	54	13	1.3	16	4	53	1.6
2	THF	n.d.	3	0.4	34	3	44	0.4
3	DMF	>98	0	4	15	n.d.	94	56
4	NMP	n.d.	1	7	10	38	54	14

^[a] [Si–H]₀ = 0.43 mol·L⁻¹, [Ru(H)(Cl)(CO)(PPh₃)₃]₀ = [DCPB]₀ = 0.002 mol·L⁻¹, CO₂/C₂H₄ 1:1 mol/mol, P(CO₂) + P(C₂H₄) = 20 bar. 100 °C. 16h

^[b] Determined by integration of the ¹H NMR signals using (Me₃Si)₄Si as internal standard.

^[c] Turnover number as determined by GC-FID using *n*-dodecane as internal standard.

Given the observed partial insolubility of **Ru-1** precursor at room temperature in toluene, we decided to test the influence of the temperature, hoping to improve route A products formation.

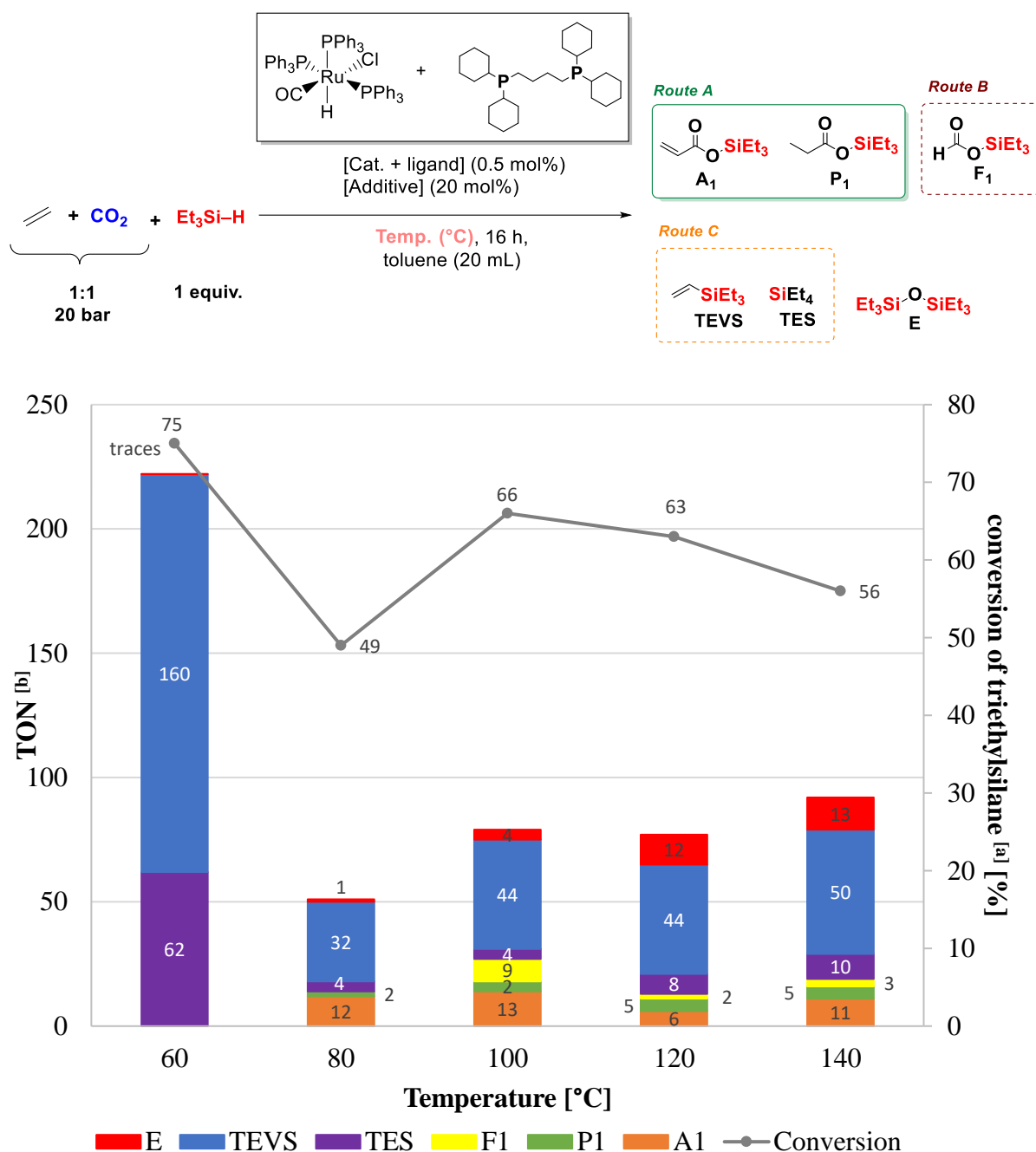


Figure I.2.5. Influence of the temperature on the selectivity toward **A1** and **P1** products.^[*]

Experiments targeting the evaluation of temperature were conducted using the **Ru-1/DCPB** catalytic system (Figure 1.2.5). Decreasing the temperature below 80 °C proved detrimental to the reaction: silylesters products **A1** and **P1** were not detected at all and mainly route C products (**TES** and **TEVS**) were observed. Increasing the temperature to 80 °C resulted

[*] Solvent (20 mL), $[\text{Si-H}]_0 = 0.43 \text{ mol}\cdot\text{L}^{-1}$, $[\text{Ru}(\text{H})(\text{Cl})(\text{CO})(\text{PPh}_3)_3]_0 = [\text{DCPB}]_0 = 0.002 \text{ mol}\cdot\text{L}^{-1}$, $[\text{KF}]_0 = 0.086 \text{ mol}\cdot\text{L}^{-1}$, $\text{CO}_2/\text{C}_2\text{H}_4$ 1:1 mol/mol, $\text{P}(\text{CO}_2) + \text{P}(\text{C}_2\text{H}_4) = 20 \text{ bar}$. [a] Determined by integration of the ^1H NMR signals vs. $(\text{Me}_3\text{Si})_4\text{Si}$ as internal standard. [b] Turnover number: TON ($\text{mol}(\text{product})\cdot\text{mol}(\text{Ru})^{-1}$) determined by GC-FID using *n*-dodecane as internal standard.

in the decrease of Et₃SiH conversion, yet allowing formation of **A1** and **P1** with an overall TON of 14. At 100 °C and above, the selectivity for route A products started to decrease to the benefit of route B and C products. Hence, the reaction has better to be conducted at 100 °C, when the best compromise between conversion and selectivity was achieved.

With the thus optimized conditions (solvent and temperature) in hand, we decided testing different ratios of the C₂H₄/CO₂ gas mixture. Under a CO₂ enriched gas atmosphere (C₂H₄/CO₂ molar ratio of 1:3) route A products were still obtained with moderate TON of 9.2 (compared to the reaction performed under a C₂H₄:CO₂ gas ratio of 1:1, Table 1.2.5, entries 1 vs. 2). Not surprisingly, the formation of the product of the hydrosilylation of CO₂, **F1**, was favored while the amounts of the products of route C decreased. Conversely, under ethylene-enriched conditions (3:1), the reactions of hydrosilylation and dehydrogenative silylation of ethylene were favored (entry 3). Route A silyl esters were obtained with TONs similar to those obtained under an equimolar ratio of C₂H₄/CO₂ gas mixture. These observations suggest that the gas concentration does not affect the elementary steps of the catalytic cycle delivering **A1** and **P1**. There are therefore at least three distinct and competitive CO₂ reduction pathways.

Table I.2.5. Catalytic results from batch experiments upon varying the relative C₂H₄ and CO₂ pressures.^[a]

Entry	C ₂ H ₄ /CO ₂ ratio	Conv. Et ₃ SiH [mol%] ^[b]	TON ^[c]					
			Route A		Route B and C			
			A1	P1	F1	TES	TEVS	E
1	1:1	54	13	1.3	16	4	53	1.6
2	1:3	34	9	0.2	28	1	16	1
3	3:1	44	13	1	traces	3	37	2

^[a] Solvent (20 mL), [Si–H]₀ = 0.43 mol·L⁻¹, [Ru(H)(Cl)(CO)(PPh₃)₃]₀ = [DCPB]₀ = 0.002 mol·L⁻¹, CO₂/C₂H₄ 1:1 mol/mol, P(CO₂) + P(C₂H₄) ≈ 20 bar. ^[b] Determined by integration of the ¹H NMR signals vs. (Me₃Si)₄Si as internal standard. ^[c] Turnover number as determined by GC-FID using *n*-dodecane as internal standard.

2.2.3. Toward metal-catalyzed synthesis of carboxylic acids from CO₂, C₂H₄ and H₂?

Encouraged by the preliminary HTS results obtained for the carboxylation reaction of C₂H₄ with Et₃SiH, we were curious to know if the successful **Ru-1**/DCPB catalytic system would deliver acrylic acid using H₂ as reductant.

Using HTS experimental tools, the different precursor/ligand combinations shown in Figure I.2.6 were introduced into reactor vials to react with C₂H₄, CO₂ and H₂ under different conditions. The tests were firstly run in toluene at 100 °C under 15 bar pressure of C₂H₄/CO₂/H₂

(1:1:1). Among the 48 combinations tested, only the Ni(cod)₂/DCPE system delivered propionic acid, yet with a very low TON = 3, as confirmed by the mass spectrum shown in Figure I.2.7.

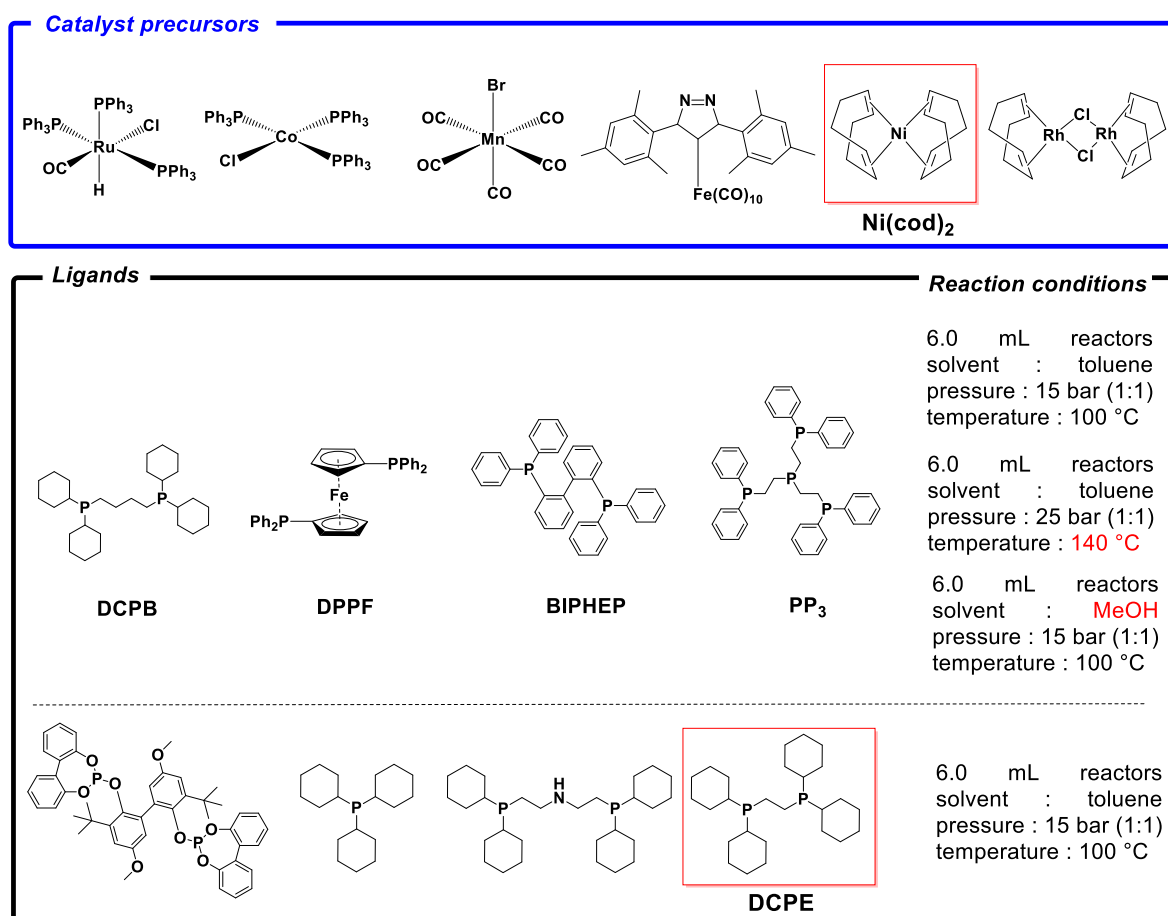


Figure I.2.6. HTS precursor/ligand combinations used for carboxylation reaction of C₂H₄ with H₂ at the REALCAT platform (Ecole Centrale de Lille, France).

Combinations of metal precursors with DCPB, DCPF, BiPheP and PP₃ ligands failed in producing carboxylic acids when increasing the temperature to 140 °C. On the other hand, switching the solvent to MeOH did not yield the corresponding methyl acrylate nor propionate esters.

Among the 96 combinations tested, only the Ni(cod)₂/DCPE system was found promising towards carboxylation reaction of C₂H₄ with H₂. Unfortunately, performing the reaction on a bench-scale autoclave failed in delivering the propionic acid previously formed in HTS. This observation pinpoints again likely the activity of the steel reactor walls.

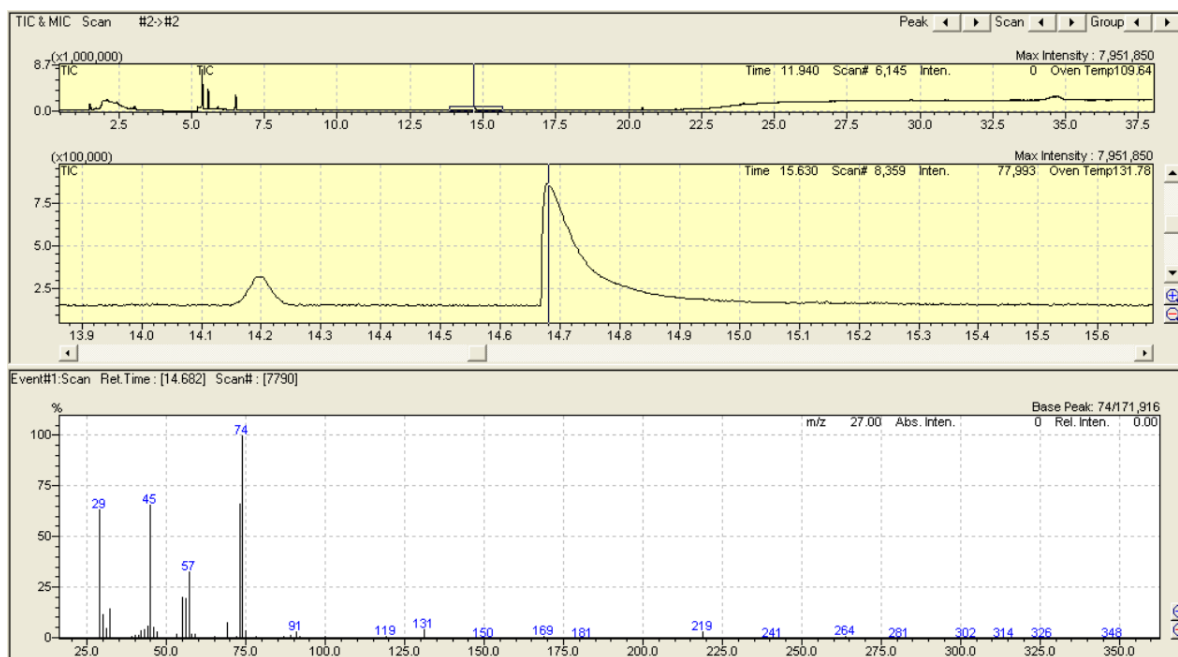


Figure I.2.7. GC-MS spectrum of the reaction medium using the $\text{Ni}(\text{cod})_2/\text{DCPE}$ system. The peak at 14.682 min refers to propionic acid ($m/z = 74$).

2.3. Conclusion

Through the state-of-the-art described in Chapter 1, several studies attempting the catalytic carboxylation reaction of ethylene with CO_2 and a reductant have been carried by using different transition metal complexes. Herein, the first metal-catalyzed synthesis of silylesters from C_2H_4 , CO_2 and HSiEt_3 was investigated, using HTS methodology. A series of *in situ*-prepared catalytic systems incorporating Ru(II), Rh(I) precursors and bidentate phosphine ligands has been probed. The catalytic production of propionate and acrylate silyl esters was evidenced by HTS and successfully implemented in batch reactor techniques. Optimization of the reaction conditions was undertaken in order to minimize side reactions; namely hydrosilylation of CO_2 and dehydrogenative silylation of ethylene. The most promising catalyst system was identified as a combination of $\text{Ru}(\text{H})(\text{Cl})(\text{CO})(\text{PPh}_3)_3$ and 1,4-bis(dicyclohexylphosphino)butane, affording encouraging TONs under a range of conditions.

2.4. References

- [1] D. Farrusseng, *Surf. Sci. Rep.* **2008**, *63*, 487–513.
- [2] J. M. Newsam, F. Schüth, *Biotechnol. Bioeng.* **1999**, *61*, 203–216.
- [3] W. F. Maier, *ACS Comb. Sci.* **2019**, *21*, 437–444.
- [4] R. A. Paciello, in *Appl. Homog. Catal. Organomet. Compd.*, Wiley-Blackwell, **2017**, pp. 1085–1096.
- [5] M. T. Reetz, M. H. Becker, H.-W. Klein, D. Stöckigt, *Angew. Chem. Int. Ed.* **1999**, *38*, 1758–1761.
- [6] C. Bosch, A. Mittasch, H. Wolf, G. Stern, *Production of Ammonia and Catalytic Agents for Use Therein*, **1913**, US1068967A.
- [7] E. Danielson, J. H. Golden, E. W. McFarland, C. M. Reaves, W. H. Weinberg, X. D. Wu, *Nature* **1997**, *389*, 944–948.
- [8] T. Fujihara, T. Xu, K. Semba, J. Terao, Y. Tsuji, *Angew. Chem. Int. Ed.* **2011**, *50*, 523–527.
- [9] Z. M. Heiden, A. P. Lathem, *Organometallics* **2015**, *34*, 1818–1827.
- [10] M. Horn, L. H. Schappele, G. Lang-Wittkowski, H. Mayr, A. R. Ofial, *Chem. – Eur. J.* **2013**, *19*, 249–263.
- [11] J. Xu, A. E. Krajewski, Y. Niu, G. S. M. Kiruba, J. K. Lee, *Chem. Sci.* **2019**, *10*, 8002–8008.
- [12] A. Tortajada, F. Juliá-Hernández, M. Börjesson, T. Moragas, R. Martin, *Angew. Chem. Int. Ed.* **2018**, *57*, 15948–15982.
- [13] F. J. Fernández-Alvarez, L. A. Oro, *ChemCatChem* **2018**, *10*, 4783–4796.
- [14] S. Lachaize, L. Vendier, S. Sabo-Etienne, *Dalton Trans.* **2010**, *39*, 8492–8500.
- [15] Y. Zhang, T. Zhang, S. Das, *Green Chem.* **2020**, *22*, 1800–1820.
- [16] “Organotransition Metal Chemistry: From Bonding to Catalysis, by John Hartwig with Contributions by Patrick J. Walsh, Geoffrey W. Coates, Charles P. Casey, Jack R. Norton, copyright 2010, published by University Science Books,” can be found under <http://www.uscibooks.com/hartwig.htm>
- [17] B. Marciniec, in *Hydrosilylation Compr. Rev. Recent Adv.* (Ed.: B. Marciniec), Springer Netherlands, Dordrecht, **2009**, pp. 3–51.
- [18] X. Ren, Z. Zheng, L. Zhang, Z. Wang, C. Xia, K. Ding, *Angew. Chem. Int. Ed.* **2016**, *56*, 310–313.
- [19] “Earth-abundant transition metal catalysts for alkene hydrosilylation and hydroboration | Nature Reviews Chemistry,” can be found under <https://www-nature-com.passerelle.univ-rennes1.fr/articles/s41570-018-0001-2>
- [20] P. Hofmann, C. Meier, W. Hiller, M. Heckel, J. Riede, M. U. Schmidt, *J. Organomet. Chem.* **1995**, *490*, 51–70.
- [21] R. Takeuchi, N. Tanouchi, *J. Chem. Soc. Chem. Commun.* **1993**, *0*, 1319–1320.
- [22] J. Wu, Q. Pan, G. L. Rempel, *J. Appl. Polym. Sci.* **2005**, *96*, 645–649.
- [23] Y. Sato, N. Hosaka, H. Inomata, K. Kanaka, *Fluid Phase Equilibria* **2013**, *344*, 112–116.

Part II

Ruthenium(II) complexes bearing bidentate phosphine ligands: catalysis and mechanistic insights towards propionate and acrylate silyl esters synthesis

Part II

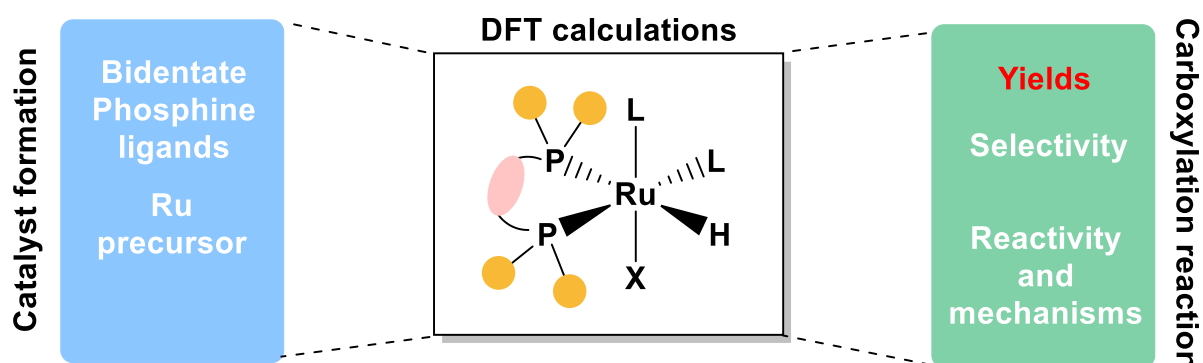
Introduction	137
Chapter 3 – Catalytic CO₂-C₂H₄ coupling mediated by ruthenium(II) complexes bearing bidentate chelating phosphines	139
3.1. Evaluation of the ligand effect on the catalytic activity	139
3.2. Towards identifying reaction intermediates: syntheses and characterization of new Ru ^{II} phosphine chelated Ru(H)(Cl)(CO)(DCPB)(PPh ₃) and Ru(H)(Cl)(CO)(DCPF)(PPh ₃) complexes.....	145
3.3. Influence of the metal/ligand ratio in ligand exchange reaction and catalysis.....	161
3.4. Reactivity of Et ₃ SiH toward ruthenium complexes	166
3.5. Conclusion.....	170
3.6. References	172
Chapter 4 – Mechanistic Investigations on the Ruthenium-Catalyzed Synthesis of Silyl Esters from C₂H₄ and CO₂	175
4.1. Background	175
4.2. Mechanistic insights on the formation of the targeted triethylsilyl acrylate (A1) and propionate (P1) products	177
4.3. Mechanistic insights on the formation of the triethylsilyl formate (F1) by-product...	205
4.4. Mechanistic insights on the formation of the triethylvinylsilane (TEVS) and tetraethylsilane (TES) by-products.....	209
4.5. Optimization of the catalytic formation of triethylsilylacrylate and propionate from CO ₂ , C ₂ H ₄ , Et ₃ SiH and additives	214
4.6. Conclusion.....	218
4.7. References	220

Part II

Introduction

Among the many possible industrial applications of carbon dioxide (CO₂), its incorporation into organic substrates to prepare added-value carboxylic acids is a field of study of growing interest. Because of kinetic inertness and thermodynamic stability of CO₂, different strategies have emerged to induce this poorly reactive molecule to undergo chemical transformations.

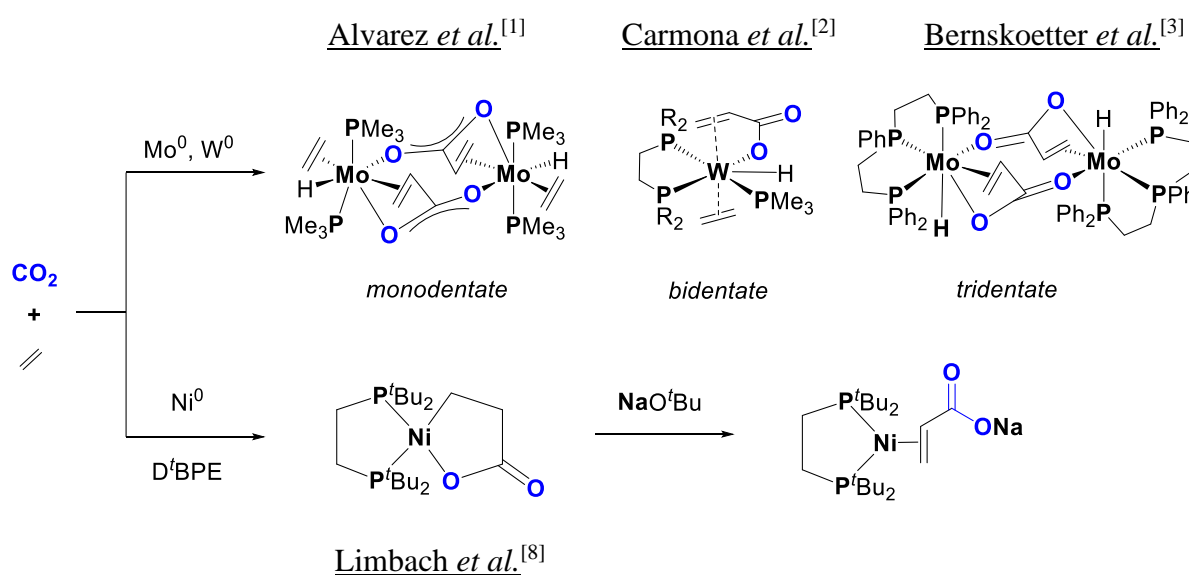
As described in the first part of this manuscript (Chapter 1), the use of highly reactive organometallic reagents in combination with metal catalysts is generally needed for converting CO₂ into carboxylic acids derivatives. Inspired by the results described in the literature, we initiated HTS experiments in order to identify suitable combinations of a catalyst precursor and a ligand for the carboxylation reaction of C₂H₄ with triethylhydrosilane as reductant (Chapter 2). Gratifyingly, one combination was found effective to some extents (in terms of activity and selectivity) for the production of acrylate and propionate silyl esters on a bench scale. However, several competitive reaction products have been detected in low to even very high TON. In order to reduce or, in the best scenario, avoid these side reactions, several strategies have been considered. The second part of this manuscript, divided into two chapters (3 and 4), is therefore focused on catalytic and mechanistic investigations carried out on the promising family of Ru(II) complexes bearing bidentate phosphine ligands. Chapter 3 describes the experimental works aiming at elucidating the role of the coordination sphere of the metal center on the reactivity and selectivity of this reductive carboxylation reaction. Having these results in hand, a collaboration with the group of Prof. L. Maron (LPCNO, INSA laboratory of Toulouse, France) was initiated to assess by DFT computations the possible catalytic cycles leading to the formation of both desired and side-products. Chapter 4 will therefore provide a selected computational data for rationalizing, validating or revoking catalytic cycles of the proposed mechanisms.



Part II

Chapter 3 – Catalytic CO₂-C₂H₄ coupling mediated by ruthenium(II) complexes bearing bidentate chelating phosphines

As described in the first chapter of the manuscript, the metal catalyzed synthesis of acrylate derivatives from CO₂ and ethylene involves generally two different pathways. The first one relies on the oxidative coupling of CO₂ and C₂H₄ on a low-valent and an electron-rich metal center, typically Mo and W complexes (Scheme II.3.1).^[1–3] The second one implies metallalactones formation *via* oxidative cyclization at the metal center, mostly known as the first step in Ni- and Pd- catalytic cycles.^[4–12]



Scheme II.3.1. Examples of molybdenum, tungsten and nickel complexes mediating the coupling of carbon dioxide and ethylene to acrylate.

In both cases, the formation of hydrido-acrylate complexes or metallacycles are proposed key intermediates in the synthesis of the acrylate motif, as it has been evidenced by theoretical calculations and experimental observations.^[4–13] These studies demonstrated that, not unexpectedly, the nature of ligands plays a crucial role in the coupling of ethylene and carbon dioxide on the metal center.

3.1. Evaluation of the ligand effect on the catalytic activity

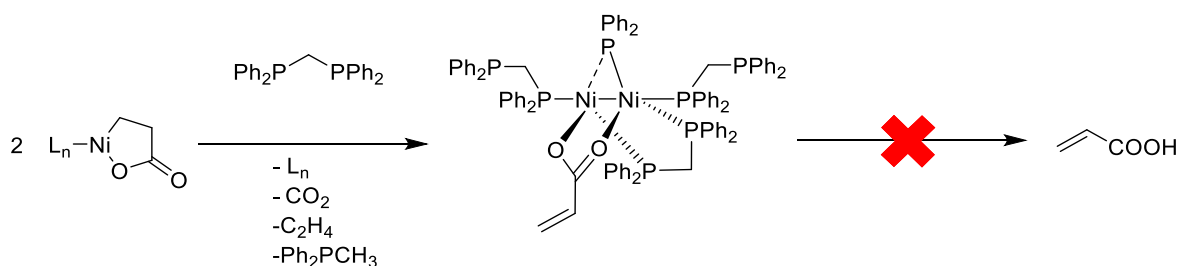
3.1.1. Background

Although early works conducted by Hoberg *et al.* used *N*-donor DBU ligand, the most investigated ligands to date in that chemistry are monodentate and bidentate chelating

phosphines. Alvarez *et al.* firstly studied the catalytic activities of Mo and W complexes with PMe_2Ph and PMe_3 ligands.^[1] It was found that Mo and W complexes readily reacted with ethylene and CO_2 , yielding the corresponding hydrido-acrylate adducts, which were not able to release acrylic acid upon reductive elimination (Scheme II.3.1).^[2,14] The DFT calculations performed by the group of Papai on the PH_3 and PMe_3 ligated Mo analogues revealed that phosphine ligands play an important role in various steps of the reaction. Their presence promotes the oxidative coupling by supplying electron density to the metal center and their dissociation governs the coordination of CO_2 .^[15] In light of these results, the group of Bernskoetter reported a Mo complex based on the use of a tridentate phosphine ligand.^[3] Thus, the zerovalent molybdenum pincer complex $[(\text{Ph}_2\text{PCH}_2\text{CH}_2)_2\text{PPh}]\text{Mo}(\text{C}_2\text{H}_4)(\text{N}_2)_2$ was found to promote C–C bond coupling between ethylene and carbon dioxide to afford a dinuclear acrylate-hydrido species (Scheme II.3.1). Kinetic and isotopic labelling studies suggested that electrophilicity and coordination geometry of the metal center may facilitate molybdenum(II) acrylate-hydrido complex formation.^[3]

On the other hand, Limbach and co-workers reported the first catalytic sodium acrylate synthesis using a nickel complex bearing a bidentate phosphine as precatalyst and NaO^tBu as base.^[8] Bis(*di-tert*-butylphosphino)ethane (D'BPE) was found to be a beneficial ligand toward the formation of the nickelalactone (Scheme II.3.1).

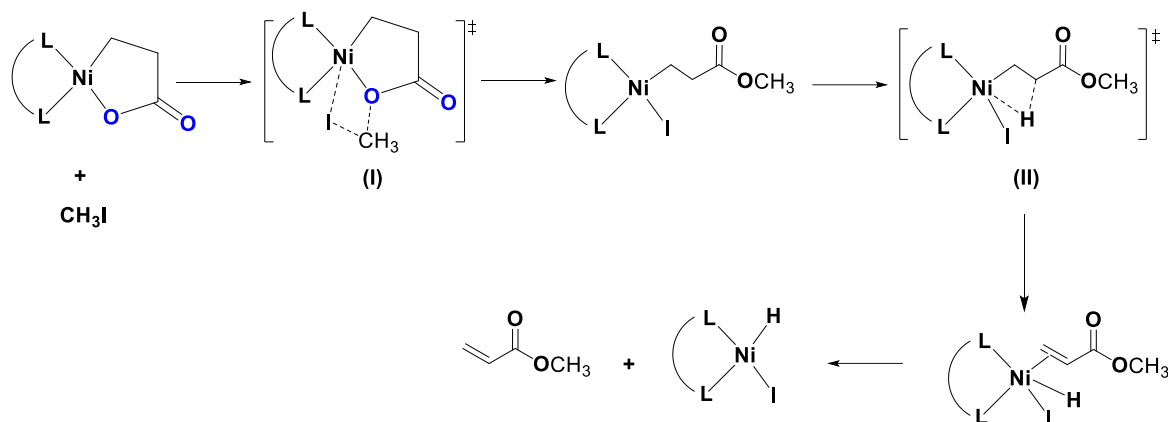
The group of Walther also described the reactivity of nickelalactones in presence of various chelating ligands.^[13] Among them, only the bis(diphenylphosphino)methane (DPPM) ligand led to the formation of a dinuclear Ni(I) complex with a bridging acrylate, through β -hydride elimination from the initial nickelalactone (Scheme II.3.2).



Scheme II.3.2. Preparation of hydrido-acrylate metal complexes.^[13]

Another strategy to induce β -hydride elimination is to cleave the M–O bond with a relevant nucleophilic interceptor and perform *in situ* reaction of the nickelacycle with methyl iodide. Using this methodology, Kühn and co-workers found that the MeI-mediated ring-opening process of nickelalactones affording methyl acrylate was ligand size sensitive (Scheme

II.3.2).^[16] In fact, the bulkiness and the bridging lengths of the bidentate ligands prevented the ring-opened intermediate (II) to undergo β -H elimination.



Scheme II.3.3. Kühn and co-workers pathway from nickelalactone to the free methyl acrylate.^[16]

The above examples evidenced that activity and reactivity of catalytic systems for C_2H_4 carboxylation reaction can be greatly influenced by the steric and electronic properties of the coordinating ligands.

3.1.2. Evaluating the catalytic performances of $\text{Ru}(\text{H})(\text{Cl})(\text{CO})(\text{PPh}_3)_3$ in combination with bidentate phosphine ligands

Considering the wide scope of chelating ligands to be explored, we firstly proceeded in evaluating the influence of the nature of various bidentate phosphine ligands on the catalytic performance, by varying the chain length of the ligand skeleton and the basicity of the P atoms through alkyl (cyclohexyl) vs. aryl (phenyl) substituents on these moieties. Dicyclohexylphosphinomethane (DCPM), dicyclohexylphosphinoethane (DCPE), dicyclohexylphosphinopropane (DCPP), 1,1'-ferrocenediyl-bis(dicyclohexylphosphine) (DCPF), 1,1'-ferrocenediyl-bis(diphenylphosphine) (DPPF) and diphenylphosphinobutane (DPPB) were used as benchmarks, as they are known to be effective ligands for the Ni-catalyzed production of acrylate from CO_2 and ethylene (Figure II.3.1).^[9,11] All catalytic tests were carried out under the optimized reaction conditions reported in Chapter 2, using $\text{Ru}(\text{H})(\text{Cl})(\text{CO})(\text{PPh}_3)_3$ (**Ru-1**) as catalyst precursor.

As shown in Table II.3.1, complexes with dicyclohexylphosphine ligands having 3 and less carbon atom backbones were found to promote routes B and C coupling reactions, although low amounts of route A products were also detectable (entries 1 to 3). Assuming that dicyclohexylphosphine ligands have bite angles similar to the reported diphenylphosphine

congeners, one can say that the P–M–P angle has a major influence on the activity and selectivity of the reaction. Indeed, extending the alkenyl backbone chain from one carbon to four increased the respective P–M–P bite angles (73 ° to 98 °),^[17] and demonstrated a positive impact on the selectivity towards **A1** and **P1** products (entries 1 to 3 vs. 4). On the other hand, the dicyclohexylphosphine DCP^{entyl} ligand with a longer five-carbon alkyl chain did not show any activity towards the route A transformation (entry 9). Interestingly, the catalytic system based on the ferrocenyl backbone (DCPF) ligand returned quite similar results compared to the successful DCPB ligand (entries 4 and 6). Although having different backbone chains, DCPF and DCPB ligands showed comparable activity probably due to their similar bite angle values (95 ° and 97 ° respectively).^[17]

Regarding the nature of the PR₂ groups, a comparison between DPPF and DCPF showed that replacement of phenyl by cyclohexyl groups increases conversions from 16% to 49% as well as selectivity toward the Route A products (entries 6 vs. 7). Moreover, in the case of the DPPB ligand, although **A1** and **P1** were still formed in small amounts, a significant decrease in selectivity was observed as compared to DCPB (entries 4 vs. 5). Whereas phenyl and cyclohexyl groups are almost similar in terms of steric bulkiness, PCy₂ moieties are much more basic than their PPh₂ counterparts, and affecting dramatically both structural arrangement and reactivity of the [(P–P)Ru] fragment. Hence, in addition to the bite angle, basicity of the P moieties is another key parameter in this process.

Replacing the cyclohexyl by cyclopentyl groups on the butylene-bridged chelating phosphine (DCP^{PB}) provided comparable results toward route A products (entries 4 vs. 8).

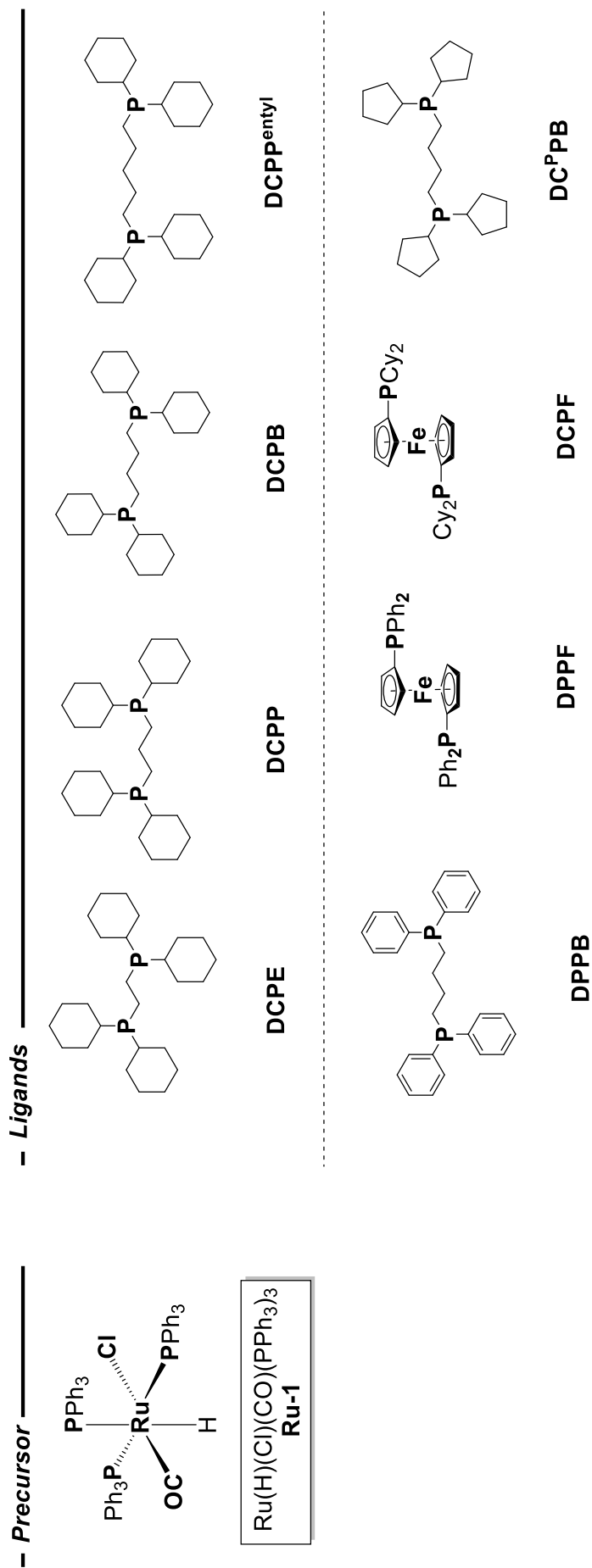


Figure II.3.1. Evaluation of bidentate phosphine ligands on the catalytic performances in C_2H_4 carboxylation reaction with CO_2 .

Table II.3.1. Evaluation of bidentate chelating phosphines for acrylate and propionate silyl esters production from CO₂, C₂H₄ and Et₃SiH.

Entry	ligand (0.5 mol%) (vs. HSiEt ₃)		Bite angle [°]	Conv. HSiEt ₃ [mol%] ^[b]	TON ^[c]					
	<i>n</i>	R			Route A products		Route B and C products			
					A1	P1	F1	TES	TEVS	E
1	1	-Cy	73 (DPPM)	>98	0	0	0	20	180	traces
2	2	-Cy	86 (DPPE)	55	traces	1.0	8.0	2.0	60	traces
3	3	-Cy	91 (DPPP)	81	traces	traces	1.0	8	66	26
4	4	-Cy	-	54	13	1.3	16	4	53	1.6
5	4	-Ph	97	54	2	6	2	14	62	traces
6	DCPF	-Cy	-	49	10	traces	0	3	26	3
7	DPPF	-Ph	95	16	traces	traces	0	20	4	traces
8	4	-Cp	-	44	12	2	9	4	48	traces
9	5	-Cy	-	>98	0	0	0	196	20	traces

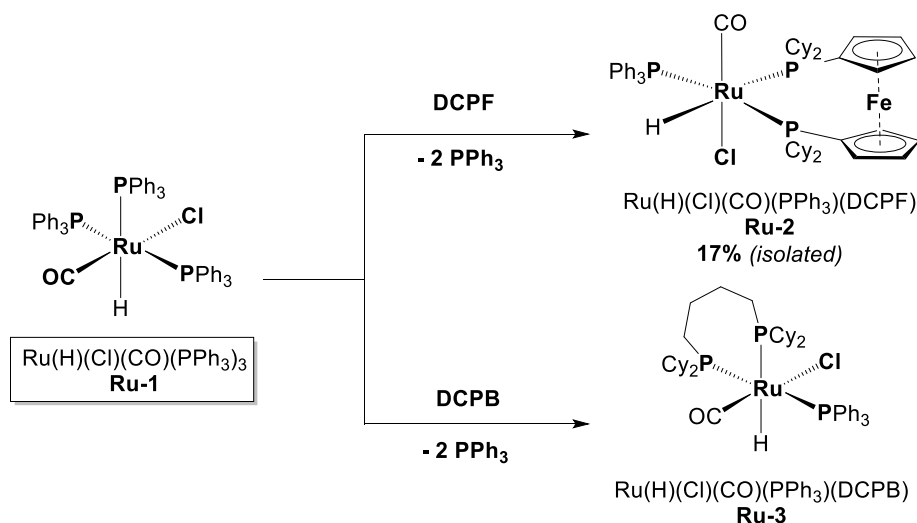
^[a] Reaction conditions: toluene (20 mL), [Si-H]₀ = 0.43 mol·L⁻¹, [Ru]₀ = [ligand]₀ = 0.002 mol·L⁻¹, CO₂/C₂H₄ 1:1 mol/mol, P(CO₂) + P(C₂H₄) = 20 bar; 16 h; results of at least duplicated experiments and averaged TON values. ^[b] Determined by integration of the ¹H NMR using (Me₃Si)₄Si as internal standard. ^[c] Turnover number as determined by GC-FID using *n*-dodecane as internal standard (mol(product).mol(Ru)⁻¹).

Therefore, the two most successful combinations enhancing selectivity toward route A products were found to be **Ru-1**/DCPB and **Ru-1**/DCPF.

3.2. Towards identifying reaction intermediates: syntheses and characterization of new Ru^{II} phosphine chelated Ru(H)(Cl)(CO)(DCPB)(PPh₃) and Ru(H)(Cl)(CO)(DCPF)(PPh₃) complexes

3.2.1. X-Ray characterization of Ru(H)(Cl)(CO)(DCPB)(PPh₃) and Ru(H)(Cl)(CO)(DCPF)(PPh₃) complexes originating from the reaction of **Ru-1** with DCPB and DCPF, respectively

To get a better insight in the nature of the catalytically active species involved in the two systems, we targeted the synthesis of Ru(H)(Cl)(CO)(DCPF)(PPh₃) and Ru(H)(Cl)(CO)(DCPB)(PPh₃) complexes, which are obvious anticipated products accessed by ligand exchange reaction of **Ru-1** with DCPF and DCPB (represented in Scheme II.3.4 namely **Ru-2** and **Ru-3**).



Scheme II.3.4. Syntheses of Ru(H)(Cl)(CO)(DCPF)(PPh₃) and Ru(H)(Cl)(CO)(DCPB)(PPh₃) complexes from **Ru-1** complexation reaction with DCPB and DCPF ligands; note that a single isomer of each complex is shown, which does not mean that other isomers are not produced.

Adapted from the procedure of Jia and co-workers,^[18] the precursor Ru(H)(Cl)(CO)(PPh₃)₃ was refluxed in the presence of DCPB or DCPF ligand (1:1 mol ratio) in toluene under argon. Upon work-up and subsequent recrystallization of the crude products, single-crystals of the expected **Ru-2** (17% isolated yield) and **Ru-3** (21% crude yield) were obtained and analysed by X-ray crystallography (Figure II.3.2.).

The solid state structures of the 18-electron complexes **Ru-2** and **Ru-3** show the DCPF and DCPB ligands bound in a *cis* fashion. These six-coordinated complexes do not however adopt an ideal octahedral geometry. Indeed, the angles between the apical phosphorous atoms and the Ru center (P3–Ru–P1, 150.78(19)° and 156.32(3)°, respectively for **Ru-2** and **Ru-3**), deviate significantly from the optimal octahedral coordination. The group of Echavarren has already reported similar observations for the 1,1'-bis(diphenylphosphino)ferrocene ruthenium hydride complex (Ru(H)(Cl)(CO)(DPPF)(PPh₃)).^[19]

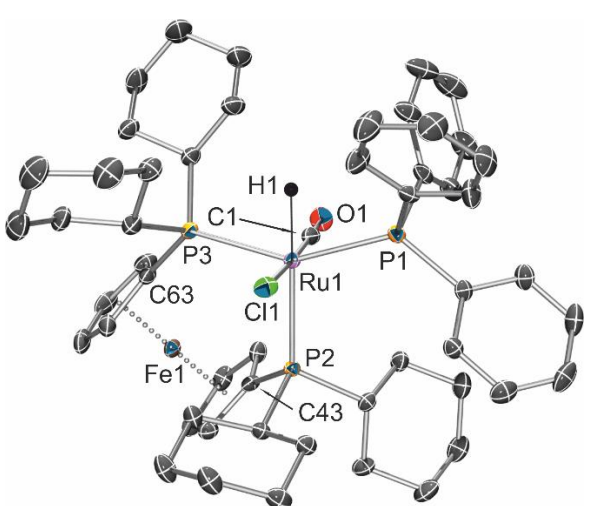
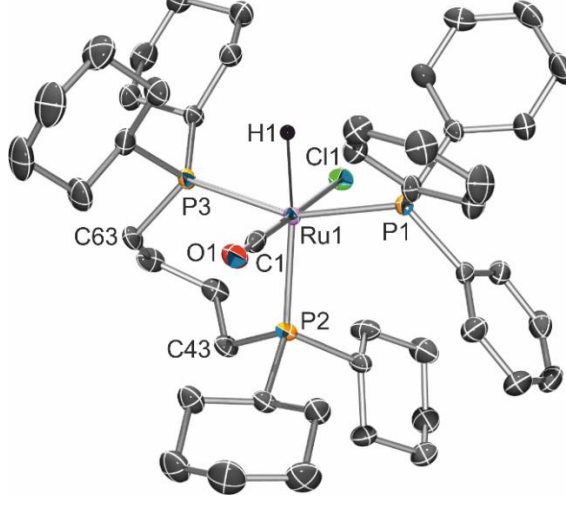
Ru(H)(Cl)(CO)(DCPF)(PPh ₃) Ru-2	Ru(H)(Cl)(CO)(DCPB)(PPh ₃) Ru-3
	
Selected bond lengths [Å]	
Ru1–H1 = 1.57(3), Ru1–C1 = 1.815(12), Ru1–P3 = 2.3810(5), Ru1–P1 = 2.3660(6), Ru1–P2 = 2.4619(5), Ru1–Cl1 = 2.465(2)	Ru1–H1 = 1.72(3), Ru1–C1 = 1.856(4), Ru1–P3 = 2.3819(8), Ru1–P1 = 2.3919(8), Ru1–P2 = 2.5039(9), Ru1–Cl1 = 2.4870(8), Ru1–C1 of 1.856(4), C1–O1 = 1.050(4)
Selected bond angles [°]	
P3–Ru1–P1 = 150.78(19), P3–Ru1–P2 = 100.83(19), P1–Ru1–P2 = 107.65(19) P2–Ru1–P3–C63 = –18.56 P3–Ru1–P2–C43 = 36.80	P3–Ru1–P1 = 156.32(3), P3–Ru1–P2 = 98.48(3), P1–Ru1–P2 = 104.95(3) P2–Ru1–P3–C63 = 5.32 P3–Ru1–P2–C43 = 18.22

Figure II.3.2. ORTEP representations of the solid-state molecular structures of ruthenium hydride complexes Ru(H)(Cl)(CO)(DCPF)(PPh₃) and Ru(H)(Cl)(CO)(DCPB)(PPh₃) (**Ru-2** and **Ru-3**) with thermal ellipsoids set at 50% probability level. Hydrogen atoms and solvent of crystallization are omitted for clarity. Selected interatomic distances and angles are given in Ångström [Å] and degree [°], respectively.

As expected, due to its localization in *trans* position to the hydride ligand, the Ru1–P2 bond in **Ru-2** and **Ru-3** (2.4619(5) and 2.5039(9) Å respectively) is longer when compared to the Ru1–P1 or Ru1–P3 bonds. Noteworthy, the solid state structures revealed respective bite angle values of the diphosphines of 100.83(19)° and 98.48(3)° for **Ru-2** and **Ru-3**. These values

were found slightly lower than those reported for the Ru(H)(Cl)(CO)(DPPF)(PPh₃) complex (102.2(1)°).^[19] The higher value observed for the DCPF ligated **Ru-2** complex might be due to the ferrocene backbone, which is generally assumed to be very flexible. In fact, the bite angle can be broadened by either opening the angle between the two cyclopentadienyl (Cp) planes or by increasing the torsion angle along the axis described by the two Cp rings.^[20] The structural data confirmed that, indeed, the cyclopentadienyl groups in **Ru-2** were staggered by 19.94° and almost parallel (dihedral angle of 2.37°).

In order to further probe the comparison between **Ru-2** and **Ru-3** and describe their steric properties, their % buried volumes (%V_{bur}, defined as the percent volume occupied by the ligand out of the total volume of a sphere centered at the metal and typically set to have a 3.5 Å radius)^[21,22] were calculated using the SambVca 2.0 web application developed by Cavallo and coworkers.^[23–25] Even though DCPB and DCPF ligands differ by their ferrocenyl and butyl backbones, **Ru-2** and **Ru-3** complexes have almost identical % buried volumes: 51.5 % and 49.3 %, respectively. However, the steric maps for **Ru-2** and **Ru-3** given in Figure II.3.3. (a) and (b) respectively, show, *via* coloured contours, that the distribution of the steric bulk around the metal is slightly different between the two complexes.

If one defines the *z* axis for these metal complexes as the P–Ru–P angle bisector, and the *xz* plane to contain the phosphorus atoms (P2 and P3), then the hindrance is much more localized on the +*x* axis edges (North and South East) for both **Ru-2** and **Ru-3**. On the other hand, the empty zones, represented in blue and white areas, indicate where the ligand retracts to allow more reactive surface for a substrate around the metal. These areas are more available within the coordination sphere of complex **Ru-3** ((b), North and South). This analysis indicates that DCPB occupies less space within the coordination sphere of the metal compared to DCPF, providing wider catalytic pockets for substrates approach (preferentially from North or South).

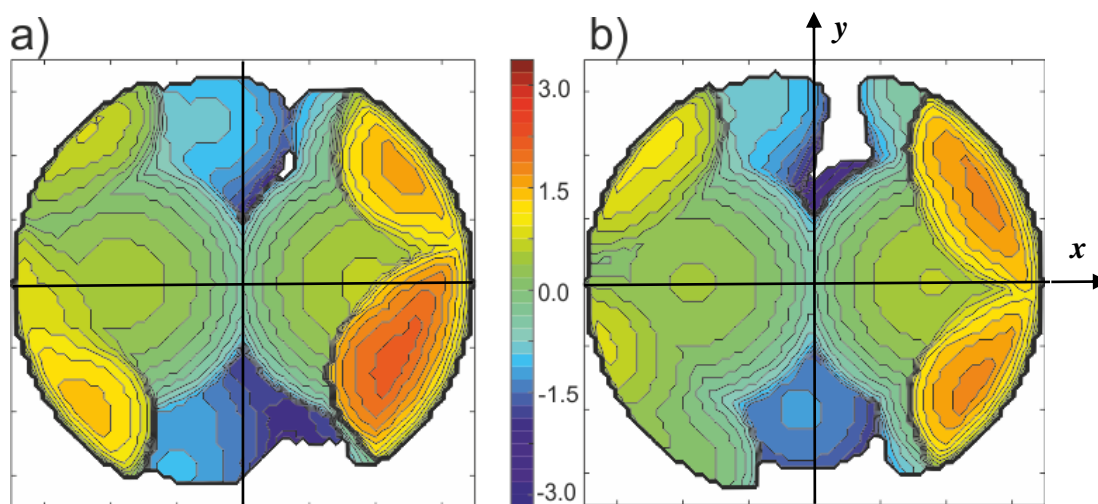


Figure II.3.3. Steric maps (computed for sphere radius of 3.5 Å) of **Ru-2** (a) and **Ru-3** (b) views “from the frontal side presented by H and Ph₃P ligands”. Positive values of the isocontour lines refer to the frontal half-sphere, which is the half sphere where the chelating ligand protrudes towards the substrates.

3.2.2. NMR studies of the reaction of **Ru-1** with DCPF: formation of **Ru(H)(Cl)(CO)(PPh₃)(DCPF)** complex (**Ru-2**)

The above crystallographic data obtained confirmed the formation of the expected **Ru-2** and **Ru-3** by ligand exchange of **Ru-1** with the corresponding DCPB and DCPF. We then wondered if these ruthenium complexes bearing bidentate phosphine ligands (and the isomers isolated by crystallization) were the ones exclusively being formed from the complexation/ligand exchange reaction. Thus, multinuclear NMR analyses were performed on the crude reaction mixtures resulting from the ligand complexation reactions.

In the room temperature ¹H NMR spectrum of the crude reaction mixture resulting from the reaction of **Ru-1** with DCPF, the corresponding series of resonances for PPh₃ (▲), Fe(C₅H₈)₂ (■) and P(C₆H₁₁)₂ (●) fragments were identified (Figure II.3.4). A key resonance, observed at δ_H = -7.5 ppm as a doublet of triplets, is diagnostic of the presence of Ru–H species that displays coupling with three phosphorus atoms of three coordinated phosphine ligands (²J_{P-H} of 102 and 26 Hz); this is the only resonance observed in the hydride region and does integrate for 1H as compared to the Fe(C₅H₈)₂ (■, 8H) and the two P(C₆H₁₁)₂ (●, 44H) fragments. On the other hand, the ³¹P{¹H} NMR spectroscopy revealed the presence of free PPh₃ at δ_P = -5.2 ppm as the complex was prepared *in situ*, as well as three new patterns at 48.6 (*dd*), 35.9 (*dd*), and 11.8 (*m*) ppm (Figure II.3.5). Each signal was integrating for one P atom, suggesting that only one species, holding three non-equivalent P nuclei, is present in solution. In addition, the signal

at δ_P 11.8 ppm (▼) showed additional splitting in ^{31}P NMR spectroscopy ($^2J_{P-H}$ 102 Hz), being in line with *trans* P-H coupling phenomenon.

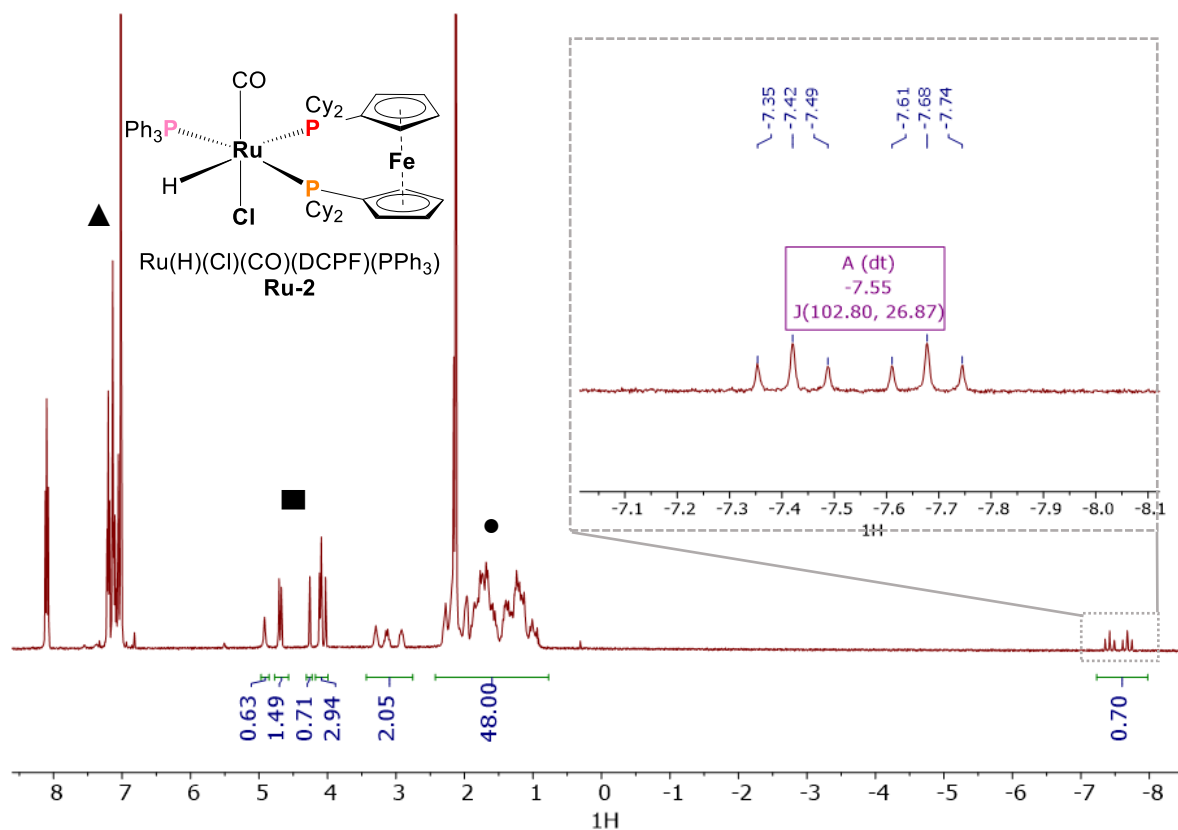


Figure II.3.4. ^1H NMR spectrum (400 MHz, $\text{toluene-}d_8$, 25 °C) of crude **Ru-2** obtained from the reaction of **Ru-1** with DCPF (1 equiv).

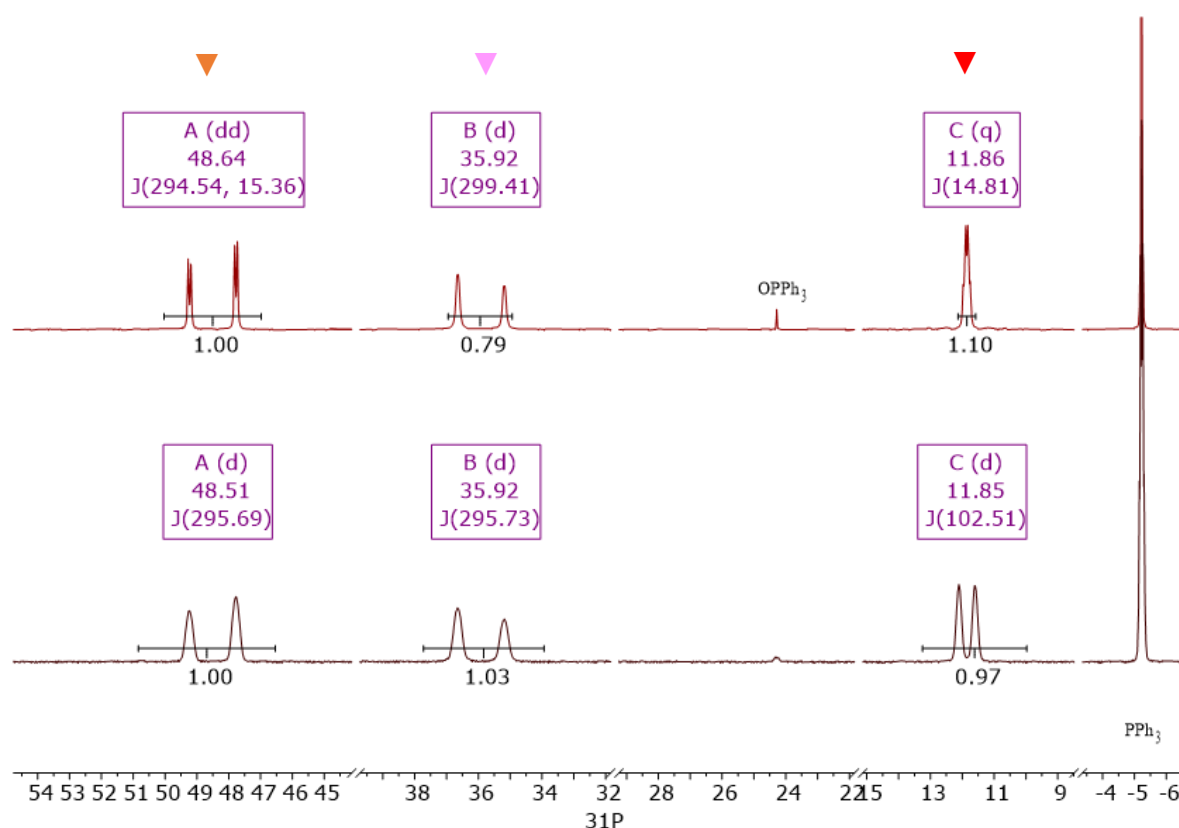


Figure II.3.5. $^{31}\text{P}\{^1\text{H}\}$ (top) and ^{31}P (bottom) NMR spectra (202 MHz, toluene- d_8 , 25 °C) of crude **Ru-2** obtained from the reaction of **Ru-1** with DCPF (1 equiv).

A complementary 2D HMQC ^1H - ^{31}P NMR experiment (Annexe II.3.17) established correlations between P and H nuclei, also allowing to assign all the observed ^{31}P NMR signals to the corresponding phosphorus nuclei of the coordinated DCPF (\blacktriangledown) and PPh_3 (\blacktriangledown) in a single **Ru-2** species. In support to our observations, $^2J_{\text{P-P trans}}$ and $^2J_{\text{P-P cis}}$ coupling constants values (295 Hz and 15 Hz respectively) were found consistent with those reported for isostructural ruthenium(II) carbonyl hydrido ($\text{Ru}(\text{H})(\text{Cl})(\text{CO})(\text{DPPF})(\text{PPh}_3)$) complexes bearing chelating diphosphines ($^2J_{\text{P-P trans}} = 306$ Hz and $^2J_{\text{P-P cis}} = 11$ Hz).^[19]

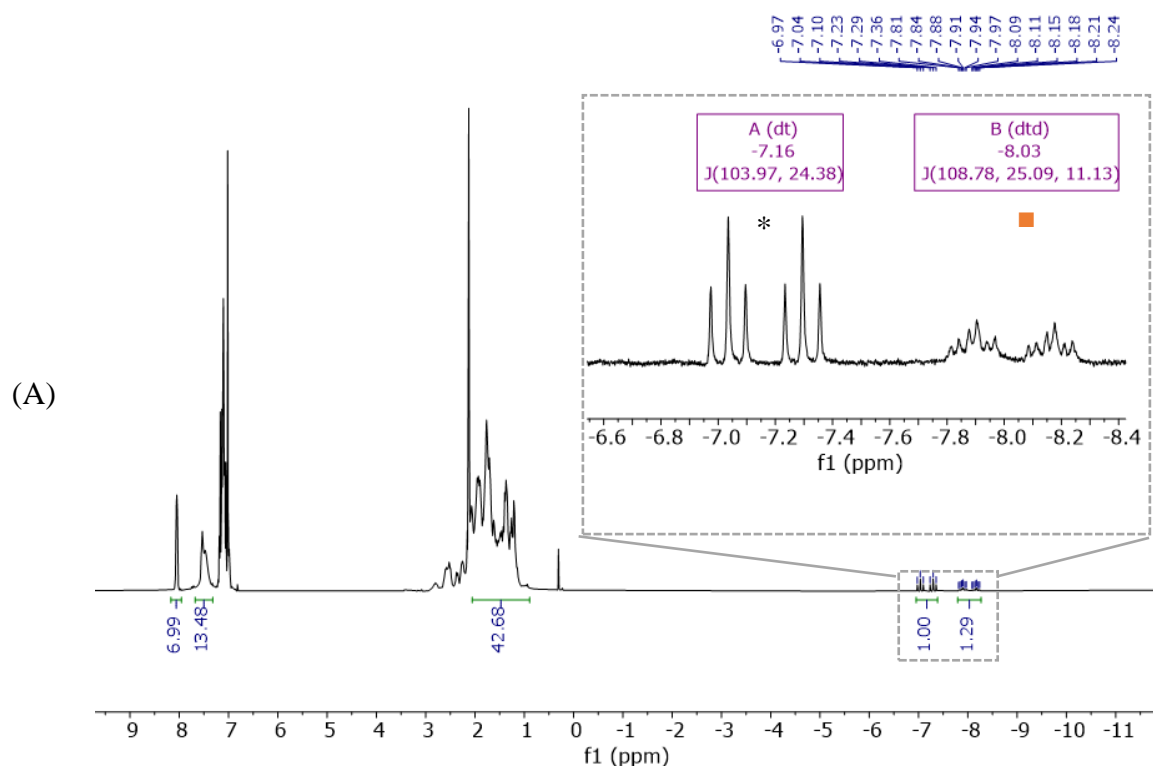
Hence, the above spectroscopic data were completely consistent with quantitative and selective formation of **Ru-2** $\text{Ru}(\text{H})(\text{Cl})(\text{CO})(\text{DCPF})(\text{PPh}_3)$ with the structure established by X-ray crystallography.

3.2.3. NMR studies of the reaction of **Ru-1** with DCPB: formation of $\text{Ru}(\text{H})(\text{Cl})(\text{CO})(\text{DCPB})(\text{PPh}_3)$ (**Ru-3**)

Unlike the **Ru-2** complex, the NMR data obtained for the crude mixture resulting from the *in situ* synthesis of **Ru-3** by reaction of **Ru-1** with DCPB (1 equiv) appeared to be complicated.

In fact, considering the crop of colourless **Ru-3** (X-ray suitable) crystals obtained, the pink crude solution (in toluene as solvent) suggested that $\text{Ru}(\text{H})(\text{Cl})(\text{CO})(\text{DCPB})(\text{PPh}_3)$ is not necessarily the only product arising from the **Ru-1**/DCPB complexation reaction.

In fact, the room-temperature ^1H NMR spectrum of the crude **Ru-3** (Figure II.3.6, (A)) revealed the presence of two set of signals in the hydride region: a well defined doublet of triplet at $\delta_{\text{H}} -7.1$ ppm (*), with characteristic *trans* and *cis* couplings ($^2J_{\text{P-H trans}} = 104$ and $^2J_{\text{P-H cis}} = 25$ Hz), and an unidentified multiplet signal at $\delta_{\text{H}} -8.03$ ppm (■), respectively integrating in a 1:1.3 ratio. Moreover, in the most upfield region of the $^{31}\text{P}\{^1\text{H}\}$ NMR spectrum (Figure II.3.6 B (top)), beside the singlet resonance from the free PPh_3 ($\delta_{\text{P}} -5.2$ ppm), two signals located at $\delta_{\text{P}} 16.7$ and 18.6 ppm, in a ratio of 1:0.6 were observed. These two latter signals exhibit a large P–P coupling constant in the ^{31}P coupled NMR spectrum (Figure II.3.6 B (bottom)), and they are most likely attributed to a P nucleus located *trans* to a hydride ($^2J_{\text{P-H trans}} = 104$ Hz). These observations suggest that, in contrast to **Ru-2**, the reaction of the formation of **Ru-3** is less selective and at least, two hydrido species are generated under these conditions.



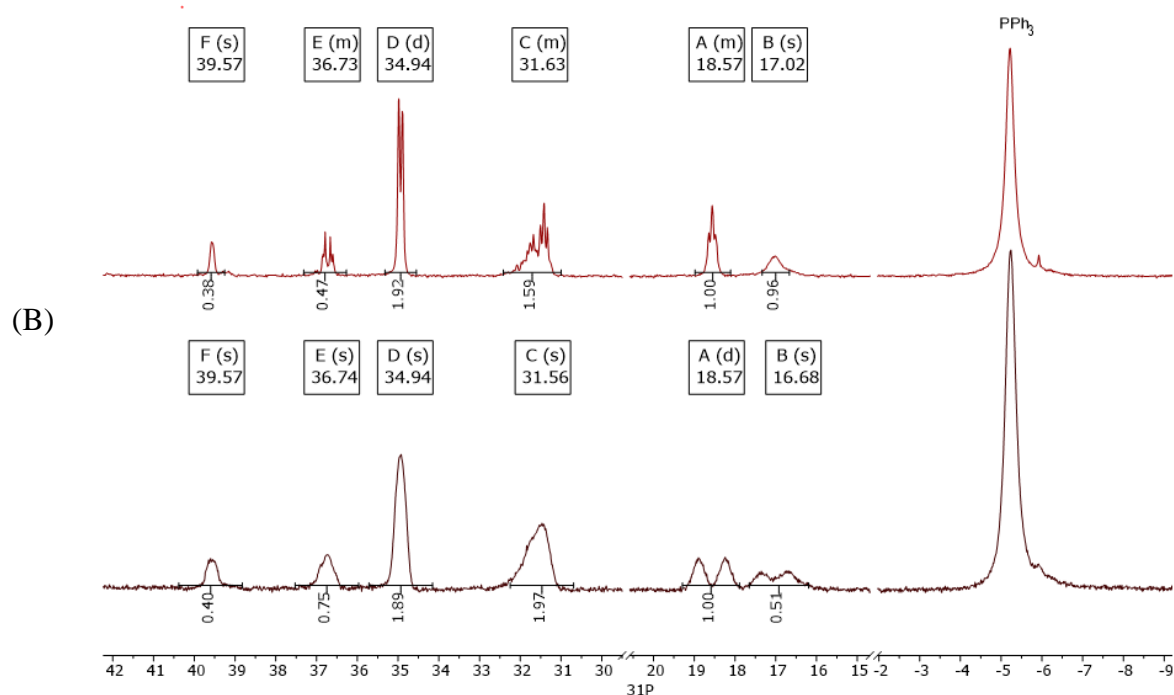


Figure II.3.6. NMR spectra of crude **Ru-3** mixture obtained from the reaction of **Ru-1** with DCPB (1 equiv): (A) ^1H (400 MHz, toluene- d_8 , 25 °C), (B, top) $^{31}\text{P}\{^1\text{H}\}$ (162 MHz, C_6D_6 , 25 °C), (B, bottom) ^{31}P (162 MHz, toluene- d_8 , 25 °C).

Interestingly, a series of variable temperature (VT) $^{31}\text{P}\{^1\text{H}\}$ NMR experiments (Figure II.3.7) showed that, upon heating up to 77 °C and then cooling down to –8 °C, the resonance at δ_{P} 34.9 ppm, initially appearing as a doublet at 25 °C, resolves into an AB spin system with measurable coupling constants of $^2J_{\text{P-P trans}} = 280$ Hz and $^2J_{\text{P-P cis}} = 16.5$ Hz. The two resonances overlap at room temperature appearing as a single doublet, but resolved into two doublets of doublets at –8 °C (blue δ_{P} 33.2 and red δ_{P} 35.4 ppm) and 70 °C (blue δ_{P} 37.0 and red δ_{P} 34.2 ppm), with a strong roof effect.^[a] A similar phenomenon has been already described by Ledger *et al.* for a series of ruthenium pincer complexes, and was explained by an intramolecular motion within the backbone of the chelating ligands.^[26]

^[a] When chemical shift difference between two nuclei in hertz ($\Delta\nu = \nu_0\delta$) is much less to order of magnitude as the J coupling constants between them ($\frac{\Delta\nu}{J} \leq 1$), then second order effects appear, often preventing detailed interpretation of the signals, or giving incorrect coupling constants. A universally observed effect is that, in case of AB system, as chemical shifts become comparable to couplings ($\frac{\Delta\nu}{J} \approx 1$), the inner peaks become taller and the outer peaks shorter. The peaks "lean" towards each other, this is called the "roof effect."

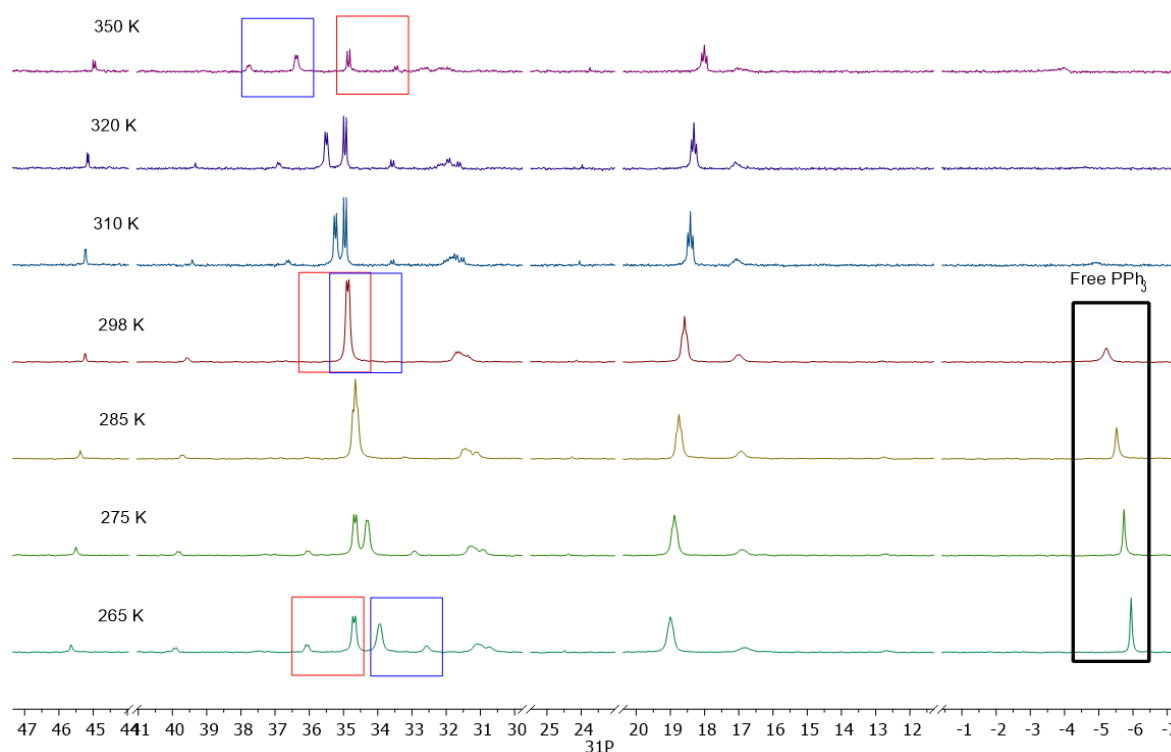


Figure II.3.7. VT $^{31}\text{P}\{^1\text{H}\}$ NMR (toluene- d_8 , 202 MHz, $-8\text{ }^\circ\text{C}$ to $77\text{ }^\circ\text{C}$) spectra of the hydride region of crude **Ru-3** obtained from the reaction of **Ru-1** with DCPB (1 equiv).

In order to determine the exact configurations of the complexes in solution, additional 2D ^1H - ^{31}P HMQC NMR experiments were conducted at $77\text{ }^\circ\text{C}$. Because of the different coupling constants ($^2J_{\text{P-H}}$ around 20 and 100 Hz), two spectra were recorded, optimized for each $^2J_{\text{P-H}}$ to give a better coupling resolution.

At $-8\text{ }^\circ\text{C}$, the NMR spectrum with 100 Hz coupling constants, the ^1H resonance at $\delta_{\text{H}} - 7.09$ ppm correlates with the ^{31}P signal at 19 ppm and thus can be assigned to the phosphine coordinated *trans* with respect to the hydride (►, Figure II.3.8, A). Moreover, the ^{31}P signal at 19 ppm can be assigned to a $\text{P}(\text{Cy})_2$ fragment of DCPB since it correlates with the ^1H -cyclohexyl patterns at 2.1 ppm (►, Figure II.3.8, (A)).

In the NMR spectrum with 20 Hz coupling constant, the hydride pattern at $\delta_{\text{H}} - 7.09$ ppm correlates with the two *dd* ^{31}P signals located at δ_{P} 33.5 and 34.7 ppm respectively (►, Figure II.3.8, (B)). These two patterns were attributed to the coordinated $\text{P}(\text{Cy})_2$ fragment and PPh_3 , respectively correlating with the protons in the aliphatic (■) and aromatic regions (■).

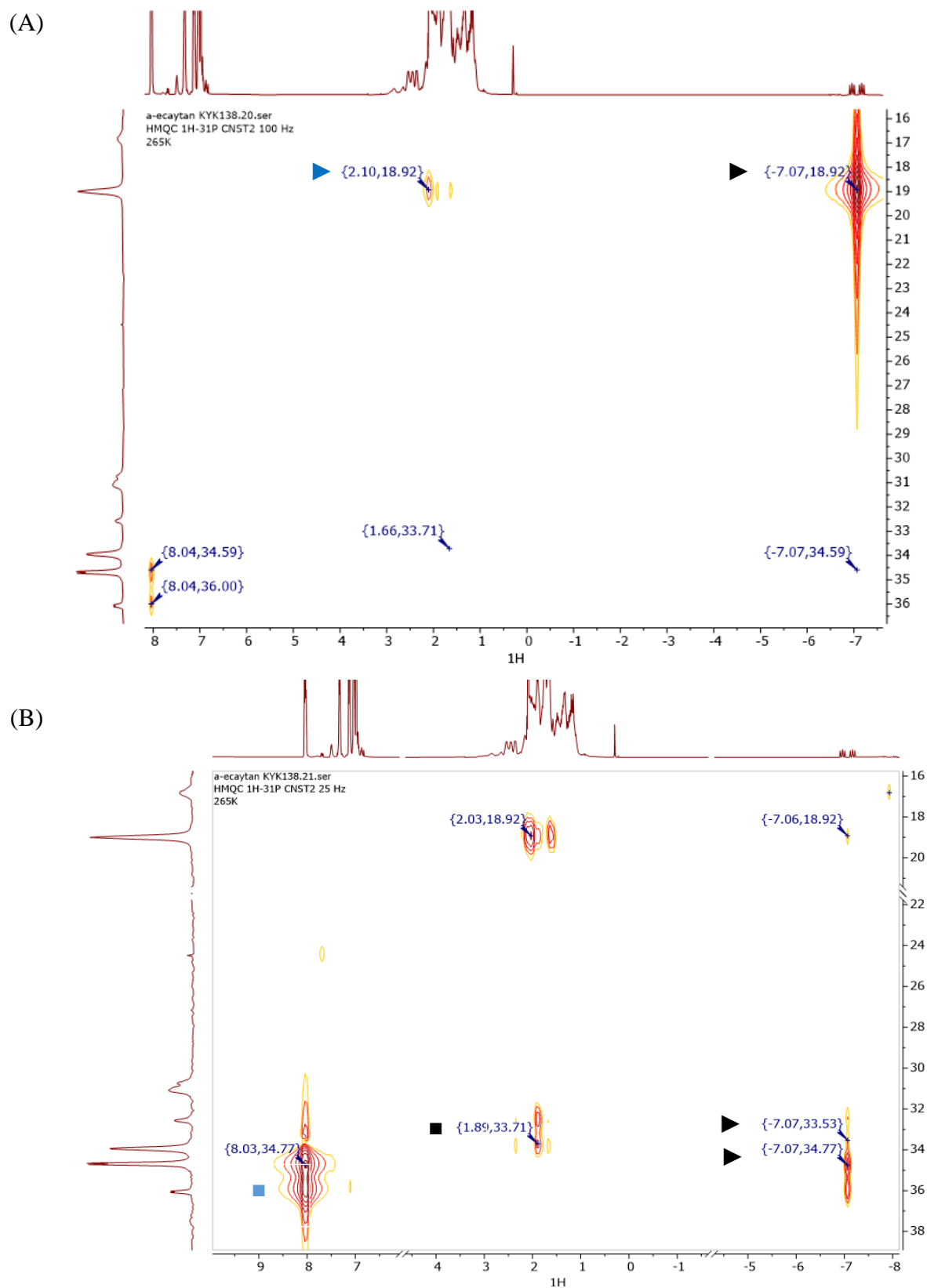


Figure II.3.8. ^1H - ^{31}P HMQC NMR correlation spectra of the hydride to the phosphorus atoms of crude **Ru-3** obtained from the reaction of **Ru-1** with DCPB (1 equiv) in toluene- d_8 optimized for (A) 100 Hz coupling constant at 350 K and (B) 25 Hz coupling constant at 265 K.

A series of selective ^{31}P -decoupled ^1H NMR experiments were also performed in order to simplify the hydride region of the NMR spectrum. At $77\text{ }^\circ\text{C}$, irradiation at the selected frequency of 7212 Hz eliminated coupling with the *cis* P-nuclei (Figure II.3.9., (*)).^[b] The resulting NMR data signal became a doublet resonance with a coupling constant $^2J_{\text{P-H trans}}$ of 104 Hz . In the same fashion, irradiating at the selected frequency of 3645 Hz suppressed the *trans* P-nucleus coupling, affording a simple triplet with $^2J_{\text{P-H cis}}$ of 23.5 Hz (Figure II.3.9. (B)).

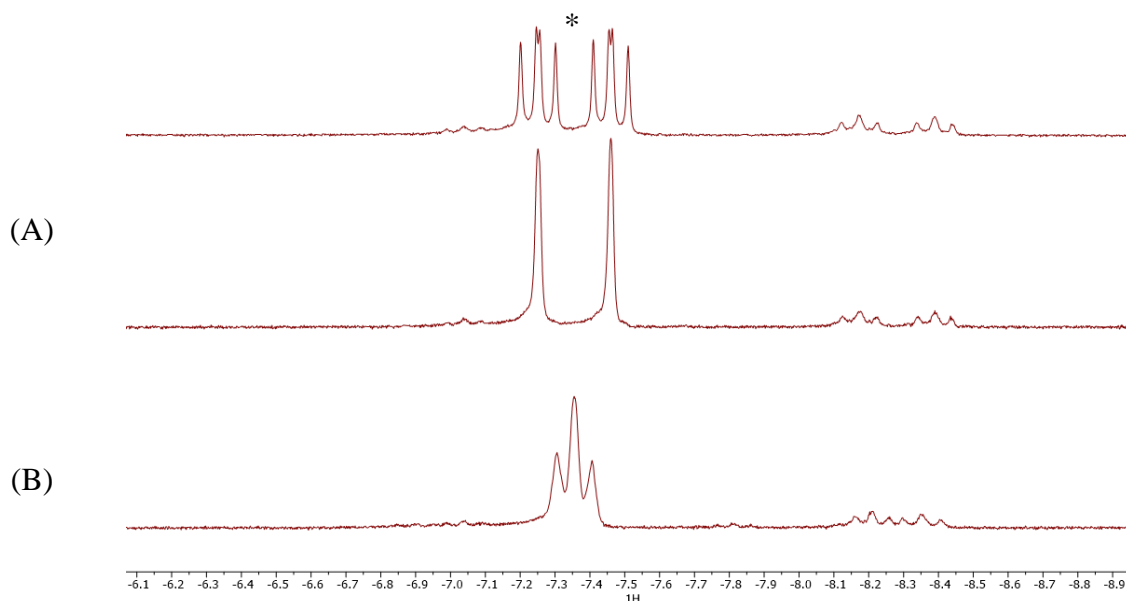


Figure II.3.9. High temperature selective homo-decoupling $^1\text{H}\{^{31}\text{P}\}$ NMR spectra (hydride region) of crude material obtained from the reaction of **Ru-1** with DCPB (1 equiv) (500 MHz , toluene- d_8 , $77\text{ }^\circ\text{C}$) (A) irradiation at the selected frequency of 7212 Hz (B) irradiation at the selected frequency of 3645 Hz .

To observe any possible exchange between the different species present in solution, a ^{31}P - ^{31}P EXSY NMR experiment was recorded (Figure II.3.10.). Yet, the data recorded in a range of different mixing times (50 – 500 ms) did not show any exchange between the coordinated phosphines patterns, excluding any equilibrium phenomena in solution (slower or of the same magnitude than the NMR timescale).

^[b] Specific proton decoupling experiment also known as band-selective or narrowband.

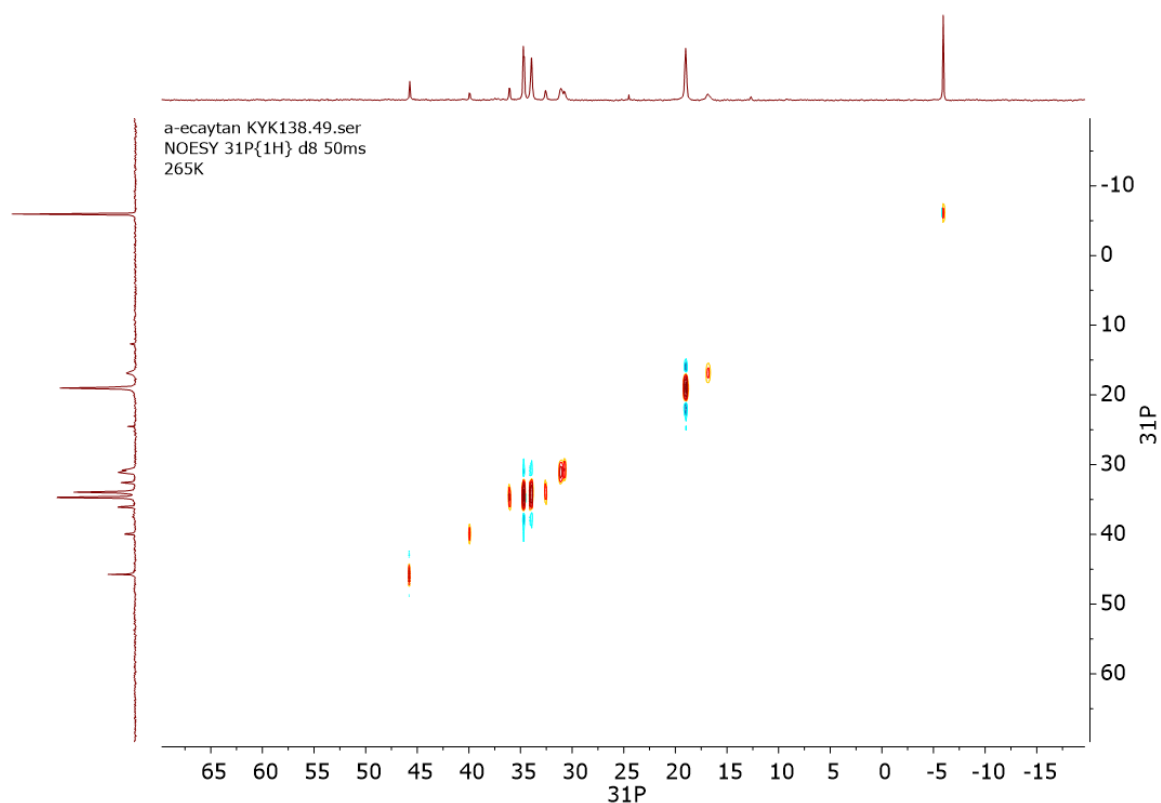


Figure II.3.10. ^{31}P - ^{31}P EXSY spectrum (500 MHz, toluene- d_8 , -8°C) of crude **Ru-3** obtained from the reaction of **Ru-1** with DCPB (1 equiv).

Although the collected NMR data were not obvious to reconcile, the structure of the major species present in the crude mixture was clarified and was assigned to the geometry of **Ru-3** observed in the solid state, that is, in which the bidentate DCPB ligand is coordinated in a *cis* fashion. A summary of the collected data can be visualized by a δ/J diagram (Figure II.3.11).

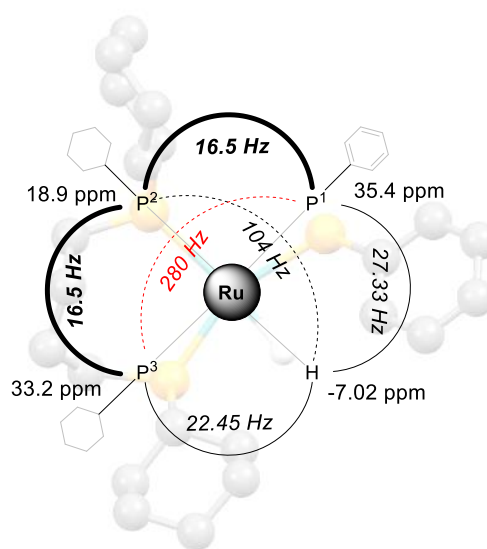
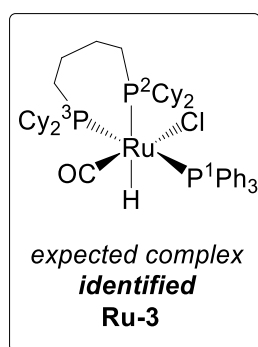


Figure II.3.11. NMR chemical shift / 2J *trans* and *cis* coupling constant (δ/J) diagram of **Ru-3** complex in toluene- d_8 .

Moreover, to comfort these observations, Flow Injection Analysis-Atmospheric Pressure Photoionization mass spectrometry (FIA-APPI performed at COBRA, Rouen, France) confirmed the formation of the expected **Ru-3** complex, as judged from the observation of the molecular peak at $m/z = 877$ and the good match between the experimental and calculated isotopic patterns (Figure II.3.12.).

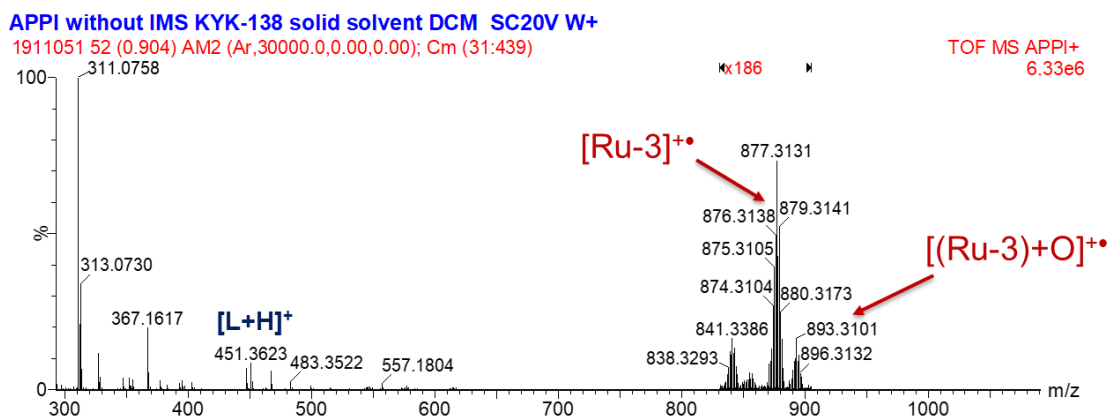


Figure II.3.12. FIA-APPI mass spectrum of the crude mixture of complex $\text{Ru(H)(Cl)(CO)(DCPB)(PPh}_3\text{)}$ (**Ru-3**).

Regarding the nature of the non-identified hydride species, associated to the multiplet signal appearing at $\delta_{\text{H}} -8.03$ ppm (■) in the room temperature ^1H NMR spectrum (Figure II.3.6. (A)), different hypotheses can be envisioned. One could assume that a positional isomers of **Ru-3** might be formed during the complexation **Ru-1** with DCPB, resulting in the observed additional patterns at $\delta_{\text{H}} -8.03$ ppm. In fact, the later exhibited both $^2J_{\text{P-H trans}}$ and $^2J_{\text{P-H cis}}$ coupling constants of 103 Hz and 25 Hz, respectively (Figure II.3.6. (A)). Therefore, these observations suggest that the unknown species possesses a hydride atom located in *cis* and *trans* position to P nuclei. Moreover, correlations were observed on the figure II.3.13 between the same multiplet at $\delta_{\text{H}} -8.03$ ppm and the ^{31}P patterns at $\delta_{\text{P}} 16.8$ (*d*, $^2J_{\text{P-H trans}} = 103$ Hz), $\delta_{\text{P}} 30.9$ (*m*) and $\delta_{\text{P}} 45.7$ ppm (*br s*). Looking at other conceivable configurations for **Ru-3** (Scheme II.3.5.), one possibility would be to arrange the triphenylphosphine P^1Ph_3 ligand in *cis* position to the DCPB ligand. In this configuration, the $^2J_{\text{P}_1-\text{P}_2 trans}$ is suppressed. The absence of a $^2J_{\text{P-P trans}}$ coupling in the recorded ^{31}P NMR spectra shown in Figures II.3.6. and II.3.7 supports this hypothesis. In accordance with these NMR findings, another possible position isomer of **Ru-3** would be to set the P^1Ph_3 ligand *trans* to the hydride, as shown in Scheme II.3.5. In theory, NMR data similar to those described above should be observed.

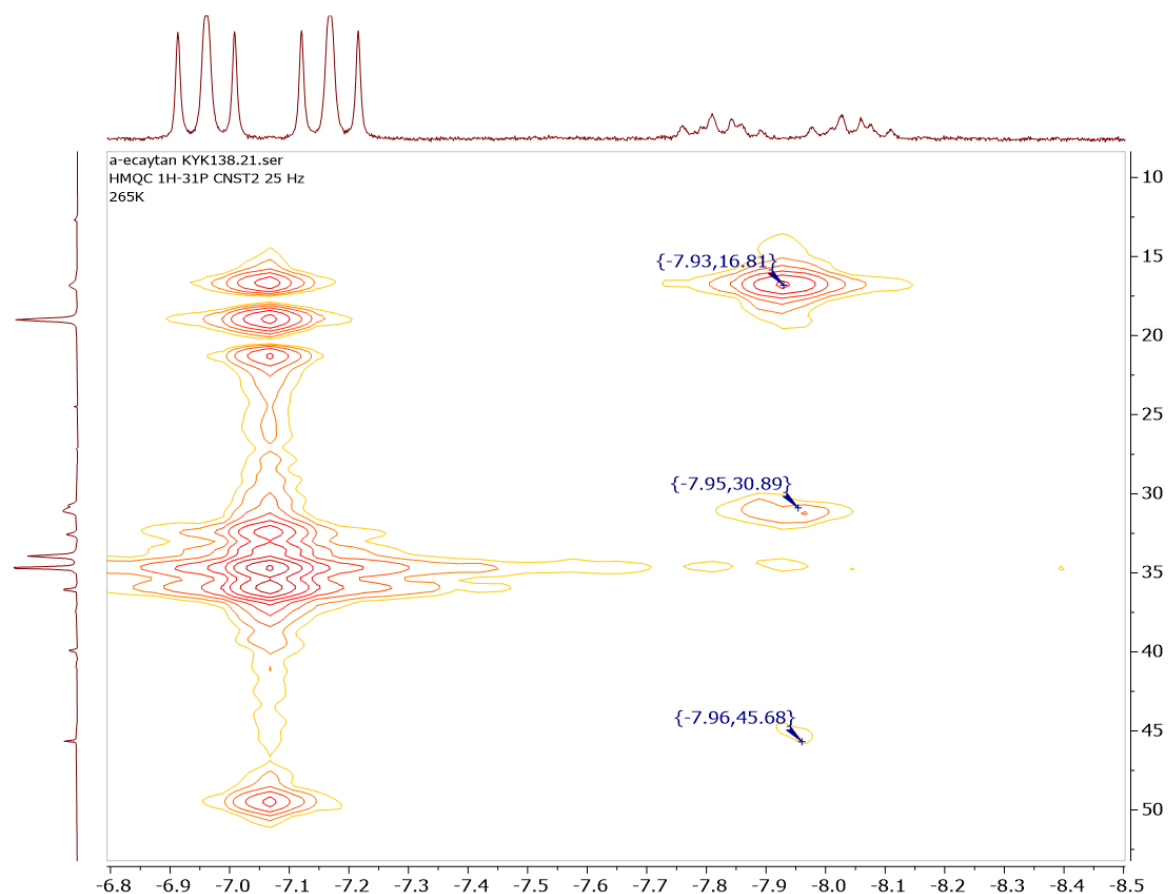
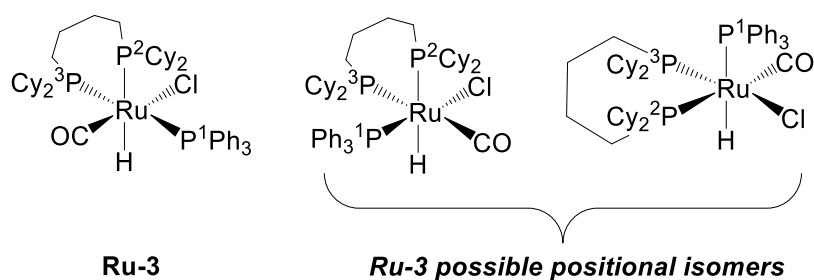


Figure II.3.13. ^1H - ^{31}P HMQC NMR correlation spectrum (toluene- d_8 , 202 MHz, -8°C) of the hydride to the phosphorus atoms of crude **Ru-3** obtained from the reaction of **Ru-1** with DCPB (1 equiv).

Since no other massive peaks were observed by GC-MS, except for those of the oxidized **Ru-3** ($\text{C}_{47}\text{H}_{67}\text{O}_2\text{P}_3\text{ClRu}^+$), which could be formed before or during sample injection, one could assume that the second unidentified species is in fact a positional isomer of **Ru-3**.



Scheme II.3.5. Representation of the possible positional isomers of **Ru-3**.

In addition to the NMR studies, we attempted different crystallization procedures/conditions on the crude reaction medium of **Ru-3**. Single crystals grown by slow evaporation of the corresponding solutions were analysed by XRD: **Ru-3-A** (from neat methanol), **Ru-3-B** (from CH_2Cl_2) and **Ru-3-C** (from heptane), shown in Figure II.3.14.

The DCPB ligand flexibility raises the chance of an arm-off η^1 coordination, more likely to form stabilized bimetallic complexes. In fact, a “spanned” coordination mode is observed in crystals of **Ru-3-A**, possessing two bridging ligands between the two metal centers (Figure II.3.14, (A)), whereas a *cis*-chelation mode is observed in **Ru-3-B** and **Ru-3-C** (Figure II.3.14, (B) and (C)). From a retrosynthetic point of view, the synthesis of three halogeno bridges species generally combines a complex having two halogeno ligands and one free coordination site with a complex having one halogeno ligand and two free coordination sites.^[27] Similar dinuclear complexes have already been described for the activation of small and inert molecules such as nitrous oxide (N₂O).^[28]

When looking at their molecular structures, all of the three complexes are free from PPh₃ ligands, illustrating the easy, complete removal of the latter. For example, **Ru-3-A** possesses two weakly coordinated methanol molecules instead of two PPh₃, forming adducts exhibiting C_s molecular symmetry. In fact, the complete decoordination of either of the two “labile” ligands, PPh₃ and CO, on the **Ru-3** catalyst, was studied by DFT calculations. The BDE for PPh₃ was calculated to be 19.7 kcal·mol⁻¹ (ΔH) whereas CO has stronger BDE (60.0 kcal·mol⁻¹), confirming that PPh₃ dissociation is the most feasible step. On the other hand, the decoordination of the chloride atom would result in a (positively) ion-charged complex and would be a higher endothermic process as evidenced for the CO ligand.

Yet, the formation of bimetallic ruthenium complexes in which two metal fragments are connected by halogeno bridges was unexpected. Moreover, even though the removal of PPh₃ ligand is conceivable thermodynamically, the disappearance of the hydride ligands remains surprising and no explanation could be given to clarify their fate.

Unfortunately, dimeric complexes **Ru-3-A-C** were not obtained in sufficient amounts to be characterized by NMR spectroscopy nor to be tested in catalysis. At this stage, these crystal structures evidence that the DCPB ligand is flexible enough to coordinate either as a chelate in a monometallic or bimetallic species, or as a bridging ligand between two metal centers in dinuclear species. However, since these compounds were obtained from different crystallization solvents/conditions, there is no evidence that such species might be formed under our catalytic reaction conditions.

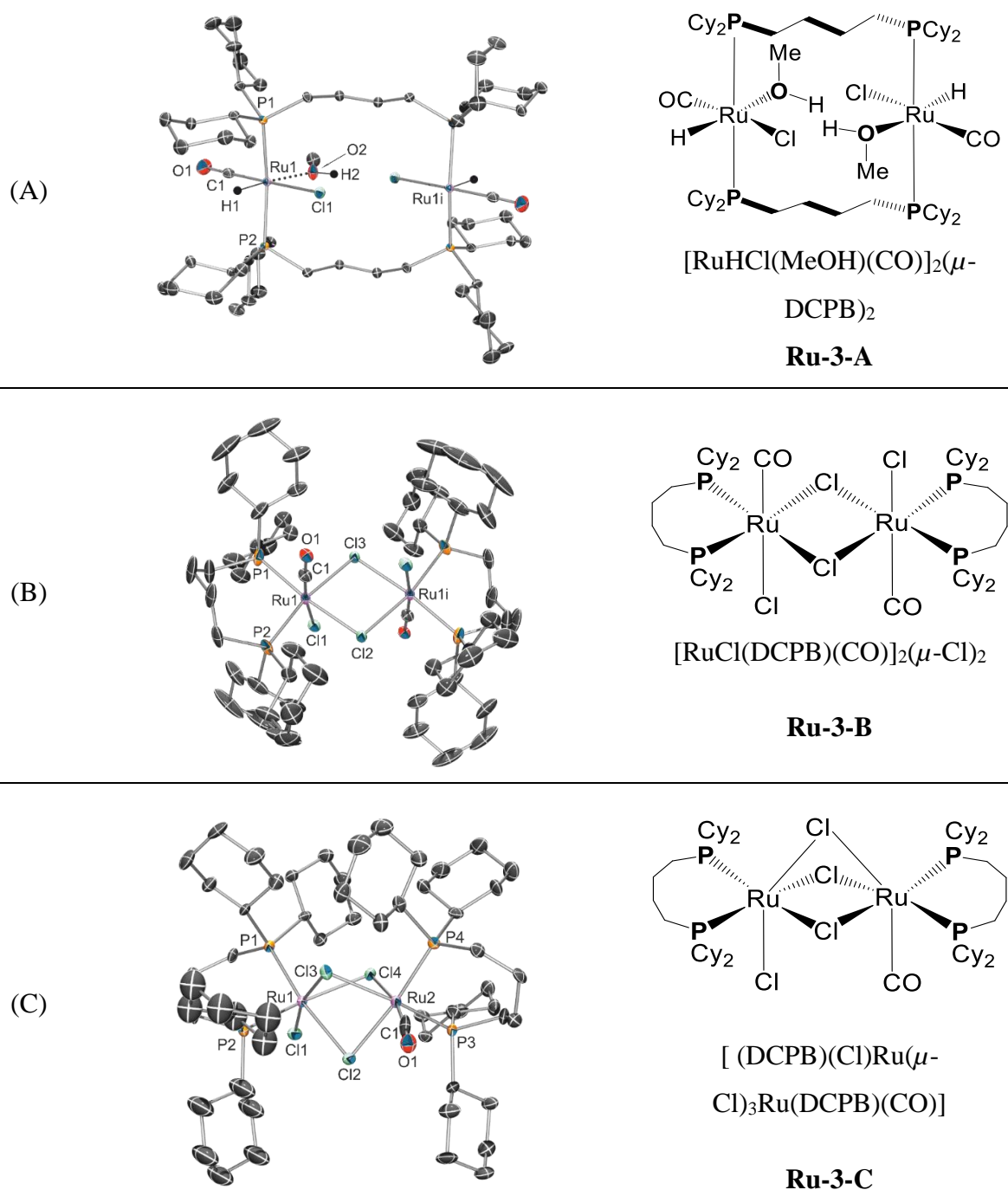


Figure II.3.14. ORTEP representation of the solid-state structures of dimeric ruthenium complexes $[\text{RuHCl}(\text{MeOH})(\text{CO})]_2(\mu\text{-DCPB})_2$ (A), $[\text{RuCl}(\text{DCPB})(\text{CO})]_2(\mu\text{-Cl})_2$ (B) and $[(\text{DCPB})(\text{Cl})\text{Ru}(\mu\text{-Cl})_3\text{Ru}(\text{DCPB})(\text{CO})]$ (C) with thermal ellipsoids set at 50% probability level. Hydrogen atoms and one molecule of MeOH in (A) are omitted for clarity.

Table II.3.2. Selected interatomic distances [Å] and angles [°] for **Ru-3-A**, **Ru-3-B** and **Ru-3-C**.

Ru-3-A			
Ru1–Cl1	2.4664(5)	Ru1–O2	2.3135(15)
Ru1–H1	1.51(2)	Ru1–P1	2.3701(5)
Ru1–P2	2.3778(5)	Ru1···Ru1i	6.612
Ru1–C1	1.809(2)	H1∠Ru1–O2	174.80(9)
C1∠Ru1–O2	98.97(8)	C1∠Ru1–P2	92.89(7)
C1∠Ru1–P1	90.67(6)	O2∠Ru1–P2	94.14(4)
P1∠Ru1–O2	98.28(4)	P1∠Ru1–P2	166.38(18)
C1∠Ru1–Cl1	176.94(7)	O2∠Ru1–Cl1	83.65(4)
P2∠Ru1–Cl1	88.48(17)	H1∠Ru1–Cl1	91.90(9)
Ru-3-B			
Ru1–Cl1	2.479(2)	Ru1–C1	1.72(2)
Ru1–Cl2	2.4647(12)	Ru1–P1	2.3642(13)
Ru1–Cl3	2.4886(11)	Ru1–P2	2.3338(13)
Ru1···Ru1i	3.784		
Cl2∠Ru1–Cl3	87.96(5)	C1∠Ru1–Cl3	92.20(7)
P2∠Ru1–Cl3	173.32(5)	P1∠Ru1–Cl3	88.12(4)
P2∠Ru1–P1	98.47(5)	P1∠Ru1–C1	86.80(7)
Ru-3-C			
Ru2–Cl2	2.4947(17)	Ru2–C1	1.690(4)
Ru2–Cl3	2.4961(18)	Ru2–P3	2.3070(19)
Ru2–Cl4	2.4330(17)	Ru2–P4	2.3205(18)
Ru1···Ru2	3.368	Ru1–Cl1	2.425(3)
Ru1–P1	2.3018(18)	Ru1–P2	2.3035(18)
P1∠Ru1–Cl2	173.27(6)	C1∠Ru2–P3	95.2(4)
P1∠Ru1–Cl3	93.67(6)	C1∠Ru2–P4	90.2(4)
P1∠Ru1–Cl4	98.75(6)	P4∠Ru2–P3	93.58(6)

3.3. Influence of the metal/ligand ratio in ligand exchange reaction and catalysis

3.3.1. Influence of the Ru(H)(Cl)(CO)(PPh₃)₃/DCPB ratios in complexation reaction

In order to evaluate the intrinsic catalytic activity of Ru catalysts, the development of a synthetic methodology allowing a cleaner preparation of both mono- or bimetallic complexes is required. Therefore, we started evaluating different metal to ligand (**Ru-1**/DCPB) ratios striving to promote the formation of either catalytic precursor in a more selective manner. Thus, a series of NMR-scale experiments in toluene-*d*₈ were conducted at 100 °C under argon. ¹H and ³¹P NMR spectroscopy data were then recorded at room temperature (Figures II.3.15 and II.3.16, respectively).

As previously observed, the reaction using an equimolar ratio of **Ru-1** and DCPB revealed, in the corresponding ¹H NMR spectrum (Figure II.3.15 (A)), the presence of a set of

doublet of triplets in the hydride region at $\delta_{\text{H}} -7.1$ ppm (*, $J_{\text{P-H,trans}} = 104.0$ Hz, $J_{\text{P-H,cis}} = 24.3$ Hz), from the **Ru-3** complex, and a multiplet at $\delta_{\text{H}} -8.0$ ppm (■) belonging to an unidentified species, in a ratio of 1:3.4. Unlike the Shlenck-tube scale complexation reaction, J. Young NMR scale reaction mixture exhibited a higher ratio of the unidentified hydride species, which might be due to the higher local concentration of **Ru-1** and DCPB and to the absence of stirring, causing low homogenization of the reaction mixture.

The $^1\text{H}\{^{31}\text{P}\}$ NMR data showed the presence of four major singlets in the hydride region, at $\delta_{\text{H}} -7.1$, -8.05 , -8.07 and -8.10 ppm and a minor one at $\delta_{\text{H}} -7.09$ ppm (Figure.II.3.15 (B)). Of the four sets of signals, only the singlet at $\delta_{\text{H}} -7.1$ ppm could be associated to the formerly *dt* observed at $\delta_{\text{H}} -7.1$ ppm in the regular ^1H NMR spectrum corresponding to the hydride ligand of the **Ru-3** complex. The remaining patterns suggested that those three or possibly four additional species are present in the mixture and account for ca. 77% of the total hydrido complexes.

Performing the reaction with a molar ratio of 2:1 (**Ru-1**/DCPB) resulted in a significant decrease of the intensity of the resonances at $\delta_{\text{H}} -8.0$ ppm (■), in the corresponding ^1H NMR spectrum (Figure II.3.15 (C)), as well as those of the signals at $\delta_{\text{P}} 31.7$ and 16.9 ppm (▼) in the $^{31}\text{P}\{^1\text{H}\}$ NMR spectrum (Figure.II.3.16 (C)). A minor hydride species is observable at $\delta_{\text{H}} -6.7$ ppm. Under these conditions, **Ru-3** is formed in a 70% yield, based on the overall phosphorous resonances.

Addition of a larger excess (1:4) of ligand with respect to **Ru-1** precursor disfavoured the formation of **Ru-3**, as shown by the diminution of the intensities of the corresponding resonances in both ^1H and $^{31}\text{P}\{^1\text{H}\}$ NMR spectra (Figure.II.3.15 (E) and Figure.II.3.16 (D)). In the hydride region, the initially presumed multiplet at $\delta_{\text{H}} -8.0$ ppm (■) evolved into a well-resolved doublet of triplets, featuring coupling constant values characteristic of a hydride nucleus coupled with three nuclei ($J_{\text{P-H,trans}} = 108.4$ Hz, $J_{\text{P-H,cis}} = 25.2$ Hz). Unfortunately, the lack of structural and NMR spectroscopy data hampered any further molecular elucidation. The same observations were recorded when a **Ru-1**/DCPB ratio of 1:2 was employed, suggesting that any surplus of ligand reduces the selectivity toward the formation of **Ru-3** complex.

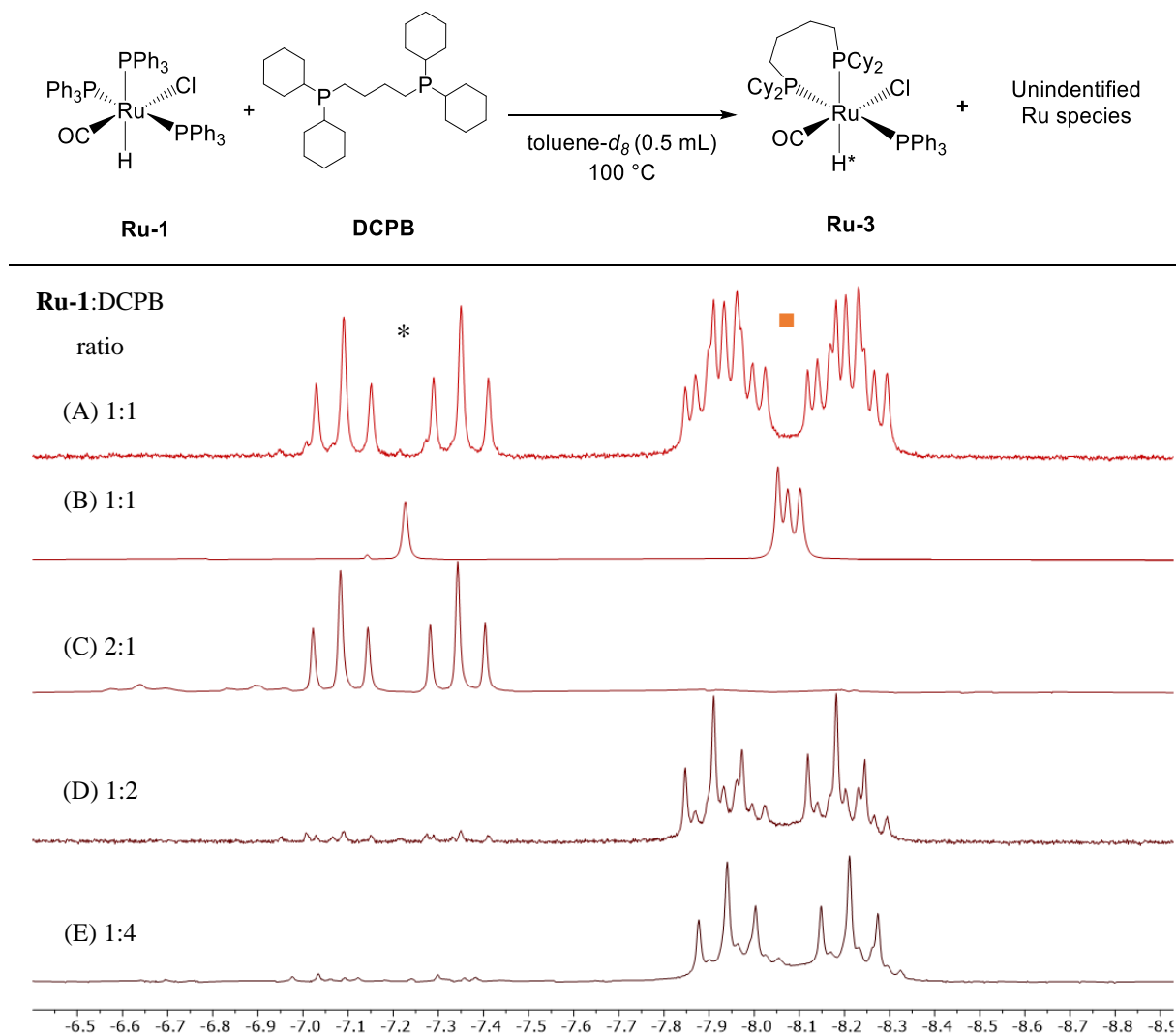


Figure II.3.15. Stack plot of ^1H NMR spectra (A, C, D, E) and $^1\text{H}\{^{31}\text{P}\}$ NMR spectrum (B) of the hydride region (400 MHz, toluene- d_8 , 25 $^\circ\text{C}$) of the crude mixtures resulting from the reaction of different **Ru-1**/DCPB ratios under argon atmosphere.

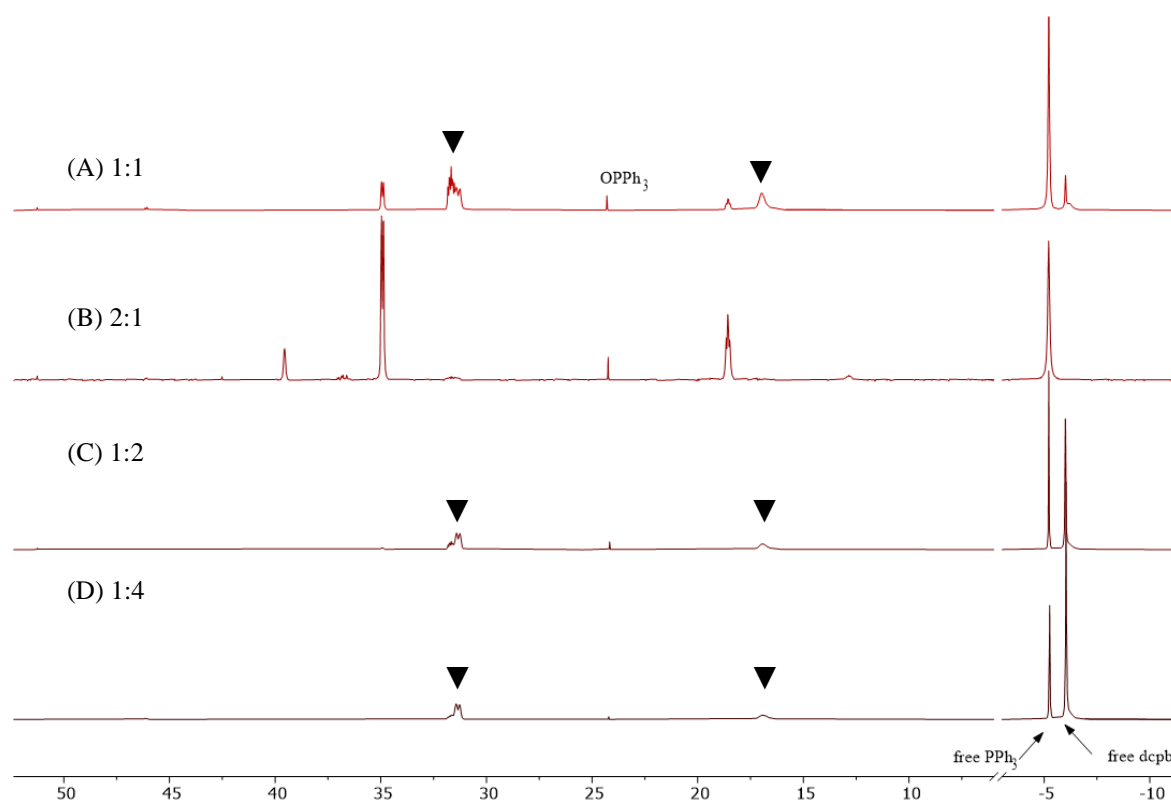


Figure II.3.16. Stack plot of $^{31}\text{P}\{^1\text{H}\}$ NMR spectra (162 MHz, toluene- d_8 , 25 °C) of the crude mixtures resulting from the reaction of different **Ru-1**:DCPB ratios under argon atmosphere.

On the other hand, performing the same equimolar reaction (**Ru-1**/DCPB) in THF- d_8 or CD_2Cl_2 solvents did not prevent the formation of the unidentified species, and led even to the appearance of an additional pattern at δ_{P} 39.2 ppm in the $^{31}\text{P}\{^1\text{H}\}$ NMR spectra (see Annexes Figure II.3.21. and Figure II.3.22.).

Then, we conducted NMR-scale reactions with a **Ru-1**/DCPB 1:1 ratio under an equimolar mixture of C_2H_4 : CO_2 gases (1 bar) to assess the catalytic behaviour of the mixture of species generated. Comparison of the ^1H NMR spectra showed no differences whether the experiment was conducted under inert or C_2H_4 / CO_2 atmosphere; both hydride patterns at -7.1 ppm (*) and δ_{H} -8.0 ppm (■) were observed in an average ratio of 1:0.4 (see Annexes Figure II.3.23.).

From the results obtained, it became clear that depending on the proportion between the precursor and the ligand, formation of **Ru-3** might be favoured over other species and *vice versa*. Unfortunately, attempts to properly isolate and authenticate either species remained unsuccessful.

3.3.2. Application to catalysis

On the next step, we carried out catalytic ethylene carboxylation experiments using different molar ratio of **Ru-1**:DCPB combinations.

First of all, we conducted the reaction in absence of DCPB ligand. High conversion of Et₃SiH was reached (Table II.3.3, entry 1) and route C products (**TEVS** and **TES**) were, however, the main compounds formed. These results attested that **Ru-1** precursor is able to catalyze, by itself, the hydrosilylative and dehydrogenative silylation reactions of C₂H₄ with Et₃SiH.

On the other hand, conducting the experiment with a 2:1 **Ru-1**/DCPB ratio increased **A1** and route C turn over numbers (entry 2). The use of an excess of ligand (4 equiv *vs.* **Ru-1**) caused a decrease of the Et₃SiH conversion from 54 to 38 % (entry 4 *vs.* 5), and formation of the route A products (**A1** and **P1**) was observed in lower TONs than those reported using an equimolar **Ru-1**:DCPB ratio.

These observations suggested that the (main) active species toward route A products might best arise from an equimolar or ruthenium-enriched mixture of **Ru-1** and DCPB. As previously observed by NMR spectroscopy, working under these conditions favored the formation of the **Ru-3** complex, suggesting that under these reaction conditions promoting its formation, the latter species is the main, if not the only active precursor toward the desired reduction carboxylation products of C₂H₄ and CO₂.

Table II.3.3. Catalytic results from batch experiments using various **Ru-1**/DCPB combinations.^[a]

Entry	Ru-1 /DCPB molar ratio	Conv. Et ₃ SiH [mol%] ^[b]	TON					
			Route A products			Route B and C products		
			A1	P1	F1	TES	TEVS	E
1	1:0	92	traces	traces	0	10	42	traces
2	2:1	57	20	2	10	8	98	1
3	1:2	43	6	2	0	5	26	traces
4	1:1	54	13	1.3	16	4	53	1.6
5	1:4	38	4	1	0	1	22	traces

^[a] Reaction conditions: toluene (20 mL), $[\text{Si-H}]_0 = 0.43 \text{ mol}\cdot\text{L}^{-1}$, $[\text{Ru}]_0 = 0.002 \text{ mol}\cdot\text{L}^{-1}$, $\text{CO}_2/\text{C}_2\text{H}_4$ 1:1 mol/mol, $\text{P}(\text{CO}_2) + \text{P}(\text{C}_2\text{H}_4) = 20 \text{ bar}$ ^[b] Determined by integration of the ^1H NMR peaks using $(\text{Me}_3\text{Si})_4\text{Si}$ as internal standard. ^[c] Yields as determined by GC-FID using *n*-dodecane as internal standard.

3.4. Reactivity of Et_3SiH toward ruthenium complexes

3.4.1. Stoichiometric reaction of **Ru-1**, DCPB and Et_3SiH

One could ask if the reductant, Et_3SiH , interferes in the complexation reaction of **Ru-1** with DCPB and/or with the complex resulting from the reaction of the precursor with the ligand. Thus, an NMR-scale reaction was performed between equimolar amounts of **Ru-1**, DCPB and Et_3SiH in toluene- d_8 under Ar atmosphere (1 bar) at 100 °C for 2 h. The room temperature ^1H NMR spectrum of the resulting reaction mixture (Figure II.3.17., (A)) exhibited three different resonances in the hydride region.

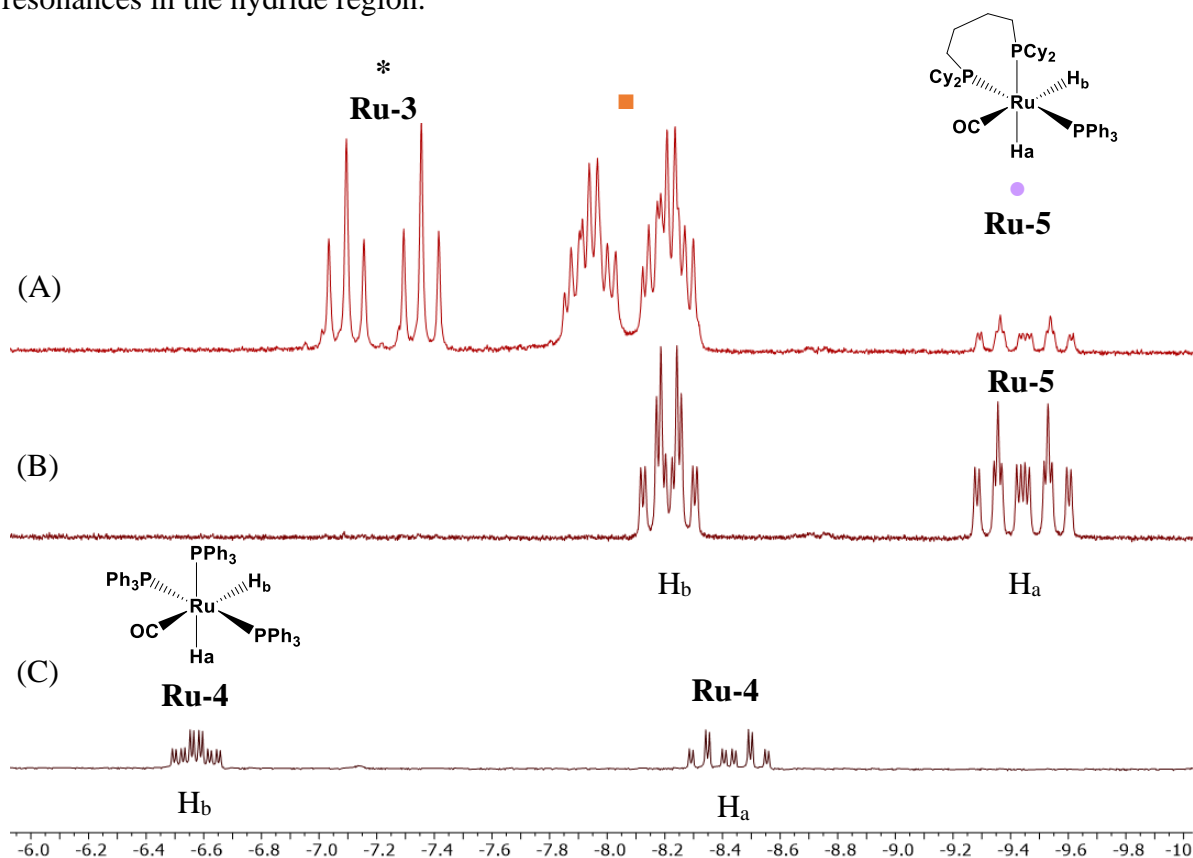


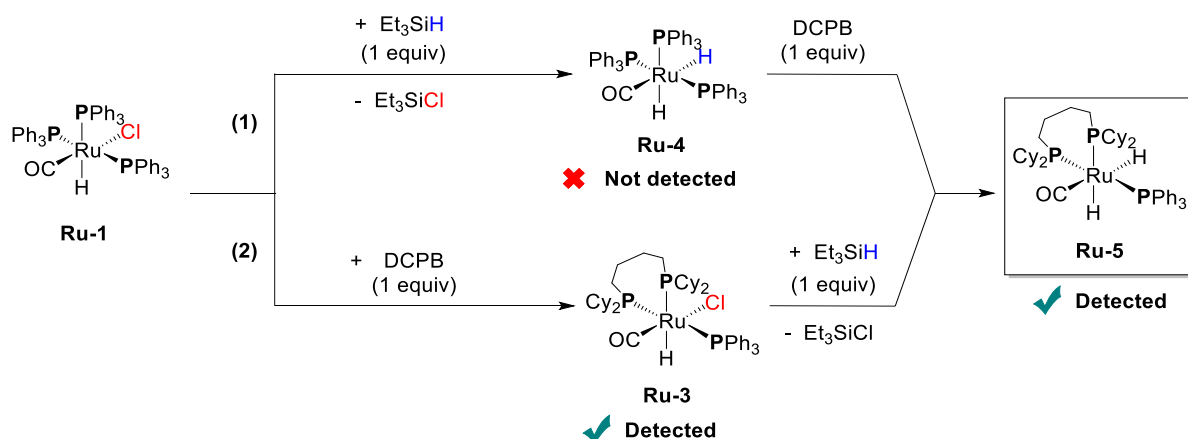
Figure II.3.17. Stack plot of the room temperature ^1H NMR spectra (400 MHz, toluene- d_8 , 25 °C) (hydride region): (A) *in situ* reaction mixture of **Ru-1**, DCPB and Et_3SiH in toluene- d_8 under argon at 100 °C for 2 h (B) $\text{Ru}(\text{H})_2(\text{CO})(\text{DCPB})(\text{PPh}_3)$ (**Ru-5**) and (C) $\text{Ru}(\text{H})_2(\text{CO})(\text{PPh}_3)_3$ (**Ru-4**) complexes.

In addition to the previously reported **Ru-3** doublet of triplets at $\delta_{\text{H}} -7.1 \text{ ppm}$ (*) and multiplet at $\delta_{\text{H}} -8.0 \text{ ppm}$ (■), a new pattern appearing at $\delta_{\text{H}} -9.4 \text{ ppm}$ (●) as a *dddd* indicated the presence of a new hydride species, featuring coupling with four inequivalent nuclei. The nature of the latter was unequivocally identified to be bis(hydride) complex

$\text{Ru}(\text{H})_2(\text{CO})(\text{DCPB})(\text{PPh}_3)$ (**Ru-5**), which was prepared in a separate experiment from the parent $\text{Ru}(\text{H})_2(\text{CO})(\text{PPh}_3)_3$ (**Ru-4**) precursor and DCPB (*vide infra*).

Two possible scenarios for the formation of **Ru-5** can be given (Scheme II.3.6). One possibility is, first, the reduction of **Ru-1** with Et_3SiH to $\text{Ru}(\text{H})_2(\text{CO})(\text{PPh}_3)_3$ (**Ru-4**), which subsequently undergoes ligand exchange with DCPB ligand and release one equivalent of chlorotriethylsilane (pathway (1)). Historically, generation of ruthenium hydride bonds from parent ruthenium chloride species using silyl hydrides has proven efficient,^[29–31] confirming that such reactivity is in fact expected.

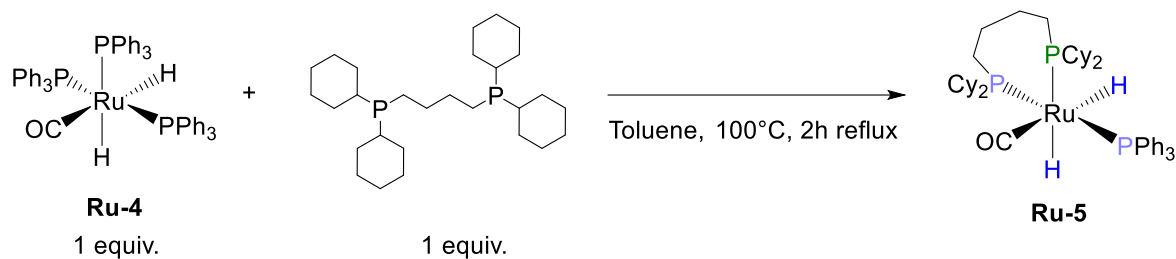
Another pathway is formation of **Ru-3** complex first, followed by its reduction into dihydro complex **Ru-5** (pathway (2)). Since complex **Ru-4** was not detected by ^1H NMR spectroscopy in the reaction medium, we assumed that route 2 is more likely to occur.



Scheme II.3.6. Possible pathways for complex **Ru-5** formation from **Ru-1** and DCPB ligand in presence of Et_3SiH .

3.4.2. Synthesis, characterization and catalytic activity of the dihydrido $\text{Ru}(\text{H})_2(\text{CO})(\text{DCPB})(\text{PPh}_3)$ complex

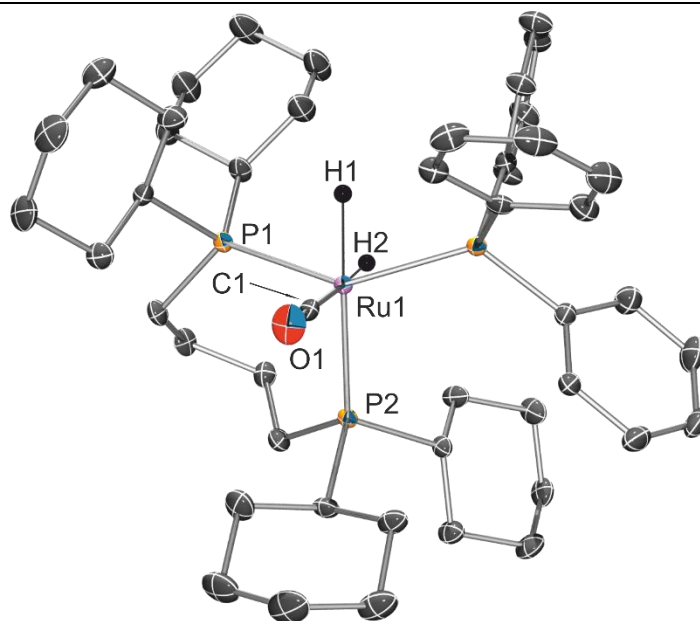
After exploring the reactivity of monohydride ruthenium(II) complexes, we decided to investigate the catalytic efficiency of dihydro ruthenium complexes, since their formation in the reaction medium has been observed by means of NMR spectroscopy. Complex **Ru-5** was obtained from the corresponding dihydro precursor $\text{Ru}(\text{H})_2(\text{CO})(\text{PPh}_3)_3$ (**Ru-4**) upon mixing with one equivalent of DCPB ligand (77% yield, Scheme II.3.7).



Scheme II.3.7. Synthesis of complex $\text{Ru}(\text{H})_2(\text{CO})(\text{DCPB})(\text{PPh}_3)$ (**Ru-5**).

The molecular structure of **Ru-5** in the solid state was elucidated *via* X-ray diffraction analysis of crystals obtained from a saturated solution of the corresponding complex in heptane. As shown in Figure II.3.18., the DCPB ligand is bound to the Ru center in a *cis* fashion, with a bite angle of $100.80(4)^\circ$. The Ru–CO bond in complex **Ru-5** ($1.902(5) \text{ \AA}$) is longer when compared to the Ru1–C1 bond ($1.856(4) \text{ \AA}$) in the monohydride **Ru-3** complex. This is due to the positioning of the carbonyl ligand *trans* to the hydride, which exhibits largest *trans* influence in comparison to the chloride congener in **Ru-3**.^[32] In the same manner, the longer Ru1–H2 bond compared to the Ru1–H1 ($1.70(5)$ and $1.54(5) \text{ \AA}$ respectively) results from the stronger *trans* influence of the CO group compared to that of the phosphine PR_3 .

Ru(H)₂(CO)(DCPB)(PPh₃)
Ru-5



Selected bond lengths [Å]

Ru1–H1 = 1.54(5), Ru1–H2 = 1.70(5), Ru1–C1 = 1.902(5), Ru1–P3 = 2.3234(11), Ru1–P1 = 2.3261(11), Ru1–P2 = 2.3932(11), Ru1–C1 = 1.902(5), C1–O2 = 1.144(6)

Selected bond angles [°]

P3–Ru1–P1 = 144.67(4), P3–Ru1–P2 = 107.42(4), P1–Ru1–P2 = 100.80(4)

Figure II.3.18. ORTEP representation of the solid-state molecular structure of ruthenium hydride complex Ru(H)₂(CO)(DCPB)(PPh₃) (**Ru-5**) with thermal ellipsoids set at 50% probability level. Hydrogen atoms omitted for clarity. Selected interatomic distances and angles are given in Ångström [Å] and degree [°], respectively.

The NMR resonances of complex **Ru-5** in toluene-*d*₈ solution were found in accordance with the solid-state structure. The key resonances in the hydrido region of the ¹H NMR spectrum (Figure II.3.17, (B)) include: a *dddd* at δ_H –8.0 ppm from Ru-(H_b), and a *dddd* splitting pattern from Ru-(H_a) at δ_H –9.4 ppm ($J_{PH, trans} = 70$ Hz, $J_{PH, cis} = 32$ and 26 Hz and $J_{HH, cis} = 5.8$ Hz).

The bis(hydride) precursors Ru(H)₂(CO)(PPh₃)₃ (**Ru-4**), Ru(H)₂(CO)(PPh₃)₃/DCPB and Ru(H)₂(CO)(DCPB)(PPh₃) were then evaluated in reductive carboxylation of C₂H₄ under regular catalytic conditions (Table II.3.4). The **Ru-4** precursor mimicked the reactivity of the **Ru-1** precursor, and higher selectivity towards route C products (**TEVS** and **TES**, entries 1 and 3) was also observed. Such results were in fact expected since the Ru(H)(Cl)(CO)(PPh₃)₃ precursor (**Ru-1**) is fully converted to the Ru(H)₂(CO)(PPh₃)₃ precursor (**Ru-4**) in the presence of Et₃SiH as it was shown by the previous experiments using equimolar amounts of the reagents. Therefore, Et₃SiH is not only involved in the formation of silylated compounds from CO₂ and C₂H₄, but also reduces monohydride-chloro species to their dihydride congeners.

Table II.3.4. Catalytic results from batch experiments with different Ru precursors and combinations.^[a]

Entry	Precursor/ligand (1:1, 0.5 mol%)	Conv. Et ₃ SiH [mol%] ^[b]	TON					
			Route A products			Route B and C products		
			A1	P1	F1	TES	TEVS	E
1	Ru(H)(Cl)(CO)(PPh ₃) ₃	92	traces	traces	0	10	42	traces
2	Ru(H)(Cl)(CO)(PPh ₃) ₃ / DCPB	54	13	1.3	16	4	53	1.6
3	Ru(H) ₂ (CO)(PPh ₃) ₃	47	traces	0	0	13	82	0
4	Ru(H) ₂ (CO)(PPh ₃) ₃ / DCPB	43	19	1.1	7	2	9	1
5	Ru(H) ₂ (CO)(DCPB)(PPh ₃)	51	22	2	9	4	10	1.3

^[a] Reaction conditions: toluene (20 mL), [Si–H]₀ = 0.43 mol·L⁻¹, [Ru]₀ = [ligand]₀ = 0.002 mol·L⁻¹, CO₂/C₂H₄ 1:1 mol/mol, P(CO₂) + P(C₂H₄) = 20 bar; results of at least duplicated experiments and averaged yields values. ^[b] Determined by integration of the ¹H NMR signals using (Me₃Si)₄Si as internal standard. ^[c] Yields as determined by GC-FID using *n*-dodecane as internal standard.

The *in situ* combination of **Ru-4** with DCPB afforded the route A products (**A1**, **P1**) with TONs values closely similar to those obtained with **Ru-1**:DCPB, while decreasing those of route B (**F1**) and route C products (entries 2 vs. 4). Interestingly, using the well-defined readily available precursor Ru(H)₂(CO)(DCPB)(PPh₃) allowed to increase TON of **A1** up to 22, as compared to a TON of 13 initially achieved with **Ru-1**/DCPB combination (entries 5 vs. 2). Moreover, the formation of **TEVS** and **TES** products was lowered.

3.5. Conclusion

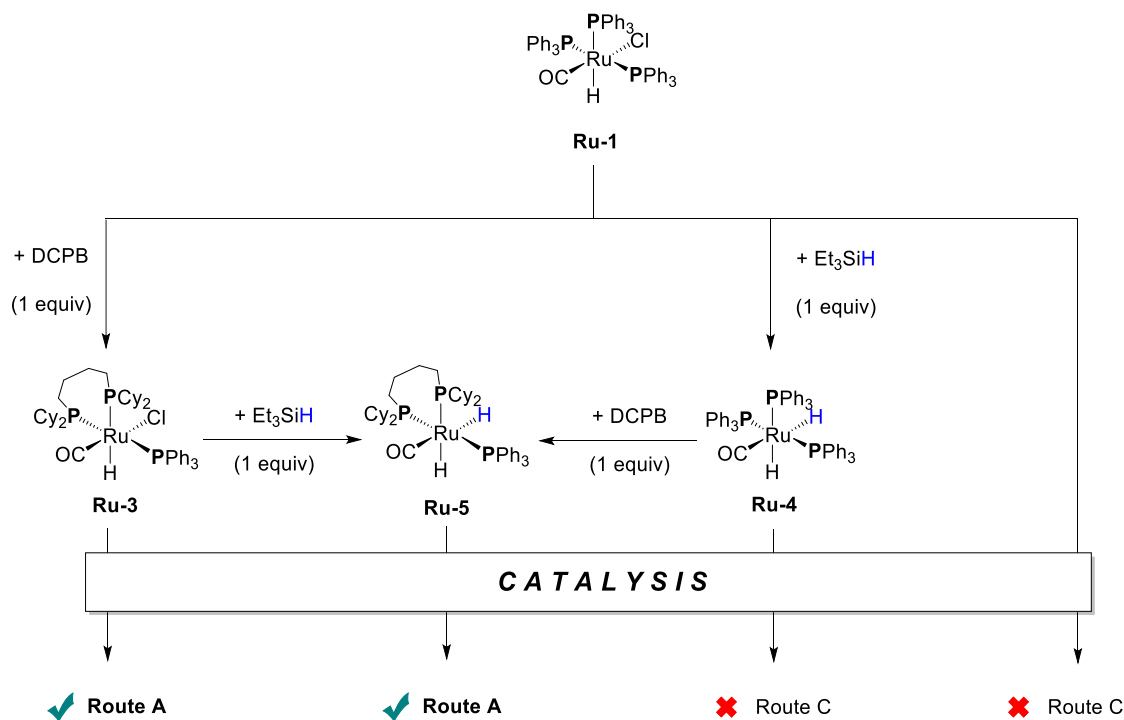
Upon optimizing the reaction conditions of ethylene reductive carboxylation reaction, complementary studies towards the identification of active species arising from the Ru(H)(Cl)(CO)(PPh₃)₃/DCPB and Ru(H)(Cl)(CO)(PPh₃)₃/DCPF combinations were performed.

X-ray diffraction and NMR spectroscopy studies confirmed the formation of the expected bidentate phosphine-coordinated complexes Ru(H)(CO)(Cl)(DCPF)(PPh₃) and Ru(H)(CO)(Cl)(DCPB)(PPh₃). In particular, the solution NMR data pointed out that the ligand exchange reaction between **Ru-1** and DCPB yielding the anticipated **Ru-3** complex is not

selective, and depends on the precursor/ligand ratio. The formation of other Ru(II) hydride species was observed and the nature of the latter was identified, according to the collected NMR data, as a mixture of possible isomers of **Ru-3**.

Crystallizations in different solvents/conditions of the crude product resulting from the ligand exchange reaction of **Ru-1**/DCPB afforded several bimetallic and dimeric structures, identified by XRD study. Given the flexibility of the 4-carbon backbone chain of the DCPB ligand, formation of such dinuclear species was not unexpected. Thus, the formation of bimetallic complexes in reaction medium under catalytic conditions remains a possible scenario. On the other hand, stoichiometric experiments also demonstrated the role of triethylsilane (Et_3SiH) in reducing monohydride-chloro species into their corresponding dihydride counterparts. As a result, new hydrido species might be formed in the presence of a reductant, rendering their identification even more complicated.

Some of the above mentioned hydride complexes were isolated, characterized and tested in catalysis. Different activities and selectivities towards the targeted acrylate and propionate silyl esters products were observed. The fact that they afforded the routes A, B and C products suggests that they might also be precursors of different other active species, each initiating a different catalytic cycle. The investigations carried out in the objective of distinguishing the species that favours route A are summarized below (Scheme II.3.8).



Scheme II.3.8. New ruthenium hydride species favouring route A pathway.

3.6. References

- [1] R. Alvarez, E. Carmona, D. J. Cole-Hamilton, A. Galindo, E. Gutierrez-Puebla, A. Monge, M. L. Poveda, C. Ruiz, *J. Am. Chem. Soc.* **1985**, *107*, 5529–5531.
- [2] A. Galindo, A. Pastor, P. J. Perez, E. Carmona, *Organometallics* **1993**, *12*, 4443–4451.
- [3] W. H. Bernskoetter, B. T. Tyler, *Organometallics* **2011**, *30*, 520–527.
- [4] H. Hoberg, D. Schaefer, *J. Organomet. Chem.* **1983**, *251*, c51–c53.
- [5] H. Hoberg, Y. Peres, A. Milchereit, *J. Organomet. Chem.* **1986**, *307*, C38–C40.
- [6] H. Hoberg, Y. Peres, C. Krüger, Y.-H. Tsay, *Angew. Chem. Int. Ed. Engl.* **1987**, *26*, 771–773.
- [7] H. Hoberg, A. Ballesteros, A. Sigan, C. Jégat, D. Bärhausen, A. Milchereit, *J. Organomet. Chem.* **1991**, *407*, C23–C29.
- [8] M. L. Lejkowski, R. Lindner, T. Kageyama, G. É. Bódizs, P. N. Plessow, I. B. Müller, A. Schäfer, F. Rominger, P. Hofmann, C. Futter, S. A. Schunk, M. Limbach, *Chem. – Eur. J.* **2012**, *18*, 14017–14025.
- [9] C. Hendriksen, E. A. Pidko, G. Yang, B. Schäffner, D. Vogt, *Chem. – Eur. J.* **2014**, *20*, 12037–12040.
- [10] Z. R. Greenburg, D. Jin, P. G. Williard, W. H. Bernskoetter, *Dalton Trans.* **2014**, *43*, 15990–15996.
- [11] N. Hugué, I. Jevtovikj, A. Gordillo, M. L. Lejkowski, R. Lindner, M. Bru, A. Y. Khalimon, F. Rominger, S. A. Schunk, P. Hofmann, M. Limbach, *Chem. – Eur. J.* **2014**, *20*, 16858–16862.
- [12] S. Manzini, A. Cadu, A.-C. Schmidt, N. Hugué, O. Trapp, R. Paciello, T. Schaub, *ChemCatChem* **2017**, *9*, 2269–2274.
- [13] R. Fischer, J. Langer, A. Malassa, D. Walther, H. Görls, G. Vaughan, *Chem. Commun.* **2006**, 2510–2512.
- [14] Rafael. Alvarez, Ernesto. Carmona, Agustin. Galindo, Enrique. Gutierrez, J. M. Marin, Angeles. Monge, M. L. Poveda, Caridad. Ruiz, J. M. Savariault, *Organometallics* **1989**, *8*, 2430–2439.
- [15] G. Schubert, I. Pápai, *J. Am. Chem. Soc.* **2003**, *125*, 14847–14858.
- [16] S. Y. T. Lee, M. Cokoja, M. Drees, Y. Li, J. Mink, W. A. Herrmann, F. E. Kühn, *ChemSusChem* **2011**, *4*, 1275–1279.
- [17] M.-N. B. (née Gensow), Z. Freixa, P. W. N. M. van Leeuwen, *Chem. Soc. Rev.* **2009**, *38*, 1099–1118.
- [18] S. H. Liu, S. T. Lo, T. B. Wen, I. D. Williams, Z. Y. Zhou, C. P. Lau, G. Jia, *Inorganica Chim. Acta* **2002**, *334*, 122–130.
- [19] A. Santos, J. Lopez, J. Montoya, P. Noheda, A. Romero, A. M. Echavarren, *Organometallics* **1994**, *13*, 3605–3615.
- [20] P. Dierkes, P. W. N. M. van Leeuwen, *J. Chem. Soc. Dalton Trans.* **1999**, 1519–1530.
- [21] A. Poater, F. Ragone, S. Giudice, C. Costabile, R. Dorta, S. P. Nolan, L. Cavallo, *Organometallics* **2008**, *27*, 2679–2681.
- [22] H. Clavier, S. P. Nolan, *Chem. Commun.* **2010**, *46*, 841–861.
- [23] A. Poater, B. Cosenza, A. Correa, S. Giudice, F. Ragone, V. Scarano, L. Cavallo, *Eur. J. Inorg. Chem.* **2009**, *2009*, 1759–1766.
- [24] L. Falivene, R. Credendino, A. Poater, A. Petta, L. Serra, R. Oliva, V. Scarano, L. Cavallo, *Organometallics* **2016**, *35*, 2286–2293.
- [25] “SambVca - Home Page,” can be found under <https://www.molnac.unisa.it/OMtools/sambvca2.1/index.html>
- [26] A. E. W. Ledger, A. Moreno, C. E. Ellul, M. F. Mahon, P. S. Pregosin, M. K. Whittlesey, J. M. J. Williams, *Inorg. Chem.* **2010**, *49*, 7244–7256.

- [27] K. Severin, *Chem. – Eur. J.* **2002**, *8*, 1514–1518.
- [28] A. G. Tskhovrebov, E. Solari, R. Scopelliti, K. Severin, *Organometallics* **2012**, *31*, 7235–7240.
- [29] H. Kono, Y. Nagai, *Chem. Lett.* **1974**, *3*, 931–932.
- [30] H. Kono, N. Wakao, Y. Nagai, *Chem. Lett.* **1975**, *4*, 955–956.
- [31] H. Kono, N. Wakao, K. Ito, Y. Nagai, *J. Organomet. Chem.* **1977**, *132*, 53–67.
- [32] “Organotransition Metal Chemistry: From Bonding to Catalysis, by John Hartwig with Contributions by Patrick J. Walsh, Geoffrey W. Coates, Charles P. Casey, Jack R. Norton, copyright 2010, published by University Science Books,” can be found under <http://www.uscibooks.com/hartwig.htm>

Chapter 4 – Mechanistic Investigations on the Ruthenium-Catalyzed Synthesis of Silyl Esters from C₂H₄ and CO₂

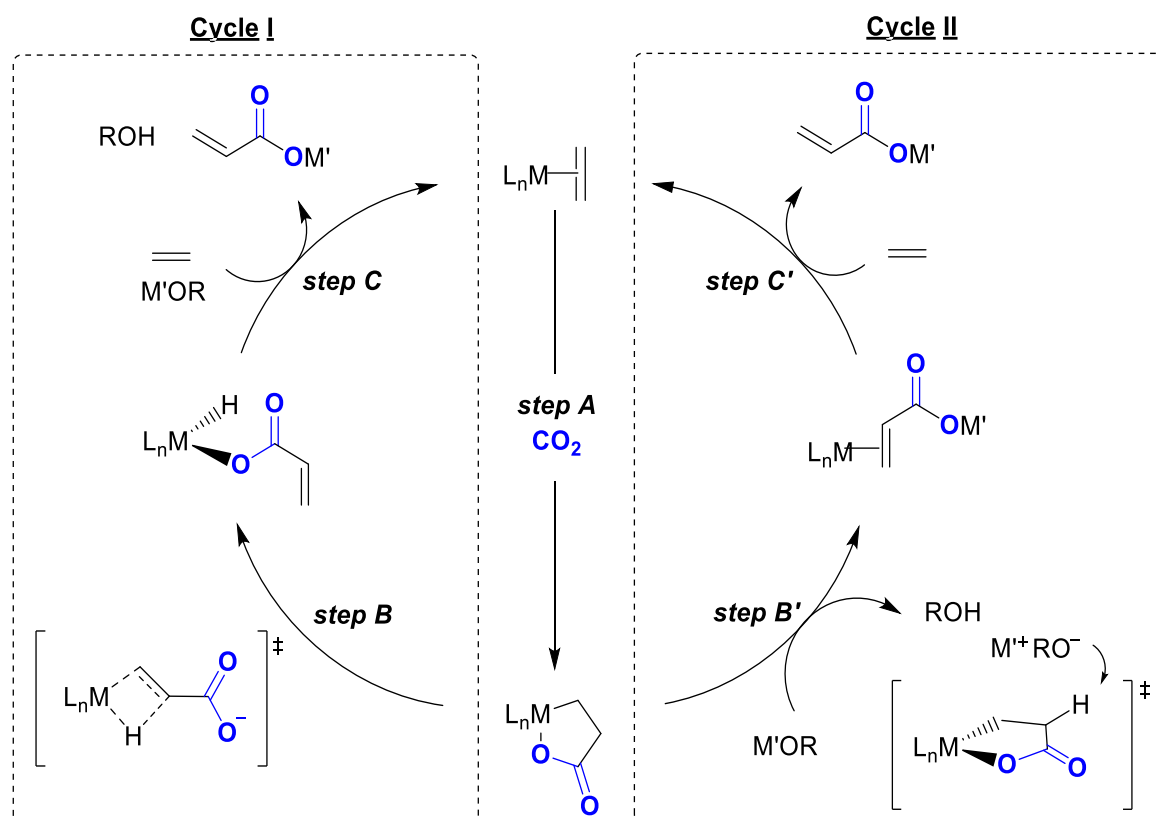
Computational studies described in sections 4.2.3, 4.3.2. and 4.4.2 were performed in collaboration with the group of Prof. L. Maron (LPCNO, INSA Toulouse). Unless otherwise stated, all DFT calculations obtained through this partnership were carried out by Dr. R. Thayalan.

4.1. Background

While investigations on the CO₂/C₂H₄ coupling reaction for acrylate formation mediated by Ni complexes are the most widespread in literature, studies with other transition metal complexes such as Pd, Mo, W, Ti, V, Zr, Fe and Rh have also been reported (see Chapter 1, Part I).^[1–9] Yet, a really efficient catalytic system has still not been identified so far. According to the different experimental and theoretical studies discussed in the literature,^[10–16] the essential step of the proposed catalytic cycles most involves a low valent complex, which undergoes oxidative cyclization of C₂H₄ and CO₂, to form a metallalactone species (Scheme II.4.1., step A). This first elementary step then gives rise to two possible pathways.

The first one is the cleavage of the metallalactone ring into a mixed hydrido-acrylato complex upon β-H elimination (Scheme II.4.1., Cycle I, step B). In the case of Ni-based systems, this step remains apparently the most challenging one due to the high stability of the nickelalactones.^[17–20] Moreover, the generally high BDE of the M–H and M–O bonds of hydrido-metal-acrylato intermediates present substantial kinetic barriers for elimination of the free acrylic acid (Cycle I, step C). To overcome this problematic step, nucleophilic interceptors (bases, additional phosphine ligands, methylating reagents or Lewis acids) are often added to promote the reductive elimination of the acrylate salt and eventually regenerate the zerovalent C₂H₄-coordinated complex.

The second possible catalytic pathway involves the direct base-mediated deprotonation of the metallacycle (Cycle II, step B'). The resulting π-coordinated acrylate complex undergoes a further ligand exchange with C₂H₄ to regenerate the zerovalent complex and releases the acrylate salt (step C').

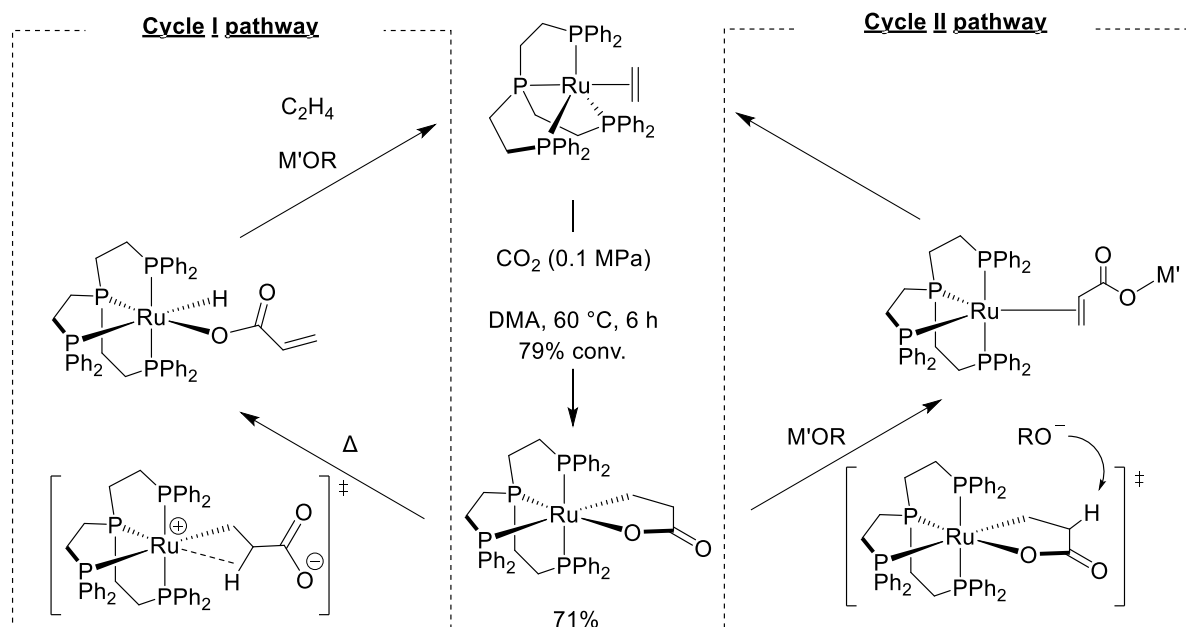


Scheme II.4.1. Proposed mechanisms for the formation of acrylate salts from C_2H_4 and CO_2 .^[21]

More recently, this chemistry was expanded to other promising homogeneous transition metal systems. For example, Iwasawa and co-workers reported the first example of a ruthenolactone, by using an electron-rich Ru(0) complex incorporating a tetradentate phosphine ligand (PP_3) (Scheme II.4.2).^[21,22] Until then, the proposed formation of ruthenacyclic species was mostly limited to olefinic and acetylenic substrates, using Ru(0) carbonyl or CpRu(II) species as precursors,^[23–25] and to some other works employing $Ru_3(CO)_{12}$ –phosphine systems for the hetero-Pauson-Khand $[2+2+1]$ cycloaddition^[26–28] as well as for oxidative cyclization of dienes with carbonyl compounds.^[29–31]

As previously proposed for Ni-based systems,^[11,16,32–34] the mechanistic investigations conducted by Iwasawa *et al.* on the cleavage of the five-membered ruthenolactone, generated from oxidative coupling of CO_2 and C_2H_4 , was considered to proceed through two possible mechanisms:^[21] the first proposed pathway is the M–O bond cleavage, generating a cationic ruthenium intermediate by dissociation of a carboxylate anion, and eventually leading to the formation of a hydrido-acrylate complex via β -H elimination (Scheme II.4.2, Cycle I). Further ligand exchange with C_2H_4 releases the free acrylic acid salt and regenerates the zerovalent complex.

Formation of such a cationic intermediate is thought to be facilitated with the stronger electron donation and/or steric bulkiness of the PP_3 ligand, which accelerates the dissociation of the carboxylate group. On the other hand, the authors also suggested the cleavage and the direct deprotonation of the ruthenolactone in the presence of KO^tBu as a possible alternative pathway (Scheme II.4.2., Cycle II).^[22]



Scheme II.4.2. Possible reaction mechanism proposed by Iwasawa *et al.* for the cleavage of ruthenolactone. Both *cis*-acrylato(hydrido) ruthenium and ruthenolactone species structures were confirmed by X-Ray analyses.^[21,22]

Taking into account these different kinetic and mechanistic data, we aimed at elucidating and developing a better understanding of the catalytic cycle behind silyl esters formation, including CO_2 and C_2H_4 side reactions, in the presence of our most effective catalytic system, *i.e.* $Ru(H)(Cl)(CO)(PPh_3)_3/DCPB$ (**Ru-1**/DCPB).

4.2. Mechanistic insights on the formation of the targeted triethylsilyl acrylate (A1) and propionate (P1) products

4.2.1. $Ru(H)(Cl)(CO)(PPh_3)(DCPB)$ mediated coupling of CO_2 and C_2H_4 : formation of the $[Ru(Cl)(CO)(DCPB)(\kappa^2O,O-CO_2CH=CH_2)]$ (**Ru-6**)

In order to understand the reductive functionalization of CO_2 and C_2H_4 into silyl esters in the presence of **Ru-1** and DCPB, to identify key intermediates, propose a mechanism toward their formation and to the subsequent release of silyl esters, we performed a series of stoichiometric reactions monitored by NMR spectroscopy.

A mixture of **Ru-1** and DCPB (1:1, 4.0 mmol·L⁻¹ in toluene) was treated under 20 bar of CO₂/C₂H₄ mixture (1:1 mol/mol) in an autoclave over 16 h at 100 °C. The reaction mixture was then cooled down to room temperature and transferred into a J.-Young NMR tube. Unexpectedly, in the up-field region of the room temperature ¹H NMR spectrum of the crude reaction mixture, no hydride species were detected (Figure II.4.1.). On the other hand, three down field shifted vinylic signals were observed at δ_H 5.2, 5.9 and 6.3 ppm with a 1:1:1 integration ratio.

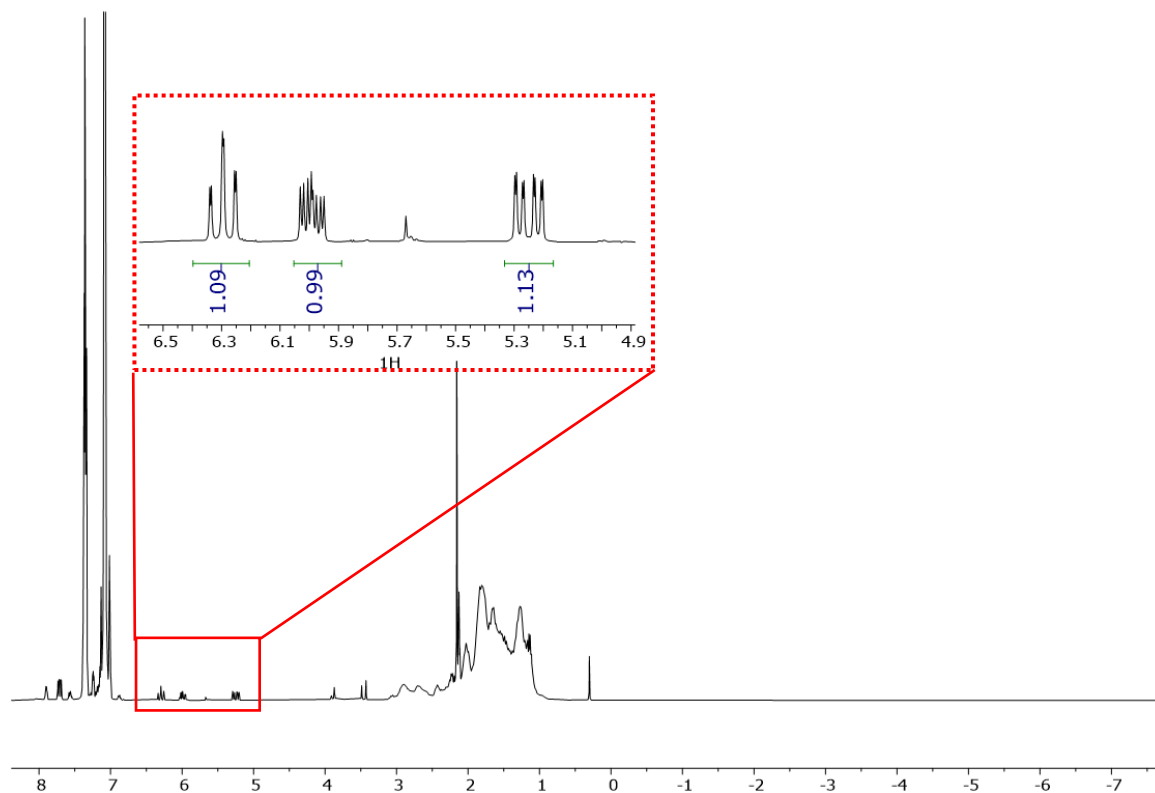
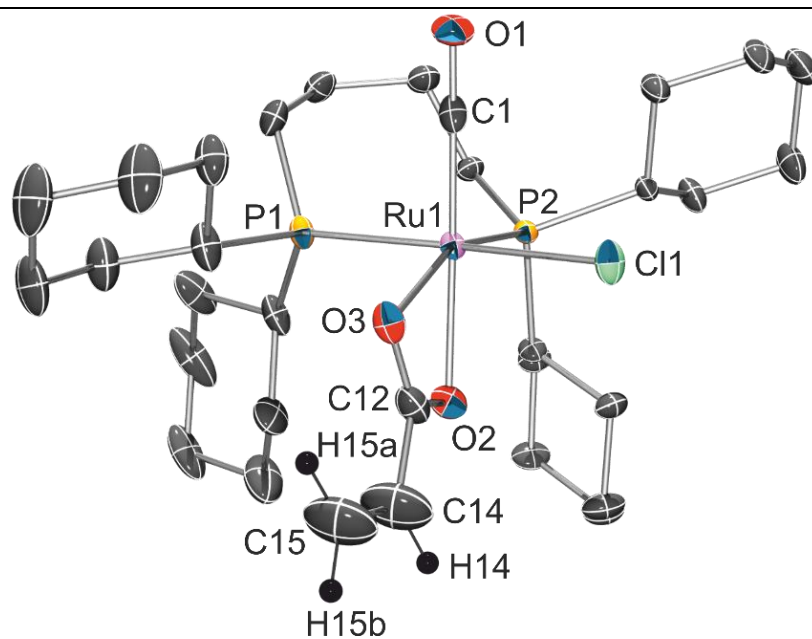


Figure II.4.1. ¹H NMR spectrum (500 MHz, toluene-*d*₈, 25 °C) of the crude reaction mixture of **Ru-1** and DCPB (1:1, 4.0 mmol·L⁻¹ in toluene) obtained under 20 bar of CO₂/C₂H₄ (1:1) after 16 h at 100 °C.

From the above crude mixture, single crystals suitable for X-ray diffraction analysis were grown from a heptane solution at room temperature. The X-ray crystallographic study allowed us to formulate the isolated complex as *cis*-[Ru(Cl)(CO)(DCPB)(κ²O, O-CO₂CH=CH₂)] (*cis*-**Ru-6**, Figure II.4.2.). The formation of such acrylate complex evidences the oxidative coupling of CO₂ and C₂H₄ but also opens up an attractive synthetic route directly to *cis*-**Ru-6** in substantial quantities (67% crude yield of *cis* and *trans* isomers).^[a]

^[a] Yields are determined by integration of the ³¹P NMR peaks *vs.* those of the standard (OPPh₃) and confirmed by integration of the ¹H NMR peaks *vs.* those of the standard (TMSS, Tetramethylsilane)

The solid-state molecular structure of *cis*-**Ru-6** exhibits a six-coordinated Ru atom in a distorted compressed octahedral environment (*i.e.* where the equatorial bonds are longer than the axial bonds). Two coordination sites are occupied by the bidentate DCPB phosphine ligand in a *cis* equatorial arrangement and two others are occupied by the bidentate acrylate ligand, with a κ^2 coordination to the metal center *via* the two carboxyl oxygen atoms. The other two ligands are Cl and CO in *cis*-position.

**Ru-6**

Selected bond lengths [Å]

Ru1–Cl1 = 2.4363(9), Ru1–C1 = 1.826(4), Ru1–P1 = 2.3338(9), Ru1–P2 = 2.2893(8), Ru1–O2 = 2.166(3), Ru1–O3 = 2.246(2), C1–O1 = 1.155(4), C14–C15 = 1.284(8), C12–O2 = 1.275(5), C12–O3 = 1.265(5)

Selected bond angles [°]

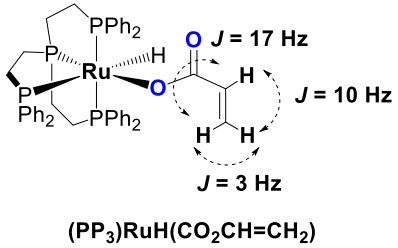
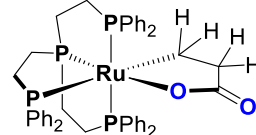
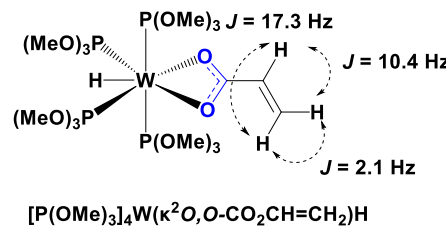
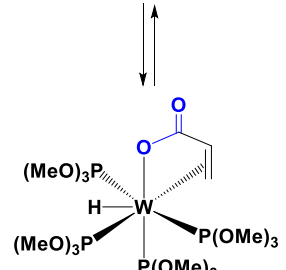
P1–Ru1–P2 = 93.58(3), P1–Ru1–O3 = 91.13(7), P1–Ru1–O2 = 94.44(7), P1–Ru1–Cl1 = 89.07(11), C1–Ru1–P2 = 92.40(11), C1–Ru1–Cl1 = 90.90(11), O3–Ru1–Cl1 = 83.17(7), P1–Ru1–Cl1 = 173.94(3), P2–Ru1–Cl1 = 92.48(3), O2–Ru1–C1 = 168.46(12), O3–Ru1–P2 = 157.72(7), O3–Ru1–C1 = 109.45(12), C12–C14–C15 = 122.2(6), O3–Ru1–O2 = 59.55(10)

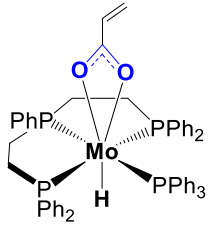
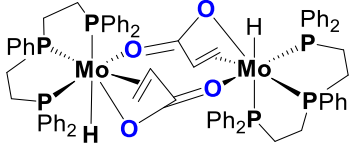
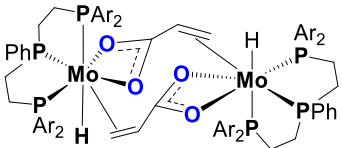
Figure II.4.2. ORTEP representation of the solid-state molecular structure of the ruthenium-acrylate complex *cis*-[Ru(Cl)(CO)(DCPB)(κ^2 O,O-CO₂CH=CH₂)] (*cis*-**Ru-6**) with thermal ellipsoids at 50% probability level. Hydrogen atoms omitted for clarity. Selected interatomic distances and angles are given in Ångström [Å] and degree [°], respectively.

The coordination geometry in this complex is remarkably similar to that in Mo and W complexes reported by Bernskoetter and co-workers (Table II.4.1.), yet, to our knowledge, *cis*-**Ru-6** is the first example of a κ^2 -O,O acrylate ruthenium complex ever reported.

The *cis* L–Ru–L angles are close to the ideal 90° value except for the O3–Ru1–Cl1 (83.17(7) Å), reflecting the repulsive interaction between the bulky DCPB phosphine and the acrylate ligand. This seems to result from close contact between the cyclohexyl ring and the vinylic fragment. The bidentate acrylate group subtends an angle of only 59.55(10)° at the ruthenium atom.

Table II.4.1. NMR data of the reported Ru, W and Mo acrylate species.

Entry	Acrylate species	δ_{H} (ppm), $^2J_{\text{HH}}$ (Hz)	δ_{C} (ppm)
		C_6D_6	C_6D_6
1 ^[21,22]	 <p>(PP₃)RuH(CO₂CH=CH₂)</p>	6.55 (dd, 17.0, 3.0 Hz, CO ₂ CH=CH ₂) 5.50 (dd, 10.0, 3.0 Hz, CO ₂ CH=CH ₂) 6.94 (dd, 17.0, 10.0 Hz, CO ₂ CH=CH ₂)	172.7 (s, CH ₂ CO ₂)
2 ^[21,22]		DMSO- <i>d</i> ₆	DMSO- <i>d</i> ₆
		0.82-0.74 (m, 2H, CH ₂ CH ₂ CO ₂), 0.20-0.05 (m, 2H, RuCH ₂ CH ₂ CO ₂)	189.0 (d, 10.8 Hz, CH ₂ CO ₂)
		23 °C C_6D_6	23 °C, toluene- <i>d</i> ₈
3 ^[35]	 <p>[P(OMe)₃]₄W(κ^2O, O-CO₂CH=CH₂)H</p>	5.15 (dd, 2.1, 10.4 Hz, CO ₂ CH=CH ₂) 5.89 (dd, 10.4, 17.3 Hz, CO ₂ CH=CH ₂) 6.12 (dd, 2.1, 17.4 Hz, CO ₂ CH=CH ₂)	174.3 (CO ₂ CHCH ₂)
	 <p>[P(OMe)₃]₄W(κ^3C, C, O-CO₂CH=CH₂)H</p>	–60 °C toluene- <i>d</i> ₈	23 °C, toluene- <i>d</i> ₈
4 ^[35]		2.19 (br, 1H, CO ₂ CH=CH ₂) 2.73 (br, 1H, CO ₂ CH=CH ₂) 4.33 (br dd, 8.5, 8.7 Hz, 1H, CO ₂ CH=CH ₂)	179.0 (CO ₂ CHCH ₂)

5 ^[36]	 <p>(Triphos)Mo(H)(PPh₃)(κ²O,O-CO₂CH=CH₂)</p>	<p>23 °C C₆D₆</p> <p>4.68 (dd, 2.0, 10.4 Hz, CO₂CH=CH₂) 5.15 (dd, 10.4, 17.2 Hz, CO₂CH=CH₂) 5.48 (dd, 2.0, 17.2 Hz, CO₂CH=CH₂)</p>	Two quaternary signals not located.
6 ^[36]	 <p>{[(Ph₂PCH₂CH₂)₂PPh]Mo(CO₂CH=CH₂)₂}</p>	<p>25 °C C₆D₆</p> <p>1.12–3.20, 3.70, 3.99 (m, PCH₂ and CH=CH₂)</p>	<p>23 °C C₆D₆</p> <p>192.3 (CO₂CH=CH₂)</p>
7 ^[37]	 <p>{[(Ar₂)₂PCH₂CH₂]₂PPh]Mo(H)(CO₂CH=CH₂)₂}</p>	<p>23 °C C₆D₆</p> <p>1.7–2.2, 2.18, 3.65, (m, PCH₂ and CH=CH₂)</p>	n.d.

On the other hand, the acrylate chelate distances show C12–O values intermediate between single and double bonds (C12–O2 = 1.275(5) and C12–O3 = 1.265(5) Å), as previously reported for acetate RuH(O₂C–CH₃)(PPh₃)₃^[38] and formate RuH(O₂CH)(PPh₃)₃^[39] species (for which average C–O bonds distances of 1.259(18) and 1.25(6) Å were reported, respectively).

The Ru–O3 distance (2.246(2) Å) is significantly longer than the sum of the covalent radii (2.12 Å),^[40] indicating a weak coordination to the Ru atom. This observation suggests the idea of an easy cleavage of the Ru–O bond. On the other hand, the Ru–O2 distance value (2.166(3) Å) is close to that reported for ruthenolactone species (Table II.4.1., entry 2, 2.180 Å^[22]), testifying of a Ru–O covalent bond. Both the Ru–O3 and Ru–O2 distances are comparable to the Ru–O distances reported for the acetate RuH(O₂CMe)(PPh₃)₃ (2.198(13) and 2.210(10) Å)^[38] and the formate RuH(O₂CH)(PPh₃) (2.29(4) and 2.23(3) Å)^[39] ruthenium complexes. However, the two Ru–O distances are significantly different, with the Ru–O3 bond length of 0.08 Å longer than Ru–O2, while it is at most 0.06 Å in the acetate and formate complexes, and 0.03 Å in the [(Ph₂PCH₂CH₂)₂PPh]Mo(H)(PPh₃)(κ²O,O-C₃H₃O₂)^[41] complex. This difference probably results from the strong *trans* influence exerted by the CO ligand, which is not present in the abovementioned Ru and Mo complexes.

The ^1H NMR spectrum of the crystals does not display any differences with that of the crude mixture, exhibiting the same vinylic patterns as observed before, *i.e.* δ_{H} 5.2, 5.9 and 6.3 ppm, in a relative integration ratio of 1:1:1 (Annexes, Figure II.4.24). The chemical shifts of the vinylic protons of **Ru-6** are comparable to those described for $\kappa^2\text{-O,O-Mo}$ and **W** (Table II.4.1., entries 3 and 5).^[35,42] The ^1H - ^1H COSY NMR spectrum (Figure II.4.3) confirms coupling between the vinylic proton nuclei. Moreover, according to the NMR spectroscopic data related to the formation of ruthenolactone species (Table II.4.1., entry 2), such complexes are not present in the crude mixture since no corresponding signals were detected in the up field region.

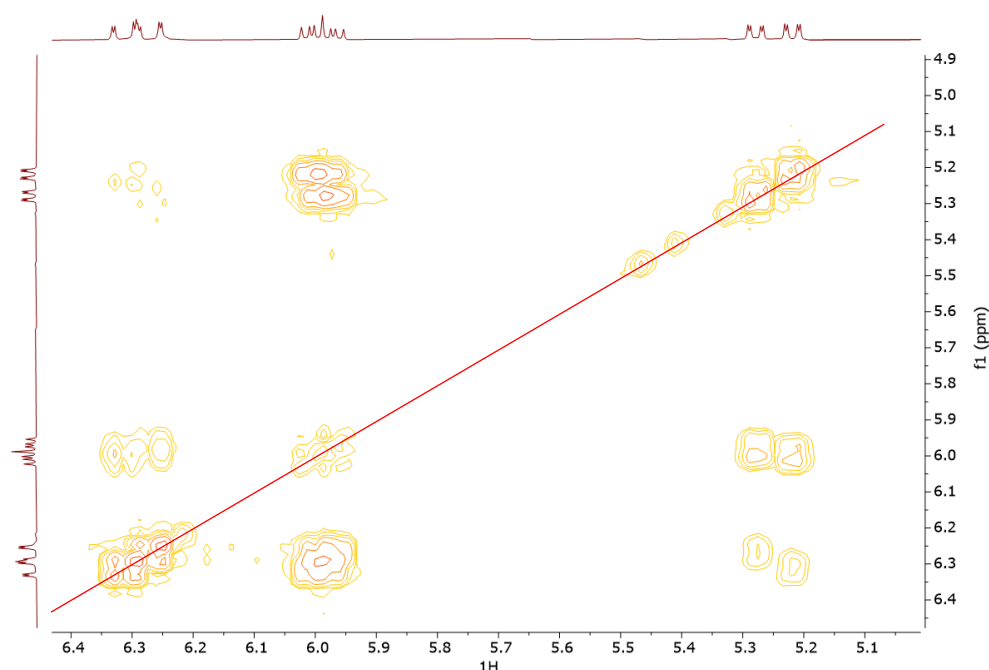
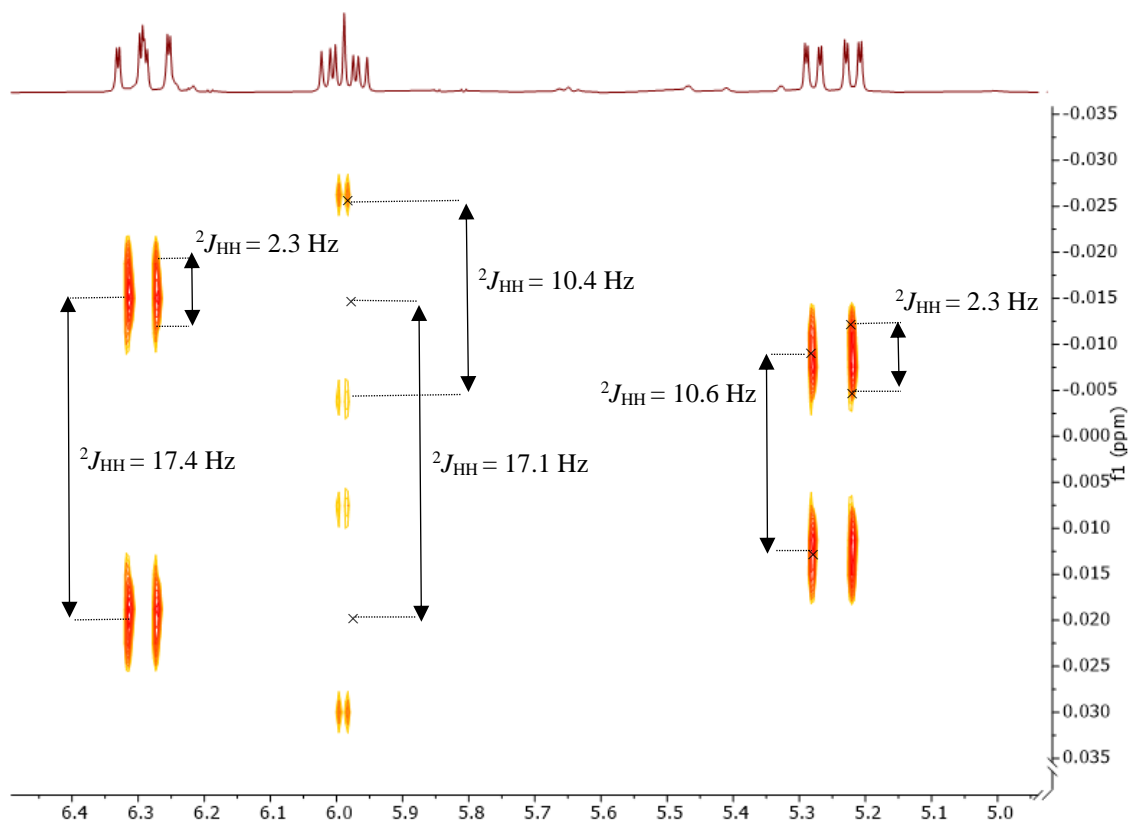


Figure II.4.3. ^1H - ^1H COSY NMR spectrum (500 MHz, toluene- d_8 , 25 °C) of the vinylic region of the crude **Ru-6** complex.

To fully understand the nature of all coupling constants of the observed patterns and to identify the coupled spin systems, 2D J-Resolved experiments were undertaken.^[b] At room temperature, the spectrum revealed that the apparent “doublet of doublets of doublets” (*ddd*) at δ_{H} 5.2 ppm is actually two overlapping *dd*, with $^2J_{\text{HH}}$ coupling constants of 2.3 and 10.6 Hz (Figure II.4.4. (A)). The pattern at δ_{H} 5.9 ppm is also to be separated into two *dd* (four vertical spots of similar intensities, $^2J_{\text{HH}} = 17.1$ and 10.4 Hz), as well as the signal at δ_{H} 6.3 ppm (two *dd* with $^2J_{\text{HH}} = 17.4$ and 2.3 Hz). These observations clearly indicate that two distinct sets of signals, in a 1.4:1 molar ratio, are overlapping in the vinylic region of the ^1H NMR spectrum.

^[b] 2D J-Res experiment is a 2D-NMR technique that helps resonance multiplicities identification. J-Res NMR spectrum has the chemical shift along one axis and the proton-proton coupling along the other axis.

(A) 25 °C



(B) 100 °C

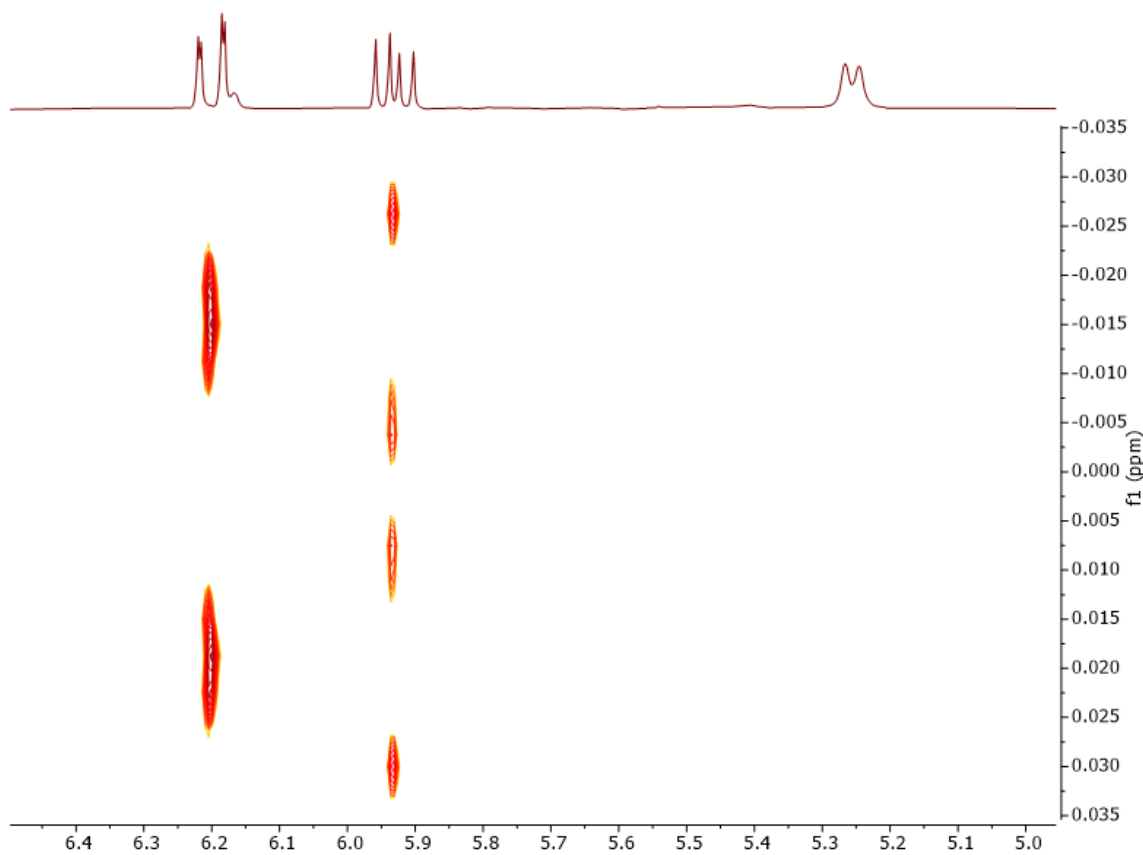


Figure II.4.4. J-Res ^1H NMR spectra (500 MHz, toluene- d_8) of the vinylic region of the crude **Ru-6** complex at (A) 25 °C, (B) 100 °C.

Since both the crude mixture and the isolated crystals gave the same ^1H NMR spectrum, we presume that the **Ru-6** crystals are either constituted of a single isomer, which interconverts/isomerizes in solution, or a mixture of two distinct acrylate species, of which only one was identified (analysed) by X-ray diffraction.

To further assess these hypotheses, a series of multidimensional/variable temperature NMR experiments were conducted on the crude mixture. While increasing progressively the temperature, a coalescence of the signals at δ_{H} 5.2, 5.9 and 6.3 ppm was observed at ca. 50 °C, and up to 100 °C, the ^1H NMR spectra was simplified (Figure II.4.5). The most downfield signals at δ_{H} 5.9 and 6.3 ppm appeared as two sets of well-defined doublet of doublets ($^2J_{\text{HH}} = 17.1, 10.4$ Hz and $^2J_{\text{HH}} = 17.4, 2.3$ Hz, respectively), as confirmed by the 2D J-Resolved experiment conducted at 100 °C (Figure II.4.4. (B)). On the other hand, the signal at δ_{H} 5.2 ppm remained fairly broad, even at 100 °C. The above NMR experiments show that, in toluene- d_8 solution at room temperature, the vinylic resonances are consistent with the presence of two types of acrylate fragments coordinated to a metal center.

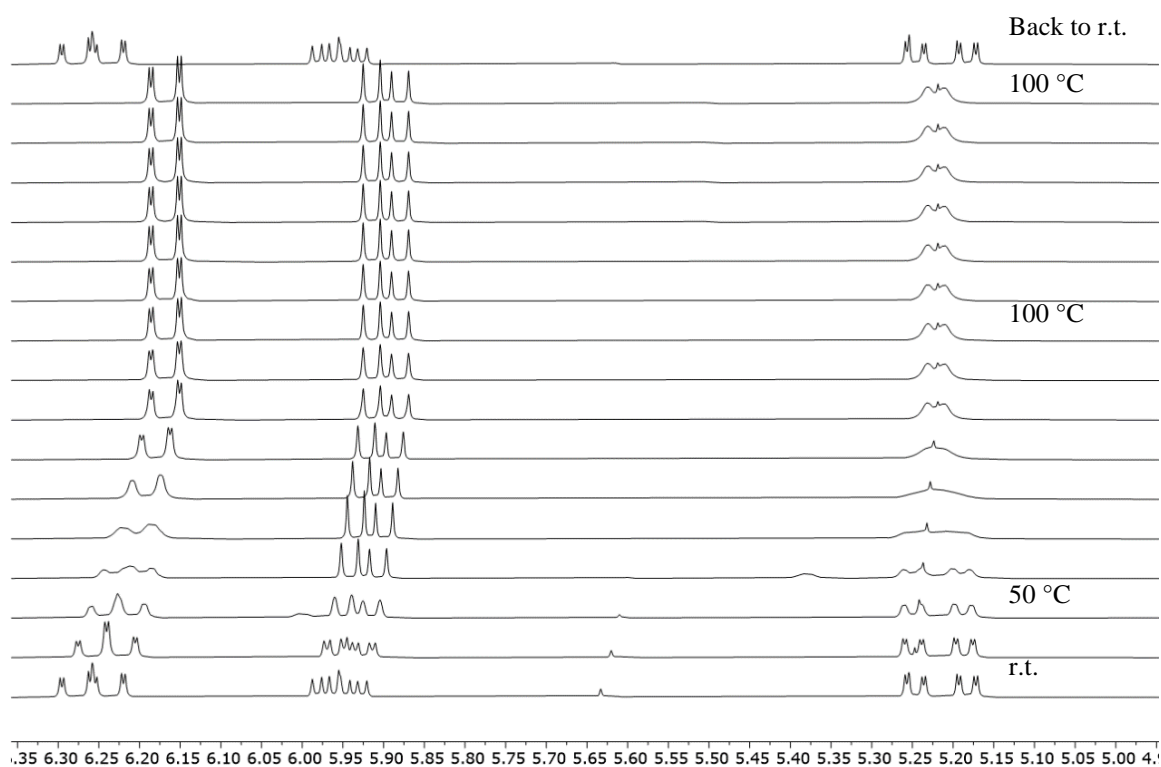


Figure II.4.5. ^1H VT NMR spectra (500 MHz, toluene- d_8) of the vinylic region of the crude **Ru-6** complex.

Moreover, the ^1H - ^{13}C HMBC NMR spectroscopy at r.t. evidenced a $^3J_{\text{CH}}$ coupling between the signals of the vinylic protons at δ_{H} 5.23, 5.27, 6.25 and 6.34 ppm and two carbon resonances at δ_{C} 181.6 and 183.3 ppm (Figure II.4.6.). These observations indicate clearly the

presence of two types of carboxylic compounds, likely differing by the mutual organization of the ligands in the Ru coordination sphere.

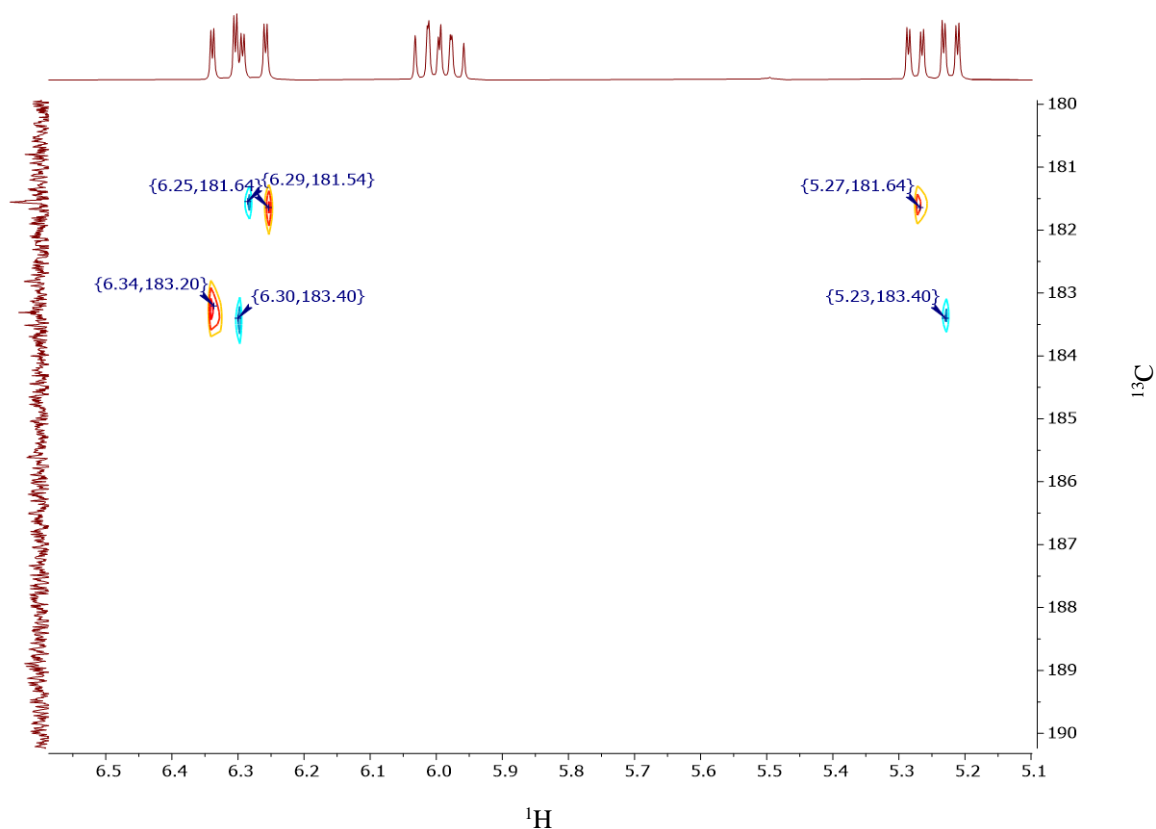


Figure II.4.6. ^1H - ^{13}C HMBC NMR spectra of the vinylic region of the crude **Ru-6** complex (500 MHz, $\text{toluene-}d_8$, 25 °C).

The presence of two main species in a 1.4:1 molar ratio was further evidenced in the $^{31}\text{P}\{^1\text{H}\}$ NMR spectrum performed on the crude **Ru-6** compound. First, two sets of doublets appearing at δ_{P} 39.2 and 60.1 ppm ($^2J_{\text{P-P}} = 23.3$ Hz) were observed, integrating for one P atom each (Figure II.4.7.). In addition to the signal from the free PPh_3 ($\delta_{\text{P}} -5.2$ ppm), a sharp singlet at 50.6 ppm, integrating for two P atoms, was observed.

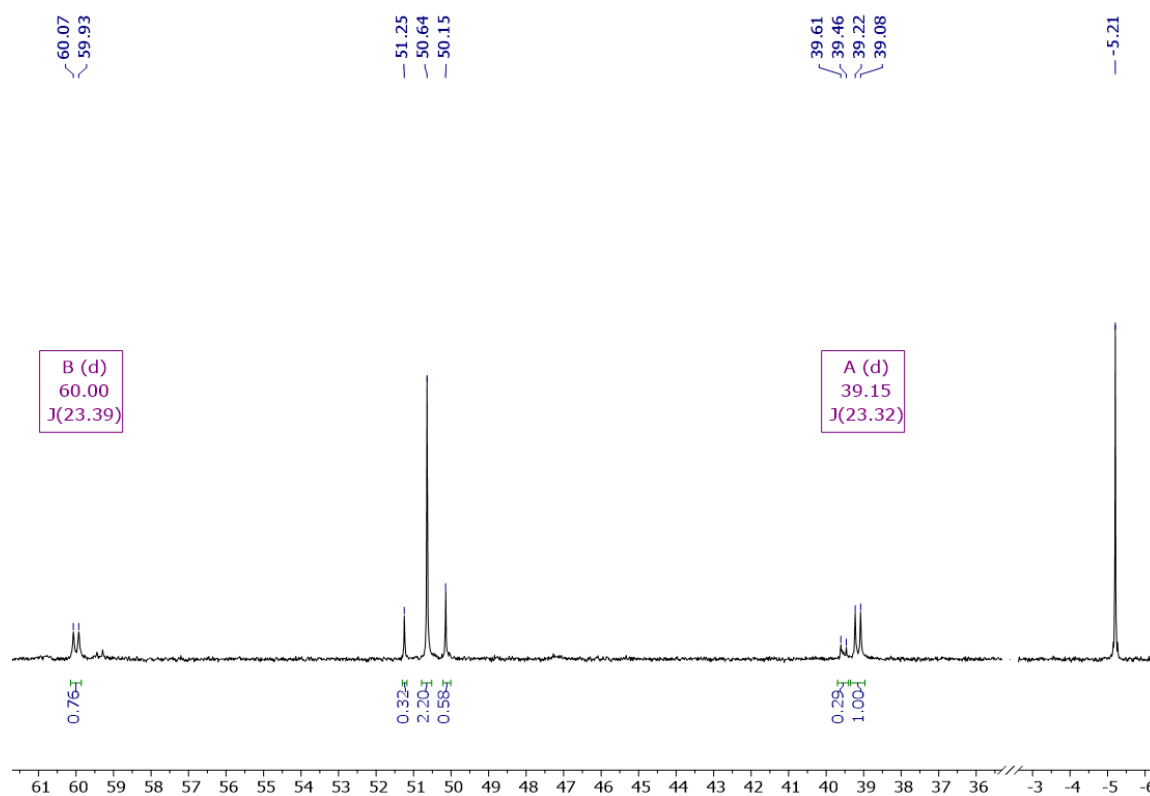
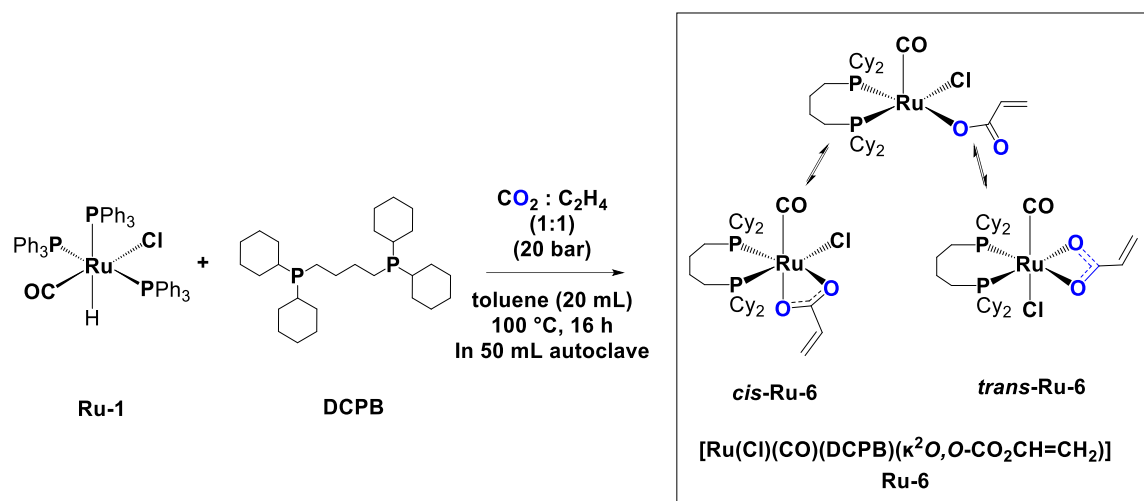


Figure II.4.7. $^{31}\text{P}\{^1\text{H}\}$ spectrum of the **Ru-6** crystals (202 MHz, toluene- d_8 , 25°C).

Altogether, these NMR spectroscopic data seem to indicate the presence of isomeric species differing in a *cis* and *trans* acrylate positioning *vs.* the DCPB ligand (Scheme II.4.3.). In fact, since the *cis*-**Ru-6** arrangement generates an unequivocal environment around the P nuclei of the DCPB ligand, the later will appear as two distinct sets of doublets in the ^{31}P NMR spectrum, as previously observed at δ_{P} 39.2 and 60.1 ppm. On the other hand, the *trans*-**Ru-6** isomer configuration implies two magnetically equivalent P nuclei, which should appear as a singlet pattern. This is consistent with the previously observed singlet, detected at δ_{P} 50.6 ppm. The $^{31}\text{P}\{^1\text{H}\}$ spectrum also shows the presence of minor signals at δ_{P} 51.3, 59.9, 39.5 (*d*) and 50.2 ppm, implying the presence of other unidentified species within the crude **Ru-6** product.



Scheme II.4.3. Synthesis of ruthenium acrylate **Ru-6** complex and possible isomerism.

Moreover, additional ^1H - ^{31}P HMQC experiments conducted on the **Ru-6** isomers mixture, at room temperature, showed perfect correlation between the doublets at δ_{P} 39.2 and 60.1 ppm, the singlet at δ_{P} 50.6 ppm and the protons of the aliphatic region (Figure II.4.8.). These observations confirm that the above mentioned P atoms are indeed part of the DCPB ligand, since they are coupling with the hydrogen atoms of the Cy groups and the butyl carbon chain.

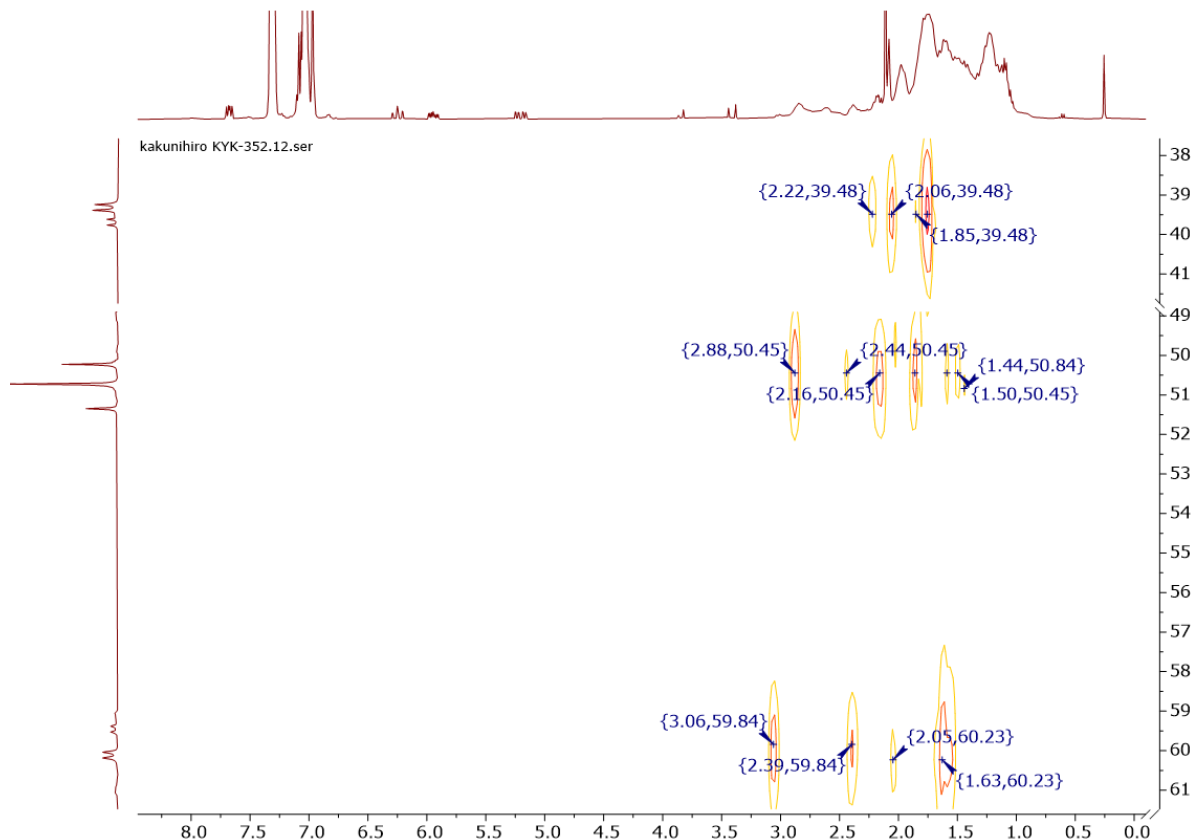


Figure II.4.8. ^1H - ^{31}P HMQC NMR correlation spectrum (400 MHz, toluene- d_8 , 25°C) of crude **Ru-6** complex.

To explain the presence of both the *cis*- and the *trans*-[Ru(Cl)(CO)(DCPB)(κ²O,*O*-CO₂CH=CH₂)] isomers in solution, we supposed that an intramolecular process, which interchanges the Cl ligand with the acrylate fragment, might take place, as shown in Scheme II.4.3.

In fact, ³¹P{¹H} VT NMR experiments conducted at high temperatures (100 °C) show that both doublet signals at δ_P 39.2 and 60.1 ppm, characteristic of the *cis* isomer, start slowly disappearing, while the singlet pattern of the *trans* species remains present and broadened (Figure II.4.9.). Back to room temperature, both sets of signals reappear. Hence, these observations are in agreement with an interconversion phenomena of the *cis* and *trans* isomers upon heating in solution.

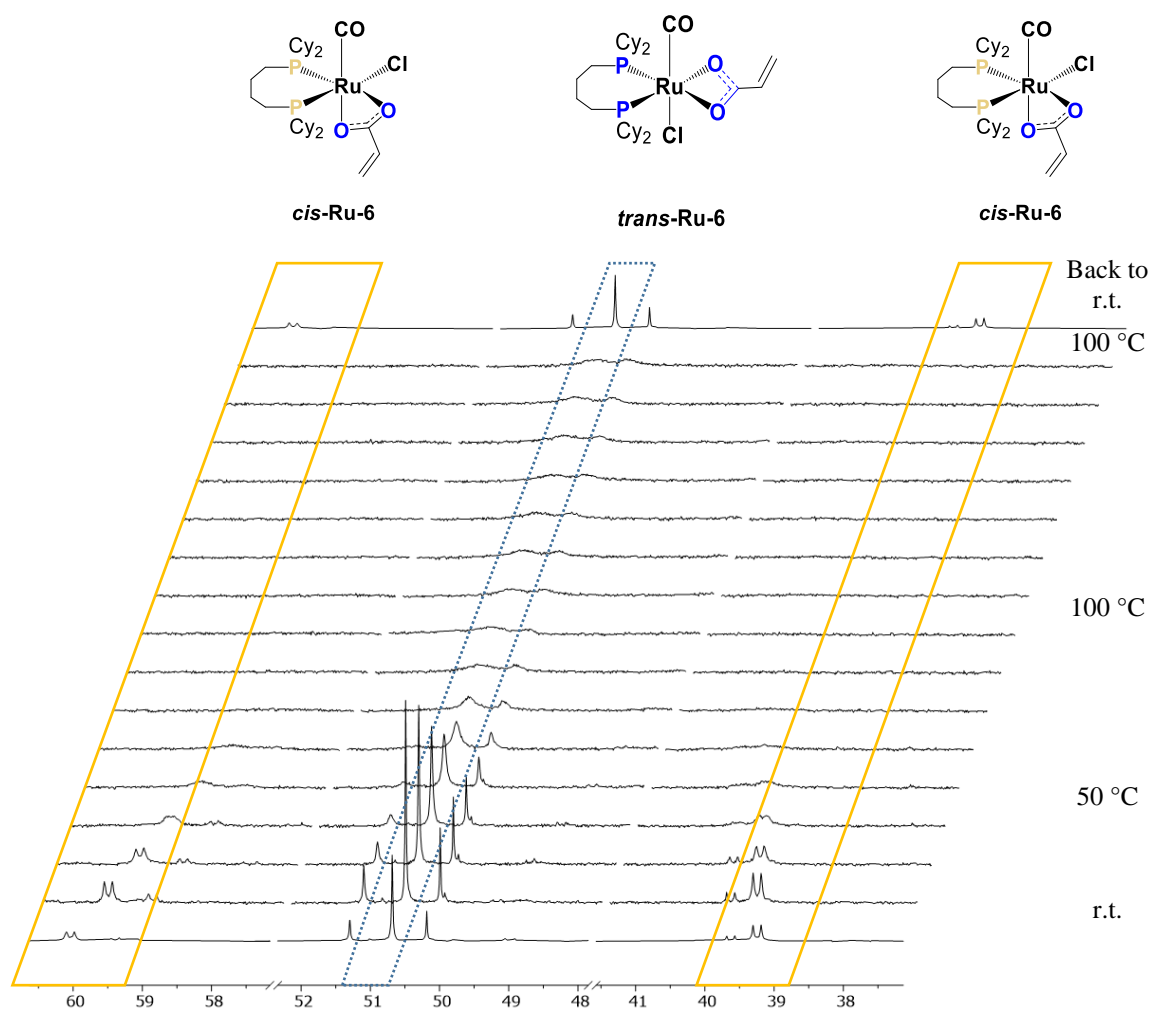


Figure II.4.9. ³¹P{¹H} VT NMR spectra (500 MHz, toluene-*d*₈) of the crude **Ru-6** isomers mixture.

The dynamic *cis* ↔ *trans* isomerization monitored in toluene-*d*₈ by ¹H NMR spectrometry at eight different temperatures, ranging from room temperature to 100 °C, was

also studied by line shape analysis (Figure II.4.10.). Rate constants k were determined for each temperatures.

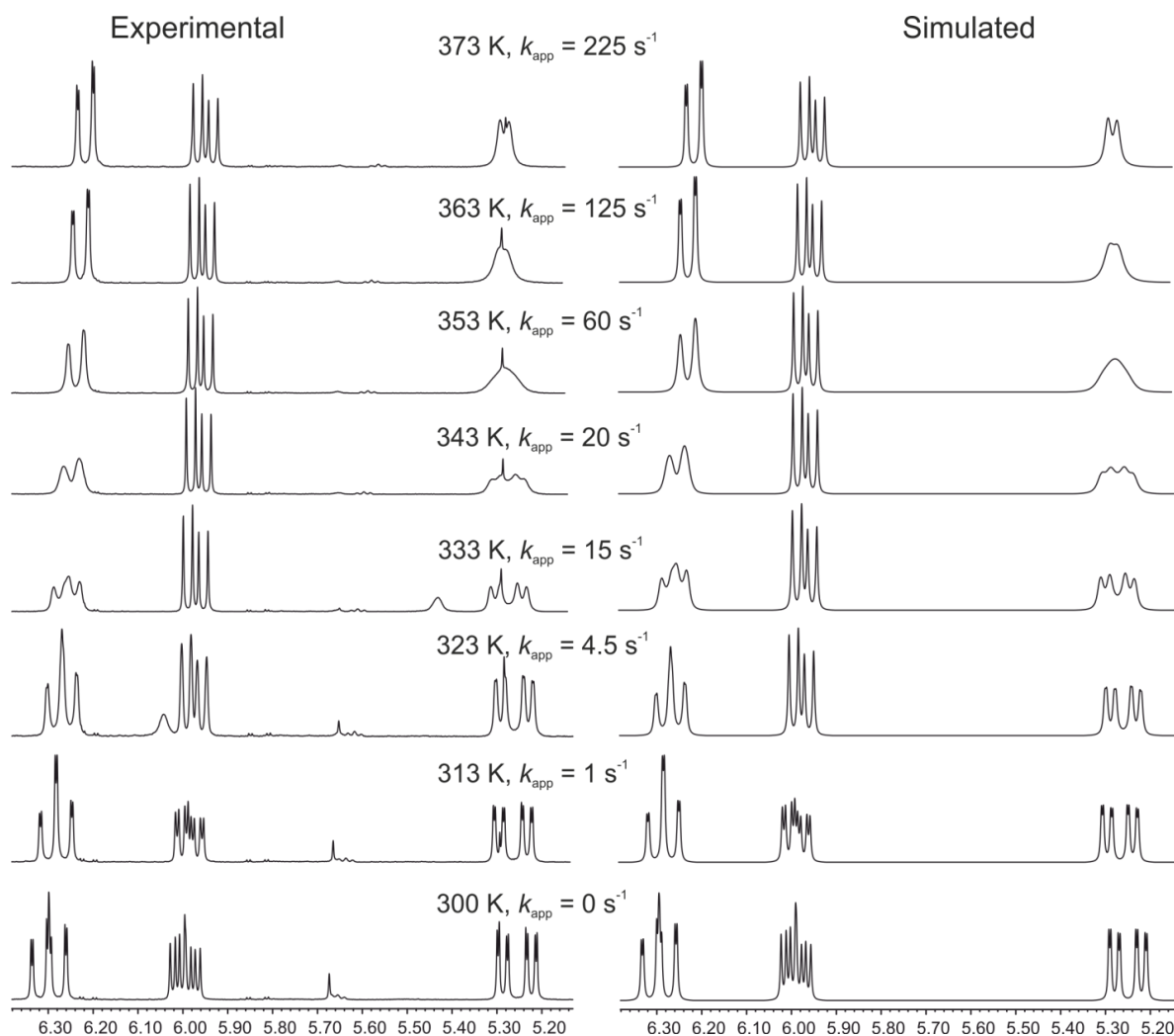


Figure II.4.10. Rate constants k determination by ^1H NMR spectrometry (500 MHz, toluene- d_8) at various temperatures.

The Eyring plot $\ln(k/T) = f(T^{-1})$ (Figure II.4.11.) was then drawn from the computed values of the first order reaction rates, allowing to determine the corresponding activation thermodynamic parameters for $\text{Ru}(\text{Cl})(\text{CO})(\text{DCPB})(\kappa^2\text{O}, \text{O}-\text{CO}_2\text{CH}=\text{CH}_2)$ isomerization ($\Delta H^\ddagger = 20(1) \text{ kcal}\cdot\text{mol}^{-1}$; $\Delta S^\ddagger = 5(2) \text{ cal}\cdot\text{mol}^{-1}$), using the following equation :

$$\ln k/T = -\frac{\Delta H^\ddagger}{RT} + \ln \frac{k_B}{h} + \frac{\Delta S^\ddagger}{R}$$

The linear fitting ($R^2 = 0.981$) gave a Gibbs enthalpy of activation of $\Delta G^\ddagger_{298} = 18.2(7) \text{ kcal}\cdot\text{mol}^{-1}$. These results are consistent with the presence of two **Ru-6** isomers, for which the *cis* \leftrightarrow *trans* isomerization in toluene- d_8 solution is observed at temperatures above 70 °C. The

slightly positive activation entropy suggests a dissociative process, consistent with that shown in Scheme II.4.3.

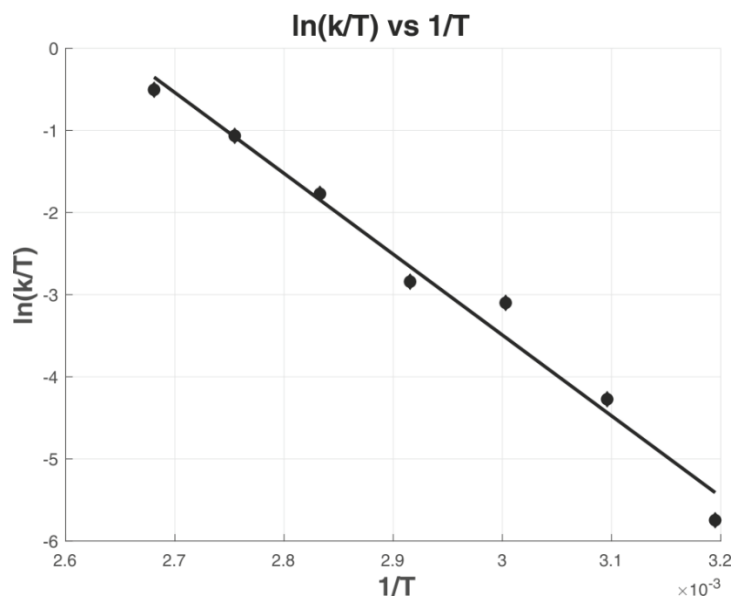


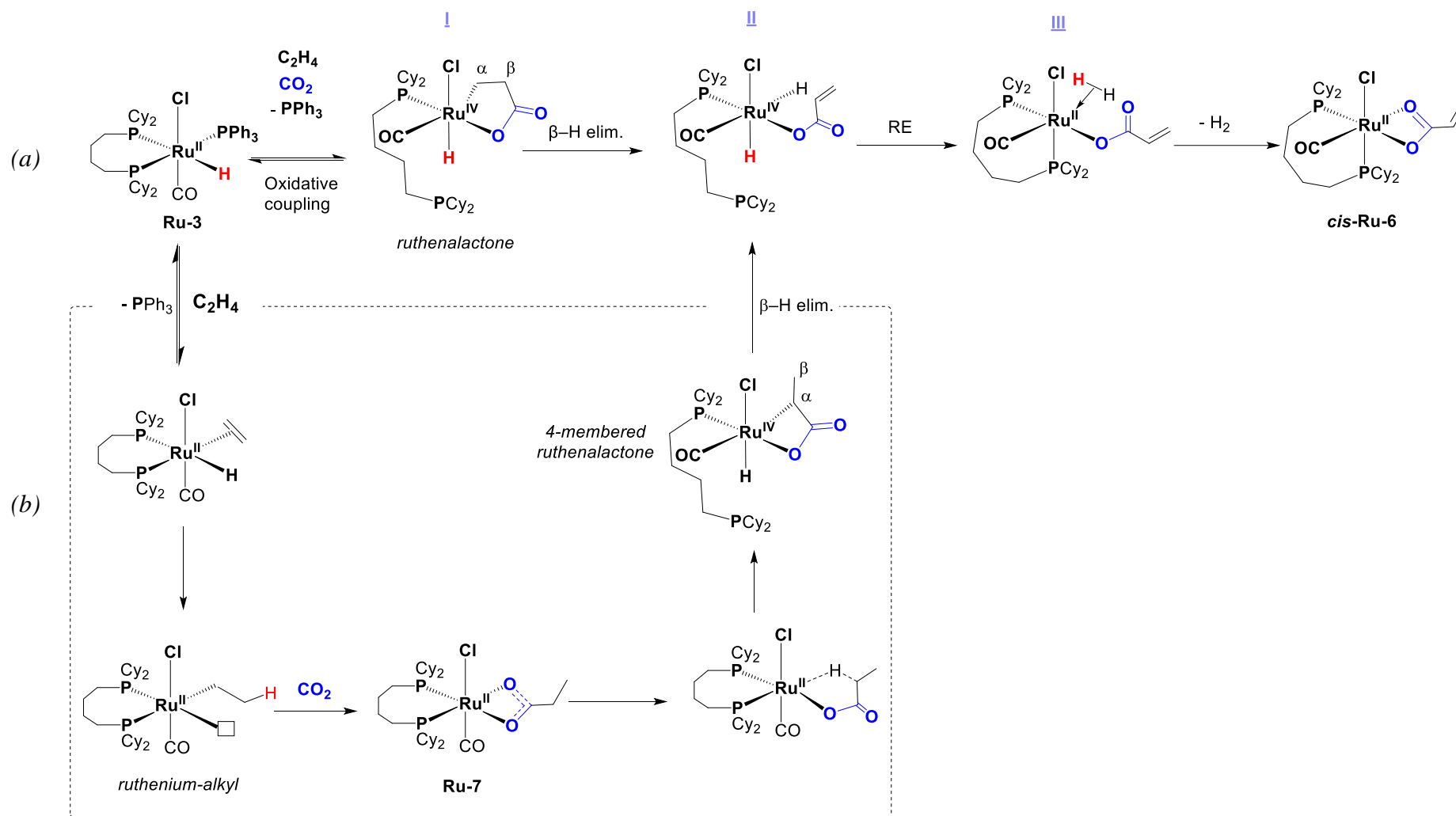
Figure II.4.11. Eyring plot of $\ln(k/T) = f(T^{-1})$ for the isomerization reactions of $\text{Ru}(\text{Cl})(\text{CO})(\text{DCPB})(\kappa^2\text{O},\text{O}-\text{CO}_2\text{CH}=\text{CH}_2)$ *trans* \leftrightarrow *cis* in toluene- d_8 . The solid line is the best fit with activation parameters.

4.2.2. Possible mechanism for the formation of Ru-6

In comparison to the rather well-established formation of ruthenolactones, the mechanism leading to unsaturated κ^2 -*O,O*-acrylate Ru complexes remains largely unclear. Yet, taking into account the experimental evidences, it is reasonable to assume that the first step in the formation of **Ru-6** is to dissociate the PPh_3 ligand, generating therefore a vacant site within the metal coordination sphere. Following this step, two conceivable pathways for the CO_2 - C_2H_4 coupling are suggested (Scheme II.4.4):

(a) concomitant oxidative coupling of C_2H_4 and CO_2 to afford a five-membered ruthenolactone (**I**), which would undergo β -H elimination, hence resulting in a putative Ru(IV) dihydrido acrylate species (**II**), followed by the loss of H_2 ;

(b) preliminary coordination of C_2H_4 onto the vacant site, leading to the formation of an intermediate $\text{Ru}(\text{H})(\text{Cl})(\text{CO})(\text{DCPB})(\text{CH}_2=\text{CH}_2)$. Next, C_2H_4 would insert into the Ru-H bond to yield a Ru(II)-alkyl species. Then, CO_2 insertion into the Ru-C bond would afford a Ru(II) propionate species (**Ru-7**). Subsequent α -C-H activation would afford a 4-membered ruthenolactone, followed by a β -H elimination step resulting in a dihydrido acrylate species (**II**), followed by the loss of H_2 to give the final **Ru-6**.



Both routes (a) and (b) rely on the assumption of the existence of several putative species (4- and 5-membered ruthenolactones and ruthenium alkene or alkyl species), for which our spectroscopic investigations on their formation have not led to any experimental evidences.

To gain deeper understanding in the different mechanisms proposed, DFT computational studies were undertaken in collaboration with the LPCNO laboratory, Toulouse, France.

4.2.3. Computational studies

The genesis of the acrylate complex **Ru-6**, from the coupling reaction between C₂H₄ and CO₂ in the presence of **Ru-1**/DCPB combination, has been addressed theoretically. However, additional computations are necessary to conclude on the mechanism of its formation.

4.2.4. Release of triethylsilyl acrylate from acrylate-ruthenium **Ru(Cl)(CO)(DCPB)(κ²O, O-CO₂CH=CH₂)** and regeneration of **Ru(H)(Cl)(CO)(DCPB)(PPh₃)**

Following the facile preparation of a CO₂–C₂H₄ derived ruthenium acrylate complex (**Ru-6**), we intended to explore the release of the desired acrylate product from the metal center. Given the Ru–O bond distance values determined by X-ray diffraction studies and the moderate oxophilicity of the ruthenium atom, this is assumed to constitute a feasible step.^[43]

*i. Addition of Et₃SiH to **Ru-6***

In a first approach, Et₃SiH (1 equiv) was added to crude **Ru-6**, at room temperature in toluene-*d*₈; then, the reaction mixture was heated progressively up to 100 °C. The ¹H VT NMR spectra showed progressive and complete disappearance of the Ru-acrylate species signals in the vinylic region and the formation of new sets of doublet of doublets (Figure II.4.12.). Total consumption of the Ru-acrylate species was already achieved at 50 °C. The signals from the newly formed vinylic product appeared at δ_H 5.3, 6.0 and 6.2 ppm (at r.t.) and are identical to those of the previously synthesized triethylsilyl acrylate (**A1**) (²J_{HH trans} = 17.4, ²J_{HH cis} = 10.2 and ²J_{HH gem} = 1.7 Hz). Hence, addition of Et₃SiH successfully consumes **Ru-6** and produces silyl acrylate ester compound in less than 30 min, under mild conditions.

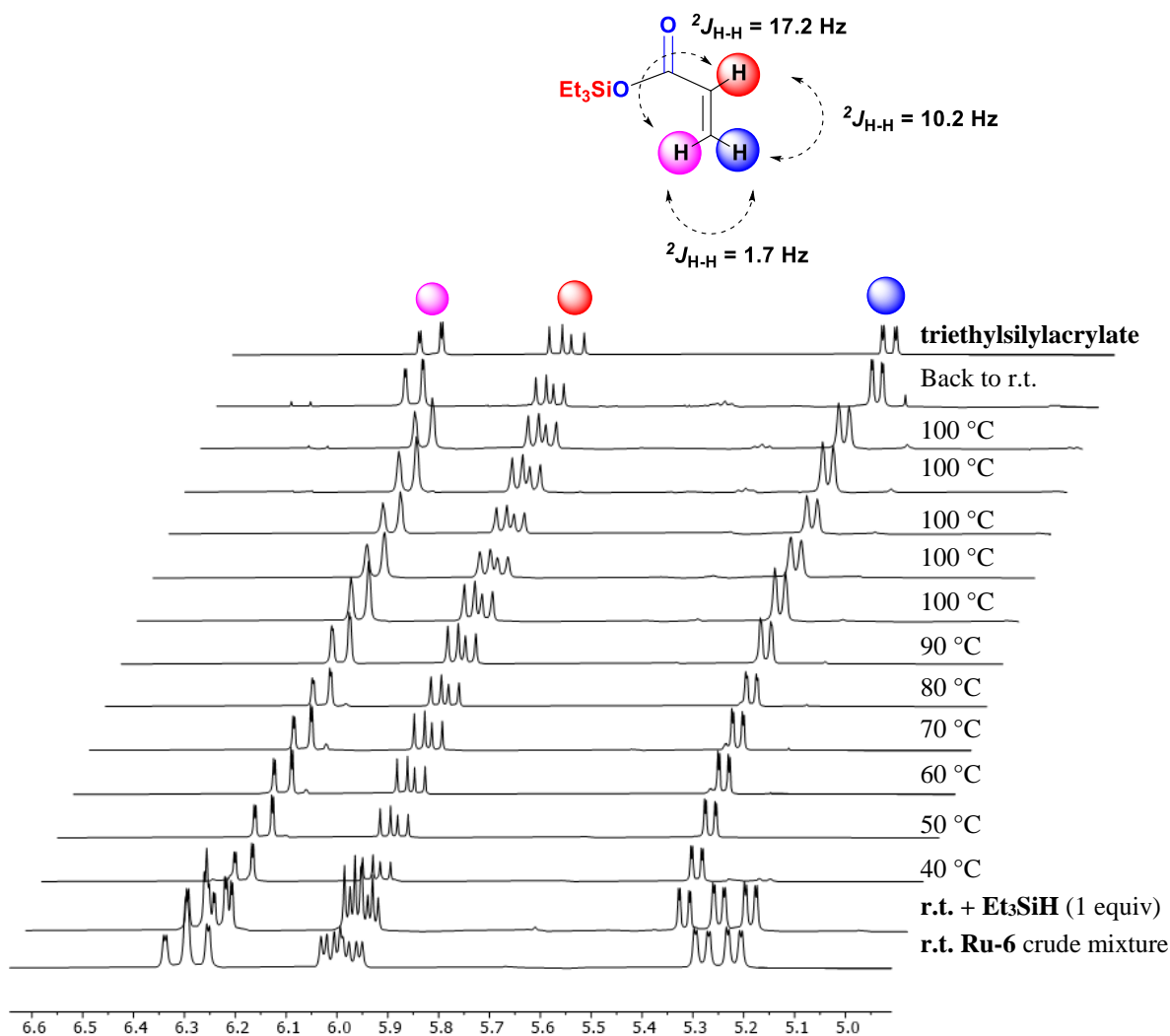


Figure II.4.12. VT ${}^1\text{H}$ NMR spectra (500 MHz, toluene- d_8) of the vinylic region of crude **Ru-6** mixture after adding 1 equivalent of Et_3SiH .

Along with the release of the organic product, triethylsilyl acrylate, the formation of at least three different metal hydride-containing species was detected by ${}^1\text{H}$ NMR spectroscopy. As shown in Figure II.4.13., immediate formation of a doublet of triplets at $\delta_{\text{H}} -7.2$ ppm was observed after addition of Et_3SiH . Based on the chemical shift and the coupling constant values (${}^2J_{\text{HP trans}} = 104$ and ${}^2J_{\text{HP cis}} = 24$ Hz), the complex formed is unambiguously assigned to the previously characterized **Ru-3** species, $\text{Ru}(\text{H})(\text{Cl})(\text{CO})(\text{DCPB})(\text{PPh}_3)$ (Part II, chapter 3). As the temperature kept increasing, other unidentified species started to form, as observed by the growing multiplets in the hydride region of the ${}^1\text{H}$ NMR spectra.

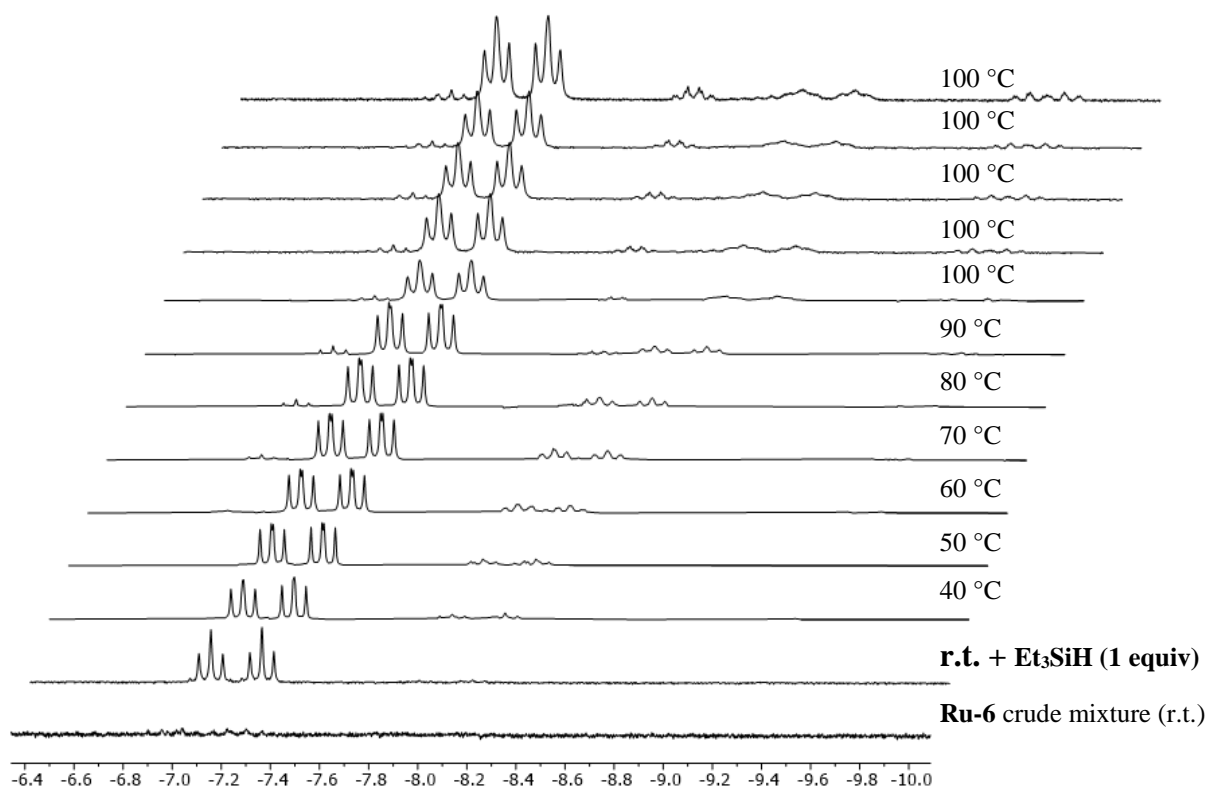


Figure II.4.13. VT ^1H NMR spectra (500 MHz, toluene- d_8) of the hydride region from the reaction of crude **Ru-6** and 1 equivalent of Et_3SiH .

In the VT $^{31}\text{P}\{^1\text{H}\}$ NMR spectra shown in Figure II.4.14., the formation of **Ru-3** was further confirmed by the presence of the characteristic signals at δ_{P} 18.6 and 35 ppm (indicated by the red arrows), formed as soon as Et_3SiH was added. As the temperature increased, new signals were observed, confirming the presence of newly formed P-containing species (δ_{P} 31.6, 39.9, 43.5, 47.8 and 48.9 ppm); identified as supposedly **Ru-3** isomers (Part II, Chapter 3).

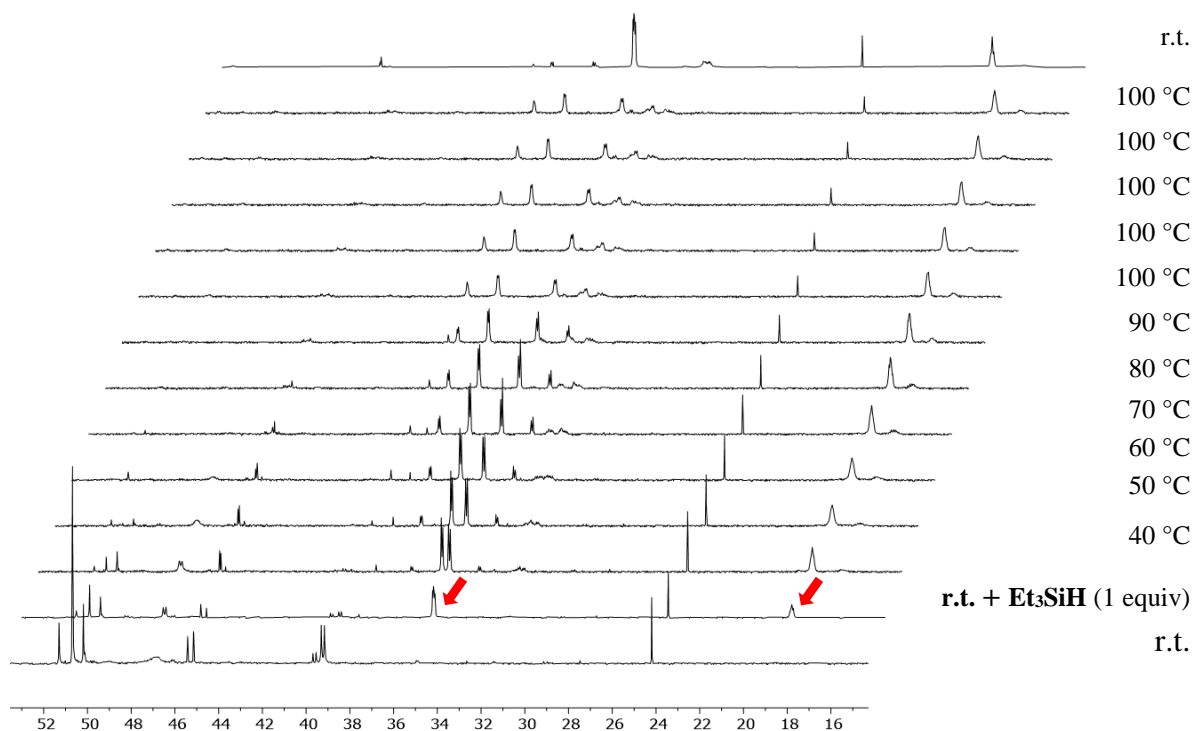
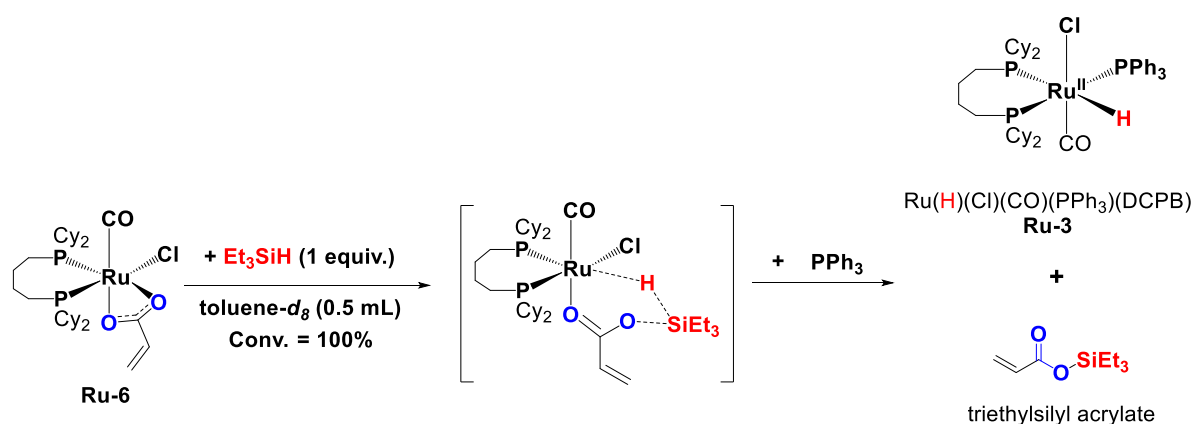


Figure II.4.14. $^{31}\text{P}\{^1\text{H}\}$ VT NMR spectra (202 MHz, toluene- d_8) of the reaction mixture of crude **Ru-6** with 1 equivalent of Et_3SiH .

In summary, the NMR monitoring data confirmed that the CO_2 -derived acrylate fragment can be easily released from the **Ru-6** coordination sphere upon treatment with Et_3SiH , affording selectively the organic product triethylsilyl acrylate and regenerating the **Ru-3** complex (Scheme II.4.5.) along with other unidentified hydrido Ru species. From these results, it appears that the hydrosilane plays a dual role in the catalytic cycle; delivering the silylester function as well as recovering the catalytic hydrido **Ru-3** species.



Scheme II.4.5. Formation of **Ru-3** and of triethylsilyl acrylate upon reaction of Et_3SiH with **Ru-6**.

ii. Addition of Et_3SiD to **Ru-6**

In order to confirm the role of the hydride function of Et_3SiH to recover the **Ru-3** hydrido complex, the stoichiometric reaction of crude **Ru-6** with Et_3SiD was investigated.^[c]

The VT ^1H NMR monitoring of the vinylic region showed, as expected, progressive decrease of the **Ru-6** vinylic signals and apparition of new broad multiplets (Figure II.4.15). These patterns accounted for 20% of the consumed Et_3SiD .

The complexity of the signals did not allow to clearly confirm the formation of the targeted (D_1)-triethylsilyl acrylate. However, it is certain that the deuterated triethylsilane played a role in the formation of new, non-identified acrylic compounds, as observed in Figure II.4.15.

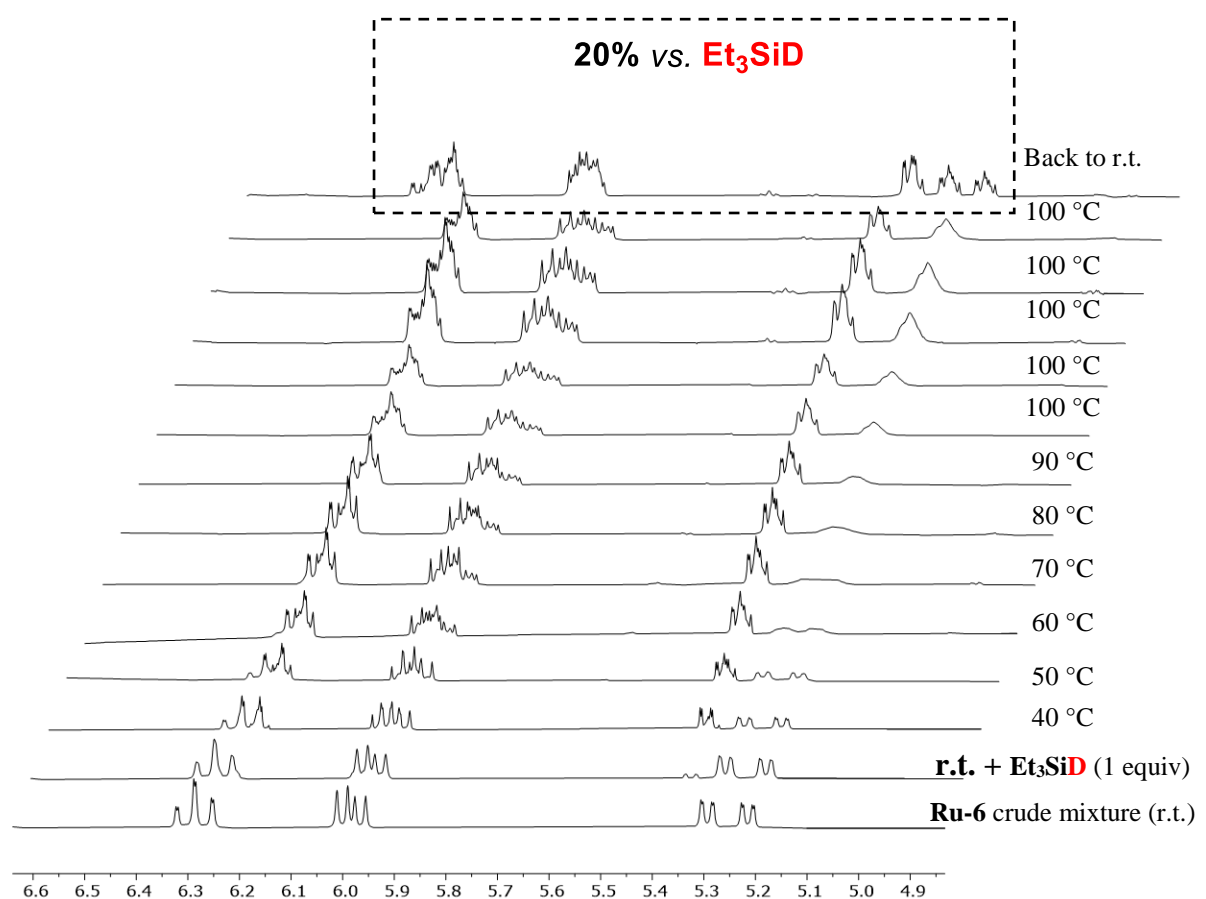


Figure II.4.15. VT ^1H NMR spectra (500 MHz, toluene- d_8) of the hydride region of the crude **Ru-6** mixture after adding 1 equivalent of Et_3SiD .

^[c] Et_3SiD > 98% atom D (^1H NMR spectroscopy). One equivalent of Et_3SiD vs. **Ru-1** initially introduced.

One can assume that, in the presence of an excess amount of Et_3SiD , H/D exchange might take place between the vinylic protons of the present acrylic products and the Si–D function. In fact, the $^{13}\text{C}\{^1\text{H}\}$ NMR spectrum (Figure II.4.16) not only showed several resonances in the δ_{C} [165;175 ppm] region, indicating the presence of at least four carbonyl compounds incorporating a quaternary carbon (typically $(\text{O})\text{C}=\text{O}$), but also revealed two new sets of triplets at δ_{C} 134.7 ppm implying a ^{13}C –D coupling. Therefore, possible exchange could explain, after addition of Et_3SiD , the broad multiplets observed at room temperature in the vinylic region.

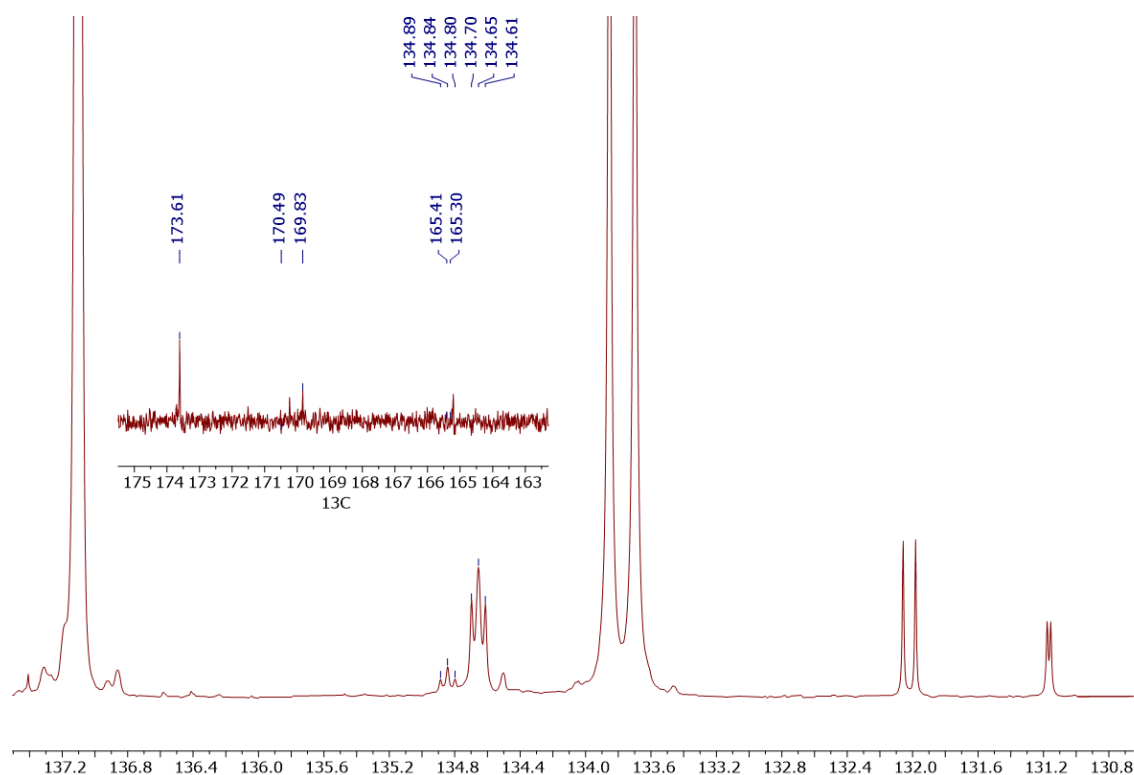


Figure II.4.16. $^{13}\text{C}\{^1\text{H}\}$ NMR spectrum (126 MHz, toluene- d_8 , 25 °C) of the reaction mixture of crude **Ru-6** after adding 1 equivalent of Et_3SiD .

More surprisingly, in the VT ^1H NMR hydride region of the spectra, the increase of the doublet of triplet signal, characteristic of the hydride **Ru-3** complex, was still observed (Figure II.4.17., 43% vs. Et_3SiD). The VT $^{31}\text{P}\{^1\text{H}\}$ NMR experiments confirmed as well the formation of **Ru-3** with the presence of the diagnostic multiplet and doublet at δ_{P} 18.6 and 35 ppm, respectively.

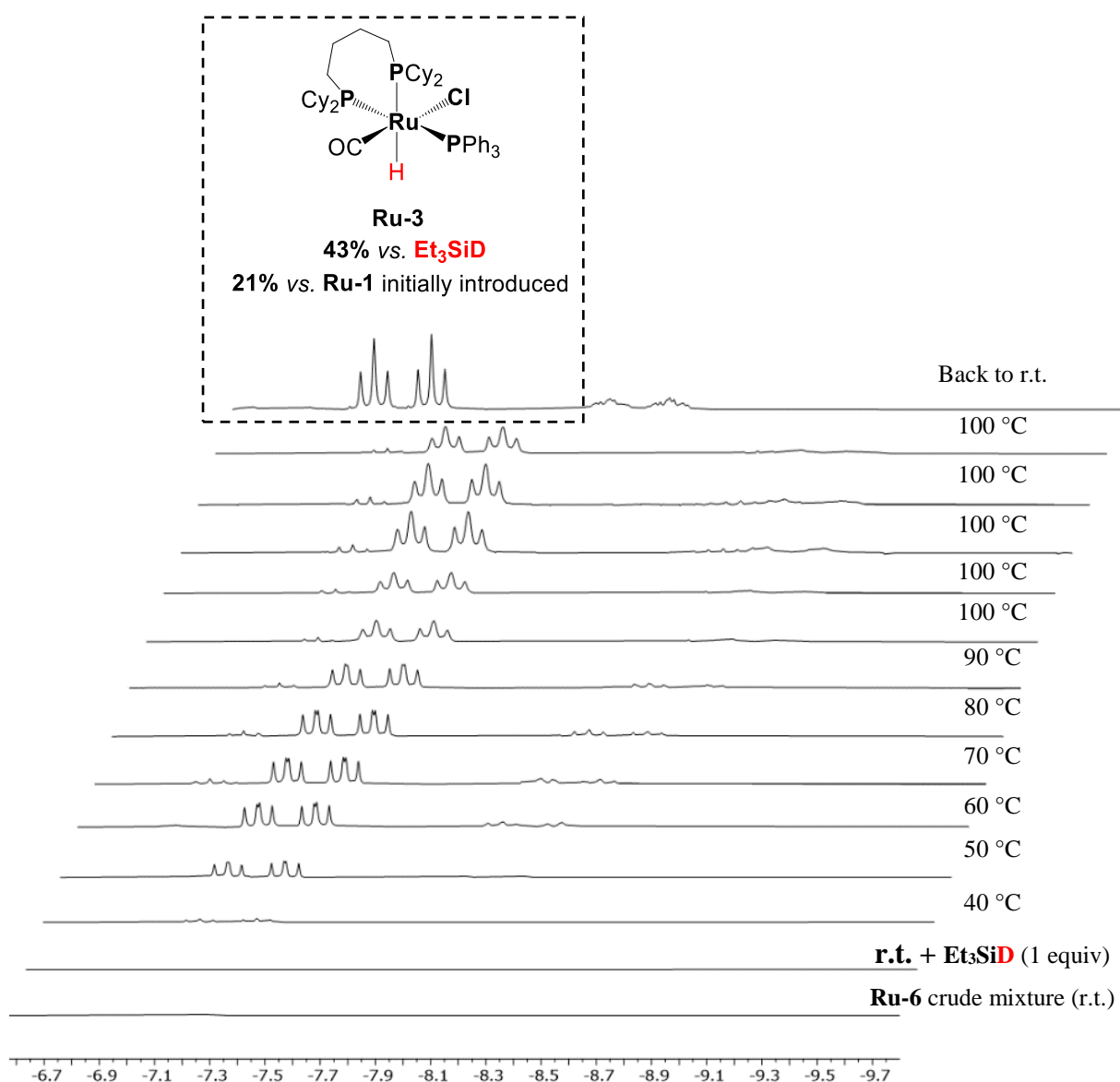


Figure II.4.17. VT ^1H NMR spectra (500 MHz, toluene- d_8) of the hydride region of the reaction of crude **Ru-6** with 1 equivalent of Et_3SiD .

Although no sources of hydride (H nor D) were introduced within the reaction vessel, the apparition of a hydride species is not in agreement with the proposed reaction scenario depicted in Scheme II.4.5. Indeed, if we suppose that Et_3SiD releases the acrylate, the deuterated analogue of **Ru-3**, that is $\text{RuD}(\text{Cl})(\text{CO})(\text{PPh}_3)(\text{DCPB})$, should be formed in the reaction mixture and no hydride pattern in the ^1H NMR spectra should be observed. One may suggest, in fact, the involvement of another source of hydride in the formation of **Ru-3**.

In addition to stoichiometric investigations, catalytic experiments using deuterium-labelled Et_3SiD were carried out under usual reaction conditions.^[d] When analysing by GC-MS

^[d] Solvent (20 mL), $[\text{Si-D}]_0 = 0.43 \text{ mol}\cdot\text{L}^{-1}$, $[\text{Ru}(\text{H})(\text{Cl})(\text{CO})(\text{PPh}_3)_3]_0 = [\text{DCPB}]_0 = 0.002 \text{ mol}\cdot\text{L}^{-1}$, $\text{CO}_2/\text{C}_2\text{H}_4$ 1:1 mol/mol, $\text{P}(\text{CO}_2) + \text{P}(\text{C}_2\text{H}_4) = 20 \text{ bar}$.

the crude reaction mixtures, the targeted products, that is triethylsilyl acrylate (**A1**) and triethylsilyl propionate (**P1**), were not found deuterated, as indicated by the molecular peaks and fragmentation analyses. The TONs values determined for production of **A1** and **P1** (10 and 1, respectively) were comparable to those obtained with Et₃SiH. These observations suggest that the most possible explanation on the fate of the D atom is the formation of non-analyzed/detected gaseous products such as D₂, HD, CDH₂CH₃ or CDH₃ (CO₂ over-reduction with D₂ or HD).

In order to verify this hypothesis, high pressure IR^[e] and Gas-Layer Chromatography (GLC)^[f] analyses of the crude gas phase, recovered from the reactor after completion of the catalytic ethylene carboxylation reaction using Et₃SiH (16h, 100°C), were performed. The GLC data revealed the absence H₂ or CH₄, whereas the high pressure IR gas-phase spectra displayed three bands in the νCH region at 1889, 2047 and 2895 cm⁻¹, possibly consistent with the formation of C₂H₆.

*ii. Addition of H₂ to **Ru-6***

In the next step of our mechanistic investigations, we exposed the **Ru-6** complex to an H₂ atmosphere, under different pressures, temperatures and reaction times. In a separated experiment carried out under 15 bar H₂ pressure, and further workup,^[g] crystals suitable for XRD analysis were obtained from the crude reaction mixture. The X-ray crystallographical analysis of those crystals confirmed the isolation of the propionate complex [Ru(Cl)(CO)(DCPB)(κ²-O,O-CO₂CH₂CH₃)] (**Ru-7**) (Figure II.4.18.). This compound most likely originates from hydrogenation of the parent **Ru-6** acrylate complex (Scheme II.4.6.).

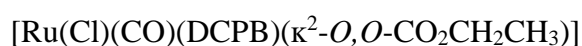
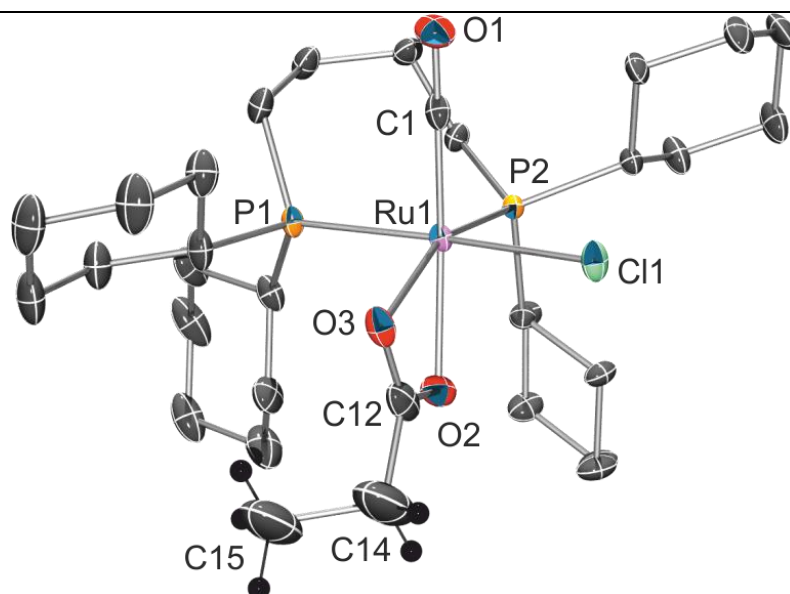
Furthermore, NMR spectroscopy of the crude mixture showed the complete consumption of the acrylate species (disappearance of the vinylic signals) as well as the formation of new hydride species, among them, the **Ru-3** complex.^[h] The presence of the latter species is interesting since it proves the possibility of regenerating the initial **Ru-3** catalyst using H₂, a green and atom efficient reductant.

^[e] Performed by Dr. A. Benidar and Prof. R. Georges at the Institut de Physique de Rennes, UMR 6251, Université de Rennes 1

^[f] Performed by Dr. T. Labasque, Géosciences Rennes, UMR 6118, Université de Rennes 1

^[g] Single crystals suitable for X-ray diffraction analysis were grown by slow evaporation of a heptane/toluene solution at room temperature.

^[h] The presence of propionic acid was investigated as well by NMR spectroscopy. Yet, the ¹³C NMR data did not show any characteristic signals for this compound.

**Ru-7**

Selected bond lengths [Å]

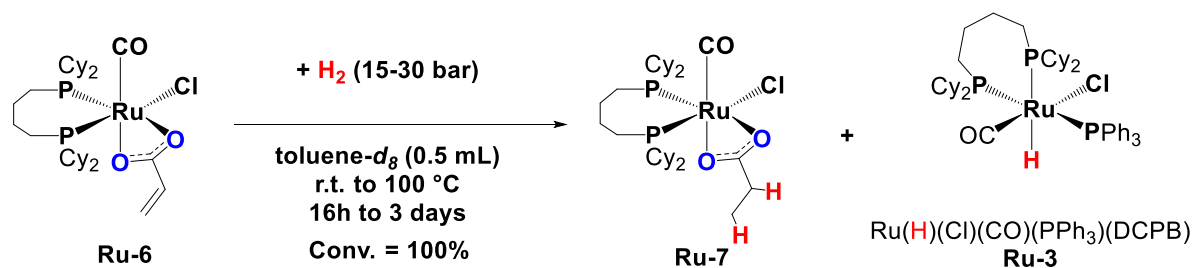
Ru1–Cl1 = 2.4383(8), Ru1–C1 = 1.824(3), Ru1–P1 = 2.3369(8), Ru1–P2 = 2.2901(7), Ru1–O2 = 2.172(2), Ru1–O3 = 2.238(2), C1–O1 = 1.155(4), C14–C15 = 1.559(7), C12–O2 = 1.279(4), C12–O3 = 1.252(5)

Selected bond angles [°]

P1–Ru1–P2 = 93.61(3), P1–Ru1–O3 = 91.10(6), P1–Ru1–O2 = 93.63(6), P1–Ru1–C1 = 89.08(10), C1–Ru1–P2 = 92.13(9), C1–Ru1–Cl1 = 91.42(10), O3–Ru1–Cl1 = 83.18(6), P1–Ru1–Cl1 = 174.11(3), P2–Ru1–Cl1 = 92.24(3), O2–Ru1–C1 = 167.95(11), O3–Ru1–P2 = 158.56(7), O3–Ru1–C1 = 108.86(11), C12–C14–C15 = 110.7(5), O3–Ru1–O2 = 59.39(9)

Figure II.4.18. ORTEP representation of the solid-state molecular structure of the ruthenium propionate complex $[(\text{DCPB})\text{Ru}(\text{Cl})(\text{CO})(\kappa^2\text{-}O,O\text{-CO}_2\text{CH}_2\text{CH}_3)]$ (**Ru-7**) with thermal ellipsoids at 50% probability level. Hydrogen atoms omitted for clarity. Selected interatomic distances and angles are given in Ångström [Å] and degree [°], respectively.

As for the **Ru-6** acrylate complex, the structural data of **Ru-7** revealed a six-coordinated Ru atom, having two coordination sites occupied by the bidentate DCPB phosphine ligand in a *cis* equatorial arrangement and two others occupied by the bidentate propionate ligand in a κ^2 coordination mode. The Cl and CO ligands are coordinated in *cis*-fashion to the metal center.



Scheme II.4.6. Hydrogenation of the C=C bond of **Ru-6** leading to **Ru-7**.

A longer C14–C15 bond length was observed in comparison to the C14=C15 distance of the **Ru-6** complex (1.559(7) vs. 1.284(8) Å, respectively), consistent with the formation of a Csp³–Csp³ bond. Moreover, the C12–C14–C15 angle value of 110.7(5) Å confirms the sp³ hybridized character of the C14 atom.

As previously observed with the **Ru-6** acrylate complex, the *cis* L–Ru–L angles are close to the ideal 90° value except for the O3–Ru1–C11 (83.18(6) Å). This likely reflects the repulsive interaction between the bulky DCPB phosphine and the propionate ligand.

iii. Addition of MeOH to Ru-6

Next, the reaction of (crude) **Ru-6** in presence of MeOH (1.5 equiv) was monitored by NMR spectroscopy while heating progressively to 100 °C. Knowing that, from a thermodynamic point of view, H₂ cannot eliminate by itself the free acid from the parent carboxylate, we intended to shift thermodynamics and recover acidic functions in a form of the corresponding esters by using MeOH as nucleophilic additive.

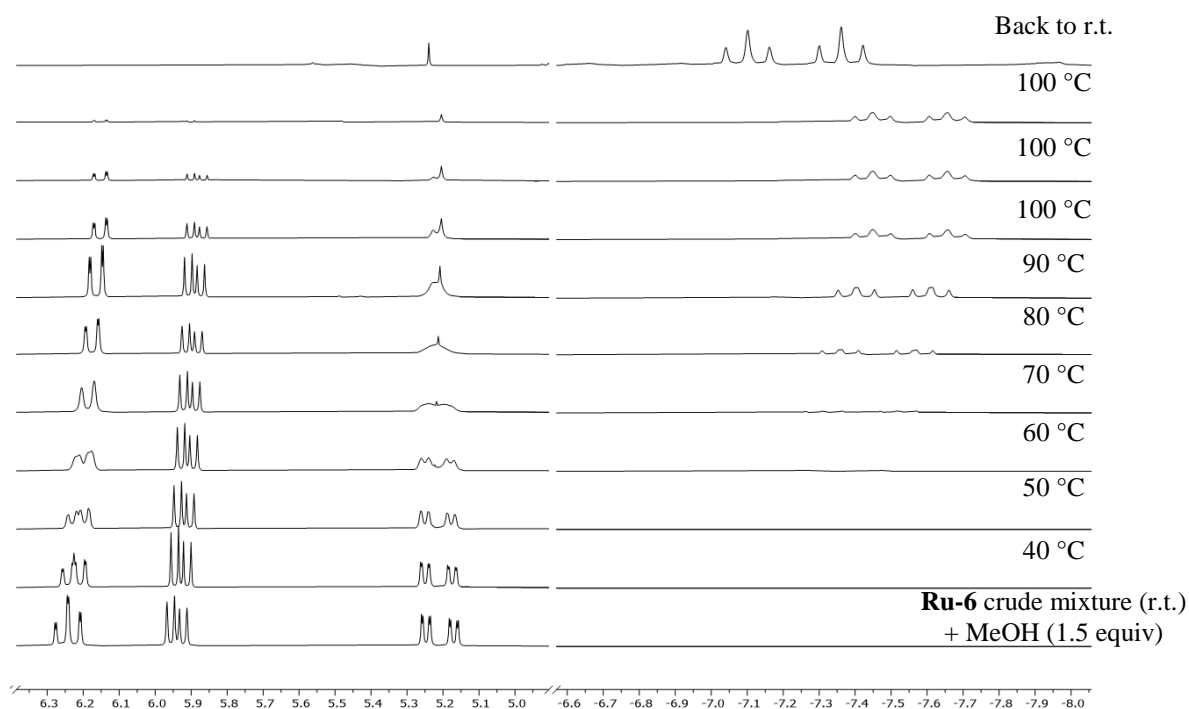


Figure II.4.19. VT ¹H NMR spectra (500 MHz, toluene-*d*₈) of the vinylic and hydride regions of the reaction of crude **Ru-6** with 1 equivalent of MeOH.

As shown in Figure II.4.19, the multiplicity of the vinylic signals started to evolve when the temperature reached 70 °C. The *gem*-hydrogen in *trans* position to the carboxy moiety of the C=C system started broadening, while the two other H vinylic signals became sharper. At the same time, in the hydride region, the doublet of triplets (δ_{H} 7.46 ppm) characteristic of the **Ru-3** complex started to grow. After heating for 1 h at 100 °C, the signals of the acrylic species completely disappeared. On the other hand, in the hydride region, a doublet of triplet, characteristic of the **Ru-3** complex, was observed (the ³¹P{¹H} NMR spectrum showed the presence of unidentified phosphorus containing species see Annexes, Figure II.4.26.).

In the ¹³C NMR spectrum, several signals were observed in the down field region (Figure II.4.20., bottom). In particular, the singlet at δ_{C} 161 ppm indicated the presence of a carbonyl moiety. When compared to the ¹³C NMR spectra of the products that might be formed from the reaction of **Ru-6** with MeOH (*i.e.* methyl formate, methyl acrylate, methyl propionate or propionic acid), none of them matched with the observed signal; the formation of methyl formate was also discarded by ¹H NMR.

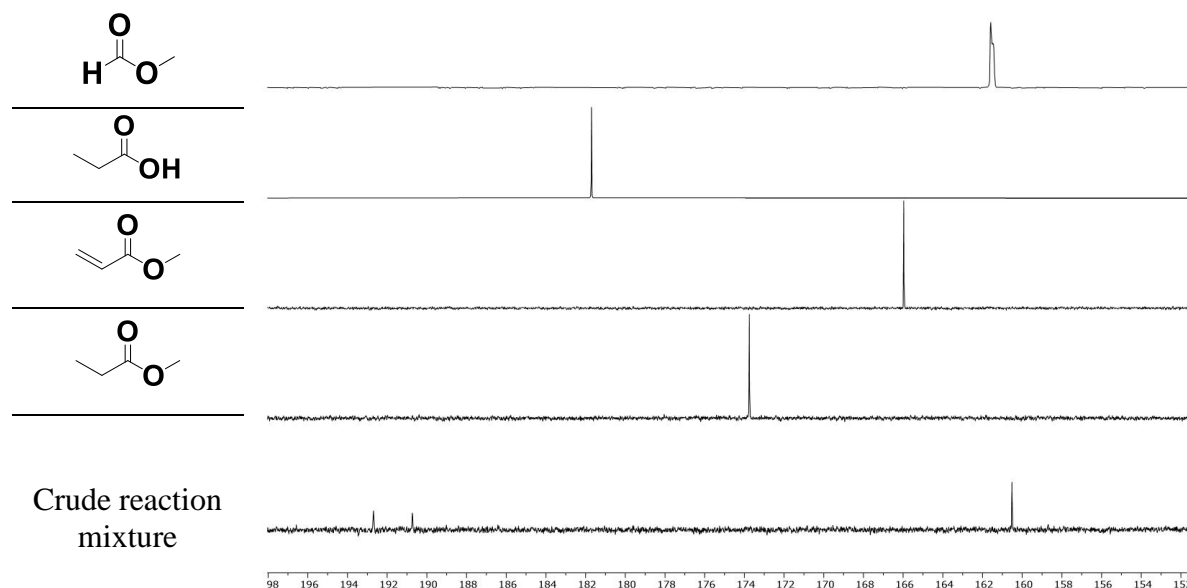
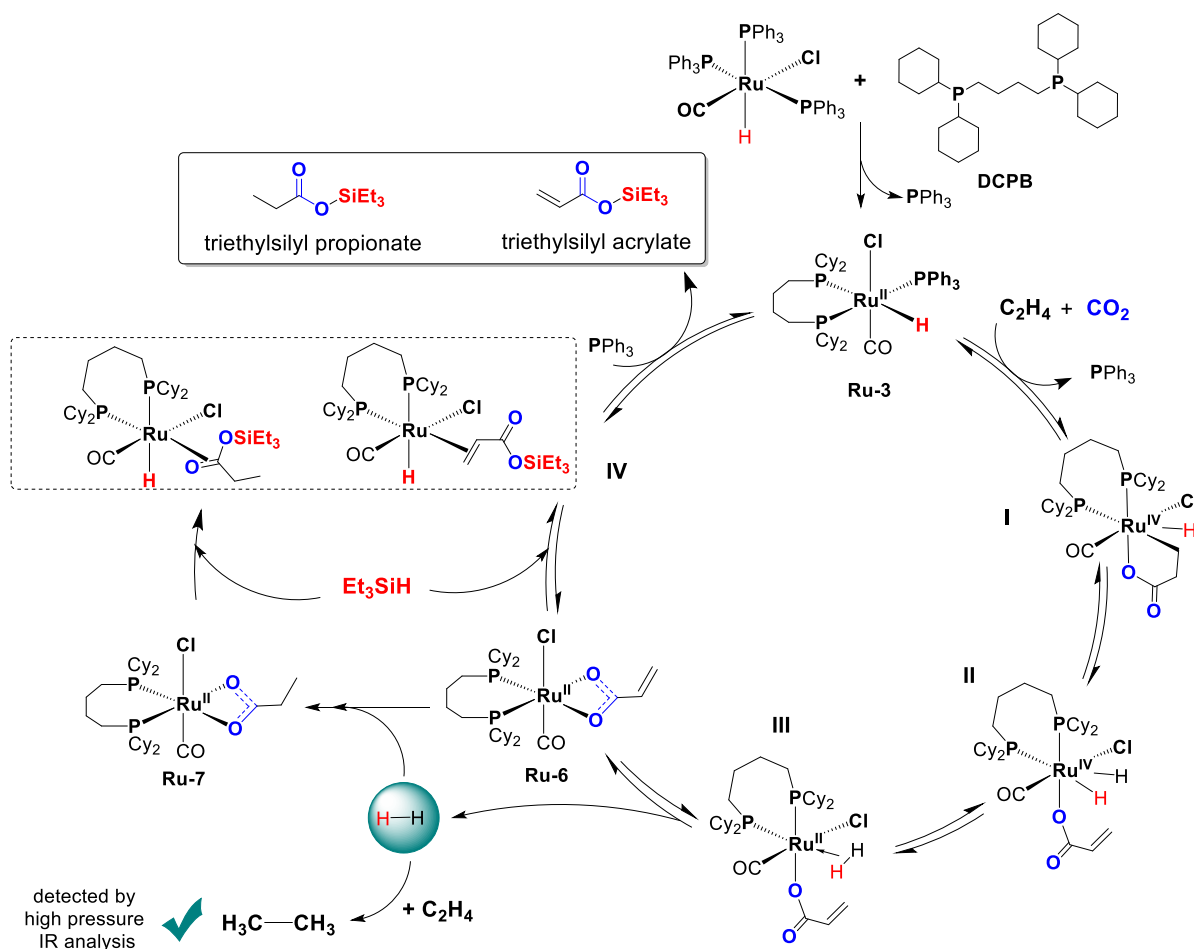


Figure II.4.20. ^{13}C NMR spectra (101 MHz, toluene- d_8 , 25 °C) of (from top to bottom) methyl formate, propionic acid, methyl propionate, methyl acrylate and the crude reaction mixture of **Ru-6** and 1.5 equivalent of MeOH.

From these results, it appeared that the spectroscopic footprints of the expected methyl esters do not correspond to the products formed by reacting **Ru-6** with MeOH. To gain deeper knowledge on the reactivity of the latter with **Ru-6**, further investigations are in progress in the objective of identifying the nature of the products observed.

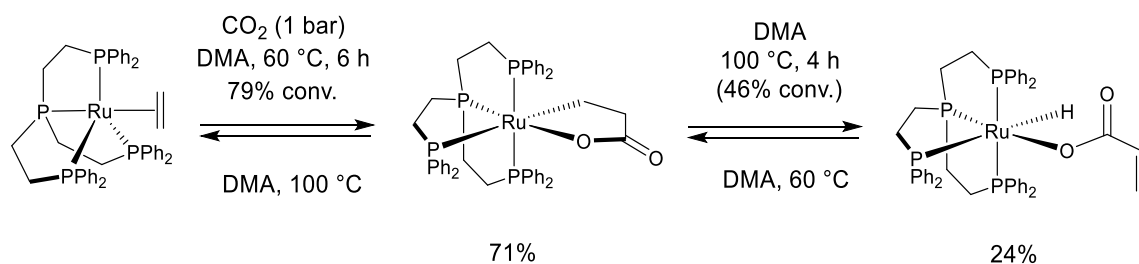
4.2.5. Possible mechanism for the formation of **Ru-6** and **Ru-7** leading to triethylsilyl acrylate and triethylsilyl propionate

Taking into account the above results, a possible mechanism for the formation of **A1** and **P1** is proposed in Scheme II.4.7. First, **Ru-3** complex is obtained by complexation of **Ru-1** with DCPB and release of 1 equiv of PPh_3 . Then, the oxidative coupling of CO_2 and C_2H_4 would afford a putative (not observed) ruthenolactone(IV) species (**I**). Indeed, since the formation and isolation of ruthenolactone species has already been described by Iwasawa *et al.*, we supposed that the most probable pathway to access **Ru-6** complex also could involve such ruthenacycle intermediate.



Scheme II.4.7. Proposed mechanism for the formation of **A1** and **P1**.

The hypothetical ruthenolactone(IV) species would then generate a (dihydrido)ruthenium(IV) acrylate complex (**II**) through a (facile and fast) β -H elimination step. The feasibility of the ruthenacycle to undergo efficient β -H elimination has already been reported by Iwasawa *et al.* upon heating, and without any additive, giving access to the isolated and identified *cis*-acrylato(hydrido)ruthenium(II) complex (Scheme II.4.8).^[21,22] The reaction was found to be reversible upon heating at 60 °C in DMA during 24 h.



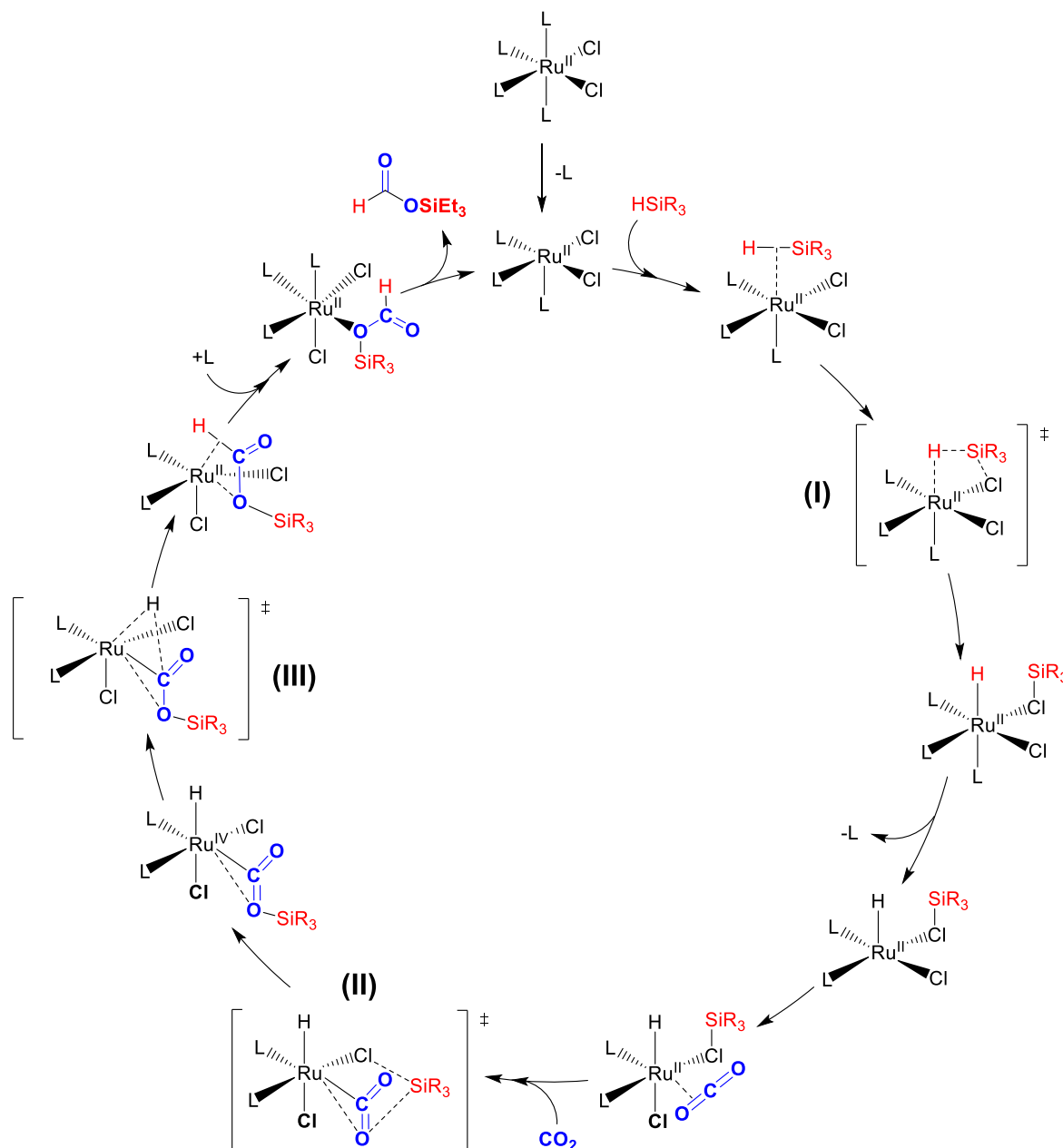
Scheme II.4.8. Reactivity of ruthenolactone upon heating.^[21,22]

using $\text{RuH}_2(\text{PMe}_3)_4$ complex and operating under supercritical CO_2 (entry 2). Based on the previous results, the group of Pitter found that the cheap precursor $\text{RuCl}_3 \cdot n\text{H}_2\text{O}$ generates in acetonitrile the $\text{trans}-[\text{Ru}^{\text{II}}\text{Cl}(\text{MeCN})_5]^+[\text{Ru}^{\text{III}}\text{Cl}_4(\text{MeCN})_2]^-$ complex, resulting in excellent TON (entry 3).^[49,50]

Table II.4.2. Examples of ruthenium catalysts for silyl formate formation.

Entry	Catalysts	Hydrosilane	T [°C]	CO ₂ (atm)	TON
1 ^[46]	$\text{RuCl}_2(\text{PPh}_3)_3$	HSiMeEt_2	100	30	28
2 ^[51]	$\text{RuH}_2(\text{PMe}_3)_4$	HSiMeEt_2	90	(scCO ₂) 200	62
3 ^[49,50]	$\text{trans}-[\text{Ru}^{\text{II}}\text{Cl}(\text{MeCN})_5]^+[\text{Ru}^{\text{III}}\text{Cl}_4(\text{MeCN})_2]^-$	Me_2PhSiH	80	14	465
4 ^[52]	$\text{RuCl}_2(\text{MeCN})_4$	Me_2PhSiH	85	20	495
5 ^[53]	$[\text{Ir}(\text{H})(\text{cis-cyclooctene})(\text{CF}_3\text{SO}_3)(\text{b-is}(\text{pyridine-2-yloxy})\text{methylsilane})]$	$(\text{Me}_3\text{SiO})_2\text{MeSiH}$	75	8	50
6 ^[54]	$[\text{Rh}_2(\text{OAc})_4]$	Me_2PhSiH	50-70	1	106-180
7 ^[55]	$\text{Cu}(\text{OAc})_2\text{H}_2\text{O}$	Me_2PhSiH	100	1	8100

In 2007, the same group proposed a mechanism based on the modified Chalk–Harrod mechanism and corroborated it by DFT calculations (Scheme II.4.10.).^[52,56] The first step is the dissociation of one MeCN ligand from the dichloride precursor to generate the five-coordinated Ru^{II} active species $[\text{Ru}^{\text{II}}\text{Cl}_2(\text{MeCN})_3]$. Next, it was proposed that the hydrosilane molecule binds the metal centre through η^2 -(Si–H) coordination to affords intermediate **I**, from which the successive decoordination of an additional MeCN molecule and coordination of CO_2 leads to intermediate **II**. Ligand reorganization in **II** yields intermediate **III**, followed by coordination of one molecule of MeCN and release of the corresponding silyl formate product, regenerating the active species.



Scheme II.4.10. Computed mechanism of the hydrosilylation of CO_2 involving the neutral complex $[\text{Ru}^{\text{II}}\text{Cl}_2(\text{MeCN})_4]$ as catalyst resting state by Deglmann *et al.*^[52]

So far, ruthenium complexes prevailed for the synthesis of silyl formate from CO_2 . Nowadays, other numerous catalysts are known (Table II.4.2., entries 5 to 7), including metal-free Frustrated Lewis pairs (FLPs), organocatalysts and metal species with or without $\text{B}(\text{C}_6\text{F}_5)_3$.^[45] For instance, Piers *et al.* reported in 2010 an FLP system consisting of 2,2,6,6-tetramethylpiperidine (TMP) and $\text{B}(\text{C}_6\text{F}_5)_3$ for reducing CO_2 into CH_4 in the presence of Et_3SiH .^[44]

In summary, CO_2 hydrosilylation has attracted several research groups, as it constitutes an important and feasible challenge for CO_2 utilization and transformation. Moreover, the

value-added reaction product, silyl formate, is interesting in its own or as an intermediate towards other attractive compounds such as formic acid, methanol and formamides.

Therefore, as judged from the literature data, the presence of product **F1** among the silylated esters is not surprising since CO₂ hydrosilylation has been proven a thermodynamically favoured chemical process.

4.3.2. Catalytical hydrosilylation of CO₂ using **Ru-3** complex; DFT calculations and mechanism

The ability of the **Ru-3** complex to achieve CO₂ hydrosilylation using Me₃SiH^[i] was investigated by DFT calculations in the frame of our collaboration with the LPCNO team.

First of all, in order to activate the *in situ* generated catalyst **Ru-3**, one of the ligands must be removed (decoordinated), so that one of the substrates could approach the vacant site around the metal center. Two different models have therefore been considered:

(a) In the **ligand dissociation model**, complete dissociation of either of the two ligands (PPh₃ and CO) were considered. The enthalpy for PPh₃ dissociation was calculated to be $\Delta H = 19.7 \text{ kcal}\cdot\text{mol}^{-1}$ whereas CO exhibited stronger BDE ($60.0 \text{ kcal}\cdot\text{mol}^{-1}$). Therefore, PPh₃ dissociation was found to be the most facile process, being in agreement with the already described experimental findings.

(b) In the **open-arm model**, decooordination of one of the phosphorus atoms of the chelating DCPB ligand was considered.

Since the calculations predicted high-lying transition states in the open-arm model, the PPh₃ ligand dissociation model was chosen as the starting point for the hydrosilylation reaction calculations. CO₂ coordinates to the available active site of the catalyst (**26**) and stabilizes the intermediate **2** by $2 \text{ kcal}\cdot\text{mol}^{-1}$ (Figure II.4.21.). Insertion of CO₂ into the Ru–H bond *via* an activation barrier of $6.5 \text{ kcal}\cdot\text{mol}^{-1}$ (**TS14**) led to the formation of the formate intermediate (**27**). Next, addition of Me₃SiH (**28**) and formate fragment silylation proceeds *via* a transition state with a low activation barrier (**TS15** = $9.1 \text{ kcal}\cdot\text{mol}^{-1}$ from **28**), leading to the formation of

^[i] Some simplifications were made to reduce calculation costs. When catalytic reactions of CO₂ and C₂H₄ were conceived using Ru(H)(CO)(Cl)(PPh₃)(DCPB) (**Ru-3**) as (pre)catalyst and hydrosilane as reductant, trimethylsilane (Me₃SiH) was considered instead of triethylsilane (Et₃SiH).

trimethylsilyl formate (**29**). Finally, its release results in the regeneration of the **Ru-3** species (**1**), making the overall reaction exothermic by $-13 \text{ kcal}\cdot\text{mol}^{-1}$.

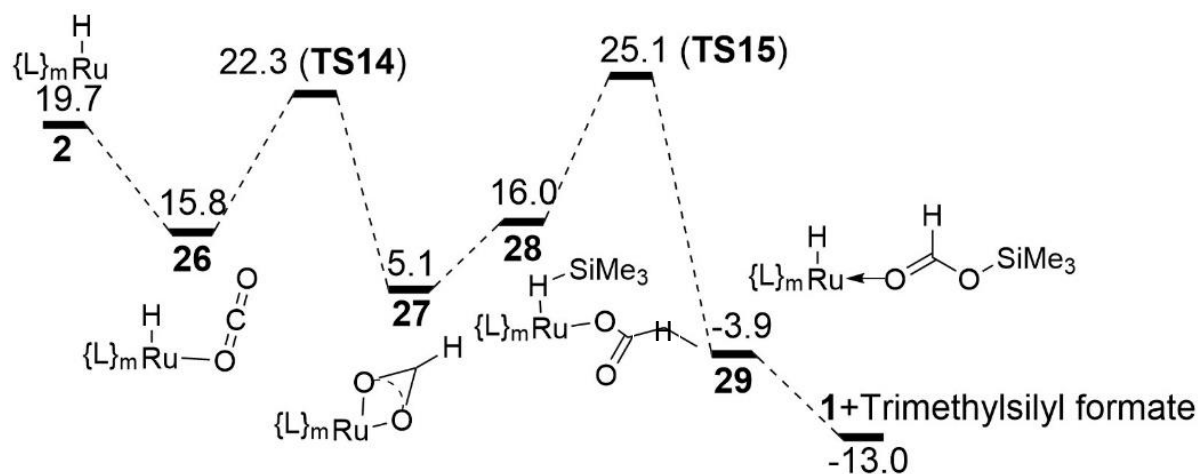


Figure II.4.21. Computed enthalpy reaction profile for CO_2 hydrosilylation using the ligand (PPh_3) dissociation model pathway on the **Ru-3** complex. Relative energies are represented in $\text{kcal}\cdot\text{mol}^{-1}$.

Hence, the DFT calculations revealed that the initial step for the hydrosilylation reaction of CO_2 is first activation of CO_2 , which takes place by transferring the H^- unit to the coordinated CO_2 . Here, we assume that the formation of a formate-type intermediate is accurate since similar stable complexes have been reported in the literature ($\text{RuH}(\text{O}_2\text{CH})(\text{PPh}_3)^{[39]}$). The presence of R_3SiH resulted in intermediates with side-on coordination (**29**), allowing silyl transfer to CO_2 and regeneration of **Ru-3**. We believe that the calculated key intermediates for the Me_3SiH reaction are similar in energy with those of Et_3SiH , which was used in our catalytic experiments. The overall process is thermodynamically favourable, in agreement with the observed experimental results.

4.4. Mechanistic insights on the formation of the triethylvinylsilane (TEVS) and tetraethylsilane (TES) by-products

4.4.1. State-of-the-art

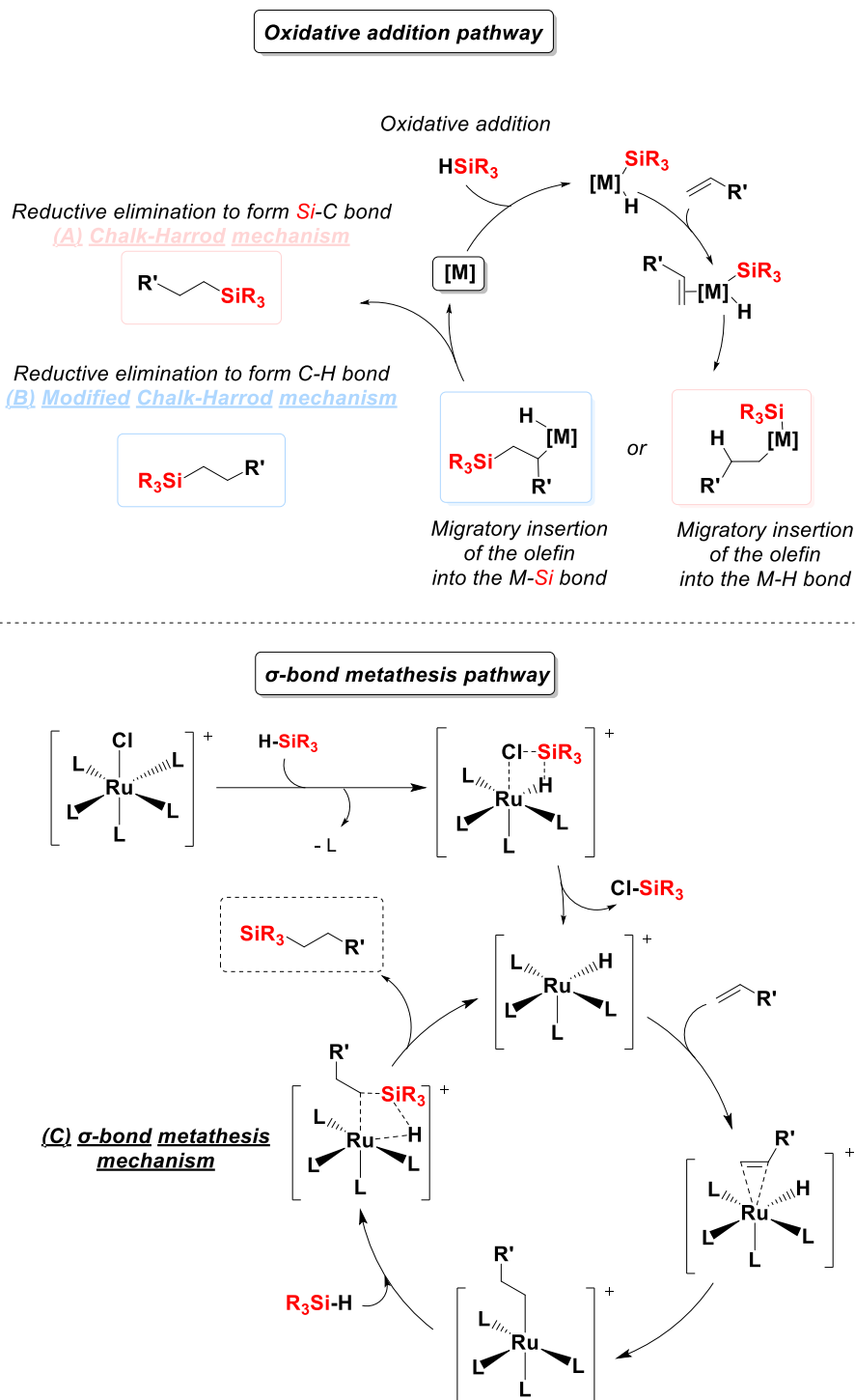
i. Hydrosilylation of alkenes

Hydrosilylation of alkenes, is the addition of a silicon–hydrogen bond across the $\text{C}=\text{C}$ π -bond to form a new alkylsilane.^[57] Although many complexes have been reported to catalyse this reaction, complexes of platinum, rhodium and palladium are the most common ones.^[58] Typically, hydrosilylation of alkenes affords terminal alkylsilanes as the major anti-Markovnikov regioisomer and hydrosilylation of vinylarenes usually generates the branched

alkylsilane (Markovnikov products).^[59] The regioselectivity (and stereoselectivity) of olefin hydrosilylation depends, however, on the olefin substrate and can be tuned by the structure of the catalyst (under kinetic control). In fact, alkylsilanes are value added monomers for industrial applications.^[60] For example, polysiloxanes derived from alkylsilanes have found a broad range of applications from aerospace to fine-chemical applications.^[58]

Historically, transition-metal-catalysed-hydrosilylation was first reported in the late 1950 with group 8 metal catalysts (platinum, ruthenium and iridium chlorides).^[61] Both Speier's and Karstedt's platinum catalysts, respectively $\text{H}_2\text{PtCl}_6 \cdot n\text{H}_2\text{O}$ and $\text{O}[\text{Si}(\text{CH}_3)_2\text{CH}=\text{CH}_2]_2\text{Pt}$ complexes, are frequently used in industrial processes as catalysts for hydrosilylation.^[62,63] Rhodium complexes are also known to catalyse hydrosilylation of olefins, and the Wilkinson's catalyst was one of the earliest used for this purpose.^[64] Palladium complexes in combination with chiral monodentate phosphine ligand (e.g. (S)-2-diphenylphosphino-1,1'-binaphthyl [(S)-H-MOP]), were also reported to be efficient for asymmetric hydrosilylation of 1-alkenes.^[65,66] Today, many other catalysts based on cobalt, ruthenium, rhodium and platinum are well-documented to catalyse hydrosilylation of alkenes allowing to access different types of products according to the chosen catalyst and the parent hydrosilane.^[67,68]

Overall, addition of a hydrosilane to a metal center involves either an oxidative addition of the Si–H bond to the metal (Scheme II.4.11. (A) and (B)) or a metathesis transition state (Scheme II.4.11. (C)). Since oxidative addition commonly requires an increase in the oxidation state of the metal by two units, a 16-electron (or less) metal center is needed. When oxidative addition is not possible (especially for the early transition metals) or not favored, a σ -bond metathesis reaction pathway is then most probable.^[69,70]



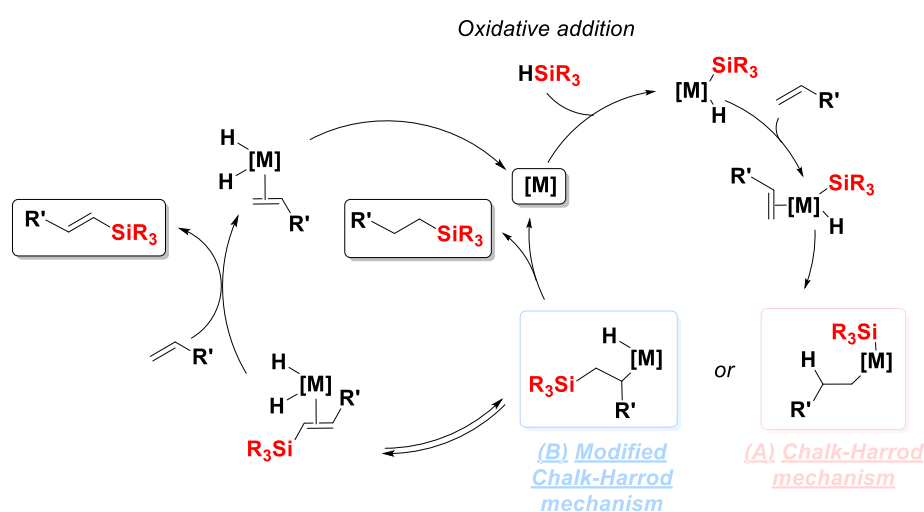
Scheme II.4.11. (A) Chalk-Harrod and (B) modified Chalk-Harrod mechanisms along with (C) σ -bond metathesis mechanism.

ii. Dehydrogenative silylation of alkenes

Being in competition with hydrogenative silylation, the dehydrogenative silylation of olefins is a process giving access to vinylsilanes. In the field of ruthenium catalysed reactions, the dehydrogenative silylation of styrene and its *p*-substituted derivatives with Et_3SiH gave vinylsilanes in high yields when using $\text{Ru}_3(\text{CO})_{12}$.^[71] The bis(dihydrogen)ruthenium complex

$\text{RuH}_2(\text{H}_2)_2(\text{PCy}_3)_2$ has been also demonstrated to selectively catalyse dehydrogenative coupling of C_2H_4 providing vinyltriethylsilane.^[72] Other catalysts incorporating noble metals such as rhodium, iridium, platinum, and palladium have been reported for the dehydrogenative silylation of alkenes.^[73] More recently, examples with earth-abundant metal catalysts including iron, cobalt, nickel, copper, and manganese catalytic systems have emerged.^[58]

One possible mechanism to dehydrogenative silylation is shown in Scheme II.4.12. The silylalkyl intermediate generated through the modified Chalk-Harrod mechanisms can undergo β -hydride elimination to form an olefin–dihydride complex. Reinsertion of an olefin and displacement of the vinylsilane from the metal results in dehydrogenative silylation.



Scheme II.4.12. Chalk-Harrod and modified Chalk-Harrod mechanisms along with dehydrogenative silylation mechanism.^[74]

Despite their usefulness, the products of hydrosilylation and dehydrogenative silylation, observed through our catalytic studies, were not the targeted compounds we initially targeted to obtain. Nevertheless, these transformations were thoroughly investigated by DFT calculations to further understand the origin of the selectivities observed for the **Ru-1**/DCPB catalytic system.

4.4.2. Catalytic hydrosilylation and dehydrogenative silylation of C_2H_4 using the **Ru-3** system; DFT calculations and mechanism proposal

Using both the PPh_3 and DCPB arm ligand dissociation models previously described in section 4.3.2., DFT studies were conducted on the hydrosilylation and dehydrosilylative silylation of C_2H_4 .

In the PPh_3 ligand removing scenario, Me_3SiH addition to the Ru(II) catalyst active site (**30**) is followed by H_2 release ($\text{TS16} = 15.4 \text{ kcal}\cdot\text{mol}^{-1}$) resulting in the formation of a Ru–Si bond (**31**) (Figure II.4.22.). The endothermic process of C_2H_4 addition in the next step leads to intermediate **32**. Next, insertion of the alkene ($\text{TS17} = 13.9 \text{ kcal}\cdot\text{mol}^{-1}$) to the Ru–Si bond results in the formation of a $\beta\text{-H}$ agostic interaction in **33**. The low barrier for the $\beta\text{-H}$ elimination, through $\text{TS18} = 3.9 \text{ kcal}\cdot\text{mol}^{-1}$, results in trimethylvinylsilane. The dissociation of the trimethylvinylsilane and regeneration of the catalyst from **34** is slightly exothermic.

DFT calculations also predicted that the addition of Me_3SiH (**35**) to **33** is possible. In an alternate pathway, the insertion of the hydride from Me_3SiH into the Ru–C bond ($\text{TS19} = 26.4 \text{ kcal}\cdot\text{mol}^{-1}$) results in the release of ethyltrimethylsilane and regeneration of **32**. The main difference between the two pathways is the significantly higher transition state (TS19) at $30.5 \text{ kcal}\cdot\text{mol}^{-1}$ compared to TS18 ($8.0 \text{ kcal}\cdot\text{mol}^{-1}$), being in excellent agreement with the higher TONs of **TEVS** vs. **TES** obtained under our experimental conditions ($100 \text{ }^\circ\text{C}$ for 16 h).

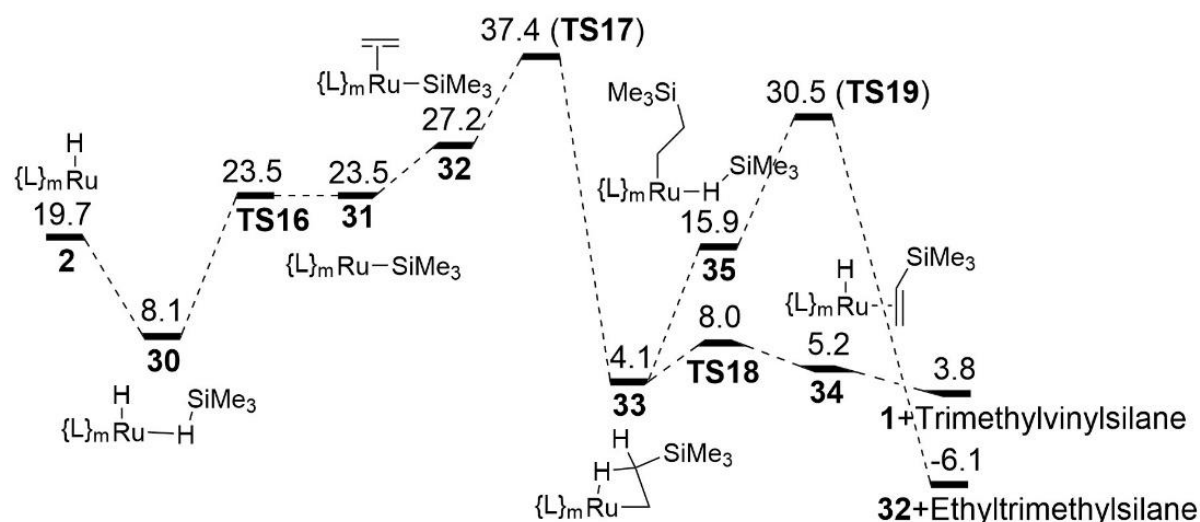


Figure II.4.22. Computed enthalpy reaction profile for C_2H_4 hydrosilylation and dehydrogenative silylation using the ligand (PPh_3) dissociation model pathway on the **Ru-3** complex. Relative energies are represented in $\text{kcal}\cdot\text{mol}^{-1}$.

Hence, hydrosilylation and dehydrogenative silylation processes of C_2H_4 with **Ru-3** complex were expected to proceed, by analogy to the work reported on hydrosilylation of olefins, *via* a mechanism similar to the modified Chalk–Harrod outlined in Scheme II.4.12.

4.5. Optimization of the catalytic formation of triethylsilylacrylate and propionate from CO₂, C₂H₄, Et₃SiH and additives

At this stage of our study, **Ru-3** complex still exhibited higher selectivities toward the unwanted **TES** and **TEVS** side products. As shown by DFT calculations, the independent parasitic reactions of C₂H₄ and CO₂ with hydrosilane were found to proceed with a low activation barrier. Therefore, to identify conditions for a more selective production of the desired carboxylation products **A1** and **P1**, we investigated the influence of several additives (Table II.4.3.).

In the literature, nucleophilic interceptors such as bases^[75] and methylating reagents,^[76–79] or Lewis acids^[33,80] or phosphine ligands^[81] are often added to promote cleavage of metallalactones and release the free acrylate products.

In our study, except for H₂O (entry 7), no significant differences in the corresponding TONs values were observed when comparing the experiments conducted in presence of KF, KPF₆, LiOTf, Al(OTf)₃ and CsF with those carried out in the absence of additives (entries 1 vs. 2–6).

Table II.4.3. Catalytic results from batch experiments upon adding additives.^[a]

Entry	Additive [mol%]	Conv. Et ₃ SiH [mol%] ^[b]	TON ^[c]					
			Route A		Route B and C			
			A1	P1	F1	TES	TEVS	E
1	none	54	13	1.3	16	4	53	1.6
2	KF [20]	56	14	4	9	4	44	4
3	KPF ₆ [10]	27	13	1	2	2	20	2
4	LiOTf [10]	62	15	2	12	11	106	4
5	Al(OTf) ₃ [10]	>98	0	0	0	50	152	8
6	CsF [20]	32	12	2	2	3	22	2
7	H ₂ O [40]	97	4	68	3	5	84	1

^[a] Solvent (20 mL), $[\text{Si-H}]_0 = 0.43 \text{ mol}\cdot\text{L}^{-1}$, $[\text{Ru}(\text{H})(\text{Cl})(\text{CO})(\text{PPh}_3)_3]_0 = [\text{DCPB}]_0 = 0.002 \text{ mol}\cdot\text{L}^{-1}$, $\text{CO}_2/\text{C}_2\text{H}_4$ 1:1 mol/mol, $P(\text{CO}_2) + P(\text{C}_2\text{H}_4) = 20 \text{ bar}$. ^[b] Determined by integration of the ^1H NMR peaks using $(\text{Me}_3\text{Si})_4\text{Si}$ as internal standard. ^[c] Turnover number as determined by GC-FID using *n*-dodecane as internal standard.

In fact, addition of water much affected Et_3SiH conversion and selectivities towards Route A products (Figure II.4.23.). With only 0.1 equiv (*vs.* Et_3SiH) of H_2O , a slightly higher conversion of Et_3SiH and a dramatic increase in the formation of **P1** were observed. With more water (0.2 and 0.4 equiv), the formation of propionate was favored over acrylate with higher corresponding TONs of 42 and 68. Yet, addition of 0.8 equiv did not seem to be beneficial to the system, decreasing the overall TON to 48.

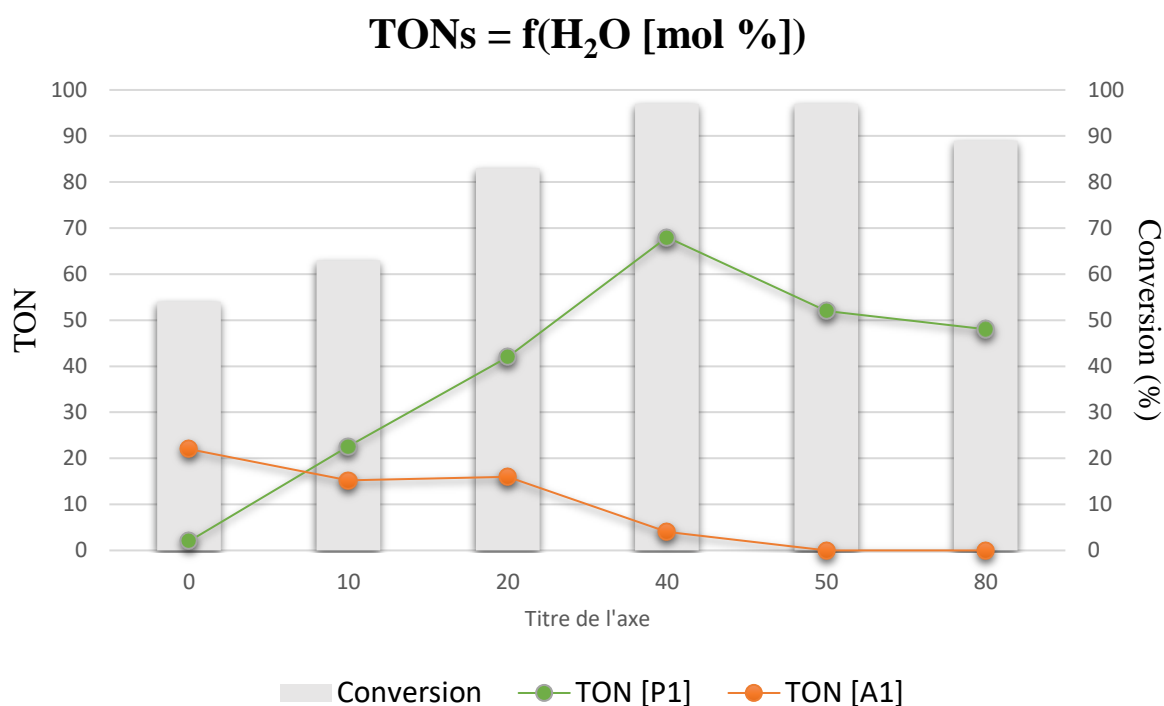


Figure II.4.23. Influence of adding water on the selectivity toward A1 and P1 products.^[j]

Isotopic experiments revealed that the reaction of CO_2 , C_2H_4 and Et_3SiH in the presence of D_2O (40 mol%) selectively afforded $\text{CH}_3\text{CHD}\text{COOSiEt}_3$ as the main product (among **F1**, **TES**, **TEVS**), deuterated at the β -position, as revealed by the ^{13}C NMR spectrum (Figure II.4.24.).

^[j] Solvent (20 mL), $[\text{Si-H}]_0 = 0.43 \text{ mol}\cdot\text{L}^{-1}$, $[\text{Ru}(\text{H})(\text{Cl})(\text{CO})(\text{PPh}_3)_3]_0 = [\text{DCPB}]_0 = 0.002 \text{ mol}\cdot\text{L}^{-1}$, $\text{CO}_2/\text{C}_2\text{H}_4$ 1:1 mol/mol, $P(\text{CO}_2) + P(\text{C}_2\text{H}_4) = 20 \text{ bar}$. ^[c] Determined by integration of the ^1H NMR signals using $(\text{Me}_3\text{Si})_4\text{Si}$ as internal standard. ^[d] Turnover number: TON ($\text{mol}(\text{product})\cdot\text{mol}(\text{Ru})^{-1}$) determined by GC-FID using *n*-dodecane as internal standard.

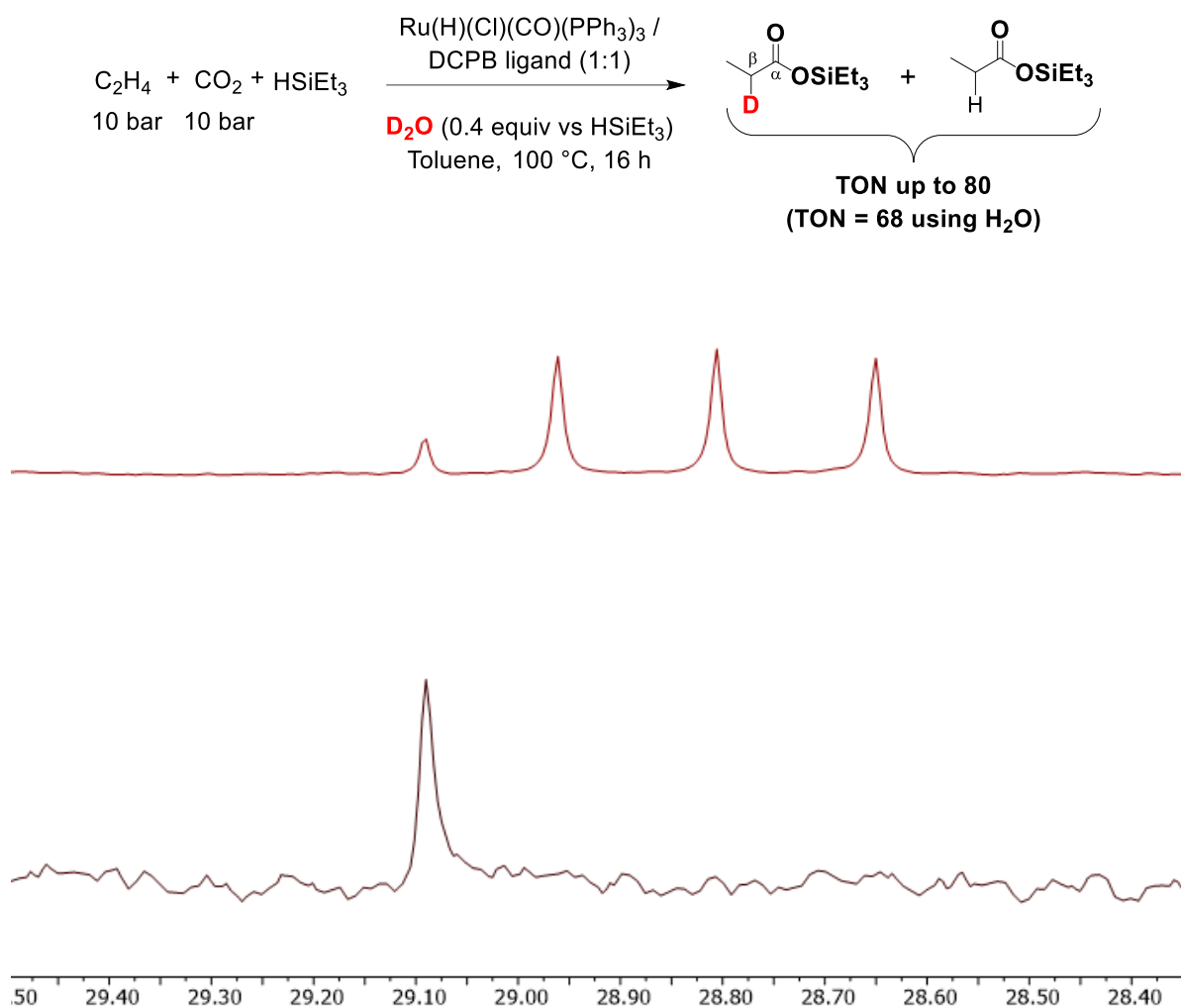
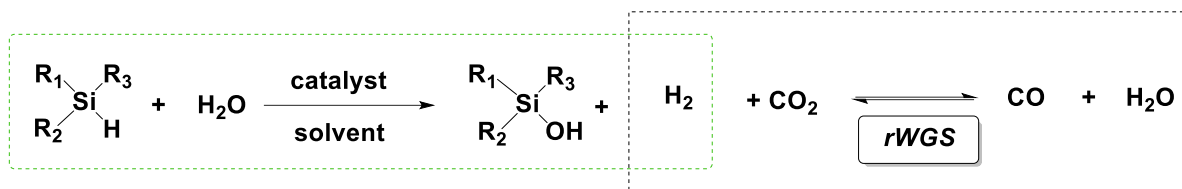


Figure II.4.24. ^{13}C NMR spectra (101 MHz, toluene- d_8 , 25 °C) of the quaternary region of (top) the crude mixture obtained from isotopic experiments of CO_2 , C_2H_4 and Et_3SiH reaction in the presence of D_2O (40 mol%) and (bottom) triethylsilylpropionate (**P1**).

Previous work by Ruben and co-workers explored the use of water in site-selective hydrocarboxylation of unsaturated hydrocarbons with CO_2 : in the case of olefins, linear carboxylic acids are formed through hypothetical hydrometallation.^[82] In our case, it is still unclear how H_2O interferes.

Addition of water to the system might involve other side reactions as well. For example the catalytic oxidation of silanes to silanols using H_2O and/or molecular oxygen as oxidants has already been reported (Scheme II.4.13.).^[83,84] The only by-products of this reaction are H_2 and/or H_2O . Therefore, in the presence of H_2 in the closed system, one can think of the possible involvement of the CO gas, generated from CO_2 , H_2 and Et_3SiH , in the formation of silylesters under the present reaction conditions.



Scheme II.4.13. Catalytic oxidation of silanes to silanols using H₂O and/or molecular oxygen as oxidants.

Although we have not been able to identify whether or not CO is generated in the reaction medium, we were able to detect, by GC-MS analysis, the presence of triethylsilanol in the crude reaction mixture ($m/z = 103$). Moreover, we have conducted catalytic experiments under CO atmosphere instead of CO₂. Using the combination Ru(H)(Cl)(CO)(PPh₃)₃/DCPB (1:1) under usual conditions, both in the presence and absence of water, neither of the acrylate (**A1**) or propionate (**P1**) silyl esters were observed (Table II.4.4). This suggests that there is no reverse-water gas shift process operating in our system. Such conclusion is also consistent with the fact that formation of **A1** and **P1** is observed when CO₂/C₂H₄/Et₃SiH react in the absence of water (chapter II); indeed, although the reduction of CO₂ to CO by Et₃SiH may be envisioned, C₂H₄ carbonylation processes shall require a nucleophile which is usually water or an alcohol.

Table II.4.4. Catalytic results from batch experiments performed under CO/C₂H₄ atmosphere.^[a]

Entry	Additive [mol%]	Conv. Et ₃ SiH [mol%] ^[b]	Yield ((mol(product).mol(Et ₃ SiH) ⁻¹)x100) ^[c]						
			Route A products		Route B and C products				
			A1	P1	F1	TES	TEVS	E	
1	None	36	0	0	0	traces	traces	0	
2	H ₂ O [40]	44	0	0	0	traces	traces	0	

^[a] Reaction conditions: toluene (20 mL), [Si-H]₀ = 0.43 mol·L⁻¹, [Ru(H)(Cl)(CO)(PPh₃)₃]₀ = [DCPB]₀ = 0.002 mol·L⁻¹, CO/C₂H₄ 1:1 mol/mol, P(CO) + P(C₂H₄) = 20 bar; results of at least duplicated experiments and averaged yields values; among several unknown products, allyl-triethylsilyl ether (CH₂=CHCH₂OSiEt₃) was identified by GC-MS. ^[b] Determined by integration of the ¹H NMR signals using (Me₃Si)₄Si as internal standard.

^[c] Yields as determined by GC-FID using *n*-dodecane as internal standard.

4.6. Conclusion

In this chapter, the mechanistic studies and rational approaches were outlined to fully understand the catalytic formation of silyl esters using **Ru-3** complex as precatalyst.

In view of the recently published mechanistic works by Iwasawa and co-workers on Ru catalysed carboxylation of ethylene,^[21,22] one might assume that a five-membered ruthenolactone, generated by oxidative cyclization of C₂H₄ and CO₂, should also be produced in our reaction mixture. Surprisingly, such species were not observed either by NMR spectroscopy studies or XRD analyses. However, a different key intermediate complex, of molecular formula Ru(Cl)(CO)(DCPB)(κ²O, O-CO₂CH=CH₂), was isolated from the reaction mixture as a mixture of *cis* and *trans* isomers (vs. the DCPB ligand) and characterized. This evidenced the effective coupling of CO₂ with C₂H₄ in the presence of **Ru-3** complex. Two mechanisms were proposed to explain the formation of the Ru-acrylate species: the first one implies a putative 5-membered ruthenolactone intermediate, whereas the second one involves a ruthenium-alkyl and a 4-membered ruthenolactone species. Nevertheless, additional DFT calculations are still necessary to shed light on the mechanisms of formation of **A1** and **P1**.

Stoichiometric reactions also conducted on the Ru(Cl)(CO)(DCPB)(κ²O, O-CO₂CH=CH₂) mixture of *cis* and *trans* isomers, with respect to different reductants (Et₃SiH, H₂ and MeOH), aimed at releasing the corresponding carboxylate fragment as either an acid or an ester reaction product. Although deuterium labelling experiments using Et₃SiD confirmed the complete consumption Ru(Cl)(CO)(DCPB)(κ²O, O-CO₂CH=CH₂), rational explanation for the formation of Ru(H)(Cl)(CO)(DCPB)(PPh₃) in our reaction medium, regardless the reductant used, could not be given so far. Some answers could be obtained through a detailed study of the **Ru-6** acrylate fragment release mechanism, which could proceed through production of gaseous D₂ or HD.

Since the **Ru-1**/DCPB combination gave also rise to side-products, originated from hydrosilylation of CO₂ and C₂H₄ and from dehydrosilylative silylation of C₂H₄, DFT calculations have been conducted to probe the different side reaction mechanisms starting from **Ru-3** complex. The electron-rich nature of the metal center in **Ru-3** and the availability of a vacant coordination site by facile dissociation of PPh₃ ligand make this complex suitable for C₂H₄ and CO₂ activation and further hydrosilylation.

Finally, aiming at improving the efficiency and selectivities toward **A1** and **P1** production, different additives were tested in catalysis. It was found that addition of substoichiometric amounts of water was beneficial to the system by increasing the TONs for the formation of **P1**. However, non-negligible production of **TES** and **TEVS** was also observed.

4.7. References

- [1] T. T. Adamson, S. P. Kelley, W. H. Bernskoetter, *Organometallics* **2020**, *39*, 3562–3571.
- [2] S. M. Rummelt, H. Zhong, I. Korobkov, P. J. Chirik, *J. Am. Chem. Soc.* **2018**, *140*, 11589–11593.
- [3] M. Aresta, E. Quaranta, *J. Organomet. Chem.* **1993**, *463*, 215–221.
- [4] A. Tortajada, F. Juliá-Hernández, M. Börjesson, T. Moragas, R. Martin, *Angew. Chem. Int. Ed.* **2018**, *57*, 15948–15982.
- [5] S. Manzini, N. Huguet, O. Trapp, T. Schaub, *Eur. J. Org. Chem.* **2015**, *2015*, 7122–7130.
- [6] A. Vavasori, L. Calgaro, L. Pietrobon, L. Ronchin, *Pure Appl. Chem.* **2018**, *90*, 315–326.
- [7] S. C. E. Stieber, N. Huguet, T. Kageyama, I. Jevtovikj, P. Ariyananda, A. Gordillo, S. A. Schunk, F. Rominger, P. Hofmann, M. Limbach, *Chem. Commun.* **2015**, *51*, 10907–10909.
- [8] S. Manzini, N. Huguet, O. Trapp, R. A. Paciello, T. Schaub, *Catal. Today* **2017**, *281*, 379–386.
- [9] S. Manzini, A. Cadu, A.-C. Schmidt, N. Huguet, O. Trapp, R. Paciello, T. Schaub, *ChemCatChem* **2017**, *9*, 2269–2274.
- [10] I. Pápai, G. Schubert, I. Mayer, G. Besenyi, M. Aresta, *Organometallics* **2004**, *23*, 5252–5259.
- [11] D. C. Graham, C. Mitchell, M. I. Bruce, G. F. Metha, J. H. Bowie, M. A. Buntine, *Organometallics* **2007**, *26*, 6784–6792.
- [12] P. N. Plessow, A. Schäfer, M. Limbach, P. Hofmann, *Organometallics* **2014**, *33*, 3657–3668.
- [13] W. Guo, C. Michel, R. Schwiedernoch, R. Wischert, X. Xu, P. Sautet, *Organometallics* **2014**, *33*, 6369–6380.
- [14] G. Yang, B. Schöffner, M. Blug, E. J. M. Hensen, E. A. Pidko, *ChemCatChem* **2014**, *6*, 800–807.
- [15] A. Julián, J. Guzmán, E. A. Jaseer, F. J. Fernández-Alvarez, R. Royo, V. Polo, P. García-Orduña, F. J. Lahoz, L. A. Oro, *Chem. – Eur. J.* **2017**, *23*, 11898–11907.
- [16] Y. Li, Z. Liu, J. Zhang, R. Cheng, B. Liu, *ChemCatChem* **2018**, *10*, 5669–5678.
- [17] H. Hoberg, D. Schaefer, *J. Organomet. Chem.* **1983**, *251*, c51–c53.
- [18] H. Hoberg, Y. Peres, A. Milchereit, *J. Organomet. Chem.* **1986**, *307*, C38–C40.
- [19] H. Hoberg, Y. Peres, C. Krüger, Y.-H. Tsay, *Angew. Chem. Int. Ed. Engl.* **n.d.**, *26*, 771–773.
- [20] H. Hoberg, K. Jenni, K. Angermund, C. Krüger, *Angew. Chem. Int. Ed. Engl.* **1987**, *26*, 153–155.
- [21] K. Takahashi, Y. Hirataka, T. Ito, N. Iwasawa, *Organometallics* **2020**, *39*, 1561–1572.
- [22] T. Ito, K. Takahashi, N. Iwasawa, *Organometallics* **2019**, *38*, 205–209.
- [23] B. M. Trost, F. D. Toste, A. B. Pinkerton, *Chem. Rev.* **2001**, *101*, 2067–2096.
- [24] B. M. Trost, M. U. Frederiksen, M. T. Rudd, *Angew. Chem. Int. Ed.* **2005**, *44*, 6630–6666.
- [25] T. Kondo, *Bull. Chem. Soc. Jpn.* **2011**, *84*, 441–458.
- [26] N. Chatani, T. Morimoto, Y. Fukumoto, S. Murai, *J. Am. Chem. Soc.* **1998**, *120*, 5335–5336.
- [27] N. Chatani, *Chem. Rec.* **2008**, *8*, 201–212.
- [28] T. Kondo, M. Nomura, Y. Ura, K. Wada, T. Mitsudo, *J. Am. Chem. Soc.* **2006**, *128*, 14816–14817.
- [29] J. C. Leung, L. M. Geary, T.-Y. Chen, J. R. Zbieg, M. J. Krische, *J. Am. Chem. Soc.* **2012**, *134*, 15700–15703.
- [30] L. M. Geary, B. W. Glasspoole, M. M. Kim, M. J. Krische, *J. Am. Chem. Soc.* **2013**, *135*, 3796–3799.

- [31] B. Y. Park, T. P. Montgomery, V. J. Garza, M. J. Krische, *J. Am. Chem. Soc.* **2013**, *135*, 16320–16323.
- [32] C. Hendriksen, E. A. Pidko, G. Yang, B. Schöffner, D. Vogt, *Chem. – Eur. J.* **2014**, *20*, 12037–12040.
- [33] D. Jin, T. J. Schmeier, P. G. Williard, N. Hazari, W. H. Bernskoetter, *Organometallics* **2013**, *32*, 2152–2159.
- [34] D. Jin, P. G. Williard, N. Hazari, W. H. Bernskoetter, *Chem. – Eur. J.* **n.d.**, *20*, 3205–3211.
- [35] J. M. Wolfe, W. H. Bernskoetter, *Dalton Trans.* **2012**, *41*, 10763–10768.
- [36] W. H. Bernskoetter, B. T. Tyler, *Organometallics* **2011**, *30*, 520–527.
- [37] B. S. Hanna, A. D. MacIntosh, S. Ahn, B. T. Tyler, G. T. R. Palmore, P. G. Williard, W. H. Bernskoetter, *Organometallics* **2014**, *33*, 3425–3432.
- [38] A. C. Skapski, F. A. Stephens, *J. Chem. Soc. Dalton Trans.* **1974**, 390–395.
- [39] I. S. Kolomnikov, A. I. Gusev, G. G. Aleksandrov, T. S. Lobeeva, Y. T. Struchkov, M. E. Vol'pin, *J. Organomet. Chem.* **1973**, *59*, 349–351.
- [40] B. Cordero, V. Gómez, A. E. Platero-Prats, M. Revés, J. Echeverría, E. Cremades, F. Barragán, S. Alvarez, *Dalton Trans.* **2008**, 2832–2838.
- [41] Y. Zhang, B. S. Hanna, A. Dineen, P. G. Williard, W. H. Bernskoetter, *Organometallics* **2013**, *32*, 3969–3979.
- [42] T. Ito, K. Takahashi, N. Iwasawa, *Organometallics* **2018**, DOI 10.1021/acs.organomet.8b00789.
- [43] K. P. Kepp, *Inorg. Chem.* **2016**, *55*, 9461–9470.
- [44] A. Berkefeld, W. E. Piers, M. Parvez, *J. Am. Chem. Soc.* **2010**, *132*, 10660–10661.
- [45] F. J. Fernández-Alvarez, A. M. Aitani, L. A. Oro, *Catal. Sci. Technol.* **2014**, *4*, 611–624.
- [46] H. Koinuma, F. Kawakami, H. Kato, H. Hirai, *J. Chem. Soc. Chem. Commun.* **1981**, 213–214.
- [47] T. C. Eisenschmid, R. Eisenberg, *Organometallics* **1989**, *8*, 1822–1824.
- [48] P. G. Jessop, T. Ikariya, R. Noyori, *Chem. Rev.* **1999**, *99*, 475–494.
- [49] A. Jansen, H. Görls, S. Pitter, *Organometallics* **2000**, *19*, 135–138.
- [50] A. Jansen, S. Pitter, *J. Mol. Catal. Chem.* **2004**, *217*, 41–45.
- [51] P. G. Jessop, *Top. Catal.* **1998**, *5*, 95.
- [52] P. Deglmann, E. Ember, P. Hofmann, S. Pitter, O. Walter, *Chem. – Eur. J.* **2007**, *13*, 2864–2879.
- [53] R. Lalrempuia, M. Iglesias, V. Polo, P. J. Sanz Miguel, F. J. Fernández-Alvarez, J. J. Pérez-Torrente, L. A. Oro, *Angew. Chem. Int. Ed.* **2012**, *51*, 12824–12827.
- [54] S. Itagaki, K. Yamaguchi, N. Mizuno, *J. Mol. Catal. Chem.* **2013**, *366*, 347–352.
- [55] K. Motokura, D. Kashiwame, A. Miyaji, T. Baba, *Org. Lett.* **2012**, *14*, 2642–2645.
- [56] S. B. Duckett, R. N. Perutz, *Organometallics* **1992**, *11*, 90–98.
- [57] B. Marciniak, *Coord. Chem. Rev.* **2005**, *249*, 2374–2390.
- [58] “Organotransition Metal Chemistry: From Bonding to Catalysis, by John Hartwig with Contributions by Patrick J. Walsh, Geoffrey W. Coates, Charles P. Casey, Jack R. Norton, copyright 2010, published by University Science Books,” can be found under <http://www.uscibooks.com/hartwig.htm>, **n.d.**
- [59] H. Group, “Book,” can be found under <https://hartwig.cchem.berkeley.edu/book/>, **n.d.**
- [60] *Gelest Inc* **n.d.**
- [61] J. L. Speier, J. A. Webster, G. H. Barnes, *J. Am. Chem. Soc.* **1957**, *79*, 974–979.
- [62] J. L. Speier, in *Adv. Organomet. Chem.* (Eds.: F.G.A. Stone, R. West), Academic Press, **1979**, pp. 407–447.

- [63] B. Karstedt, *Platinum Complexes of Unsaturated Siloxanes and Platinum Containing Organopolysiloxanes*, **1973**, US3775452A.
- [64] F. de Charentenay, J. A. Osborn, G. Wilkinson, *J. Chem. Soc. Inorg. Phys. Theor.* **1968**, 787–790.
- [65] Y. Uozumi, T. Hayashi, *J. Am. Chem. Soc.* **1991**, *113*, 9887–9888.
- [66] K. Kitayama, Y. Uozumi, T. Hayashi, *J. Chem. Soc. Chem. Commun.* **1995**, 1533–1534.
- [67] T. Tuttle, D. Wang, W. Thiel, J. Köhler, M. Hofmann, J. Weis, *Organometallics* **2006**, *25*, 4504–4513.
- [68] Y. Maruyama, K. Yamamura, I. Nakayama, K. Yoshiuchi, F. Ozawa, *J. Am. Chem. Soc.* **1998**, *120*, 1421–1429.
- [69] J. Y. Corey, J. Braddock-Wilking, *Chem. Rev.* **1999**, *99*, 175–292.
- [70] J. Y. Corey, *Chem. Rev.* **2016**, *116*, 11291–11435.
- [71] Y. Seki, K. Takeshita, K. Kawamoto, S. Murai, N. Sonoda, *Angew. Chem. Int. Ed. Engl.* **1980**, *19*, 928–928.
- [72] M. L. Christ, S. Sabo-Etienne, B. Chaudret, *Organometallics* **1995**, *14*, 1082–1084.
- [73] W. Lu, C. Li, X. Wu, X. Xie, Z. Zhang, *Organometallics* **2020**, *39*, 3780–3788.
- [74] S. Lachaize, L. Vendier, S. Sabo-Etienne, *Dalton Trans.* **2010**, *39*, 8492–8500.
- [75] M. L. Lejkowski, R. Lindner, T. Kageyama, G. É. Bódizs, P. N. Plessow, I. B. Müller, A. Schäfer, F. Rominger, P. Hofmann, C. Futter, S. A. Schunk, M. Limbach, *Chem. – Eur. J.* **2012**, *18*, 14017–14025.
- [76] C. Bruckmeier, M. W. Lehenmeier, R. Reichardt, S. Vagin, B. Rieger, *Organometallics* **2010**, *29*, 2199–2202.
- [77] S. Y. T. Lee, M. Cokoja, M. Drees, Y. Li, J. Mink, W. A. Herrmann, F. E. Kühn, *ChemSusChem* **2011**, *4*, 1275–1279.
- [78] P. N. Plessow, L. Weigel, R. Lindner, A. Schäfer, F. Rominger, M. Limbach, P. Hofmann, *Organometallics* **2013**, *32*, 3327–3338.
- [79] S. Y. T. Lee, A. A. Ghani, V. D’Elia, M. Cokoja, W. A. Herrmann, J.-M. Basset, F. E. Kühn, *New J. Chem.* **2013**, *37*, 3512–3517.
- [80] D. Jin, P. G. Williard, N. Hazari, W. H. Bernskoetter, *Chem. – Eur. J.* **2014**, *20*, 3205–3211.
- [81] R. Fischer, J. Langer, A. Malassa, D. Walther, H. Görls, G. Vaughan, *Chem. Commun.* **2006**, 2510–2512.
- [82] M. Gaydou, T. Moragas, F. Juliá-Hernández, R. Martin, *J. Am. Chem. Soc.* **2017**, *139*, 12161–12164.
- [83] T. Mitsudome, S. Arita, H. Mori, T. Mizugaki, K. Jitsukawa, K. Kaneda, *Angew. Chem. Int. Ed.* **2008**, *47*, 7938–7940.
- [84] T. Mitsudome, A. Noujima, T. Mizugaki, K. Jitsukawa, K. Kaneda, *Chem. Commun.* **2009**, 5302–5304.

General conclusion and perspectives

Carbon dioxide conversion into value-added chemicals through C–C bond-forming reactions has gained considerable interest, as it might constitute a conceivable solution to gradually renounce to the use of fossil fuels in favour of more sustainable carbon resources. In the literature, particular attention has been devoted to the conversion of CO₂ into carboxylic acids, given their important role in the manufacture of various relevant compounds for the chemical industry. Unfortunately, the use of CO₂ as raw material in synthetic transformations has to withstand with its significant inertness. For decades, these features implied that heavily polarized and highly reactive organometallic co-reagents would be needed for converting CO₂ into carboxylic acid derivatives, associated to the co-production of significant amounts of wastes.

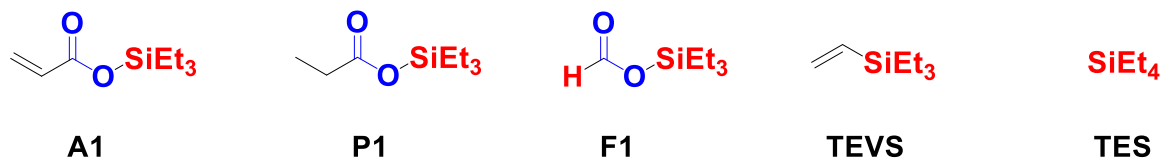
Through this work devoted to CO₂ valorisation and transformation, we sought at providing new synthetic methodology for producing carboxylic acid derivatives using CO₂, as an inexpensive and renewable feedstock.

In the first part of the manuscript, we brought together the studies and the major mechanistic hypotheses put forward, over the last three decades, aiming at finding catalytic CO₂ fixation techniques for the straightforward production of carboxylic acids. More specifically, we were interested in the discovery and elaboration of homogeneous catalytic processes for the efficient coupling of CO₂ with alkenes to form industrially relevant commodity and fine chemicals.

The preliminary studies carried out with our collaborators, experts in high-throughput screening (HTS) techniques (Argonne National Laboratory, IL, USA and Realcat platform of UCCS, Lille, France), have exploited around 150 different combinations of ligands and transition metal precursors across the Periodic Table, each tested individually in C₂H₄–CO₂ coupling using as reducing agent, the readily available and easy-to-handle, Et₃SiH. The highly tunable activity of hydrosilanes, by the substituents at the silicon atom, make them competitive reducing agents to organometallic hydrides, and they, indeed, appeared well-suited for preliminary investigations.

General conclusion

The two relevant silyl esters **A1** and **P1** have been unequivocally identified and quantified by GC and GC-MS analyses as significant products of some promising catalytic systems.



However, in the context of C_2H_4 - CO_2 coupling reaction in the presence of a reductant, the latter reagent can potentially be responsible for parasitic reactivities, by either reacting independently with C_2H_4 or CO_2 . Therefore, these first HTS results allowed us to sort the catalytic systems capable of producing **A1** and **P1** while attempting to avoid **F1**, **TEVS** and **TES** by-products. Among them, Ru based metal precursors, in combination with bidentate phosphine ligands, have shown propensity to afford, after optimization of the reaction conditions, the targeted silyl esters **A1** and **P1** in higher selectivities, reaching maximum TONs of 13 and 68, respectively. Ru monohydride complexes bearing DCPB and DCPF diphosphine ligands were found to be promising candidates for these studies, as they have demonstrated straightforward CO_2 insertion chemistry to yield the corresponding carboxylates silyl esters.

To further optimize these systems, we then sought at identifying the catalytically active Ru-species formed during the coupling of CO_2 and C_2H_4 , capable of delivering **A1** and **P1**. Acquiring detailed structural information about key intermediates and side-products would allow determining the actual operative catalytic mechanism and improve selectivities toward the silyl esters formation pathway.

Therefore, a significant part of this work has focused on the utilization of NMR techniques to understand the reactivity of the most promising $Ru(H)(Cl)(CO)(PPh_3)_3/DCPB$ (**Ru-1/DCPB**) system. The expected $Ru(H)(CO)(Cl)(DCPB)(PPh_3)$, obtained from the complexation reaction of the precursor and ligand, could not be selectively formed and other hydride compounds were detected by multinuclear NMR spectroscopy. By varying the metal-to-ligand ratio, proportion between the hydride species formed changed, evidencing that one couple of precursor/ligand might give rise to not only one, but several complexes, each probably initiating a different catalytic pathway or, at least, imparting its own selectivities towards the different products. We also realized that the presence of hydrosilane reductant can modify the nature of the species formed, by converting $Ru(H)(CO)(Cl)(DCPB)(PPh_3)$ into its dihydride

$\text{Ru}(\text{H})_2(\text{CO})(\text{DCPB})(\text{PPh}_3)$ congener. Gratifyingly, the latter turned out to be an efficient precursor towards **A1** and **P1** silyl esters formation. In future works, it could be interesting to explore further the reactivity of such $(\text{H})_2$ -complexes with CO_2 , since preliminary studies have shown that the latter does not lead to the formation of intermediate species similar to those observed with $\text{Ru}(\text{H})(\text{CO})(\text{Cl})(\text{DCPB})(\text{PPh}_3)$.

In fact, although various species might be involved in the catalytic coupling of CO_2 , C_2H_4 , Et_3SiH in the presence of $\text{Ru}(\text{H})(\text{Cl})(\text{CO})(\text{PPh}_3)_3/\text{DCPB}$, we were able to isolate and characterize the first example of $\kappa^2\text{-O,O}$ acrylate ruthenium complex ever reported; $\text{Ru}(\text{Cl})(\text{CO})(\text{DCPB})(\kappa^2\text{O,O-CO}_2\text{CH=CH}_2)$ (**Ru-6**). From 1D and 2D spectroscopic NMR data, a *cis* \leftrightarrow *trans* isomerization process for **Ru-6** was evidenced in solution. The presence of the acrylate fragment in both isomers certifies the effective oxidative coupling of CO_2 and C_2H_4 . Reactivity studies of **Ru-6** with Et_3SiH corroborated the successful release of the corresponding acrylic ester **A1**, providing therefore experimental evidence of the role of the Ru-acrylate species as a key intermediate towards **A1** formation.

The question of generating **Ru-6** from $\text{Ru}(\text{H})(\text{CO})(\text{Cl})(\text{DCPB})(\text{PPh}_3)$ remains however unsolved, since no experimental evidences have validated the proposed mechanisms towards its formation. Ongoing DFT calculations are in progress to obtain more detailed information on the nature of the structures of the complexes involved. In parallel, it would be pertinent to study the reactivity of the deuterated $\text{Ru}(\text{D})(\text{CO})(\text{Cl})(\text{DCPB})(\text{PPh}_3)$ complex in the coupling of CO_2 and C_2H_4 , in order to know the fate of the labelled D atom. Ideally, these investigations must be supported by ^2D NMR experiments and should include extensive chromatographic analyses of both the gas and liquid phase reaction mixtures, as potential gaseous deuterated compounds might be formed. Moreover, for a better understanding of the elementary steps involved in the catalytic cycle, ^{13}C isotopic labelling studies using $^{13}\text{CO}_2$ can help identifying additional CO_2 -derived products.

If these pending data help confirming the proposed mechanistic hypotheses, we could then consider varying the reaction conditions to improve the selectivities toward the formation of the targeted esters and hamper the abilities of the **Ru-1/DCPB** system to catalyse side processes. In fact, the most recent optimization studies showed that addition of H_2O to the one-pot catalytic mixture increased remarkably the production of **P1**, although it is still unclear how water interferes in the reaction mechanism of its formation.

General conclusion

These additional informations could also be helpful understanding and rationalizing the reasons behind the difference of reactivity observed in the early studies using different hydrosilanes (Ph_3SiH , $(\text{EtO})_3\text{SiH}$) and alkenes (styrene, hex-1-ene, cyclohexene).

In the longer term, it would be interesting to study the role of the coordination sphere of the Ru-center on the catalytic activity by varying either the nature of the X and/or L ligands or modifying the coordination number around the metal.

Through a multidisciplinary approach, involving several experimentations, spectroscopic and theoretical modeling techniques, this work has led, we hope, to a better understanding of Ru-based catalytic activation and conversion of CO_2 . Projects for CO_2 valorisation and utilisation, such as the one described in this manuscript, will hopefully continue to breed and complete each other, leading may be one day, to the development of efficient industrial processes using CO_2 as feedstock. Relying on renewable carbon resources could, in the most optimistic scenario, provide long-term solutions to the increasing accumulation of CO_2 in the atmosphere, but will certainly not solve, by itself, the climate crisis Earth is facing today.

Experimental section

Experimental section

Experimental section

Chapter 2 – Efficient catalytic systems toward carboxylation reaction of C ₂ H ₄ with CO ₂ : from discovery to optimization by means of High Throughput Experimentation.....	233
Generalities	233
• HTS experiments.....	233
• High pressure autoclave catalysis reaction.....	234
• GC analyses.....	234
• NMR.....	235
• Silylesters syntheses.....	235
Typical procedures.....	235
• HTS	235
• High pressure autoclave catalysis reaction.....	236
• Syntheses of silylesters.....	236
• Silyl esters retention coefficient determination for calibration	237
Chapter 3 – Catalytic CO ₂ -C ₂ H ₄ coupling mediated by ruthenium(II) complexes bearing bidentate chelating phosphines	242
Generalities	242
Typical procedures.....	242
• Syntheses of ligands	242
• High pressure autoclave catalysis reaction with additive.....	243
Chapter 4 – Mechanistic investigations on the ruthenium-catalyzed synthesis of silyl esters from C ₂ H ₄ and CO ₂	243
Generalities	243
• Crystal structure determination	244
Typical procedures.....	245
• Syntheses of new ruthenium(II) complexes	245
• Evaluation of thermal stability the (DCPB)Ru complexes.....	247
• Synthesis of [Ru(Cl)(CO)(DCPB)(CO ₂ CH=CH-κ ² -O,O)] complex (Ru-6).....	248
• Release of triethylsilylacrylate (A1) from Ru-6 and Ru-1 complex regeneration.....	248
• Synthesis of [Ru(Cl)(CO)(DCPB)(CO ₂ CH ₂ CH ₃ -κ ² -O,O)] complex (Ru-7).....	249
• Computational details.....	249
Annexes.....	254

Experimental section

The experimental part is divided into 3 sections corresponding respectively to chapter 2, 3 and 4 of the manuscript. All experimental procedures included in the manuscript's body text are described herein.

Chapter 2 – Efficient catalytic systems toward carboxylation reaction of C₂H₄ with CO₂: from discovery to optimization by means of High Throughput Experimentation

Generalities

- HTS experiments

Catalytic tests were carried out on the REALCAT platform (University of Lille, France) in a Screening Pressure Reactor system (SPR) from Unchained Labs (London, UK) equipped with 24 stainless steel 6 mL-vials/reactors for high-throughput screening (Figure S1). Temperature, pressure, and flow profiles were controlled automatically based on a user-defined recipe software.

All catalyst precursors and ligands were handled in a MB-Unilab PlusSP (MBraun) glove box for sample preparation under controlled atmosphere, unless otherwise stated. Solvents were purified over alumina columns using MBraun system (toluene) and degassed or dried over Mg. Starting materials were purchased from Alfa, Strem, Acros, Fluorochem or Aldrich, and used as received.

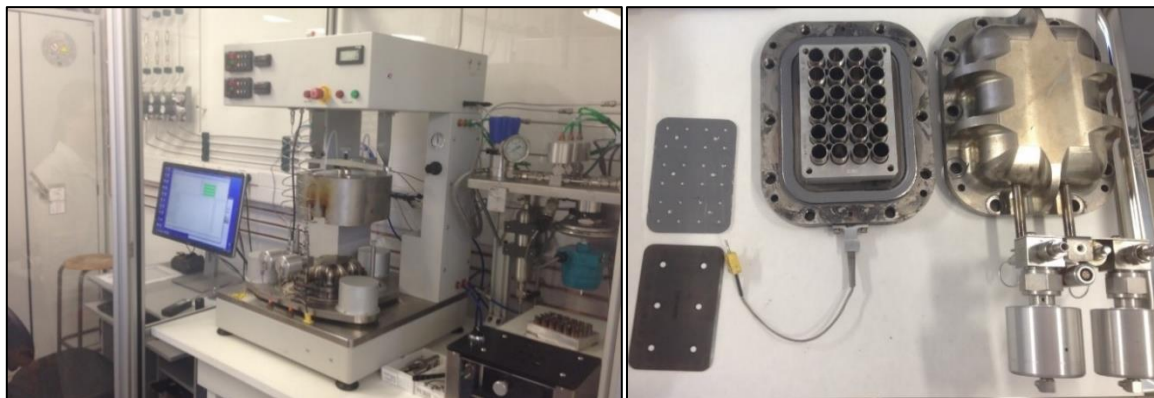


Figure S1. Screening Pressure Reactor (SPR) automated system (left) equipped with 24 stainless steel 6 mL-reactors (right).

- High pressure autoclave catalysis reaction

All manipulations were performed at the Organometallics: Materials and Catalysis laboratories, University of Rennes 1 (Institut des Sciences Chimiques de Rennes), under a purified Ar atmosphere using standard Schlenk techniques or in a glovebox. Solvents were distilled from Na/benzophenone (THF, Et₂O) and Na/K alloy (toluene, pentane) under argon, degassed thoroughly and stored under argon prior to use.

- GC analyses

A GC chromatograph (Shimadzu GC 2010 PLUS, Kyoto, Japan) equipped with a ZB-WAX Plus column (30 m × 0.25 mm × 0.25 μm) and a FID (flame ionization detector) was used to analyze the carboxylation reaction mixtures (temperature of injector: 250 °C, temperature of detector: 280 °C; temperature of column: 50 °C for 5 min then gradient of 6 °C.min⁻¹ until 280°C ; flow rate of helium: 22.1 mL.min⁻¹). GC-MS (Shimadzu QP 2014 SE gas chromatograph, Kyoto, Japan) equipped with a Supelco Equity-5 column (30 m × 0.25 mm × 0.25 μm) was used to ensure precision in the identification of the products. Preparation of the samples was follow:

Once the high pressure reactor was cooled down to room temperature and depressurized, 0.5 mL of a dodecane solution (0.09 M) was added to the crude mixture and stirred for 5 min, then submitted to GC-FID analysis. For GC-MS analysis, the mixture was first diluted in HPLC grade toluene (dilution factor of 15) then injected.

- NMR

NMR spectra were recorded on Bruker AV III 400 MHz and Bruker AV III HD 500 MHz spectrometers fitted with BBFO probes at 25 °C, unless otherwise stated. Chemical shifts are reported in ppm *vs* SiMe₄ using the residual solvent resonances. Assignment of resonances was made from 2D ¹H–¹H COSY, ¹H–¹³C HSQC and HMBC NMR experiments. Coupling constants are given in Hertz. The following abbreviations and their combinations are used: br, broad; s, singlet; d, doublet; t, triplet; q, quartet; m, multiplet. Deuterated solvents (benzene-*d*₆, toluene-*d*₈, THF-*d*₈; >99.5% D, Deutero GmbH and Eurisotop) were thoroughly dried by standard methods, distilled immediately before use and stored over 3/4 Å molecular sieves.

- Silylesters syntheses

Triethylsilyl formate (**F1**) was synthesized according to reported literature procedure.^[1] Hexaethyldisiloxane (**E**), tetraethylsilane (**TES**) and triethylvinylsilane (**TVS**) were purchased from Alfa or Aldrich, and used as received.

Typical procedures

- HTS

In a typical reductive carboxylation reaction, combinations of the precursors and ligands (1:1 ratio, 0.5 mol% *vs* hydrosilane) were placed in each reactor inside the glovebox. Next, Et₃SiH (0.86 mmol, 139 μL) was added by syringe followed by addition of dry and degassed toluene (2.0 mL). The reactors were then sealed and the catalytic tests were performed with a mixture of C₂H₄/CO₂ (molar ratio 1:1) set constant at 15-17 bar and at 100 °C for 16 h under vortex stirring (600 rpm). The reactors were then cooled to room temperature. After the run, the crude mixtures were taken out from the reactors, filtered through an Agilent 0.2 μm PTFE filter and analyzed by GC-FID and GC-MS.

GC sample preparation: in a glass vial were introduced 100 μL of crude mixture in 1.0 mL of HPLC grade toluene.

¹ J. Chen, L. Falivene, L. Caporaso, L. Cavallo, E. Y.-X. Chen, *J. Am. Chem. Soc.* **2016**, *138*, 5321–5333.

Experimental section

- High pressure autoclave catalysis reaction

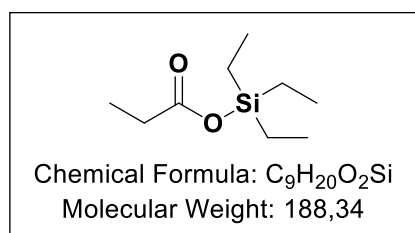
A 50 mL-stainless steel autoclave equipped with a magnetic stir bar was charged under argon with a solution of the desired metal precursor (0.043 mmol), ligand (0.043 mmol), and triethylsilane (8.6 mmol, 1.4 mL). Toluene (20 mL) was then introduced with syringe and the reactor was immediately pressurized with C₂H₄/CO₂ mixture (1:1 molar ratio) at the desired pressure (typically 20 bar). The reaction mixture was stirred (500 rpm) at the required temperature for 16 h using an oil bath. The reactor was then cooled down to room temperature, vented off and the reaction mixture was filtered through an Agilent 0.2 μm PTFE filter. The crude mixture was analyzed by both ¹H NMR spectroscopy (using (Me₃Si)₄Si as standard) and GC-FID (using *n*-dodecane as internal standard).

Samples preparation:

GC-FID and GC-MS: a standard solution of *n*-dodecane in HPLC grade toluene was prepared (C = 0.09 M) and 0.5 mL of the solution was added to the crude reaction mixture once the reactor was depressurized. After 5 min stirring, 100 μL of the mixture were added to 1.0 mL of HPLC grade toluene in a vial and injected for analysis.

NMR sample preparation: a standard solution of [(CH₃)₃Si]₄Si in CDCl₃ (C = 0.03 M) was prepared and 0.25 mL was added to 0.25 mL of the crude reaction mixture in a pre-heated NMR tube.

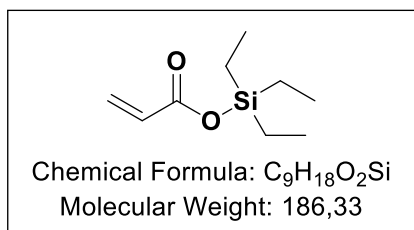
- Syntheses of silylesters



Synthesis of Triethylsilylpropionate (P1).

Chlorotriethylsilane (7.4 mL, 44 mmol) was slowly added to a solution of propionic acid (3.3 mL, 43 mmol) and pyridine (3.5 mL, 44 mmol) in CH₂Cl₂ (20 mL) at 0 °C. The resulting mixture was stirred at ambient temperature for 1 h before the reaction was quenched at 0 °C with saturated aqueous NaHCO₃ solution (40 mL). After the evolution of gas ceased, the aqueous layer was extracted with Et₂O (3 x 20 mL), the combined organic phases were successively washed with saturated aqueous NaHCO₃ solution NaHCO₃, dried over MgSO₄ and evaporated. The desired triethylsilyl propionate was obtained after distillation under reduced pressure (P = 8 mbar, T bath = 80 °C, T head column = 58 °C), as a colorless liquid (6.0 mL, 65 %). ¹H NMR (400 MHz, 25 °C, Chloroform-*d*₁): δ 2.34 (q, *J*_{H-H} = 7.5, 2H, CH₂CH₃), 1.11 (t, *J*_{H-H} = 7.5, 3H, CH₂CH₃), 0.97 (t, *J*_{H-H} = 8.3, 9H, Si-CH₂CH₃), 0.76 (qd, *J*_{H-H} = 7.8 and 1.1, 6H, Si-CH₂CH₃). ¹³C{¹H} NMR (101 MHz, 25 °C, Chloroform-*d*₁): δ

175.03 (C=O), 29.09 (CH₃CH₂), 9.34 (CH₃CH₂), 6.46 (Et), 4.51 (Et). **ESI-MS** (*m/z*): obsvd: 159 (C₇H₁₅O₂Si⁺, M⁺ – Et), calculated for C₉H₂₀O₂Si: 188.12.



Synthesis of Triethylsilylacrylate (A1).

Chlorotriethylsilane (7.4 mL, 43.8 mmol) was slowly added to a solution of acrylic acid (1.44 g, 44.0 mmol) and pyridine (3.5 mL, 44.0 mmol) in CH₂Cl₂ (20 mL) at 0 °C. The resulting mixture was stirred at ambient temperature for 1 h before the reaction was quenched at 0 °C with saturated aqueous NaHCO₃ solution (40 mL). After the evolution of gas ceased, the aqueous layer was extracted with Et₂O (3 x 20 mL), the combined organic phases were successively washed saturated aqueous NaHCO₃ solution, dried over MgSO₄ and evaporated. The desired triethylsilyl propionate was obtained after distillation under reduced pressure (P = 8 mbar, T bath = 80 °C, T head column = 58 °C), as a colorless liquid (4.7 mL, 52 %). **¹H NMR** (400 MHz, 25 °C, Chloroform-*d*₁): δ 6.34 (dd, *J*_{H-H} = 17.2 and 1.6, 1H, HC=CH₂), 6.08 (dd, *J*_{H-H} = 17.2 and 10.2, 1H, HC=CH₂), 5.81 (dd, *J*_{H-H} = 10.3 and 1.6, 1H, HC=CH₂), 1.00 (t, *J*_{H-H} = 1.0, 9H, Si-CH₂CH₃), 0.79 (qd, *J*_{H-H} = 7.7 and 1.2, 6H, Si-CH₂CH₃). **¹³C{¹H} NMR** (101 MHz, 25 °C, Chloroform-*d*₁): δ 166 (C=O), 130.85 (HC=CH₂), 130.18 (HC=CH₂), 6.79 (Et), 6.42 (Et). **ESI-MS** (*m/z*): obsvd: 157 (C₇H₁₃O₂Si⁺, M⁺ – Et), calculated for C₉H₂₀O₂Si: 186.11.

- Silyl esters retention coefficient determination for calibration

Linear correlations for each product were determined as follow :

$$\frac{m(\text{compound})}{m(\text{IS})} = k * \frac{A(\text{compound})}{A(\text{IS})}$$

Where m_{compound} = compound weight (mg)

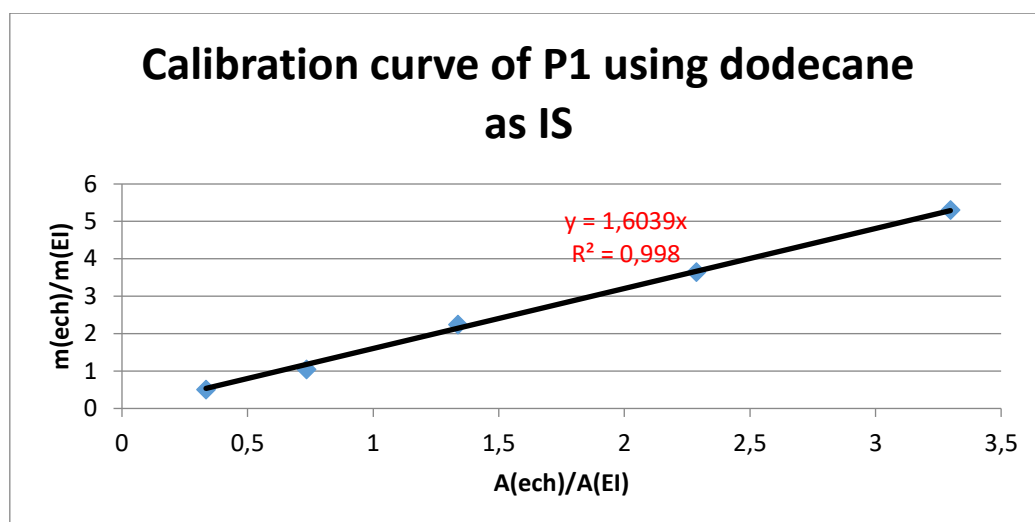
m_{IS} = internal standard (IS) weight (mg)

A_{compound} = pic area of the compound

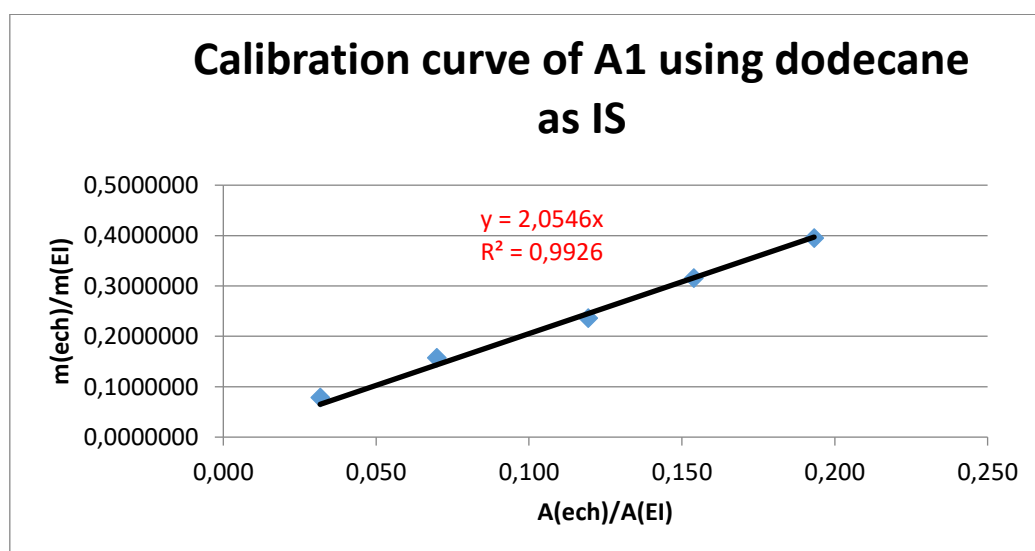
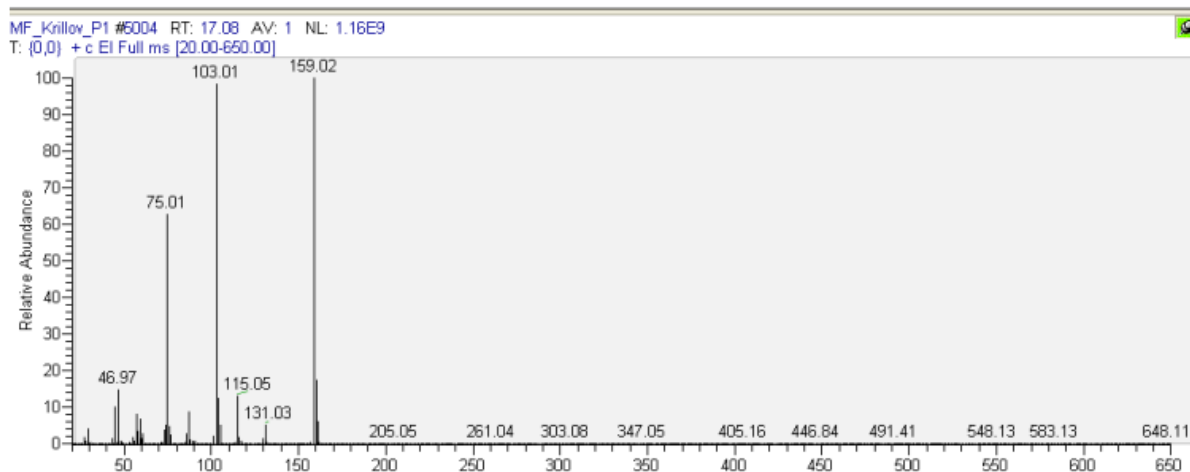
A_{IS} = pic area of the internal standard (IS)

k = retention coefficient

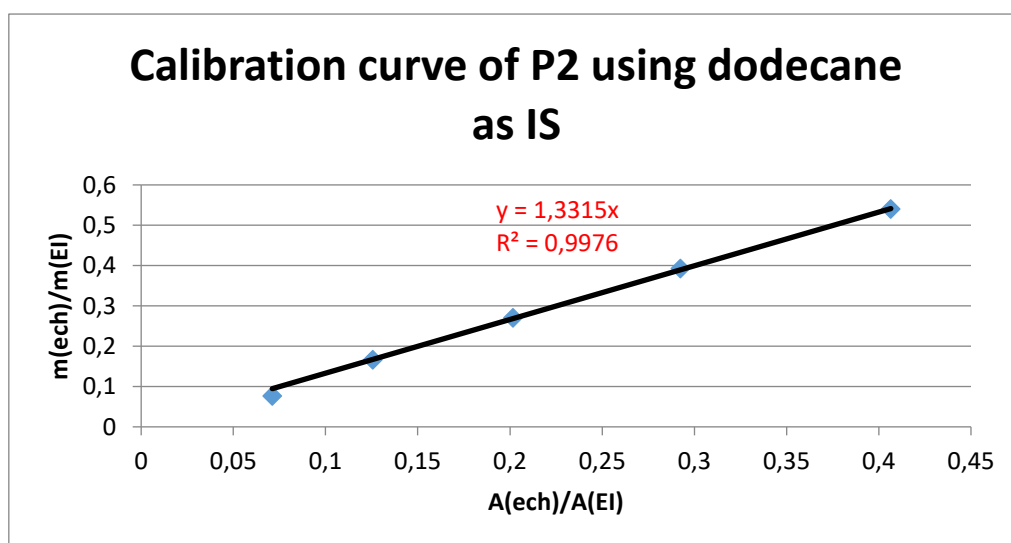
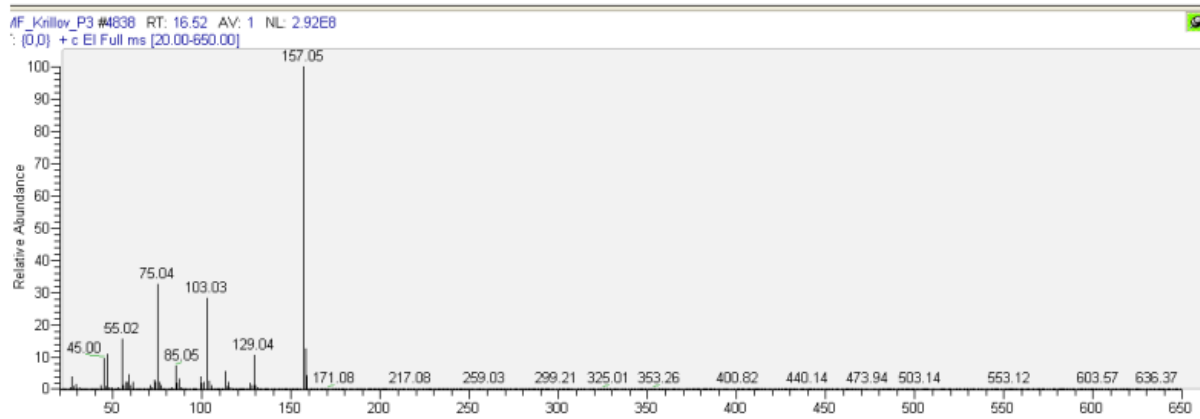
Experimental section



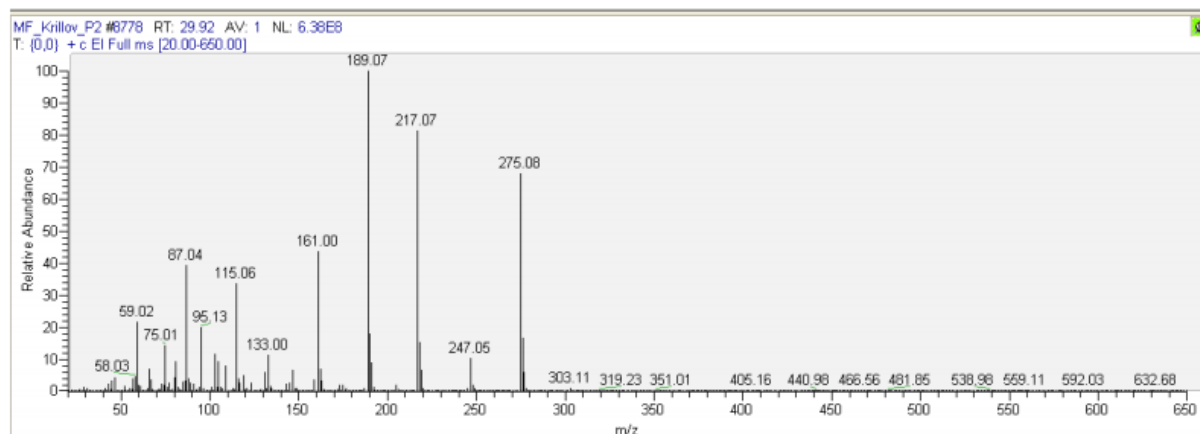
P1, $t_{R=}$ 10.6 min (GC-FID), $t_{R=}$ 11.402 min (GC-MS)



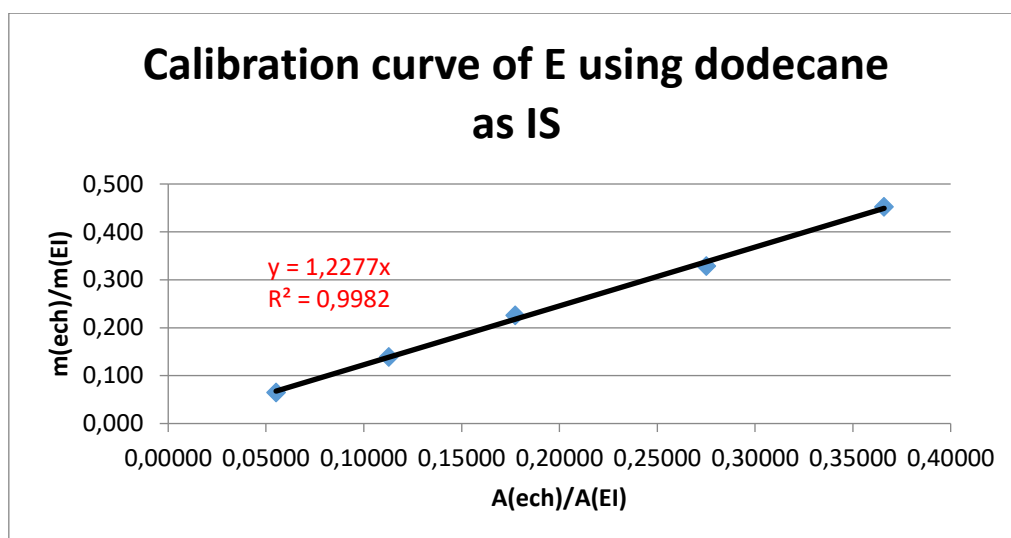
A1, $t_{R=}$ 10.4 min (GC-FID), $t_{R=}$ 11.199 min (GC-MS)



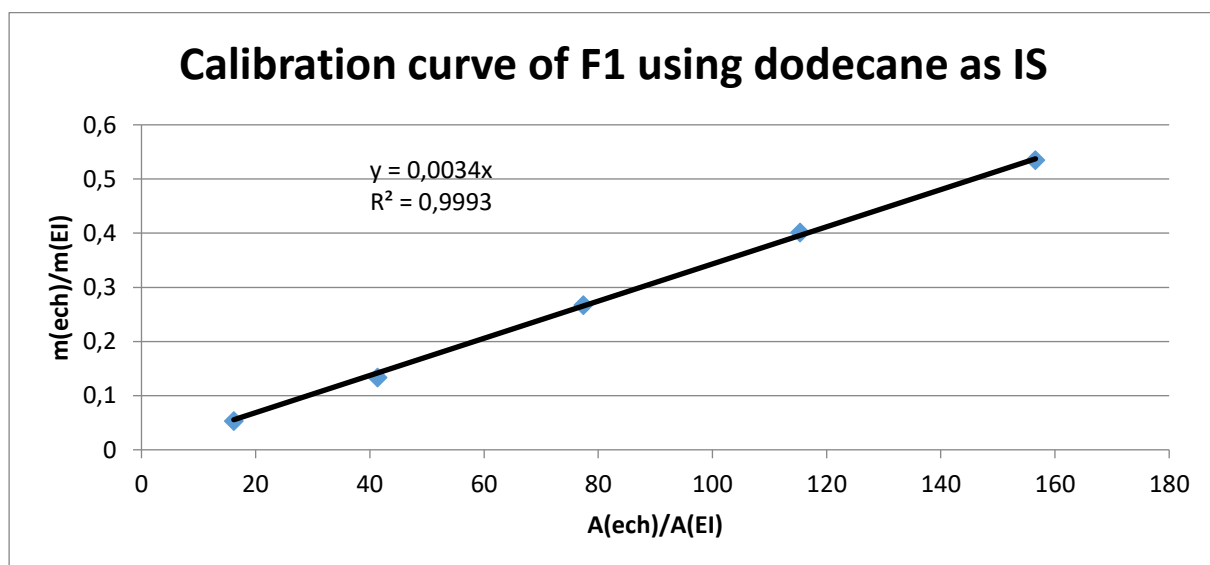
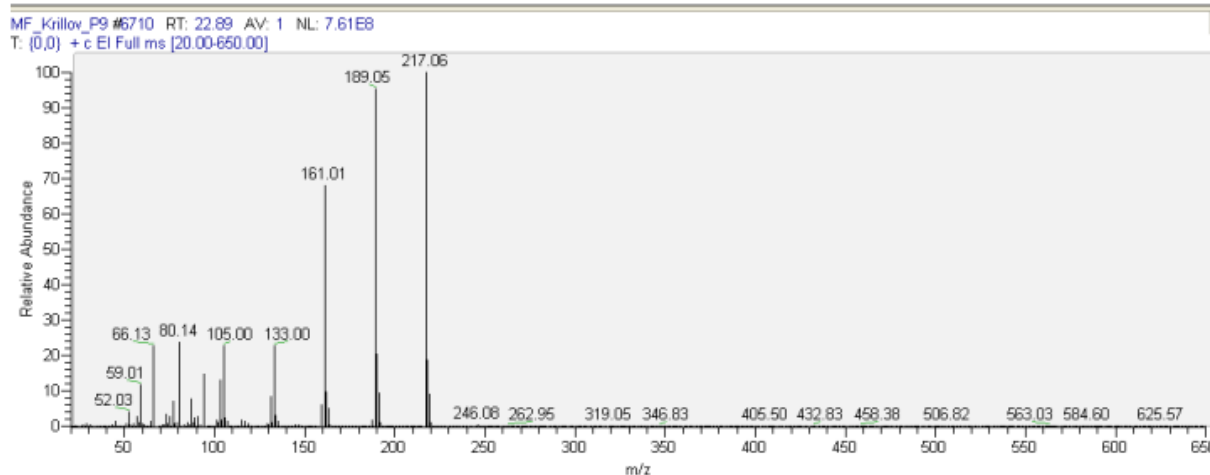
P2, $t_R = 22.417$ min (GC-FID), $t_R = 21.847$ min (GC-MS)



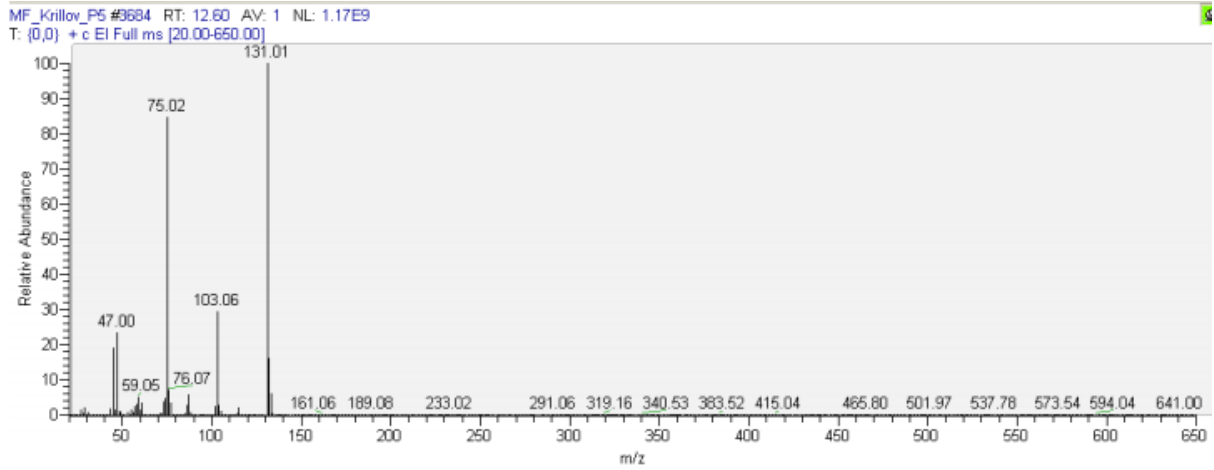
Experimental section



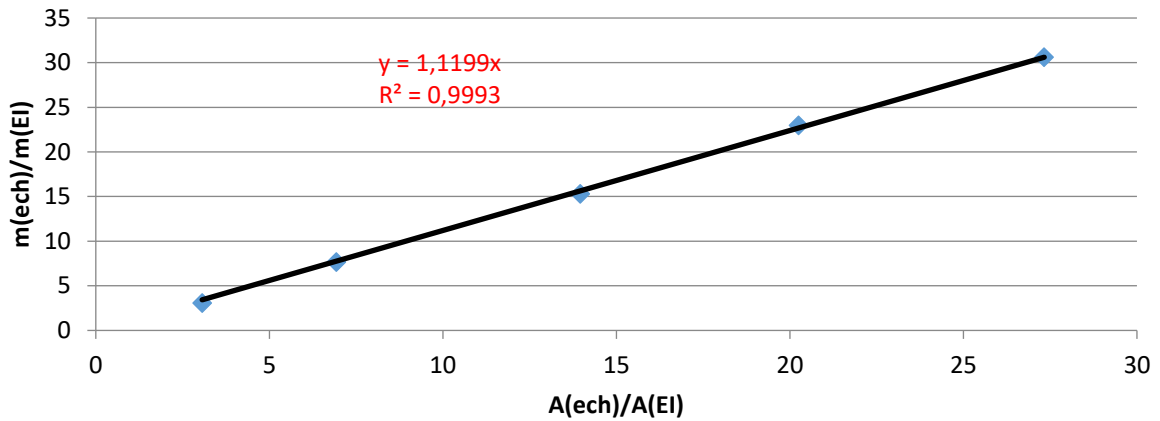
E, $t_{R} = 15.5$ min (GC-FID), $t_{R} = 14.2$ min (GC-MS)



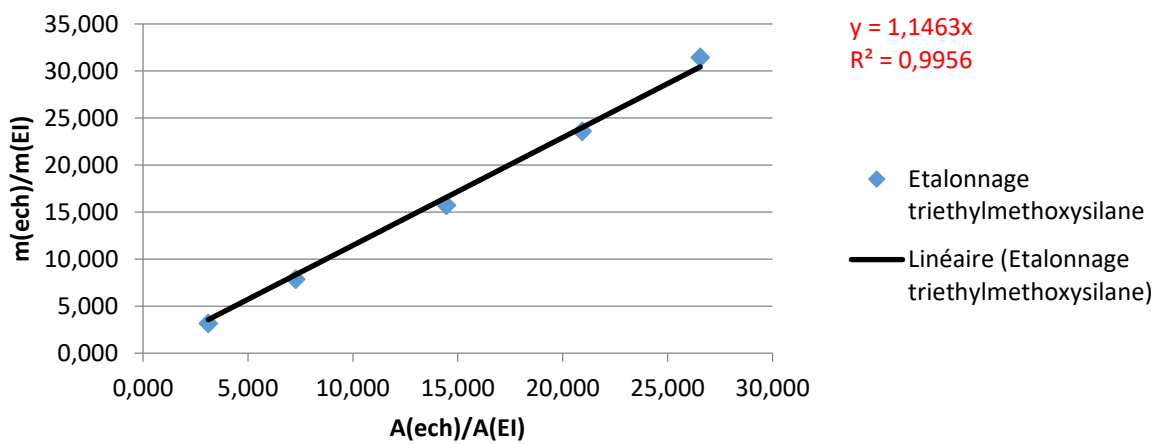
F1, $t_{R} = 7.4$ min (GC-FID), $t_{R} = 7.2$ min (GC-MS)



Calibration curve of TEVS using dodecane as IS



Calibration curve of TES using dodecane as IS



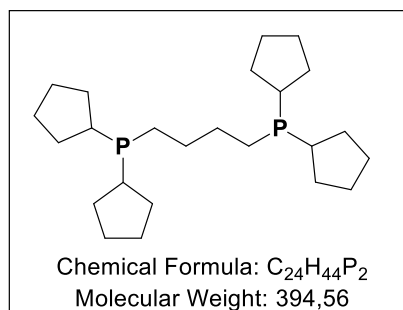
Chapter 3 – Catalytic CO₂-C₂H₄ coupling mediated by ruthenium(II) complexes bearing bidentate chelating phosphines

Generalities

The glassware, NMR tubes and autoclave reactors were dried at 120 °C before use. NMR spectra were recorded on Bruker AV III 400 MHz and Bruker AV III HD 500 MHz spectrometers fitted with BBFO probes at 25 °C, unless otherwise stated. Chemical shifts are reported in ppm vs SiMe₄ using the residual solvent resonances. Assignment of resonances was made from 2D ¹H-¹H COSY, ¹H-¹³C HSQC and ¹H-³¹P HMBC NMR experiments. Coupling constants are given in Hertz. The following abbreviations and their combinations are used: br, broad; s, singlet; d, doublet; t, triplet; q, quartet; m, multiplet. Deuterated solvents (benzene-*d*₆, toluene-*d*₈, THF-*d*₈; >99.5% D, Deutero GmbH and Eurisotop) were thoroughly dried by standard methods, distilled immediately before use and stored over 3/4 Å molecular sieves.

Typical procedures

- Syntheses of ligands



Synthesis of 1,4-bis(dicyclopentylphosphino)butane.

1,4-bis(dicyclopentylphosphino)butane was prepared using a similar literature procedure as that reported for the synthesis of 1,5-bis(dicyclohexylphosphino)pentane.^[2]

Preparation of [Cp₂PLi·(THF)]_∞.^[3]

To a solution of Cp₂PH (0.91 mL, 5.0 mmol) in THF (40 mL) was added *n*-BuLi (2.03 mL of 2.5 M solution in hexanes, 5.08 mmol). After the stirring for 1 h at room temperature, the solvent was removed under vacuum. The product was obtained as a yellow powder. Next, a Schlenk flask was charged with [Cp₂PLi·(THF)]_∞ (1.38 g, 5.0 mmol) and suspended in dry 1,4-dioxane (15 mL) at room temperature. Then, 1,4-dibromobutane (0.3 mL, 2.5 mmol) was added dropwise via syringe, promptly producing a colourless solution. The solution was stirred at room temperature for 2 h yielding a white suspension. The resulting suspension was filtered via cannula and 1,4-dioxane was removed in vacuo to give a colourless solid. This residue was dissolved in dry ethanol (15 mL) upon warming up to 40 °C. 1,4-

² A. J. Martínez-Martínez, B. E. Tegner, A. I. McKay, A. J. Bukvic, N. H. Rees, G. J. Tizzard, S. J. Coles, M. R. Warren, S. A. Macgregor, A. S. Weller, *J. Am. Chem. Soc.* **2018**, *140*, 14958–14970.

³ R. A. Bartlett, M. M. Olmstead, P. P. Power, *Inorg. Chem.* **1986**, *25*, 1243–1247.

bis(dicyclopentylphosphino)butane was obtained as a colorless crystalline solid by storing the resulting solution at 277 K for 24 h (641 mg, 1.63 mmol, 65%). $^1\text{H NMR}$ (400 MHz, Toluene- d_8): δ 1.90 – 1.39 (m, 44H). $^{31}\text{P}\{^1\text{H}\}$ NMR (162 MHz, Toluene- d_8) δ -5.75. $^{13}\text{C}\{^1\text{H}\}$ NMR (101 MHz, Toluene- d_8): 36.64 (d, $J = 13.4$), 31.19 (d, $J = 17.7$), 30.40 (d, $J = 13.8$), 28.98 (dd, $J = 13.8, 9.7$), 26.43 (d, $J = 7.2$), 26.09 (d, $J = 6.3$), 25.11 (d, $J = 17.3$). **ESI-MS** (m/z): obsvd: 395.2992 (M^+), calculated for ($\text{C}_{24}\text{H}_{45}\text{P}_2$): 395.2991.

- High pressure autoclave catalysis reaction with additive

In a typical high pressure reaction with H_2O , a 50 mL-stainless steel autoclave equipped with a magnetic stir bar was charged under argon with a solution of the desired metal precursor (0.043 mmol), ligand (0.043 mmol), and triethylsilane (8.6 mmol, 1.4 mL). Next, deionized and degassed water (3.4 mmol, 31 μL) were introduced followed by toluene (20 mL). The reactor was then immediately pressurized with $\text{C}_2\text{H}_4/\text{CO}_2$ mixture (1:1 molar ratio) at the desired pressure (typically 20 bar). The reaction mixture was stirred (500 rpm) at the required temperature for 16 h. The reactor was then cooled down to room temperature, vented off and the reaction mixture was filtered through an Agilent 0.2 μm PTFE filter. The crude mixture was analyzed by both $^1\text{H NMR}$ spectroscopy (using $(\text{Me}_3\text{Si})_4\text{Si}$ as standard) and GC-FID (using *n*-dodecane as internal standard).

Chapter 4 – Mechanistic investigations on the ruthenium-catalyzed synthesis of silyl esters from C_2H_4 and CO_2

Generalities

All samples were prepared at 25 °C in a Jacomex glove box under an inert argon atmosphere, and under vacuum / argon ramp using Schlenk techniques.

NMR tubes equipped with J. Young valves were used for all NMR experiments. The glassware, NMR tubes and autoclave reactors were dried at 120 °C before use. Solvents were distilled from Na/benzophenone (THF, Et_2O) and Na/K alloy (toluene, pentane) under argon, degassed thoroughly and stored under argon prior to use. Deuterated solvents (benzene- d_6 , toluene- d_8 , THF- d_8 ; >99.5% D, Deutero GmbH and Eurisotop) were thoroughly dried by standard methods, distilled immediately before use and stored over 3/4 Å molecular sieves.

Experimental section

Starting materials were purchased from Alfa, Strem, Acros, Fluorochem or Aldrich, and used as received. $(\text{PPh}_3)_3\text{Ru}(\text{H})_2\text{CO}$ and $\text{Ru}(\text{H})(\text{Cl})(\text{CO})(\text{PPh}_3)(\text{DPPF})$ were synthesized according to a reported procedure,^[4,5] as well as deuterated triethylsilane (Et_3SiD).^[6]

NMR spectra were recorded on Bruker AV III 400 MHz and Bruker AV III HD 500 MHz spectrometers fitted with BBFO probes at 25 °C, unless otherwise stated. Chemical shifts are reported in ppm vs SiMe_4 using the residual solvent resonances. Assignment of resonances was made from 2D ^1H - ^1H COSY, ^1H - ^{13}C HSQC and ^1H - ^{31}P HMBC NMR experiments. Coupling constants are given in Hertz. The following abbreviations and their combinations are used: br, broad; s, singlet; d, doublet; t, triplet; q, quartet; m, multiplet.

- Crystal structure determination

Diffraction data were collected at 100 K using a Bruker APEX CCD diffractometer with graphite-monochromatized $\text{MoK}\alpha$ radiation ($\lambda = 0.71073 \text{ \AA}$). A combination of ω and θ scans was carried out to obtain a unique data set. The crystal structures were solved by direct methods, remaining atoms were located from difference Fourier synthesis followed by full-matrix least-squares refinement based on F2 (programs SIR97 and SHELXL-97).^[7] Many hydrogen atoms could be located from the Fourier difference analysis. Other hydrogen atoms were placed at calculated positions and forced to ride on the attached atom. The hydrogen atom positions were calculated but not refined. All non-hydrogen atoms were refined with anisotropic displacement parameters. Crystal data and details of data collection and structure refinement for the compounds are given in Table S1. Crystal data, details of data collection and structure refinement for all compounds (CCDC 2017569 and 2017570, respectively) can be obtained from the Cambridge Crystallographic Data Centre via www.ccdc.cam.ac.uk/data_request/cif.

⁴ H. Samouei, V. V. Grushin, *Organometallics* **2013**, *32*, 4440–4443.

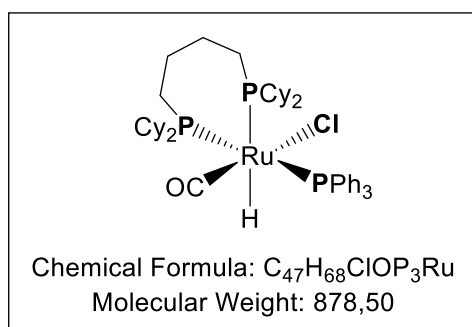
⁵ A. Santos, J. Lopez, J. Montoya, P. Noheda, A. Romero, A. M. Echavarren, *Organometallics* **1994**, *13*, 3605–3615.

⁶ P.-W. Long, T. He, M. Oestreich, *Org. Lett.* **2020**, *22*, 7383–7386.

⁷ (a) G. M. Sheldrick, SHELXS-97, Program for the Determination of Crystal Structures, University of Goettingen (Germany), **1997**; (b) G. M. Sheldrick, SHELXL-97, Program for the Refinement of Crystal Structures, University of Goettingen (Germany), **1997**. (c) Sheldrick, G. M. *Acta. Cryst.* **2008**, *A64*, 112–122.

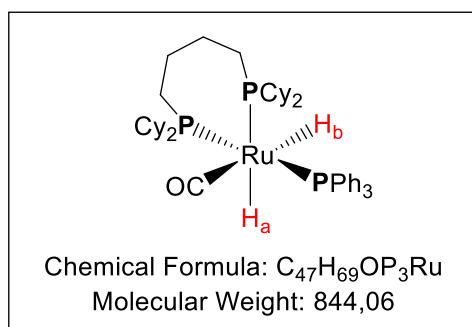
Typical procedures

- Syntheses of new ruthenium(II) complexes



Synthesis of $Ru(H)(Cl)(CO)(Cy_2P-(CH_2)_4-PCy_2)(PPh_3)$. A mixture of $Ru(H)(Cl)(CO)(PPh_3)_3$ (466 mg, 0.49 mmol) and DCPB (220 mg, 0.49 mmol) in toluene (30 mL) was refluxed for 1 h. The solvent was then removed under vacuum. Hexanes (30 mL) were added and the mixture was stirred for 30 min. The solution was filtered in order to remove the unreacted

$Ru(H)(Cl)(CO)(PPh_3)_3$ and PPh_3 . Volatiles were stripped under vacuum to leave an oily brown residue. Methanol (30 mL) was added to the residue and the mixture was stirred for 3 h to give a pinkish precipitate. The solid was filtered under argon, washed with methanol (2×20 mL) and dried under vacuum (90 mg, 0.10 mmol, 21%, mixture of two hydride species in a 1:0.4 ratio). X-ray quality crystals of $Ru(H)(Cl)(CO)(DCPB)(PPh_3)$ were obtained from a concentrated toluene solution by slow evaporation at room temperature. **1H NMR** (400 MHz, 25 °C, Toluene- d_8): δ 8.05 (m, 5H, $P(C_6H_5)_3$), 7.11–7.03 (m, 10H, $P(C_6H_5)_3$), 2.71–0.84 (m, $(C_6H_{11})_2P-C_4H_8-P(C_6H_{11})_2$, overlap with residual solvent signals), -7.16 (dt, $^2J_{P-H trans} = 103.9$ and $^2J_{P-H cis} = 24.3$, 1H, $Ru-H$). **$^{31}P\{^1H\}$ NMR** (162 MHz, 25 °C, Toluene- d_8): δ 34.9 (d, $^2J_{P-P cis} = 14.2$, 2P, $Ru-P_{cis}Cy_2$ and $Ru-P_{cis}Ph_3$), 18.6 (t, $^2J_{P-P cis} = 14.7$, 1P, $Ru-P_{trans}Cy_2$). **$^{31}P\{^1H\}$ NMR** (202 MHz, 32 °C, Toluene- d_8): δ 35.2 (d, $^2J_{P-P cis} = 13.82$, 1P, $Ru-P_{cis}Ph_3$), δ 34.9 (d, $^2J_{P-P cis} = 15.79$, 1P, $Ru-P_{cis}Cy_2$), 18.4 (t, $^2J_{P-P cis} = 14.95$, 1P, $Ru-P_{trans}Cy_2$). **$^{13}C\{^1H\}$ NMR** (126 MHz, 77 °C, Toluene- d_8) δ 204.62 ($C\equiv O$), 135.21, 134.30, 128.86, 127.80, 30.19, 29.03, 28.12, 26.74, 24.95, 23.11. **APPI-MS** (m/z): obsvd: 877.3331 ($[Ru]^+$), calculated for $C_{47}H_{68}ClOP_3Ru$: 878.3215.

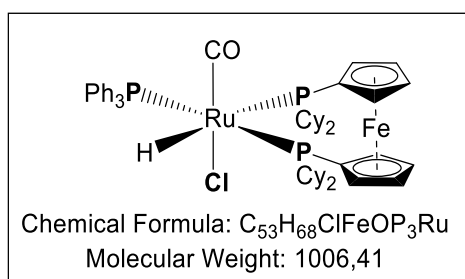


Synthesis of $Ru(H)_2(CO)(DCPB)(PPh_3)$. A mixture of $(PPh_3)_3Ru(H)_2CO$ (1.0 g, 1.1 mmol) and $Cy_2P(CH_2)_4PCy_2$ (0.49 g, 1.1 mmol) in Toluene (30 ml) was refluxed for 1 h. The solvent was removed completely under vacuum. Fifty millilitres of hexane was added and the mixture was stirred for 30 min. The solution was filtered through a filtration cannula to remove the unreacted $RuHCl(CO)(PPh_3)_3$.

The solvent was removed under vacuum to give an oily residue. Methanol (50 ml) was added

Experimental section

to the residue and the mixture was stirred for 3 h to give a white-pink precipitate. The white solid was collected on a filter frit and washed with methanol and dried under vacuum. $^1\text{H NMR}$ (400 MHz, 25 °C, Toluene- d_8) δ 7.99 (m, 5H, $\text{P}(\text{C}_6\text{H}_5)_3$), 7.22 – 7.12 (m, 6H, $\text{P}(\text{C}_6\text{H}_5)_3$), 7.11 – 7.04 (m, 3H, $\text{P}(\text{C}_6\text{H}_5)_3$), 2.50 – 0.64 (m, 54H, $(\text{C}_6\text{H}_{11})_2\text{P}-\text{C}_4\text{H}_8-\text{P}(\text{C}_6\text{H}_{11})_2$), -8.17 (dtd, Ru–H_b, $^2J_{\text{P-Hb cis}} = 28.0$, 21.6, $^2J_{\text{Ha-Hb cis}} = 6.0$ Hz), -9.39 (dddd, Ru–H_a, $^2J_{\text{P-Ha trans}} = 69.6$, $^2J_{\text{P-Ha cis}} = 32.0$, 26.4, $^2J_{\text{Ha-Hb cis}} = 5.9$ Hz, 1H). $^{31}\text{P}\{^1\text{H}\}$ NMR (162 MHz, 25 °C, Toluene- d_8): δ 62.27 (dd, $^2J_{\text{P-P trans}} = 219$, 13.9, Ru– PPh_3), 53.28 (q, $^2J_{\text{P-P cis}} = 16$, 14.2, Ru– PCy_2), 48.96 (dd, $^2J_{\text{P-P trans}} = 219$, 16.6, Ru– PCy_2). $^{13}\text{C}\{^1\text{H}\}$ NMR (101 MHz, toluene- d_8) δ 208.67 (C \equiv O), 141.83 (d, $^1J_{\text{P-C}} = 36.1$ Hz), 134.79 (d, $J = 11.7$ Hz), 127.59, 41.35 (d, $^1J_{\text{P-C}} = 31.0$ Hz), 30.66, 30.07, 29.72, 25.73, 23.64 (d, $^1J_{\text{P-C}} = 5.3$ Hz). **ESI-MS** (m/z): obsvd: 843.3526 ($[\text{Ru}]^+$), calculated for ($\text{C}_{47}\text{H}_{69}\text{OP}_3\text{Ru}$): 843.35266.



Synthesis of $\text{Ru}(\text{H})(\text{Cl})(\text{CO})(\text{DCPF})(\text{PPh}_3)$. Using a protocol similar to that described above for $\text{Ru}(\text{H})(\text{Cl})(\text{CO})(\text{DCPB})(\text{PPh}_3)$, $\text{Ru}(\text{H})(\text{Cl})(\text{CO})(\text{DCPF})(\text{PPh}_3)$ was prepared from $\text{Ru}(\text{H})(\text{Cl})(\text{CO})(\text{PPh}_3)_3$ (492 mg, 0.52 mmol) and DCPF (303 mg, 0.52 mmol). The resulting yellow solid was

collected on a filter frit and washed with methanol (25 mL) and dried under vacuum (90 mg, 0.09 mmol, 17 %). X-ray quality crystals of $\text{Ru}(\text{H})(\text{Cl})(\text{CO})(\text{DCPF})(\text{PPh}_3)$ were obtained from a concentrated toluene solution by slow evaporation at room temperature. $^1\text{H NMR}$ (400 MHz, 25 °C, Toluene- d_8): δ 7.90–7.77 (m, 5H, $\text{P}(\text{C}_6\text{H}_5)_3$), 7.63–6.98 (m, 10H, $\text{P}(\text{C}_6\text{H}_5)_3$), 4.73–2.42 (m, 10H, $\text{Fe}(\text{C}_5\text{H}_8)_2$), 2.29–0.38 (m, 46H, $(\text{C}_6\text{H}_{11})_2\text{P}-\text{Fe}(\text{C}_5\text{H}_8)_2-\text{P}(\text{C}_6\text{H}_{11})_2$), -7.85 (dt, $^2J_{\text{P-H trans}} = 101.9$ and $^2J_{\text{P-H cis}} = 26.7$, 1H, Ru–H). $^{31}\text{P}\{^1\text{H}\}$ NMR (162 MHz, 25 °C, Toluene- d_8): 48.50 (dd, $^2J_{\text{P-P trans}} = 295.5$ and $^2J_{\text{P-P cis}} = 17.0$, 1P, Ru– $\text{P}_{\text{cis}}\text{Ph}_3$), 35.92 (d, $^2J_{\text{P-P trans}} = 296.1$, 1P, Ru– $\text{P}_{\text{cis}}\text{Cy}_2$), 12.44–11.40 (m, 1P, Ru– $\text{P}_{\text{trans}}\text{Cy}_2$). $^{13}\text{C}\{^1\text{H}\}$ NMR (126 MHz, 25 °C, toluene- d_8): δ 202.74 (C \equiv O), 134.6, 133.7, 128.8, 127.4, 75.9, 74.9, 74.1, 72.4, 70.2, 69.9, 69.6, 68.2, 41.9, 39.4, 36.6, 36.1, 32.8, 31.8, 30.5, 29.5, 28.6, 28.4, 28.13, 27.8, 27.7, 27.4, 27.1, 26.8, 26.2. **ESI-MS** (m/z): obsvd: 1005.5482 ($[\text{Ru}\cdot\text{H}]^+$), calculated for ($\text{C}_{53}\text{H}_{68}\text{ClFeOP}_3\text{Ru}$): 1006.41.

Table S1. Summary of Crystal and Refinement Data for Ru(H)(Cl)(CO)(DCPF)(PPh₃) (**Ru-2**) and Ru(H)(Cl)(CO)(DCPB)(PPh₃) (**Ru-3**)

	Ru-2	Ru-3
Empirical formula	C ₆₀ H ₇₅ ClFeOP ₃ Ru	C ₄₇ H ₆₈ ClOP ₃ Ru
Formula weight	1097.48 g/mol	878.44 g/mol
Temperature, K	150(2) K	150(2) K
Wavelength, Å	0.71073 Å	0.71073 Å
Crystal system	triclinic	orthorhombic
Space group	<i>P</i> -1	<i>P</i> 2 ₁ 2 ₁ 2 ₁
a, Å	12.4039(9) Å	13.7530(16) Å
b, Å	15.7021(12) Å	14.6594(17) Å
c, Å	16.1327(13) Å	21.801(3) Å
β, deg	83.168(3) °	90 °
Volume, Å ³	2967.5(4) Å ³	4395.4(9) Å ³
Z	2	4
Density (calc.), g/cm ³	1.228 g.cm ⁻³	1.327
Absorption coefficient, mm ⁻¹	0.661 mm ⁻¹	0.561
Crystal size, mm ³	0.600 x 0.590 x 0.380 mm	0.400 x 0.240 x 0.180 mm
Reflections collected	68135	73494
Independent reflections	13538 [^a R(int) = 0.0496]	10109 [^a R(int) = 0.0376]
Max. and min. transmission	0.778, 0.647	0.904, 0.823
Data / restraints / parameters	13538 / 0 / 635	10109 / 0 / 481
Final R indices [I>2σ(I)]	^c R ₁ = 0.0342, ^d wR ₂ = 0.0755	^c R ₁ = 0.0274, ^d wR ₂ = 0.0606
R indices (all data)	^c R ₁ = 0.0453, ^d wR ₂ = 0.0825	^c R ₁ = 0.0307, ^d wR ₂ = 0.0633
^b Goodness-of-fit on F ²	1.073	1.142
Largest diff. peak, e.Å ⁻³	0.783, -0.828	0.720, -0.513

$$^a R(\text{int}) = \frac{\sum |F_o^2 - \langle F_o^2 \rangle|}{\sum F_o^2}$$

$$^c R_1 = \frac{\sum ||F_o| - |F_c||}{\sum |F_o|}$$

$$^d wR_2 = \left\{ \frac{\sum [w(F_o^2 - F_c^2)^2]}{\sum [w(F_o^2)^2]} \right\}^{1/2}$$

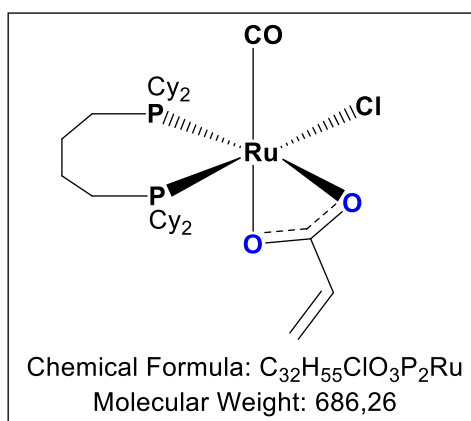
$$w = 1. / [\sigma(F_o^2) + (aP)^2 + bP] \text{ with } P = [2F_c^2 + \text{Max}(F_o^2, 0)] = 3$$

- Evaluation of thermal stability the (DCPB)Ru complexes

In a typical a J. Young NMR tube was introduced the Ru precursor (0.043 mmol) and the ligand (0.043 mmol) and dissolved in deuterated toluene (0.5 mL). The Ar atmosphere was replaced by 1 atm

Experimental section

- Synthesis of $[\text{Ru}(\text{Cl})(\text{CO})(\text{DCPB})(\text{CO}_2\text{CH}=\text{CH}-\kappa^2-O,O)]$ complex (**Ru-6**)



A 50 mL-stainless steel autoclave equipped with a magnetic stir bar was charged under argon with $\text{Ru}(\text{H})(\text{Cl})(\text{CO})(\text{PPh}_3)_3$ (0.043 mmol, 41 mg), DCPB ligand (0.043 mmol, 20 mg), and dry toluene (20 mL). The reactor was immediately pressurized with a $\text{C}_2\text{H}_4/\text{CO}_2$ mixture (1:1 molar ratio) of 20 bar. The reaction mixture was stirred (500 rpm) at 100 °C for 16 h. The autoclave was then cooled down to room

temperature, depressurized and the reaction mixture transferred into a Schlenk flask under argon. The solvent was then removed *in vacuo* and the crude mixture was treated with heptane (5-10 mL) and stirred for 1 h to precipitate the generated PPh_3 . Cannula filtration allowed to recover the liquid phase which was concentrated to give X-ray quality crystals of $[\text{Ru}(\text{Cl})(\text{CO})(\text{DCPB})(\text{CO}_2\text{CH}=\text{CH}-\kappa^2-O,O)]$. **^1H NMR for *cis*-Ru-6** (500 MHz, 25 °C, Toluene- d_8): δ 6.23 (dd, $^2J_{\text{H-H trans, gem}} = 17.4, 2.2$ Hz, 1H), 5.89 (dd, $^2J_{\text{H-H trans, cis}} = 17.4, 10.5$ Hz, 1H), 5.17 (dd, $^2J_{\text{H-H cis, gem}} = 10.5, 2.3$ Hz, 1H), 2.02 – 0.81 (m, 52H, $(\text{C}_6\text{H}_{11})_2\text{P}-\text{C}_4\text{H}_8-\text{P}(\text{C}_6\text{H}_{11})_2$). **$^{31}\text{P}\{^1\text{H}\}$ NMR** (202 MHz, Toluene- d_8) δ 59.98 (d, $^2J_{\text{P-P cis}} = 22.8$ Hz), 39.17 (d, $^2J_{\text{P-P cis}} = 23.4$ Hz). **$^{13}\text{C}\{^1\text{H}\}$ NMR** (126 MHz, 25 °C, Toluene- d_8): δ 198.84 (C \equiv O), 181.95 (C=O), 132.39, 126.61, 40.83, 30.33, 29.98, 29.71, 26.36, 23.52. **ESI-MS** (m/z): obsvd: 651.2670 ($[\text{Ru}-\text{Cl}]^+$), calculated for $(\text{C}_{32}\text{H}_{55}\text{ClO}_3\text{P}_2\text{Ru})$: 686.26.

- Release of triethylsilylacrylate (**A1**) from **Ru-6** and **Ru-1** complex regeneration

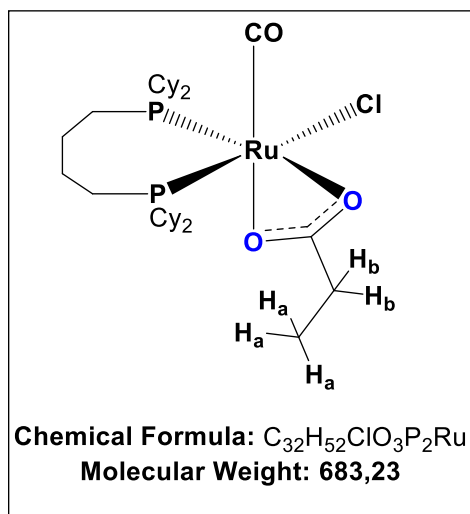
Using Et_3SiH :

Ru-6 complex generated above was introduced in a J. Young NMR tube and dissolved in toluene- d_8 (0.5 mL). Et_3SiH (0.043 mmol, 6.9 μL) and $(\text{Me}_3\text{Si})_4\text{Si}$ (0.0120 mmol) were then added to the solution and the tube was immediately sealed, introduced into the spectrometer for monitoring, and heated progressively to 100 °C.

Using MeOH:

Reaction of **Ru-6** with MeOH (0.129 mmol, 5.2 μL) was performed using the same procedure.

- Synthesis of $[\text{Ru}(\text{Cl})(\text{CO})(\text{DCPB})(\text{CO}_2\text{CH}_2\text{CH}_3\text{-}\kappa^2\text{-O,O})]$ complex (**Ru-7**)



A 50 mL-stainless steel autoclave equipped with a magnetic stir bar was charged under argon with **Ru-6** (0.043 mmol) and dry toluene (20 mL). The reactor was immediately pressurized with H_2 (15-30 bar). The reaction mixture was stirred (500 rpm) at 100 °C for 16 h. The autoclave was then cooled down to room temperature, depressurized and the reaction mixture transferred into a Schlenk flask under argon. The solvent was then removed *in vacuo* and the crude mixture was treated with heptane (5-10 mL) and stirred

for 1 h to precipitate the generated PPh_3 . Cannula filtration allowed to recover the liquid phase which was concentrated to give X-ray quality crystals of $\text{Ru}(\text{OOC}_3\text{H}_7)(\text{Cl})(\text{CO})(\text{DCPB})$. ^1H NMR for **Ru-7** (500 MHz, 25 °C, Toluene- d_8): δ 2.15 (q, $^2J_{\text{Hb-Ha}} = 7.6$ Hz, 2 H_b), δ 2.15 (t, $^2J_{\text{Ha-Hb}} = 7.6$ Hz, 3 H_a), 2.10 – 0.80 (m, 52H, $(\text{C}_6\text{H}_{11})_2\text{P-C}_4\text{H}_8\text{-P}(\text{C}_6\text{H}_{11})_2$). $^{31}\text{P}\{^1\text{H}\}$ NMR (500 MHz, 25 °C, Toluene- d_8) assignments of many signals was impossible because of the poor quality of the NMR data. $^{13}\text{C}\{^1\text{H}\}$ NMR (500 MHz, 25 °C, Toluene- d_8) assignments of many signals was impossible because of the poor quality of the NMR data 204.13 (C \equiv O), 192.23(C=O), 190.25 (C=O). NMR data for **Ru-7** are reported in Annexes, Figures II.4.27 to 31.

- Computational details

All calculations were carried out with the Gaussian 09 suite of programs.^[8] Ruthenium atoms were treated with the very small core Stuttgart–Dresden effective core potential associated with its adapted basis sets and additional *f* and *g* polarization functions.⁹ Carbon, hydrogen and

⁸ Gaussian 09, Revision **D.01**, Frisch, M. J.; Trucks, G. W.; Schlegel, H. B.; Scuseria, G. E.; Robb, M. A.; Cheeseman, J. R.; Scalmani, G.; Barone, V.; Mennucci, B.; Petersson, G. A.; Nakatsuji, H.; Caricato, M.; Li, X.; Hratchian, H. P.; Izmaylov, A. F.; Bloino, J.; Zheng, G.; Sonnenberg, J. L.; Hada, M.; Ehara, M.; Toyota, K.; Fukuda, R.; Hasegawa, J.; Ishida, M.; Nakajima, T.; Honda, Y.; Kitao, O.; Nakai, H.; Vreven, T.; Montgomery, J. A., Jr.; Peralta, J. E.; Ogliaro, F.; Bearpark, M.; Heyd, J. J.; Brothers, E.; Kudin, K. N.; Staroverov, V. N.; Kobayashi, R.; Normand, J.; Raghavachari, K.; Rendell, A.; Burant, J. C.; Iyengar, S. S.; Tomasi, J.; Cossi, M.; Rega, N.; Millam, M. J.; Klene, M.; Knox, J. E.; Cross, J. B.; Bakken, V.; Adamo, C.; Jaramillo, J.; Gomperts, R.; Stratmann, R. E.; Yazyev, O.; Austin, A. J.; Cammi, R.; Pomelli, C.; Ochterski, J. W.; Martin, R. L.; Morokuma, K.; Zakrzewski, V. G.; Voth, G. A.; Salvador, P.; Dannenberg, J. J.; Dapprich, S.; Daniels, A. D.; Farkas, Ö.; Foresman, J. B.; Ortiz, J. V.; Cioslowski, J.; Fox, D. J. Gaussian, Inc., Wallingford CT, **2009**.

⁹ (a) Andrae, D.; Haeussermann, U.; Dolg, M.; Stoll, H.; Preuss, H. *Theor. Chim. Acta* **1990**, 77, 123-141. (b) Martin, J. M. L.; Sundermann, A. *J. Chem. Phys.* **2001**, 114, 3408-3420.

Experimental section

oxygen atoms were described with a 6-31G(d,p) double- ζ basis set.^[10] Silicon and phosphorous atoms have been treated with the small core Stuttgart-Dresden effective core potential associated with its adapted basis set and additional *d* polarization functions.^[11] Calculations were carried out at the DFT level of theory with the hybrid functional B3PW91.^[12] Solvation energies were evaluated by a self-consistent reaction field (SCRF) approach based on accurate numerical solutions of the Poisson-Boltzmann equation by using the SMD solvation model.^[13] Toluene was used as solvent. All geometries were optimized without any symmetry restriction and the nature of the extrema was verified by analytical frequency calculations. The calculation of electronic energies and enthalpies of the extrema of the potential energy surface (minima and transition states) were performed at the same level of theory as the geometry optimizations. Enthalpies were obtained at T = 298 K within the harmonic approximation.

¹⁰ Hehre, W. J.; Ditchfield, R.; Pople, J. A. *J. Chem. Phys.* **1972**, *56*, 2257-2261.

¹¹ Bergner, A.; Dolg, M.; Kuechle, W.; Stoll, H.; Preuss, H. *Mol. Phys.* **1993**, *80*, 1431.

¹² (a) Becke, A. D. *J. Chem. Phys.* **1993**, *98*, 5648-5652. (b) Burke, K.; Perdew, J. P.; Yang, W. in *Electronic Density Functional Theory: Recent Progress and New Directions*, Eds: Dobson, J. F.; Vignale, G.; Das, M. P., Plenum, New York, **1998**.

¹³ Marenich, A. V.; Cramer, C. J.; Truhlar, D. G. *J. Phys. Chem. B* **2009**, *113*, 6378-6396.

Table S2. Summary of Crystal and Refinement Data for [(DCPB)Ru(Cl)(CO)(CO²CH=CH-κ²-O, O)] (**Ru-6**) and [(DCPB)Ru(Cl)(CO)(CO₂CH₂CH₃-κ²-O, O)] (**Ru-7**)

	Ru-6	Ru-7
Empirical formula	C ₃₂ H ₅₅ ClO ₃ P ₂ Ru	C ₃₂ H ₅₇ ClO ₃ P ₂ Ru
Formula weight	686.22 g/mol	688.23 g/mol
Temperature, K	150(2) K	150(2) K
Wavelength, Å	0.71073 Å	0.71073 Å
Crystal system	monoclinic	monoclinic
Space group	P 2 ₁ /c	P 2 ₁ /c
a, Å	11.3737(4) Å	11.4179(4) Å
b, Å	16.0327(7) Å	16.0443(7) Å
c, Å	19.0099(8) Å	19.0367(13) Å
β, deg	103.1370(10) °	103.203(3) °
Volume, Å ³	3375.8(2) Å ³	3395.2(3) Å ³
Z	4	4
Density (calc.), g/cm ³	1.350	1.346
Absorption coefficient, mm ⁻¹	0.668	0.664
Crystal size, mm ³	0.180 x 0.140 x 0.070 mm	0.240 x 0.130 x 0.050 mm
Reflections collected	31509	20665
Independent reflections	7696 [^a R(int) = 0.0352]	7647 [^a R(int) = 0.0387]
Max. and min. transmission	0.954, 0.777	0.967, 0.874
Data / restraints / parameters	7696 / 0 / 346	7647 / 1 / 347
Final R indices [I > 2σ(I)]	^c R ₁ = 0.0489, ^d wR ₂ = 0.1018	^c R ₁ = 0.0424, ^d wR ₂ = 0.0950
R indices (all data)	^c R ₁ = 0.0582, ^d wR ₂ = 0.1078	^c R ₁ = 0.0550, ^d wR ₂ = 0.1027
^b Goodness-of-fit on F ²	1.244	1.040
Largest diff. peak, e.Å ⁻³	1.345, -1.183	1.847, -1.276

$$^a R(\text{int}) = \frac{\sum |F_o^2 - \langle F_o^2 \rangle|}{\sum F_o^2}$$

$$^c R_1 = \frac{\sum ||F_o| - |F_c||}{\sum |F_o|}$$

$$^d wR_2 = \left\{ \frac{\sum [w(F_o^2 - F_c^2)^2]}{\sum [w(F_o^2)^2]} \right\}^{1/2}$$

$$w = 1. / [\sigma(F_o^2) + (aP)^2 + bP] \text{ with } P = [2F_c^2 + \text{Max}(F_o^2, 0)] = 3$$

ANNEXES

Annexes

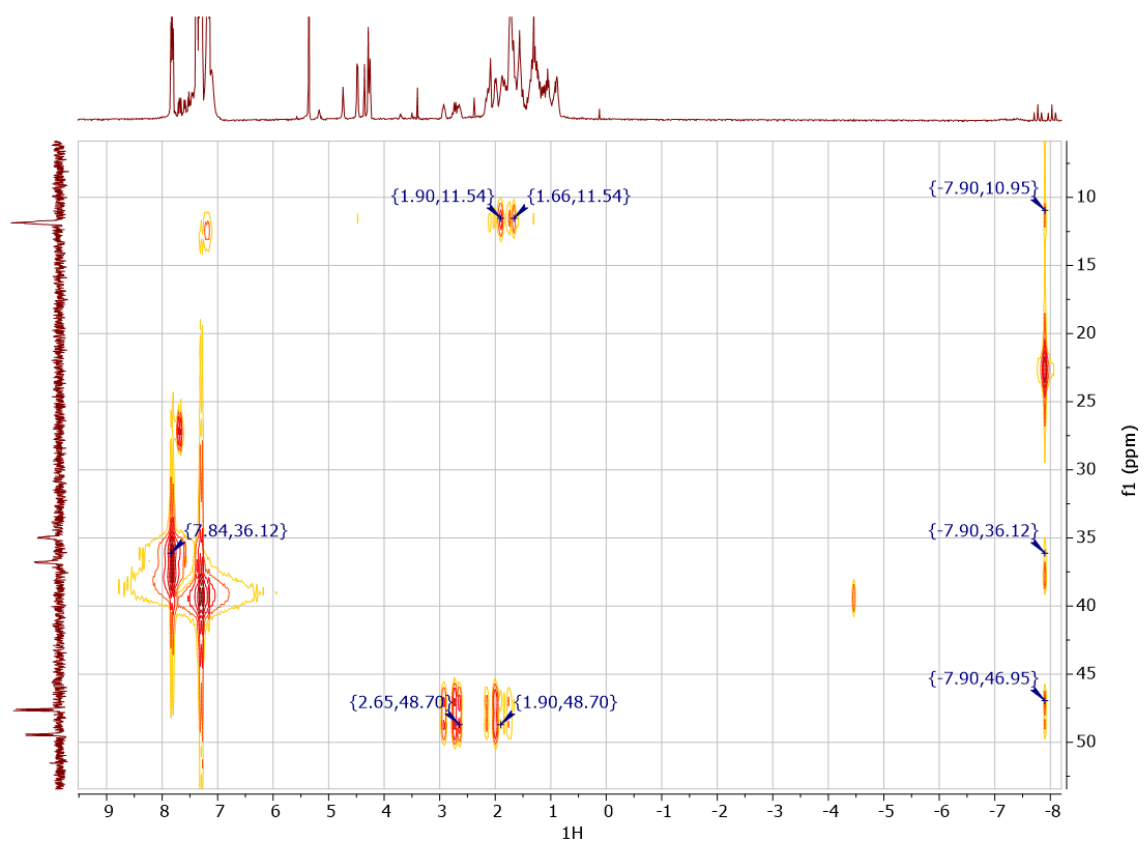


Figure II.3.17. ^1H - ^{31}P HMBC NMR spectrum of **Ru-2** in toluene- d_8 at 25 °C.

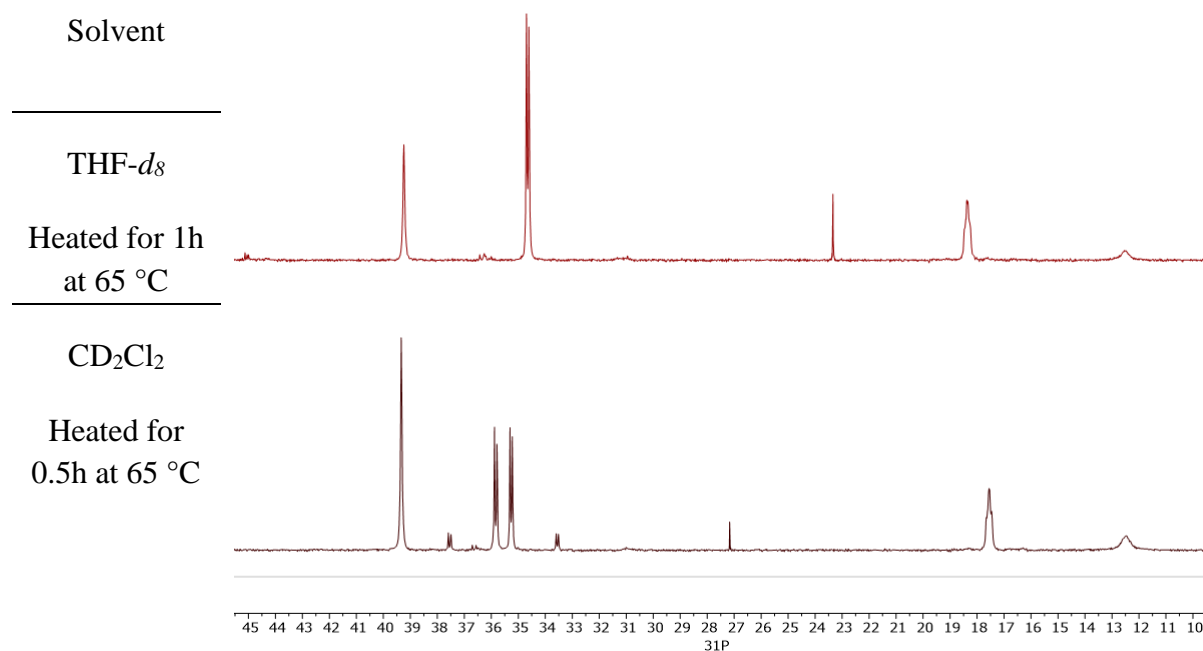


Figure II.3.21. $^{31}\text{P}\{^1\text{H}\}$ NMR spectra of the crude mixtures resulting from the reaction of **Ru-1**:DCPB (1:1) under Ar atmosphere in THF- d_8 and CD_2Cl_2 at 25 °C.

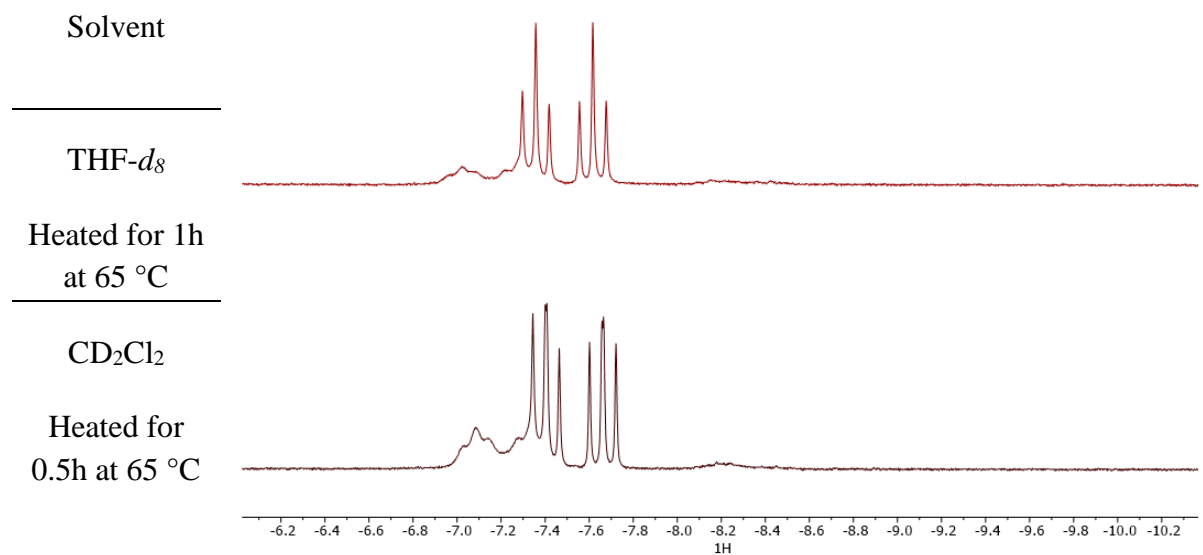


Figure II.3.22. ^1H NMR spectra of the crude mixtures resulting from the reaction of **Ru-1**:DCPB (1:1) under Ar atmosphere in THF- d_8 and CD_2Cl_2 at 25 °C.

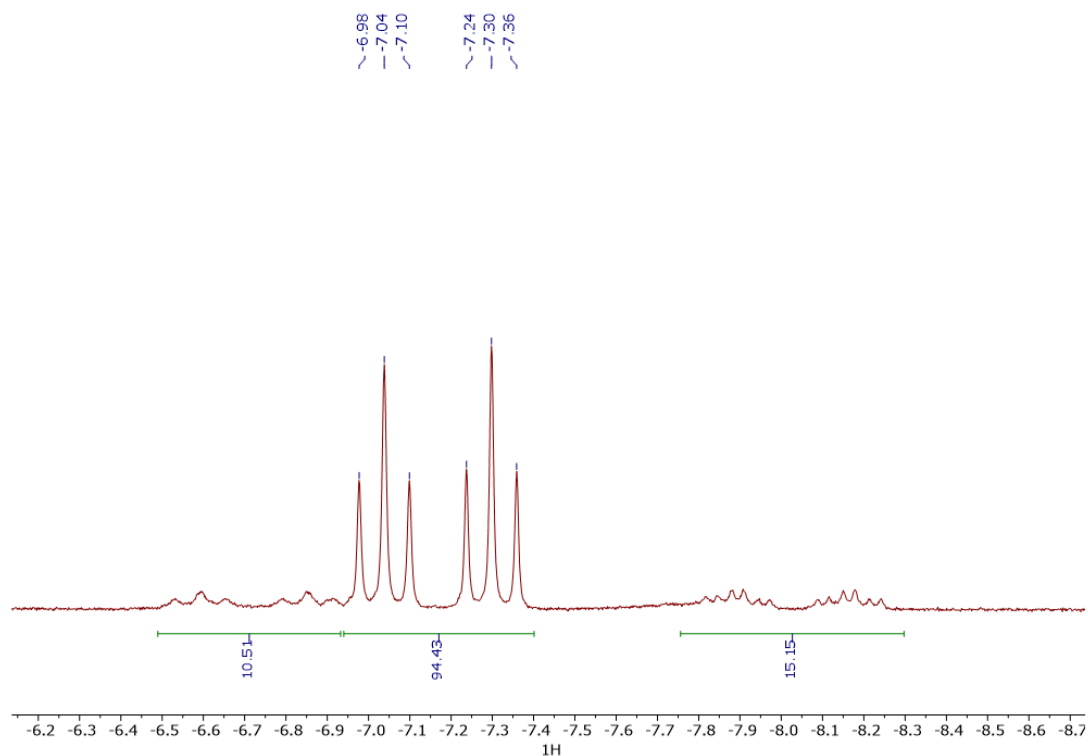


Figure II.3.23. ^1H NMR spectrum (400 MHz, toluene- d_8 , 25 °C) of the crude mixture resulting from the reaction of **Ru-1**:DCPB (1:1) under CO_2 : C_2H_4 atmosphere (1:1).

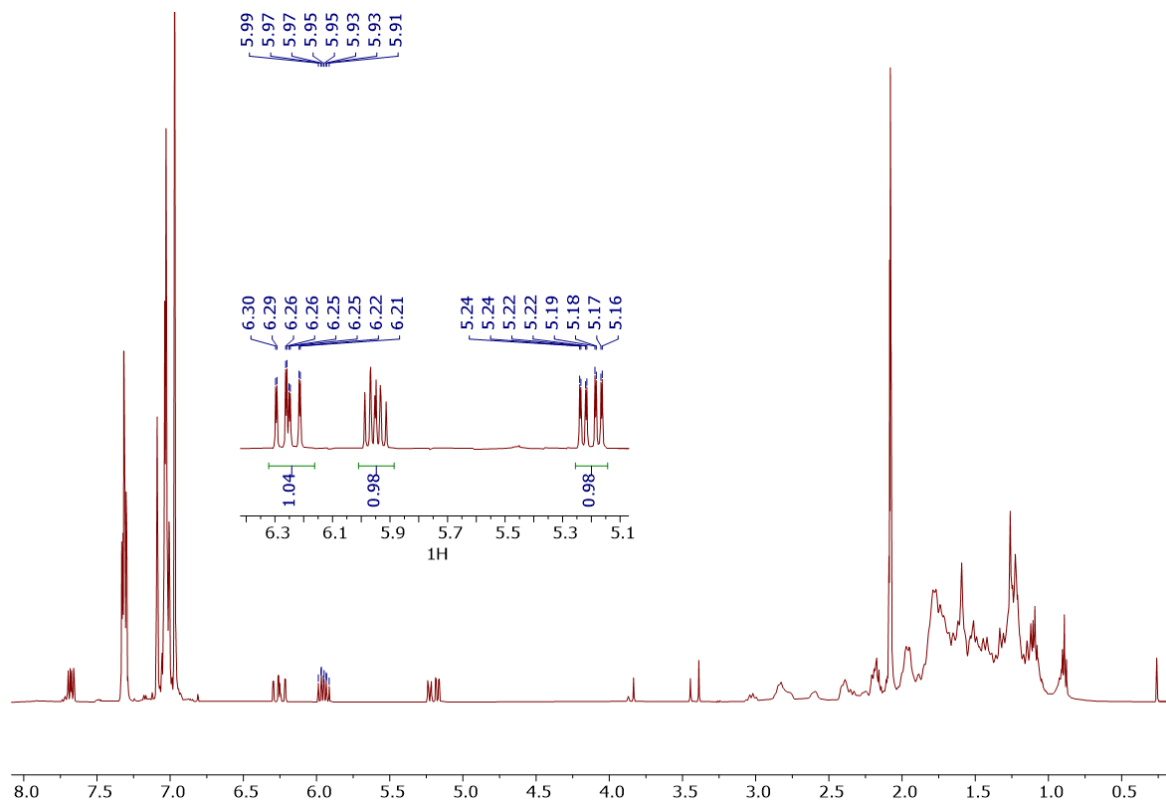


Figure II.4.24. ^1H NMR spectrum (500 MHz, toluene- d_8 , 25 °C) of the **Ru-6** isolated crystals.

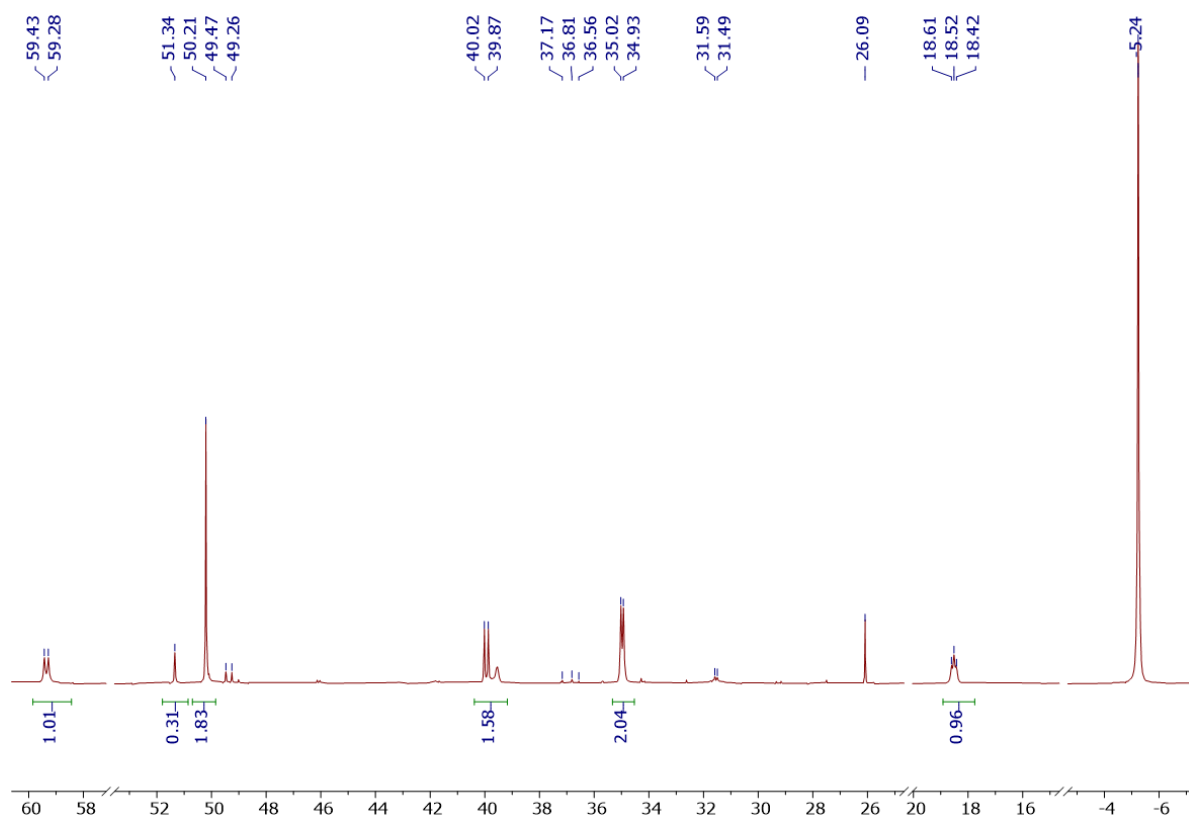


Figure II.4.26. ^{31}P NMR spectrum (500 MHz, toluene- d_8 , 25 °C) of the mixture of **Ru-6** isomers after adding 1.5 equiv of MeOH.

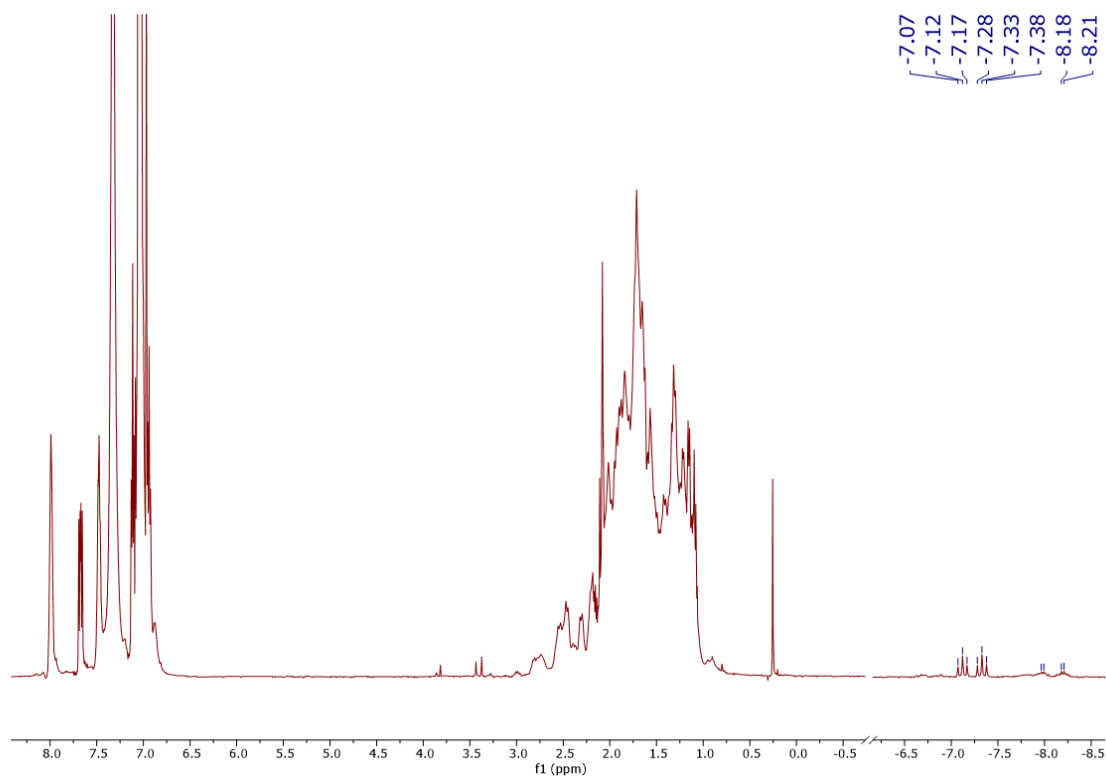
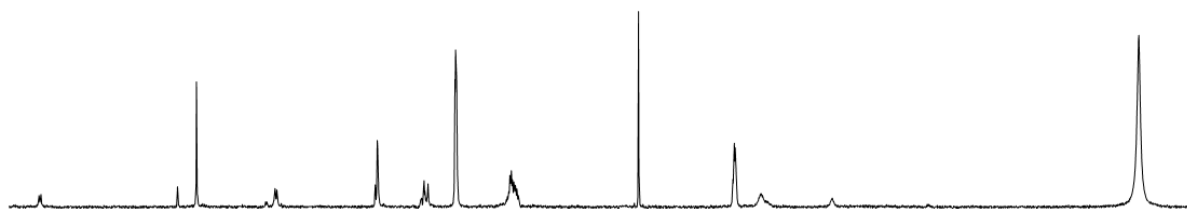


Figure II.4.27. ^1H NMR spectrum (500 MHz, toluene- d_8 , 25 °C) of the **Ru-6** crude mixture after reacting under an atmosphere of H_2 (30 bar) for 16h at 100 °C.

kakunihiro KYK-439.22.fid
31Pdec



kakunihiro KYK-439.21.fid
31P

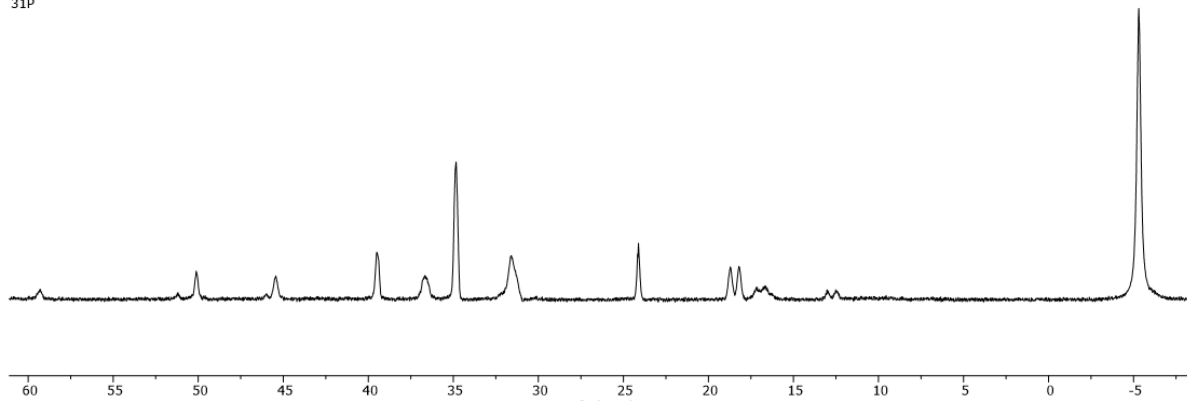


Figure II.4.28. $^{31}\text{P}\{^1\text{H}\}$ (top) and ^{31}P (bottom) NMR spectra (500 MHz, toluene- d_8 , 25 °C) of the **Ru-6** crude mixture after reacting under an atmosphere of H_2 (30 bar) for 16h at 100 °C.

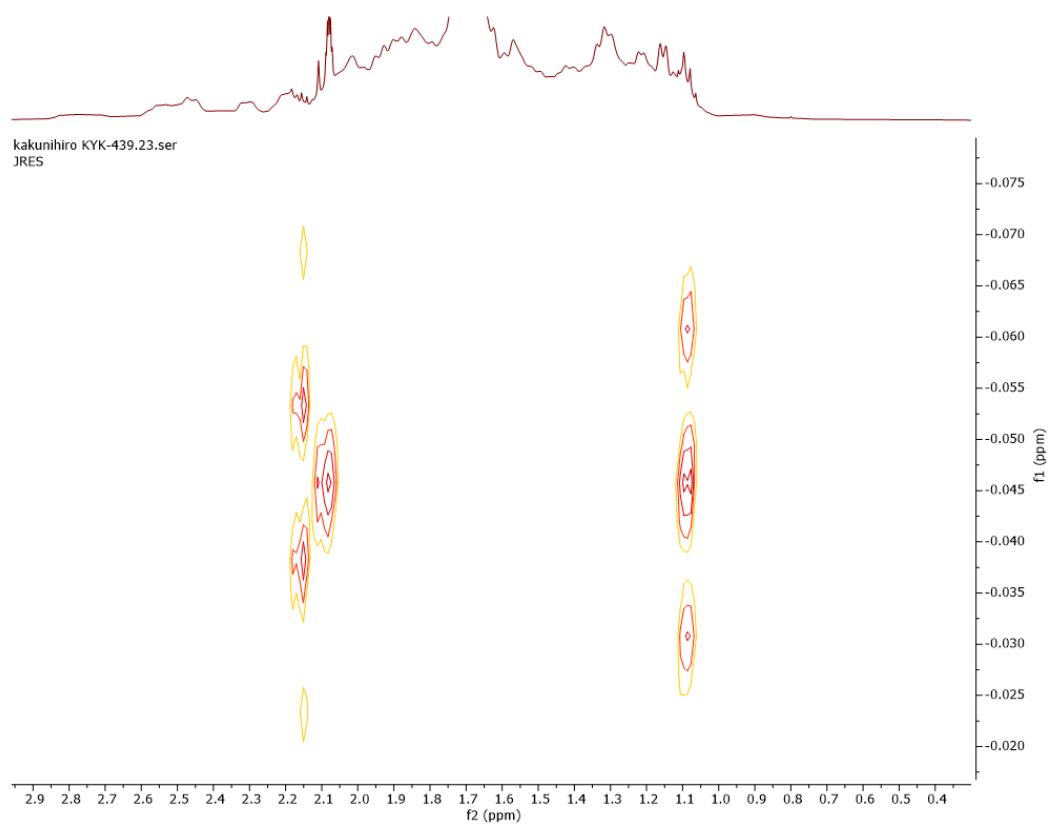


Figure II.4.29. J-Res ^1H NMR spectra (500 MHz, toluene- d_8 , 25 °C) of the aliphatic region of the **Ru-6** crude mixture after reacting under an atmosphere of H_2 (30 bar) for 16h at 100 °C.

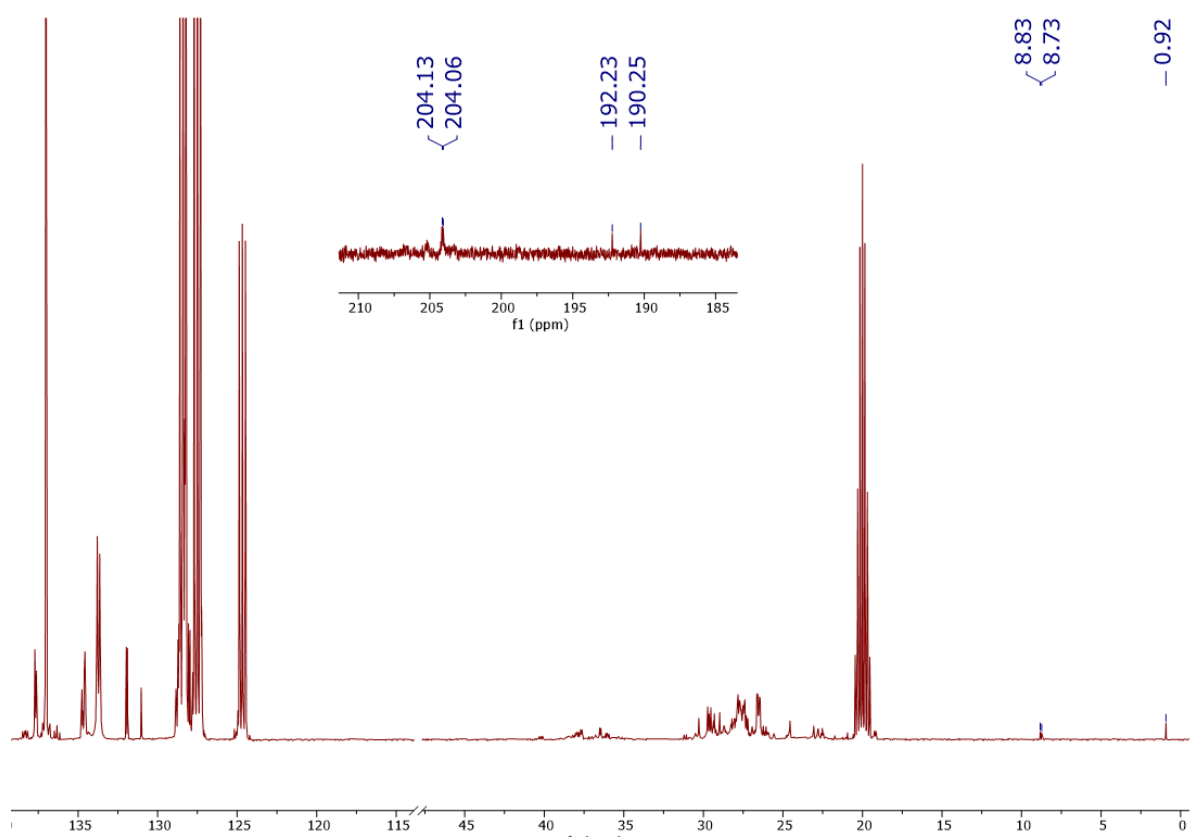


Figure II.4.30. $^{13}\text{C}\{^1\text{H}\}$ NMR spectrum (126 MHz, toluene- d_8 , 25 °C) of the **Ru-6** crude mixture after reacting under an atmosphere of H_2 (30 bar) for 16h at 100 °C.

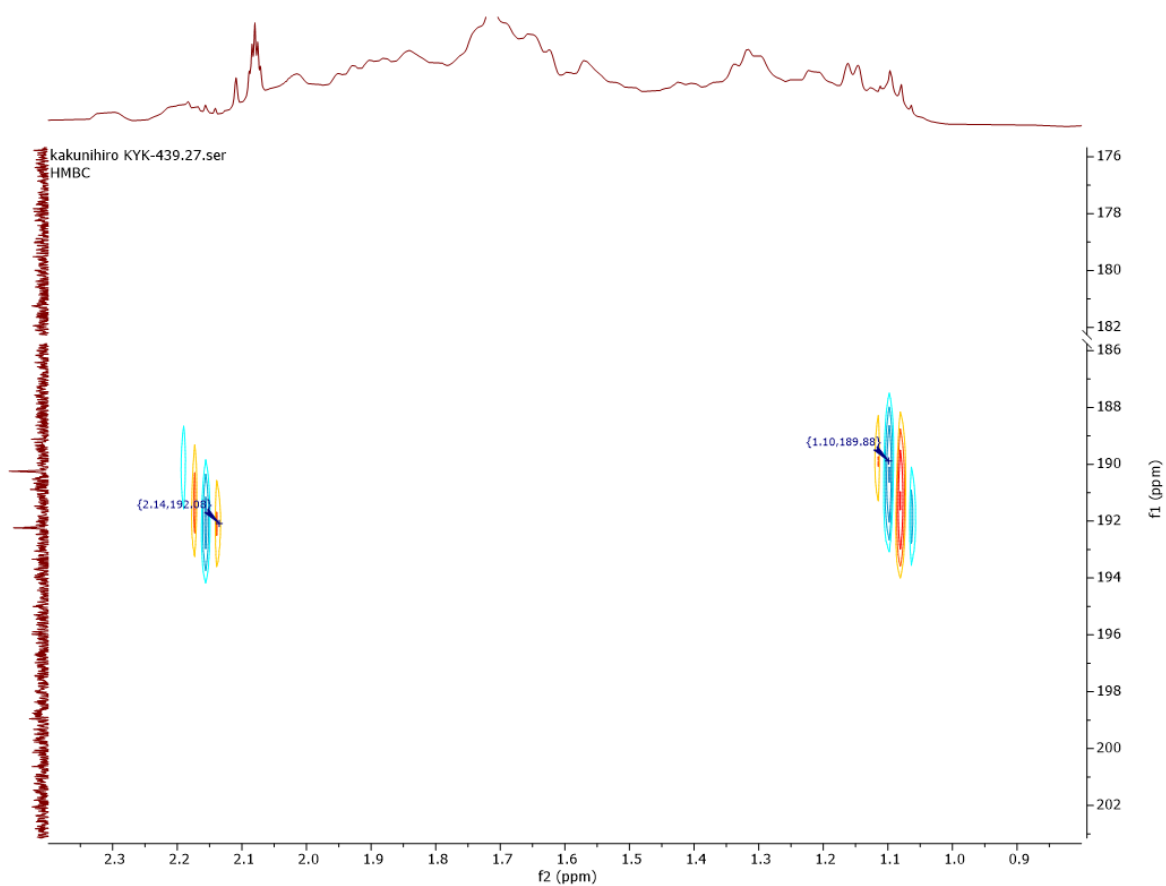


Figure II.4.31. ^1H - ^{13}C HMBC NMR spectrum of the aliphatic region (500 MHz, toluene- d_8 , 25 °C) of the **Ru-6** crude mixture after reacting under an atmosphere of H_2 (30 bar) for 16h at 100 °C.

Compte-rendu en langue française

Introduction générale

Compte tenu des conséquences socio-environnementales du réchauffement climatique, diverses sources d'énergie renouvelables ont été explorées pour remplacer les combustibles fossiles, utilisées à la fois pour couvrir les besoins énergétiques et comme source de carbone dans la synthèse de molécules à haute valeur ajoutée. En effet, l'exploitation et l'utilisation de ces ressources non-renouvelables sont aujourd'hui responsables de plus de 60% des émissions de dioxyde de carbone (CO₂) anthropiques dans l'atmosphère (37 Gt de CO₂ anthropique/an).^[1] Afin de tirer parti de l'abondance de ce gaz, le développement de nouvelles transformations chimiques à partir du CO₂ connaît un intérêt croissant au sein de la communauté scientifique puisqu'il permettrait un remplacement progressif des hydrocarbures fossiles au profit de ressources carbonées renouvelables, et ce pour accéder à des produits de chimie fine.

Mais afin d'utiliser le CO₂ comme brique élémentaire pour la synthèse de molécules carbonées, deux aspects principaux sont à prendre en compte : surmonter les barrières cinétiques et thermodynamiques des réactions utilisant le CO₂.

En effet, la barrière thermodynamique élevée de ce gaz inerte le rend difficilement réactif ($\Delta G_f^\circ = -393,52 \text{ kJ/mol}$).^[2] La plupart des réactions de conversion du CO₂ sont endergoniques et nécessitent donc des quantités importantes d'énergie pour le faire réagir.^[3] Celles-ci peuvent être amenées soit sous forme physique (électricité, lumière) ou chimique (substrats de réaction très réactifs). Cet apport doit cependant provenir d'une source décarbonée pour avoir un bilan carbone qui soit favorable. Par ailleurs, afin de diminuer les différentes barrières énergétiques mises en jeu et accroître la sélectivité de la réaction, l'utilisation de catalyseurs robustes, rapides, efficaces et sélectifs est nécessaire.^[4]

De manière générale, deux approches principales pour convertir le CO₂ en produits à valeur ajoutée pour la chimie fine peuvent être considérées. La première consiste en la réduction directe du CO₂, appelée « réduction verticale » par Cantat *et al.* (figure 1), pour produire, par exemple, du méthanol (pour une application hydrocarbures) ou de l'acide formique (vectorisation de l'hydrogène).^[4] Cette méthodologie nécessite une grande quantité d'énergie et de puissants agents réducteurs (par exemple H₂). La deuxième approche, non-réductrice (c'est-à-dire que l'état d'oxydation +IV du carbone est maintenu), est utilisée pour produire de nouvelles liaisons chimiques entre le CO₂ et un substrat, pour ainsi former des molécules fonctionnalisées comme l'urée, les carbonates, carboxylates, lactones ou carbamates (« utilisation horizontale », figure 1). Bien qu'ils jouent un rôle important dans l'économie actuelle

et pour la synthèse des carburants de demain, ces produits chimiques ne couvrent pas l'ensemble des matières premières nécessaires à la synthèse de tous les produits chimiques sur le marché.^[5] En effet, pour accéder à aux fonctions classiques de la chimie organique telles que les acides carboxyliques, les amides, les éthers, etc., les molécules issues de la pétrochimie (hydrocarbures) sont traditionnellement utilisées comme réactifs de départ, impliquant des réactions multi-étapes coûteuses énergétiquement. Ainsi, pour élargir la gamme de composés directement disponibles à partir du CO₂ et concurrencer la pétrochimie, de nouvelles méthodes visant à combiner à la fois la réduction du CO₂ et la formation de liaisons C–C, C–N et C–O doivent être développées (« transformations diagonales », figure 1). Les transformations diagonales idéales, pour lesquelles l'état d'oxydation de l'atome de carbone du CO₂ varie de +III (pour les acides carboxyliques) à –II (pour les éthers), devraient assurer une économie d'énergie et un bilan carbone positif.

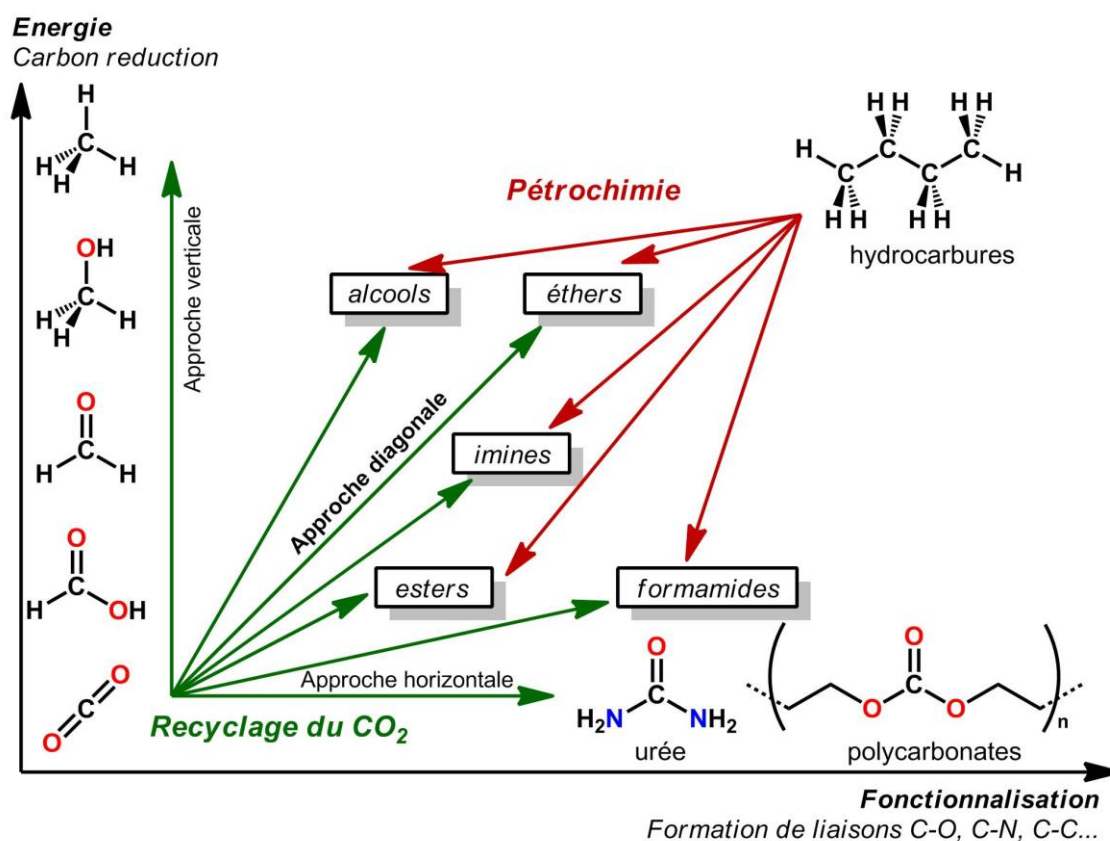


Figure 1. Comparaison des différentes stratégies pour le recyclage du CO₂, illustré par Cantat *et al.*^[4]

Pourtant, les exemples viables restent rares et à ce jour, seuls quelques procédés utilisant du CO₂ ont été industrialisés, comme la synthèse de l'urée, le méthanol, le méthane, l'acide salicylique, les carbonates organiques et inorganiques, les polymères (**Schéma 1**). Aujourd'hui, la synthèse d'urée (130 Mt/an) et de méthanol (2,7 Mt/an) sont les principaux consommateurs

de CO₂ (pur ou dérivé du CO par la réaction du gaz à l'eau, en anglais *Water Gas Shift* (WGS)).^[6]

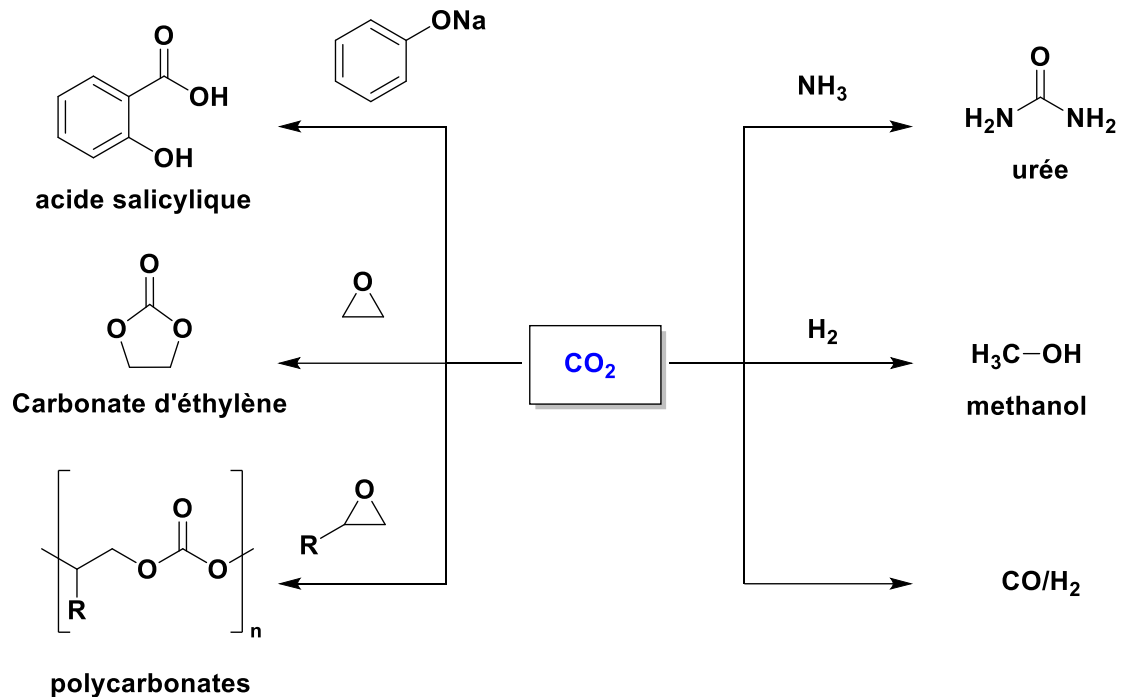


Schéma 1. Procédés industriels utilisant le CO₂ comme matière première.

Parmi les nombreuses réactions étudiées, une « réaction de rêve » n'a cessé d'intriguer les domaines académiques et industriels : la synthèse directe de l'acide acrylique directement à partir du CO₂ et de l'éthylène comme matières premières.^[7] En effet, cette voie de synthèse est, en principe, industriellement très intéressante. Elle permettrait non seulement d'utiliser le CO₂, peu cher et abondamment disponible, mais aussi d'envisager l'utilisation d'éthylène renouvelable, provenant par exemple de la déshydratation du bioéthanol, qui pourrait présenter un réel intérêt environnemental.^[8] Ainsi, elle permettrait d'éviter la formation de déchets, générés par les réactions de synthèses organiques d'acides carboxyliques classiques, et ce tout en garantissant une meilleure économie d'atomes. En effet, l'introduction directe d'un groupement carboxylique demande des procédures élaborées et/ou nécessitant des conditions sévères. Les voies de synthèses les plus couramment utilisées sont classées en trois grands types de réactions^[9] :

- Oxydation d'alcools primaires, d'aldéhydes et d'alcènes à l'aide de réactifs oxydants forts (KMnO₄, réactif de Jones, periodinane de Dess-Martin)

- Hydrolyse des nitriles en acides carboxyliques

- Réactions consécutives d'un substrat organométallique hautement énergétique, porteur d'un carbone nucléophile, avec du CO₂ (dont l'atome de carbone électrophile), formant les sels carboxylates correspondants, suivi d'un traitement acide aqueux fort aboutissant à l'acide carboxylique

La dernière stratégie de synthèse repose sur l'insertion directe du CO₂ dans une liaison C–métal polarisée et est donc promue en utilisant des quantités stœchiométriques de substrat organométalliques hautement nucléophiles, tels que des réactifs de Grignard ou des espèces d'organolithium ou d'organoaluminium.

Cependant, la faible chimiosélectivité de ces réactifs a orienté les recherches vers la conception de réactions de couplage catalysées par des métaux de transition.^[10] Suite à la compréhension des différents modes de liaison du CO₂ à un centre métallique, le développement de techniques de carboxylation catalysée et utilisant des réactifs organométalliques moins basiques/nucléophiles ont vu le jour.

Il y a plus de quatre décennies, les études pionnières conduites indépendamment par les groupes de Höberg et Carmona ont permis de proposer un cycle catalytique hypothétique pour le couplage du CO₂ et C₂H₄ pour former de l'acide acrylique/dérivés acrylates^[11–21]. Les études mécanistiques conduites sur les complexes de Ni, Mo/W et Pd ayant permis de prouver le couplage effectif entre le CO₂ et C₂H₄ et suggèrent des voies similaires pour ces métaux. Bien qu'encourageantes, ces voies catalytiques présentent encore aujourd'hui de nombreux obstacles.

Par exemple, dans le cas des systèmes les plus étudiés, principalement utilisant des complexes au Ni, le processus global est fortement endothermique, donc défavorable ($\Delta G_R^0 = 10,2 \text{ kcal}\cdot\text{mol}^{-1}$)^[22] et des espèces cycliques stables, appelées nickelalactones sont formées (**Schéma 2**). Des calculs théoriques ont montré que la barrière cinétique de l'étape de β -Hydrure élimination est particulièrement élevée ($\Delta G^\ddagger = +42.5 \text{ kcal}\cdot\text{mol}^{-1}$) en raison de la forte déformation du cycle à cinq chaînons qui empêche les interactions agostiques Ni \cdots H.^[11,23,24] Par conséquent, la scission de la liaison Ni–C n'a pas lieu et la transformation en acrylate est difficile. Pour induire la β -H élimination, des études expérimentales indiquent que l'activation de la liaison M–O pourrait surmonter la barrière de dissociation énergétique de la liaison. Pour y parvenir, l'utilisation récente de quantités sur-stœchiométriques de nucléophiles, de bases ou de réactifs acides de Lewis ont été investiguées.^[10]

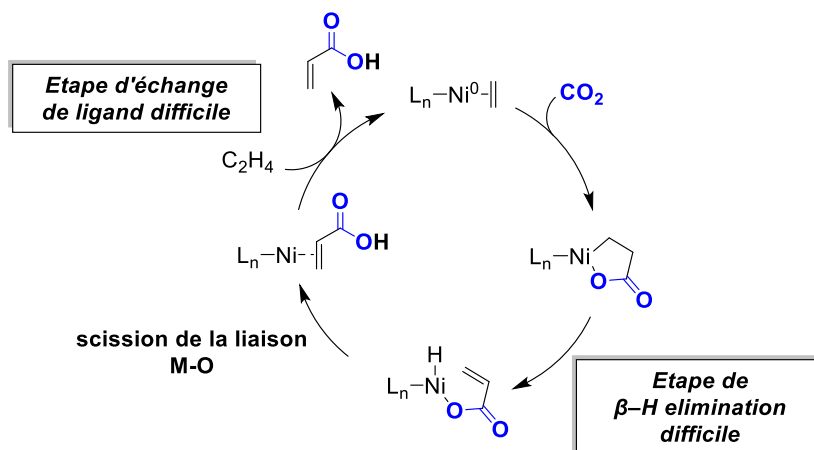


Schéma 2. Cycle hypothétique pour la formation directe d'acide acrylique à partir du CO₂ et de l'éthylène, catalysée par des complexes au Ni.^[10]

Concernant les centres métalliques du groupe VI, ces derniers semblent induire un couplage oxydatif du CO₂ et C₂H₄ ainsi qu'une β-H élimination plus facilement qu'avec les systèmes au Ni. Alors que le couplage se produit à température et pression ambiante avec des complexes au Mo et W, des pressions élevées de gaz (~40 bar) sont en effet nécessaires dans le cas des complexes de Ni. Cependant, la forte oxophilie des complexes acrylate de Mo et W est un obstacle à l'élimination réductrice de l'acrylate, qui ne peut être surmonté qu'en utilisant des bases fortes (BuLi) ou des électrophiles forts (MeI).^[17,19,21,25]

Ce n'est que récemment qu'une nouvelle stratégie a été reportée par les groupes indépendants de Limbach et Vogt,^[26,27] présentant les premières applications catalytiques de systèmes à base de Ni (**Schéma 3, (a)**) et de Pd et utilisant différentes bases afin de déprotoner la métallalactone. Le rôle de la base a été effectivement attribué à sa capacité à extraire l'un des protons acides de la lactone en position α au groupe carbonyle. D'autre part, les auteurs ont souligné que les bases fortes soumises à de hautes pressions de CO₂, réagissent et forment avec celui-ci des carbonates stables, devenant donc inutiles pour la déprotonation directe de la métallalactone. Pour y remédier, une méthodologie de carboxylation en deux étapes a été développée, durant laquelle des cycles de pressurisation et de dépressurisation sont répétés. A cela sont également nécessaires des quantités en large excès de base inorganiques et, de réducteurs, dans certains cas. Sous ces conditions, des TONs maximum de 10 en acrylate de sodium ont été obtenus à l'aide d'un catalyseur au Ni (**Schéma 3, (a)**),^[27] et de 514 en présence de Pd (**Schéma 3, (b)**).^[28]

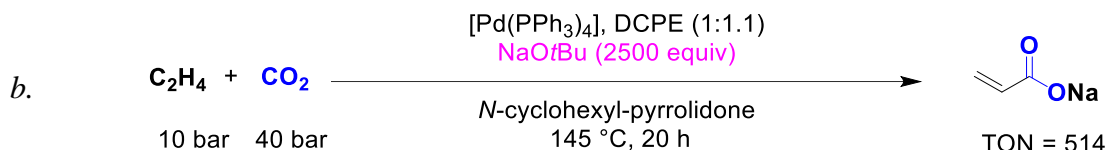
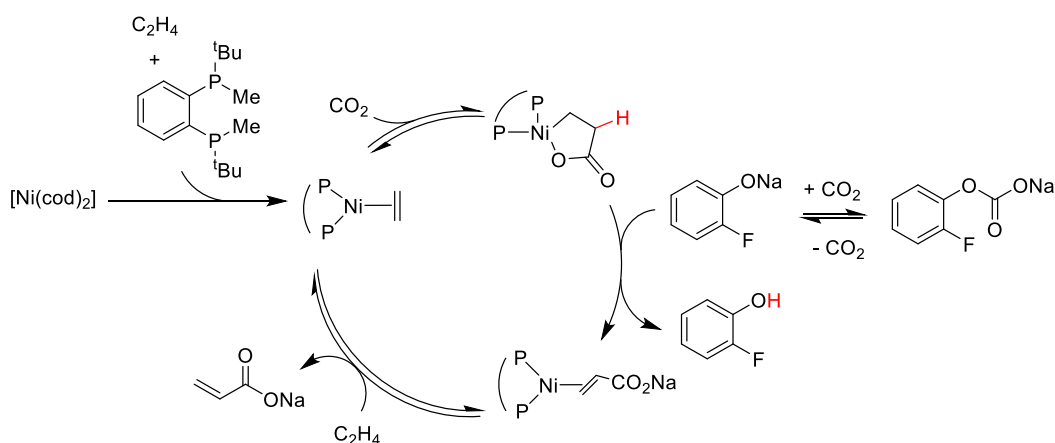
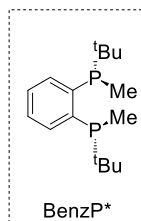
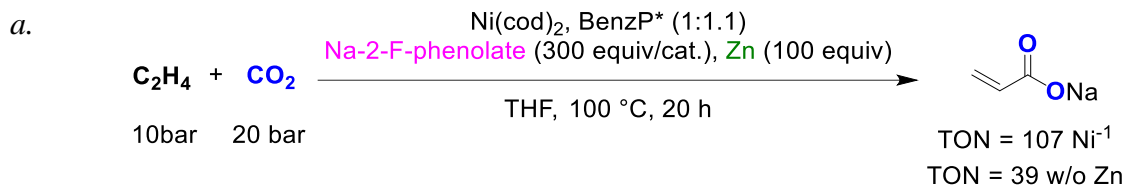


Schéma 3. Formation de sel d'acrylate de sodium à partir de CO₂ et C₂H₄ (a) catalysée au Ni, en présence de large excès de base (2-F-phenolate de sodium) et de réducteur (Zn) et le cycle catalytique proposé pour cette réaction (b) catalysée au Pd, en présence de large excès de base (tBuONa).^[27,28]

Objectifs du projet de thèse

Au vu des performances limitées des catalyseurs les plus prometteurs de la littérature, le but de ce projet est d'explorer et de développer de nouveaux systèmes catalytiques homogènes permettant la carboxylation réductrice de l'éthylène en acides carboxyliques.

Ainsi, dans la toute première phase du projet, l'identification de systèmes catalytiques prometteurs pour la réaction de couplage entre le CO₂ et C₂H₄ s'appuiera sur l'utilisation de techniques de criblage à haut débit (HTS). En supposant que le cycle catalytique menant à la formation des acides désirés nécessite la formation d'une espèce metalallactone hypothétique, l'emploi d'un agent réducteur adéquat permettrait de scinder le cycle à cinq chaînons et libérer l'acide. Idéalement, l'utilisation du dihydrogène (H₂) permettrait de rendre le processus

inoffensif, entièrement efficace en terme d'économie d'atomes et attractif sur le plan industriel/économique (réaction cible, **Schéma 4**). Cependant, en raison des nombreuses réactions parasites liées à l'emploi de H_2 , cet objectif ne sera étudié qu'une fois les mécanismes réactionnels mis en jeu clairement élucidés. En remplacement de H_2 , les hydrosilanes, faciles d'accès et à manipuler, inoffensifs et relativement peu coûteux (bien qu'encore non viables industriellement), sont largement utilisés comme agents réducteurs pour de nombreux groupes fonctionnels.^[29] Compte tenu de leur réactivité modulable des et leur facilité de manipulation (liquides stables), les hydrosilanes sont des réducteurs intéressants et compétitifs par rapport aux réducteurs organométalliques.

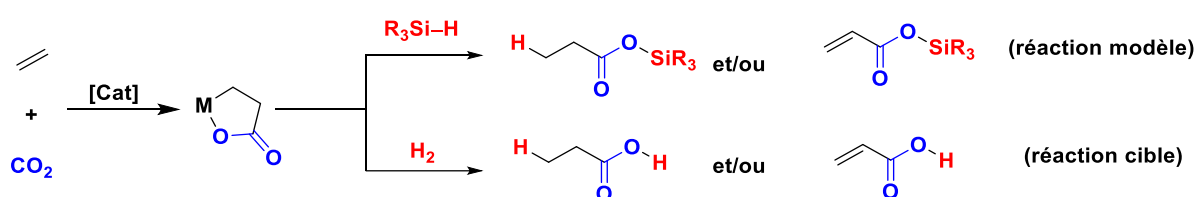


Schéma 4. Proposition de carboxylation réductrice d'éthylène en acides carboxyliques ou esters silyliques, catalysées par un métal de transition.

De plus, la formation favorisée de la liaison Si–O (Energie de Dissociation de Liaison (EDL) = 110 kcal·mol⁻¹)^[30], liée à l'oxophilie de l'atome de silicium, facilite la formation d'esters silylés et donc la transformation réductrice du CO₂. De plus, l'activation relativement facile de la liaison Si–H (EDL = 91 kcal·mol⁻¹ pour SiH₄ par rapport à la plus forte liaison H–H non-polaire EDL = 104 kcal·mol⁻¹ pour H₂) fait des hydrosilanes d'efficaces réducteurs même lorsqu'employés dans des conditions relativement douces.

La deuxième phase du projet est consacrée à l'optimisation de la productivité à l'échelle du laboratoire (en réacteurs autoclaves) pour accéder aux esters silylés.

Parallèlement à ces études catalytiques, la compréhension de la réactivité des espèces catalytiques vis-à-vis du CO₂, de l'éthylène et des hydrosilanes, l'acquisition d'informations structurales détaillées des principaux intermédiaires et sous-produits, participeront à la détermination du ou des mécanisme(s) catalytique(s) mis en jeu. Dans une perspective à plus long terme, les données fondamentales collectées permettront l'extrapolation du modèle établi pour l'éthylène à d'autres alcènes et/ou réducteurs chimiques.

Chapitre 2 – Systèmes catalytiques efficaces pour la réaction de carboxylation du C₂H₄ en présence de CO₂ : de la découverte à l'optimisation au moyen de l'expérimentation à haut débit

A travers l'état de l'art décrit dans la littérature, différents complexes de métaux de transition ont été étudiés pour la réaction de carboxylation catalytique de l'éthylène en présence de CO₂ et d'un réducteur. Bien que des résultats encourageants ont été décrits, des lacunes importantes doivent être surmontées. En effet, ces techniques nécessitent encore souvent l'utilisation de quantités stœchiométriques de réactifs organométalliques ou pré-fonctionnalisés, ainsi que de quantités stœchiométriques d'additifs organométalliques ou métalliques, produisant des quantités importantes de déchets, et entravant ainsi leur application potentielle industrielle. De plus, les systèmes catalytiques les plus prometteurs présentent un faible TON, traduisant un manque d'efficacité. Aujourd'hui, l'existence d'un système catalytique simple et compatible avec les groupes fonctionnels pour la carboxylation de substrats faiblement polarisés avec du CO₂ n'est toujours pas d'actualité.

Ainsi, la première synthèse d'esters silylés catalysée par un métal de transition, à partir de C₂H₄, CO₂ et triéthylsilane (HSiEt₃), a été étudiée en utilisant la méthodologie de criblage à haut débit en collaboration avec la plateforme de Realcat (Villeneuve d'Ascq, France). Le HSiEt₃ a été sélectionné comme réducteur car il présente à la fois une bonne capacité à donner son atome d'hydrure et une bonne nucléophilie.

Une série de précurseurs au Ru et Rh, à savoir [Ru(*p*-cymène)Cl₂]₂, Ru(H)(Cl)(CO)(PPh₃)₃, bis(*n*-octanoate) de rhodium(II), Rh(Cl)(PPh₃)₃ et [RhCl(COD)]₂, en combinaison avec un ensemble de ligands diphosphines présentant des propriétés stéréoélectroniques variables, a été testée en catalyse (figure 2).^[31]

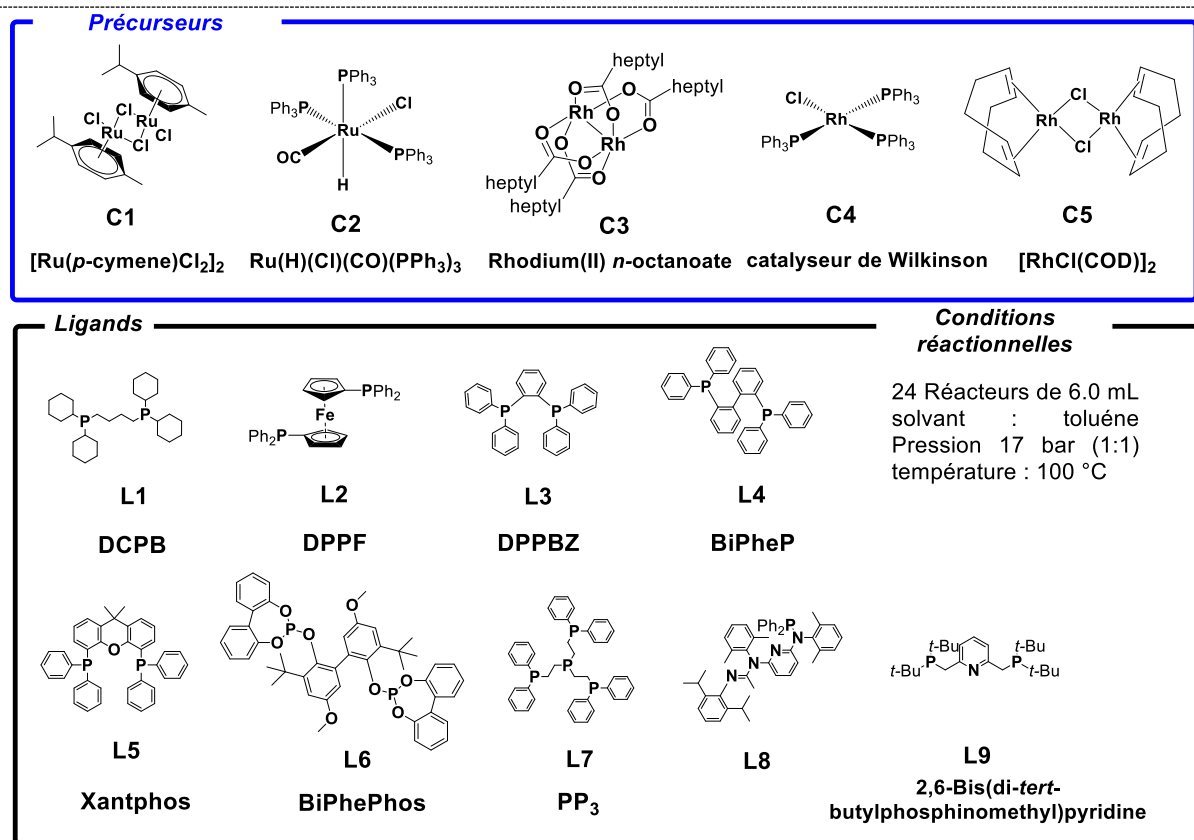
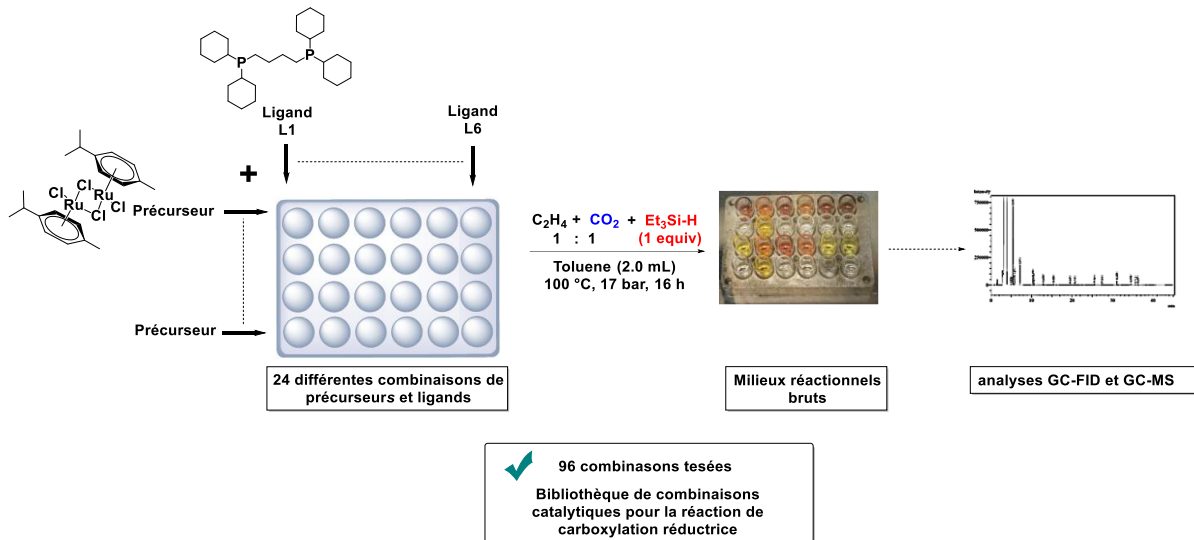


Figure 2. Combinaisons de précurseurs/ligands utilisées en criblage à haut débit sur la plateforme REALCAT (Ecole Centrale de Lille, France).

Après un temps de réaction donné (16 h), les analyses en chromatographie gazeuse ont montré des mélanges bruts contenant divers produits dans la phase liquide (les produits gazeux tels que CO, CH₄, H₂ n'ont pas été recherchés). Le **Schéma 5** représente les voies réactionnelles possibles pouvant se produire, en parallèle, ainsi que les différents produits observés.

Le propionate de triéthylsilyle (**P1**) et l'acrylate de triéthylsilyle (**A1**) (Voie A), produits d'intérêt issus de la réaction de carboxylation réductrice de l'éthylène, ont été obtenus avec

succès par certaines combinaisons de catalyseur/ligand (tableau 1). Dans certains cas, des traces des produits de la réaction de sur-réduction de **A1** en **A2**, **A3** puis propène et **P1** en **P2**, **P3** puis propane, ont été détectées (**Schéma 5**, Voie A).

A noter que pour chaque étape de sur-réduction de **A2** et **P2**, une molécule d'hexaéthylidisiloxane (**E**) est générée comme sous-produit. D'autre part, le formiate de triéthylsilyle (**F1**) issu de la réaction d'hydrosilylation du CO₂, a également été identifié. Ce dernier peut aussi être soumis à une série de réactions de sur-réduction conduisant au méthane (Voie B).^[32] Cependant, les deux voies réactionnelles produisant les TONs les plus élevés sont celles de la voie C, à savoir l'hydrosilylation et le couplage déshydrogénatif de l'éthylène avec l'hydrosilane, produisant du tétraéthylsilane (**TES**) et du triéthylvinylsilane (**TEVS**), respectivement.^[33] Tout au long de cette étude, dire que la sélectivité envers la réaction de carboxylation catalytique du C₂H₄, en présence de HSiEt₃, est améliorée signifie que les TONs des produits de la voie A souhaitée sont augmentés, tandis que ceux des voies indésirables B et C sont abaissés. La production catalytique d'esters silylés **A1** et **P1** (produits de la voie A ciblée) a donc été mise en évidence par HTS puis transposée avec succès aux réacteurs autoclaves (tableau 1). L'optimisation des conditions de réaction a été réalisée afin de minimiser les réactions secondaires; à savoir l'hydrosilylation du CO₂ et la silylation déshydrogénative de l'éthylène. Le système catalytique le plus prometteur a été identifié comme la combinaison de Ru(H)(Cl)(CO)(PPh₃)₃ et de 1,4-bis(dicyclohexylphosphino)butane, offrant les plus TONs élevés pour **A1** et **P1** (entrée 3').

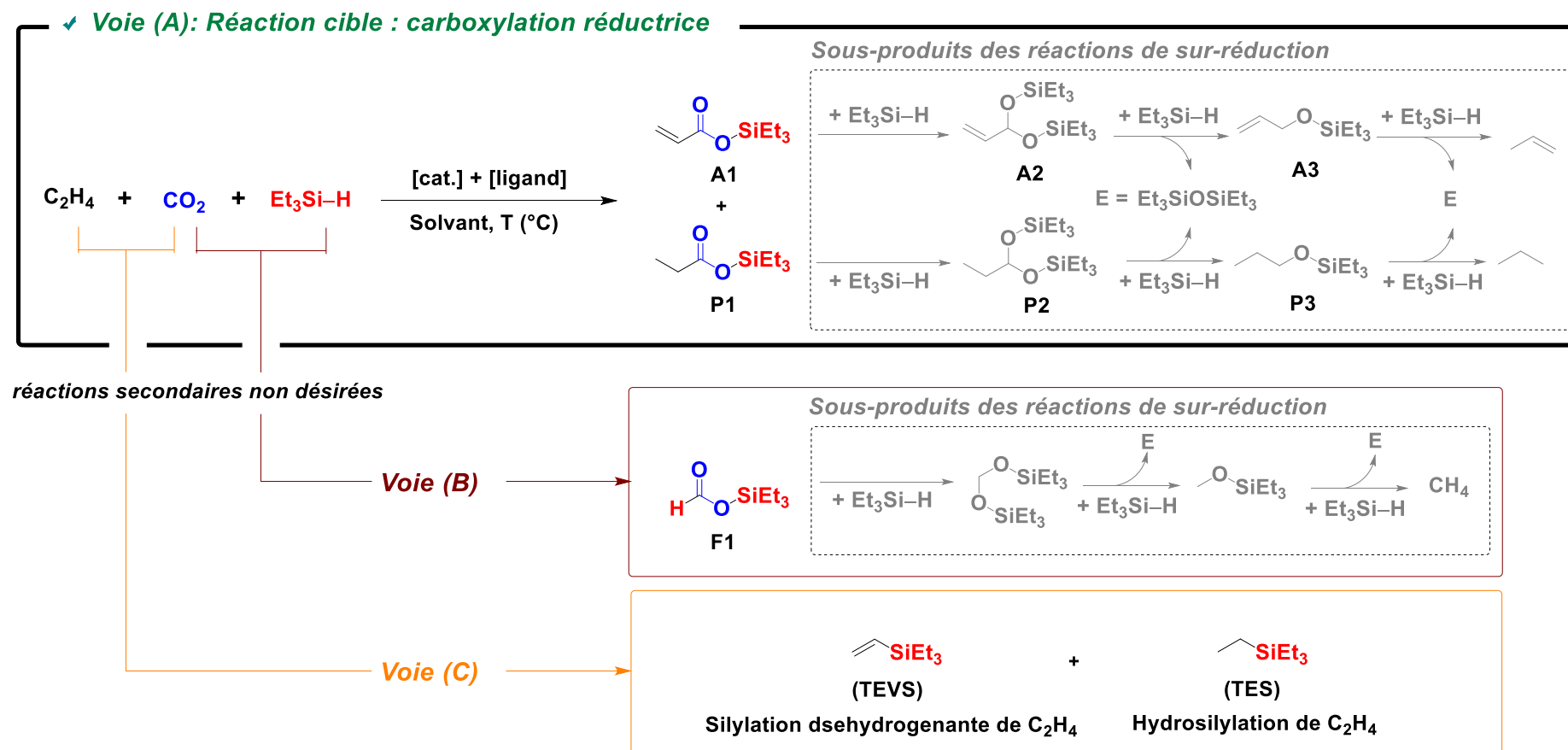
Schéma 5. Les différentes voies réactionnelles possibles de la réaction de couplage du CO_2 avec C_2H_4 en présence de $HSiEt_3$.

Tableau 1. Activités catalytiques des différentes combinaisons de précurseurs/ligands testées en criblage à haut débit (entrées 1 à 4) et à l'échelle de réacteurs autoclaves (entrées 1' à 4') pour la réaction catalytique de carboxylation de C₂H₄ en présence de CO₂ et HSiEt₃.

Entrée	Précurseur / ligand (1:1, 0,5 mol%) (vs HSiEt ₃)	Conv. HSiEt ₃ [mol%] ^[b]	TON (mol(produit)·mol(Ru) ⁻¹) ^[c]					
			Produits de la voie A		Produits des voies B et C			
			A1	P1	F1	TES	TEVS	E
1	[Ru(<i>p</i> -cymene)Cl ₂] ₂ / DCPB	>98	0,4	traces	141	55		2
1'		>98	0	0	0	180	traces	traces
2	Ru(H)(Cl)(CO)(PPh ₃) ₃ / PP ₃	8	18	traces	34	0		0
2'		29	0	0	0	traces	2	0
3	Ru(H)(Cl)(CO)(PPh ₃) ₃ / DCPB	92	0,3	traces	72	102		0
3'		54	13	1,3	16	4	53	1,6
4	[Ru(<i>p</i> -cymene)Cl ₂] ₂ / DPPF	>98	0,2	traces	79	103		4
4'		67	0	3	0	74	16	2
5	Ru(H)(Cl)(CO)(PPh ₃) ₃ / DPPF	92	0,3	traces	72	102		0
5'		16	0,2	0,4	0	10	4	0,4

Les résultats surlignés en gris ont été conduits à l'échelle de réacteurs autoclaves. Conditions réactionnelles : toluène (20 mL), [Si-H]₀ = 0,43 mol·L⁻¹, [Ru]₀ = [ligand]₀ = 0,002 mol·L⁻¹, CO₂/C₂H₄ 1:1 mol/mol, P(CO₂) + P(C₂H₄) = 20 bar; 16 h; expériences dupliquées. ^[b] Déterminée par intégration des signaux en RMN ¹H en utilisant le (Me₃Si)₄Si comme standard interne. ^[c] TONs déterminés par GC-FID en utilisant le *n*-dodécane comme standard interne.

Chapitre 3 – Couplage catalytique entre le CO₂ et C₂H₄ opéré par des complexes de ruthénium(II) porteurs de phosphines chélatantes bidentées

En parallèle des études d'optimisation des conditions de réaction, des études complémentaires ont montré qu'en faisant varier la nature des ligands phosphines bidentés, et ce en modifiant la longueur de chaîne du squelette du ligand et/ou la basicité des atomes de phosphores (substituants alkyle *vs* aryle, cyclohexyle *vs* phényle), les performances catalytiques s'en trouvaient impactés. Les tests catalytiques ont été effectués en utilisant Ru(H)(Cl)(CO)(PPh₃)₃ (**Ru-1**) comme précurseur. L'emploi du ligand DCPF (1,4-bis(dicyclohexylferrocenyl)butane) a montré une augmentation de la sélectivité envers les produits de la voie A. Ainsi, les deux combinaisons les plus prometteuses en termes de sélectivité ont été identifiées comme étant **Ru-1**/DCPB et **Ru-1**/DCPF. Afin de mieux comprendre la nature des espèces catalytiquement actives impliquées dans les deux systèmes, nous avons ciblé la synthèse de Ru(H)(Cl)(CO)(DCPF)(PPh₃) et Ru(H)(Cl)(CO)(DCPB)(PPh₃), qui sont des produits anticipés issus de la réaction d'échange de ligand entre **Ru-1** et DCPF, et **Ru-1** et DCPB (représentés dans le Schéma 6, à savoir **Ru-2** et **Ru-3**, respectivement).

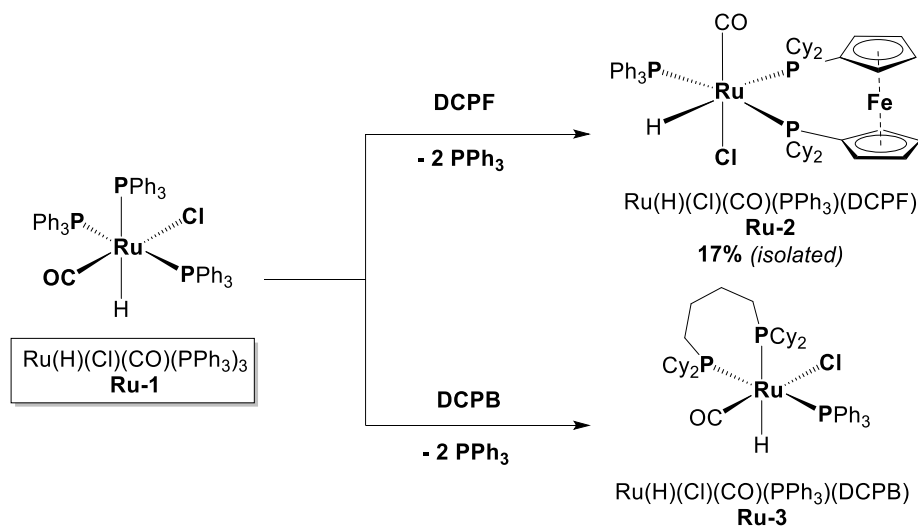


Schéma 6. Synthèses des complexes Ru(H)(Cl)(CO)(DCPF)(PPh₃) et Ru(H)(Cl)(CO)(DCPB)(PPh₃) à partir de la réaction de complexation de **Ru-1** avec les ligands DCPB et DCPF. A noter qu'un seul isomère de chaque espèce est représenté.

Des études de diffraction des rayons X et de spectroscopie RMN ont confirmé la formation des complexes attendus bidentés **Ru-2** et **Ru-3**. En particulier, les données RMN en solution ont montré que la réaction d'échange de ligand entre **Ru-1** et DCPB ne fournissait pas sélectivement **Ru-3**. La formation d'espèces hydrures de Ru a été observée. A partir des données RMN recueillies, ces dernières correspondraient à des isomères de position possibles de **Ru-3** (Schéma 7). Par ailleurs, il a été observé qu'en faisant varier le rapport molaire entre le précurseur et le ligand, la proportion de ces espèces diminuait.

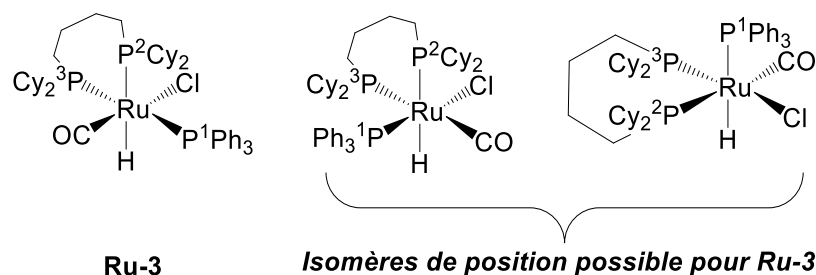


Schéma 7. Représentation des structures moléculaires des isomères de position possibles de **Ru-3**.

D'autre part, les essais de cristallisations du mélange réactionnel brut de **Ru-3** dans différents solvants et sous différentes conditions, ont montré la formation de structures bimétalliques (identifiées par étude XRD). Compte tenu de la flexibilité de la chaîne carbonnée du ligand DCPB, la formation de telles espèces dinucléaires n'est pas surprenante. Ainsi, la formation de complexes bimétalliques dans le milieu réactionnel, et sous nos conditions catalytiques, reste un scénario possible. Leurs activités quant à la formation des esters silylés n'ont cependant pas pu être évaluées en raison des faibles quantités proprement isolés.

D'autre part, des expériences stœchiométriques ont également démontré le rôle du HSiEt₃ pour la réduction des complexes de ruthénium monohydrure chlorés en leurs homologues dihydrures (**Ru-4**, Schéma 8). En conséquence, de nouvelles espèces hydrures pourraient se former en présence du réducteur silylé, rendant l'identification des espèces actives encore plus compliquée. Le complexe **Ru-4** peut également réagir avec un équivalent du ligand DCPB pour former le complexe Ru(H)₂(CO)(DCPB)(PPh₃) (espèce V, **Ru-5**), qui peut également être obtenu par réaction de **Ru-3** en présence de HSiEt₃ (IV).

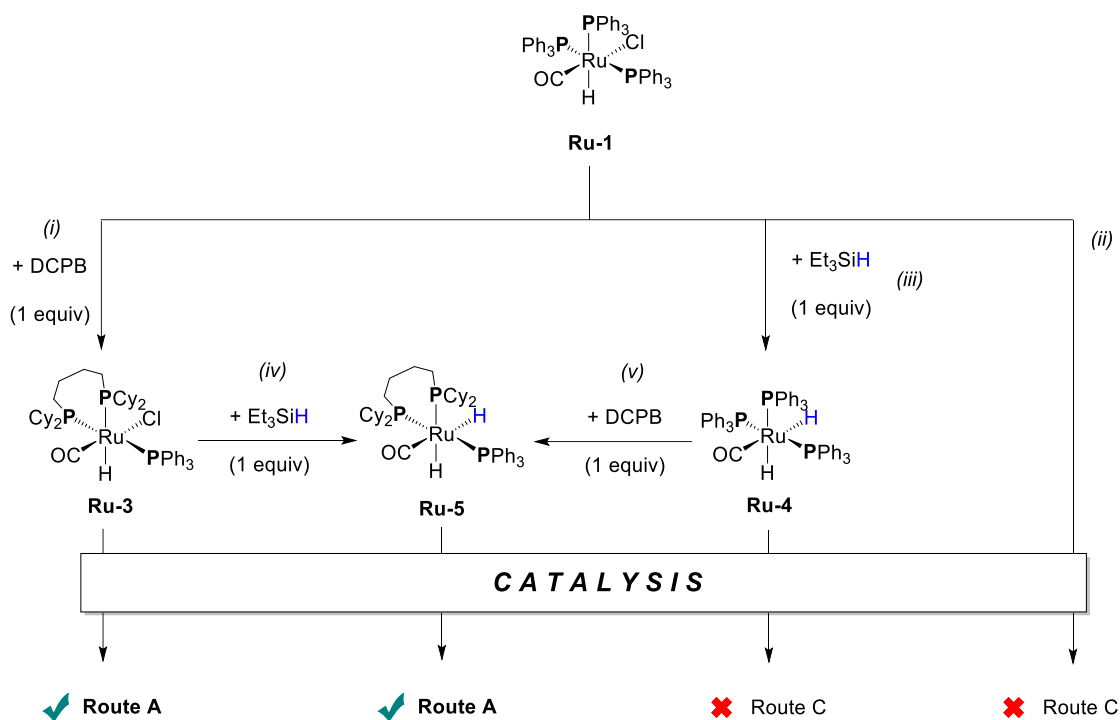


Schéma 8. Nouveaux complexes mono- et di-hydrures de ruthénium obtenus à partir de **Ru-1**.

Les complexes mono- et di-hydrures mentionnés ci-dessus ont été isolés, caractérisés et testés en catalyse. Différentes activités et sélectivités vis-à-vis des produits ciblés, les esters **A1** et **P1**, ont été observées (tableau 2). Ces résultats indiquent donc que plusieurs espèces menant aux composés ciblés de la voie A sont potentiellement actives, chacune initiant un cycle catalytique différent. D'autre part, ces espèces ont également fourni les produits des voies B et C, à savoir les sous-produits non désirés **F1**, **TEVS** et **TES** (tableau 2), suggérant que ces complexes sont également impliqués dans d'autres cycles catalytiques.

Les investigations menées dans l'objectif de distinguer l'espèce qui privilégie la voie A sont résumées sur le Schéma 8. Les complexes **Ru-3** et **Ru-5** étant identifiés comme les plus prometteurs.

Tableau 2. Activités catalytiques de différents précurseurs au ruthénium et ligands testés à l'échelle de réacteurs autoclaves pour la réaction catalytique de carboxylation de C_2H_4 en présence de CO_2 et $HSiEt_3$.^[a]

Entrée	Précurseur/ligand (1:1, 0,5 mol%)	Conv. $HSiEt_3$ [mol%] ^[b]	TON					
			Produits de la voie A			Produits des voies B et C		
			A1	P1	F1	TES	TEVS	E
1	$Ru(H)(Cl)(CO)(PPh_3)_3$ Ru-1	92	traces	traces	0	10	42	traces

2	Ru-1 / DCPB	54	13	1,3	16	4	53	1,6
3	$\text{Ru}(\text{H})_2(\text{CO})(\text{PPh}_3)_3$ Ru-4	47	traces	0	0	13	82	0
4	Ru-4 / DCPB	43	19	1,1	7	2	9	1
5	$\text{Ru}(\text{H})_2(\text{CO})(\text{DCPB})(\text{PPh}_3)$ Ru-5	51	22	2	9	4	10	1,3

^[a] Conditions réactionnelles: toluène (20 mL), $[\text{Si-H}]_0 = 0,43 \text{ mol}\cdot\text{L}^{-1}$, $[\text{Ru}]_0 = [\text{ligand}]_0 = 0,002 \text{ mol}\cdot\text{L}^{-1}$, $\text{CO}_2/\text{C}_2\text{H}_4$ 1:1 mol/mol, $\text{P}(\text{CO}_2) + \text{P}(\text{C}_2\text{H}_4) = 20 \text{ bar}$; expériences dupliquées. ^[b] Déterminée par intégration des signaux en RMN ^1H en utilisant le $(\text{Me}_3\text{Si})_4\text{Si}$ comme standard interne. ^[c] TONs déterminés par GC-FID en utilisant le *n*-dodécane comme standard interne.

Chapitre 4 – Etudes mécanistiques de la synthèse catalysée au ruthénium d'esters silylés à partir de C_2H_4 et CO_2

Les études mécanistiques ainsi que les approches rationnelles décrites dans le présent manuscrit se sont focalisées sur l'élucidation du mécanisme expliquant la formation catalytique des esters silylés à partir du complexe **Ru-3**.

Au vu des travaux récemment publiés par le groupe d'Iwasawa pour la carboxylation de l'éthylène, catalysée par un complexe zérovalent de ruthénium (**Schéma 9**),^[34,35] nous pourrions supposer qu'une ruthénalactone (cycle à cinq chaînons), générée par la cyclisation oxydative de C_2H_4 et de CO_2 , pourrait être générée dans notre mélange réactionnel.

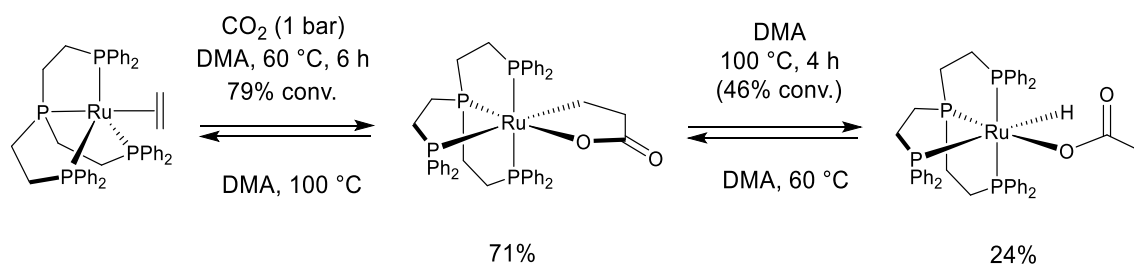


Schéma 9. Synthèse d'une ruthénalactone publiée par le groupe d'Iwasawa.^[34,35]

Etonnamment cependant, de telles espèces n'ont pas été observées dans notre milieu réactionnel. En revanche, un complexe intermédiaire clé, de formule moléculaire $\text{Ru}(\text{Cl})(\text{CO})(\text{DCPB})(\kappa^2\text{O}, \text{O}-\text{CO}_2\text{CH}=\text{CH}_2)$ (**Ru-6**, **Schéma 10**), a été caractérisé et isolé, et ce, pour la première fois. Celui-ci, en solution, a été observé sous la forme d'un mélange d'isomères *cis* et *trans* (positionnement du groupement acrylate par rapport au ligand DCPB).

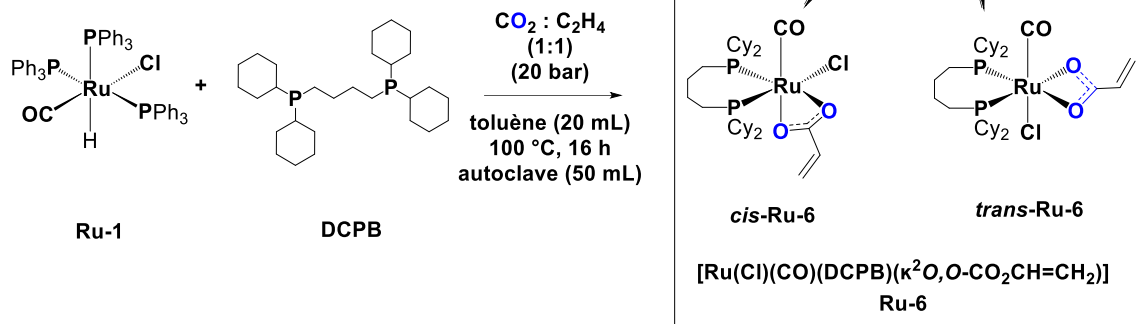


Schéma 10. Synthèse du complexe **Ru-6** en réacteur autoclave (50 mL). Illustration des formes d'isomérisme possibles entre les complexes *cis*-**Ru-6** et *trans*-**Ru-6**.

De par la présence du fragment acrylate, le couplage entre le CO_2 et C_2H_4 en présence du complexe **Ru-3** a bien été démontré. Contrairement à la formation établie des ruthénolactones, le mécanisme conduisant aux complexes $\kappa^2\text{O},\text{O}$ -acrylate Ru insaturés reste largement méconnu.

Cependant, compte tenu des preuves expérimentales, il est raisonnable de supposer que la première étape pour la formation de **Ru-6** consiste à dissocier le ligand PPh_3 , générant ainsi un site vacant dans la sphère de coordination du métal. Suite à cette étape, deux voies envisageables pour le couplage CO_2 - C_2H_4 sont proposées (**Schéma 11**) :

(a) la première implique un couplage oxydatif entre le C_2H_4 et CO_2 pour former un intermédiaire hypothétique ruthénolactone à 5 chaînons (espèce I), qui subirait par la suite une β -H élimination, aboutissant ainsi à un complexe d'acrylate de Ru(IV) (espèce II), suivie de la perte de H_2 ;

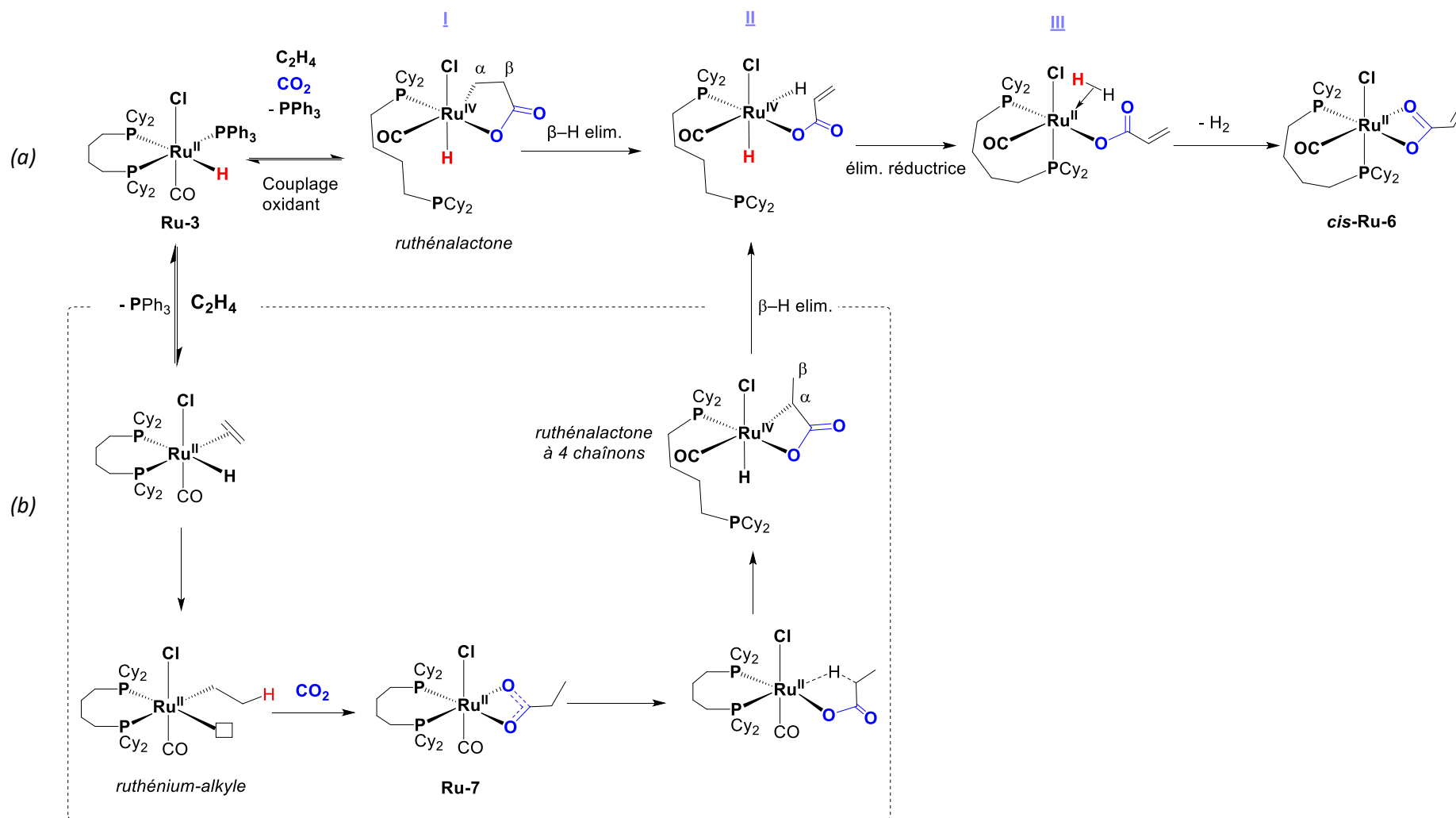


Schéma 11. Propositions de mécanismes réactionnel pour la formation du complexe **Ru-6** à partir de **Ru-1** et de DCPB sous une atmosphère de $\text{CO}_2\text{-C}_2\text{H}_4$ via (a) un intermédiaire ruthénolactone à 5 chaînons (b) une espèce ruthénium-alkyle et un intermédiaire ruthénolactone à 4 chaînons.

(b) la seconde débute par la coordination préliminaire de C_2H_4 au site vacant, conduisant à la formation d'un intermédiaire $Ru(H)(Cl)(CO)(DCPB)(CH_2=CH_2)$. Ensuite, C_2H_4 s'insérerait dans la liaison $Ru-H$ pour donner une espèce $Ru(II)$ -alkyle, suivi de l'insertion de CO_2 dans la liaison $Ru-C$ pour former le propionate de $Ru(II)$ (**Ru-7**). Une activation ultérieure de la liaison $\alpha-C-H$ formerait une ruthénalactone à 4 chaînons. Enfin, une étape de $\beta-H$ d'élimination générerait l'espèce acrylate (II), qui suite à la perte de H_2 donnerait **Ru-6**.

La suite des études mécanistique s'est concentrée sur l'étude des réactions stœchiométriques conduites sur le mélange d'isomères *cis* et *trans* de l'espèce **Ru-6**, visant à libérer les fragment carboxylate sous la forme d'un acide ou d'un ester.

En présence de $HSiEt_3$, la formation du complexe **Ru-3** a été observé, indiquant donc la rupture de la liaison covalente $Ru-O$, la création d'une liaison $Ru-H$, le départ du groupement acrylate et son remplacement par un ligand PPh_3 (Schéma 12, gauche). De plus, les données de suivi RMN ont confirmé la formation sélective de **A1**. Le fragment d'acrylate dérivé du CO_2 a donc facilement été libéré de la sphère de coordination de **Ru-6** lors de son traitement avec $HSiEt_3$ et régénérant le complexe **Ru-3**. A partir de ces résultats, le rôle de l'hydrosilane dans le cycle catalytique a été identifié comme double; libérer l'ester et régénérer l'espèce catalytique **Ru-3**.

D'autre part, exposer le complexe **Ru-6** à une atmosphère H_2 , a permis d'isoler des cristaux dont l'analyse cristallographique aux rayons X a montré la formation du complexe propionate $[Ru(Cl)(CO)(DCPB)(\kappa^2O,O-CO_2CH_2CH_3)]$ (**Ru-7**) (Schéma 12, milieu). Ce composé est issu de l'hydrogénation du complexe **Ru-6** parent.

Enfin, le suivi en spectroscopie RMN de la réaction stœchiométrique de **Ru-6** avec 1.5 équivalent de $MeOH$ a montré l'apparition de **Ru-3** et la formation de produits carboxylés dont la nature exacte n'a pas pu être identifiée.

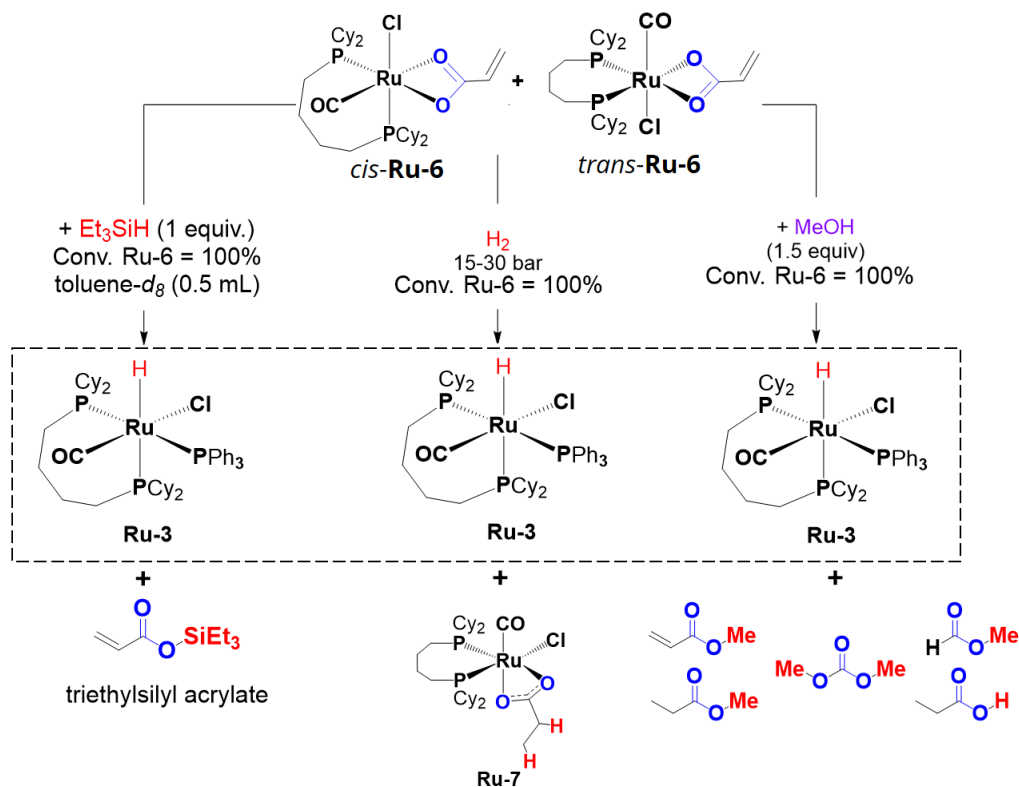


Schéma 12. Réactions stœchiométriques des complexes *cis*-**Ru-6** et *trans*-**Ru-6** en présence de différents réducteurs : de gauche à droite, HSiEt₃, H₂ et MeOH.

Compte tenu des résultats ci-dessus, un mécanisme possible pour la formation de **A1** et **P1** est proposé au **Schéma 13**. Tout d'abord, le complexe **Ru-3** est obtenu par complexation de **Ru-1** avec DCPB et libération d'un équivalent de PPh₃. Ensuite, le couplage oxydatif de CO₂ et C₂H₄ donnerait une espèce hypothétique (non observée) de ruthénalactone (IV) (I). En effet, puisque la formation et l'isolement des espèces de ruthénalactone ont déjà été décrits par Iwasawa *et al.*, la voie d'accès la plus probable au complexe **Ru-6** a donc supposé l'implication d'un tel intermédiaire.

La ruthénalactone (IV) générerait alors un complexe d'acrylate (dihydrido) ruthénium (IV) (**Schéma 13**, espèce II) par une étape de β-H d'élimination (facile et rapide). La possibilité pour le ruthénacycle de subir une élimination efficace du β-H a déjà été rapportée par le groupe d'Iwasawa par simple chauffage.^[34,35]

Par la suite, l'élimination de H₂ du complexe **III** donnerait accès au **Ru-6**, ainsi que **Ru-7** par réaction d'hydrogénation de la liaison C=C. Enfin, la réaction de **Ru-6** et **Ru-7** avec le l'hydrosilane libérerait les esters **A1** et **P1** et régénérerait l'espèce **Ru-3**.

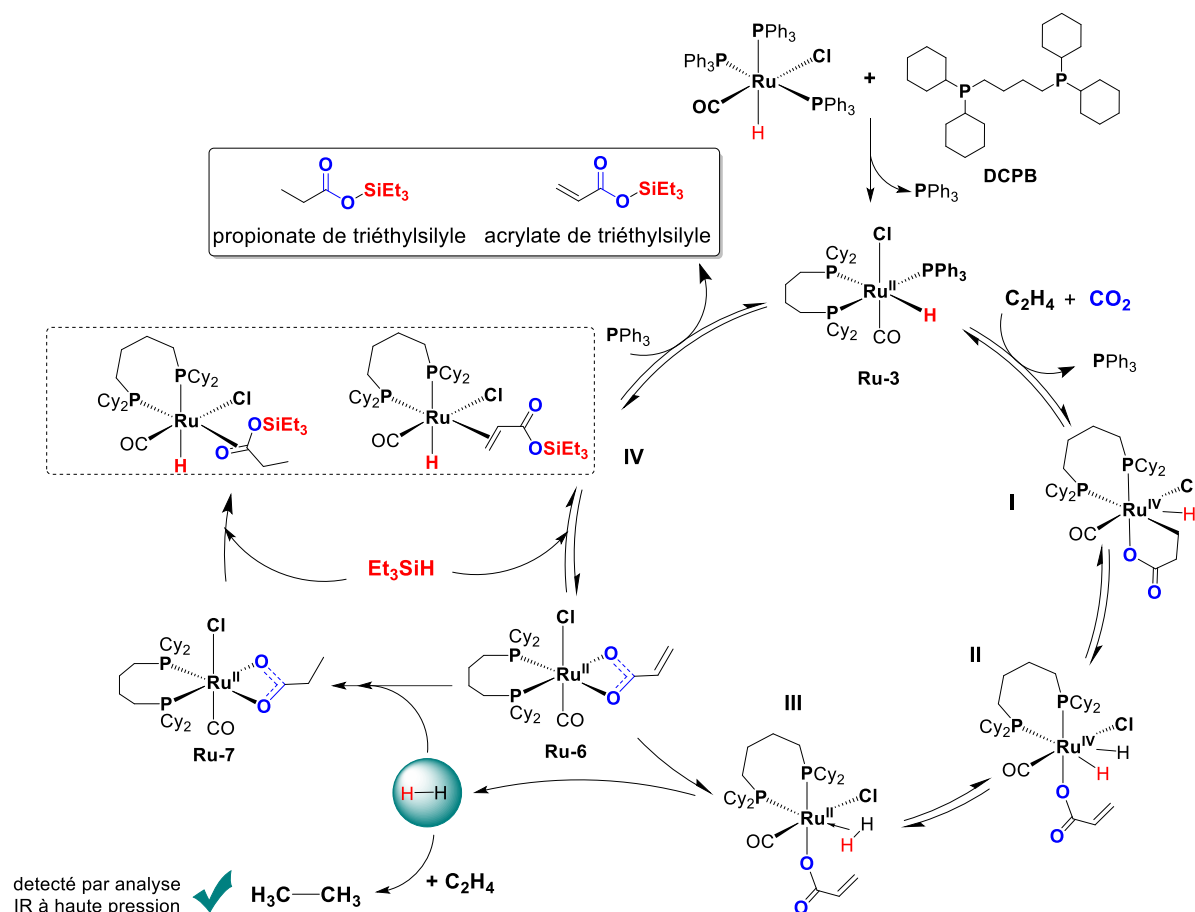


Schéma 13. Proposition de mécanisme réactionnel pour la formation de **A1** et **P1** à partir de **Ru-3**.

Par ailleurs, étant donné que la combinaison **Ru-1**/DCPB a également donné lieu aux sous-produits des voies B et C, provenant de l'hydrosilylation de CO_2 et de C_2H_4 ainsi que de la silylation déshydrogénative de C_2H_4 , des calculs DFT ont été effectués pour élucider les mécanismes de ces réactions secondaires à partir du complexe **Ru-3**. La nature riche en électrons du centre métallique de **Ru-3** et la disponibilité d'un site de coordination vacant par la dissociation facile du ligand PPh_3 rendent ce complexe adapté à l'activation du C_2H_4 et du CO_2 , suivies de l'hydrosilylation de ces derniers.

Enfin, dans le but d'améliorer l'efficacité et la sélectivité de notre système catalytique vis-à-vis de la production de **A1** et **P1**, différents additifs ont été testés en catalyse. Il a été constaté que l'ajout d'eau en quantité sur-stoechiométriques (40 mol% vs. HSiEt_3) était bénéfique au système, permettant d'augmenter la production de **P1** (TON de 1,3 sans eau et 68 avec eau). Le mécanisme d'action en présence d'eau est soumis aux calculs DFT afin de comprendre son rôle au sein de la sphère de coordination et son implication dans la formation privilégiée de **P1** par rapport à **A1**.

Conclusion et perspectives

L'utilisation du CO₂ comme source de carbone représente une méthodologie clé vers le développement de procédés chimiques durables. Au cours des dernières décennies, des efforts considérables ont été réalisés dans le domaine des réactions de carboxylation, utilisant le CO₂ comme matière première pour produire des acides carboxyliques et leurs dérivés, qui sont des composés intéressants pour la synthèse de chimie fine. Leur préparation comprend plusieurs méthodes bien établies et malgré leur efficacité, les réactions de carboxylation catalysées par des métaux de transition ont connu une croissance exponentielle, puisqu'elles permettent l'utilisation d'une plus large variété de partenaires de couplage, tout en améliorant la compatibilité des groupes fonctionnels.

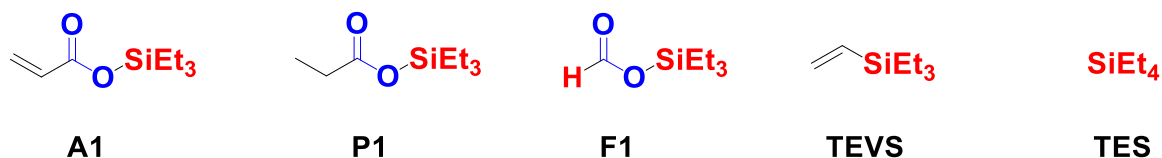
Cependant, ces réactions catalysées ont nécessité l'utilisation de co-réactifs organométalliques fortement polarisés et hautement réactifs pour convertir le CO₂ en dérivés d'acide carboxylique, et générant ainsi des quantités importantes de déchets.

A travers ce travail, nous avons cherché à développer un nouveau système catalytique pour la production de dérivés d'acides carboxyliques à partir du couplage C₂H₄-CO₂, en utilisant comme agent réducteur le HSiEt₃, facilement disponible et facile à manipuler. La réactivité modulable des hydrosilanes, de par leurs substituants sur l'atome de silicium, en fait des agents réducteurs compétitifs vis-à-vis des hydrures organométalliques.

Les études préliminaires menées avec nos collaborateurs, experts des techniques de criblage à haut débit (HTS) (Argonne National Laboratory, IL, USA et plateforme Realcat de l'UCCS, Lille, France), ont étudié environ 150 combinaisons différentes de ligands et de précurseurs catalytiques.

Certains systèmes catalytiques prometteurs ont fourni les deux esters silylés ciblés **A1** et **P1**, qui ont été identifiés et quantifiés par analyses GC et GC-MS.

Cependant, la réaction de couplage C₂H₄-CO₂ en présence de HSiEt₃ présente des réactivités parasites. En effet, le réducteur réduit les esters ciblés en leurs homologues gazeux, ou encore réagit indépendamment avec C₂H₄ ou CO₂. Ainsi, ces premiers résultats HTS nous ont permis de trier les systèmes catalytiques capables de produire **A1** et **P1** tout en essayant d'éviter les sous-produits **F1**, **TEVS** et **TES**.



Les précurseurs métalliques à base de Ru, en combinaison avec des ligands phosphines bidentés, ont montré une prédisposition à fournir, après optimisation des conditions réactionnelles, des sélectivités plus élevées envers **A1** et **P1**, en atteignant des TONs maximum de 13 et 68, respectivement. Les complexes mono- et di-hydrure de Ru, porteurs d'un ligand diphosphine DCPB et DCPF, se sont avérés être des candidats prometteurs pour des études mécanistiques.

Ainsi, nous avons cherché à identifier les espèces de Ru catalytiquement actives formées lors du couplage de CO₂ et C₂H₄, et capables de délivrer **A1** et **P1**. L'acquisition d'informations structurales détaillées sur les intermédiaires clés et les sous-produits ont permis de proposer un cycle catalytique.

Des calculs DFT en cours pour obtenir des informations plus détaillées sur la nature des structures des complexes mises en jeu. En parallèle, pour une meilleure compréhension des étapes élémentaires impliquées dans le cycle catalytique, des études de marquage isotopique ¹³C à l'aide de ¹³CO₂ peuvent aider à identifier des produits complémentaires dérivés du CO₂.

Si ces données en attente aident à confirmer les hypothèses mécanistiques proposées, nous pourrions alors envisager de faire varier les conditions réactionnelles pour améliorer les sélectivités envers la formation des esters ciblés et entraver les capacités du système **Ru-1**/DCPB à catalyser les réactions parasites.

Les études d'optimisation menées en parallèle ont montré que l'ajout de H₂O au mélange catalytique *in situ* augmentait remarquablement la production de **P1**, bien que l'on ne sache toujours pas comment l'eau interfère dans le mécanisme réactionnel de sa formation.

Ces informations supplémentaires pourraient également être utiles pour comprendre et rationaliser les différences de réactivité observées.

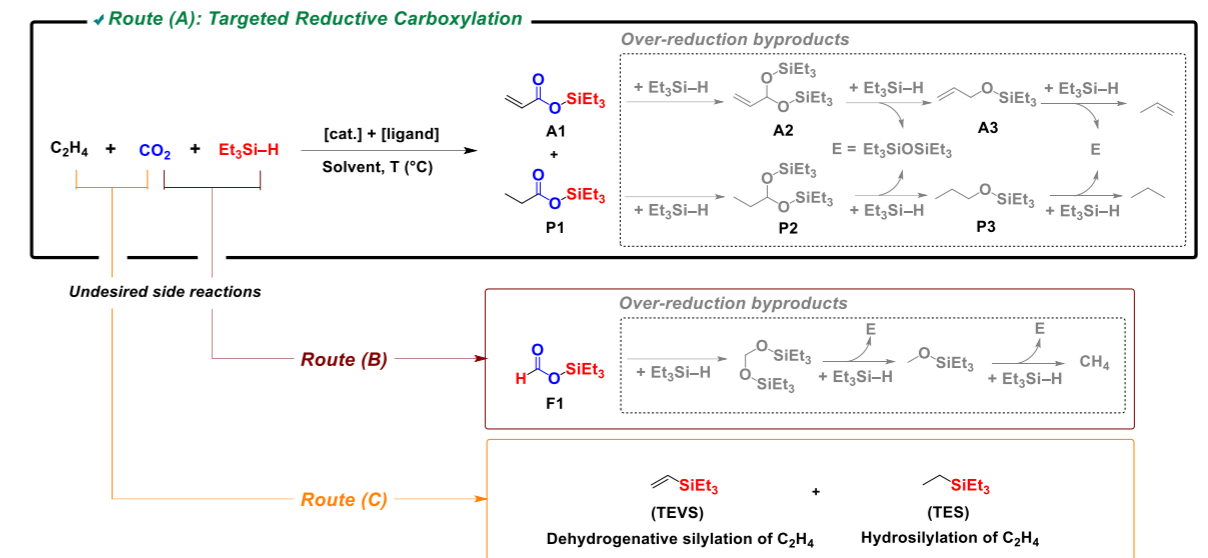
A plus long terme, il serait intéressant d'étudier le rôle de la sphère de coordination du centre Ru sur l'activité catalytique en faisant varier soit la nature des ligands X et/ou L soit en modifiant le nombre de coordination autour du métal.

Grâce à une approche multidisciplinaire, impliquant plusieurs techniques expérimentales, spectroscopiques et modèles théoriques, ce travail a conduit, nous l'espérons, à une meilleure compréhension de l'activation du CO₂ en présence de catalyseurs au Ru. Les projets de valorisation et d'utilisation du CO₂ comme matière première, tels que celui décrit dans ce manuscrit, continueront, espérons-le, à fleurir, menant peut-être un jour au développement de procédés industriels efficaces. S'appuyer sur des ressources renouvelables en carbone pourrait, dans le scénario le plus optimiste, fournir des solutions à long terme à l'accumulation croissante du CO₂ dans l'atmosphère, mais ne résoudra certainement pas, à lui seul, la crise climatique à laquelle la Terre est confrontée aujourd'hui.

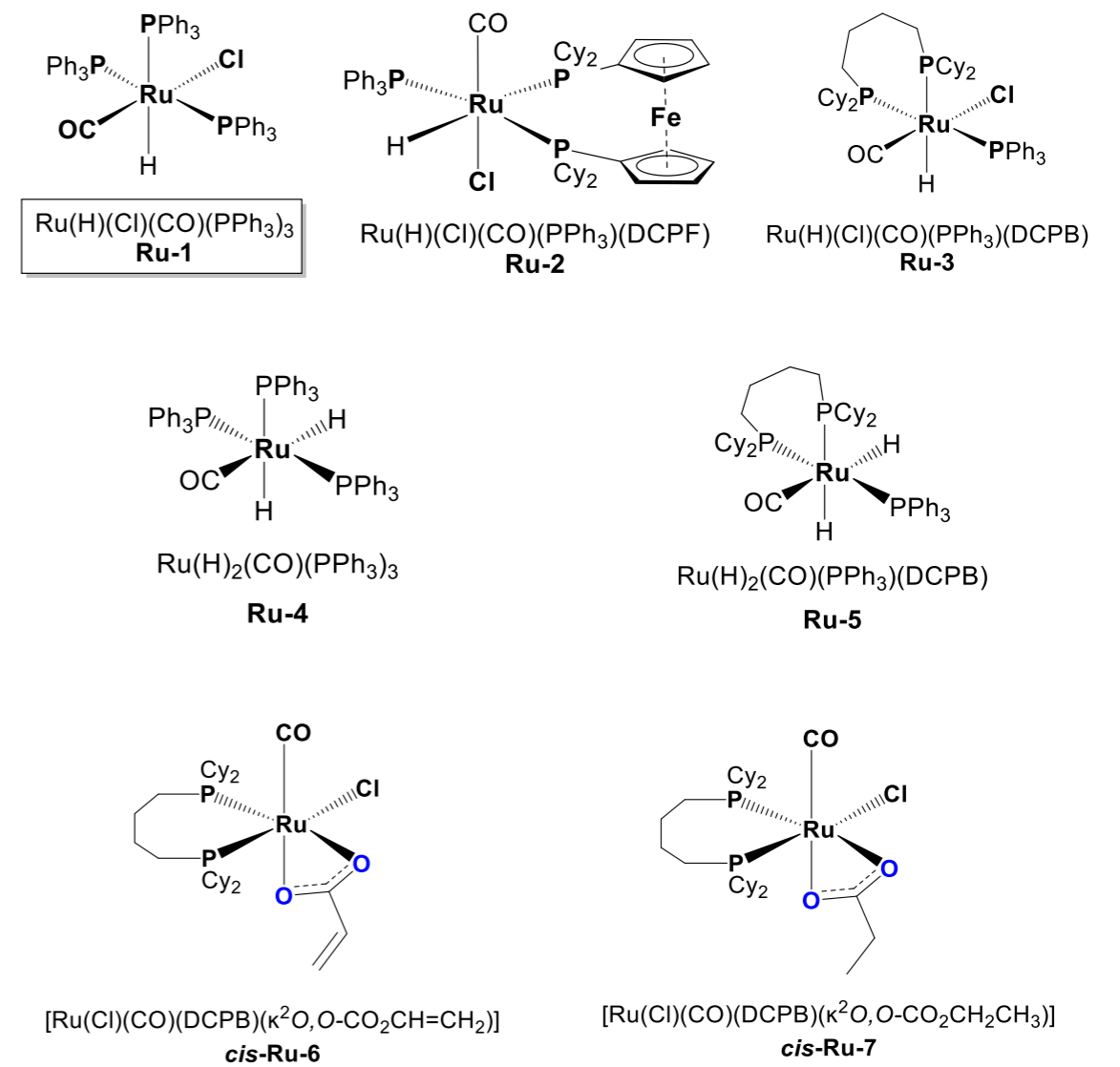
Références bibliographiques

- [1] H. Ritchie, M. Roser, *Our World Data* **2020**.
- [2] T. Allison, **1996**, DOI 10.18434/T42S31.
- [3] S. Topham, A. Bazzanella, S. Schiebahn, S. Luhr, L. Zhao, A. Otto, D. Stolten, in *Ullmanns Encycl. Ind. Chem.*, American Cancer Society, **2014**, pp. 1–43.
- [4] C. Das Neves Gomes, O. Jacquet, C. Villiers, P. Thuéry, M. Ephritikhine, T. Cantat, *Angew. Chem. Int. Ed.* **2012**, *51*, 187–190.
- [5] “Valorisation chimique du CO₂ : état des lieux. Quantification des bénéfiques é...,” can be found under <https://www.ademe.fr/valorisation-chimique-co2-etat-lieux-quantification-benefices-energetiques-environnementaux-evaluation-economique-trois-voies-chimiques>, **n.d.**
- [6] “Putting CO₂ to Use – Analysis,” can be found under <https://www.iea.org/reports/putting-co2-to-use>, **n.d.**
- [7] M. Limbach, in *Adv. Organomet. Chem.* (Ed.: P.J. Pérez), Academic Press, **2015**, pp. 175–202.
- [8] “Surfactants from Renewable Resources | Wiley,” can be found under <http://www.wiley.com/en-us/Surfactants+from+Renewable+Resources-p-9780470760413>, **n.d.**
- [9] Jonathan Clayden, Nick Greeves, Stuart Warren, *Organic Chemistry Second Edition*, **2012**.
- [10] A. Tortajada, F. Juliá-Hernández, M. Börjesson, T. Moragas, R. Martin, *Angew. Chem. Int. Ed.* **2018**, *57*, 15948–15982.
- [11] H. Hoberg, A. Ballesteros, A. Sigan, C. Jegat, A. Milchereit, *Synthesis* **1991**, *1991*, 395–398.
- [12] H. Hoberg, Y. Peres, C. Krüger, Y.-H. Tsay, *Angew. Chem. Int. Ed. Engl.* **n.d.**, *26*, 771–773.
- [13] H. Hoberg, A. Ballesteros, A. Sigan, C. Jegat, D. Bärhausen, A. Milchereit, *J. Organomet. Chem.* **1991**, *407*, C23–C29.
- [14] H. Hoberg, A. Ballesteros, A. Sigan, *J. Organomet. Chem.* **1991**, *403*, C19–C22.
- [15] H. Hoberg, Y. Peres, A. Milchereit, *J. Organomet. Chem.* **1986**, *307*, C38–C40.
- [16] H. Hoberg, D. Schaefer, G. Burkhart, C. Krüger, M. J. Romão, *J. Organomet. Chem.* **1984**, *266*, 203–224.
- [17] R. Alvarez, E. Carmona, D. J. Cole-Hamilton, A. Galindo, E. Gutierrez-Puebla, A. Monge, M. L. Poveda, C. Ruiz, *J. Am. Chem. Soc.* **1985**, *107*, 5529–5531.
- [18] R. Alvarez, E. Carmona, M. L. Poveda, R. Sanchez-Delgado, *J. Am. Chem. Soc.* **1984**, *106*, 2731–2732.
- [19] Rafael. Alvarez, Ernesto. Carmona, Agustin. Galindo, Enrique. Gutierrez, J. M. Marin, Angeles. Monge, M. L. Poveda, Caridad. Ruiz, J. M. Savariault, *Organometallics* **1989**, *8*, 2430–2439.
- [20] M. Álvarez, A. Galindo, P. J. Pérez, E. Carmona, *Chem. Sci.* **2019**, *10*, 8541–8546.
- [21] A. Galindo, A. Pastor, P. J. Perez, E. Carmona, *Organometallics* **1993**, *12*, 4443–4451.
- [22] D. C. Graham, C. Mitchell, M. I. Bruce, G. F. Metha, J. H. Bowie, M. A. Buntine, *Organometallics* **2007**, *26*, 6784–6792.
- [23] G. Schubert, I. Pápai, *J. Am. Chem. Soc.* **2003**, *125*, 14847–14858.
- [24] I. Pápai, G. Schubert, I. Mayer, G. Besenyi, M. Aresta, *Organometallics* **2004**, *23*, 5252–5259.
- [25] W. H. Bernskoetter, B. T. Tyler, *Organometallics* **2011**, *30*, 520–527.
- [26] C. Hendriksen, E. A. Pidko, G. Yang, B. Schäffner, D. Vogt, *Chem. – Eur. J.* **2014**, *20*, 12037–12040.
- [27] N. Hugué, I. Jevtovikj, A. Gordillo, M. L. Lejkowski, R. Lindner, M. Bru, A. Y. Khalimon, F. Rominger, S. A. Schunk, P. Hofmann, M. Limbach, *Chem. – Eur. J.* **2014**, *20*, 16858–16862.
- [28] S. Manzini, A. Cadu, A.-C. Schmidt, N. Hugué, O. Trapp, R. Paciello, T. Schaub, *ChemCatChem* **2017**, *9*, 2269–2274.
- [29] T. Fujihara, T. Xu, K. Semba, J. Terao, Y. Tsuji, *Angew. Chem. Int. Ed.* **2011**, *50*, 523–527.
- [30] Z. M. Heiden, A. P. Lathem, *Organometallics* **2015**, *34*, 1818–1827.
- [31] K. Kunihiro, S. Heyte, S. Paul, T. Roisnel, J.-F. Carpentier, E. Kirillov, *Chem. – Eur. J.* **2021**, *27*, 3997–4003.
- [32] F. J. Fernández-Alvarez, L. A. Oro, *ChemCatChem* **2018**, *10*, 4783–4796.
- [33] S. Lachaize, L. Vendier, S. Sabo-Etienne, *Dalton Trans.* **2010**, *39*, 8492–8500.
- [34] T. Ito, K. Takahashi, N. Iwasawa, *Organometallics* **2019**, *38*, 205–209.
- [35] K. Takahashi, Y. Hirataka, T. Ito, N. Iwasawa, *Organometallics* **2020**, *39*, 1561–1572.

Possible products of the coupling reaction of CO₂ with C₂H₄ in the presence of Et₃SiH.



Chemdraw drawings of the synthesized and characterized Ru complexes.



Titre : Activation du CO₂ pour la formation d'acides et d'esters carboxyliques, catalysée par des précurseurs au ruthénium

Mots clés : CO₂ – C₂H₄ – carboxylation – ruthénium – phosphine – mécanisme – esters silyliques

Résumé : Au cours des dernières décennies, l'utilisation du CO₂ comme matière première carbonée a suscité un intérêt considérable de par sa non toxicité et son abondance. Le CO₂ représente une ressource renouvelable attrayante pour pallier à la consommation massive de ressources fossiles et aux difficultés environnementales liées à leur exploitation. Plus récemment, le développement de nouvelles stratégies de synthèse d'acides carboxyliques, molécules polyvalentes pour la chimie fine, ont vu le jour. Néanmoins, en raison de la stabilité inhérente du CO₂, l'utilisation de substrats hautement réactifs et générateurs de déchets est souvent nécessaire. Le présent travail doctoral s'est intéressé au développement de nouveaux systèmes pour les réactions de carboxylation réductrice, catalysées par des métaux de transition, permettant de s'affranchir de co-réactifs polluants.

Ces travaux de thèse s'intéressent d'abord à l'étude de l'activité de différents systèmes catalytiques, préalablement sélectionnés au travers d'une étude de la littérature existante. En utilisant une approche de criblage à haut débit, certains systèmes prometteurs pour la réaction de carboxylation réductrice du C₂H₄, en présence du réducteur Et₃SiH, ont été identifiés puis optimisés en termes de conversion et de sélectivité. La seconde partie du manuscrit vise à la compréhension des mécanismes réactionnels donnant accès aux esters d'alkyle et d'alcényl silylés désirés. Elle décrit en particulier l'élucidation structurale des espèces catalytiques intermédiaires générées *in situ* à partir de précurseurs au ruthénium et de ligands phosphine bidentés. Les connaissances acquises à travers des études RMN expérimentales, complétées par des calculs DFT, ont permis de proposer plusieurs mécanismes réactionnels potentiellement mis en jeu.

Title : Catalytic activation of CO₂ towards carboxylic acids and esters mediated by ruthenium precursors

Keywords : CO₂ – C₂H₄ – carboxylation – ruthenium – phosphine – mechanism – silyl esters

Abstract : In recent decades, the use of CO₂ as a carbon source has gained considerable interest due to its non-toxicity and abundance. CO₂ represents an attractive renewable resource to decrease the massive consumption of fossil fuels as well as the environmental difficulties associated with their exploitation. More recently, the development of new strategies for carboxylic acids synthesis has emerged as these compounds are versatile starting materials for the fine chemical industry. However, due to the inherent stability of CO₂, the use of highly reactive and waste-generating substrates is often needed. The present project finds interest in developing new systems for reductive carboxylation reactions, catalyzed by transition metals, allowing to avoid the use of polluting co-reactants. This work first focuses on the study of different catalytic systems activities, previously selected through a literature study.

Using a high throughput screening approach, some promising systems for the reductive carboxylation reaction of C₂H₄, in the presence of the reducing agent Et₃SiH, have been identified and then optimized in terms of conversion and selectivity. The second part of the manuscript aims at understanding the corresponding reaction mechanisms giving access to the targeted alkyl and alkenyl silyl esters. In particular, it describes the structural investigations carried out on the catalytic intermediate species generated *in situ* from ruthenium precursors and bidentate phosphine ligands. The knowledge acquired through experimental NMR studies, supplemented by DFT calculations, allowed to propose several reaction mechanisms potentially involved.